Rock Fabric Study of the Northern Lebombo and Rooi Rand Dyke Swarms – Regional and Local Implications

By:

Warwick W. Hastie

Submitted in fulfilment of the degree Doctor of Philosophy

In the Discipline of Geological Sciences

School of Agricultural, Earth and Environmental Sciences

College of Agriculture, Engineering and Science

University of KwaZulu-Natal,

Durban

South Africa

2012

- Preface -

- SUPERVISOR'S APPROVAL -

As the candidates supervisor I have/have not approved this dissertation for submission and examination.

Signature: _____ Date: _____

Prof. Michael K. Watkeys

As the candidates co-supervisor I have/have not approved this dissertation for submission and examination.

Signature:  Date: _____

Prof. Charles Aubourg

- CANDIDATES DECLARATION -

I ..... declare that:

(i) The research reported in this thesis, except where otherwise indicated, is my original work.

(ii) This thesis has not been submitted for any degree or examination at any other university.

(iii) This thesis does not contain other persons' data, pictures, graphs or other information, unless specifically acknowledged as being sourced from other persons.

(iv) This thesis does not contain other persons' writing, unless specifically acknowledged as being sourced from other researchers. Where other written sources have been quoted, then:

a) their words have been re-written but the general information attributed to them has been referenced;

b) where their exact words have been used, their writing has been placed inside quotation marks, and referenced.

(v) Where I have reproduced a publication of which I am author, co-author or editor, I have indicated in detail which part of the publication was actually written by myself alone and have fully referenced such publications.

(vi) This thesis does not contain text, graphics or tables copied and pasted from the Internet, unless specifically acknowledged, and the source being detailed in the thesis and in the References sections.

Signed: _____ Date: _____

- Acknowledgements -

This project has taken over 5 years to complete, beginning as a MSc. project and has benefitted greatly from input from many people. There are so many people to thank, whose small or large gifts of guidance and help have had a profound effect on this thesis and my "geological" life over the past years. I apologise if I have forgotten anyone.

First and foremost I would like to thank my supervisor and co-supervisor. Prof. Watkeys, you have been an inspirational character since first year and still now during the completion of this thesis. You have been patient, insightful and most of all helped me to bring this project up to the standard it has (hopefully!) reached.

Prof. Charles (Charly) Aubourg, you have been a great co-supervisor from the outset of this project, and very patient with me. You have been gracious enough to introduce me to some top class scientists, your family, friends, the French Alps and the French way of life.

I am extremely grateful to both Prof. Watkeys and Charly (Prof. Aubourg) for the opportunity to be a part of a joint French - South African co-operation, and to the NRF (National Research Foundation) and CNRS (*Centre National de la Recherche Scientifique*) for funding and travel and research expenses respectively. Bernard Henry of the IPGP (*Institut de Physique du Globe de Paris*) was most gracious to allow me the use of some of the finest magnetic facilities in the world. I must extend my gratitude also to Alain Vauchez and Luiz Morales at the University of Montpelier for allowing me the use of the EBSD facility.

At the University of Cergy-Pontoise I would like to thank Dominic Frizon de Lamotte, Christian David, Phillipe Robion, Ronan Hebert and Jean-Christian Colombier who were extremely hospitable during my three stays. Each of you helped me at some stage, from laboratory work to stimulating discussions about this work. The postgraduate students in France, particularly Nico, Lisa, Camille, Fabien and Matthieu were extremely welcoming and friendly. Thank you very much. I will always remember my visits to France with fondness.

Back in South Africa I would like to extend my gratitude to Prof. Steve McCourt, former head of the School of Geological Sciences. You are someone I could always go to for help and advice regarding the seemingly never-ending administrative issues faced by post-grads. You have done a super-human job of keeping the department going, which has had a direct impact on the completion of this work. Within the department I am also indebted to Arthur Peterson and Mukesh Seyambu for help with the converted chainsaw drill, and its maintenance. Mukesh made more than 180 thin sections which have been used in the SPO analysis. This work has proved critical Mukesh, so thank you kindly. Steve Hughes, Kent Gravelet-Blondin, Gareth Driemeyer and Peter Horvath helped with sampling in Swaziland. Dr. Matt Brayshaw helped enormously by introducing me to the SPO and Ellipsoid programs.

Another postgraduate (now staff member) who has helped me along the way is Dr. Andrew Green. You kept me sane during our all too frequent tea breaks, geo-braai's and other shenanigans. I wish you and Lauren well in your careers.

To my non-geology friends, a big "thank you" as well. Without having great friends to go fishing with, climbing with, or just hanging out, I would have surely lost my mind long ago.

To my kindred spirit, girlfriend and best-friend Michelle, thanks seem inadequate. You came into my life at a particularly difficult time during the writing and publication of papers of which this thesis consists. Your encouragement and belief in me will never be forgotten.

Finally, to my family…I love you more than anything in the world, and the realisation that you have let me pursue my studies further in spite of any financial or personal gain is a profound one. I'm sure it has not been easy having a sometimes manic post-grad living in the house, but I hope to be as self-sacrificing as you have demonstrated is possible one day.

"*The visitor from another planet would look at the evidence and come up with a sensible hypothesis. If a … geophysicist were to … present her with the plume theory, the visitor would certainly say "What the Hell is that*?"

Prof. Don L. Anderson (California Institute of Technology)

(From: www.mantleplumes.org)

- Abstract -

This thesis comprises three new works which document the investigation of magma flow direction in 32 mafic dykes of the Northern Lebombo and Rooi Rand dyke swarms of southern Africa. These dyke swarms are an integral igneous component of the Lebombo rifted volcanic margin that developed during the formation of the Karoo Large Igneous Province ~183 million years ago. The northeast trending Sabi monocline and the west-northwest trending Okavango dyke swarm intersect with the northern Lebombo, forming a conspicuous triple-junction-like geometry. The triple junction, along with geochemical and petrological evidence, has led researchers to hypothesise that a mantle plume may be responsible for its formation, and consequently that lateral injection of magma occurred during the emplacement of these dyke swarms. Characteristic studies of magma flow direction in dykes have often used one technique (e.g. anisotropy of magnetic susceptibility) to determine the origin of flow-related petrofabric. This is achieved by measuring (directly, or geophysically) the crystallised grains that have imbricated along dyke margins because of the simple shear of magma along the wall rock during emplacement. Thus, both the direction and absolute sense of magma flow in presently solidified dykes can be quantified. In contrast, this study investigates and compares 1) the origin of magnetic fabric, 2) the origin of the plagioclase petrofabric and 3) macroscopic flow-related structures (where available) in dykes of the Northern Lebombo and Rooi Rand dyke swarms. The microscopic and submicroscopic methods employed include measuring the anisotropy of magnetic susceptibility and mineral shape preferred orientation. Results show that the bulk magnetic fabric in the Rooi Rand dyke swarm is generally sub-parallel to the dyke plane. This is type-A fabric. Further investigation of the shape preferred orientation of plagioclase and opaque (magnetite grains) reveals an additional inverse fabric in 30% of the data. This is type-B fabric. It is proposed that the type-B petrofabric (which is in most cases not coaxial with the magnetic fabric) was acquired during increased grain interaction during late-stage magma flow associated with increasing viscosity and decreasing magma pressure. Three dimensional fabric shape tensors and grain-size and shape data show that the most common grain-size classes with modest shape ratios ($1.80 < r < 2.20$), are predominantly associated with type-A fabric in the Rooi Rand dyke swarm. Conversely, grains with increasing r values show a tendency toward type-B fabric. Textural information and crystal size distributions are consistent with late-stage nucleation and growth of plagioclases < 80 μm in size. This late-stage, rapid nucleation of plagioclase groundmass significantly affected the final fabric that developed, apparently related to grains increasing in anisotropy because of rapid undercooling. If only type-A fabric in the Rooi Rand dyke swarm is considered on a regional scale it suggests that both inclined (sub-vertical) and lateral magma flow has occurred. This is also supported by the shape preferred orientation of plagioclase. Magnetic fabric in the Northern Lebombo dyke swarm is of magmatic origin in ~50% of the samples and is carried predominantly by stoichiometric magnetite. The anisotropy of magnetic susceptibility and shape preferred orientation data show remarkable agreement and at the dyke and regional scale tend to support lateral magma flow from the north in the youngest dykes. Thus, the petrofabric of the Northern Lebombo dyke swarm is interpreted to have developed as a result of lateral magma flow from the Karoo triple junction. Proof of the influence of a mantle plume in the development of the Karoo triple junction remains inconclusive from petrofabric studies alone, but appears to be unlikely in light of this and other work documenting the composition and age of the dyke swarms and the extrusive components of the Karoo Large Igneous Province.

- Contents -

-page-

- Chapter 1 -

Introduction

1.1. Research Objective

The principal objective of this study was to investigate the original magma flow direction in two dyke swarms in southern Africa. These two dyke swarms, the Northern Lebombo dyke swarm (NLDS) and the Rooi Rand dyke swarm (RRDS), are north-south (N–S) striking mafic dyke swarms which are parallel to the Lebombo faulted monocline which is essentially a volcanic rifted margin (Watkeys, 2002). The Lebombo formed during the development of the Karoo Large Igneous Province (LIP) from ~183–174 million years (Ma) ago (Jourdan et al., 2004).

The Lebombo monocline has long been considered the southern branch of the Karoo triple junction, centred on Mwenezi (formerly Nuanetsi) in southern Zimbabwe (Burke and Dewey, 1973). From this triple junction an additional two dyke swarms extend: the Okavango dyke swarm (ODS) to the west-northwest (WNW) and the Save-Limpopo dyke swarm (SLDS) to the northeast (NE) (Le Gall et al., 2005). The conspicuous triple-rift geometry of these dyke swarms, along with geochemical and petrological evidence, suggests that a mantle plume may be responsible for its formation (White and McKenzie, 1989). As a result, it is likely that such a plume may have provided the magmatic source and indeed the driving pressure for the development of these dykes.

Therefore, this work examines evidence of emplacement and flow-related fabric within the petrofabric of the NLDS and RRDS. The research can be framed best by the following seven research questions:

1. To what extent does evidence for magma flow in the NLDS and RRDS exist?
2. How do the discovered flow directions relate to the mantle plume model which predicts lateral magma flow away from a central magma source?

3. How reliable is the measurement of the anisotropy of magnetic susceptibility (AMS) in finding the orientation of petrofabric(s) in mafic dykes?
4. Is the measurement of the mineral shape-preferred orientation (SPO) of constituent grains a more rigorous test of petrofabric orientation?
5. How do results of the analytical techniques compare to field evidence of magma flow direction?
6. Are there any other processes besides magma flow which may affect the fabric origin and/or orientation in these dykes?
7. Is there any relationship between mineral grain-size or morphology and imbricated magmatic fabric?

It should be noted, therefore that the regional implications of this work relate to understanding the nature of the magma flow history in the NLDS and RRDS (questions 1 and 2). The local implications relate to questions 3–7, which appraise whether the techniques (AMS and SPO) and the results gleaned from them are sensible and reliable predictors of magmatic petrofabrics. As will become evident, the results of these methods can be contradictory. Hence one of the main objectives of this work was to investigate possible pitfalls of interpretation when confronted with the "best" result of a particular technique, most notably AMS. This work is presented first in the thesis, as it develops the necessary framework in which the regional work on the dyke swarms can be correctly interpreted.

1.2. Structure & Layout of Thesis

This submission is composed of three current publications accepted and published in international, peer-reviewed journals. A fourth paper, combining the work presented here with previous work of Aubourg et al. (2008) and Curtis et al. (2008) is currently being submitted to the journal "Gondwana Research".

This paper is essentially a review of the current knowledge of the flow directions in 5 dyke swarms of the Karoo LIP and how they relate to the current understanding of how Karoo magmatism developed in southern Gondwana. It is a combination of the geological

background of the Karoo LIP presented in Chapter 3 and the work presented in Chapter 6 in combination with the regionally significant petrofabric of the RRDS. This overview, presented in Chapter 7, explores the regional significance of magma flow in dykes within the Karoo LIP (see Appendix B for the manuscript of Paper IV).

The accepted and published papers are as follows, in the order they appear in this thesis:

- Paper I: Hastie, W.W., Aubourg, C., Watkeys, M.K., 2011. When an "inverse" fabric is not inverse: an integrated AMS-SPO study in MORB-like dykes. Terra Nova 23, 49–55.
- Paper II: Paper IV: Hastie, W.W., Watkeys, M.K., Aubourg, C., (in press). Characterisation of grain-size, shape and orientation of plagioclase in the Rooi Rand dyke swarm. Tectonophysics. DOI: 10.1016j.tecto.2012.10.035.
- Paper III: Hastie, W.W., Watkeys, M.K., Aubourg, C., 2011. Significance of magnetic and petrofabric in Karoo-feeder dykes, northern Lebombo. Tectonophysics 513, 96–111.

This work has also generated two conference presentations (Appendix B) and an instructional/technical manual related to the use of SPO-2003 software (Appendix C):

- Hastie, W.W., Aubourg, C., Watkeys, M.K., 2009. Orthogonal AMS and SPO fabrics in the MORB-like Rooi-Rand dyke swarm of South Africa and Swaziland. Abstracts, 11th biennial conference and exhibition of the South African Geophysical Association (SAGA). Mbabane, Swaziland, p. 66.
- Hastie, W.W., Watkeys, M.K., Aubourg, C., 2011. Problems associated with interpreting magmatic fabrics. 23rd Colloquium for African Geology (CAG-23). Abstracts, University of Johannesburg, South Africa, p. 180.
- Hastie, W.W., 2012. Mineral Shape Preferred Orientation: A guide to using "SPO-2003" and "Ellipsoid-2003" software.

It must be strongly stated that the authorship of the papers reflects only the advisory and editorial roles played by the supervisor (Prof. M.K. Watkeys) and co-supervisor (Prof. C. Aubourg) of this work. The first author (W.W. Hastie) was responsible for:

- Sample collection and preparation (Prof. Watkeys and Prof. Aubourg collected samples in the NLDS during 2006, before the commencement of this research project in 2007).
- The operation of all analyses (AMS and SPO). Introduction to the relevant equipment and continuing supervision in this regard was carried out by Prof. C. Aubourg during 2007 and 2008.
- The collation and interpretation of data. The interpretation naturally required the knowledge and experience of both supervisors, but the final conclusions drawn; particularly with respect to previous work, are entirely those of W.W. Hastie.
- The devising and completion of the SPO study and model of fabric acquisition as published in Papers I and II.
- The writing, editing and preparation of all manuscripts and all figures.
- All submission, editorial, peer-review and revision processes related to the publication of the manuscripts.

There is no "Results" section (*sensu stricto*) in this thesis because all the results are contained within the papers (Chapters 4–7). Supplementary data which accompanies the published papers is provided within the relevant chapter for the sake of continuity, clarity and completeness. The papers have been re-formatted (e.g. fonts, referencing, pagination, figures, numbering etc.) to maintain a single style throughout the thesis. The papers are, however, provided in their published format in Appendix A. References for the introductory and background chapters are provided at the end of Chapter 3. The references for Chapters 7 and 8 are provided at the end of Chapter 8.

1.3. Overview of Chapters

Chapter 1 introduces the outline and scope of the study, in particular the relevant background to dykes, dyke swarms and their mechanism of emplacement is covered

because their geometry and the stress field to which dykes are subjected affect their orientation and indeed the direction of magma flow within them. Chapter 2 expands further upon the relevant methodological and theoretical background to this study. In particular, the methods of AMS and minerals SPO are discussed, as are the ways in which data is presented and interpreted.

Chapter 3 deals with the regional geology of the Karoo LIP of which the dyke swarms are a part. The magmatism involved the eruption of continental flood basalts (CFBs), fed by accompanying intrusions between 183 Ma and 174 Ma. The volcanic sequences reach a thickness of between 1.5 and 12 km and overly the uppermost sedimentary rocks of the Karoo Supergroup, represented in South Africa by arenaceous rocks of the Clarens Formation. Rarely, the volcanic rocks are unconformable to Archaean terranes, such as the Limpopo Belt in southern Zimbabwe and basement of the Kaapvaal Craton. The three main crustal components through which magma erupted and intruded include the Kaapvaal and Zimbabwe Cratons and the intervening Limpopo Belt.

The Karoo triple junction is within the Limpopo Belt, centred over Mwenezi in southern Zimbabwe. Within these rift systems are dyke swarms associated with volcanism during the Jurassic (the west-northwest striking Okavango dyke swarm and the northeast striking Save-Limpopo dyke swarm). In places, such as the NLDS, certain dyke suites have been directly linked to overlying volcanic rocks. In other areas, such as the RRDS, there is no known extrusive equivalent. Thus, in Chapter 3 the relationship between the Lebombo monocline, Karoo triple junction and the dyke swarms is explored. This includes an overview of the geochemical and geochronological aspects of the extrusive and intrusive components. These relate to the distribution of Karoo magmatism through time and, importantly, the current understanding and debate surrounding the origin of the Karoo LIP.

Chapter 4 deals with comparison between 3-D mineral SPO and AMS, thermally altered AMS fabric in basaltic rocks and proposes the acquisition of an apparently “inverse” fabric due to late-stage effects of viscous magma flow. In general, studies involving the

use of AMS in mafic magmatic rocks focus on results which reveal flow-related fabrics. However, with increasing use of this technique, it has become evident that much data are overlooked when fabrics appear to be "inverse" (i.e. in unexpected orientations with respect to a dyke plane or volcanic flow surface). Generally, when such inversion is found, it is ascribed to the single domain state (SD) of very fine-grained magnetite. This is because the maximum magnetic susceptibility is found to be orthogonal to the grain's long axis. Increasingly, however, researchers have found evidence for genetic causes of inverse fabrics rather than magnetic domain causes.

As a result Chapter 4 examines how the magnetic fabric in dykes of the RRDS relates to the true petro-fabric (defined by plagioclase and opaque grains) and therefore provides an explanation for the origin of the magnetic fabric as it applies to the stage of magma flow being examined, i.e. late-stage adjustment of relatively large grains. Thus by directly comparing the 3-D SPO fabric of plagioclase and opaque grains to typical AMS data, it can be shown that the "inverse" fabric exists in ~40% of both AMS and SPO fabrics, hence refuting the notion that SD magnetite is the sole cause of the fabric inversion in basaltic dykes.

Chapter 5 deals further with the petrography, grain-size and shape parameters of the mineral plagioclase in dykes of the RRDS. A number of authors (Ildefonse and Fernandez, 1988; Benn and Allard, 1989; Kattenhorn, 1994) have found differences in fabric orientation according to grains of different shape ratios (where shape ratio r = long-axis / short-axis). In general these workers found that low shape ratios ($r < 1.5$) were less likely to reach an imbricated angle. It was hypothesised, therefore, that there may be an "ideal" grain-size and/or shape that has reached a stable, type-A fabric (within 30° of the dyke plane). Thus, in Chapter 5 the SPO of plagioclase in 16 samples is investigated in relation to the grain-size and grain shape. The results show that type-A and type-B fabric coexist within the RRDS while the grain-size and shape of plagioclase are essentially independent. There is no discernable correlation between the grain-size of plagioclase and the type of fabric it develops. Rather, type-A fabric is defined by plagioclase grains in the 12–13 μm size range with modest shape ratios (1.80–2.20).

There is also an apparent correlation between increasing grain anisotropy and type-B fabric – comparable to the findings of Dragoni et al. (1997). This result is somewhat surprising, as it has been previously shown that larger grains (phenocrysts) are more likely to interact during magma flow and crystallisation, coming to rest in a tiled, imbricated fashion.

The crystal size distribution (CSD) of the RRDS, and the igneous textures, are consistent with late growth of these grains – probably as a result of relatively rapid undercooling. Nucleation was likely heterogeneous involving early growth of phenocrysts at depth prior to intrusion. This is comparable to the results of Chapter 3, although it appears that rapid nucleation of the plagioclase groundmass at a late-stage has affected the final SPO much more than grain interaction has. The hypothesis of strongly interacting grains attempting to rotate in a highly viscous magma is therefore unlikely to be the sole mechanism of type-B fabric development.

Chapter 6 provides the main regional-scale results of the study pertaining to the NLDS, contrasting the results of AMS and mineral SPO study in these dykes. There are suites of dykes in the NLDS that are distinct in relative age, orientation and composition. The results from studying 14 dykes of varying relative ages are consistent with early, upward flow in the oldest dykes, and lateral magma flow from the north in the youngest dykes. This has implications for the hypothesis of a Karoo mantle plume, and for understanding the magmatic history of the Karoo triple junction. The interpretation of the magma flow directions in dykes of the RRDS is presented in Chapter 7. This work follows on from Chapters 4 and 5, but has not been presented or published elsewhere. Additionally to the RRDS and NLDS, Chapter 7 brings together magma flow data from the ODS and Underberg dyke swarm (UDS) of southern Africa and the Straumsvola and Jutulrøra dyke swarms (SDS and JDS respectively) of Antarctica.

This chapter relates the results of these studies to the timing and duration of Karoo and associated magmatism and the mantle plume hypothesis for the development of the Karoo LIP. The aim is to constrain the regional sense of magma flow in dykes of the

Karoo LIP to the time of their formation in order to more critically assess the mantle plume hypothesis.

Chapter 8 concludes the thesis, bringing together the salient findings with respect to the small-scale (local) findings in the RRDS and the regional AMS and SPO results that impact upon the current understanding of the development of the Karoo triple junction and the various dyke swarms associated with the Karoo LIP.

- Chapter 2 -

Theoretical Background & Methodology

2.1. Context of Study

Dykes are fractures through which magma moves, feeding into volcanic centres or fissures from the magma source below (Figure 2.1). They are thus the "plumbing" to surface volcanic processes, and understanding them from various geological standpoints is fundamental to understanding magma movement in the crust. Individual dyke geometry and structure as witnessed in the field has often been used to differentiate between vertically and laterally intruded dykes (Delaney et al., 1986; Pollard, 1987; Bussel, 1989).

This is based on features such as broken bridges and dyke offsets (vertical intrusion) as well as regional trends in dyke population, such that dyke numbers decrease and compositions become more evolved with increasing distance from the source (lateral intrusion) (Gudmundsson, 1990a).

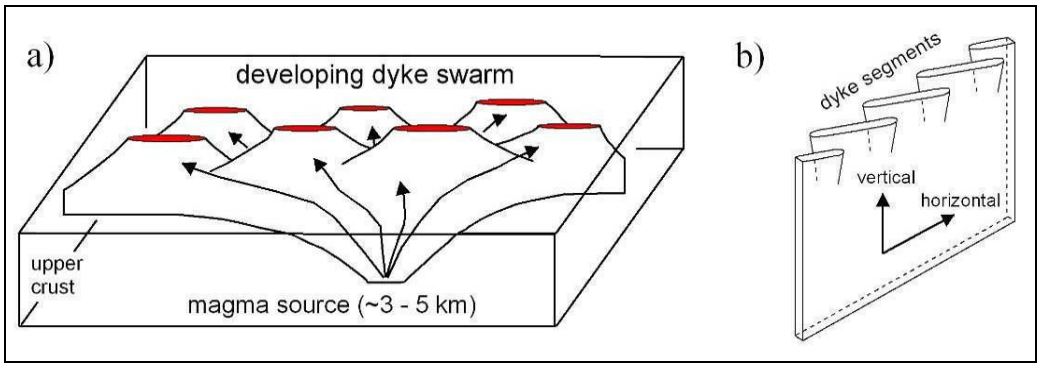

Figure 2.1: (**a**) 3-D sketch illustrating proximal vertical magma intrusion and distal lateral intrusion in a dyke swarm in the upper crust (Archanjo et al., 2000) and (**b**) Schematic diagram of a dyke plane with vertically intruding dyke segments (Poland et al., 2004).

However, in dykes and sills, it has been demonstrated that the orientation of various other features such as grooves and vesicles may provide a local (dyke-scale) indication of the direction of magma flow (Correa-Gomes et al., 2001; Philpotts and Philpotts, 2007) due to the effect of simple shear of the magma along the intrusion walls. If, however, macroscopic features are absent from the margins of dykes in the field it is necessary to employ microscopic or submicroscopic methods to picture any preferred orientation caused by simple shear between the magma and the intrusion walls. A number of authors have investigated the shape and preferred orientation of anisotropic grains which have crystallised in a moving magma, whether in a dyke, sill or larger intrusion (e.g. Cruden, 1990; Ernst, 1990; Baer, 1995; Lister, 1995; Launeau and Robin, 1996) (Figure 2.2).

It has subsequently emerged that constituent grains or phenocrysts in the magma tend to be imbricated (albeit weakly) along the intrusion walls, providing a sense of magma flow direction. This phenomenon has allowed geologists to investigate [1] the origin of the source magma (e.g. vertically flowing or horizontally flowing magma), [2] the rate of magma influx (Cruden, 1990), [3] rheology and grain interaction in crystallising fluid (Launeau and Cruden, 1998) and [4] diapiric "ballooning" of intermediate and felsic intrusions (Ramsay, 1989).

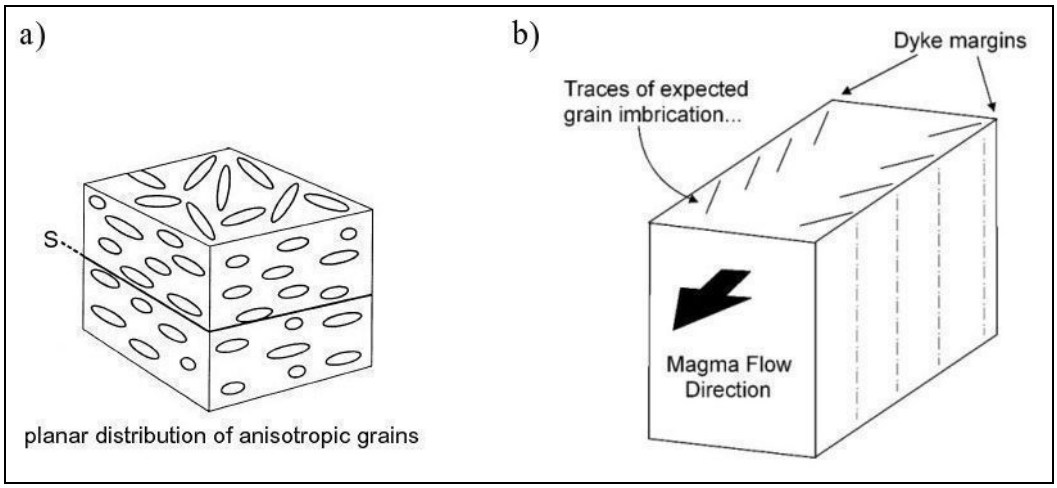

Figure 2.2: (**a**) Schematic diagram (not to scale) showing planar preferred orientation of anisotropic grains in a theoretical sample (Borradaile and Lagroix, 2001) and (**b**) 3-D schematic illustration of the potential distribution of grains (not to scale) against the margins of a dyke resulting from the simple shear effects induced by the magma flow vector shown (modified from Gil-Imaz et al., 2006).

This study focuses on the implications of the magma source for understanding the geodynamics of the NLDS and RRDS, and considers the significance of flow related petrofabric in these dykes in order to better understand their origin.

2.2. Dyke Emplacement

2.2.1. Introduction & Scope

The review of dyke emplacement conditions which follows is restricted to the most relevant conditions. These provide the necessary physical background to the work which is presented here as there are a myriad structural features and generally considered conditions necessary for dyke emplacement. The reader is referred to the following literature for additional information regarding the emplacement conditions and tectonic relevance of dykes and dyke swarms: Shaw (1980), Spence and Turcotte (1985), Delaney et al. (1986), Pollard (1987), Bruce and Huppert (1990), Hoek (1994), Kattenhorn (1994), Uken and Watkeys (1997) and Reeves (2000).

2.2.2. Rock Fracturing & Crack Propagation

The intrusion of dykes is strongly controlled by the stress regime in the crust into which they intrude because the stress regime controls the propagation of the initial fractures (Shaw, 1980). It is generally considered that natural rocks inherently contain significant numbers of microscopic cracks (Griffith fractures), such that the crack tips propagate as a result of compression ($+\sigma_1$) in, and directed toward, the plane of suitably orientated cracks; with extension in the orthogonal (σ_3) direction (Griffith, 1924; Spera, 1980). This results from tensile stresses which develop in the crack tips, as they propagate through the rock (Pollard, 1987; Turcotte, 1990).

If magma intrudes into these fractures the dilation of the fracture is dependent initially on the magma pressure exceeding the lithostatic pressure, resulting in the intrusion tips propagating toward σ_1 in newly formed hydraulic fractures (Spera, 1980). Further propagation of the intrusion results from the elastic deformation of the host rock around the dyke tip (process zone), which may contain a vapour phase, resulting in a decreasing pressure gradient developing from the magma source to the dyke tip (Figure 2.3) (Pollard,

1987; Hoek, 1994). Spera (1980) also indicates that the presence of a low viscosity fluid reduces the overall rock strength, thereby assisting fracture propagation.

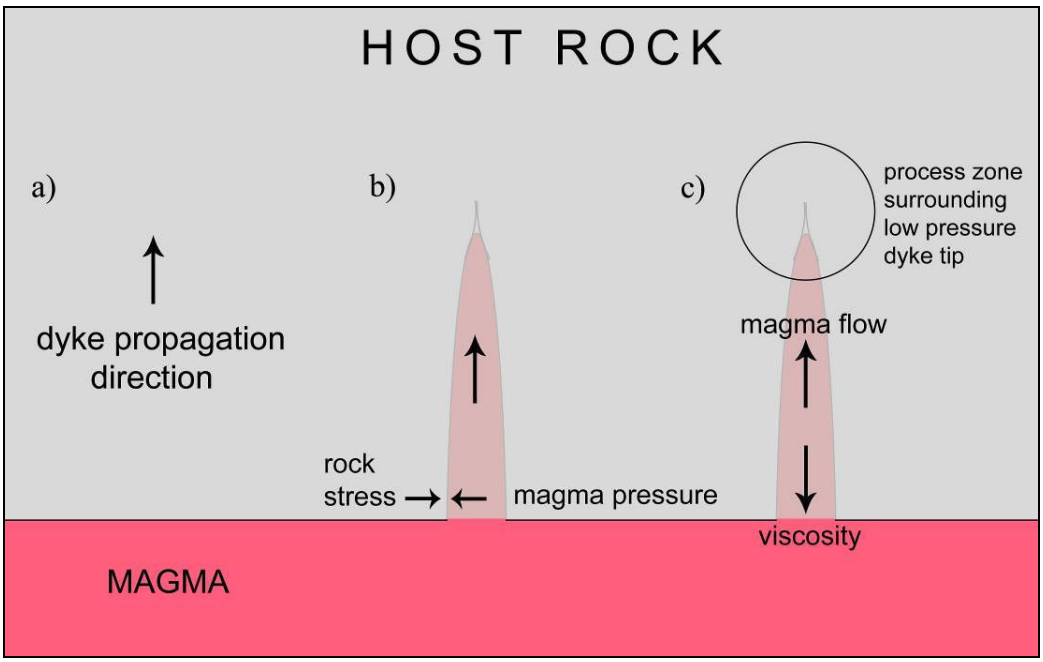

Figure 2.3: Schematic illustration of processes involved in the propagation of (and movement of magma within) a vertical dyke in host rock (not to scale), (**a**) Stress conditions in the host rock are such that fractures will propagate upward, and the plane is perpendicular to this section, (**b**) Propagation of a magma filled fracture (dyke) continues as the magma pressure exceeds the lithostatic pressure, (**c**) Viscosity (as well as gravity and friction) resists the upward movement of magma (modified from Hoek, 1994).

Propagation may, however, be under greater influence by pre-existing fractures and local stress conditions around the dyke tip, especially if the process zones of adjacent dykes interact (Nicholson and Pollard, 1985). Other factors, such as a pre-existing foliation or conjugate tensile fractures (Pollard, 1987) may strongly influence dilation and propagation directions (Delaney et al., 1986). This is discussed further in Sections 2.2.3 and 2.2.5.

With respect to effective stress – that stress available to fracture the rock – it is evident that rock fracturing related to magma intrusion cannot occur under conditions of equal stress because effective stress will be zero. Thus it is the relationship amongst magma pressure, rock stress and the "*ability of extensional fracture*" that allows the development

of magma flow paths (Shaw, 1980). It is evident from Equation 1 that as fluid pressure (λ) tends toward the value of 1, the depth to which extensional fracturing occurs increases (modified from Shaw, 1980):

$$d_{max} = \sigma \div [\rho g (1-\lambda)] \quad (1)$$

Where: d_{max} = depth to which fracturing extends

σ = compressive stress (σ_1 is vertical in this case)

ρ = density

g = acceleration due to gravity

In a more quantitative sense, if magma pressure (P_f) is approximately equal to lithostatic pressure (P_{lith}), then fractures will only open in a plane perpendicular to the least compressive stress, σ_3, such that the fracture tip will propagate toward σ_1 (Spera, 1980).

Furthermore, Shaw (1980) also notes that the initial melt increments are orientated, indicating that stress and strain developed through igneous processes are coeval with melting. It appears then that strain and deformation rates, coupled with variations in magma density and pressure can result in a number of potential paths for fracture formation, therefore not necessarily parallel to σ_1. This is also true of the movement of fracture margins relative to one another during the emplacement of magma.

2.2.3. From Fractures to Dykes

Loading of a fracture due to the emplacement of magma results in the two margins of a fracture moving relative to one another (Kanninen and Popelar, 1985; Pollard and Fletcher, 2005). Within a three dimensional reference frame (X, Y and Z) there are three possible fracture "modes" which can develop (Figure 2.4). Mode I fractures occur when the margins open relative to one another. Mode II fractures involve a sliding motion and Mode III fractures involve a tearing motion. The overall stress and the magnitude thereof is controlled by the fracture geometry and loading conditions, but the differentiation of fracture modes arises from the local stress component distribution at the fracture tip due to the relative movement of the margins.

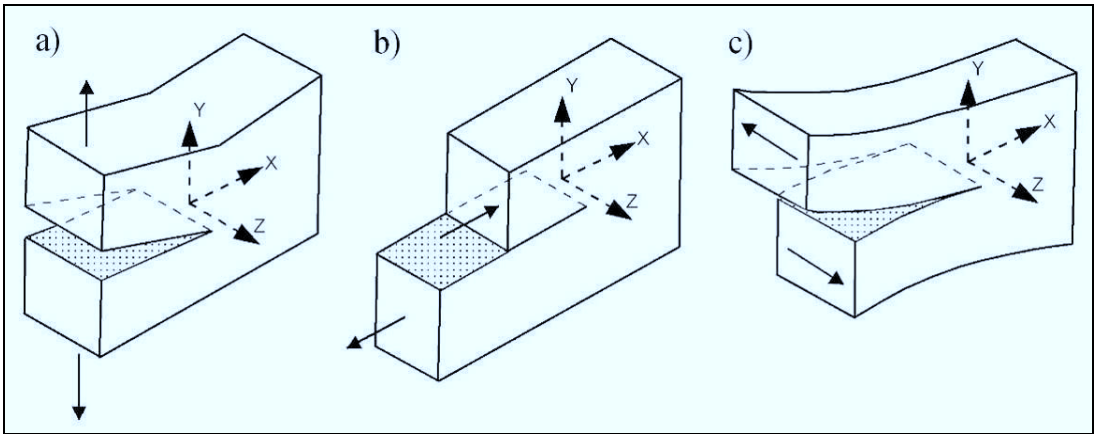

Figure 2.4: Idealised diagram illustrating the three principle fracture modes which can be expected to form during the fracture of brittle material. Note the XYZ coordinate system which defines the reference frame and the relative directions of movement of the fracture margins, (**a**) Mode I fracture, (**b**) Mode II fracture and (**c**) Mode III fracture (modified from Pollard and Fletcher, 2005).

These differences have profound effects on the geometry of dykes which propagate from fractures of varying modes (Pollard and Fletcher, 2005) (Figure 2.5).

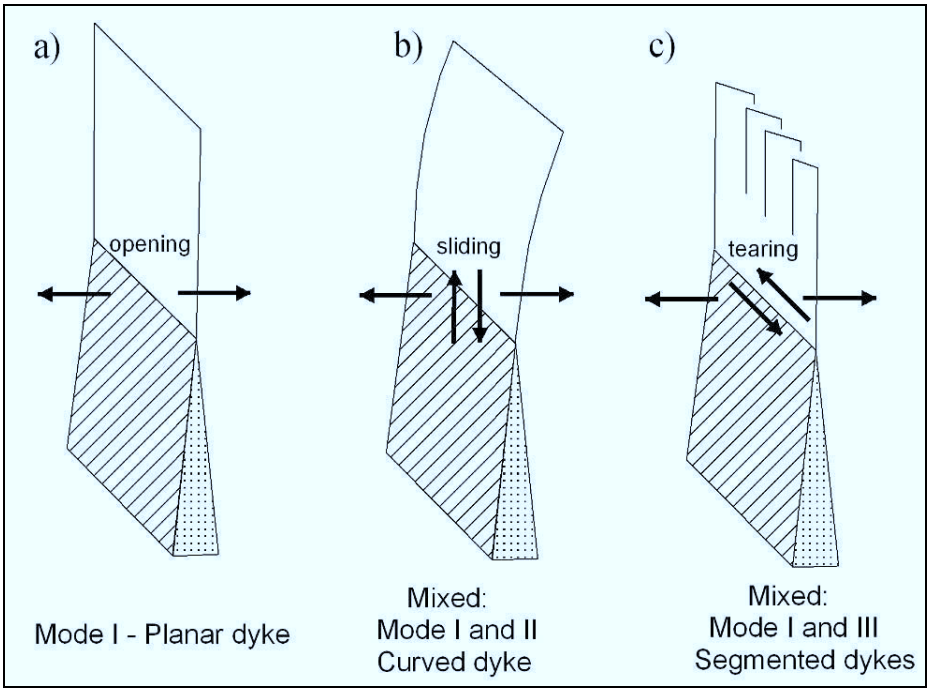

Figure 2.5: Expected dyke geometry based on vertical magma emplacement into (**a**) Mode I fractures, (**b**) mixed Mode I and II fractures and (**c**) mixed Mode I and III fractures (modified from Pollard, 1987).

A pure Mode I fracture will allow the development of a planar dyke. A mixed Mode I and II fracture will result in dykes with curved margins. *En echelon* dyke segments result from intrusion into mixed Mode I and III fractures. It is important to note that the *propagation direction* of a fracture as it is filled with magma is not synonymous with the *magma flow direction*. These two directions may in fact be orthogonal (see Section 2.2.5).

2.2.4. Arrest of Dyke Propagation

Three factors assist in the arrest of magma, [1] temperature difference between the magma and wall rocks, which decreases as crystallisation progresses, [2] friction between the magma and wall rocks and [3] loss of magma pressure/supply (Hoek, 1994; Lister, 1995). These factors are moderated by parameters such as dyke length, thickness and initial temperature of the wall rock and magma (Bruce and Huppert, 1990). Seismic studies suggest that strain induced in wall rocks surrounding a dyke is released elastically (Shaw, 1980). Pollard (1987) also indicates that the relaxation of elastic strain in a propagating dyke decreases the energy of the system, preventing further propagation. This is most likely to occur due to a drop in magma pressure in the magma reservoir (Pollard, 1987). A mafic dyke of about 1 m in thickness is likely to take ~7 days to solidify, whereas dykelets 10 mm thick may freeze within 60 seconds (Jaeger, 1959). The flow of magma, wall rock interaction, and the cooling history of a dyke must have an effect on the resulting rock fabric. Thus, careful interpretation of flow related fabric found along dyke margins must allow for the possibility that the fabric does not reflect the initial and instantaneous magma flow.

2.2.5. Dyke Geometry & Palaeostress

Palaeostress analysis of dykes, or other planar intrusions is based on certain features (such as orientation) of a dyke and the fracture through which it intruded (Pollard, 1987). Examples have been described above, such that the longitudinal axis of dykes can be in the orientation of the maximum compressive stress, σ_1 during the time of intrusion (Pollard, 1987). The expansion direction of the dyke will then be directed toward the minimum compressive stress, σ_3.

For a dyke of length 2a, the tensile stress (σ^r_1) it is subjected to is related to a 'stress intensity factor' S_i, as shown in Equation 2 (Pollard, 1987):

$$S_i = \sigma^r_1(\Pi a)^{1/2} \quad (2)$$

From S_i, and other components, it is possible to determine the magnitude of σ^r_1, which is useful in that S_i relates proportionally to the stress components at the dyke tip, which itself is under the influence of the stress field, as illustrated in Equation 3 (Pollard, 1987):

$$S_i \sim (P_f - S)\sqrt{(\Pi a)} - \sqrt{(8L/\Pi)} \quad (3)$$

Where: P_f = fluid pressure, S = remote stress and L = dyke tip length unoccupied by magma.

If the dilation of two previously adjacent points outside the dyke margin is perpendicular to the dyke margins, it is evidence that the plane of the dyke is parallel to one of the principal stress axes, with the dilation direction being normal to σ_3 (Pollard, 1987; Bussel, 1989). Magma flow in most dykes will have lateral and vertical components, which are not necessarily related to the propagation direction but rather the dyke geometry as discussed previously (Figure 2.6).

Certainly *en echelon* dyke segments, although propagating laterally (Figures 2.5c and 2.6b) must be fed from a magma source beneath the segments. Only if these segments join through bent and broken bridges of host rock can lateral magma transport occur.

Once again it must be reiterated that palaeostress considerations are only reliable for newly formed hydraulic fractures as pre-existing fractures may be intruded by magma and dilate *irrespective of the stress regime* (Nicholson and Pollard, 1985; Pollard, 1987). Also, if σ_3 is close in magnitude to the other principal stresses, the fracture orientations may be controlled by other factors, such as a pre-existing foliation or conjugate tensile fractures which develop at 45° to σ^r_1 (Pollard, 1987). The interaction of process zones, as

is likely in *en echelon* segments of mixed Mode I and III dykes, also complicates the resolution of the overall stress field (Delaney et al., 1986; Pollard, 1987; Wickham, 1987). Thus palaeostress analysis on dykes based on field characteristics should be carried out with caution.

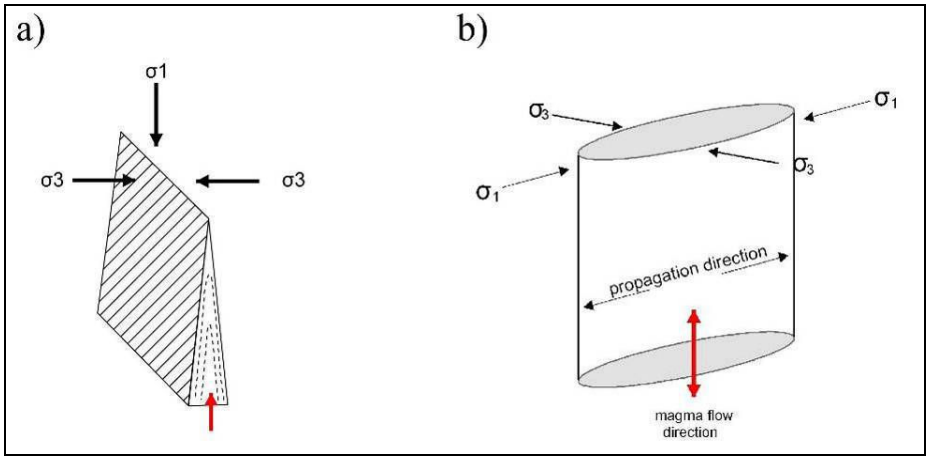

Figure 2.6: (**a**) Idealised model of a vertically intruding Mode I dyke in a divergent margin setting (vertical σ_1). Dilation is perpendicular to the dyke margins and magma flow is in the plane of σ_1 and σ_2, (**b**) vertically intruding dyke under horizontal tensile conditions (representative of an *en echelon* segment of mixed Mode I and III dyke). The bulk flow direction of magma is orthogonal to the propagation direction in this case.

In addition to palaeostress analysis, the orientation and geometry of the dyke margins also provide significant information about the magma flow direction. The theory, methods and application of these techniques to dyke analysis form the subject of Section 2.5.

2.2.6. Dyke Emplacement in Divergent Margins

Divergent margins are by definition regions of horizontal minimum compressive stress (σ_3), induced by slab-pull or the spreading effects of mantle upwelling below the lithosphere, such as a plume. This divergence results in fracturing under essentially tensile conditions. Dyke intrusion into tensile fractures (Griffith, 1924; Delaney et al., 1986; Pollard, 1987), which propagate perpendicular to σ_3, is common in such regions; most notably at mid-oceanic ridges (MORs). However, fractures, and indeed dykes will also propagate along lines of weakness, including pre-existing fractures and/or faults,

which may have formed under the same tectonic regime as that involved in the dyking (Delaney et al., 1986; Gudmundsson, 1990a).

The propagation direction and style of dyking is dependant on magma overpressure, which if greater than the overlying vertical pressure will result in sill formation. Also, the nature of stress in the host rock can determine the style, given that rock with a low vertical tensile strength may be more easily intruded by laterally propagating dykes (Gudmundsson, 1990b). This is also true of melts which reach their level of neutral buoyancy (Lister and Kerr, 1990). Nevertheless, dyke intrusion in divergent margins is governed by essentially upward magma flow from magma reservoirs, with lateral magma flow being a minor component of the magma migration of dyke swarms (Gudmundsson, 1990a). Modelling of stress fields around crustal magma chambers in divergent margins suggests that lateral magma flow in bladed dykes would be most likely at relatively high crustal levels, in cases of a magma chamber under *tensile conditions*. However, it is more typical that magma chambers, even in tensional regimes, are subject only to their own internal magma pressure, which favours vertical magma emplacement (Gudmundsson, 1990a).

Callot et al. (2001) studied dolerite dykes from a coastal dyke swarm in East Greenland generated during the opening of the North Atlantic in the Tertiary. Their results indicate that 40% of the dykes from this volcanic margin involved lateral flow from a local, and relatively shallow (3–4 km), magma source (Figure 2.7).

Similar results have been found in dykes on the Isle of Skye (Geoffroy and Aubourg, 1997) and Iceland, suggesting that shallow magmatic centres exist in volcanic margins resulting in focused magmatic accretion. In areas of crustal thinning, such as MORs, dyke swarms are directly linked to the formation of new oceanic crust, which is fundamental to the formation of divergent plate boundaries during continental break-up (Gudmundsson, 1990a). True extension in the crust, such as during rifting, results from negative minimum compressive stress ($-\sigma_3$) and vertical maximum compressive stress (σ_1). Under such conditions, lateral magma flow in dykes can be expected, as opposed to sill

emplacement under conditions of $+\sigma_3$. However, during simple shear, maximum compressive stress will have an angular component, and the resulting extension will be asymmetrical.

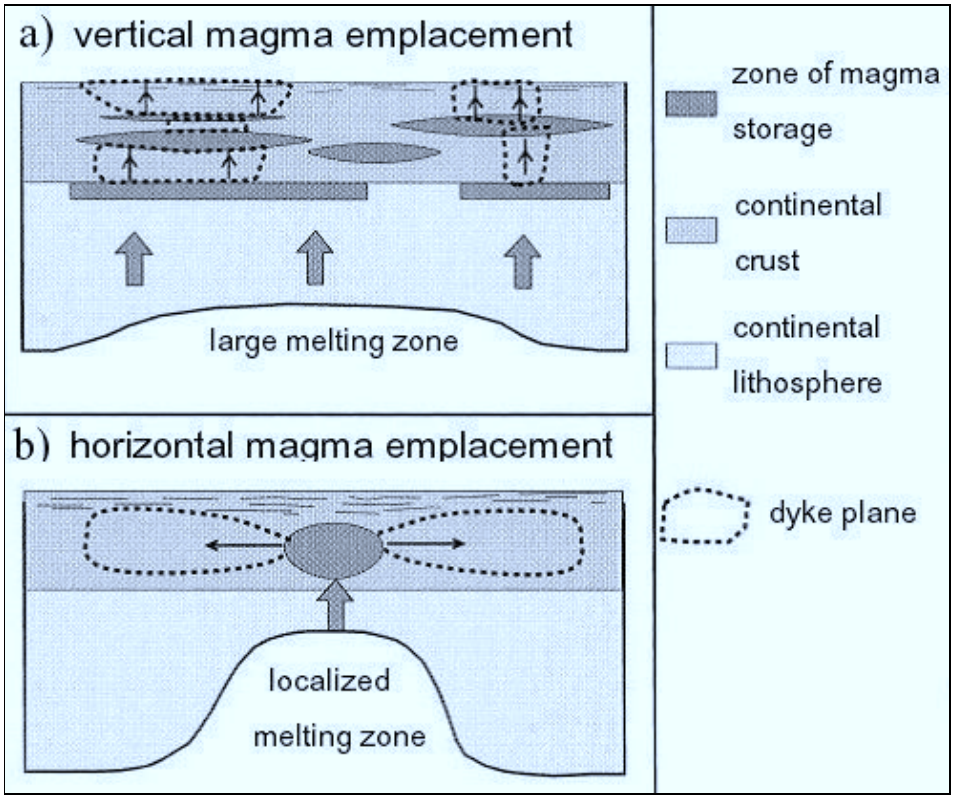

Figure 2.7: Cross sections illustrating (**a**) a large magmatic source feeding vertically intruding dykes and (**b**) laterally intruding dykes fed by a shallow magmatic source (from Callot et al., 2001).

2.3. Sampling

Sampling dykes thicker than 1 m and sampling within 10 cm of the dyke margin increases the chances of gaining good flow direction data from intrusions using AMS (Tauxe et al., 1998; Rochette et al., 1999). Sampling for this project followed this principle as far as possible, in spite of limitations of outcrop preservation and suitability for drilling. Between 6 and 10 orientated core samples of 40–200 mm in length were taken from a single site using a hand-held petroleum powered drill with a hollow, 25 mm diameter diamond-tipped drill tube. Each site represents a single dyke margin with 6 to

10 cores collected from each opposing margin (Figure 2.8) which is necessary for finding imbrication of magnetic fabric (Knight and Walker, 1988; Tauxe et al., 1998).

Figure 2.8: Plan view photograph taken in the field, showing the sampled western margin of a Rooi Rand dyke (demarcated in red). Note the drill in the top right corner. Tape measure for scale is 1 m in length. North is toward the top of the photograph.

Each sample was orientated in the field using a core-orientator with both a magnetic and sun compass. A total of 224 samples were collected from the NLDS, 212 from the northern RRDS (in Swaziland) and 154 samples from the central RRDS (please see field sketches and tabulated data in Appendix E). Thus, representative samples from a total of 32 dykes were collected. Tabulated AMS and SPO data for the NLDS can also be found in Chapter 6.

2.4. Anisotropy of Magnetic Susceptibility

2.4.1. Introduction

Since the 1960's the anisotropy of magnetic susceptibility (AMS) has become a standard tool for the analysis of rock fabrics, most notably characterising possible flow related linear and planar fabrics in volcanic, intrusive and metamorphic rocks (Khan, 1962; Ellwood, 1978; Knight and Walker, 1988; Tarling and Hrouda, 1993). AMS is represented graphically as an ellipsoid derived from a second-rank tensor. The ellipsoid is quantitative and its shape and orientation (as well as scalar data) can be described. For studying dykes, the AMS ellipsoids are determined from opposing margins of an intrusion, i.e. per site, which provide constraint on the original magma flow orientation (Geoffroy et al., 2002).

2.4.2. Principles of AMS

The application of a magnetic field to minerals results in a response from the minerals known as induced magnetisation. This can be measured for any mineral, although the induced magnetic response of certain minerals, such as magnetite (Fe_3O_4), is greater than for silicates. The mean susceptibility includes contributions from ferromagnetic grains (*K*-ferro), paramagnetic grains (*K*-para) and diamagnetic grains (*K*-dia) where *K*-ferro>> *K*-para >>*K*-dia. This is because the response of ferromagnetic grains to an induced field enhances the field, and such minerals therefore have a high magnetic susceptibility (Butler, 1992). The total number of grains which contribute to the AMS signal in one ~10 cc drill core sample may number in the billions.

Susceptibility (*K*) can be related to magnetisation (M) thus in Equation 4:

$$M = KH = K\,(B \div \mu_0) \qquad (4)$$

Where: M = magnetisation in magnetic dipole moment per unit vol. (A/m)

H = strength of the applied field (A/m)

B = magnetic field measured in Tesla

μ_0 = permeability of the free space ($4\pi \times 10^{-7}$ henry/m)

Borradaile and Henry (1997) state that "*a symmetrical second-rank tensor represents the anisotropy of low field susceptibility*". In order to determine anisotropy, susceptibility is measured along six or more suitably dispersed directions. This provides six equations to solve for the six unknown terms of the susceptibility tensor. Thus, six independent terms are needed to evaluate the tensor and fix the directions and magnitudes of the principal susceptibilities. These can be written as s_1 to s_6 thus:

$$s_1 = K_{11} \qquad s_4 = K_{12\,(21)}$$
$$s_2 = K_{22} \qquad s_5 = K_{23\,(32)}$$
$$s_3 = K_{33} \qquad s_6 = K_{13\,(31)}$$

Where: K = the susceptibility tensor

The first step in finding the AMS ellipsoid is assessing whether the eigenvalues define a truly triaxial ellipsoid or not. This has to be known with some degree of confidence, as only six measurements (which would satisfy the tensor) are not sufficient. Where N number of directional susceptibility values is measured; eigenvalues and eigenvectors (τ) are calculated by iterative diagonalisation of a 6 element matrix. Thus, a minimum of 6 discrete orientations measurements must be made in order to resolve the 6 tensor elements AMS (Borradaile and Jackson, 2004). To this end, F statistics can be calculated for each tensor to show whether data are isotropic ($\tau_1 = \tau_2 = \tau_3$) or not ($\tau_1 > \tau_2 > \tau_3$) (Hext, 1963). Furthermore, this is why the 15 position measurement procedure for samples is widely used (Jelinek, 1978).

2.4.3. Statistical Confidence Regions & Bootstrapping

One approach to defining regions of 95% confidence on AMS stereoplots is the bootstrap method. It can be used for determining confidence regions of directions or axes (Fisher et al., 1987) and does not depend on the F test (Tauxe et al., 1998). Bootstrapping randomly re-samples the original samples of N measurements up to 10 000 times (paradata sets). These paradata sets are essentially replacement data calculated from random samples with the mean and standard deviation of data from the entire site. One site is one dyke

margin in this case. In this method, at least 95% of the eigenvalues and eigenvectors must fall within the confidence limits in order to be considered for further interpretation. Each of the paradata sets contains *N* orientations which duplicate some of the original measurements and omit others. The distribution of the eigenparameters is determined by bootstrapping the paradata. The mean orientation of each re-sample is then plotted, the mean orientations of which produce a simple elliptical concentration (Tauxe et al., 1998). The density distribution of these concentrations are contoured to reflect the confidence region (Tauxe et al., 1998; Borradaile and Jackson, 2004). The confidence regions shown in AMS plots in the remainder of this thesis are 95% confidence limits calculated by this method within the AMS plotting program "Tclamswin" (Equi-4 Software, v.1.4.0).

2.4.4. The AMS Ellipsoid

The AMS ellipsoid is shown in three dimensions by means of an ellipsoid which reflects the proportions of three principal eigenvectors ($K_{max} > K_{int} > K_{min}$ or $K1 > K2 > K3$) of the second-rank tensor (Jelinek, 1981; Tarling and Hrouda, 1993). The magnetic lineation is referred to as $K1$ and the pole to magnetic foliation as $K3$. Hence AMS studies document both a linear and planar (foliation) element (Figure 2.9). Note that in this thesis "K_m" denotes susceptibility while "K_{max}" denotes the maximum principal axis.

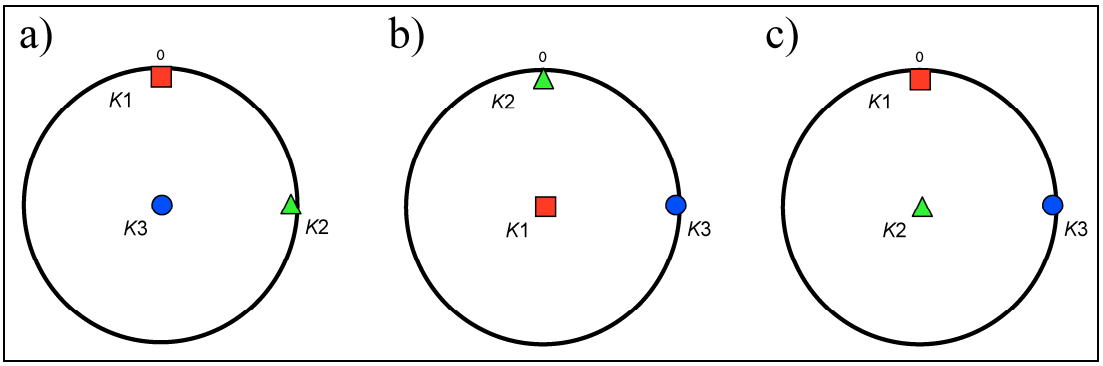

Figure 2.9: AMS ellipsoid axes represented on a lower hemisphere, equal area projection, (**a**) Horizontal foliation (plane to $K3$) and north-south horizontal lineation ($K1$), (**b**) north-south striking vertical foliation with vertical lineation, (**c**) north-south striking foliation with north-south horizontal lineation. The same symbols for $K1$ (■), $K2$ (▲) and $K3$ (●) shown here are retained throughout this thesis.

Scalar data are also obtained from AMS studies, including the bulk susceptibility: K_m = ([$K1$ + $K2$ + $K3$] ÷ 3). The anisotropy factor (P') and the shape parameter (T) are calculated as shown in Equations 5 and 6 respectively (Jelinek, 1981). The reader is referred to Tarling and Hrouda (1993) for a comprehensive overview of the physical and mathematical principles of AMS in geological applications.

$$P' = exp\sqrt{2\left[\left(ln\frac{K_{max}}{K_{mean}}\right)^2 + \left(ln\frac{K_{int}}{K_{mean}}\right)^2 + \left(ln\frac{K_{min}}{K_{mean}}\right)^2\right]} \quad (5)$$

$$T = \frac{ln\,(K_{int} / K_{min}) - ln\,(K_{max} / K_{int})}{ln\,(K_{int} / K_{min}) + ln\,(K_{max} / K_{int})} \quad (6)$$

2.4.5. Mineralogical Control

Because paramagnetic minerals have induced fields parallel to the applied field, their susceptibilities are positive (Table 2.1). Diamagnetic minerals, conversely, have negative susceptibilities. Some minerals carry a magnetisation in the absence of an applied field, termed remanent magnetisation, which occurs in the first of the transition group elements. Only ferromagnetic and ferrimagnetic minerals have this property, although an antiferromagnetic mineral, such as hematite, may have parasitic magnetism arising from consistent and stable lattice imperfections (Tarling and Hrouda, 1993).

Minerals such as multi-domain (MD) magnetite, pyrrhotite, hematite and phyllosilicates are the most common carriers of magnetic susceptibility which have a “normal” magnetic fabric (Rochette et al., 1999). Some minerals do result in “inverse” fabrics because the maximum susceptibility is not parallel to the elongation of the mineral, e.g. tourmaline, cordierite and single domain (SD) magnetite (Potter and Stephenson, 1988; Rochette et al., 1999).

However, the shape fabric of minerals in a rock does not necessarily correlate to AMS fabric because it may be controlled by distribution anisotropy (Hargraves et al., 1991; Rochette et al., 1999), although Gaillot et al. (2006) have shown that the degree to which magnetic grain interaction affects mean AMS is overstated, and hence abnormal fabrics may arise from one or more other contributing factors.

Table 2.1: Magnetic and physical properties of relevant common rocks and important magnetic species.

Rock[4] / Mineral[1,2,3]	*K_m (μSI Units)*	*Density(g.cm^{-3})*	*Curie Temperature[4]*
mafic igneous rock	$5.5\times10^{-5} – 1.2\times10^{-2}$	2.79	-
felsic igneous rock	$3.8\times10^{-6} – 8.2\times10^{-3}$	2.61	-
magnetite	$2.0\times10^{6} – 5.7\times10^{6}$	5.18	585°C
maghemite	$2.0\times10^{6} – 2.5\times10^{6}$	4.9	645°C
pyrrhotite	3.2×10^{6}	4.62	320°C
hematite	4.0×10^{-3}	5.26	685°C

[1]Borradaile and Henry (1997)
[2]Herrero-Bervera et al. (2002)
[3]Borradaile and Jackson (2004)
[4]Hunt et al. (1995)

To summarise, a magnetic fabric found using AMS originates from the magnetic signal of anisotropic grains which are non-randomly distributed within a given sample (Hargraves et al., 1991; Tarling and Hrouda, 1993).

2.5. Dyke Geometry & Magma Flow Analysis

2.5.1. Macroscopic Field Evidence

As alluded to in the beginning of this chapter, the orientation and geometry of dyke margins provide significant information about the magma flow direction. For instance, consider dyke segments intruding into newly formed mixed Mode I and III fractures which develop *en echelon* geometry relative to one another (Figure 2.10). The propagation direction of the fractures is toward each other (i.e. laterally); however, it

should be evident that the magma itself cannot flow laterally on a regional scale. Instead, magma will flow sub-parallel to the marginal axis of the *en echelon* segments and/or any bent or broken bridges which result from the joining of the segments. Thus accurately measuring the plunge of these segments and/or bridges provides a relatively quick yet reliable estimate of the magma flow direction in the field.

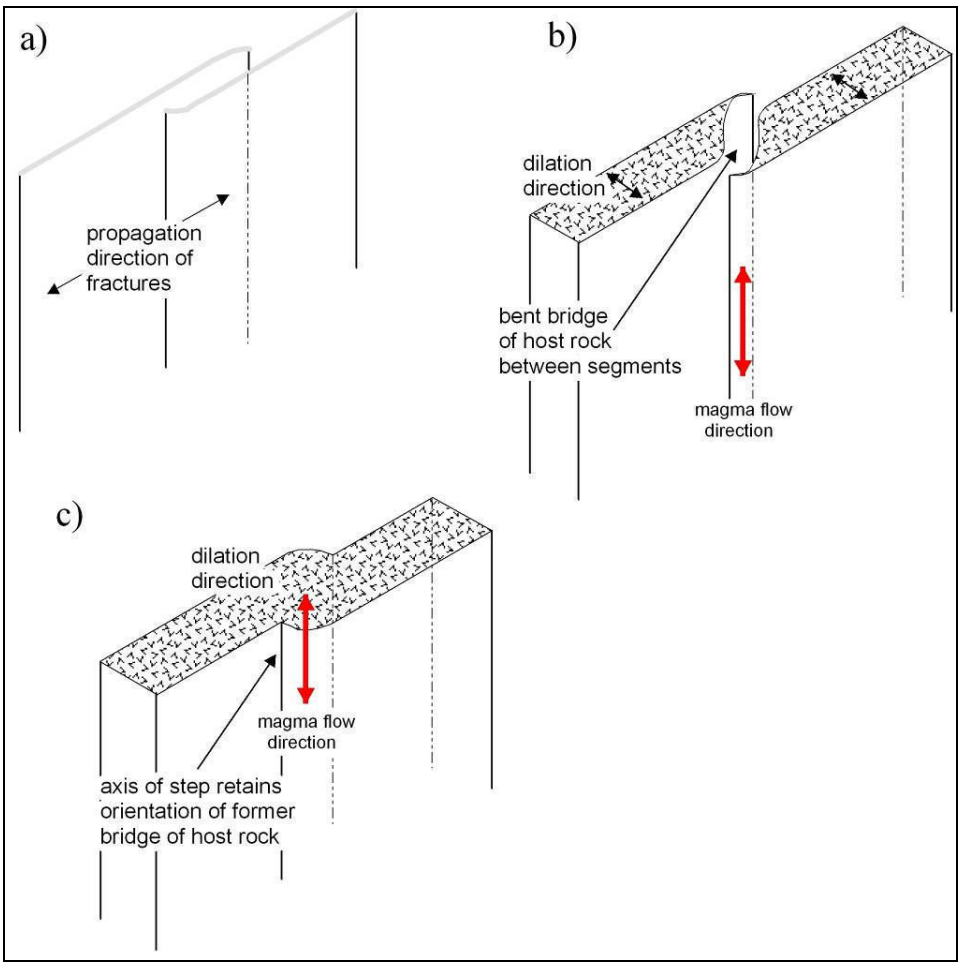

Figure 2.10: Model of a progressively dilating vertically intruding *en echelon* dyke array showing (**a**) newly formed hydraulic fractures. Note the propagation direction, (**b**) formation of bent bridge in host rock and (**c**) magma flow direction is parallel to the dyke segments (modified from Bussel, 1989).

In addition, it is possible to utilise smaller macroscopic features to determine the original magma flow direction. These features are the result of magma shearing against the wall

rock, and hence these features are most likely to be preserved within or close to the chill margin of the dyke (Figure 2.11).

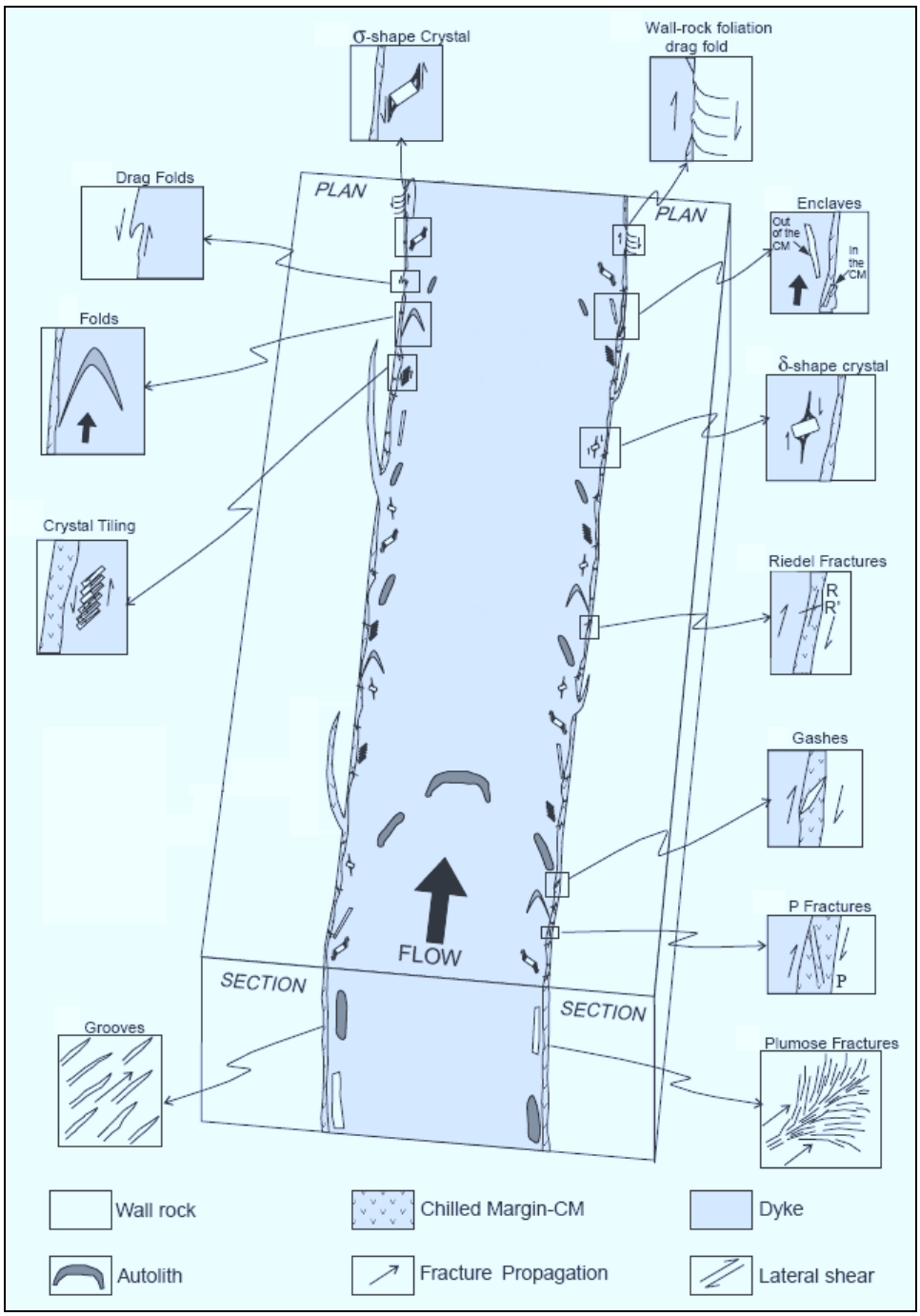

Figure 2.11: Theoretical dyke shown in plan and section view, illustrating an array of macroscopic to microscopic features which may be recognised along a dyke margin. These may provide some constraint on the original magma flow direction. Not to scale (modified from Correa-Gomes et al., 2001).

Large features found along dyke margins (centimetre scale or larger) may include folds, drag folds, grooves, lineations and plumose features. Smaller scale features include crystal tiling (imbrication) along the chill margins, sheared grains (σ-structures), rotated grains (δ-structures) and gashes and fractures. The shape preferred orientation (SPO) of grains within a dyke margin is typically studied microscopically.

2.5.2. Magnetic Fabric & Magma Flow

The technique of measuring anisotropy of magnetic susceptibility (AMS) probes the microscopic to submicroscopic petrofabric scale. Rochette et al. (1999) identifies two basic AMS fabric types; "normal" and "inverse". A normal AMS fabric is one in which *K*1 is parallel to the statistical mineral alignment of elongate grains (Rochette et al., 1999; Borradaile and Lagroix, 2001). In the case of a dyke, the magnetic foliation will be sub-parallel to the magmatic foliation developed from the alignment of mineral grains along the dyke wall (Figure 2.12). This is referred to as **type-A** fabric.

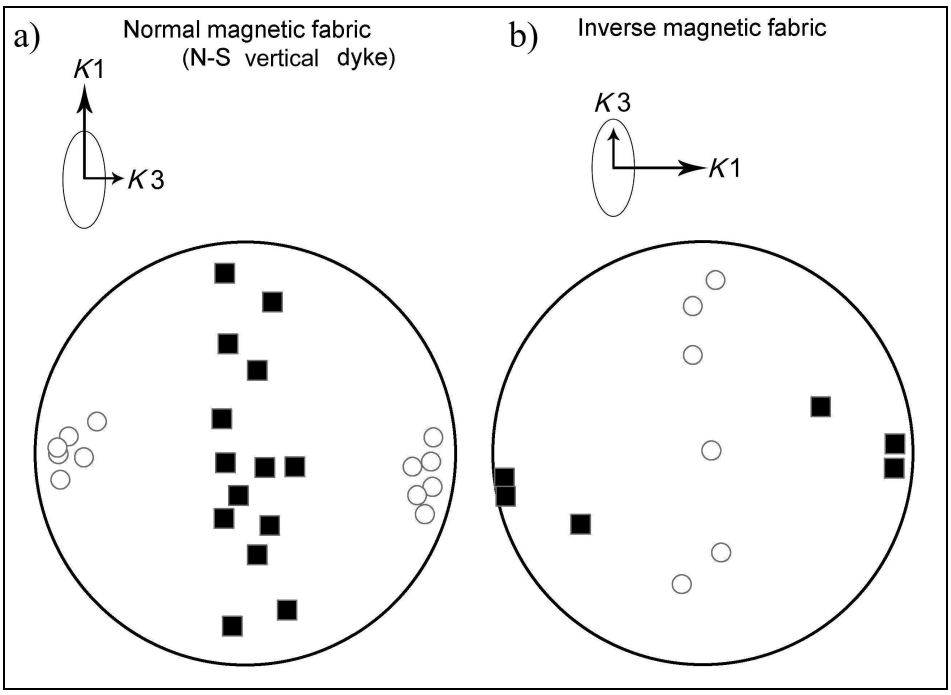

Figure 2.12: (**a**) Normal (type-A) and (**b**) inverse (type-B) AMS fabrics for north-south trending vertical dykes. Squares = *K*1, circles = *K*3 (*K*2 not shown). Insets represent the relative orientation of the AMS ellipsoid to the grain orientation (not to scale) (modified from Rochette et al., 1999).

It has been found, however, that some AMS fabric has $K1$ at a high angle to the dyke plane and thus $K3$ within and parallel to the dyke plane. Such fabric will be referred to as **type-B** fabric throughout this thesis. The same inversion of axes may occur between $K2$ and $K1$ or $K2$ and $K3$ (Rochette et al., 1999; Borradaile and Lagroix, 2001).

For the case of type-A fabric in a dyke, the $K1$ axis direction has been used as an indicator of flow direction, based on the assumption that the long axis of anisotropic grains (whether magnetic or not) will align to the direction of magma flow (Ellwood, 1978; Knight and Walker, 1988; Poland et al., 2004). However, it has been shown that even in cases of type-A fabric, the proportion of $K1$ axes parallel to the magmatic foliation approximates the proportion perpendicular to the dyke margins. This is due to the effect of $K1$ axes being zone axes to the distribution of $K3$ axes (pole of foliation) (Henry, 1997; Callot and Guichet, 2003).

It is recognised that imbrication of inequant grains along dyke margins at angles of < 30° during magma flow can occur. Thus, Geoffroy et al. (2002) proposed a method for using the imbrication of the magnetic foliation to find the magma flow direction as opposed to only relying on the $K1$ axes directions (Figure 2.13).

If the foliation dips at ~30° or more and intersects the dyke plane horizontally (intersection lineation plunge = 0°) it is indicative of vertical flow (Figure 2.13a). Conversely, vertical foliations imbricated about the dyke plane indicate purely horizontal magma flow (intersection lineation plunge = 90°) (Figure 2.13b). It is approximately this orientation of fabric found by Aubourg et al. (2008) which allowed the inference of an overall lateral magma flow direction in the ODS.

Magma flow on the regional scale can be understood in a similar way. The general approach here is to focus on the imbrication of the foliations relative to the dyke plane in predominantly oblate shaped fabric (Aubourg et al., 2002; Geoffroy et al., 2002) while also factoring in the orientation of $K1$ axes (in prolate fabrics). The identical approach can be taken with mineral SPO data, as is demonstrated in Chapters 6 and 7.

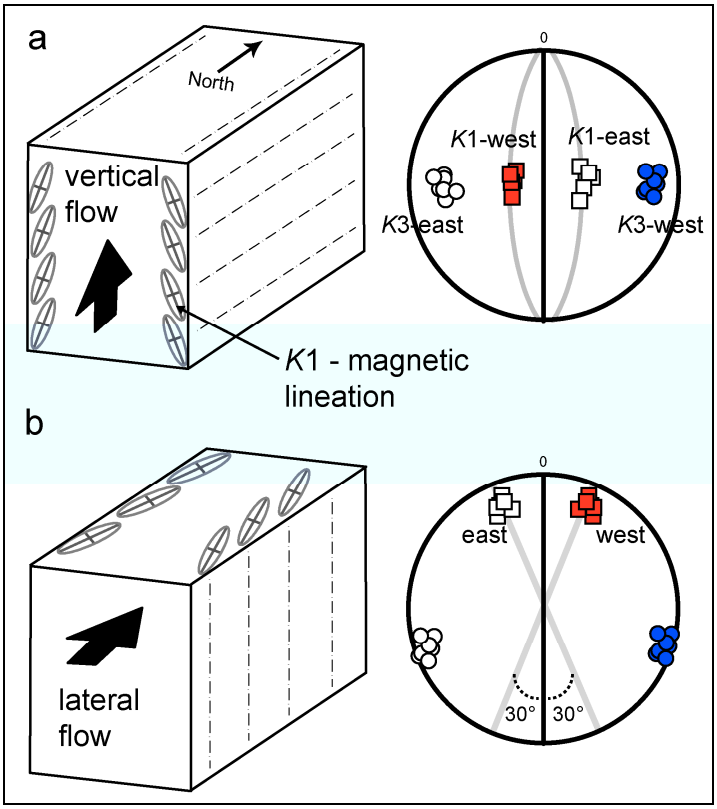

Figure 2.13: (**a**) Idealised imbrication pattern of magnetic fabric in a north-south trending, vertical dyke, consistent with vertical flow, (**b**) Idealised imbrication of magnetic fabric due to lateral magma flow from the south (east and west refer to opposing margins of the dyke). Red squares = *K*1 axes, blue circles = *K*3 axes. Grey lines are the magnetic foliations (modified from Geoffroy et al., 2002 and Gil-Imaz et al., 2006).

The finding of vertical flow (Figure 2.14a) and lateral flow (Figure 2.14b) across a suite of dykes or a dyke swarm is important in a regional sense. This is because the flow history is strongly controlled by the disposition of the melt source (e.g. broad vs. narrow melt zone, see Figure 2.14), the characteristics of the crust (e.g. nature and orientation of stress) and the magma (e.g. overpressure, viscosity, neutral buoyancy level and volatile content). This is done by plotting all the data together in order to observe and interpret the AMS, or other petrofabric, on a regional scale (Rochette et al., 1991; Tamrat and Ernesto, 1999; Callot et al., 2001; Aubourg et al., 2002; Archanjo and Launeau, 2004).

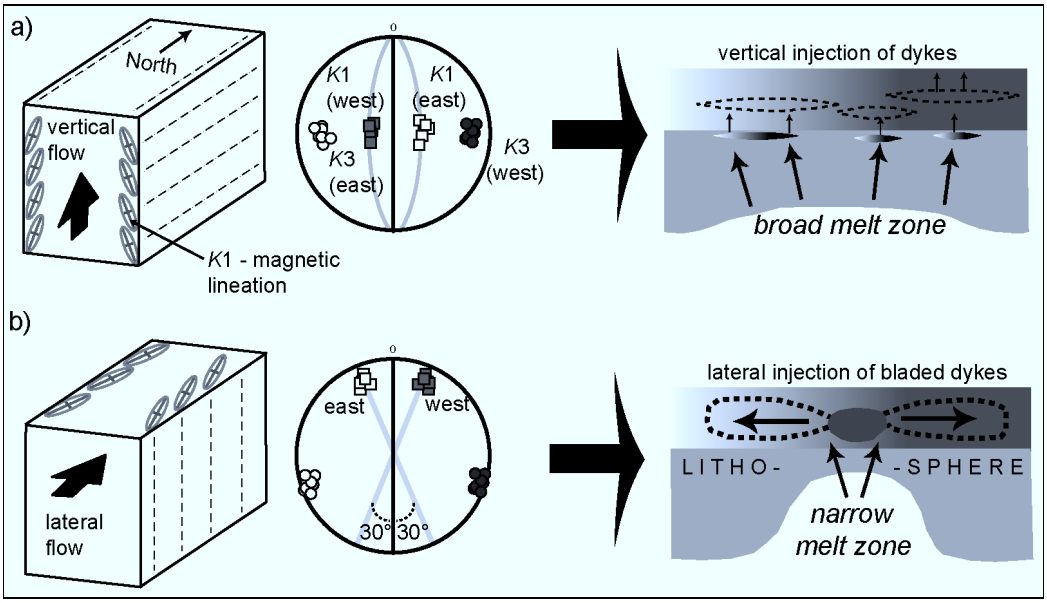

Figure 2.14: Schematic diagrams of a vertical, N–S striking dyke indicating idealised AMS fabric orientation resulting from (a) vertical intrusion of magma and (b) lateral intrusion of magma. Dyke plane is shown as N-S striking black line and the magnetic foliations in grey. Intermediate axes (*K*2) have been omitted for clarity. Not to scale (modified from Geoffroy et al., 2002 and Gil-Imaz et al., 2006). The application of AMS in determining the mode of dyke emplacement is illustrated by the simplified sketches on the right of each end-member of flow type (re-drawn from Callot et al., 2001). Lateral injection of bladed dykes is commonly associated with mantle plumes.

This regional AMS fabric is shown in dyke co-ordinates, where data have been rotated in accordance with the orientations of the dykes from which data were collected. This essentially "normalizes" the data for ease of viewing and interpretation (Rochette et al., 1991; Callot et al., 2001; Aubourg et al., 2008). In such a framework it is easiest to observe and interpret the imbrication of the fabric (the bulk foliation as determined by the grouping of *K*3 axes), should it occur. Thus, for example, if a mantle plume is involved in the injection of dykes from a local, narrow melt zone, it is expected that flow will be lateral (Ernst and Baragar, 1992; Fialko and Rubin, 1999) (Figure 2.15).

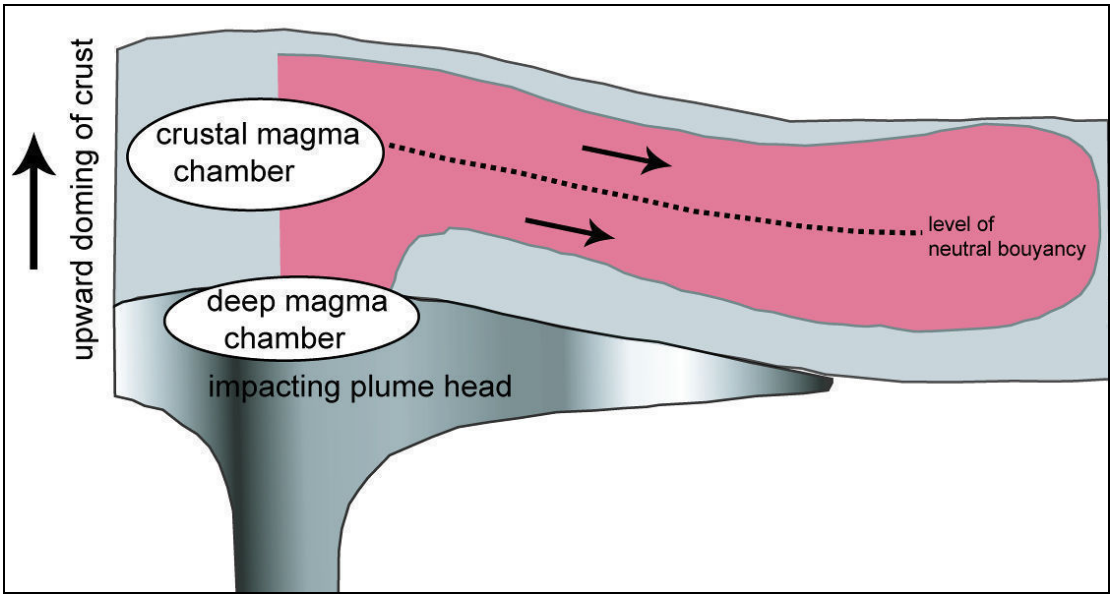

Figure 2.15: Schematic figure showing proposed lateral flow (arrows) of a dyke along the level of neutral magma buoyancy in the crust (not to scale). Note the doming caused by plume-related uplift (re-drawn from Fialko and Rubin, 1999).

The "normalised" regional data presented in the following chapters has been contoured on an equal area stereonet and type-B fabric has been omitted.

2.6. Critical Factors in AMS Interpretation

One of the major drawbacks of using AMS is the potential for uncertainty with regard to the origin of the magnetic fabric. Certainly there are a number of examples of magnetic fabric resulting from secondary processes, such as alteration, metasomatism or metamorphism. However, even primary magnetic fabric may show irregular or unexpected orientations. The possible origins of these fabrics (including axes interchange) have been documented and modelled (Dragoni et al., 1997; Cañón-Tapia and Chávez-Álvarez, 2004). A number of hypotheses, tested models, field data and other relevant examples from the literature are briefly presented below for the purpose of contextualising the focus of the remainder of this study.

2.6.1. Magma Flow

- Horizontal magma flow may occur at shallow depths in bladed dykes which radiate outwards away from a vertically fed, centralised source (e.g. Figure 2.1).
- Dragoni et al. (1997) first demonstrated cyclical rotation of particles during magma flow within a dyke. Thus the principle susceptibility axes pictured in any study may not necessarily reflect the expected flow fabric (Cañón-Tapia and Chávez-Álvarez, 2004).
- Magma pressure may drop once a dyke reaches the Earth's surface as a lava flow. This may result in magma sagging back down, possibly obliterating evidence of shear on dyke walls (Aubourg et al., 2002; Philpotts and Philpotts, 2007). Also, the contraction of dyke walls (positive σ_3) may squeeze magma within the dyke, obliterating primary flow fabric.

2.6.2. Sampling

- An unresolved issue in AMS studies is the relationship between the chilled margin width and the area of sampling which produces "good" AMS results (Tauxe et al., 1998). If a dyke has intruded and crystallised rapidly along the margins, the AMS results should be well grouped and reflect a magmatic fabric. However, if the rate of flow is slow, and possibly turbulent, this may result in weak shearing along the margins, and consequent poorly developed fabric is sampled. This may also hold true for dyke wall melt-back which will tend to disturb or obliterate any original flow fabric.

2.6.3. Grain Size & Orientation

- The orientation and distribution of grain size populations may impact on the nature of the AMS fabric which is being measured. i.e. strongly elongate grains should align more readily to the flow direction, and/or the magnetic grains may be of a later generation.
- Cañón-Tapia and Chávez-Álvarez (2004) demonstrate that more elongate grains ($0.3 < r < 0.95$) yield imbrication consistent with the magma flow direction. Also,

flattened grains, although yielding similar results, will be more likely to result in type-B fabric, given *K*1 axes inversion in sub-equant grains.

2.6.4. Composition

- It has been found that MORB-like dykes in Oman had greater amounts of inverse (type-B) fabric than calc-alkali dykes, suggesting a whole-rock compositional control on the distribution of magnetic phases, probably due to the order of phase crystallisation (Rochette et al., 1991; Cañón-Tapia and Chávez-Álvarez, 2004).
- It has been suggested that the presence of relatively pure magnetite in samples is indicative of a non-primary origin, although exsolution of titanomagnetite or metasomatic processes is not uncommon (Rochette et al., 1999).

2.6.5. Fluids & Alteration

- Hydrothermal alteration of primary magnetite can result in intergrowths of titanomagnetite, titanomaghemite and hematite. An investigation into the effects of such alteration indicates that bulk susceptibility and P' are affected, but not the direction of ellipsoid axes, which is of primary interest in this study (Krása and Herrero-Bervera, 2005). It is likely, then, that "good" AMS results may be the result of strong shape anisotropy or that newly formed minerals from alteration processes mimic the existing fabric.
- The predominance of pure magnetite and lack of titanomagnetite and/or ilmenite indicates that residual titanomagnetite which remains after exsolution processes may become overwhelmed in the magnetic signal by the pure magnetite, which has a higher susceptibility (Butler, 1992).
- Altered samples containing titanomagnetite altered to titanomaghemite were found by Krása and Herrero-Bervera (2005) to have red halos and internal reflections (hematite) around and within the grains. Microprobe work indicates that altered grains lose Fe in favour of increasing Ti, which is consistent with maghemitisation. However, grain size variation is such that smaller grains may be late-stage, pure magnetite – which dominates the magnetic signal.

- Dykes exsolve fluid as they crystallise, especially at the tip. This fluid may firstly assist in the alteration of potentially useful magnetic grains, and secondly weaken the dyke margins with respect to their contraction as magma pressure drops. Thus fluid processes may be important for understanding chemical and structural adjustment of the measured AMS fabric.
- In a sheeted dyke swarm, such as the RRDS, there may be significant thermal disturbance of the magnetic fabric because of the re-intrusion of magma into older dykes and associated heating.

2.6.6. Magnetic Domain

- It is generally considered that AMS exploits the susceptibility of MD grains which carry type-A fabric.
- However, SD magnetite is known to have the maximum susceptibility axis ($K1$) parallel to the short axis due to spontaneous magnetic saturation along the grain length. This is often used as an explanation for instances of $K1$ - $K3$ axes interchange (Rochette et al., 1999).

From the overview above it is clear that there is a wide ranging field of study which has begun to deal with at least some of the above mentioned "complications" in AMS studies. A more detailed study of these factors, focusing on type-B fabric and its potential origin is the focus of Chapters 4 and 5. It is important to critically evaluate which fabric can be reliably used in the interpretation of magma flow in dykes (Chapters 6 and 7), particularly if they carry type-B fabric.

2.7. AMS Measurements

AMS measurements were undertaken in the Departement de Sciences de la Terre et Environment at the University of Cergy-Pontoise, Neuville Sur-Oise, France. Samples were analysed using a Kappabridge KLY-3 anisotropy magnetometer, according to the standard 15 position procedure of Jelinek (1978). Recorded data of the principle orientations of the AMS tensor are plotted as lower hemisphere equal area projections in geographic co-ordinates using the programme "Tclamswin" (Equi-4 Software, v.1.4.0).

2.8. Data Analysis & Treatment

For the purposes of sampling and analysis one dyke comprises 2 sites, each representing the two opposing margins. Each site consists of a number of samples (between 3 and 12, depending on factors mentioned previously). Each sample was prepared and measured independently, but later grouped according to the site (margin) and dyke to which it belongs. Projections of the principle AMS axes *K*1 and *K*3 were prepared for each site (Figure 2.16).

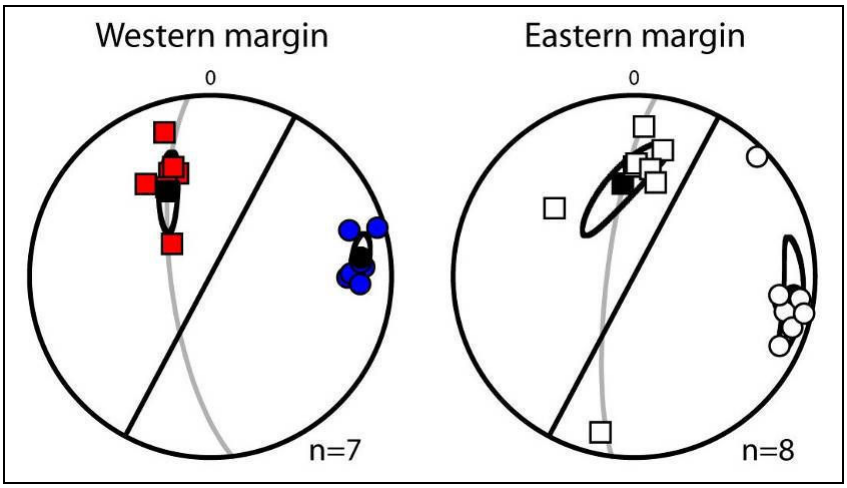

Figure 2.16: Example of a lower hemisphere, equal area projection of AMS data for site WH-07-07 (central RRDS). Closed symbols = western margin. Open symbols = eastern margin. Confidence ellipses are shown (bootstrap method - see discussion in Section 2.4.3) (Tauxe et al., 1998). Squares = *K*1, circles = *K*3 (pole of foliation), *K*2 not shown for clarity. Foliations are shown in grey, and dyke planes in black.

Density diagrams of *K*1 and *K*3 are produced for each site, followed by two orientation corrections. First, all the data are rotated about a vertical axis into a north-south plane. Secondly, all the data are then un-tilted according to the dip of their respective dykes (~70–90°) in order to bring all the data into a vertical plane, assuming that the dip was induced by the eastward tilting of the sedimentary rocks and basalts of the Lebombo monocline (discussed in Chapter 3). Following these corrections, the data of all margins are merged, thus producing four stereographic projections of orientation and tilt corrected density data, two for the eastern margins (*K*1 and *K*3) and two for the western margins (*K*1 and *K*3) of all sites. These data are presented as density diagrams of the principal susceptibility axes, as this allows for easy identification of the statistical distribution and

concentration of the axes orientations with reference to any structural direction (Rochette et al., 1992).

2.9. Measurements & Experimental Background

2.9.1. Characteristic & Isothermal Remanent Magnetisation

Before any interpretation of AMS data can be made, it is essential to understand the magnetic mineralogy of the samples (see Chapters 4, 6 and 7). This involves several analytical procedures which provide information relating to grain size and composition.

Characteristic remanent magnetisation (ChRM) in dykes can be acquired during the cooling of magma. ChRM is determined through cleaning of the natural remanent magnetisation (NRM). NRM is carried only by ferromagnetic minerals. ChRM may help in dating an igneous body because it is records the palaeomagnetic pole at the time of crystallisation.

Isothermal remanent magnetisation (IRM) is a remanence imparted to a sample in a laboratory by a fixed external magnetic field under isothermal conditions. Thermal demagnetisation of IRM is recognised as a relatively simple means of determining the unblocking temperature (T_{ub}) of a sample and the coercivity, which reveals information about the mineral species responsible for the magnetic signal in a sample (Lowrie, 1990). This is because the unblocking temperature is slightly less than the Curie temperature (Tc) for known mineral species, which is essentially unique to that mineral, as shown in Table 2.2 (Butler, 1992).

Table 2.2: The range of unblocking and Curie temperatures, coercivity and the magnetisation at saturation of common magnetic minerals encountered in basalt (O'Reilly, 1984; Hunt et al., 1995).

Mineral	Maximum unblocking temperature / Curie Temperature	Coercivity	Maximum saturation magnetisation (A/m)
Coarse Ti-poor magnetite (metasomatism)	580°C / 580°C	soft	4.8×10^5
Fine Ti-poor magnetite (metasomatism)	~450°C / 580°C		
Ti-rich magnetite (common in basalt)	<300°C / <300°C	soft	$<4.8 \times 10^5$
Maghemite (γFe_2O_3)	~640°C	soft	4.2×10^5
Hematite (αFe_2O_3)	685°C-400°C / 685°C	hard	2.0×10^3
Iron sulphide (pyrrhotite)	<320°C / ~320°C	soft to medium	1.3×10^5

2.9.2. Impulse Magnetisation

An ASC impulse magnetiser was used to induce a magnetic field in three principle directions in each of the samples used for monitoring of IRM. Each sample was subjected to the following applied fields:

1) Z = 1.2 Tesla (T) (hard – parallel to sample length)
2) Y = 0.5 T (medium – perpendicular to sample strike)
3) X = 0.1 T (soft – perpendicular to Y-direction)

2.9.3. Alternating Field (AF) Demagnetisation

This was applied using an AGICO AF-demagnetiser. The field strength used was 20 mT, applied for a few seconds per sample. After demagnetisation the sample was subjected to IRM monitoring.

2.9.4. NRM and IRM Measurements

These procedures were carried out on an AGICO JR-6A apparatus, with automated high speed sample spinner. Parameters were set for 'automated', 'high speed' and 'cylindrical'. REMA-6 software was used for operation and data recording.

2.9.5. Thermal Demagnetisation

Samples monitored for magnetic mineralogy were heated in an automated furnace, at a rate of 10°C / min. to the desired temperature. Samples were heated for 45 minutes at temperatures below 300°C and 30 minutes at temperatures above 300°C. After heating, the samples were cooled in a null magnetic field to room temperature.

2.9.6. Susceptibility vs. Temperature – KT Curves

The change in mean magnetic susceptibility with temperature is a reliable measure of the magnetic mineralogy of a given sample. The procedure involves stepwise thermal demagnetisation of powdered samples in an argon atmosphere (to prevent oxidation during heating) within a Kappabridge KLY-3 apparatus under low-field. Curie temperatures were determined by the inflection point method applied using the differential curve. This method can also detect temperature sensitive magnetic transitions, which provide further constraint on the mineralogy. The analyses in this study were carried out at the Institut de Physique du Globe de Paris (IPGP), France.

2.10. Mineral Shape Preferred Orientation

2.10.1. Introduction

Despite the increasing use of AMS to study rock petrofabric, it is still useful, and often necessary, to supplement AMS data with the true representation of the silicate and/or opaque mineral fabric. In similar and recent AMS studies, the use of mineral shape preferred orientation (SPO) is very limited, mostly due to the laborious nature of thin section preparation and the image analysis (Callot et al., 2001; Aubourg et al., 2002). The intention here, however, is to present a more detailed, data intensive and true three dimensional study of mineral SPO. The instructional manual presented in Appendix D

provides further detail of the methods and procedures applied in SPO study, as do the methods laid out in Chapters 4, 5 and 6.

2.10.2. Dyke Petrofabric as Evidence of Magma Flow

Magmatic flow, especially in relatively low viscosity melts, results in rigid-body rotation of crystals in the magma. Sub-magmatic flow involves crystal interference because of the lowered melt fraction during crystallisation (Passchier and Trouw, 1998). As a result, the recognition of magmatic flow in the rock fabric is usually in the form of an SPO of inequant grains, such as plagioclase or the pyroxenes. Although this preferred orientation will define the magmatic fabric, it may not necessarily define the magma flow sense. It is acceptable as an indicator of the average flow direction for comparison with other data, such as AMS however. Only if undeformed (rigid-body rotated), imbricated grains are found on either margin of an intrusion or flow is it a reliable indicator of flow sense. Because there is no evidence of post-intrusion deformation of the RRDS or NLDS, it is assumed that the petrofabric along the dyke margins in synonymous with the magmatic fabric.

2.10.3. Previous Work

Some of the earliest studies of igneous fabrics are associated with plutonic diapirs (e.g. (Ramsay, 1989; Cruden, 1990), although they were dealt with more for the purposes of dilation and structural emplacement, including solid-state strain analysis. Studies of mineral SPO formed under 'sub-magmatic' conditions include Gay (1966, 1968), Willis (1977), Ferguson (1979), Blumenfeld and Bouchez (1988), Kattenhorn (1994) and Baer (1995). Most of the pioneering work and software development in studying SPO has arisen from the research of Patrick Launeau into methods of comparing SPO's with AMS, and evidently the determination of magma flow from such data (Launeau and Robin, 1996; Launeau and Cruden, 1998; Launeau, 2004). Although concern may arise when SPO and AMS results are divergent, Cañón-Tapia and Chávez-Álvarez (2004) point out that typical low-field AMS measurements measure the bulk susceptibility of the sample, and not a single phase, especially if magnetic sub-fabrics are present. Slight

deviations in the orientation of the petrofabric from the magnetic fabric are therefore to be expected (Archanjo and Launeau, 2004).

2.10.4. Defining the SPO

This is done by producing three orthogonal, orientated thin sections per sample. In this study each thin section corresponds to a plane of the drill core sample of known orientation. Thus sections *XY*, *XZ* and *ZY* are produced; with *XY* being parallel to the top of the core; *XZ* is a vertical section parallel to the plunge direction of the core and *ZY* at right angles to *XY* and *XZ* (Figure 2.17) (note: these axes are entirely unrelated to those discussed in Section 2.9.2 regarding impulse magnetisation). Defining the orientation of the thin sections is rigorous: the dip of the *XY* plane (top of the core) is equal to [90° – plunge angle (α)] of the core and the strike using the right-hand rule (RHR) is [azimuth of the core + 90°] (Figure 2.18). By way of geometry, the *XZ* section always has a dip of 90°, and the strike is equal to the azimuth direction of the core. The *ZY* section has a dip equal to the amount of plunge of the core, and the strike is [azimuth – 90°].

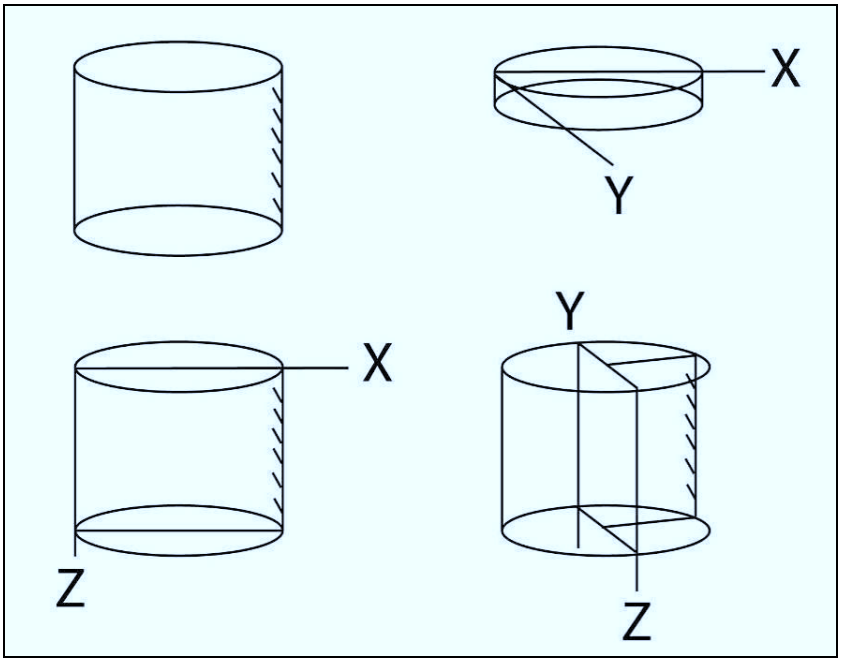

Figure 2.17: Illustration showing the three relevant planes (*XZ*, *XY*, *ZY*) exploited for making three orthogonal thin sections from a drill core. Each core is ~22 mm in height and 25 mm in diameter. The tick marks shown verge downwards along the plunge of the core (adapted from Archanjo and Launeau, 2004).

For the purposes of analysis, it is further necessary to define the "X" direction for each section, if it is assumed that each surface is defined as having two orthogonal directions *X* and *Y*. For the *XY* section, the "X" direction is equal to the azimuth, and for the *ZY* section, "X" is equal to [azimuth ± 180°]. The "X" direction of the *XZ* section is equal to [azimuth – 90°].

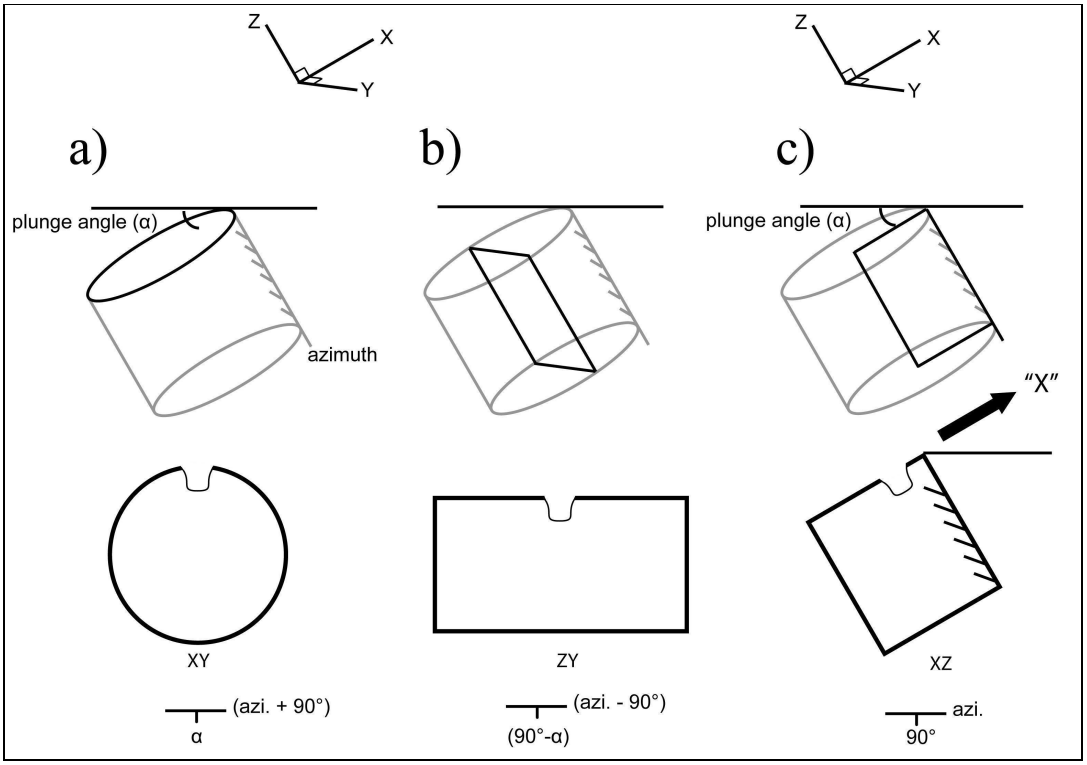

Figure 2.18: Schematic diagram of AMS cores showing *XYZ* sections used for mineral SPO analysis: (**a**) Section *XY*; dip and strike = [90°-α], [azimuth + 90°], (**b**) Section *ZY*; dip and strike = [α°], [azimuth – 90°], (**c**) Section *XZ*; dip and strike = [90°], [azimuth]. The apparent "X" direction for *XY*, however, is (90° + α). Note the notches cut into each orientated block.

Measuring the 2-D ellipse of the mineral fabric in a single thin section is achieved using the freely available "SPO-2003" software (Launeau and Robin, 1996). This image analysis software determines grain orientations and fabric intensities on filtered images taken from orientated rock thin sections (Figure 2.19). Plagioclase grains in each section are digitally filtered using Adobe® Photoshop® into circular Bitmap images in order to remove the remaining phases that are not considered and to reduce edge effects. The Bitmap images are then analysed using SPO-2003 (Launeau and Cruden, 1998), using the

inertia tensor method, as it is directly comparable to AMS. Between 130 and 2800 grains per thin section are indexed, with a resulting minimum of ~1000 grains per sample. Each photomicrograph is analysed using the inertia tensor method, as it is directly comparable to the AMS tensor.

Figure 2.19: Photomicrograph on the left, with filtered Bitmap image of plagioclase grains of section 07D-*ZY* on the right. Using rounded images reduces edge effects which may distort true grain orientations. Both images are 9 mm wide.

From such data it is possible to determine the three dimensional shape preferred orientation (SPO) of grains within a single drill core sample using the "Ellipsoid-2003" software. This defines the shape and orientation parameters of the SPO tensor (without scale factor) in three dimensions. This provides a direct comparison to the AMS ellipsoid (Launeau and Cruden, 1998; Launeau, 2004). Thus a direct comparison between the 3-D SPO and AMS is possible, and may also provide constraint on the relative age of the opaque/oxide grains with respect to the silicate (plagioclase etc.) framework by comparing the orientation the magnetic fabric to the magmatic fabric (e.g. Launeau and Cruden, 1998). Note that AMS axes nomenclature (*K*1, *K*2, *K*3) is replaced in SPO by *L*1, *L*2 and *L*3 respectively to avoid confusion.

- Chapter 3 -

The Karoo Large Igneous Province

3.1. Introduction

In this section the Karoo Large Igneous Province (LIP) and associated magmatism within Gondwana is discussed, paying particular attention to the distribution and compositional types of magma in the Karoo LIP. The distribution and relative age of intrusive components of southern Africa and Dronning Maud Land, as well as the Karoo triple junction are considered. Relevant geochronology contextualises the dyke swarms with respect to the bulk of the magmatism.

3.2. Regional Distribution

The Karoo LIP comprises a large number of volcanic and intrusive components, which in South Africa alone have been studied for more than 70 years (e.g. Du Toit, 1929; Cox et al., 1967; Duncan et al., 1984; Ellam et al., 1992; Jourdan et al., 2009). There has not been a collation of the existing and more recent work on the Karoo LIP since Erlank (1984), but readers are referred to Jourdan et al. (2009) who provide an updated synthesis of the current understanding of Karoo magmatism.

The Karoo LIP extends across southern Africa, covering ~3×10^6 km^2 (Eales et al., 1984) and is contemporaneous with other igneous provinces, including the Ferrar Province of Antarctica (Figure 3.1) (Kyle et al., 1981; Encarnación et al., 1996; Zhang et al., 2003), the associated Kirkpatrick basalts and various intrusive components of west Dronning Maud Land and the Tasman dolerites of Australasia (Elliot, 1975; Fleming et al., 1995).

Geochronology indicates that the bulk of the magmatism occurred between ~183 Ma and ~178 Ma, but continued up to ~174 Ma with the intrusion of the RRDS in the southern Lebombo monocline (Duncan et al., 1997; Jourdan et al., 2005; Jourdan et al., 2007b, c).

The Lebombo is in fact a N–S striking, easterly dipping structure comprising a highly magmatic and rifted volcanic margin (Bristow, 1982; Watkeys, 2002; Klausen, 2009).

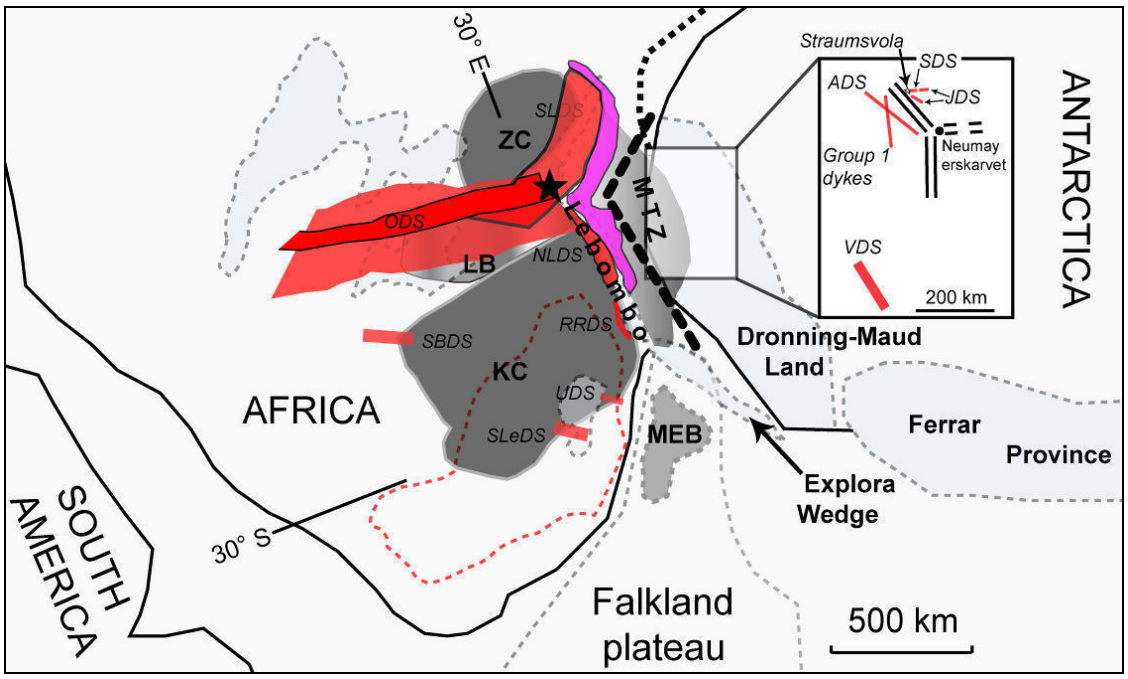

Figure 3.1: Schematic map of southern Gondwana at ~170 Ma showing the broad pre-Karoo crustal structure (solid) with the Karoo and associated volcanic provinces overlaid (in light grey with dashed outline). Note the positions (in bold text) of the Lebombo monocline, the Falkland Plateau, the Explora Wedge, Dronning Maud Land, the Ferrar Province, the Kaapvaal Craton (KC), Zimbabwe Craton (ZC), Limpopo Belt (LB), the Mozambique thinned-zone (MTZ) and the Maurice-Ewing Bank (MEB). The Jurassic dyke swarms are shown in red (ODS=Okavango dyke swarm, SLDS=Save-Limpopo dyke swarm, NLDS=Northern Lebombo dyke swarm, RRDS=Rooi Rand dyke swarm, UDS=Underberg dyke swarm, SBDS=Southern Botswana dyke swarm, SLeDS=Southern Lesotho dyke swarm). The SW-1 dyke swarm of Mozambique is shown in pink (see Section 3.4). The incipient rift shown in the MTZ is from Jokat et al. (2003). Inset over Antarctica shows the two regions of the Jutulrøra dyke swarm (JDS), the Straumsvola dyke swarm (SDS), the Alhmannryggen dyke swarm (ADS), the Vestfjella dyke swarm (VDS) and the Group 1 dyke swarm. Note the triple rift system in Antarctica that converges on Neumayerskarvet (Ferraccioli et al., 2005). The black star at the convergence of the ODS and SLDS shows the position of Mwenezi. The full extent of the ODS is illustrated as it comprises a heavily intruded zone (darker) bounded by regions of decreasing dyke density, reaching > 300 km in width. Note the overlap of the SLDS with the ODS, and the overlap of the ODS with the NLDS. The extent of sill intrusion in South Africa (red dashed outline) is also shown. The present coastline of Mozambique is shown as a heavy dashed black line to the north of the MTZ (re-drawn from White and McKenzie, 1989; Storey et al., 1992; Encarnación et al., 1996; Storey and Kyle, 1997; Watkeys, 2002; Jourdan et al., 2004; Ferraccioli et al., 2005; Riley et al., 2006; Curtis et al., 2008).

The voluminous, low-Ti, tholeiitic magmas which characterise much of the Karoo LIP erupted within 3–4.5 Ma as continental flood basalts (CFBs) now preserved mainly in

Lesotho and western Botswana (Jourdan et al., 2007a, c). The volcanic sequences of the Lebombo reach a thickness of 1.5–12 km and overlie the uppermost arenaceous rocks of the Karoo Supergroup (Clarens Formation) (Eales et al., 1984; Watkeys, 2002). There is also an associated network of dolerite sills extending throughout most of the Karoo basin of South Africa (Figure 3.1).

The dyke swarms associated with the Karoo LIP have become increasingly studied as they provide structural, geochemical and geochronological information about their own development, and that of the entire Karoo. These include, but are not limited to, the ODS (Reeves, 1978; Elburg and Goldberg, 2000; Reeves, 2000; Le Gall et al., 2002, 2005; Jourdan et al., 2004; Aubourg et al., 2008) and the NLDS and RRDS of the Lebombo monocline (Saggerson et al., 1983; Armstrong et al., 1984; Watkeys, 2002; Jourdan et al., 2006; Klausen, 2009; Hastie et al., 2011a, b) (Figure 3.1). The dyke swarms and Karoo triple junction are discussed in further detail in Section 3.4.

Along with the ODS and Lebombo monocline, another dyke swarm, the Save-Limpopo dyke swarm (SLDS) (Jourdan et al., 2006) converges on Mwenezi (formerly Nuanetsi) in southern Zimbabwe (Figure 3.1). The SLDS is found primarily within the Sabi monocline (or Save-Limpopo monocline) which developed during normal faulting in the Permian (Watkeys, 2002). The intersection of the monoclines and the ODS produces a conspicuous triple junction. This geometry has been used (other than compositional and geochemical data) as evidence for the role played by a mantle plume in its formation (Burke and Dewey, 1973; White and McKenzie, 1989; Campbell and Griffiths, 1990; Cox, 1992; Ernst and Buchan, 1997; Storey and Kyle, 1997; White, 1997). Before further discussion of the timing and duration of the eruptive and intrusive phases it is necessary to examine the distribution and relevant petrology of the rock types within the Karoo LIP.

3.3. Igneous Stratigraphy & Petrology

Volcanic rocks of Karoo LIP range from earliest nephelinites and picrites to continental tholeiites and rhyolites (Eales et al., 1984). There has been much geochemical study performed on the compositionally diverse igneous rocks of the Karoo LIP (Cox et al.,

1967; Duncan et al., 1984; Sweeney and Watkeys, 1990; Hergt et al., 1991; Ellam et al., 1992; Sweeney et al., 1994; Riley et al., 2006). These findings have a significant bearing on the mantle plume model for the Karoo LIP, and are summarised below.

The most primitive rock types are centred on the Karoo triple junction (Figure 3.2) and consist of the incompatible element enriched Mashikiri Formation nephelinites and the Letaba Formation picrites (Bristow, 1982; Bristow, 1984). The triple junction, at the northern termination (Mwenezi) of the Lebombo monocline, is within the Limpopo Belt (discussed further in Section 3.4) while the remainder of the N–S trending structure occupies a position along the eastern edge of the Archaean Kaapvaal Craton (Figure 3.1).

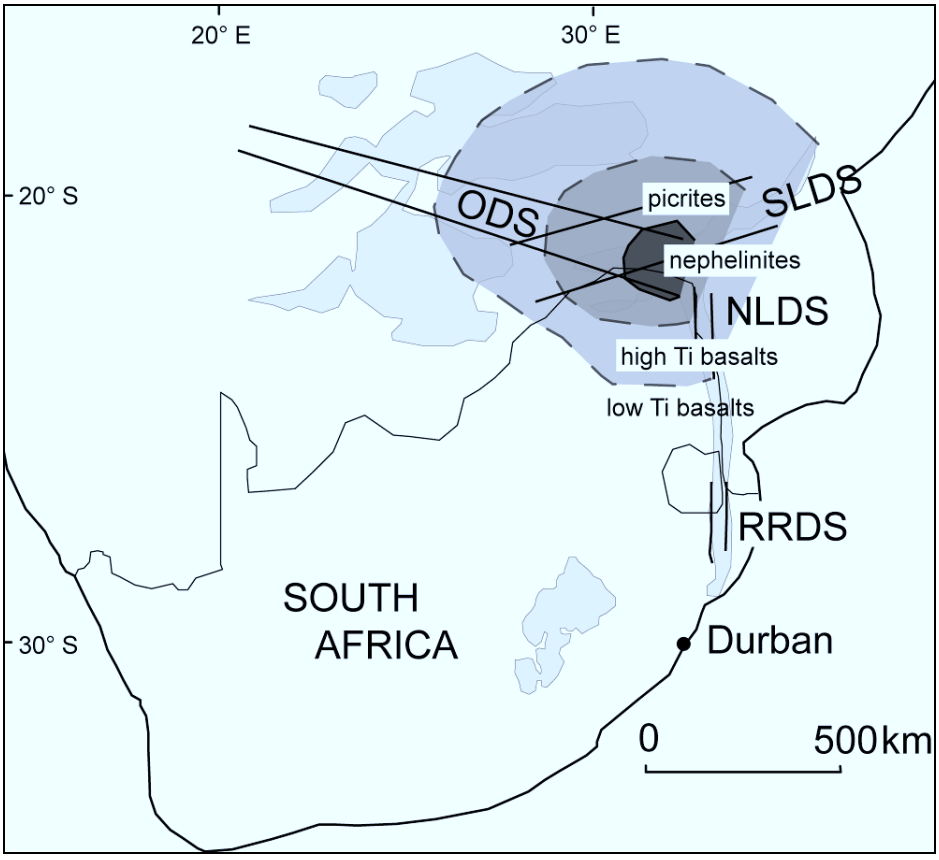

Figure 3.2: Schematic map of the outcrop of the Karoo LIP (lightest grey) in southern Africa, illustrating the concentric distribution of nephelinites, picrites and high- and low-Ti basalts with respect to the Karoo triple junction centred on Mwenezi, southern Zimbabwe (re-drawn from Jourdan et al., 2004; Klausen, 2009).

The Mashikiri Formation overlies the arenaceous Clarens Formation, which in the northern Lebombo directly overlies Precambrian basement. The Mashikiri Formation is not as laterally extensive north-to-south as the overlying volcanics of the Lebombo Group, which include the Letaba Formation picrites and Sabie River Formation basalts. There are units of rhyolite (flows and intrusions) within the basalts of the Sabie River Formation known as the Olifants Beds (Bristow, 1982; Riley et al., 2004). The youngest volcanics of the Lebombo are the Jozini and Mbuluzi Formation rhyolites and rhyodacites (Watkeys 2002; Klausen 2009).

The Mashikiri nephelinites display enrichment of incompatible trace elements which reflect melting of an ancient, metasomatically-enriched sub-continental lithospheric mantle (SCLM) (Ellam and Cox, 1989; Hawkesworth et al., 1999; Jourdan et al., 2007a). The Letaba Formation picrites (MgO 10–24%) of the northern Lebombo monocline are more voluminous than the nephelinites and reach a maximum thickness of 4 km. They may have been derived from the SCLM (Bristow et al., 1984; Ellam and Cox, 1989) or from mixing between asthenospheric mantle and SCLM (Ellam and Cox, 1991; Sweeney et al., 1991) or from a heterogeneous source (Ellam, 2006).

The voluminous continental flood basalts and associated dykes and sills which followed the primitive volcanics at ~182 Ma are low in MgO (2% < MgO < 9%) and possess a variation in Ti and Zr across southern Africa. Specifically, basalts in the northern Lebombo and further north into Zimbabwe are high-Ti (TiO_2 > 2%), whilst basalts of the southern Lebombo, Lesotho, central Botswana and central Namibia are low-Ti (Figure 3.2) (Cox et al., 1967; Duncan et al., 1984; Jourdan et al., 2007a) and those of the Lebombo have calc-alkaline affinities (low-K tholeiites) (Duncan, 1987). This distinction is attributed to differences in melting, resulting in 30–40% of the incompatible elements in the high-Ti basalts being derived from the lithospheric mantle (Sweeney and Watkeys, 1990; Sweeney et al., 1994). Indeed Ellam and Cox (1989) have shown, using Sm-Nd systematics that the Karoo yields a Proterozoic eruption “isochron” which demonstrates mixing in the melt source region. This is also evident from the background levels of crustal contamination and generally MORB-like signature of incompatible elements (Cox

and Bristow, 1984; Hawkesworth et al., 1984). Bristow et al. (1984) also find evidence for a heterogeneous mantle source for the bulk of the Karoo basalts in the $^{87}Sr/^{86}Sr$ ratios, although these authors find no convincing evidence for interaction of the melts with crustal material. The low-Ti basalts were possibly derived from an asthenospheric source which equilibrated with refractory lithospheric mantle (Sweeney et al., 1991). The voluminous basaltic volcanism was followed by the eruption of the Jozini and Mbuluzi Formation rhyolites which cap the Lebombo monocline (Riley et al., 2004). This was followed by the intrusion of the RRDS in the southernmost region of the Lebombo (Armstrong et al., 1984).

The Ferrar Province is exposed along the length of the Transantarctic Mountains and comprises the Dufek intrusion as well as massive, laterally extensive dolerite sills (Elliot et al., 1999) and pyroclastics capped by the Kirkpatrick basalts (Kyle et al., 1981; Elliot and Fleming, 2000). The Ferrar Province is dominated by low-Ti tholeiitic basalts which were most likely derived from a lithospheric mantle source (Hergt et al., 1991). The extensional rift-like structure along which the Ferrar magmas intruded has been suggested as the reason for its linear extent (Storey et al., 1992) (Figure 3.1). It has also been suggested that the Ferrar is indicative of a linear melting anomaly caused by a long-lived subduction zone on the southern margin of Gondwana (Cox, 1992; Storey, 1995). However, some workers argue that the Ferrar and related magmas were emplaced from the Weddell Sea triple junction (Elliot and Fleming, 2000, 2004; Leat, 2008; Luttinen et al., 2010). This is discussed in further detail in Section 3.6.

The mafic rocks of Dronning Maud Land are comparable to those in southern Africa with two varieties, DM1 and CT1 (Riley et al., 2005 and Luttinen et al., 1998 respectively) being similar to the low-Ti compositions of southern Africa (DM = Dronning Maud, CT = chemical type). Luttinen et al. (1998) provide general geochemical and isotopic data from the basalts and dykes of Vestfjella, in Dronning Maud Land. Using Sr and Nd isotopes, they differentiate 4 magma types (CT1–CT4) which can be identified in related lavas and dykes. Dolerite dykes belonging to the CT4 magma type are the only OIB-like (ocean island basalt) magmas known from Karoo-age magmatism. The CT1 magma type

is tholeiitic, most likely derived from an Archaean, sub-lithospheric mantle source. The CT2 and DM2 magma types have MORB affinities similar to the RRDS and most likely derive from an asthenospheric source. There is also a high-Ti basalt composition (Group 4 basalts of Riley et al., 2005). The ferro-picrite CT3 magma type does not have a comparable composition within the Karoo LIP of southern Africa and is thought to be derived from early mantle plume melts (Riley et al., 2005).

The evidence for structural control on the distribution of basaltic compositions in southern Africa is found in compositional changes (e.g. low-Ti to high-Ti) that occur across basement boundaries through which the basalts erupted (Proterozoic mobile belts vs. Archaean cratons) (Cox et al., 1967; Duncan et al., 1984; Watkeys, 2002; Jourdan et al., 2004, 2006). Field relationships and geochronology show that the lithospheric architecture has also controlled the development of the Karoo triple junction and associated dyke swarms (Watkeys, 2002; Jourdan et al., 2004; Le Gall et al., 2005).

This has also been shown in Dronning Maud Land by Luttinen et al. (2010) who identify Grunehogna province magmas and Maud province magmas on the basis of geochemistry and Nd and Sr isotope data. In brief, the authors indicate that the Grunehogna magma type shows evidence of recycled oceanic crust in the parent magma, and that the magmas most likely derived from the partial melting of eclogite-bearing asthenospheric mantle. Contamination has occurred, with high-Ti types showing evidence of lithospheric mantle contamination and low-Ti types showing evidence of crustal contamination. The Maud province magma type, however, derived from relatively low-pressure partial melting of lithospheric mantle associated with rifting in the region of the Weddell Sea triple junction. This is a broadly similar pattern to the distribution of magma types across the southern African cratonic regions (high-Ti) and the central (Lesotho) Karoo and Botswana areas (low-Ti).

3.4. Dykes of the Karoo & Associated LIP's

There are three main dyke swarms associated with the Karoo triple junction (SLDS, NLDS, ODS; Jourdan et al., 2004), four more isolated swarms (RRDS, UDS, SLeDS,

SBDS; Armstrong et al., 1984; Riley et al., 2006; Jourdan et al., 2007a) and at least five dyke swarms in Dronning Maud Land (Curtis et al., 2008) (Figure 3.1).

The Karoo triple junction at Mwenezi is situated within the Limpopo Belt and comprises both the earliest (nephelinites, picrites) and latest (Mwenezi igneous complex) manifestations of Karoo magmatism. The Limpopo Belt comprises poly-metamorphosed rocks that represent an Archaean collision between the Kaapvaal and Zimbabwe Cratons. These deformed cratonic and volcano-sedimentary rocks have a strong ENE-trending fabric which has been exploited by both faulting (Watkeys, 2002) and dyking (Uken and Watkeys, 1997; Jourdan et al., 2004) since the Proterozoic.

The ENE-trending SLDS comprises predominantly fine to medium grained dolerite dykes emplaced within the central and northeastern regions of the Limpopo Belt, extending for ~600 km from SE Botswana (the Tuli basin) to the NE of the Limpopo Belt. The SLDS is 50–100 km wide and comprises vertical to sub-vertically dipping dykes. These dykes have been dated to 180.4±0.7–178.9±0.8 Ma although a significant proportion of the dykes are Proterozoic in age (Le Gall et al., 2002; Jourdan et al., 2005, 2006). Field relationships indicate that this dyke orientation (ENE to NE) predate dykes of the NLDS and ODS, particularly evident from the picritic dykes of the Mwenezi region having intruded in this orientation (Watkeys, 2002).

The NLDS is hosted by the basaltic and other volcanic units, as well as the Clarens Formation, of the Lebombo. Dykes of the N–S trending NLDS comprise several generations of feeder dykes which can be directly correlated with volcanic units of the Sabie River Formation basalts (D1 and D2 generation), the Jozini Formation (D3 generation) and possibly the Movene Formation basalts (D4 dykes) within the Lebombo monocline (Klausen, 2009). In other areas, such as the ODS and RRDS, the dykes intrude the basalts of the Karoo, and have no known extrusive equivalents. The D1 to D4 nomenclature is indicative of relative dyke ages, such that D4 dykes are the youngest, and tend to strike NW, similar to the ODS. Two radiogenic ages of 181.4±0.7 and 182.3±1.7 Ma have been found for the NLDS (Jourdan et al., 2005). As yet, no Proterozoic age

dykes have been recognised in the NLDS, suggesting that the N–S dyke trend developed in the Lebombo monocline during the Jurassic in response to E–W extension (Watkeys, 2002).

The WNW-trending ODS is ~1500 km in length, reaching ~300 km in width, where it overlaps with the northernmost Lebombo and the SLDS (Jourdan et al., 2006) (Figure 3.1). It converges with the Lebombo monocline and SLDS at Mwenezi (Jourdan et al., 2004). Dykes of the ODS have intruded Precambrian basement (central and northwestern regions of the Limpopo Belt) and sedimentary and volcanic rocks of the Karoo Supergroup within the Tuli basin (Smith, 1984; Elburg and Goldberg, 2000; Le Gall et al., 2005; Aubourg et al., 2008). The orientation of the ODS has been recognised as essentially a reactivation of an older structural trend evident in both the Kaapvaal and Zimbabwe Cratons (Watkeys, 2002). From field evidence, Le Gall et al. (2005) inferred a NNW-SSE dilation direction for the dykes, a similar direction to that inferred for the SLDS.

The ODS was first described as a post-Karoo (Cretaceous) dyke swarm associated with a failed rift axis (Reeves, 1978, 2000), i.e. an aulacogen. Uken and Watkeys (1997) considered the ODS to be Karoo in age. Indeed, subsequent work has shown a predominantly Karoo-age with ~13% of the dykes being Proterozoic in age (Elburg and Goldberg, 2000; Le Gall et al., 2002, 2005). Dykes of the ODS have been dated to 179±1.2–178.4±1.1 Ma, with the Proterozoic component providing ages of 851±6–1672±7 Ma (Jourdan et al., 2004). The dykes are doleritic in composition; dominated by plagioclase (35–45%), clinopyroxene (20–35%) and Fe-Ti oxides. Both high-Ti and low-Ti varieties occur (Elburg and Goldberg, 2000; Aubourg et al., 2008).

The youngest dyke swarm in the Karoo LIP is the RRDS (173.9±0.7 Ma) which post-dates the main Karoo flood basalts (Jourdan et al., 2007b, c). The MORB-like RRDS is a N–S trending dyke swarm found in the southern Lebombo monocline, extending ~180 km from the Msunduze River in KwaZulu-Natal northwards to central Swaziland. The 10–22 km thick swarm intruded the Sabie River Formation and Beaufort Group, just to

the west of the Lebombo monocline (Marsh, 1987; Marsh, 2002; Watkeys, 2002). The steeply dipping (> 80°), generally N–S striking dykes of the RRDS in the central area give way to more shallowly dipping (50°–70°) NNE–SSW striking dykes in the north (in Swaziland). The RRDS most likely originated from the melting of an upwelling asthenosphere, as is typical during lithospheric rupture during the early stages of continental break-up (Armstrong et al., 1984; Meth, 1996; Saggerson et al., 1983). The Explora Wedge probably developed at this time (Cox, 1992; Leinweber and Jokat, 2012) (Figure 3.1). As previously mentioned, the CT2 and DM2 magma types of Dronning Maud Land have MORB affinities similar to the RRDS (Luttinen et al., 1998) which is consistent with the coeval development of the Lebombo monocline and Explora Wedge.

There are additional dyke swarms in southern Africa which require introduction, as they are relevant to the tectonomagmatic characteristics of the Karoo LIP. These are the southern Botswana and southern Lesotho dyke swarms (SBDS and SLeDS respectively) and the NW–SE striking Underberg dyke swarm (UDS) (Riley et al., 2006) (Figure 3.1). The SBDS and SLeDS are shown only in the interest of completeness, because magma flow and geochronological studies have not been conducted on these swarms.

Dykes of the UDS are fine- to medium-grained dolerites with intergranular and/or sub-ophitic textures. The UDS intruded sedimentary sequences of the Permo-Triassic Beaufort Group and the overlying Molteno, Elliot and Clarens Formations. The UDS is geochemically similar to the low-Ti basalts of Lesotho (and the SLeDS); although field relationships and geochronology confirm that the dykes are younger than the Lesotho basalts. Riley et al. (2006) provide an age of ~176 Ma for the intrusion of the UDS. These authors have found that the strike of the dykes is remarkably uniform (130°–140°), which differs slightly from the ODS and SBDS (110–120°). The UDS was derived from sub-lithospheric melts involving some crustal contamination (Riley et al., 2006). AMS measurements have been undertaken on three dykes of the UDS.

In addition, there is the Olifants River dyke swarm (ORDS, not shown) which was once thought to be related to the Karoo LIP, but has been shown to be older than ~800 Ma

(Marsh, 2002; Jourdan et al., 2006). The ORDS extends south-westward from the Lebombo monocline following an Archaean/Proterozoic dyking direction (Uken and Watkeys, 1997; Watkeys, 2002). It is common to find that NE–SW striking dykes are truncated by NW–SE striking dykes – which is the orientation of the ODS. For example, the SLDS overlaps with the ODS and has been dated to 180.4±0.7–178.9±0.8 Ma (Le Gall et al., 2002; Jourdan et al., 2005, 2006) although Proterozoic ages have been found (728±3–1683±18 Ma, n=14). Karoo dykes do not generally occur in the 0°–40° orientation, which is best explained by the SW–NE strike of the Proterozoic age dykes of the SLDS.

Karoo-age dyke swarms in Dronning Maud Land include the Alhmannryggen (178 Ma), Straumsvola (178–176 Ma) and Vestfjella (177 Ma) dyke swarms (ADS, SDS and VDS respectively). There are two older dyke swarms, the Group 1 dykes of the Alhmannryggen region (~190 Ma) (Riley et al., 2005) and the Jutulrøra dyke swarm (JDS) (~205 Ma). The JDS consists predominantly of low-Ti tholeiitic dykes that trend NNW–SSE. The SDS, which is mainly restricted to the Straumsvola area (Figure 3.1), is predominantly doleritic in composition and was emplaced between 178.5 Ma and 174.8 Ma (concordant $^{40}Ar/^{39}Ar$ isochron age of 174.8±2.0 Ma). Heinonen et al. (2010) have shown that the VDS comprises two geochemically distinct suites – an enriched, OIB-like type and a depleted, MORB-like type.

The youngest dyke phase of the SDS yielded an age of 170.9±1.7 Ma (younger than the Lebombo rhyolites). These younger dykes, including phonolitic and lamprophyric compositions, cross-cut the dolerite dykes. Curtis et al. (2008) propose two distinct phases of mafic dyke emplacement rather than a protracted magmatic history. From field, structural and AMS data these authors assert that the dykes were sourced locally. For example, power-law distribution of the dyke thicknesses and spacing indicates that the dykes generally become more widely spaced ~25 km south of Straumsvola. This may reflect a spatial variation in magma pressure, such that the SDS was emplaced under higher magmatic pressure than the JDS; the restricted orientations thereof indicating that

the JDS was bound to the stress field of the host rock and not the magma pressure driving emplacement.

Despite attributing the origin of these dykes to a mantle plume (Curtis et al., 2008), it is evident that the majority of these dykes are low-Ti tholeiites, similar to the bulk of the Karoo mafic dykes and lava flows. Interestingly, these compositions are also found off-craton in Antarctica in the same manner as the Grunehogna magma type (Luttinen et al., 2010) and the low-Ti tholeiites of the southern Lebombo (Sweeney and Watkeys, 1990).

An important structural feature of this region of Dronning Maud Land is un-named triple rift system first described by Ferraccioli et al. (2005). It was discovered beneath the Antarctic ice sheet in west Dronning Maud Land and converges on Neumayerskarvet, which is near the southern termination of the ADS (Figure 3.1). The convergent rifts of this triple junction are occupied by Jurassic-age volcanic rocks and alkaline and tholeiitic intrusions (Ferraccioli et al., 2005; Curtis et al., 2008). Riley et al. (2005) observed in the Ahlmannryggen region that initial crustal dilation due to dyking was N–S oriented (190 Ma) followed at 178 Ma by regional NW–SE oriented dilation. Ferraccioli et al. (2005) demonstrate, however, that extension in these rifts cannot be accounted for by dyke dilation alone, and suggest considerable crustal thinning prior to, or post-dyking. These authors also argue that the triple junction geometry and the ferro-picrite composition of certain dykes are consistent with derivation from an early mantle plume (~190 Ma?), although the Jurassic dyke swarms described above do not coincide geometrically with these rifts (Figure 3.1). The same is clear in the dyke swarms of the Karoo LIP (e.g. the RRDS, SLeDS and UDS).

There is a "new" dyke swarm that has been recognised geophysically within the Mozambique thinned-zone (MTZ) (Figure 3.1) that is known as the SW-1 dyke swarm (or Mozambique dyke swarm) (Mekonnen, 2004). There is virtually nothing known about or published regarding these dykes. However, its prominent NNE strike direction and presence within the MTZ suggests that it intruded later (~170 Ma) than the Karoo LIP in

response to extension between SE Africa and Antarctica (Jokat et al., 2003; Mekonnen, 2004).

3.5. Geochronology of the Karoo LIP

3.5.1. Overview

As illustrated already, the Karoo LIP comprises many components; volcanic and intrusive, with contemporaneous and overlapping volcanism spread across southern Africa and Antarctica. Handling the observed and resolved field relationships and the radiogenic age-data can therefore be somewhat cumbersome. Thus, an overview of the salient and reliable dates from the growing number of data on the Karoo is provided, which better constrain the ages of particular lithologies and events (and the duration of Karoo magmatism).

Although Jourdan et al., (2007b) provide a thorough analysis and review of the development of the Karoo LIP based on $^{40}Ar/^{39}Ar$ geochronology, there are new data (Curtis et al., 2008) and previously determined ages on the Antarctic components of the Karoo LIP which have not been discussed (Heimann et al., 1994; Zhang et al., 2003; Riley et al., 2005). Thus, a concise chronostratigraphy of the major components of the Karoo LIP is presented (Figure 3.3). The source references for the ages are shown below the key in Figure 3.3. The assembly of ages shown is not exhaustive, but is restricted to ages determined by the $^{40}Ar/^{39}Ar$ and U-Pb methods on single plagioclase and zircon grains respectively (i.e. no bulk sample / bulk rock / groundmass ages). A synopsis of the reliability of these ages, and the omission of others, is presented below because this impacts on what geologically significant conclusions can be drawn from this chronostratigraphy.

3.5.2. Reliability of Ages

Firstly, whole-rock ages (including those determined using K/Ar and Rb/Sr) are excluded because their meaning is highly debatable (Jourdan et al., 2005). Also, only Jurassic ages are shown for dyke swarms in which Proterozoic ages have also been found (the SLDS and ODS).

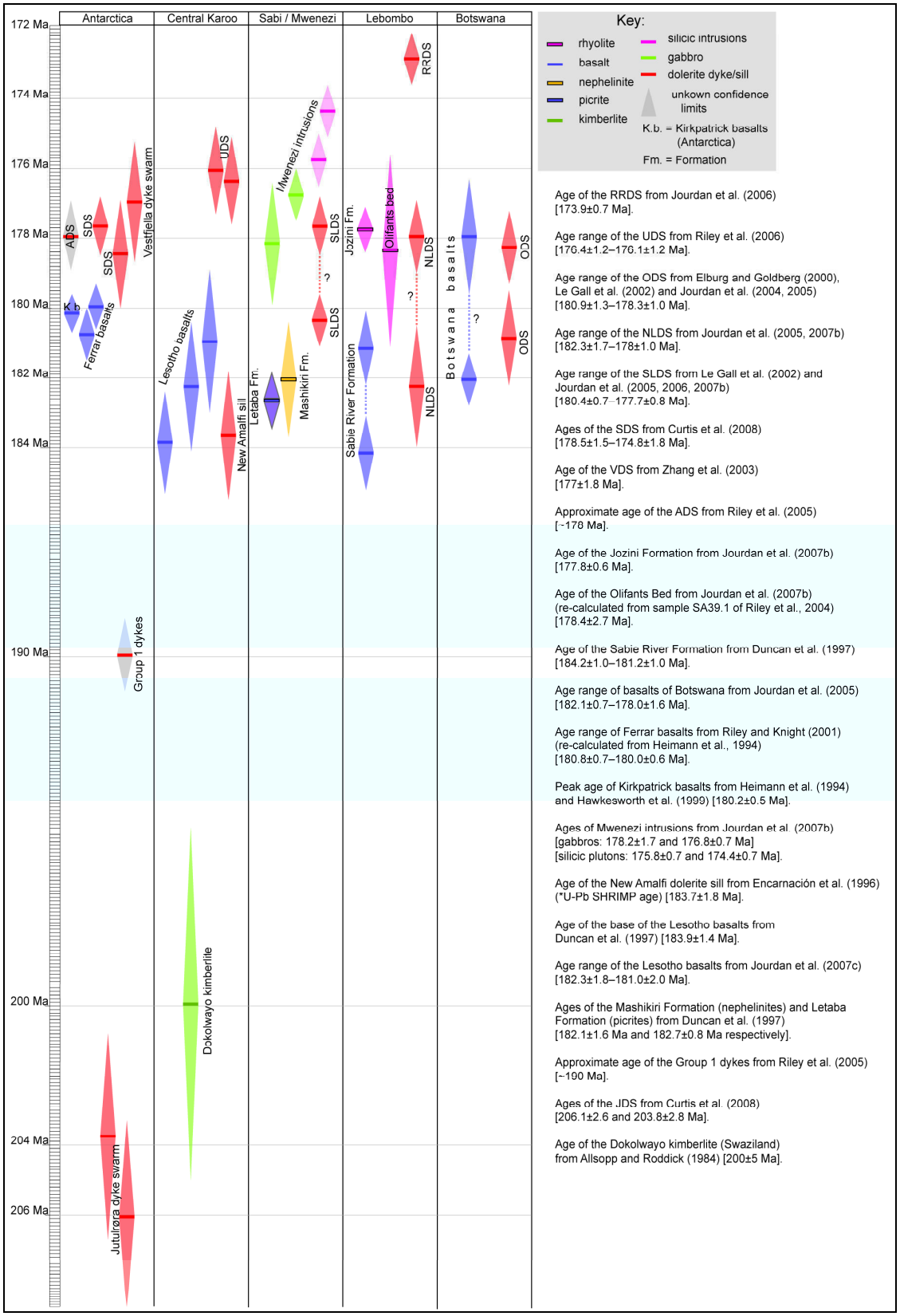

Figure 3.3: Chronostratigraphy of the major regions of the Karoo LIP and associated igneous provinces. Note that ages are shown in solid colours with lighter shaded error bars. The smallest age increments are 0.1 Ma. RRDS=Rooi rand dyke swarm, UDS=Underberg dyke swarm, ODS=Okavango dyke swarm, SLDS=Save-Limpopo dyke swarm, NLDS=Northern Lebombo dyke swarm, SDS=Straumsvola dyke swarm, VDS=Vestfjella dyke swarm, ADS=Alhmannryggen dyke swarm, JDS=Jutulrøra dyke swarm. See Section 3.5.2 for discussion of age reliability.

There is some concern about the ages found by Riley et al. (2005) for the Group 1 dykes and the ADS. These authors indicate that the criteria necessary to define an age plateau during step-heating in the $^{40}Ar/^{39}Ar$ method were generally not met and the effects of alteration and/or excess ^{40}Ar make distinguishing any age differences uncertain. These criteria are: [1] at least 70% of the ^{39}Ar must be released, [2] a minimum of three successive steps in the age plateau must be evident and [3] the integrated age of the plateau should (within 2σ confidence limits) agree with each apparent age increment of the plateau (Jourdan et al., 2007b).

This probably relates to making age determinations on the groundmass of 2 samples which can be problematic because of mineralogical alteration (Jourdan et al., 2007c). These ages have, therefore, only been included in the interest of completeness and they are shown with "unknown" confidence limits.

The age of 180.2±2.7 Ma found for the lowermost Olifants Bed (rhyolite flow within the Sabie River Formation basalt) is a reliable regression age (Figure 3a of Riley et al., 2004). The other ages determined (U-Pb zircon ages) are discordant. Unfortunately, this includes the ages determined for the Jozini Formation rhyolites, which also have provided older ages (182.1±2.9 Ma) than the rhyolites stratigraphically beneath them. Thus, these ages are not included here.

Jourdan et al. (2007b) re-calculated the U-Pb age of Riley et al. (2004) in order to compare it to $^{40}Ar/^{39}Ar$ ages, and found the age to be 178.4±2.7 Ma. This is essentially indistinguishable from the age of 177.8±0.6 Ma found for the Jozini Formation rhyolites (Jourdan et al., 2007b), although these evidently overlie the rhyolite flow within the Sabie River Formation. Duncan et al. (1997) determined $^{40}Ar/^{39}Ar$ ages of the Jozini rhyolites, but these may represent cooling ages (Riley et al., 2004) and are therefore not considered here.

The re-calculation of ages by Riley and Knight (2001) on the basalts of the Ferrar Province was done because ages calibrated to older standards (e.g. McClure Mountain

Hornblende, MMhb-1 at 523.1±2.6 Ma) cannot be compared reliably to those calibrated to newer standards (e.g. Hb3gr hornblende at 1072 Ma). See Jourdan et al. (2007c) for further discussion about the intercalibration of radiometric ages within the Karoo LIP.

3.5.3. Progression & Duration of the Karoo LIP

If the oldest (~184 Ma) and youngest (~174 Ma) ages are considered as reliable, there is an approximate duration of 10 Ma for the Karoo LIP *sensu stricto*. The older age (~205 Ma) for the JDS is most likely a legitimate pre-Karoo LIP age. However, there is evidence of older volcanism in southern Africa from this time. For example, there is evidence of small volumes of volcaniclastic material associated with diatreme-like vents within the Molteno, Elliot and Clarens Formations and andesitic to dacitic dome complexes (McClintock et al., 2008). Although no absolute ages are known, the field relationships do suggest that they pre-date the earliest mafic eruptions of Karoo LIP proper. Furthermore, it has been shown that the Dokolwayo kimberlite (Swaziland) intruded during the deposition of the Karoo Supergroup, but is older than the uppermost sedimentary units (Molteno and Clarens Formations). Dokolwayo has been dated to 200±5 Ma ($^{40}Ar/^{39}Ar$ age on phlogopite) (Allsopp and Roddick, 1984).

It is clear from Figure 3.3 that there was an overlap of basalt eruption (Lesotho and Lebombo) and sill intrusion with volcanic and intrusive activity in the northern Lebombo (NLDS). If the dyking activity in the northern Lebombo is assumed to have been continuous, it overlaps consistently with the age ranges of both the SLDS and ODS. The voluminous outpourings of flood basalts in northern Botswana occurred over this time, from ~182–178 Ma, while those of southern Botswana erupted from ~185–181 Ma (Jourdan et al., 2005).

At approximately the same time volcanic activity that gave rise to the Ferrar Province began in Antarctica, with clearly later dyking of the VDS and SDS (Zhang et al., 2003; Curtis et al., 2008) and a remarkable lack of concomitant basalt eruption. This is consistent with the earlier findings of Riley and Knight (2001), who showed that the bulk

of Ferrar magmatism occurred at ~180 Ma, approximately 3 Ma after the bulk of Karoo magmatism in southern Africa.

There is a dearth of ages for the Sabie River Formation which, on the basis of the interbedded Olifants Bed, suggests that it may have erupted until ~178 Ma, although Jourdan et al. (2007b) suggests that it may have only erupted over a 2–3 Ma period. The Sabie River Formation was fed from the D2 dyke generation of the NLDS (Klausen, 2009).

By this time in the Lebombo volcanism had progressed to more rhyolitic outpourings and intrusive activity in the Sabi/Mwenezi region, culminating in the youngest intrusive activity (silicic and syenite intrusions) of the northern Karoo LIP. This was likely contemporaneous with the intrusion of the ODS and SLDS (Jourdan et al., 2007b). The ~176 Ma old UDS intruded at this time in the central Karoo region, cross-cutting the basalts of Lesotho, while the youngest Karoo LIP-related magmatism is represented in the southern Lebombo by the intrusion of the RRDS at ~174 Ma.

Besides the D2 dyke generation of the NLDS, there is little evidence to suggest that the dykes were feeders flowing from the Karoo triple junction to the now preserved basaltic volcanic pile. While many of the sills may be comparable in age to the basalts (see Jourdan et al., 2007c), the dyke swarms are not. For example, to the southeast of the main Lesotho basalts is the UDS which is ~176 Ma in age compared to ~183 Ma for the basalts. The same is true of the ADS and VDS in Antarctica, and SLDS and RRDS.

There is also evidence of diachronous magmatism in field evidence (Watkeys, 2002) and the broad geochronological data (Jourdan et al., 2004). Early primitive melts erupted at the Karoo triple junction, followed by volcanism and early dykes (earliest dykes of the NLDS) in the south and central (Lesotho basalts) regions, followed by further dyking in the north (ODS) and Antarctica (early SDS), rhyolitic volcanism in the Lebombo virtually synchronous with Antarctic magmatism and finally an apparent return to activity

in the south (UDS and RRDS). Magmatism of the Mwenezi Igneous Complex appears to span this period of late dyking (178–174 Ma).

3.6. Mantle Plume Origin for the Karoo LIP

Burke and Dewey (1973) were the first to postulate a link between mantle plumes and the Karoo triple junction. To account for the geometry of the triple junction, and volcanism further to the northeast, they proposed two possible mantle plume positions: one at the triple junction (Figure 3.4a) and one in the lower Zambezi Valley (Figure 3.4b).

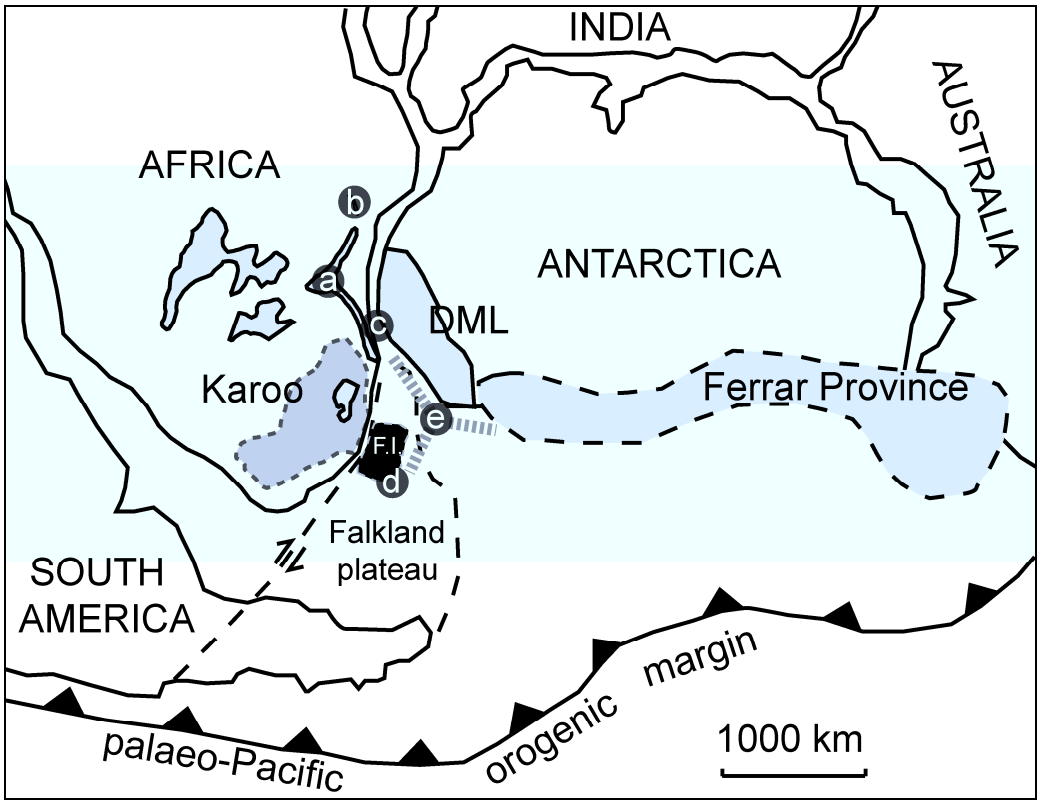

Figure 3.4: Regional schematic map of the Karoo LIP and associated magmatic provinces (shown in grey). Area of major sill intrusion in South Africa is shown in darker grey with a dashed outline. DML=Dronning Maud Land. The plume positions shown (**a–d**) are from (**a**) Burke and Dewey (1973); Storey (1995), (**b**) Burke and Dewey (1973), (**c**) Cox (1989); White and McKenzie (1989); Storey et al. (1992); White (1997); Curtis et al. (2008), (**d**) "megaplume" of Storey and Kyle (1997), (**e**) Weddell Sea triple junction of Elliot and Fleming (2000) (F.I.=Falkland Islands) (regional map modified from Cox, 1992 and Riley et al., 2006).

White and McKenzie (1989), however, proposed a much broader (~2000 km diameter) plume situated at the juncture between Antarctica and the Lebombo (~450 km ENE of

Maputo) to account for the contiguous magmatism of Dronning Maud Land and the Karoo (Figure 3.4c). Campbell and Griffiths (1990) and Storey (1995) upheld the idea of a plume head impacting directly beneath the triple junction itself, to account for its geometry and the composition and distribution of the nephelinites and picrites (Figure 3.2).

Cox (1989) showed that drainage patterns of rivers of the northern Lebombo break along an arc that coincides with the circumference of the plume position proposed by White and McKenzie (1989). This area may have been underplated by a hot, low density upwelling from the mantle, an idea upheld by White (1997) who also suggest that uplift across an area of up to 2000 km in diameter occurred above the plume head. It is difficult, however, to infer uplift caused by a mantle plume in the Mwenezi region because it has been a long-lived palaeo-high (a horst-like structure) since the Permo-Carboniferous (Watkeys, 2002).

It has also been suggested that the axis of the proposed plume was not necessarily responsible for the primitive rocks centred on Mwenezi (Cox, 1992). The ENE-striking fabric and relative structural weakness of the Limpopo Belt has influenced the position of the primitive lithologies, an idea upheld later by specific geochronological and structural studies (Le Gall et al., 2002; Watkeys, 2002; Jourdan et al., 2004; Le Gall et al., 2005).

The mantle plume origin for the Karoo LIP suggested by White (1997) is a modified version – with stretching of the lithosphere from ~150 km to 50–60 km depth. This would have allowed for decompression melting brought about by an upwelling mantle plume to occur. White (1997) favours a plume centred off the Kaapvaal Craton because a plume would have thermally perturbed the sub-continental lithosphere; an unlikely scenario given the eruption of Proterozoic and older diamonds through the Craton during the emplacement of post-Karoo Jurassic and Cretaceous-age kimberlites. Storey and Kyle (1997) suggest that a "megaplume" ($\geq$ 2000 km diameter) positioned on the pre-break up position of the Falkland Plateau (Figure 3.4d) can account best for the contiguous magmatism across the region.

There are also compositional factors of the Karoo LIP that are consistent with mantle plume melting. The earliest magmatism in the Karoo is composed of picrites and nephelinites (Bristow, 1984) which are geochemically compatible with uncontaminated plume-derived melt (White, 1997). Furthermore, Sweeney et al. (1994) have suggested that the more evolved high-Fe basalts in the central region of the Lebombo are consistent with mantle plume melting. This is echoed by Riley et al. (2005) who suggest that the ferro-picrite CT3 magma type is derived from a mantle plume melt.

Indeed, the early nephelinites and picrites which centre on the Karoo triple junction may be accounted for in this fashion. There are few OIB-like compositions in the Karoo (except the CT4 magma type of Luttinen et al., 1998), a melt composition generally regarded as being plume-derived. It is only igneous provinces younger than the Karoo, such as the Paraná, Etendeka and the Deccan Traps that display isotopic and major and trace element signatures comparable to OIB (Hawkesworth et al., 1999). Regardless, some models suggest that OIB can originate from sub-lithospheric fractionation (Anderson, 1985).

The vast majority of the Karoo magmas are low-Ti tholeiites (Hawkesworth et al., 1999) and it is quite consistent with a mantle plume that a progression from primitive to tholeiitic compositions exists. Although high-Ti compositions are indeed widespread in the Karoo, there is the conspicuous link between crustal architecture and the occurrence of these compositions: low-Ti compositions tend to occur over mobile belts, while high-Ti compositions occur over cratonic basement (Cox et al., 1967). This has been attributed to sub-continental lithospheric mantle (SCLM) control on the melts produced (Sweeney and Watkeys, 1990; Sweeney et al., 1994).

The siliceous, high field strength element-depleted signature in the Ferrar Province is believed to be the result of sedimentary contamination of the mantle source, most likely because of subduction (Hergt et al., 1991). Cox (1992) also indicates that the linear extent of the Ferrar Province in Antarctica is most likely beyond the extent of a proposed mantle plume(s). Encarnación et al. (1996) provided the first evidence for the geochronological

link between the Ferrar Province and the Karoo LIP, indicating a subduction related process to account for the linear extent and geochemistry of the basalts. The suggestions that a plume may be more linear in extent (Storey and Kyle, 1997; White, 1997), or that a number of non-interacting plumes operated simultaneously in different regions (Storey and Kyle, 1997) seems possible, but speculative in light of other evidence. Some workers suggest that the Ferrar magmas were emplaced from the Weddell Sea triple junction (Elliot and Fleming, 2000) (Figure 3.4e) and Leat (2008) also suggests that the magma source for the laterally emplaced Ferrar magmas was in the rift between SE Africa and Antarctica.

Central to the plume hypothesis are the Karoo triple junction and associated dyke swarms. Previous work has shown that there are a number of characteristics of the dyke swarms which strongly question the validity of a mantle plume origin for the Karoo LIP. The Karoo triple junction was undoubtedly an active feature of the Karoo LIP, but its history is linked firmly to lithospheric architecture and its pre-Jurassic past (Watkeys, 2002; Jourdan et al., 2004). For example, the Lebombo monocline occupies the eastern edge of the Kaapvaal Craton and the structural trend of the Limpopo Belt has been exploited by the SLDS. Indeed, the area of maximum basalt thickness in Lesotho lies conspicuously on the southern boundary of the Kaapvaal Craton where it is adjacent to granite-gneiss terranes of the Proterozoic Namaqua-Natal Metamorphic Province.

Furthermore, geochronology shows two important features of the radiating dyke swarms of the Karoo triple junction. Firstly, there are a significant number of dykes in the ODS and SLDS that are Proterozoic in age, suggesting that the orientation of these two swarms was determined prior to Karoo magmatism (Uken and Watkeys, 1997; Watkeys, 2002; Le Gall et al., 2002, 2005; Jourdan et al., 2004). Secondly, dating of basalts quite clearly shows a progression in age from south to north (Lesotho, 183 Ma; Botswana, 178 Ma) while the intrusion of Jurassic dykes in southern Africa appears to have progressed from the NLDS to the SLDS and ODS and finally to the UDS and RRDS (Watkeys, 2002).

The dyke swarms of the Karoo LIP around southern Africa do not form part of a singular volcanic feeder system, as most of the dyke swarms (ODS, RRDS, SLeDS, UDS) cross-cut the basalts. This is reflected in the geochronology which shows that the ODS and RRDS post-date the main Karoo volcanic event by at least 3 Ma. This seems counterintuitive given the classic model of radial injection of dykes from a triple junction (Ernst and Baragar, 1992), simultaneously feeding overlying volcanics. Furthermore, short-lived (~2–5 Ma), high volume magmatism is not strictly applicable to the Karoo LIP; although the volumetrically significant tholeiitic, CFB component did erupt relatively rapidly (Jourdan et al., 2005).

Taking the entire igneous component of the Karoo into consideration it is evident that magmatism extended over the period 183–174 Ma, almost twice the duration that has been suggested for other LIP's and is atypical of the classical model of short lived, rapid magmatism driven by an active plume (Jourdan et al., 2004, 2006). This relatively long duration is suggestive of long-term magma storage and a lack of preservation of primitive melt compositions. The south-to-north migration of magmatism also appears to have been too rapid for it to have occurred as a result of the crust migrating over a plume head (Jourdan et al., 2007b). Magmatism at Mwenezi and in the Lebombo monocline appears to be the longest-lived (183–174 Ma) compared to the other arms of the triple junction (Watkeys, 2002; Jourdan et al., 2007b). The 174 Ma old RRDS most likely represents an isolated dyking event, given its restricted occurrence, age and unique MORB-like composition. The youngest Karoo volcanic activity is preserved as the predominantly felsic Mwenezi igneous complex which intrudes rhyolites in the Mwenezi trough (Watkeys, 2002). Such diversity in distribution and age is difficult to reconcile with a mantle plume.

It has been asserted that vigorous output of large volumes of magma is linked to active crustal extension caused by mantle plumes (Richards et al., 1989; White, 1997). This would suggest, in the case of the Karoo, a relatively short period of magmatism followed rapidly by continental break-up, i.e. within ~10 Ma as is typical of other LIPs. Jourdan et al. (2005) indicate that the bulk of Karoo magmatism occurred over ~6 Ma, resulting in

calculated eruption volumes of ~0.3 $km^3.yr^{-1}$, approximately a third of the rate for the Central Atlantic Magmatic Province (CAMP) (Marzoli et al., 1999). If, for example, full oceanisation occurred at this time (consistent with rapid rifting caused by a plume), it would still imply a long-lived thermal incubation of at least 10 Ma, which is odds with a mantle plume. In addition, the first sea-floor anomalies of southern Gondwana are ~155 Ma old (Goodlad et al., 1982). This puts ~28 Ma between the onset of magmatism and oceanisation, which seems too protracted a time for a plume to have heated the lithosphere without it rupturing (Storey et al., 1992). However, if new sea-floor magnetic data are considered (Leinweber and Jokat, 2012), which puts the earliest sea-floor spreading at 166 Ma, there is a shorter period of 8 Ma following the intrusion of the RRDS before sea-floor spreading initiated.

Workers generally agree that, whichever mechanism operated, there was clearly a temperature elevation in the mantle that gave rise to melting (Cox, 1989; White and McKenzie, 1989; Sweeney et al., 1994). Indeed, Cox (1992) suggests that there may have been interplay between a hinterland plume (Karoo) and more distal subduction along the Pacific margin of southern Gondwana (Ferrar, Antarctica). A similar idea is echoed by Jourdan et al. (2007a), who indicate that the isotope and trace element geochemistry of the Karoo magmas are compatible with a combination of isolation of mantle source regions and enrichment processes that may have involved a mixed mantle plume contribution. Cox (1992) also speculated that the slightly earlier beginning of subduction may have triggered the upwelling of a mantle plume, an idea which is explored in Chapter 7 (O'Neill et al., 2009).

It is of interest, therefore, to investigate whether the dyke swarms of the Karoo LIP and those of Dronning Maud Land can provide any convincing evidence for lateral intrusion from a point source. A scenario involving lateral magma flow from the Karoo triple junction would be expected under the influence of an active mantle plume – an idea explored with regard to the NLDS in Chapter 6 and the other dyke swarms of the Karoo LIP in Chapter 7.

3.7. References

Allsopp, H.L., Roddick, J.C., 1984. Rb-Sr and ^{40}Ar-^{39}Ar age determinations on phlogopite micas from the pre-Lebombo Group Dokolwayo kimberlite pipe. Geological Society of South Africa Special Publication 13, 267–272.

Anderson, D.L., 1985. Hotspot magmas can form by fractionation and contamination of MORB. Nature 318, 145–149.

Archanjo, C.J., Launeau, P., 2004. Magma flow inferred from preferred orientations of plagioclase of the Rio Cearf-Mirim dyke swarm (NE Brazil) and its AMS significance. In: Martin-Hernandez, F., Luneburg, C.M., Aubourg, C., Jackson, M. (Eds.), Magnetic Fabric: Methods and applications. Geological Society of London Special Publication 238, 285–298.

Archanjo, C.J., Trindade, R.I., Macedo, J.W.P., Araújo, G., 2000. Magnetic fabric of a basaltic dyke swarm associated with Mesozoic rifting in northeastern Brazil. South American Journal of Earth Sciences 13, 179–189.

Armstrong, R.A., Bristow, J.W., Cox, K.G., 1984. The Rooi Rand dyke swarm, southern Lebombo. In: Erlank, A.J. (Eds.), Petrogenesis of the volcanic rocks of the Karoo province. Geological Society of South Africa Special Publication 13, 77–86.

Aubourg, C., Giordano, G., Mattei, M., Speranza, F., 2002. Magma flow in sub-aqueous rhyolitic dikes inferred from magnetic fabric analysis (Ponza Island, W. Italy). Physics and Chemistry of the Earth 27, 1263–1272.

Aubourg, C., Tshoso, G., Le Gall, B., Bertrand, H., Tiercelin, J.-J., Kampunzu, A.B., Dyment, J., Modisi, M., 2008. Magma flow revealed by magnetic fabric in the Okavango giant dyke swarm, Karoo igneous province, northern Botswana. Journal of Volcanology and Geothermal Research 170, 247–261.

Baer, G., 1995. Fracture propagation and magma flow in segmented dykes: Field evidence and fabric analyses, Makhtesh Ramon, Israel. In: Baer, G., Heimann, A. (Eds.), Physics and Chemistry of Dykes. Balkema, Rotterdam, 125–140.

Benn, K., Allard, B., 1989. Preferred mineral orientations related to magmatic flow in ophiolite layered gabbros. Journal of Petrology 30, 925–946.

Blumenfeld, P., Bouchez, J.-L., 1988. Shear criteria in granite and migmatite deformed in the magmatic and solid state. Journal of Structural Geology 10, 361–372.

Borradaile, G.J., Henry, B., 1997. Tectonic applications of magnetic susceptibility and its anisotropy. Earth Science Reviews 42, 49–93.

Borradaile, G.J., Jackson, M., 2004. Anisotropy of magnetic susceptibility (AMS): magnetic petrofabrics of deformed rocks. In: Martin-Hernandez, F., Luneburg, C.M., Aubourg, C., Jackson, M. (Eds.), Magnetic Fabric: Methods and applications. Geological Society of London Special Publication 238, 299–360.

Borradaile, G.J., Lagroix, F., 2001. Magnetic fabrics reveal upper mantle flow fabrics in the Troodos Ophiolite Complex, Cyprus Journal of Structural Geology 23, 1299–1317.

Bristow, J.W., 1982. Geology and structure of Karoo volcanic and sedimentary rocks of the northern and central Lebombo. Transactions of the Geological Society of South Africa 85, 167–178.

Bristow, J.W., 1984. Nephelinites of the north Lebombo and south-east Zimbabwe. In: Erlank, A.J. (Eds.), Petrogenesis of the volcanic rocks of the Karoo province. Geological Society of South Africa Special Publication 13, 87–104.

Bristow, J.W., Allsopp, H.L., Erlank, A.J., Marsh, J.S., Armstrong, R.A., 1984. Strontium isotope characterization of Karoo volcanic rocks. In: Erlank, A.J. (Eds.), Petrogenesis of the volcanic rocks of the Karoo province. Geological Society of South Africa Special Publication 13, 295–329.

Bruce, P.M., Huppert, H.E., 1990. Solidification and melting along dykes by the laminar flow of basaltic magma. In: M.P. Ryan (Eds.), Magma Transport and Storage. John Wiley & Sons, New York, 87–101.

Burke, K., Dewey, J.F., 1973. Plume generated triple junctions: key indicators in applying plate tectonics to old rocks. Journal of Geology 81, 406–433.

Bussel, M.A., 1989. A simple method for the determination of the dilation direction of intrusive sheets. Journal of Structural Geology 11, 679–687.

Butler, R.F., 1992. Paleomagnetism: magnetic domains to geologic terranes. Blackwell Scientific Publications, Boston, 319 pp.

Callot, J.P., Geoffroy, L., Aubourg, C., Pozzi, J.P., Mege, D., 2001. Magma flow directions of shallow dykes from the East Greenland volcanic margin inferred from magnetic fabric studies. Tectonophysics 335, 313–329.

Callot, J.P., Guichet, X., 2003. Rock texture and magnetic lineation in dykes: a simple analytical model. Tectonophysics 366, 207–222.

Campbell, I.H., Griffiths, R.W., 1990. Implications of mantle plume structure for the evolution of flood basalts. Earth and Planetary Science Letters 99, 79–93.

Cañón-Tapia, E., Chávez-Álvarez, M.J., 2004. Theoretical aspects of particle movement in flowing magma: implications for the anisotropy of magnetic susceptibility of dykes. In: Martin-Hernandez, F., Luneburg, C.M., Aubourg, C., Jackson, M. (Eds.), Magnetic Fabric: Methods and Applications. Geological Society of London Special Publication 238, 227–249.

Correa-Gomes, L.C., Souza Filho, C.R., Martins, C.J.F.N., Oliveira, E.P., 2001. Development of symmetrical and asymmetrical fabrics in sheet-like igneous bodies: the role of magma flow and wall-rock displacements in theoretical and natural cases. Journal of Structural Geology 23, 1415–1428.

Cox, K.G., 1989. The role of mantle plumes in the development of continental drainage patterns. Nature 342, 873–877.

Cox, K.G., 1992. Karoo igneous activity, and the early stages of the break-up of Gondwanaland. In: Storey, B.C., Alabaster, T., Pankhurst R.J. (Eds.), Magmatism and the Causes of Continental Break-up. Geological Society of London Special Publication 68, 37–148.

Cox, K.G., Bristow, J.W., 1984. The Sabie river basalt Formation of the Lebombo monocline and south-east Zimbabwe. In: Erlank, A.J. (Eds.), Petrogenesis of the volcanic rocks of the Karoo province. Geological Society of South Africa Special Publication 13, 125–147.

Cox, K.G., MacDonald, R., Hornung, G., 1967. Geochemical and petrogenetic provinces in the Karoo basalts of southern Africa. American Mineralogist 52, 1451–1474.

Cruden, A.R., 1990. Flow and fabric development during the diapiric rise of magma. Journal of Geology 98, 681–698.

Curtis, M.L., Riley, T.R., Owens, W.H., Leat, P.T., Duncan, R.A., 2008. The form, distribution and anisotropy of magnetic susceptibility of Jurassic dykes in H.U. Sverdrupfjella, Dronning Maud Land, Antarctica. Implications for dyke swarm emplacement. Journal of Structural Geology 30, 1429–1447.

Delaney, P.T., Pollard, D.D., Ziony, J.I., McKee, E.H., 1986. Field relations between dikes and joints: emplacement processes and paleostress analysis. Journal of Geophysical Research 91, 4920–4938.

Dragoni, M., Lanza, R., Tallarico, A., 1997. Magnetic anisotropy produced by magma flow: theoretical model and experimental data from Ferrar dolerite sills (Antarctica). Geophysical Journal International 128, 230–240.

Du Toit, A.L., 1929. The volcanic belt of the Lebombo: a region of tension. Transactions of the Royal Society of South Africa. 18, 189–218.

Duncan, A.R., 1987. The Karoo igneous province - a problem area for inferring tectonic setting from basalt geochemistry. Journal of Volcanology and Geothermal Research 32, 13–34.

Duncan, A.R., Erlank, A.J., Marsh, J.S., 1984. Regional geochemistry of the Karoo igneous province. In: Erlank, A.J. (Eds.), Petrogenesis of the Volcanic Rocks of the Karoo Province. Geological Society of South Africa Special Publication 13, 355–388.

Duncan, R.A., Hooper, P.R., Rehacek, J., Marsh, J.S., Duncan, A.R., 1997. The timing and duration of the Karoo igneous event, southern Gondwanaland. Journal of Geophysical Research 102, 18127–18138.

Eales, H.V., Marsh, J.S., Cox, K.G., 1984. The Karoo igneous province: An introduction. In: Erlank, A.J. (Eds.), Petrogenesis of the volcanic rocks of the Karoo province. Geological Society of South Africa Special Publication 13, 1–26.

Elburg, M., Goldberg, A., 2000. Age and geochemistry of Karoo dolerite dykes from northeast Botswana. Journal of African Earth Sciences 31, 539–554.

Ellam, R.M., 2006. New constraints on the petrogenesis of the Nuanetsi picrite basalts from Pb and Hf isotope data. Earth and Planetary Science Letters 245, 153–161.

Ellam, R.M., Carlson, R.W., Shirley, S.B., 1992. Evidence from Re–Os isotopes for plume–lithosphere mixing in Karoo flood basalt genesis. Nature 359, 718–721.

Ellam, R.M., Cox, K.G., 1989. A Proterozoic lithospheric source for Karoo magmatism: evidence from the Nuanetsi picrites. Earth and Planetary Science Letters 92, 207–218.

Ellam, R.M., Cox, K.G., 1991. An interpretation of Karoo picrite basalts in terms of interaction between asthenospheric magmas and mantle lithosphere. Earth and Planetary Science Letters 105, 330–342.

Elliot, D.H., 1975. Tectonics of Antarctica: a review. American Journal of Science 275, 45–106.

Elliot, D.H., Fleming, TH. 2000. Weddell triple junction: The principal focus of Ferrar and Karoo magmatism during initial breakup of Gondwana. Geology 28, 539–542.

Elliot, D.H., Fleming, T.H., 2004. Occurrence and Dispersal of Magmas in the Jurassic Ferrar Large Igneous Province, Antarctica. Gondwana Research 7, 223–237.

Elliot, D.H., Fleming, T.H., Kyle, P.R., Foland, K.A., 1999. Long-distance transportation of magmas in the Jurassic Ferrar Large Igneous Province, Antarctica. Earth and Planetary Science Letters 167, 89–104.

Ellwood, B.B., 1978. Flow and emplacement direction determined for selected basaltic bodies using magnetic anisotropy measurements. Earth and Planetary Science Letters 41, 254–264.

Encarnación, J., Fleming, T.H., Elliot, D.H., Eales, H.V., 1996. Synchronous emplacement of Ferrar and Karoo dolerites and the early breakup of Gondwana. Geology 24, 535–538.

Erlank, A.J., 1984. Petrogenesis of the volcanic rocks of the Karoo province, Geological Society of South Africa Special Publication 13, 395 pp.

Ernst, R.E., Baragar, W.R.A., 1992. Evidence from magnetic fabric for the flow pattern of magma in the Mackenzie giant radiating dyke swarm. Nature 356, 511–513.

Ernst, R.E., Buchan, K.L., 1997. Giant Radiating Swarms: Their Use in Identifying Pre-Mesozoic Large Igneous Provinces and Mantle Plumes. Geophysical Monographs 100, 297–333.

Ernst, R.E., 1990. Magma flow directions in two mafic Proterozoic dyke swarms of the Canadian Shield: As estimated using anisotropy of magnetic susceptibility data. In: Parker, A.J., Rickwood, P.C., Tucker, D.H. (Eds.), Mafic Dykes and Emplacement Mechanisms. Balkema, Rotterdam, 231–235.

Ferguson, C.C., 1979. Rotations of elongate rigid particles in slow non-newtonian fluids. Tectonophysics 60, 247–262.

Ferraccioli, F., Jones, P.C., Curtis, M.L., Leat, P.T., 2005. Subglacial imprints of early Gondwana break-up as identified from high resolution aerogeophysical data over western Dronning Maud Land, East Antarctica. Terra Nova 17, 573–579.

Fialko, Y.A., Rubin, A.M., 1999. Thermal and mechanical aspects of magma emplacement in giant dike swarms. Journal of Geophysical Research 104, 23033–23049.

Fisher, N. I., Lewis, T., Embleton, B.J.J., 1987. Statistical Analysis of Spherical Data. Cambridge University Press, New York, 344 pp.

Fleming, T.H., Poland, K.A., Elliot, D.H., 1995. Isotopic and chemical constraints on the crustal evolution and source signature of Ferrar magmas, north Victoria Land, Antarctica. Contributions to Mineralogy and Petrology 121, 217–236.

Gaillot, P., de Saint Blanquet, M., Bouchez, J.-L., 2006. Effects of magnetic interactions in anisotropy of magnetic susceptibility: Models, experiments and implications for igneous rock fabrics quantification. Tectonophysics 418, 3–19.

Gay, N.C., 1966. Orientation of mineral lineation along the flow direction in rocks: a discussion. Tectonophysics 3, 559–564.

Gay, N.C., 1968. The motion of rigid particles embedded in a viscous fluid during pure shear deformation of the fluid. Tectonophysics 5, 81–88.

Geoffroy, L., Aubourg, C., 1997. Magma injection around plume related high-level ultramafic bodies in Skye Island: a study by AMS. EUG XI [abstract].

Geoffroy, L., Callot, J.P., Aubourg, C., Moreira, M., 2002. Is the common use of AMS in mafic dykes scientifically correct? Terra Nova 14, 183–190.

Gil-Imaz, A., Pocoví, A., Lago, M., Galé, C., Arranz, E., Rillo, C., Guerrero, E., 2006. Magma flow and thermal contraction fabric in tabular intrusions inferred from AMS analysis. A case study in a late-Variscan folded sill of the Albarracı´n Massif (southeastern Iberian Chain, Spain). Journal of Structural Geology 28, 641–653.

Goodlad, S.W., Martin, A.K., Hartnady, C.J.H., 1982. Mesozoic magnetic anomalies in the southern Natal valley. Nature 295, 686–688.

Griffith, A.A., 1924. The theory of rupture. In: Biezeno, C.B., Burgers, J.M. (Eds.), Proceedings of the first international congress on applied mechanics. J. Waltman, Delft, 55–63.

Gudmundsson, A., 1990a. Dyke emplacement at divergent plate boundaries. In: Parker, A.J., Rickwood, P.C., Tucker, D.H. (Eds.), Mafic Dykes and Emplacement Mechanisms. Balkema, Rotterdam, 47–62.

Gudmundsson, A., 1990b. Emplacement of dykes, sills and crustal magma chambers at divergent plate boundaries. Tectonophysics 176, 257–275.

Hargraves, R.B., Johnson, D., Chan, C.Y., 1991. Distribution anisotropy: the cause of AMS in igneous rocks? Geophysical Research Letters 18, 2193–2196.

Hastie, W.W., Aubourg, C., Watkeys, M.K., 2011a. When an 'inverse' fabric is not inverse: an integrated AMS-SPO study in MORB-like dykes. Terra Nova 23, 49–55.

Hastie, W.W., Watkeys, M.K., Aubourg, C., 2011b. Significance of magnetic and petrofabric in Karoo-feeder dykes, northern Lebombo. Tectonophysics 513, 96–111.

Hawkesworth, C.J., Kelley, S., Turner, S., Le Roex, A., Storey, B.C., 1999. Mantle processes during Gondwana break-up and dispersal. Journal of African Earth Sciences 28, 239–261.

Hawkesworth, C.J., Marsh, J.S., Duncan, A.R., Erlank, A.J., Norry, M.J., 1984. The role of continental lithosphere in the generation of the Karoo volcanic rocks: evidence from combined Nd- and Sr-isotope studies. In: Erlank, A.J. (Eds.), Petrogenesis of the volcanic rocks of the Karoo province. Geological Society of South Africa Special Publication 13, 341–354.

Heimann, A., Fleming, T.H., Elliot, D.H., Foland, K.A., 1994. A short interval of Jurassic continental flood basalt volcanism in Antarctica as demonstrated by $^{40}Ar/^{39}Ar$ geochronology. Earth and Planetary Science Letters 121, 19–41.

Heinonen, J.S., Luttinen, A.V., 2010. Mineral chemical evidence for extremely magnesian subalkaline melts from the Antarctic extension of the Karoo large igneous province. Mineralogy and Petrology 99, 201–217.

Henry, B., 1997. The magnetic zone axis: a new element of magnetic fabric for the interpretation of magnetic lineation. Tectonophysics 271, 325–331.

Hergt, J.M., Peate, D.W., Hawkesworth, C.J., 1991. The petrogenesis of Mesozoic Gondwana low-Ti flood basalts. Earth and Planetary Science Letters 105, 134–148.

Herrero-Bervera, E., Cañon-Tapia, E., Walker G.P.L., Tanaka, H., 2002. Magnetic fabrics study and inferred flow directions of lavas of the Old Pali Road, O'ahu, Hawaii. Journal of Volcanology and Geothermal Research 249, 1–11.

Hext, G., 1963. The estimation of second-order tensors, with related tests and designs. Biometrika 50, 353–357.

Hoek, J.D., 1994. Mafic dykes of the Vestfold Hills, East Anarctica: an analysis of the emplacement mechanism of tholeiitic dyke swarms and of the role of dyke emplacement during crustal extension (unpubl. PhD. thesis), Universiteit Utrecht, The Netherlands, 133 pp.

Hunt, C.P., Moskowitz, B.M., Banerjee, S.K., 1995. Magnetic Properties of Rocks and Minerals. In: Ahrens, T.J. (Eds.), Rock physics and phase relations. A Handbook of physical constants. American Geophysical Union, Washington, 189–204.

Ildefonse, B., Fernandez, A., 1988. Influence of the concentration of rigid markers in a viscous medium on the production of preferred orientations. An experimental contribution, 1. Non-coaxial strain. In: Geological Kinematics and Dynamics (in honor of the 70th birthday of Hans Ramberg). Bulletin of the Geological Institute University Uppsala, 14, 55–60.

Jaeger, J.C., 1959. Temperature outside a cooling sheet. American Journal of Science 257, 44–54.

Jelinek, V., 1978. Statistical processing of anisotropy of magnetic susceptibility measured on group of specimens and its applications. Studies in Geophysics and Geodynamics 22, 50–62.

Jelinek, V., 1981. Characterization of the magnetic fabric of rocks. Tectonophysics 79, 63–67.

Jokat, W., Boebel, T., König, M., Meyer, U., 2003. Timing and geometry of the early Gondwana breakup. Journal of Geophysical Research. 108, 1–15.

Jourdan, F., Bertrand, H., Féraud, G., Le Gall, B., Watkeys, M.K., 2009. Lithospheric mantle evolution monitored by overlapping large igneous provinces: Case study in southern Africa. Lithos 107, 257–268.

Jourdan, F., Bertrand, H., Sharer, U., Blichert-Toft, J., Féraud, G., Kampunzu, A.B., 2007a. Major and trace element and Sr, Nd, Hf, and Pb isotope compositions of the Karoo large igneous province, Botswana–Zimbabwe: lithosphere vs. mantle plume contribution. Journal of Petrology 48, 1043–1077.

Jourdan, F., Féraud, G., Bertrand, H., Kampunzu, A.B., Tshoso, G., Le Gall, B., Tiercelin, J.J., Capiez, P., 2004. The Karoo triple junction questioned: evidence from Jurassic and Proterozoic $^{40}Ar/^{39}Ar$ ages and geochemistry of the giant Okavango dyke swarm (Botswana). Earth and Planetary Science Letters 222, 989–1006.

Jourdan, F., Féraud, G., Bertrand, H., Kampunzu, A.B., Tshoso, G., Watkeys, M.K., Le Gall, B., 2005. Karoo large igneous province: Brevity, origin and relation to mass extinction questioned by new $^{40}Ar/^{39}Ar$ age data. Geology 33, 745–748.

Jourdan, F., Féraud, G., Bertrand, H., Watkeys, M.K., Kampunzu, A.B., Le Gall, B., 2006. Basement control on dyke distribution in Large Igneous Provinces: Case study of the Karoo triple junction. Earth and Planetary Science Letters 241, 307–322.

Jourdan, F., Féraud, G., Bertrand, H., Watkeys, M.K., 2007b. From flood basalts to the inception of oceanization: Example from the $^{40}Ar/^{39}Ar$ high-resolution picture of the Karoo large igneous province. Geochemistry, Geophysics, Geosystems 8, 989–1006.

Jourdan, F., Féraud, G., Bertrand, H., Watkeys, M.K., Renne, P.R., 2007c. Distinct brief major events in the Karoo large igneous province clarified by new $^{40}Ar/^{39}Ar$ ages on the Lesotho basalts. Lithos 98, 195–209.

Kanninen, M.F., Popelar, C.H., 1985. Advanced Fracture Mechanics. Oxford University Press, New York, 584 pp.

Kattenhorn, S.A., 1994. Mechanisms of sill and dyke intrusion (unpubl. MSc. thesis), University of Natal, Durban, South Africa, 149 pp.

Khan, M.A., 1962. The anisotropy of magnetic susceptibility of some igneous and metamorphic rocks. Journal of Geophysical Research 67, 2873–2885.

Klausen, M.B., 2009. The Lebombo monocline and associated feeder dyke swarm: Diagnostic of a successful and highly volcanic rifted margin? Tectonophysics 468, 42–62.

Knight, M.D., Walker, G.P.L., 1988. Magma flow directions in dikes of the Koolau Complex, Oahu, determined from magnetic fabric studies. Journal of Geophysical Research 93, 4301–4319.

Krása, D., Herrero-Bervera, E., 2005. Alteration induced changes of magnetic fabric as exemplified by dykes of the Koolau volcanic range. Earth and Planetary Science Letters 240, 445–453.

Kyle, P.R., Elliot, D.H., Sutter, J.P., 1981. Jurassic Ferrar Supergroup tholeiites from the Transantarctic Mountains, Antarctica, and their relationship to the initial fragmentation of Gondwana. In: Cresswell, M.M., Vella, P. (Eds.), Gondwana Five. Balkema, Rotterdam, 283–287.

Launeau, P., 2004. Mise en évidence des écoulements magmatiques par analyse d'images 2-D des distributions 3-D d'Orientations Préferentielles de Formes. Bulletin of the Geological Society of France 175, 331–350.

Launeau, P., Cruden, A.R., 1998. Magmatic fabric acquisition mechanisms in a syenite: Results of a combined anisotropy of magnetic susceptibility and image analysis study. Journal of Geophysical Research 103, 5067–5089.

Launeau, P., Robin, P.-Y.F., 1996. Fabric analysis using the intercept method. Tectonophysics 267, 91–119.

Leat, P.T., 2008. On the long-distance transport of Ferrar magmas. In: Thomson, K., Petford, N. (Eds.), Structure and Emplacement of High-Level Magmatic Systems. Geological Society of London Special Publication 302, 45–61.

Le Gall, B., Tshoso, G., Dyment, J., Kampunzu, A.B., Jourdan, F., Féraud, G., Bertrand, H., Aubourg, C., Vétela, W., 2005. The Okavango giant mafic dyke swarm (NE Botswana): its structural significance within the Karoo Large Igneous Province. Journal of Structural Geology 27, 2234–2255.

Le Gall, B., Thsoso, G., Jourdan, F., Féraud, G., Bertrand, H., Tiercelin, J.J., Kampunzu, A.B., Modisi, M., Dyment, J., Maia, M., 2002. $^{40}Ar/^{39}Ar$ geochronology and structural data from the giant Okavango and related mafic dyke swarms, Karoo igneous province, N Botswana. Earth and Planetary Science Letters 202, 595–606.

Leinweber, V.T., Jokat, W., 2012. The Jurassic history of the Africa-Antarctica Corridor - new constraints from magnetic data on the conjugate continental margins. Tectonophysics 530–531, 87–101.

Lister, J.R., 1995. Fluid-mechanical models of the interaction between solidification and flow in dykes. In: Baer, G., Heimann, A. (Eds.), Physics and Chemistry of Dykes. Balkema, Rotterdam, 115–124.

Lister, J.R., Kerr, R.C., 1990. Fluid mechanical models of dyke propagation and magma transport. In: Parker, A.J., Rickwood, P.C., Tucker, D.H. (Eds.), Mafic Dykes and Emplacement Mechanisms. Balkema, Rotterdam, 69–80.

Lowrie, W., 1990. Identification of ferromagnetic minerals in rock by coercitivity and unblocking temperature properties. Geophysical Research Letters 17, 159–162.

Luttinen, A.V., Leat, P.T., Furnes, H., 2010. Björnnutane and Sembberget basalt lavas and the geochemical provinciality of Karoo magmatism in western Dronning Maud Land, Antarctica. Journal of Volcanology and Geothermal Research 198, 1–18.

Luttinen, A.V., Rämö, O.T., Huhma, H., 1998. Neodymium and strontium isotopic and trace element composition of a Mesozoic CFB suite from Dronning Maud Land, Antarctica: Implications for lithosphere and asthenosphere contributions to Karoo magmatism. Geochimica et Cosmochimica Acta 62, 2701–2714.

Marsh, J.S., 1987. Basalt geochemistry and tectonic discrimination within continental flood basalt provinces. Journal of Volcanology and Geothermal Research 32, 35–49.

Marsh, J.S., 2002. Discussion: ‘‘The geophysical mapping of Mesozoic dyke swarms in southern Africa and their origin in the disruption of Gondwana’’ [J. Afr. Earth Sci. 30 (2000) 499–513]. Journal of African Earth Sciences 35, 525–527.

Marzoli, A., Renne, P., Piccirillo, E., Ernesto, M., Bellieni, G., De Min, A., 1999. Extensive 200-million-year-old continental flood basalts of the Central Atlantic magmatic province. Science 284, 616– 618.

McClintock, M., White, J.D.L., Houghton, B.F., Skilling, I.P., 2008. Physical volcanology of a large crater-complex formed during the initial stages of Karoo flood basalt volcanism, Sterkspruit, Eastern Cape, South Africa. Journal of Volcanology and Geothermal Research 172, 93–111.

Mekonnen, T.K., 2004. Interpretation & Geodatabase of Dykes Using Aeromagnetic Data of Zimbabwe and Mozambique (unpubl. MSc. thesis), International Institute for Geoinformation Science and Earth Observation, Enschede, The Netherlands, 72 pp.

Meth, D.L., 1996. The Geology and Geochemistry of the Rooi Rand Dyke Swarm (unpubl. MSc. thesis), University of Natal, Durban, South Africa, 189 pp.

Nicholson, R., Pollard, D.D., 1985. Dilation and linkage of echelon cracks. Journal of Structural Geology 7, 583–590.

O'Neill, C., Lenardic, A., Jellinek, A.M., Moresi, L., 2009. Influence of supercontinents on deep mantle flow. Gondwana Research 15, 276–287.

O'Reilly, W., 1984. Rock and Mineral Magnetism. Blackie & Son, Glasgow, 220 pp.

Passchier, C.W., Trouw, R.A.J., 1998. Micro-tectonics. Springer, Berlin, 283 pp.

Philpotts, A.R., Philpotts, D.E., 2007. Upward and downward flow in a camptonite dike as recorded by deformed vesicles and the anisotropy of magnetic susceptibility (AMS). Journal of Volcanology and Geothermal Research 161, 81–94.

Poland, M.P., Fink, J.H., Tauxe, L., 2004. Patterns of magma flow in segmented silicic dikes at Summer Coon volcano, Colorado: AMS and thin section analysis. Earth and Planetary Science Letters 219, 155–169.

Pollard, D.D., 1987. Elementary Fracture Mechanics Applied to the Structural Interpretation of Dykes. In: Halls, H.C., Fahrig, W.F. (Eds.), Mafic Dyke Swarms. Geological Association of Canada Special Paper 34, 5–24.

Pollard, D.D., Fletcher, R.C., 2005. Fundamentals of Structural Geology. Cambridge University Press, New York, 512 pp.

Potter, D.K., Stephenson, A., 1988. Single-domain particles in rocks and magnetic fabric analysis. Geophysical Research Letters 15, 1097–1100.

Ramsay, J.G., 1989. Emplacement kinematics of a granite diapir: the Chindamora batholith, Zimbabwe. Journal of Structural Geology 11, 191–209.

Reeves, C.V., 1978. A failed Gondwana spreading axis in southern Africa. Nature 273, 222–223.

Reeves, C.V., 2000. The geophysical mapping of Mesozoic dyke swarms in southern Africa and their origin in the disruption of Gondwana. Journal of African Earth Sciences 30, 499–513.

Richards, M.A., Duncan, R.A., Courtillot, V., 1989. Flood basalts and hot spot tracks: Plume heads and tails. Science 246, 103–107.

Riley, T.R., Curtis, M.L., Leat, P.T., Watkeys, M.K., Duncan, R.A., Millar, I.L., Owens, W.H., 2006. Overlap of Karoo and Ferrar magma types in KwaZulu-Natal, South Africa. Journal of Petrology 47, 541–566.

Riley, T.R., Knight, K.B., 2001. Age of pre-break-up Gondwana magmatism: a review. Antarctic Science 13, 99–110.

Riley, T.R., Leat, P.T., Curtis, M.L., Millar, L.L., Fazel, A., 2005. Early-Middle Jurassic dolerite dykes from western Dronning Maud Land (Antarctica): identifying mantle sources in the Karoo large igneous province. Journal of Petrology 46, 1489–1524.

Riley, T.R., Millar, L.L., Watkeys, M.K., Curtis, M.L., Leat, P.T., Klausen, M.B., Fanning, C.M., 2004. U-Pb zircon (SHRIMP) ages for the Lebombo rhyolites, South Africa: refining the duration of Karoo volcanism. Journal of the Geological Society of London 161, 547–550.

Rochette, P., Aubourg, C., Perrin, M., 1999. Is this magnetic fabric normal? A review and case studies in volcanic formations. Tectonophysics 307, 219–234.

Rochette, P., Jackson, M., Aubourg, C., 1992. Rock magnetism and the interpretation of anisotropy of magnetic susceptibility. Reviews of Geophysics 30, 209–226.

Rochette, P., Jenatton, L., Dupuy, C., Boudier, F., Reuber, I., 1991. Diabase dikes emplacement in the Oman Ophiolite: a magnetic fabric study with reference to geochemistry. In: Peters, T., Nicolas, A., Coleman, R.G. (Eds.), Ophiolite genesis and evolution of the oceanic lithosphere. Ministry of Petroleum and Minerals, Sultanate of Oman, 55–82.

Saggerson, E.P., Bristow, J.W., Armstrong, R.A., 1983. The Rooi Rand dyke swarm. South African Journal of Science 79, 365–369.

Shaw, H.R., 1980. The fracture mechanism of magma transport from the mantle to the surface. In: Hargraves, R.B. (Eds.), Physics of Magmatic Processes. Princeton University Press, Princeton, New Jersey, 201–264.

Smith, R.A., 1984. The lithostratigraphy of the Karoo Supergroup in Botswana. Bulletin of the Geological Survey of Botswana 26, 239.

Spence, D.A., Turcotte, D.L., 1985. Magma-Driven Propagation of Cracks. Journal of Geophysical Research 90, 575–580.

Spera, F.J., 1980. Aspects of magma transport. In: Hargraves, R.B. (Eds.), Physics of Magmatic Processes. Princeton University Press, Princeton, New Jersey, 265–323.

Storey, B.C., 1995. The role of mantle plumes in continental breakup: case histories from Gondwanaland. Nature 377, 301–308.

Storey, B.C., Alabaster, T., Hole, M.J., Pankhurst, R.J., Wever, H.E., 1992. Role of subduction-plate boundary forces during the initial stages of Gondwana break-up: evidence from the proto-Pacific margin of Antarctica. In: Storey, B.C., Alabaster, T., Pankhurst, R.J. (Eds.), Magmatism and the Causes of Continental Break-up. Geological Society of London Special Publication 68, 149–163.

Storey, B.C., Kyle, P.R., 1997. An active mantle mechanism for Gondwana break-up. South African Journal of Geology 100, 283–290.

Sweeney, R.J., Duncan, A.R., Erlank, A.J., 1994. Geochemistry and petrogenesis of central Lebombo basalts from the Karoo Igneous Province. Journal of Petrology 35, 95–125.

Sweeney, R.J., Falloon, T.J., Green, D.H., Tatsumi, Y., 1991. The mantle origins of Karoo picrites. Earth and Planetary Science Letters 107, 256–271.

Sweeney, R.J., Watkeys, M.K., 1990. A possible link between Mesozoic lithospheric architecture and Gondwana flood basalts. Journal of African Earth Sciences 10, 707–716.

Tamrat, E., Ernesto, M., 1999. Magnetic fabric and rock-magnetic character of the Mesozoic flood basalts of the Paranâ Basin, Brazil. Journal of Geodynamics 28, 419–437.

Tarling, D.H., Hrouda, F., 1993. The Magnetic Anisotropy of Rocks. Chapman & Hall, London, 217 pp.

Tauxe, L., Gee, J.S., Staudigel, H., 1998. Flow directions in dikes from anisotropy of magnetic susceptibility data: The bootstrap way. Journal of Geophysical Research 103, 17775–17790.

Turcotte, D.L., 1990. On the role of laminar and turbulent flow in bouyancy driven magma fractures. In: Ryan, M.P. (Eds.), Magma Transport & Storage. John Wiley & Sons, New York, 103–111.

Uken, R., Watkeys, M.K., 1997. An interpretation of mafic dyke swarms and their relationship with major mafic magmatic events on the Kaapvaal Craton and Limpopo Belt. South African Journal of Geology 100, 341–349.

Watkeys, M.K., 2002. Development of the Lebombo rifted volcanic margin of southeast Africa. In: Menzies, M.A., Klemperer, S.L., Ebinger, C.J., Baker, J. (Eds.), Volcanic Rifted Margins. Geological Society of America Special Paper 362, 27–46.

White, R.S., 1997. Mantle Plume origin for the Karoo and Ventersdorp Flood Basalts, South Africa. South African Journal of Geology 100, 271–283.

White, R.S., McKenzie, D., 1989. Magmatism at rift zones: The generation of volcanic continental margins and flood basalts. Journal of Geophysical Research 94, 7685–7729.

Wickham, S.M., 1987. The segregation and emplacement of granitic magmas. Journal of the Geological Society of London 144, 281–297.

Willis, D.G., 1977. A kinematic model of preferred orientation. Geological Society of America Bulletin 88, 883–894.

Zhang, X., Luttinen, A.V., Elliot, D.H., Larsson, K., Foland, K.A., 2003. Early stages of Gondwana breakup: The $^{40}Ar/^{39}Ar$ geochronology of Jurassic basaltic rocks from western Dronning Maud Land, Antarctica, and implications for the timing of magmatic and hydrothermal events. Journal of Geophysical Research 108, 2449–2468.

- Chapter 4 -

Terra Nova

doi: 10.1111/j.1365-3121.2010.00983.x

When an 'inverse' fabric is not inverse: an integrated AMS-SPO study in MORB-like dykes

Warwick W. Hastie,[1] Charles Aubourg[2] and Michael K. Watkeys[1]

[1]*School of Geological Sciences, University of KwaZulu-Natal, Building H1, University Road, Westville, Durban, 4001, South Africa;*
[2]*Géosciences & Environnement Cergy, University of Cergy Pontoise, 8 Le Campus, 95031 Cergy Cedex, France*

Abstract:

Magma flow direction is recorded in the macroscopic mineral petrofabric and magnetic fabric of the MORB-like Rooi Rand dyke swarm (RRDS). The bulk magnetic fabric is sub-parallel to the dyke plane, resulting from preferred orientation of grains during magma flow. This is referred to as type-A fabric. A study of mineral shape preferred orientation (SPO) reveals an additional fabric which is orthogonal to the average dyke orientation in 30% of the data. This fabric is carried by both plagioclase and opaque grains and would typically be interpreted as "inverse". It is referred to here as type-B fabric. However, because it is carried by the SPO of macroscopic grains and is in most cases not coaxial to the AMS fabric; it is interpreted as having been acquired during increased grain interaction during late-stage magma flow associated with decreasing magma pressure.

4.1. Introduction

Studies of the anisotropy of magnetic susceptibility (AMS) in magmatic rocks focus on flow-related fabrics which are significant in understanding magma emplacement conditions (Khan, 1962; Ellwood, 1978; Knight and Walker, 1988; Rochette et al., 1992; Tarling and Hrouda, 1993; Tauxe et al., 1998; Poland et al., 2004; Philpotts and Philpotts, 2007; Aubourg et al., 2008). AMS is represented as an ellipsoid, the shape and orientation of which is most relevant. In dykes, AMS ellipsoids determined from opposing margins provide constraint on the magma flow orientation if imbrication of the fabric occurs (Tauxe et al., 1998; Geoffroy et al., 2002). Minerals such as multi-domain (MD) magnetite, pyrrhotite, hematite and phyllosilicates are the most common contributors to magnetic susceptibility which have a "normal" magnetic fabric. Conversely, single-domain (SD) magnetite, which is smaller in grain size (<20 nm), can cause "inverse" magnetic fabric (Potter and Stephenson, 1988; Rochette et al., 1999). However, few AMS studies of mafic dykes have taken into account the potential complications of turbulence (Cañón-Tapia and Chávez-Álvarez, 2004) grain size differences (Archanjo and Launeau, 2004), or late-stage fabric (Philpotts and Philpotts, 2007) as possible causes for inverse or anomalous fabrics which occur frequently in rocks of MORB-like composition (Rochette et al., 1991; Cañón-Tapia and Chávez-Álvarez, 2004). The aim of this paper is to examine how the magnetic fabric in dykes of the MORB-like Rooi Rand dyke swarm (RRDS) relates to apparently inverse petrofabric. This work has a bearing on the general interpretation of magnetic fabrics as its questions whether magnetic grains mimic the silicate or opaque grain petrofabric.

4.2. Geological Setting

The RRDS is a north-south trending, 200 km long dyke swarm which extends from the Msunduze River in KwaZulu-Natal (South Africa) northwards into east-central Swaziland (Saggerson et al., 1983; Armstrong et al., 1984; Duncan et al., 1990) (Figure 4.1). The RRDS is 10-22 km in width and has intruded sedimentary rocks and basalts of the Karoo Supergroup just to the west of the main Lebombo range, which comprises rhyolites of the Jozini and Mbuluzi Formations (Eales et al., 1984).

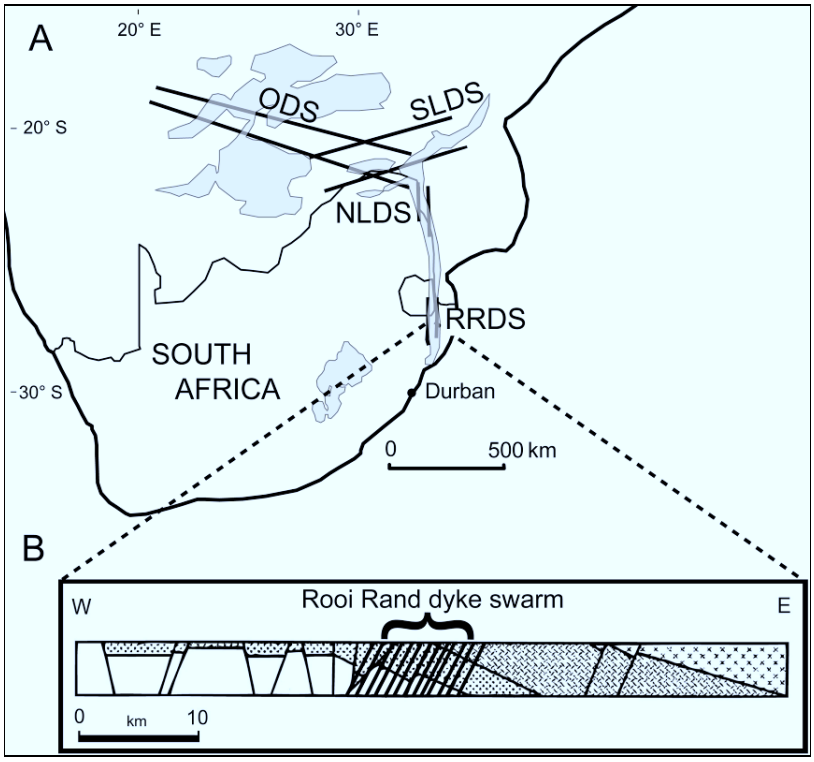

Figure 4.1: Southern Africa showing (**a**) the position and extent of the volcanic remnants of the Karoo large igneous province (shaded), RRDS = Rooi Rand dyke swarm, NLDS = Northern Lebombo dyke swarm, SLDS = Save-Limpopo dyke swarm, ODS = Okavango dyke swarm (modified from Jourdan et al., 2007). (**b**) Cross-section from west to east through the RRDS showing eastward dipping sedimentary and volcanic (ornamented) rocks of the Karoo Supergroup which comprise the Lebombo faulted monocline (modified from Watkeys, 2002).

The Lebombo developed during extensive Karoo magmatism from ~184 Ma to ~174 Ma, during which time some 3×10^6 km^3 of basaltic lava covered parts of southern Africa and Antarctica (Eales et al., 1984; Encarnación et al., 1996). The eastward tilting and domino-style faulting (Figure 4.1b) is the result of the separation of Antarctica from the southeast margin of Africa during Gondwana break-up (Eales et al., 1984; Watkeys, 2002). The apparent lack of crustal contamination in the RRDS is evidence of rapid emplacement, which occurred between 173.9 Ma and 172.1 Ma (Jourdan et al., 2007) and therefore represents the final phase of magmatic activity in the Lebombo prior to the sea-floor spreading offshore 33 Ma later (Goodlad et al., 1982; Watkeys, 2002).

4.3. Methods

The recognition of magmatic flow in rock fabric is usually in the form of a shape preferred orientation (SPO) of inequant grains, such as plagioclase. Such SPO data are useful as it helps to corroborate AMS data (Launeau and Robin, 1996; Launeau and Cruden, 1998; Cañón-Tapia and Chávez-Álvarez, 2004; Launeau, 2004).

Standard AMS samples (25 mm × 22 mm) were collected from opposing margins of dykes using a hand-held petroleum powered drill. Samples were orientated using both a magnetic compass and sun compass. A total of 40 samples from the same dykes were used for the mineral SPO study in comparison to the AMS results. The anisotropy of low-field susceptibility was measured using a Kappabridge KLY-3 apparatus at the University of Cergy-Pontoise.

In addition, the magnetic mineralogy of the samples was determined by monitoring susceptibility-temperature curves which quantify changes in mean susceptibility (K_m) with temperature (Hunt et al., 1995). This involves stepwise thermal demagnetisation of powdered samples in an argon atmosphere within a Kappabridge KLY-3 apparatus under low-field.

The method for investigating mineral SPO involves digitally filtering grains from photomicrographs of three orthogonal thin sections per sample (Figure 4.2) and analysing between 300 and 2800 grains per section in order to determine the 3-dimensional ellipsoid from the 2-dimensional SPO inertia ellipses (Launeau, 2004; Launeau and Robin, 2005). This is done by inverting the colours of the image, converting the image to greyscale, and then applying a threshold which reduces the image to only black (grains) and white. Because the plagioclase grains are larger and darker than the surrounding matrix in these colour inverted images, applying the threshold effectively removes the finer-grained matrix component.

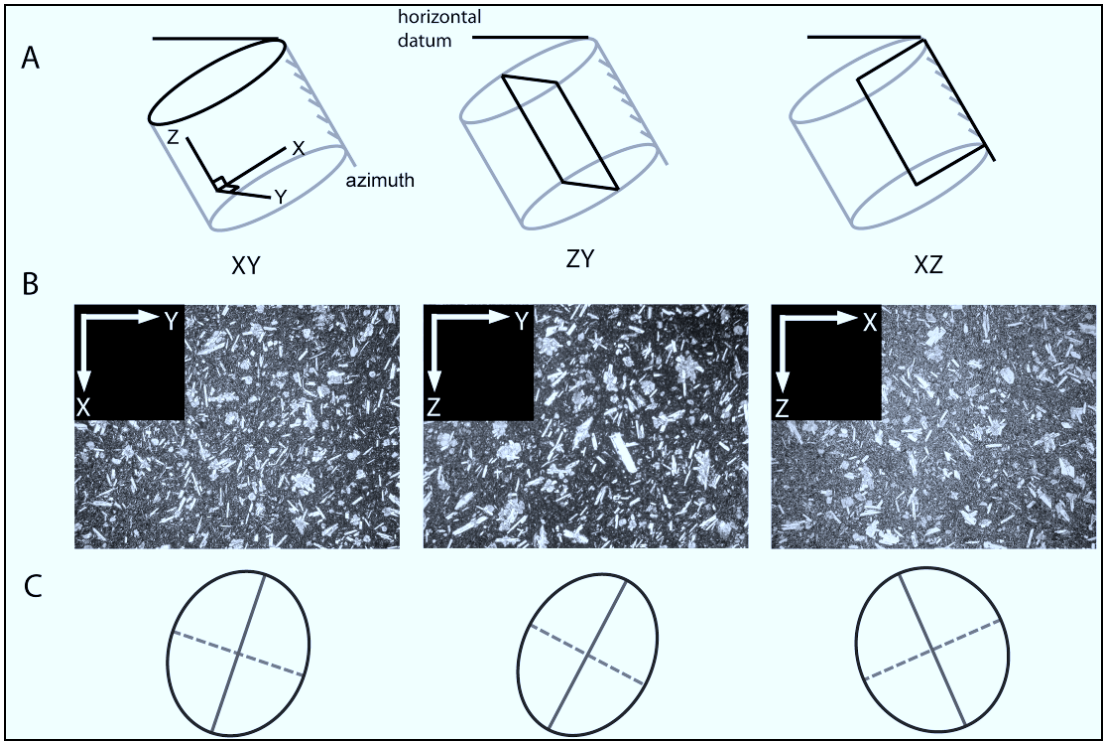

Figure 4.2: Schematic diagram (**a**) illustrating the methodology employed for producing three orthogonal thin sections from a standard 10cc drill core sample. Each drill core is cut into three orthogonal sections defined by an *XYZ* co-ordinate system. (**b**) Examples of greyscale thin section photomicrographs from dyke WH-07-08 (9mm in width). (**c**) Two dimensional inertia tensors of constituent plagioclase grains are determined from each photomicrograph before being rendered in 3-dimensions as an ellipsoid.

This is achieved using most imaging software, such as Adobe® Photoshop®. The results of SPO analysis on images in which individual grains were digitised by hand were found to be the same as those using the method described above.

The potential misfit between the 2-dimensional sectional ellipses and the 3-dimensional ellipsoid is quantified by an incompatibility index ($\sqrt{F}$), given as a percentage which is analogous to the standard deviation of the population of sectional ellipses (Launeau and Robin, 2005). A total of 6 thin sections per margin were analysed for 10 dykes, with all ellipsoids yielding $\sqrt{F}$ values < 13%.

Following the work of Park et al. (1988), 52 samples were thermally demagnetised in order to monitor changes in the orientation of the principle AMS axes, especially where

poorly grouped data or inverse fabric were encountered. Park et al. (1988) showed that the magnetic fabric of the magnetite-bearing Mealy dyke swarm was irregular and scattered in the natural state, but better grouped after heating samples to 640°C. The method used in this study involves monitoring changes in magnetic fabric after heating for 1 hour in a nil magnetic field, from room temperature to 300°C and finally 700°C. Although the results of this work are discussed (being superficially relevant to the SPO fabric), the interpretation thereof is limited due to the lack of grain-size and magnetic domain state parameters.

4.4. Results

Dykes of the RRDS are predominantly plagioclase (55 vol. %) and augite (40 vol. %) bearing and contain magnetite. Olivine may also be present (Meth, 1996). The dykes can be divided into less common plagioclase phyric (e.g., Figure 4.2b) and those with a uniform texture. Plagioclase, which can reach 3-4 mm in length, is typically euhedral to subhedral, while augite is anhedral and stubby.

The bulk magnetic fabric (23 dykes, 368 samples) of the RRDS is predominantly normal (Figure 4.3a) and carried by low-Ti magnetite – deduced from thermomagnetic curves. The mean value for K_m is $36\pm20\times10^{-3}$ SI units, which is characteristic of basaltic rocks containing ~1 vol. % magnetite. The shape of the fabric is neutral to oblate and weakly anisotropic (Figure 4.3b). Examples of susceptibility-temperature (K-T) curves for the RRDS samples, such as SZ-1, show demagnetisation of the dominant phase at ~585°C in a reversible curve (Figure 4.3c). A Hopkinson peak is also present. In other samples (Figure 4.3d) there is evidence of magnetic transitions in the temperature range 180–280°C.

The magnetic foliation is generally sub-parallel (within 35°) to the north-south striking dyke; this is referred to as type-A fabric. In contrast, magnetic foliations in ~35% of the magnetic fabric data are orthogonal to the dyke plane. Following the work of Archanjo and Launeau (2004), this fabric will be referred to as type-B.

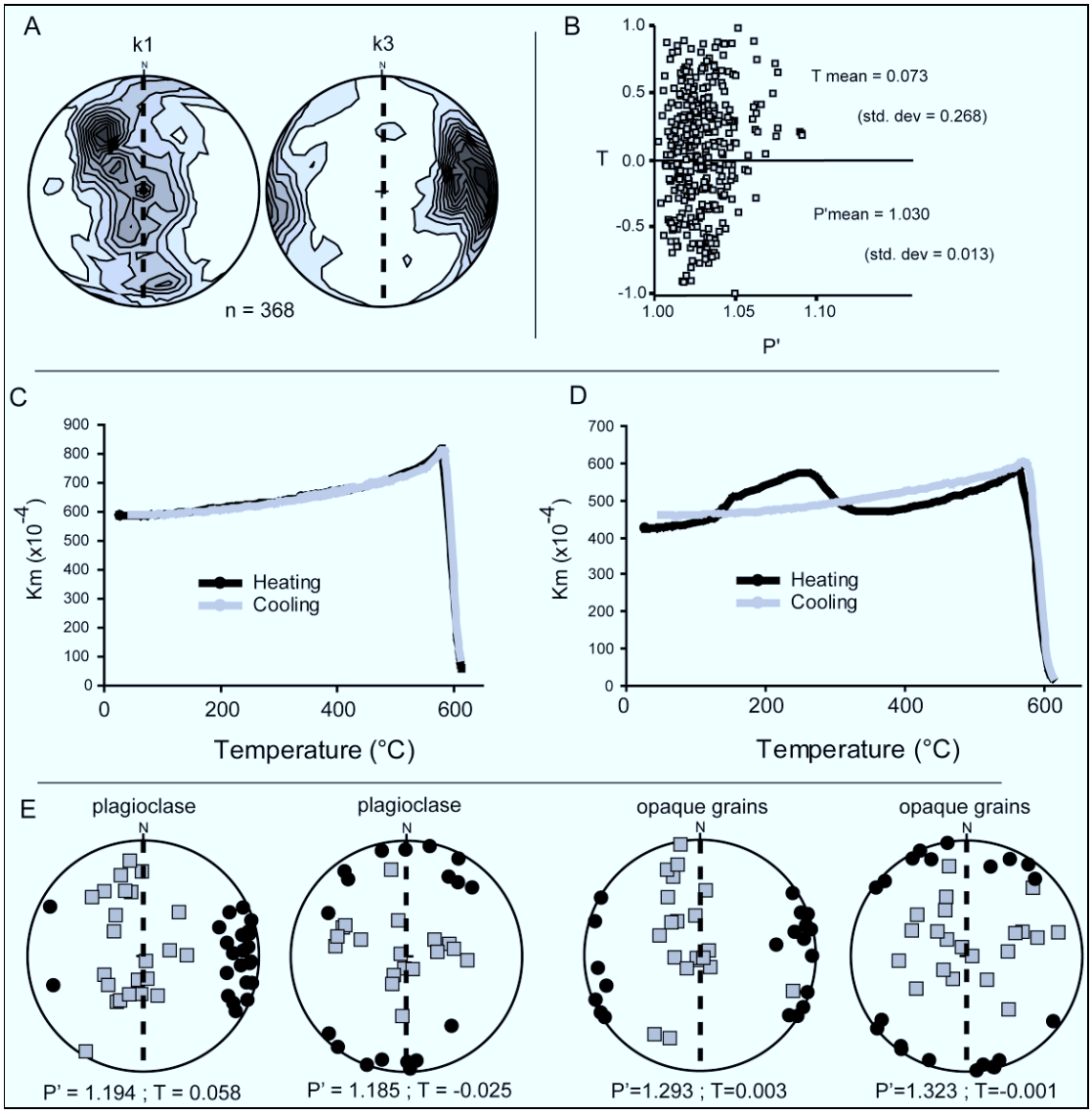

Figure 4.3: (**a**) Density diagrams (*K*1 and *K*3) of the bulk AMS fabric for the RRDS in north-south dyke co-ordinates. This fabric is predominantly type-A. (**b**) *P'*-*T* diagram of the AMS fabric illustrating a neutral to oblate shape and anisotropy < 1.10. (**c**) Susceptibility-temperature (*K*-T) curve for dyke SZ-1, illustrating reversibility and Curie temperature of 580°C. (**d**) *K*-T curve for dyke SZ-10 showing a magnetic transition during heating between 180 and 280°C. See text for discussion of results. (**e**) Mineral shape preferred orientation (SPO) data for both plagioclase and opaque grains in north-south dyke co-ordinates. Note that the type-A and type-B fabrics have been separated.

The SPO of plagioclase determined from 120 thin sections (2.1×10^5 grains) define an anisotropic (*P'* = 1.19), neutral shaped fabric (*T* = 0.04). The opaque grain fabric (*P'* = 1.31 and *T* =0.00) is remarkably similar in orientation to the plagioclase fabric, and on average is type-A (Figure 4.3e). It is coaxial to the AMS fabric in 8 dykes. However,

similarly to the AMS data, 30% of the SPO data are not comparable because the foliation plane is orthogonal to the dyke plane, i.e. type-B. The occurrence of the type-B fabric in the opaque grain fraction suggests that these macroscopic grains do not necessarily contribute significantly to the generally type-A AMS fabric.

These two fabrics are exemplified by the results of dyke SZ-4; as the SPO fabric is type-B, while the AMS fabric is type-A (Figure 4.4a). Close inspection of individual greyscale *XY* sections indicates the presence of the two fabrics in question. This is achieved by the "SPO-2003" programme, which differentiates grain populations of different orientations by colour-coding each population according to a rose of directions.

Thus, in the example, two distinct populations of plagioclase were found, one of which is type-A fabric (grey grains in Figure 4.4b), and the other type-B (black grains in Figure 4.4b). Indeed, the bulk SPO of plagioclase grains can be separated, revealing the presence of the less common but significant type-B fabric in all but one *XY* section of dyke SZ-4 (Figure 4.4c).

The thermally treated magnetic fabric of SZ-4 appears to be initially type-A, but becomes increasingly type-B after heating up to 700°C, while the bulk thermally altered AMS fabric also reflects this type-B orientation in 28% of the data (Figure 4.5). This change is associated with a 45% decrease in bulk susceptibility (K_m).

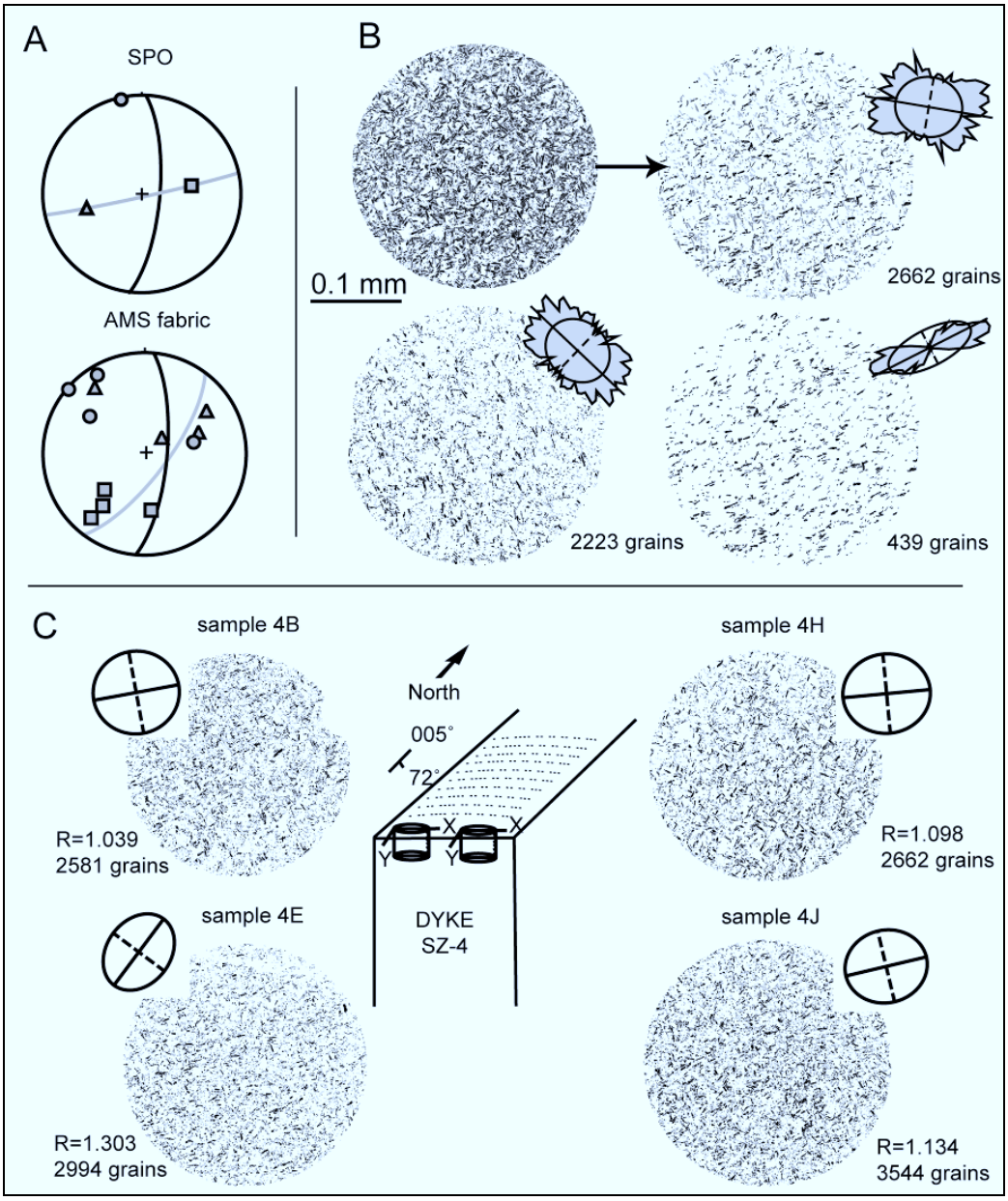

Figure 4.4: Stereographic projections (**a**) of petrofabric in dyke SZ-4 illustrating SPO fabric (plagioclase and opaques combined) and AMS fabric (type-A). (**b**) Greyscale photomicrographs of section *XY* of sample 4H illustrating the presence of two plagioclase sub-fabrics (north is to top of page). Grain populations of different orientations are differentiated according to a colour-coded rose of directions. In this example it is evident that 2 distinct populations of plagioclase coexist; one shown in grey (magmatic fabric), and the other in black (type-B component). SPO ellipses illustrate the orientation of each population. (**c**) Plagioclase SPO fabric of all *XY* sections of dyke SZ-4 showing type-B fabric (except sample 4E) as illustrated by the 2D ellipses (short axis dashed). R = long axis/short axis.

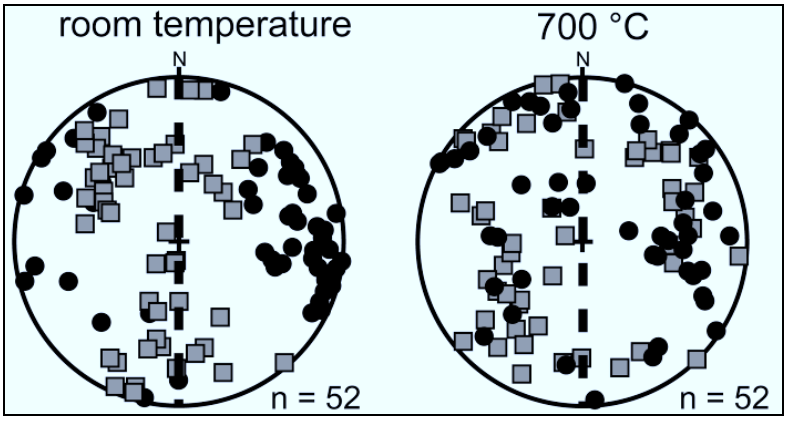

Figure 4.5: Magnetic fabric measured at room temperature and after thermally treatment to 700°C for 52 samples. All data shown are in north-south dyke co-ordinates, as indicated by the dashed black line. The initial fabric is predominantly type-A, but appears type-B after heating; this change is associated with a decrease in susceptibility. Only *K*1 (grey squares) and *K*3 (black circles) are shown.

4.5. Discussion

Demagnetisation of the dominant phase at ~585°C in a reversible K-T curve indicates the predominance of magnetite, and there is no mineralogical transformation of magnetic minerals (Smith and Prevot 1977; Henry, 2007). Magnetic transitions in the temperature range 180–280°C are likely due to the destruction of a sulphide phase during heating (Kontny et al., 2000). The presence of a Hopkinson peak just below the unblocking temperature of the K-T curves is consistent with the occurrence of very fine-grained, stoichiometric magnetite (Hopkinson, 1889; O'Reilly, 1984; Hunt et al., 1995). Magnetite of magmatic origin would typically have higher Ti content, with consequently lower Curie temperature. The unusually pure and evidently fine-grained magnetite in some samples suggests that it is of secondary origin; resulting from exsolution or metasomatic processes (Rochette et al., 1999). As a result, residual titanomagnetite remaining after exsolution processes may become overwhelmed in the magnetic signal by the pure magnetite, which has a higher susceptibility (Butler, 1992).

Obliquities may develop between fabrics defined by particles of different aspect ratios due to the relationship between the amount of shear; governed by the magma flow gradient; and the resulting fabric (Jezek et al., 1994; Cañón-Tapia and Chávez-Álvarez, 2004). During continuous grain rotation in a viscous medium, Cañón-Tapia and Chávez-

Álvarez (2004) have found that the aspect ratio primarily controls the periodicity of rotation, and oblate particles are more likely to define a type-A fabric. Similarly, Launeau and Cruden (1998) indicate that grain size differences can be reflected by different fabric orientations. Although SPO and AMS may record fabrics formed by different processes (as SPO is sensitive to grain orientation only), it is evident that the plagioclase grains and the significantly smaller magnetite grains can yield coaxial fabrics. The grain orientation in both SPO and AMS fabrics yields a type-A fabric sub-parallel to the dyke plane resulting from magmatic flow in 70% the data. This is comparable to a "steady state" fabric in which anisotropic grains rotate into the shear plane (Ildefonse et al., 1992; Launeau and Cruden., 1998). However, the type-B fabric, which in an AMS study would be interpreted as "inverse", is inconsistent with this steady-state fabric.

Changes in the orientation of thermally altered AMS fabric must be considered cautiously. If fine-grained magnetite were to dominate the natural AMS signal, it is likely that thermal alteration would lead to oxidation (and concomitant decrease in K_m, [Henry et al., 2003]), allowing the larger grains to contribute more to the AMS signal. This would result in the appearance of the type-B fabric, a result consistent with the SPO of the larger opaque grains. It is possible, however, that complex alteration may occur, resulting in growth of new grains along pre-existing fabrics (Mintsa Mi Nguema et al., 2002; Souque et al., 2002). Additionally, there is no constraint on the absolute grain-size or domain characteristics. Thus, the relationship between thermally altered magnetic fabric and the type-B SPO fabric must remain unresolved at this stage.

4.6. Type-B Fabric Acquisition

Fabric acquisition models have taken into account cyclical rotation of progressively crystallising and interacting grains (Cañón-Tapia and Chávez-Álvarez 2004), or orthogonal fabrics in which prolate grains have evidently rotated about their long axes (Philpotts and Philpotts, 2007). However, type-B fabric in the SPO of plagioclase and opaque grains and the AMS fabric suggest that (1) the very fine-grained fraction defines an early-formed type-A fabric (measured by AMS) and (2) the type-B fabric in the SPO is carried by larger plagioclase and opaque grains in 30% of the data. In a model of

progressive crystallisation it is expected that intermediate fabrics between the type-A and type-B orientations should exist. However, there is no evidence for (sub-) horizontal foliations, fabric axes inversion or scattering of axes in the fabric of the RRDS (*viz.* Figure 4.3).

In contrast, a dyke such as SZ-4 contains two distinct fabrics. Assuming that minimal phenocryst crystallisation occurs during cooling at a late stage, it is likely that mineral grains in an increasingly more viscous magma could preferentially re-orientate due to grain interaction, resulting in larger grains developing type-B fabric. Aarnes et al. (2008) have shown that significant post-emplacement flow can occur in basaltic melt (viscosity ~10^2 Pa s) that is 99% crystallised; with late-stage fluid movement occurring from the intrusion centre towards the margins. This process is driven by a steep pressure drop along the margins caused by cooling and crystallisation. The effects of a pressure drop along dyke margins may be important characteristic of sheeted dykes such as the RRDS which intrude under purely extensional conditions. The late-stage effects on finer grains which control AMS are not clear however. It is possible that the record of type-A fabric is evidence for these grains being controlled by an early formed silicate framework, but they do not mimic the late-stage fabric.

4.7. Acknowledgements

The authors acknowledge the technical staff of the University of Cergy-Pontoise and University of KwaZulu-Natal for assistance during the AMS measurements and thin section preparation. Patrick Launeau and an anonymous reviewer are thanked for their constructive comments. The authors acknowledge the NRF-CNRS co-operative "PICS" programme that funded this research. W. Hastie acknowledges a free-standing NRF Scarce Skills bursary.

4.8. References

Aarnes, I., Podladchikov, Y.Y., Neumann, E.R., 2008. Post-emplacement melt flow induced by thermal stresses: Implications for differentiation in sills. Earth and Planetary Science Letters 276, 152–166.

Archanjo, C.J., Launeau, P., 2004. Magma flow inferred from preferred orientations of plagioclase of the Rio Cearf-Mirim dyke swarm (NE Brazil) and its AMS significance. In: Martin-Hernandez, F., Luneburg, C.M., Aubourg, C., Jackson, M. (Eds.), Magnetic Fabric: Methods and applications. Geological Society of London Special Publication 238, 285–298.

Armstrong, R.A., Bristow, J.W., Cox, K.G., 1984. The Rooi Rand dyke swarm, southern Lebombo. In: Erlank, A.J., (Eds.), Petrogenesis of the volcanic rocks of the Karoo province. Geological Society of South Africa Special Publication 13, 77–86.

Aubourg, C., Tshoso, G., Le Gall, B., Bertrand, H., Tiercelin, J.J., Kampunzu, A.B., Dyment, J., Modisi, M., 2008. Magma flow revealed by magnetic fabric in the Okavango giant dyke swarm, Karoo igneous province, northern Botswana. Journal of Volcanology and Geothermal Research 170, 247–261.

Butler, R.F. 1992. Paleomagnetism: magnetic domains to geologic terranes. Blackwell Scientific Publications, Boston, 319 pp.

Cañón-Tapia, E., Chávez-Álvarez, M.J., 2004. Theoretical aspects of particle movement in flowing magma: implications for the anisotropy of magnetic susceptibility of dykes. In: Martin-Hernandez, F., Luneburg, C.M., Aubourg, C., Jackson, M. (Eds.), Magnetic Fabric: Methods and applications. Geological Society of London Special Publication 238, 227–249.

Duncan, A.R., Armstrong, R.A., Erlank, A.J., Marsh, J.S., Watkins, R.T., 1990. MORB-related dolerites associated with the final phases of Karoo flood basalt volcanism in southern Africa. In: Parker, A.J., Rickwood, P.C., Tucker, D.H. (Eds.), Mafic Dykes and Emplacement Mechanisms, Balkema, Rotterdam, 119–129.

Eales, H.V., Marsh, J.S., Cox, K.G. 1984. The Karoo igneous province: An introduction. In: Erlank, A.J. (Eds.), Petrogenesis of the volcanic rocks of the Karoo province. Geological Society of South Africa Special Publication 13, 1–26.

Ellwood, B.B., 1978. Flow and emplacement direction determined for selected basaltic bodies using magnetic anisotropy measurements. Earth and Planetary Science Letters 41, 254–264.

Encarnación, J., Fleming, T.H., Elliot, D.H., Eales, H.V., 1996. Synchronous emplacement of Ferrar and Karoo dolerites and the early breakup of Gondwana. Geology 24, 535–538.

Geoffroy, L., Callot, J.P., Aubourg, C., Moreira, M., 2002. Divergence between magnetic and plagioclase linear fabrics in dykes: a new approach for defining the flow vector using magnetic foliation. Terra Nova 14, 183–190.

Goodlad, S.W., Martin, A.K., Hartnady, C.J.H., 1982. Mesozoic magnetic anomalies in the southern Natal valley. Nature 295, 686–688.

Henry, B., 2007. Magnetic mineralogy, changes due to heating. In: Gubbins, D., Herrero-Bervera, E. (Eds.). Encyclopedia of Geomagnetism and Paleomagnetism. Springer, Dordrecht, 512–515.

Henry, B., Jordanova, D., Jordanova, N., Souque, C., Robion, P., 2003. Anisotropy of magnetic susceptibility of heated rocks. Tectonophysics 366, 241–258.

Hopkinson, J., 1889. Magnetic and other physical properties of iron at a high temperature. Philosophical Transactions of the Royal Society of London Series A 180, 443 pp.

Hunt, C.P., Moskowitz, B.M., Banerjee, S.K., 1995. Magnetic Properties of Rocks and Minerals. In: Ahrens, T.J. (Eds.), Rock physics and phase relations. A Handbook of physical constants. American Geophysical Union, Washington, 189–204.

Ildefonse, B.P., Launeau, P., Bouchez, J.L., Fernandez, A., 1992. Effect of mechanical interactions on the development of shape preferred orientations: A two-dimensional experimental approach. Journal of Structural Geology 14, 73–83.

Jezek, J.R., Melka, R., Schulman, K., Venera, Z., 1994. The behavior of rigid triaxial ellipsoidal particles in viscous flows - modeling of fabric evolution in a multiparticle system. Tectonophysics 229, 165–180.

Jourdan, F., Féraud, G., Bertrand, H., Watkeys, M.K., 2007. From flood basalts to the inception of oceanization: Example from the $^{40}Ar/^{39}Ar$ high-resolution picture of the Karoo large igneous province. Geochemistry, Geophysics, Geosystems 8, 1–20.

Khan, M.A., 1962. The anisotropy of magnetic susceptibility of some igneous and metamorphic rocks. Journal of Geophysical Research 67, 2873–2885.

Knight, M.D., Walker, G.P.L., 1988. Magma flow directions in dikes of the Koolau Complex, Oahu, determined from magnetic fabric studies. Journal of Geophysical Research 93, 4301–4319.

Kontny, A., De Wall, H., Sharp, T.G., Pósfai, M., 2000. Mineralogy and magnetic behavior of pyrrhotite from a 260°C section at the KTB drilling site, Germany. American Mineralogist 85, 1416–1427.

Launeau, P., 2004. Mise en évidence des écoulements magmatiques par analyse d'images 2-D des distributions 3-D d'Orientations Préferentielles de Formes. Bulletin of the Geological Society of France 175, 331–350.

Launeau, P., Cruden, A.R., 1998. Magmatic fabric acquisition mechanisms in a syenite: Results of a combined anisotropy of magnetic susceptibility and image analysis study. Journal of Geophysical Research 103, 5067–5089.

Launeau, P., Robin, P.-Y.F., 1996. Fabric analysis using the intercept method. Tectonophysics 267, 91–119.

Launeau, P., Robin, P.-Y.F., 2005. Determination of fabric & strain ellipsoids from measured sectional ellipses - Implementation and applications. Journal of Structural Geology 27, 2223–2233.

Meth, D.L., 1996. The geology and geochemistry of the Rooi Rand dyke swarm (unpubl. MSc. thesis). University of Natal, Durban, South Africa 189 pp.

Mintsa Mi Nguema, T., Trindade, R.I.F., Bouchez, J.L., Launeau, P., 2002. Selective thermal enhancement of magnetic fabrics from the Carnmenellis granite (British Cornwall). Physics and Chemistry of the Earth 27, 1281–1287.

O'Reilly, W., 1984. Rock and Mineral Magnetism. Blackie & Son, Glasgow, 220 pp.

Park, J.K., Tanczyk, E.I. ,Desbarats, A., 1988. Magnetic fabric and its significance in the 1400 Ma Mealy diabase dykes of Labrador, Canada. Journal of Geophysical Research 93, 13689–13704.

Philpotts, A.R., Philpotts, D.E., 2007. Upward and downward flow in a camptonite dike as recorded by deformed vesicles and the anisotropy of magnetic susceptibility (AMS). Journal of Volcanology and Geothermal Research 161, 81–94.

Poland, M.P., Fink, J.H., Tauxe, L., 2004. Patterns of magma flow in segmented silicic dikes at Summer Coon volcano, Colorado: AMS and thin section analysis. Earth and Planetary Science Letters 219, 155–169.

Potter, D.K., Stephenson, A., 1988. Single-domain particles in rocks and magnetic fabric analysis. Geophysical Research Letters 15, 1097–1100.

Rochette, P., Aubourg, C., Perrin, M., 1999. Is this magnetic fabric normal? A review and case studies in volcanic formations. Tectonophysics 307, 219–234.

Rochette, P., Jackson, M., Aubourg, C., 1992. Rock magnetism and the interpretation of anisotropy of magnetic susceptibility. Reviews in Geophysics 30, 209–226.

Rochette, P., Jenatton, L., Dupuy, C., Boudier, F., Reuber, I. 1991. Diabase dikes emplacement in the Oman Ophiolite: a magnetic fabric study with reference to geochemistry. In: Peters, T., Nicolas, A., Coleman, R.G. (Eds.), Ophiolite genesis and evolution of the oceanic lithosphere. Ministry of Petroleum and Minerals, Sultanate of Oman, 55–82.

Saggerson, E.P., Bristow, J.W., Armstrong, R.A., 1983. The Rooi Rand dyke swarm. South African Journal of Science 79, 365–369.

Smith, B.M., Prévot, M., 1977. Variation of the magnetic properties in a basaltic dyke with concentric cooling zones. Physics of the Earth and Planetary Interiors 14, 120–136.

Souque, C., Robion, P., Frizon de Lamotte, D., 2002. Cryptic magnetic fabric of tectonic origin revealed by heating of sedimentary samples from the Corbières (France). Physics and Chemistry of the Earth 27, 1253–1262.

Tarling, D.H., Hrouda, F., 1993. The Magnetic Anisotropy of Rocks. Chapman & Hall, London, 217 pp.

Tauxe, L., Gee, J.S., Staudigel, H. 1998. Flow directions in dikes from anisotropy of magnetic susceptibility data: The bootstrap way. Journal of Geophysical Research 103, 17775–17790.

Watkeys, M.K. 2002. Development of the Lebombo rifted volcanic margin of southeast Africa. In: Menzies, M.A., Klemperer, S.L., Ebinger, C.J., Baker, J. (Eds.), Volcanic Rifted Margins. Geological Society of America Special Paper 362, 27–46.

4.9. Supplementary Data

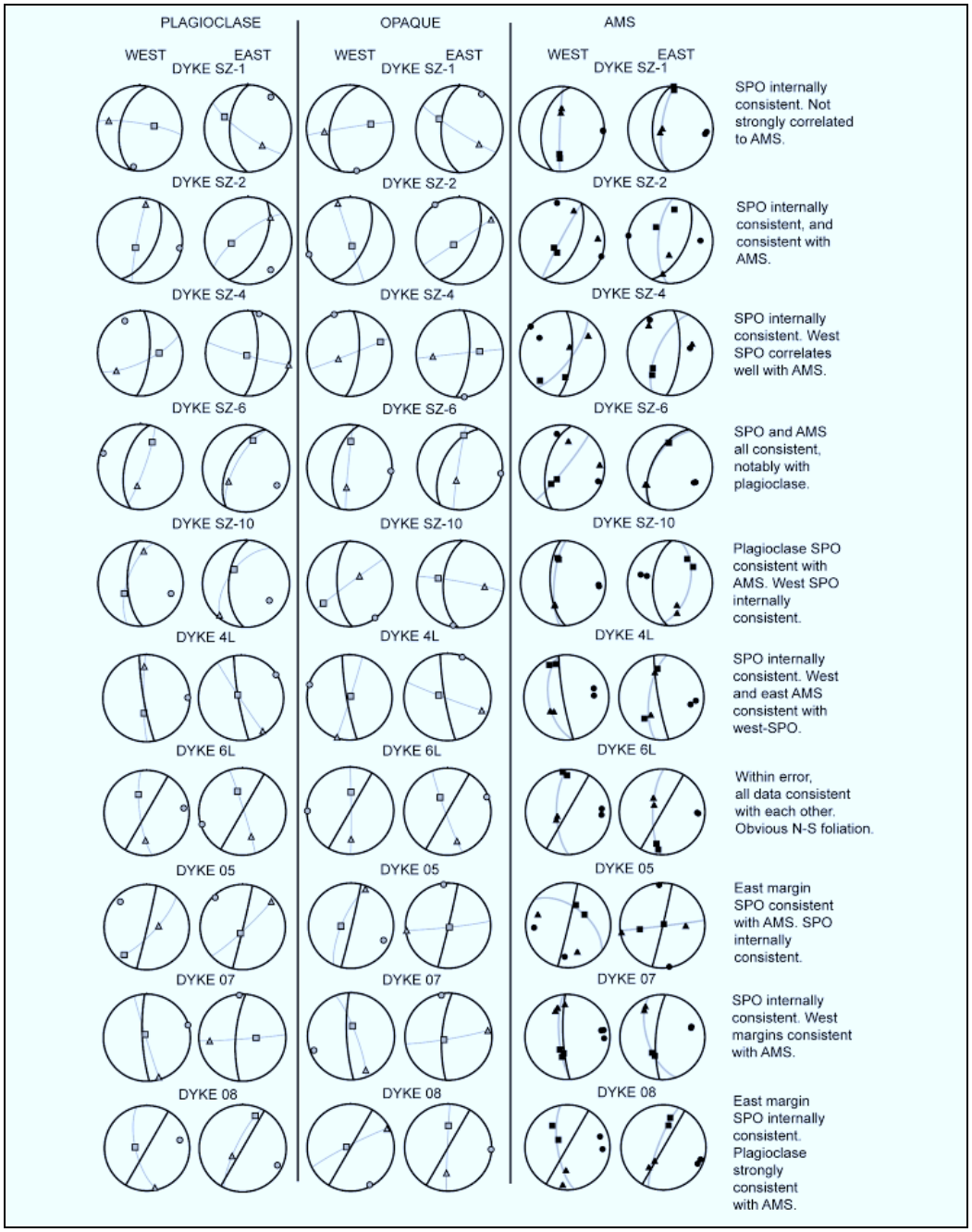

Figure 4.6: (*supplementary data*) All SPO and AMS data, presented stereographically in the lower hemisphere for all 12 dykes studied. Note that data are split into "west" and "east" margins in order to observe possible imbrication of foliations (in grey). Dyke planes shown in black. Maximum axes = square, intermediate axes = triangle, minimum axes = circle. A brief interpretation of the fabric for each dyke is given on the right. There is evidence of type-B fabric in dykes SZ-1, SZ-4, SZ-10, 4L, WH-07-05 and WH-07-07.

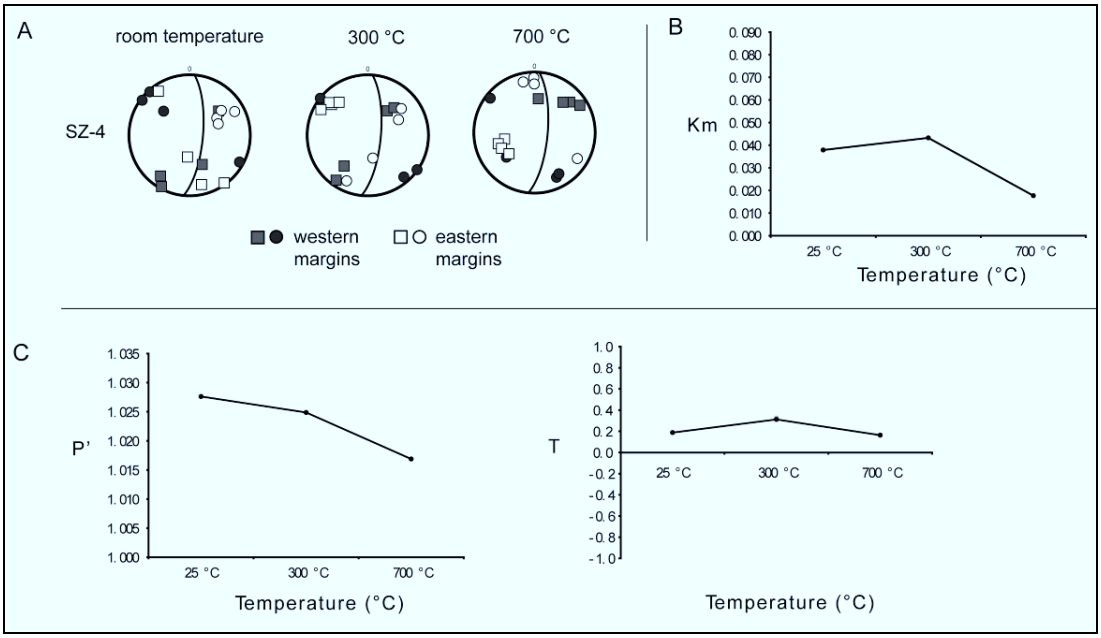

Figure 4.7: (*supplementary data*) (**a**) Magnetic fabric (AMS) of dyke SZ-4 as pictured after successive heating for 1 hour to 300ºC and 700ºC. Western and eastern margins are discriminated, as in Figure 4.6. Note that the fabric becomes increasingly type-B with heating (note position of *K*3 axes). (**b**) Susceptibility vs. temperature curve for SZ-4, indicating a decrease in K_m with heating. (**c**) Anisotropy (*P'*) and shape parameter (*T*) vs. temperature curves.

- Chapter 5 -

Tectonophysics 583 (2013) 145–157

Contents lists available at SciVerse ScienceDirect

Tectonophysics

journal homepage: www.elsevier.com/locate/tecto

Characterisation of grain-size, shape and orientation of plagioclase in the Rooi Rand dyke swarm, South Africa

Warwick William Hastie [a,*], Michael K. Watkeys [a], Charles Aubourg [b]

[a] School of Geological Sciences, Building H1, University of KwaZulu-Natal, University Road, Westville, Durban 4001, South Africa
[b] Laboratoire des Fluides Complexes et Réservoirs, UMR 5150, CNRS, TOTAL, Université de Pau et des Pays de l'Adour, Avenue de l'Université BP 1155, 64013 Pau Cedex, France

Abstract:

Magmatic (type-A) fabric co-exists with dyke-orthogonal (type-B) fabric in both the plagioclase and opaque grain fractions in dykes of the Rooi Rand dyke swarm (RRDS). We present new data from the RRDS pertaining to the size, shape, texture and orientation of plagioclase. Texturally, the samples range from intersertal to sub-ophitic and phenocrystic (plagioclase-phyric). More than 90% of plagioclase grains are < 33 μm in size and the modal size is 12.3 μm. The smallest, most abundant grains have modest shape ratios ($1.40 < r < 1.95$). Larger grains have relatively low shape ratios although grain-size and shape in the RRDS are essentially independent. Additionally, we investigate the angle between individual grains and the respective dyke margins in (sub-) horizontal thin-sections. This apparent imbrication angle, A_i, in conjunction with three dimensional fabric shape tensors and grain-size and shape data, shows that the most common grain-size class, with modest shape ratios (1.80–2.20), is predominantly associated with type-A fabric. The interaction of grains attempting to rotate in even-textured samples appears to have resulted in the lack of correlation between shape and size parameters and the orientation or intensity of the fabric, whilst grains with increasing *r* values show a tendency toward type-B fabric. Based on textural information and crystal size distribution, we suggest that plagioclase < 80 μm in size grew as a result of a late-stage nucleation event, becoming increasingly anisotropic as a result of relatively rapid undercooling. Thus, late-stage, rapid nucleation of the plagioclase groundmass significantly affected the final fabric that developed, and the interaction of large, anisotropic grains has not played as significant a role in the development of type-B fabric as previously thought.

5.1. Introduction

There have been many studies quantifying fabric development in igneous rocks, whether using anisotropy of magnetic susceptibility (AMS) (Cañón-Tapia, 2004 and references therein) or the shape preferred orientation (SPO) of minerals (Gay, 1966, 1968; Willis, 1977; Blanchard et al., 1979; Ferguson, 1979; Blumenfeld and Bouchez, 1988; Nicolas et al., 1988; Ramsay, 1989; Cruden, 1990; Kattenhorn, 1994; Baer, 1995; Launeau and Robin, 1996; Launeau and Cruden, 1998; Launeau, 2004; Romeo et al., 2007). Lattice preferred orientations (LPO / CPO) and electron back-scattered diffraction (EBSD) studies have also been applied to the study of igneous petrofabrics in gabbro (Benn and Allard, 1989), volcanic flows (Bascou et al., 2005) and dykes (Romeo et al., 2007; Chadima et al., 2009). In the study of dykes these techniques are primarily applied to determine the original flow direction of magma as this has important geodynamic implications, particularly when dealing with a dyke swarm (Ernst, 1990; Ernst and Baragar, 1992; Ernst and Duncan, 1995; Callot et al., 2001; Aubourg et al., 2008; Kissel et al., 2010).

The development of flow-related petrofabrics in mafic dykes follows the general premise that a statistically significant number of grains will become imbricated (tiled) against the dyke walls during magma flow (Blanchard et al., 1979). The recognition of this flow-related fabric is typically based on the angle between the dyke and the tiled grains being in the range ~10–30°. These grains may be phenocrysts or they may be part of the finer grained groundmass in the solidified dyke. The most basic formation of a flow-related magmatic fabric in a dyke occurs under conditions of simple shear in a magma in which constituent grains become tiled against the walls of an intrusion. This would typically develop fabric symmetrical with respect to the dyke plane. Non-symmetrical fabrics may develop for a number of reasons, including but not limited to deformation of the dyke during emplacement and grain interaction (Correa-Gomes et al., 2001; Callot and Guichet, 2003). Oblate shaped AMS fabrics have been shown to develop intersection lineations and S/C type relationships (Callot and Guichet, 2003).

There are, however, many factors which may complicate the acquisition of such an ideal magmatic fabric. This has become evident from petrofabric studies as well as proposed quantitative models which attempt to account for simultaneous grain growth, rotation, interaction and overall magmatic fabric acquisition (Willis, 1977; Benn and Allard, 1989; Dragoni et al., 1997; Launeau and Cruden, 1998; Amenta, 2001; Correa-Gomes et al., 2001; Callot and Guichet, 2003; Archanjo and Launeau, 2004). The study of sub-fabrics and the role of grain shape and rotation is well documented (see citations above and Fernandez et al., 1983; Ildefonse et al., 1992; Jezek et al., 1994). In this paper we present directly observed, two-dimensional (2-D) data pertaining to the size, shape and orientation of plagioclase grains which define the igneous petrofabric in dolerite dykes of the Rooi Rand dyke swarm (RRDS).

In a recent study, the magnetic fabric and the mineral SPO fabric of the RRDS of South Africa was presented (Hastie et al., 2011a). Inverse fabric (referred to as type-B fabric) exists in the mineral SPO of plagioclase grains in ~40% of the data. This is an igneous petrofabric in which the foliation defined by plagioclase (and some opaque grains) is orthogonal to the dyke plane. A model of late-stage fabric acquisition owing to grain interaction has been proposed to explain this fabric orientation. It was also shown that finer grain sizes (< 10 μm), particularly those measured by AMS, appeared to preserve the earliest, relict fabric (similarly to Romeo et al., 2007).

From visual inspection alone there seems to be no apparent relationship between the orientation of grains and their morphology (specifically the grain-size and shape ratio) in the RRDS. In one case (Figure 4b of Hastie et al., 2011a) it was demonstrated that the type-B fabric component could be digitally separated from the type-A (normal) fabric component. The overall fabric comprises a type-A component defined by the majority of the grains and a type-B component defined by the less abundant fraction. It is difficult to judge visually whether particular fabrics are occupied by finer, or coarser grains than the average, or by grains of a particular shape.

5.2. Grain Shape & Flow Fabric

Benn and Allard (1989) have quantified igneous fabrics in gabbro of the Oman ophiolite using mineral SPO and LPO. These authors found differences in fabric orientation according to grains of different shape ratios. In particular, low shape ratios ($r < 1.5$) were less likely to reach an imbricated angle – where r is the ratio of long (L) to short (S) axes. A similar finding has been made by Ildefonse and Fernandez (1988) as well. A study of grain-size and magmatic fabric development in a single dyke of the RRDS by Kattenhorn (1994) revealed that grains of relatively high shape-ratio ($3 < r < 10$) were found predominantly within 30° of the dyke plane. Furthermore, there is evidence that continued crystallisation (i.e. an increasing number of grains) leads to grain interaction, and therefore a higher degree of grain imbrication is achieved (stable fabric of Ildefonse et al., 1997). Laminar flow also increases the likelihood of grain imbrication. The magnitude of shear (γ) is also important, particularly when considering the magnitude of shear imparted to each of the grain populations with different shape ratios (Launeau and Cruden, 1998).

Dragoni et al. (1997) demonstrated that magma flow typically produces cyclical rotation of grains. Indeed these authors showed that, when considering AMS fabrics, the orientation of the magnetic foliation (the $K1$-$K2$ plane) oscillates between vertical and horizontal positions in mafic sills of the Ferrar Province, Antarctica. Importantly these authors were able to show that these oscillations were dependant on the value of r. For example, as r increased, the greater the time interval $K3$ spent in a vertical position – which essentially defines a type-B fabric. This is contrary to the findings of Ildefonse and Fernandez (1988) and Kattenhorn (1994).

Launeau and Cruden (1998) provide a thorough analysis of grain orientation, fabric intensity and direct measurement of igneous fabric development in the Lebel syenite (Ontario, Canada) using both AMS and mineral SPO. These authors explore the factors involved in the progressive development of the igneous petrofabric in the Lebel syenite. These include free grain rotation, grain interaction and progressive crystallisation. They find that (1) the rate of rotation of grains is proportional to r. Thus, different populations

of grains, with differing shape ratios will tend to develop their own preferred orientations provided the grains do not interact. Grains with the smallest *r* values will have rotated most, (2) fabric anisotropy (*P'*) increases with increasing γ, particularly when there is a component of pure shear (i.e. flattening). Additionally, a pure shear component greatly increases the degree of preferred orientation (Rf_{φ}) for grains of high shape ratio, (3) at high shear magnitudes ($\gamma > 6$) preferred orientations begin to show cyclicity; whereby populations of grains with differing values of *r* have more intense or less intense degrees of preferred orientation. Thus, obliquities between sub-fabrics are a function of their shape ratio and the shear magnitude, (4) progressive simple shear in a nearly crystallised magma (involving grain interaction) will result in anisotropic grains rotating into the shear plane. These grains will most likely maintain a stable orientation irrespective of grain-size and shape and (5) if grain-size is related to time then each grain-size population will have its own range of shape ratios and distribution of preferred orientation. The authors, however, indicate that the distribution of grain sizes in the Lebel syenite appears to be independent of grain shape and preferred orientation. It is thus the product of magmatic, progressive crystallisation, with strong interaction of grains during the final stages of emplacement.

More recently, Cañón-Tapia and Chávez-Álvarez (2004) performed an investigation of simulated grain movement and rotation – primarily in the context of AMS. The orientations of the principal axes of the susceptibility tensor (*K*1, *K*2 and *K*3) were monitored during continuous deformation (in this case grain rotation in a viscous medium). The simulations of particle movement focused on using groups of data with different initial orientations, and increasing shear strain. The results of these simulations showed that (1) the grain shape (*r*) primarily controls the periodicity of particle rotation, (2) the fabric intensity (anisotropy) fluctuates with particle rotation due to the original orientation and shape (*r*) of the grains, (3) oblate particles are more likely to be imbricated with *K*3 normal to the dyke plane, which is consistent with the model of Geoffroy et al. (2002) who showed that oblate fabrics tend to be "normally" imbricated, with the foliation being within ~30° of the dyke plane and (4) prolate grains are more likely to produce correctly imbricated, type-A magnetic fabric irrespective of the amount

of shear. However, areas of little or no deformation (e.g. the centre of a dyke) yield poorly grouped AMS irrespective of the value of *r*.

There are number of ways in which the above findings may be applicable to the study of the RRDS. Firstly, one might expect to find that the large, most anisotropic grains will tend to be restricted in their movement owing to their larger size, and later interaction during simple shear. Secondly, there should then be a strong relationship between the grain shape (*r*) and preferred orientation. Thirdly, the distribution of grain-size may provide, at least qualitatively, an indication of the crystallisation behaviour. The sliding of grains past one another will be important in the shear plane, presumably most evident in the foliation plane. Finally, the fabric studied in the solidified dykes is unlikely to be representative of the early history in the fabric development. Given that the Lebel syenite is of a different composition and not a sheet-like intrusive, however, it is prudent to be cautious about inappropriate comparison. The above brief synthesis suggests that there is a correlation between the orientation of a fabric and its scalar parameters – although it has not been shown previously if this can be directly applied to the grains which constitute the fabric, as we attempt to do here.

5.3. Aim

We explore the interdependence of grain-size, shape and orientation of plagioclase within the igneous petrofabric of the RRDS in an attempt to answer the following questions: (1) Is there any correlation between the size and/or shape of plagioclase grains and the angle at which they come to rest against the dyke wall? (2) Is there evidence of an ideal grain-size or grain shape which occur in a "magmatic" orientation ($\leq 30°$ from the dyke plane)? (3) Is there any correlation between magmatic fabric and the degree of preferred orientation, which is considered independent of grain-size and shape?

We thus continue, in this paper, to investigate the acquisition of petrofabric in the RRDS. However, we turn our attention here to characteristics of the grains themselves, their morphology and any influence or relationship which can be demonstrated between grain morphology, size and the petrofabric orientation. We refrain from comparison between

mineral SPO and AMS as it has been carried out previously (Hastie et al., 2011a). The results are interpreted in the context of previously published models which have simulated or demonstrated the relationships between grain-size, shape, rotation and grain interaction (Ildefonse et al., 1997) in the development of preferred orientation (Benn and Allard, 1989; Arbaret et al., 1996; Dragoni et al., 1997; Launeau and Cruden, 1998).

5.4. Geological Background

The Rooi Rand dyke swarm (RRDS) is a 200 km long, 10–20 km wide, N–S trending dyke swarm which crops out between the Msunduze River in northern KwaZulu-Natal (South Africa) and central-eastern Swaziland (Figure 5.1). The RRDS is related to the ~180 Ma old Karoo Large Igneous Province (LIP) and intruded during the final stage in the development of the Lebombo faulted monocline at ~174 Ma (Jourdan et al., 2007). Although strictly dolerites the RRDS has a MORB-like composition, the only such composition known in the Karoo LIP.

The dykes have intruded the Beaufort Group (Permo-Triassic sandstones), Clarens Formation (Triassic sandstones) and Sabie River Formation (basalts). These Formations and Groups form the uppermost part of the Karoo Supergroup. Geochronology suggests that the RRDS is younger than the rhyolites of the Jozini Formation which cap the Lebombo (Armstrong et al., 1984; Watkeys, 2002; Riley et al., 2004).

The steeply dipping (> 80°), generally N–S striking dykes of the RRDS in the central area (Figure 5.1c) give way to more shallowly dipping (50°–70°) NNE–SSW striking dykes in the north (in Swaziland) (Figure 5.1b). The eastward dip of sedimentary strata and basalts (~15°) into which the dykes have intruded suggests that the dykes intruded vertically, and hence their westward dip is the result of this eastward tilting after their intrusion.

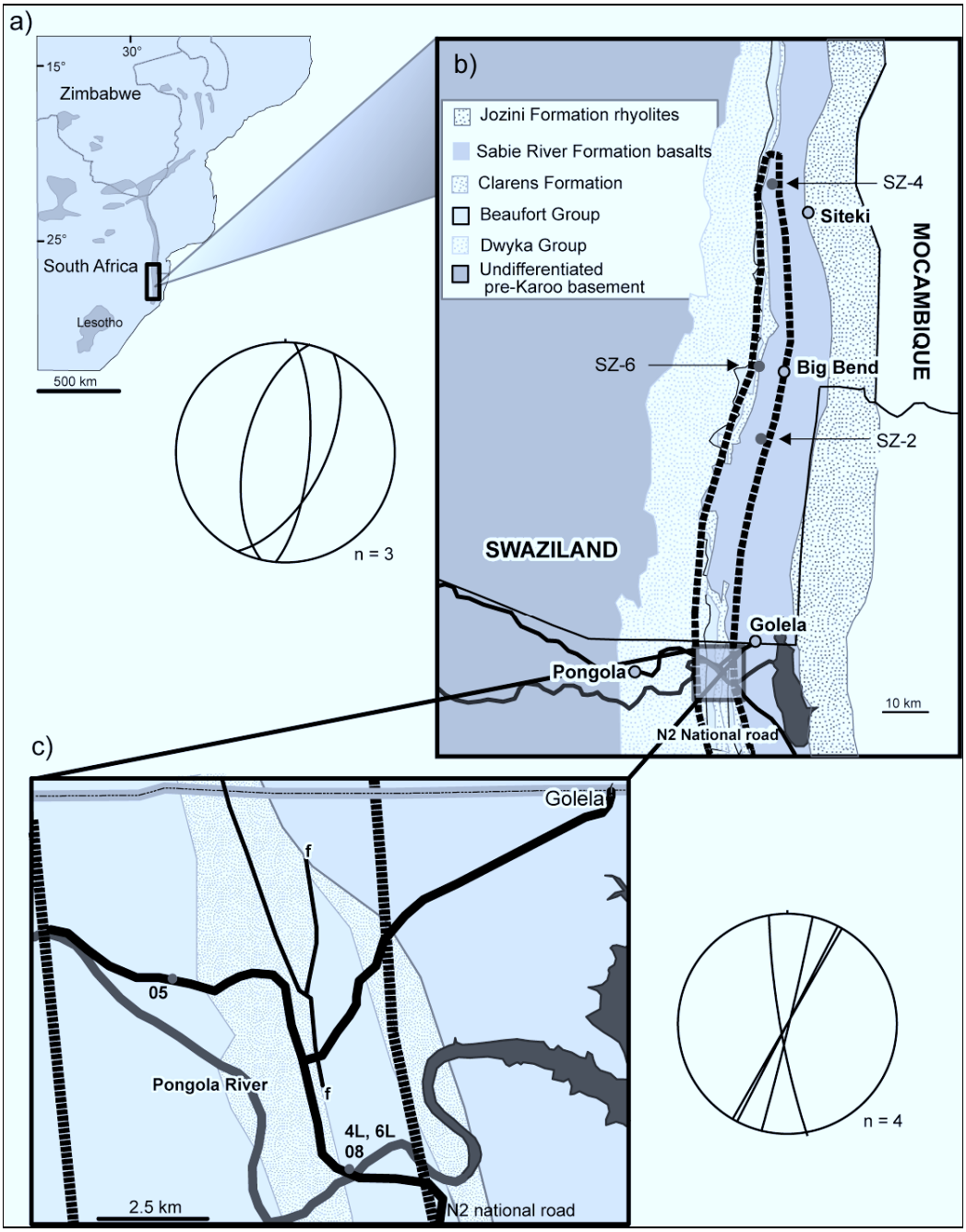

Figure 5.1: Sketch maps showing (**a**) the outcrop pattern of the volcanic rocks of the Karoo LIP in southern Africa, (**b**) the northern extent of the RRDS (outlined by broad, dashed line) in Swaziland and (**c**) the central part of the RRDS which is exposed along the Pongola River (dark grey) and N2 National Road (solid black line). Note that only the dykes relevant to this study are shown (SZ-2, SZ-4, SZ-6 and 4L, 6L, 08 and 05). Stereographic projections show the orientations of the dykes (see also Table 5.1).

Petrological and geochemical evidence indicates that the RRDS originated from the melting of an upwelling asthenosphere, as is typical of MORs (Saggerson et al., 1983; Armstrong et al., 1984; Meth, 1996). The MORB-like composition and intrusion of the RRDS into thinning crust during the earliest phase of break-up in southern Gondwana is consistent with this but this area failed to rift and produce oceanic crust along its present N–S exposure.

5.5. Methodology

5.5.1. Sampling & Basic Parameters

Samples were drilled from the two opposing chilled margins of each dyke. The samples are cylindrical drill-cores which are 22 mm × 25 mm in size. In mineral SPO studies a tensor representing the petrofabric is determined from these samples and the principal axes of the tensor are represented by $L1$, $L2$ and $L3$ ($L1 > L2 > L3$). The tensors are represented stereographically in the lower hemisphere. Scalar quantities are also determined, which quantify the anisotropy (P') and shape (T parameter). Prolate fabrics have $T < 0$ and oblate fabrics have $T > 0$. In this study the 3-D inertia tensor (see Launeau and Cruden, 1998) is calculated from 2-D ellipses determined from the bulk orientations of plagioclase in three mutually perpendicular thin-sections per sample. This method and the parameters described are discussed in further detail in Section 5.5.3.

5.5.2. Finding Magmatic Fabric

In trying to find the magma flow direction in a dyke using mineral SPO, it is the orientation of the lineation ($L1$) and foliation (the $L1$-$L2$ plane) relative to the dyke plane which is fundamentally important. Magma flow will tend to cause grains, such as plagioclase, to become tiled along the dyke walls (because of simple shear) with the long axes within and along the foliation, both of which become imbricated. If the dyke wall represents the shear plane during magma flow then the angle between the magmatic foliation and the dyke plane can be used to determine the sense of magmatic shear (Figure 5.2a) (Blanchard et al., 1979; Benn and Allard, 1989; Aubourg et al., 2002; Geoffroy et al., 2002; Callot and Guichet, 2003).

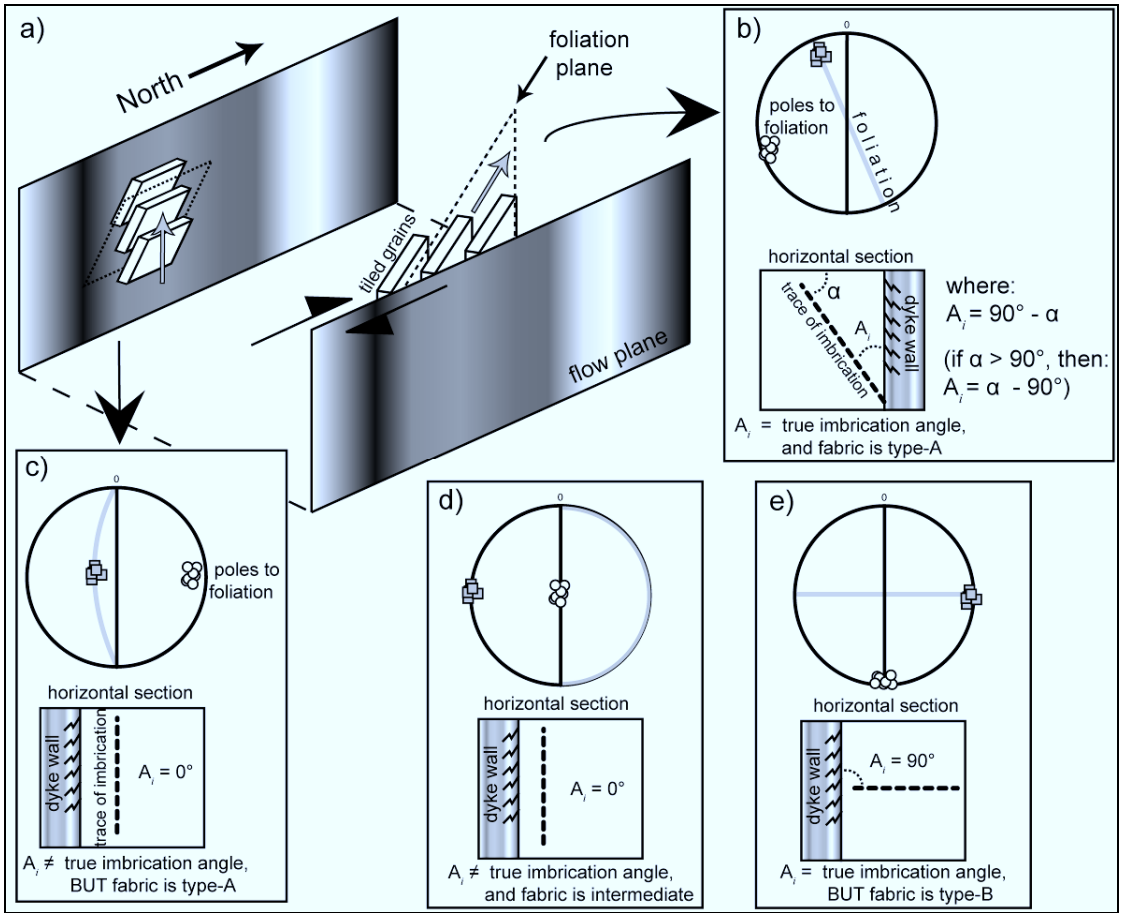

Figure 5.2: Schematic diagram summarising the approach used in this study (**a**) an idealised N–S striking dyke with tiled imbrication (after Blanchard et al., 1979) of grains along the margins (lateral flow on eastern margin and vertical flow on western margin), (**b**) stereonet showing *L*1 (grey squares) and *L*3 axes (white circles) of the 3-D tensor for lateral flow with the dyke plane (flow plane) and foliation plane (grey line) shown. Below the stereonet is a horizontal section (plan view) showing the trace of imbrication and the method of calculating the apparent imbrication angle (A_i) from angle α (measured in SPO-2003). In this case A_i is coincident with the true imbrication angle, (**c**) stereonet showing a 3-D tensor for vertical flow and horizontal section illustrating an A_i angle of zero with type-A fabric. End-member geometries of intermediate and type-B fabric are shown in (**d**) and (**e**) respectively. These illustrate how comparison of the 2-D measurement of A_i with the 3-D tensor prevents misinterpretation of the A_i angle. See text for further discussion.

The angle between the foliations (determined from each, opposing dyke margin) and the respective dyke plane can also be taken as a measure of whether the fabric is reliable as a magma flow indicator. Angles of < 30°, or between 30° and 50° are generally accepted as being flow-related (Blanchard et al., 1979; Geoffroy et al., 2002), as opposed to higher angles which are indicative of the presence of sub-fabrics or late-stage fabrics. In this paper a conservative range of 0°–30° will be considered to represent type-A fabric.

Mirrored geometry of the foliation planes provide the sense of magma flow, as they converge in the direction of magma flow (Aubourg et al., 2002; Geoffroy et al., 2002). It has been previously shown that the lineation resolved from 3-D tensorial data may be a zone axis – essentially an intersection lineation. This has been demonstrated for oblate shaped AMS fabric (Henry, 1997; Launeau and Cruden, 1998; Geoffroy et al., 2002; Callot and Guichet, 2003) and for plagioclase (Hastie et al., 2011b).

As discussed, however, magmatic fabrics may become complicated by other processes. For example, unexpected and mixed fabrics develop because (1) different grain sub-populations come to rest at different times and (2) grains are likely to interact as they move, rotate and imbricate within a crystallising magma. It is therefore necessary to consider whether there are any predictors of fabric imbrication, such as grain-size or shape factors and the reasons for the development of sub-fabrics unrelated to that which provides a sense of magma flow direction.

5.5.3. Shape Preferred Orientation

Measurement of individual grains or grain populations in 2-D is achieved using the image analysis software SPO-2003 (Launeau and Robin, 1996; Launeau, 2004). The SPO of plagioclase constitutes a direct, quantitative measure of the igneous petrofabric(s) as a whole – and is measured at the scale of individual grains and grain populations. The petrography of the samples and any significant differences between samples is therefore also important.

Most studies carried out to find the 3-D shape ellipsoid or tensor is carried out using Ellipsoid-2003 (Robin, 2002; Launeau, 2004; Launeau and Robin, 2005). The method used here is explained in Launeau and Cruden (1998) and Hastie et al. (2011a). In brief, photomicrographs of thin-sections (of known scale and orientation) are converted to binary (black and white) bitmap images, and analysed using this software. It is generally found that once the images are filtered (colour-inverted binary bitmaps) very few plagioclase grains are in contact with one another. This is ideal, as it prevents the measurement of aggregated grains as single grains. This would evidently introduce bias

in terms of grain-size, shape and also orientation. This filtering and inversion does, however, tend to reduce or even remove the smallest grain sizes (< 8 μm), a phenomenon which has been noted in previous studies (Launeau and Cruden, 1998).

From SPO-2003 it is possible to export and analyse scalar data of individual grains. This data can also be combined in 3-D using Ellipsoid-2003 to provide the inertia tensor of the petrofabric for an individual sample, or for a dyke margin. The thin-sections used (3 per sample) are mutually perpendicular, cut from standard drill-cores (22 mm × 25 mm). The arbitrary co-ordinate system used (*XYZ*) is based on the geographic orientation of each core. In this scheme, *X* is parallel to the azimuth and orthogonal to the strike of the core, *Y* is orthogonal to the azimuth and defines the strike direction and *Z* is parallel to the azimuth and plunge direction of the core.

Because the grain-size, shape and orientation of many thousands of individual grains are of primary interest here we made these measurements in 2-D sections. This is because the ellipsoid determined in 3-D is a bulk measure of all the grains, and it therefore does not provide any morphological or orientation parameters of individual grains. Our choice of samples is restricted, however, because it is most straightforward to measure the angle between the dyke walls and plagioclase grains in (sub-) horizontal thin-sections from the margins of a vertically orientated dyke with relatively straight margins. Thus, for our analyses we are restricted to *XY* and some *ZY* sections through which the dyke plane passes. We have analysed 16 samples from seven dykes of the RRDS. In the investigation of the 3-D SPO tensor, however, four samples (12 thin-sections) per dyke were analysed.

Because the angle measured between the plagioclase grains and the dyke margin is in 2-D, it is an apparent angle of imbrication, referred to here as A_i. The angle A_i is calculated by subtracting angle α measured by SPO-2003, which is the angle between the top of a thin-section and the long-axis of each individual grain (Figure 5.2b). Within SPO-2003, these orientations are determined according to a rose of directions from 0° to 90° (0° = dyke-parallel; 90° = dyke-orthogonal). We anticipate that orientation measurements in SPO-2003 do not introduce significant errors in calculating A_i, but potential errors are

more likely to derive from localised deviations in dyke orientation along the dyke margin. The orientation of thousands of individual grains (10^5) from seven dykes has been measured and it is thus possible to compare and contrast fabric types across different dykes but also maintain a sense of the fabric orientation at the smallest scale.

It must be made clear that, because A_i is an apparent angle, the true measurement of tiled imbrication (as formalised by Blanchard et al., 1979) is not necessarily measured here, except in cases where the elongation of the fabric ellipsoid defined by plagioclase is horizontal (i.e. where lateral flow is evident). This is because the trace of grains in horizontal sections will be coincident with the trace of the foliation (Figure 5.2b). This fabric is type-A. There are three other end-member situations which demonstrate how the 3-D tensor can assist in distinguishing between foliation imbrication and A_i which allows us to correctly interpret the fabric type. In the case of vertical flow (Figure 5.2a, c) the trace of grains from which A_i is calculated will be < 30° (i.e. type-A fabric) despite A_i not being coincident with the true imbrication angle. This is similar to Figure 5.2d, except that the 3-D tensor clearly illustrates intermediate fabric, which is not flow related and type-B fabric can be detected from both the 3-D tensor and A_i in horizontal thin-sections (Figure 5.2e). There can be intermediate types to those shown here, but these end-member situations demonstrate clearly how the measurement of the angle A_i it must be monitored in conjunction with the 3-D SPO tensor.

5.5.4. Grain-size

The scalar data (grain-size, shape ratio etc.) can be exported from SPO-2003 and sorted according to any chosen parameter for analysis and comparison. One difficulty encountered with measuring grain-size is that small grains may have similar shape ratios to larger grains, and thus the length of the grain axes are not representative of grain-size. Following the work of Launeau and Cruden (1998) it is reasonable to use the diameter of a circle which is of the same spatial area as each of the grains as a proxy for grain-size.

5.5.5. Grain Shape

The shape ratio (r) for each grain is the ratio of the long axis to the short axis (r = L / S). This is measured for plagioclase in 2-D sections. For each of these analyses the angle A_i is critical because it allows us to assess whether the fabric is orientated in a systematic way in each sample based on grain-size and/or shape. In addition we are able to measure the degree of preferred orientation (Rf_φ). This value provides the intensity of the preferred orientation independently of grain-size and grain shape. For each of these dykes we also present the 3-D SPO tensors.

5.6. Results

5.6.1. Igneous Textures in the RRDS

Dykes of the RRDS are generally fine to medium-grained, intergranular to plagioclase-phyric dolerites in which plagioclase is the dominant phase (55 vol. %), with the remainder comprising augite (~ 40%) and opaque oxides such as magnetite. The RRDS has not suffered any late deformation or mineral alteration, and the textures are therefore primary. There are essentially three main igneous textures evident in the dolerite dykes of the RRDS; intergranular, sub-ophitic and phenocrystic (plagioclase-phyric). Intergranular textures are most common, with plagioclase and approximately equal sized augite forming the framework of the fabric (05, 6L15, SZ-4) (Figure 5.3). The phenocrystic textures of dyke 08 comprise a fine-grained to aphanitic groundmass with plagioclase phenocrysts while 4L14 does not have an aphanitic groundmass but is nevertheless phenocrystic. Sub-ophitic textures (SZ-2, SZ-6J) are relatively coarse-grained and comprise a framework dominated by plagioclase grains, sometimes partially enclosed within augite. Plagioclase in the phenocrystic samples appears more elongate than plagioclase in the other samples and tends to be sub- to euhedral. Augite is always anhedral and generally granular in shape. As a result, investigation or quantification of fabric defined by augite could not be carried out effectively using SPO-2003.

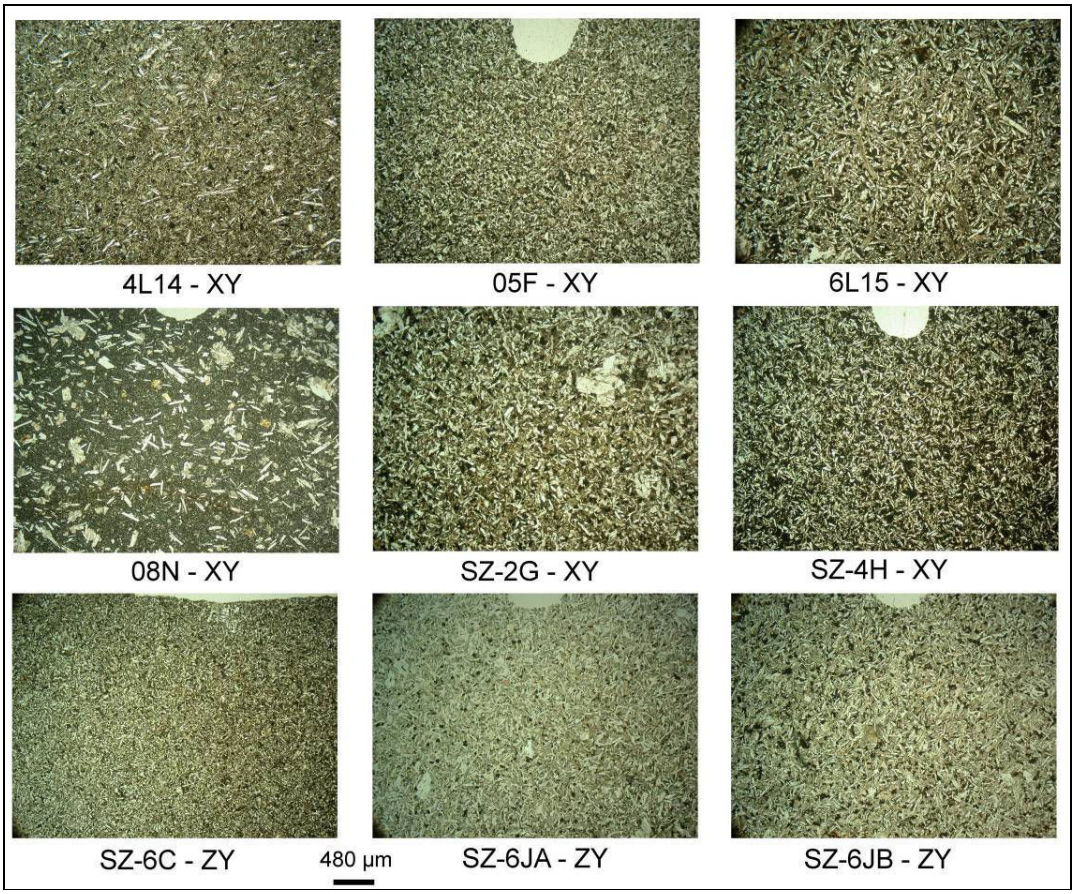

Figure 5.3: Thin-section photomicrographs (plane-polarised light) of representative sections of the samples being studied. Note that the scale is the same for all sections (see scale bar). The main textural types are intergranular (05, 6L15, SZ-4) to sub-ophitic (SZ-2, SZ-6J), as well as plagioclase-phyric examples (4L14 and 08N). See Table 5.1 for thin-section orientations.

5.6.2. Plagioclase SPO

The 3-D tensor data are shown here because the examination of the fabrics/sub-fabrics will proceed in a manner that examines the scalar and orientation parameters of plagioclase in increasingly finer detail. Thus, the 3-D SPO tensor provides an appropriate context in which to gauge the contribution of the textures investigated in 2-D to the full picture of the 3-D fabric. The data are restricted to plagioclase, because (1) plagioclase is the dominant phase, with the remainder comprising anhedral, granular augite and magnetite, (2) it is within this fabric of the RRDS that type-B fabric has been found, (3) a greater number of grains are measured in each thin-section and (4) because a greater variety of grain sizes can be studied according to the different textural types.

The 3-D inertia tensors for each margin of the seven dykes and the orientation of each dyke plane are shown in Figure 5.4. Note that two foliations are shown (in grey) per dyke as they are determined from each margin (e.g. western and eastern margin for a N–S striking dyke). The *L*1 axes vary from steeply plunging to sub-horizontal and the foliations generally dip steeply.

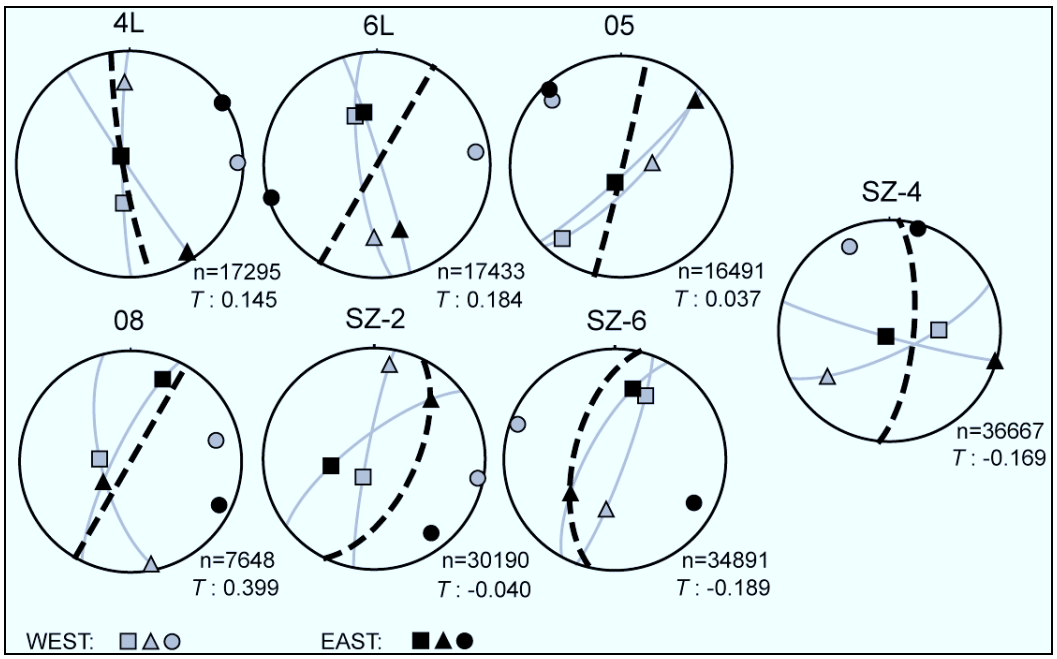

Figure 5.4: Stereographic projections of 3-D inertia tensors of the plagioclase SPO for the 7 dykes under consideration (after Figure 6 of Hastie et al., 2011a). Note that the fabric is split into two respective margins (see key; *L*1 = ■, *L*2 = ▲, *L*3 = ●). Foliations are shown in grey. Dyke plane shown as black dashed line. Note that the fabric in SZ-4 is type-B: the foliations are orthogonal to the dyke plane. The "n" value is the number of plagioclase grains measured for each dyke to construct the inertia tensors. Shape parameters (*T*) are also shown.

The angle between the foliations and the respective dyke planes are shown in Table 5.1 and it is evident that type-B fabric is found in three dykes (six margins overall). Dykes 6L and 05 do not strictly have type-B fabric, but the foliations fall just outside the 30° criterion and are not imbricated with respect to the dyke plane. Of the seven dykes being considered, only SZ-4 has type-B fabric. The remaining examples carry type-A fabric, but the foliations are only imbricated symmetrically with respect to the dyke plane in 4L.

Table 5.1: Thin-section, dyke and SPO data for the 16 samples analysed from the RRDS (*L*2 is not shown). Note that the values shown for the 3-D ellipsoids and associated foliations are those calculated for each sample (i.e. inclusive of *XY*, *XZ* and *ZY* sections for each sample).

		2-D ellipse						3-D ellipsoid						foliation		
Sample - section	dyke orient.	strike	dip	L (μm)	S (μm)	grains	√F[a]	*L*1-azi.	*L*1-plunge	*L*3-azi.	*L*3-plunge	*P′*	*T*	strike	dip	Imbrication angle
4L13 - *XY*	82°/170°	020°	10°	33	30	512	1.6%	142°	86°	002°	03°	1.157	0.078	92°	87°	05°–15°
4L14 - *XY*	82°/170°	031°	13°	14	13	825	6.4%	337°	64°	083°	08°	1.200	0.093	173°	82°	
05E - *XY*	88°/014°	268°	10°	17	15	1281	4.0%	214°	61°	118°	04°	1.183	0.140	208°	86°	
05F - *XY*	88°/014°	179°	12°	38	33	244	5.7%	168°	80°	338°	10°	1.296	-0.218	68°	80°	18°–32°
05I - *XY*	88°/014°	264°	21°	7	6	219	0.0%	174°	60°	313°	24°	1.147	0.169	43°	66°	
6L13 - *XY*	90°/030°	056°	15°	29	26	676	3.3%	340°	63°	247°	02°	1.201	-0.041	337°	88°	45°
6L15 - *XY*	90°/030°	080°	22°	29	24	212	5.9%	349°	33°	255°	06°	1.246	0.276	345°	84°	
08N - *XY*	90°/030°	358°	12°	33	28	290	7.3%	237°	68°	093°	18°	1.334	0.507	183°	72°	0°–24°
SZ-2B - *XY*	90°/026°	258°	21°	19	17	1900	5.4%	218°	73°	104°	07°	1.209	0.221	194°	83°	
SZ-2F - *XY*	90°/026°	203°	12°	15	15	1397	1.9%	195°	74°	098°	02°	1.134	-0.288	188°	88°	05°–15°
SZ-2G - *XY*	90°/026°	328°	20°	16	15	1598	1.8%	270°	59°	141°	20°	1.106	0.022	231°	70°	
SZ-4B - *ZY*	72°/005°	355°	24°	16	15	1674	3.8%	099°	46°	198°	09°	1.118	-0.556	288°	81°	70°–88°
SZ-4H - *XY*	72°/005°	185°	25°	17	16	1781	3.6%	296°	86°	205°	00°	1.135	0.133	295°	90°	
SZ-6C - *ZY*	60°/193°	274°	23°	15	13	1126	4.3%	012°	28°	107°	09°	1.173	-0.780	197°	81°	
SZ-6JA - *ZY*	56°/207°	275°	25°	16	11	1862	9.0%	012°	28°	115°	24°	1.345	-0.038	205°	66°	10°
SZ-6JB - *ZY*	56°/207°	275°	25°	17	15	1736	7.9%	016°	43°	122°	17°	1.31	0.324	212°	73°	

[a] √F value is a measure of the degree of misfit between 2-D ellipses in the construction of the 3-D ellipsoid (values of <10% are desirable) (Launeau et al., 2010).

As indicated earlier, the 3-D tensors provide some control on the apparent imbrication angle, because A_i will be significantly different from the true imbrication angle in cases where $L1$ is (sub-) vertical given that we have made 2-D measurements from (sub-) horizontal thin sections. This is acceptable for our use here because we do not make any inference regarding the direction or inclination of magma flow based on the angle A_i.

There is some variation in the shape of the fabrics being considered. The fabric of samples 4L13, 4L14, 05E, 05I, 6L15, 08N, SZ-2B, SZ-2G, SZ-4H and SZ-6JB are oblate in shape (average T: 0.196) (see Table 5.1) while the remaining six samples are near-neutral to prolate in shape (average T: -0.320). The shape parameters of the 3-D tensors shown in Figure 5.4 indicate the slight predominance (57%) of oblate fabric. The percentage anisotropy ($[P' - 1] \times 100$) of the 3-D tensors is in the range 15–24%.

5.6.3. Apparent Imbrication Angle (A_i)

Given that type-B fabric exists in the SPO of plagioclase in the RRDS it is worthwhile finding the angle A_i at the scale of individual grains from all 16 samples (Figure 5.5). A total of 31% of the grains are < 30° from the dyke plane (i.e. type-A fabric) while the remainder show a slight, but noticeable increase in frequency towards a dyke-orthogonal orientation (type-B fabric).

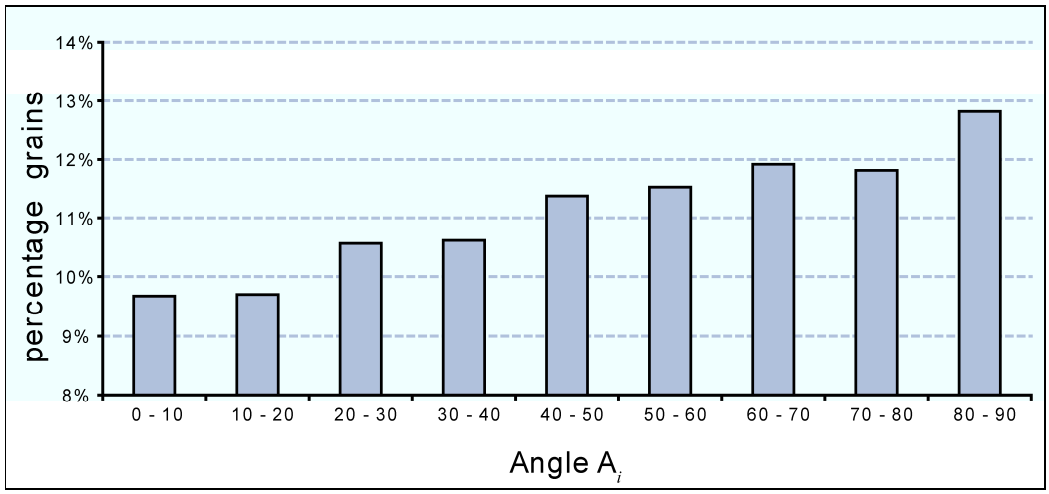

Figure 5.5: Graph illustrating the percentage of grains (total=1.7×10^5) which occupy a particular apparent angle to the respective dyke planes (A_i at 10° intervals). Note the trend of the grains towards increasingly higher angles to the dyke plane (69% of grains > 30° from the dyke plane).

From Figure 5.4, however, it is evident that the angle A_i in some dykes (4L, SZ-4, 05-east, 08-west) is unlikely to be representative of the true imbrication angle. Thus, we now present grain-size and shape data, while keeping track of the angle A_i across the size and shape classes because we are primarily interested in finding any potential correlation between these parameters and the fabric type.

5.6.4. Grain-size

The grain-size, shape and orientation of the plagioclase grains have been measured for all individual samples and for the combined data. The distribution of grain sizes is shown in Figure 5.6, and those grain-size classes with angle $A_i < 30°$ are indicated in black. This is determined by finding the mode of the angle occupied by grains across the population of grains in each size (and shape) class.

It is evident that 4L has a bimodal grain-size distribution with peaks at 9–10 μm and 20–21 μm. Dykes 05, SZ-2, SZ-4 and SZ-6 have similar, unimodal distributions that are skewed towards the coarser fraction. Standard deviations are also shown in Figure 5.6. Dyke 08 has an unusual grain-size distribution relative to the others that is most likely related to its phenocrystic texture. The apparent peak in the 60–65 μm range is a function of plotting at 5 μm intervals for grains > 60 μm.

When considering all the data it is evident that the majority of grains (90%) are < 33 μm in size. Grain sizes range from 8.50–254 μm with the most common grain-size being 12.3 μm. The median grain-size is 16.76 μm. In most cases (except 6L, 05 and 08) the grain-size classes 11–12 μm and 12–13 μm have A_i values < 30°. Dykes 6L, 05 and 08 are from the central RRDS (Figure 5.1c).

Two observations can be made regarding common trends in the angle A_i within the grain-size populations. Firstly, SZ-4 appears to have a relatively large number of grain sizes with an angle A_i of < 30°. Secondly, in samples 4L, 05, SZ-2 and to a lesser extent in SZ-6, regular intervals of grain-size populations have A_i values ≤ 30°.

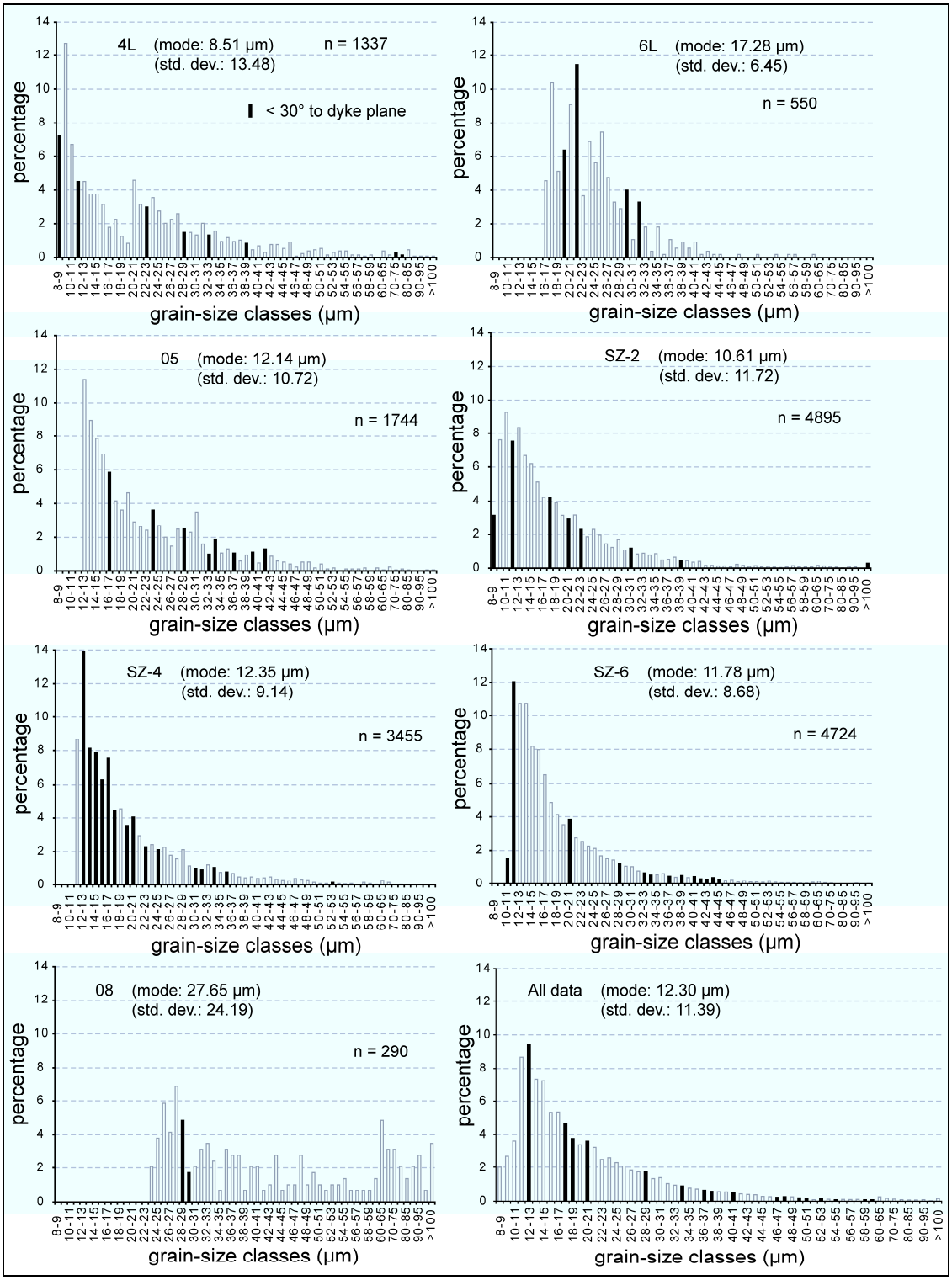

Figure 5.6: Grain-size distribution (%) of plagioclase grain sizes in 7 dykes of the RRDS. Note that grain-size classes in which the modal occurrence of angle of A_i is < 30° are shown in black. The modal grain-size of all 1.7×10^5 plagioclase grains is 12.30 µm.

5.6.5. Grain Shape

Plots of the distribution of grain shapes in the RRDS, with the modal occurrence shown, are presented in Figure 5.7. Grain shape classes with angle $A_i < 30°$ from the dyke plane are indicated in black. It was initially found that grains within the shape range 1–5 were most common (91% of all grains) and were thus investigated at 0.05 intervals. Grain shapes, however, reach maximum *r* values of 17.

It can be seen from the individual dykes that SZ-2 has the highest *r* value for modal abundance (1.80) and SZ-4 has the lowest (1.22). From the bulk analysis it is evident that the most populated shape classes are in the range 1.40–1.95 (24% of the total grains). It is interesting to note that the shape classes shown in black lie either side of this range in the plot of all the data, and 4L and SZ-2.

The distribution of grain shapes does not match that of the grain-size distribution. Indeed, a plot of grain-size vs. shape (supplementary data) demonstrates a lack of correlation between the two parameters. The significance of this may be undermined to some extent by the 2-D measurements and consequent sectional effects. Large grain sizes (> 55 μm) do, however, appear to be considerably less anisotropic than the smaller grains. The distribution of grain sizes according to angle A_i is also shown in the supplementary material. There does not appear to be any correlation between grain-size and A_i or grain shape and A_i.

If the fabric is once again scrutinised in 9 representative examples, bearing in mind the angle A_i and modal grain sizes, we observe type-A fabric in 05F, 6L15 and SZ-4H as demonstrated by the A_i values (Figure 5.8). In these examples of type-A fabric the modal grain-size is 27.8 μm, 21.4 μm and 12.3 μm respectively. In samples 05F and 6L15 there seems to be an association between these relatively large grains with relatively high Rf_φ values (~1.3) and type-A fabric. The modal grain-size in the other examples tend to be lower (8.51–11.8 μm), although in the phenocrystic sample 08N the modal grain-size is 27.7 μm, in which the highest value of Rf_φ (1.418) is also found. Values of Rf_φ range from 1.031 to 1.418.

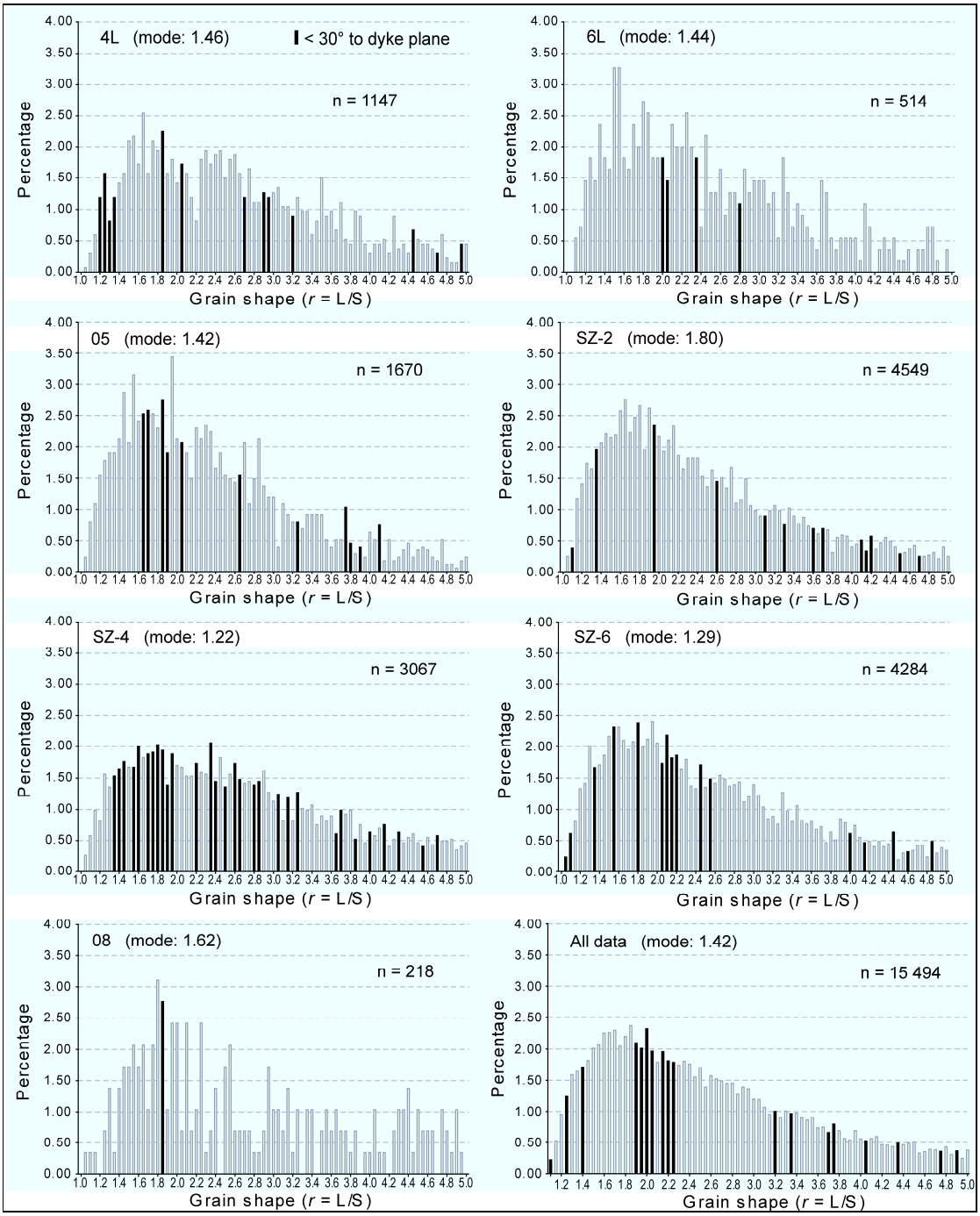

Figure 5.7: Graphs showing the distribution (%) of grain shape classes for individual and all samples. Only shape classes up to $r = 5.00$ are shown (note values of "n"). The grain shape classes 1.40–1.95 are the most populated across the entire dataset and account for 24% of the total grains.

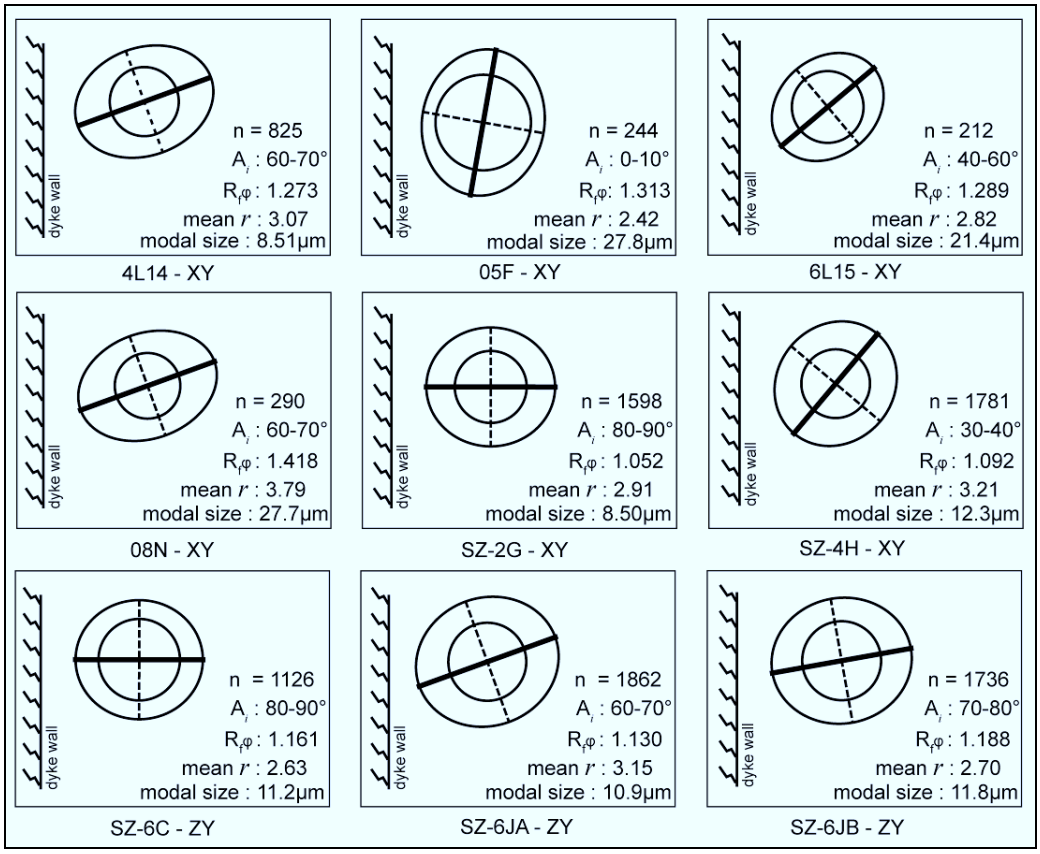

Figure 5.8: Schematic representations of selected samples showing the shape tensor (minor axis dashed) and relevant scalar, size and orientation (A_i) data, relative to the dyke wall for each sample. There is no striking correlation, although small grain sizes (~8–12 µm) with high Rf_{φ} values tend to be associated with type-B fabric (4L, SZ-2). Sample SZ-4H is contrary to this observation, however.

5.7. Discussion

5.7.1. Overview

In this study we have assessed factors related to the size, shape and orientation of plagioclase grains which define the igneous petrofabric in the Rooi Rand dyke swarm. Texturally, the samples range from intersertal, even-grained to sub-ophitic and plagioclase-phyric. The modal grain-size is 12.3 µm and 91% of plagioclase grains are < 33 µm in size. Some phenocrysts reach > 100 µm in size (max. 250 µm). The distribution of grain sizes is skewed towards the larger fraction, although plagioclase-phyric samples are less common than the sub-ophitic and even-grained samples. The most abundant grain shapes have modest *r* values; 1.40–1.95, carried by the smallest grain sizes. The larger grains tend to have relatively low shape ratios while the more anisotropic grains (*r*

> 10) are found in the populations of small grain sizes (< 55 μm). The modest Rf_{φ} values throughout (1.031–1.418) suggest that the fabric has not been affected by a component of flattening induced by pure shear (Launeau and Cruden, 1998).

By measuring the modal distribution of angle A_i across plagioclase populations of different size and shape we can show that the most common size class (12–13 μm), with modest shape ratios (1.80–2.20), appears to define the "ideal" type-A fabric (Figure 5.7). This is most evident in samples from the northern RRDS in Swaziland. Grains with shape ratios in this range account for 15% of the total plagioclase abundance. In some examples there is type-A fabric carried by slightly larger (20–21 μm), more anisotropic (4.80–4.85) grains but they do not appear in close association in the way the less anisotropic grains do.

However, the 3-D SPO tensors of some dykes and dyke margins (4L, SZ-4, 05-east, 08-west) have steep $L1$ axes, which suggests that the angle A_i may differ significantly from the true angle of tiled imbrication in these dykes. Still, the fabric in dyke 4L is oblate in shape and thus the meaning of the $L1$ tensor axis is debatable because the 3-D SPO tensor shows mirrored imbrication of the foliations with respect to the dyke plane. According to the methodology adopted in this work, therefore, this is most consistent with lateral flow and is not coincident with the lineation, which is essentially vertical.

In samples with shallowly plunging $L1$ axes in the 3-D tensor the apparent imbrication angle will be close, if not coincident, with the true imbrication angle of the long axes of the constituent plagioclase grains. This includes dykes SZ-6 and 6L and dyke margins 05-east and 08-east. If discussion is restricted to these dykes and dyke 4L it is evident that grains in the shape ratio range 1.80–2.20 tend to be imbricated within 30° of the dyke plane. Thus, our findings with respect to shape and fabric type are reasonable in these examples, notwithstanding the fact that the angle A_i is not necessarily the true imbrication angle of plagioclase. Similarly, in Figure 5.8, the tendency toward type-B fabric as r increases in small grains (< 8.50 μm) is evident in these same examples.

These results are not consistent with findings of other works which have shown fabric intensity and orientation to be a function of highly anisotropic grains. For example, Kattenhorn (1994) found in the RRDS that the most elongate grains ($3.3 < r < 10$) align within 10–25° of the dyke wall. It has been shown here that these grains constitute only ⅓ of the petrofabric and do not necessarily hold a magmatic fabric orientation.

The phenocrystic sample 08N is interesting because it has the strongest degree of preferred orientation, while displaying an angle of $A_i > 30°$. This may be related to the factors discussed above with regard to the apparent imbrication angle, or it may be indicative of a lack of grain interaction leading to obliquities developing between different shape classes. In samples in which grains are interconnected (SZ-6) grain interaction during flow of the magma must have played an important role. It is difficult to envision interacting, anisotropic grains rotating preferentially into the magmatic shear plane, particularly as crystallisation is drawing to a close. Thus, grain interaction may indeed increase the stability, but not the type of petrofabric.

It is thus questionable whether placing emphasis on the orientation and characteristics of the most anisotropic, least abundant grains is justified, particularly when comparisons are drawn between fabrics defined by grain populations of significantly different abundance. This is exemplified in dykes in which numerous, widely spaced grain-size classes have $A_i < 30°$ (4L, SZ-2, SZ-6). The difference in abundance can be accounted for by nucleation, crystallisation and fractionation processes in the magma. For example, Launeau and Cruden (1998) note that different grain-size populations represent a particular crystallisation event during progressive crystallisation.

5.7.2. Plagioclase Nucleation in the RRDS

Crystal size distribution (CSD) can be used to constrain nucleation and growth rates during crystallisation in igneous rocks – allowing for quantification of the kinetic processes involved (Kirkpatrick et al., 1979; Muncill and Lasaga, 1987; Cashman and Marsh, 1988; Marsh, 1998; Pupier et al., 2008). CSDs are typically shown as plots of the

natural logarithm of the population density (vertical axis) as a function of grain-size (horizontal axis) (Marsh, 1988; Higgins, 2000).

While we are not concerned with quantifying crystal growth rates, the CSD in the 16 samples of the RRDS may provide useful information about the nucleation and crystallisation history of these dykes. Dowty (1980) has shown that igneous textures are controlled by the interaction between the pre-cooling history of the melt, the degree of cooling and cooling rate, volatile content of the melt, oxygen fugacity and nucleation kinetics. Nucleation can be homogeneous or heterogeneous; the latter occurring when nucleation begins upon an existing phase in the magma, or along the base of a flow or margins of an intrusive body. Heterogeneous nucleation is also responsible for ophitic/sub-ophitic textures in basaltic rocks (Kirkpatrick, 1977). A relatively uniform distribution of crystal sizes is indicative of continuous nucleation and growth under conditions of constantly decreasing temperature. This tends to depress growth-rates while nucleation is not affected – provided that latent heat of crystallisation is constantly removed (Kirkpatrick, 1977; Dowty, 1980). Uniform lognormal slopes of distribution in the CSD of igneous rocks can thus be explained in essentially two ways. Either the nucleation rate increases exponentially as a function of time (growth rate is constant) or the growth rate increases exponentially as a function of crystal size (nucleation rate is constant) (Marsh, 1998; Hersum and Marsh, 2006).

There are processes which may disturb this uniformity. Sudden undercooling and a resultant burst of nucleation will cause an increase in negative slope at small grain sizes, provided the system does not equilibrate fully. Crystal fractionation will tend to steepen the slope of the correlation line at large grain sizes, while crystal accumulation will tend to develop an upwardly concave CSD curve. Once nucleation has ceased and growth becomes the dominant process the smallest grains tend to be resorbed while larger grains continue to grow (Ostwald ripening). This would cause a downward turn of the CSD curve at the smallest grain sizes (Marsh, 1998). A CSD can become “kinked” if there is crystal agglomeration (Burkhart, et al., 1980) or a difference in nucleation rate (Marsh, 1998). Interestingly, in the study of Pupier et al. (2008) it was found that changing the

crystal shape of plagioclase in their experiments had essentially no effect on the slope of the CSD. Launeau and Cruden (1998) also showed in their results that CSD was independent of grain shape.

The CSD of the 16 samples of the RRDS is shown in Figure 5.9. The distribution shows a break in slope at 80 μm (note the regression lines for the two parts of the CSD) that is consistent with the kinked CSDs described by Marsh (1998). This kinked CSD could be interpreted as a function of crystal agglomeration (Burkhart et al., 1980) – a process which tends to cause plagioclase grains to evolve from acicular to blocky shapes because of the coalescence of grains during cooling. However, if crystal agglomeration occurred at a late-stage it would tend to reduce the number of early formed small grains. Furthermore, evidence of textural coarsening (Ostwald ripening), which would also reduce the number of small grains, is not supported by the CSD.

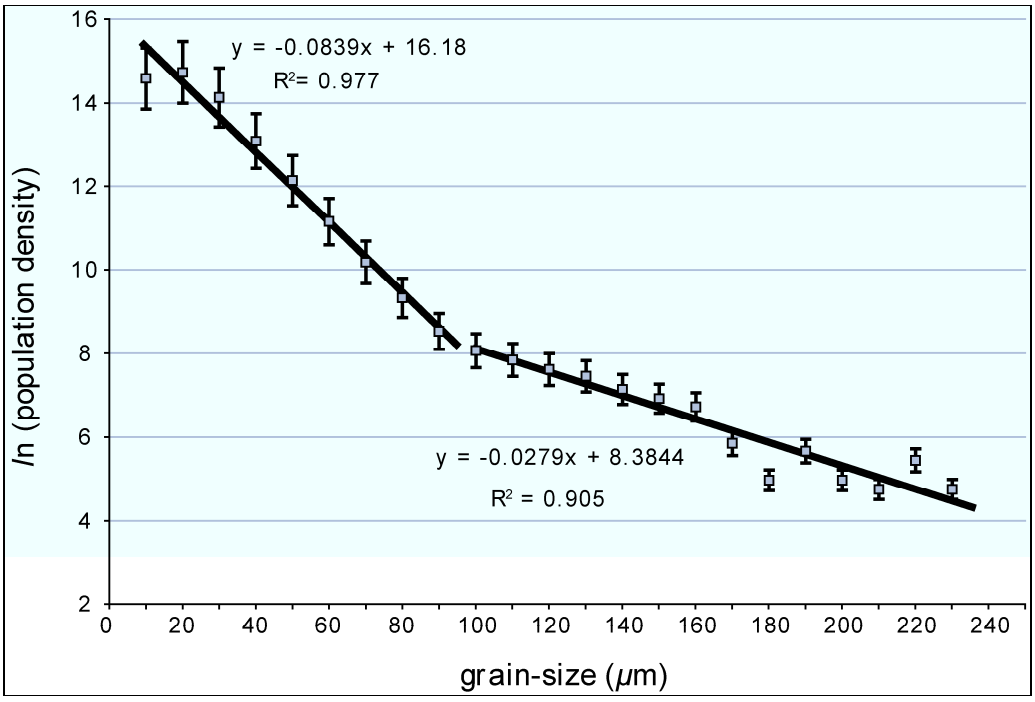

Figure 5.9: Crystal size distribution (CSD) of 1.7×10^5 plagioclase grains from 16 samples of the RRDS (error bars at 5%). There is a break in slope at 80 μm (note regression line correlation values) which is probably related to a late-stage nucleation event that gave rise to crystal growth below this grain-size (see Section 5.7.2. for discussion).

Marsh (1998) indicates that kinked CSDs are related to changes in nucleation rate which may reflect two distinct nucleation events. Marsh (1998) demonstrates that distinct events of heterogeneous nucleation provide the geological explanation for a kinked CSD derived from Makaopuhi lava lake (Hawaii). In thin-sections of samples from this basaltic lava lake there is evidence of co-precipitation of the main phases, with early growth occurring in poorly sorted clusters (heterogeneous nucleation). Larger crystals have "annexed" smaller grains, resulting in a texture comprising large, spatially separate grains which are within a groundmass of smaller grains that grew at a later stage. In phenocrystic samples, this may be a function of different environments of nucleation – phenocrysts nucleate and grow at depth, while the smaller grains grow later, potentially affected by relatively rapid undercooling at a later stage.

Kirkpatrick et al. (1979) and Muncill and Lasaga (1987) have found that the morphology of plagioclase crystals become increasingly skeletal, dendritic and fibrous with increasing undercooling. These crystal shapes are consequently more anisotropic than sub/euhedral crystals grown under equilibrium conditions. This is applicable to the textures and CSD of the RRDS. We have shown that the highest values of anisotropy ($r > 7$) occur in the smallest grains and thus are likely to have grown at a late stage, perhaps during undercooling caused by upward migration of magma while earlier crystallisation, closer to equilibrium conditions, occurred at depth.

5.8. Conclusions

It is possible to draw the following conclusions based on the results presented:

1. Grain-size and shape in the RRDS are independent, although grains > 55 μm tend to have lower *r* values than smaller grains.
2. Plagioclase grains in the 12–13 μm size range with modest shape ratios (1.80–2.20) appear to define type-A fabric. This is comparable to the work of Benn and Allard (1989) who found that imbrication is not common below an *r* value of 1.50.

3. Type-B fabric is more strongly associated with higher anisotropy, small grains (~8.50 μm).
4. The CSD and igneous textures of samples of the RRDS are consistent with heterogeneous nucleation – with phenocrysts having grown early at depth and grains < 80 μm having grown later under conditions of relatively rapid undercooling.
5. Our results are comparable to the findings of Dragoni et al. (1997) given that there is an apparent correlation between increasing grain shape (*r*) and type-B fabric. We therefore do not favour the strong interaction of grains attempting to rotate as the primary mechanism in the development of type-B fabric.

In our previous work on the SPO fabric of the RRDS we suggested that type-B fabric developed as a result of late-stage (high magma viscosity) re-orientation of the fabric caused by the interaction of large grains. Our findings in this work also suggest late-stage processes, but it seems that rapid nucleation of the plagioclase groundmass at a late-stage has more significantly affected the development of type-B fabric than the process of grain interaction.

5.9. Acknowledgements

The corresponding author would like to acknowledge a freestanding NRF Innovation Scholarship, as this work forms part of his PhD research. Carlos Archanjo and an anonymous reviewer are thanked for their reviews of this paper.

5.10. References

Amenta, R.V., 2001. Three-dimensional computer modelling of fabric evolution in igneous rocks. Computers & Geosciences 27, 477–483.

Arbaret, L., Diot, H., Bouchez, J.-L., 1996. Shape fabrics of particles in low concentration suspensions: 2D analogue experiments and application to tiling in magma. Journal of Structural Geology 18, 941–950.

Archanjo, C.J., Launeau, P., 2004. Magma flow inferred from preferred orientations of plagioclase of the Rio Cearf-Mirim dyke swarm (NE Brazil) and its AMS significance. In: Martin-Hernandez, F., Luneburg, C.M., Aubourg, C., Jackson, M. (Eds.), Magnetic Fabric: Methods and applications. Geological Society of London Special Publication 238, 285–298.

Armstrong, R.A., Bristow, J.W., Cox, K.G., 1984. The Rooi Rand dyke swarm, southern Lebombo. In: Erlank, A.J. (Eds.), Petrogenesis of the volcanic rocks of the Karoo province. Geological Society of South Africa Special Publication 13, 77–86.

Aubourg, C., Giordano, G., Mattei, M., Speranza, F., 2002. Magma flow in sub-aqueous rhyolitic dikes inferred from magnetic fabric analysis (Ponza Island, W. Italy). Physics and Chemistry of the Earth 27, 1263–1272.

Aubourg, C., Tshoso, G., Le Gall, B., Bertrand, H., Tiercelin, J.-J., Kampunzu, A.B., Dyment, J., Modisi, M., 2008. Magma flow revealed by magnetic fabric in the Okavango giant dyke swarm, Karoo igneous province, northern Botswana. Journal of Geothermal and Volcanic Research 170, 247–261.

Baer, G., 1995. Fracture propagation and magma flow in segmented dykes: Field evidence and fabric analyses, Makhtesh Ramon, Israel. In: Baer, G., Heimann, A. (Eds.), Physics and Chemistry of Dykes. A.A. Balkema, Rotterdam, 125–140.

Bascou, J., Camps, P., Dautria, J.M., 2005. Magnetic versus crystallographic fabrics in a basaltic lava flow. Journal of Volcanology and Geothermal Research 145, 119–135.

Benn, K., Allard, B., 1989. Preferred mineral orientations related to magmatic flow in ophiolite layered gabbros. Journal of Petrology 30, 925–946.

Blanchard, J.-P., Boyer, P., Gagny, C., 1979. Un nouveau critere de sens de mise en place dans une caisse filonienne: Le “pincement” des mineraux aux epontes: Orientation des minéraux dans un magma en écoulement. Tectonophysics 53, 1–25.

Blumenfeld, P., Bouchez, J.-L., 1988. Shear criteria in granite and migmatite deformed in the magmatic and solid state. Journal of Structural Geology 10, 361–372.

Burkhart, L.E., Hoyt, R.C., Oolman, T., 1980. Control of particle size distribution and agglomeration in continuous precipitations. In: Kuczynski, G.C. (Eds.), Sintering processes. Plenum, New York, 23–38.

Callot, J.P., Geoffroy, L., Aubourg, C., Pozzi, J.P., Mege, D., 2001. Magma flow directions of shallow dykes from the East Greenland volcanic margin inferred from magnetic fabric studies. Tectonophysics 335, 313–329.

Callot, J.P., Guichet, X., 2003. Rock texture and magnetic lineation in dykes: a simple analytical model. Tectonophysics 366, 207–222.

Cañón-Tapia, E., 2004. Anisotropy of magnetic susceptibility of lava flows and dykes: an historical account. In: Martín-Hernández, F., Lüneburg, C.M., Aubourg, C., Jackson, M. (Eds.), Magnetic Fabric: Methods and Applications. Geological Society of London Special Publication 238, 205–225.

Cañón-Tapia, E., Chávez-Álvarez, M.J., 2004. Theoretical aspects of particle movement in flowing magma: implications for the anisotropy of magnetic susceptibility of dykes. In: Martín-Hernández, F., Lüneburg, C.M., Aubourg, C., Jackson, M. (Eds.), Magnetic Fabric: Methods and Applications. Geological Society of London Special Publication 238, 227–249.

Cashman, K.V., Marsh, B.D., 1988. Crystal size distribution (CSD) in rocks and the kinetics and dynamics of crystallization—II: Makaopuhi lava lake. Contributions to Mineralogy and Petrology 99, 292–305.

Chadima, M., Cajz, V., Týcová, P., 2009. On the interpretation of normal and inverse magnetic fabric in dikes: Examples from the Eger Graben, NW Bohemian Massif. Tectonophysics 466, 47–63.

Correa-Gomes, L.C., Souza Filho, C.R., Martins, C.J.F.N., Oliveira, E.P., 2001. Development of symmetrical and asymmetrical fabrics in sheet-like igneous bodies: the role of magma flow and wall-rock displacements in theoretical and natural cases. Journal of Structural Geology 23, 1415–1428.

Cruden, A.R., 1990. Flow and fabric development during the diapiric rise of magma. Journal of Geology 98, 681–698.

Dowty, R., 1980. Crystal growth and nucleation theory and the numerical simulation of igneous crystallization. In: Hargraves R.B. (Eds.), Physics of Magmatic Processes. Princeton University Press, Princeton, New Jersey, 419–485.

Dragoni, M., Lanza, R., Tallarico, A., 1997. Magnetic anisotropy produced by magma flow: theoretical model and experimental data from Ferrar dolerite sills (Antarctica). Geophysical Journal International 128, 230–240.

Ernst, R.E., 1990. Magma flow directions in two mafic Proterozoic dyke swarms of the Canadian Shield: As estimated using anisotropy of magnetic susceptibility data. In: Parker, A.J., Rickwood, P.C., Tucker, D.H. (Eds.), Mafic Dykes and Emplacement Mechanisms. A.A. Balkema, Rotterdam, 231–235.

Ernst, R.E., Baragar, W.R.A., 1992. Evidence from magnetic fabric for the flow pattern of magma in the MacKenzie giant radiating dyke swarm. Nature 356, 511–513.

Ernst, R.E., Duncan, A.R., 1995. Magma flow in the Giant Botswana dyke swarm from analysis of magnetic fabric (abstract). Third International Dyke Conference. Jerusalem, Israel.

Ferguson, C.C., 1979. Rotations of elongate rigid particles in slow non-Newtonian fluids. Tectonophysics 60, 247–262.

Fernandez, A., Feybesse, J.-L., Mezure, J.-F., 1983. Theoretical and experimental study of fabrics developed by different shaped markers in two-dimensional simple shear. Bulletin of the Geological Society of France 25, 319–26.

Gay, N.C., 1966. Orientation of mineral lineation along the flow direction in rocks: a discussion. Tectonophysics 3, 559–564.

Gay, N.C., 1968. The motion of rigid particles embedded in a viscous fluid during pure shear deformation of the fluid. Tectonophysics 5, 81–88.

Geoffroy, L., Callot, J.P., Aubourg, C., Moreira, M., 2002. Divergence between magnetic and plagioclase linear fabrics in dykes: a new approach for defining the flow vector using magnetic foliation. Terra Nova 14, 183–190.

Hastie, W.W., Aubourg, C., Watkeys, M.K., 2011a. When an 'inverse' fabric is not inverse: an integrated AMS-SPO study in MORB-like dykes. Terra Nova 23, 49–55.

Hastie, W.W., Watkeys, M.K., Aubourg, C., 2011b. Significance of magnetic and petrofabric in Karoo-feeder dykes, northern Lebombo. Tectonophysics 513, 96–111.

Henry, B., 1997. The magnetic zone axis: a new element of magnetic fabric for the interpretation of the magnetic lineation. Tectonophysics 271, 325–356.

Hersum, T.G., Marsh, B.D., 2006. Igneous microstructures from kinetic models of crystallization. Journal of Volcanology and Geothermal Research 154, 34–47.

Higgins, M.D., 2000. Measurement of crystal size distributions. American Mineralogist 85, 1105–1116.

Ildefonse, B., Arbaret, L., Diot, H., 1997. Rigid particles in simple shear flow: is their preferred orientation periodic or steady-state? In: Bouchez, J.L., Hutton, D.H.W., Stephens, W.E. (Eds.), Granite: from segregation of melt to emplacement fabrics. Kluwer academic publishers, Dordrecht, l77–185.

Ildefonse, B., Fernandez, A., 1988. Influence of the concentration of rigid markers in a viscous medium on the production of preferred orientations. An experimental contribution, 1. Non-coaxial strain. In: Geological Kinematics and Dynamics (in honor of the 70th birthday of Hans Ramberg). Bulletin of the Geological Institute University Uppsala, 14, 55–60.

Ildefonse, B., Launeau, P., Bouchez, J.L., Fernandez, A., 1992. Effect of mechanical interactions on the development of shape preferred orientation: a two-dimensional experimental approach. Journal of Structural Geology 14, 73–83.

Jezek, J.R., Melka, R., Schulman, K., Venera, Z., 1994. The behavior of rigid triaxial ellipsoidal particles in viscous flows - modeling of fabric evolution in a multiparticle system. Tectonophysics 229, 165–180.

Jourdan, F., Féraud, G., Bertrand, H., Watkeys, M.K., 2007. From flood basalts to the inception of oceanization: Example from the $^{40}Ar/^{39}Ar$ high-resolution picture of the Karoo large igneous province. Geochemistry, Geophysics, Geosystems 8, 1–20.

Kattenhorn, S.A., 1994. Mechanisms of sill and dyke intrusion (unpubl. MSc thesis). University of Natal, Durban, South Africa, 149 pp.

Kirkpatrick, R.J., 1977. Nucleation and growth of plagioclase, Makapuhi and Alae lava lakes, Kilauea Volcano, Hawaii. Geological Society of America Bulletin 88, 78–84.

Kirkpatrick, R.J., Klein, L., Uhlmann, D.R., Hays, J.F., 1979. Rates and processes of crystal growth in the system Anorthite-Albite. Journal of Geophysical Research 84, 3671–3676.

Kissel, C., Laj C., Sigurdsson, H., Guillou, H., 2010. Emplacement of magma in Eastern Iceland dikes: Insights from magnetic fabric and rock magnetic analyses. Journal of Volcanology and Geothermal Research 191, 79–92.

Launeau, P., 2004. Mise en évidence des écoulements magmatiques par analyse d'images 2-D des distributions 3-D d'orientations préferentielles de formes. Bulletin of the Geological Society of France 175, 331–350.

Launeau, P., Archanjo, C.J., Picard, D., Arbaret, L., Robin, P.-Y., 2010. Two- and three-dimensional shape fabric analysis by the intercept method in grey levels. Tectonophysics 492, 230–239.

Launeau, P., Cruden, A.R., 1998. Magmatic fabric acquisition mechanisms in a syenite: Results of a combined anisotropy of magnetic susceptibility and image analysis study. Journal of Geophysical Research 103, 5067–5089.

Launeau, P., Robin, P.-Y.F., 1996. Fabric analysis using the intercept method. Tectonophysics 267, 91–119.

Launeau, P., Robin, P.-Y.F., 2005. Determination of fabric & strain ellipsoids from measured sectional ellipses – Implementation and applications. Journal of Structural Geology 27, 2223–2233.

Marsh, B.D., 1988. Crystal size distributions (CSD) in rocks and the kinetics and dynamics of crystallization, I, Theory. Contributions to Mineralogy and Petrology 99, 277–291.

Marsh, B.D., 1998. On the interpretation of crystal size distributions in magmatic systems. Journal of Petrology 39, 553–599.

Meth, D.L., 1996. The Geology and Geochemistry of the Rooi Rand Dyke Swarm (unpubl. MSc. thesis). University of Natal, Durban, South Africa, 189 pp.

Muncill, G.E., Lasaga, A.C., 1987. Crystal-growth kinetics of plagioclase in igneous systems: One-atmosphere experiments and application of a simplified growth model. American Mineralogist 72, 299–311.

Nicolas, A., Reuber, L. and Benn, K. 1988. A new magma chamber model based on structural studies in the Oman ophiolite. Tectonophysics 151, 87–105.

Pupier, E., Duchene, S., Toplis, M.J., 2008. Experimental quantification of plagioclase crystal size distribution during cooling of a basaltic liquid. Contributions to Mineralogy and Petrology 155, 555–570.

Ramsay, J.G., 1989. Emplacement kinematics of a granite diapir: the Chindamora batholith, Zimbabwe. Journal of Structural Geology 11, 191–209.

Robin, P.-Y.F., 2002. Determination of fabric and strain ellipsoids from measured sectional ellipses – theory. Journal of Structural Geology 24, 531–544.

Romeo, I., Capote, R., Lunar, R., Cayzer N., 2007. Polymineralic orientation analysis of magmatic rocks using Electron Back-Scatter Diffraction: implications for igneous fabric origin and evolution. Tectonophysics 444, 45–62.

Saggerson, E.P., Bristow, J.W., Armstrong, R.A., 1983. The Rooi Rand dyke swarm. South African Journal of Science 79, 365–369.

Watkeys, M.K., 2002. Development of the Lebombo rifted volcanic margin of southeast Africa. In: Menzies, M.A., Klemperer, S.L., Ebinger, C.J., Baker, J. (Eds.), Volcanic Rifted Margins. Geological Society of America Special Paper 362, 27–46.

Willis, D.G., 1977. A kinematic model of preferred orientation. Geological Society of America Bulletin 88, 883–894.

5.11. Supplementary Data

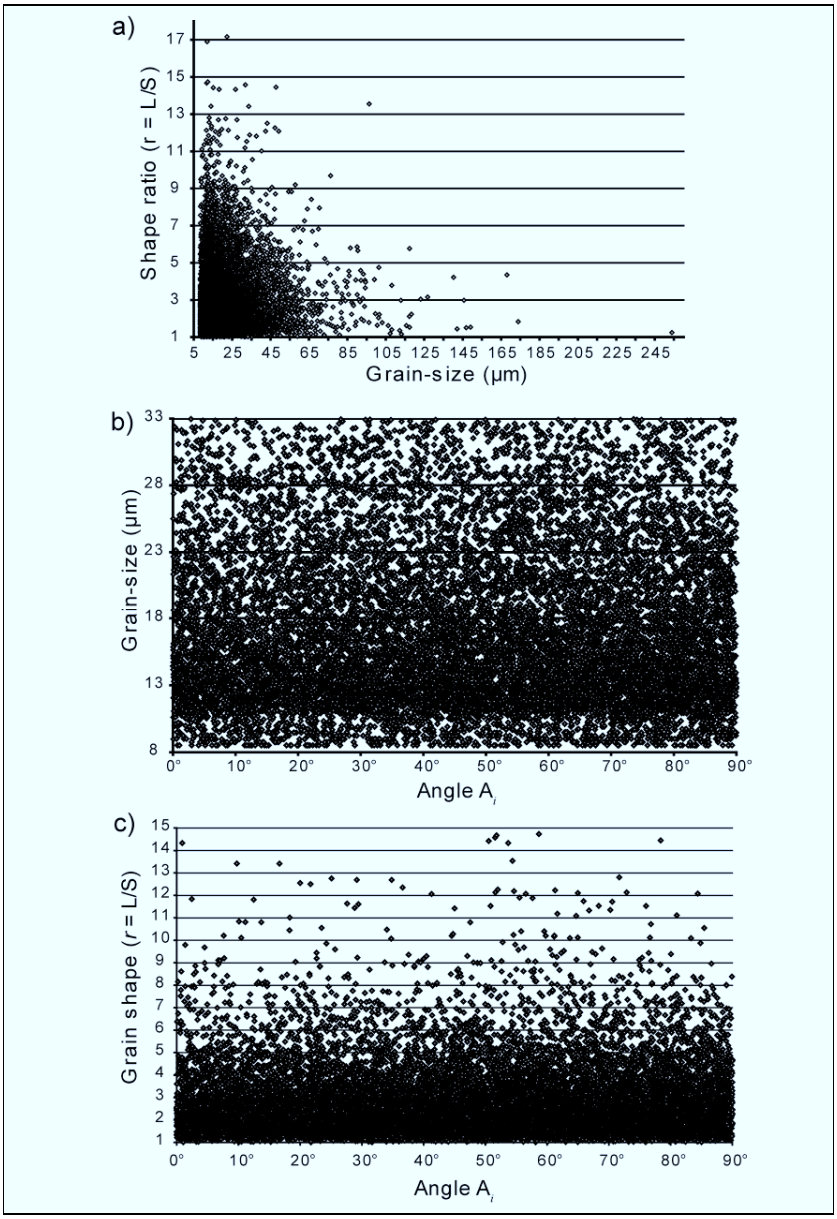

Figure 5.10: (*supplementary data*) (**a**) Plot of grain-size vs. shape showing a lack of correlation between the two parameters. Large grains (> 55 µm) do, however, appear to be less anisotropic than the smaller grains, (**b**) Plot of grain-size vs. angle A_i, again showing a lack of correlation and (**c**) Grain-shape vs. A_i.

- Chapter 6 -

Tectonophysics 513 (2011) 96–111

Contents lists available at SciVerse ScienceDirect

Tectonophysics

journal homepage: www.elsevier.com/locate/tecto

Significance of magnetic and petrofabric in Karoo-feeder dykes, northern Lebombo

Warwick W. Hastie [a,*], Michael K. Watkeys [a], Charles Aubourg [b]

[a] School of Geological Sciences, Building H1, University of KwaZulu-Natal, University Road, Westville, Durban 4001, South Africa
[b] Laboratoire des Fluides Complexes et Réservoirs, UMR 5150, CNRS, TOTAL, Université de Pau et des Pays de l'Adour, Avenue de l'Université BP 1155, 64013 Pau Cedex, France

Abstract:

The orientation of magnetic and petrofabric in 14 mafic dykes of the Northern Lebombo dyke swarm (NLDS) has been determined using the anisotropy of magnetic susceptibility (AMS) and mineral shape preferred orientation (SPO) in order to constrain the magma flow direction during dyke emplacement. The N-S striking NLDS intruded the N-S trending; 700 km long Lebombo faulted monocline between 182 and 178 Ma. The Lebombo faulted monocline, which forms the eastern-most sub-province of the Karoo large igneous province (LIP), is essentially a volcanic rifted margin with a protracted magmatic and tectonic history related to the break-up of southern Gondwana. It also forms the southern limb of the Karoo triple-rift system which has been hypothesised to have formed by a mantle plume centred on the triple junction locus. The other two arms of the rift which converge on the triple junction are the WNW trending Okavango dyke swarm (ODS) and NE trending Save-Limpopo dyke swarm (SLDS). In the NLDS it is found that the magnetic fabric, which is of magmatic origin in ~50% of the samples, is carried predominantly by stoichiometric magnetite. There is remarkable agreement between the orientations of the AMS and SPO fabrics and at least two dykes show coaxial AMS and mineral SPO fabric consistent with lateral magma flow from the north. This direction is supported by the imbrication of the foliations of the well-defined bulk AMS and plagioclase SPO fabric when viewed in a dyke co-ordinate system. Although steeply plunging maximum axes occur in the SPO fabric, their possible use as magma flow vectors is questioned because they do not necessarily mimic the elongation of plagioclase grains visible in orientated thin sections. The magnetic and petrofabric of the NLDS is interpreted to have developed during lateral magma flow from the locus of the Karoo triple junction.

6.1. Introduction

6.1.1. The Karoo Large Igneous Province

Dykes of the northern Lebombo in northeast South Africa have been directly linked to basaltic volcanism of the Karoo large igneous province (LIP) along the Lebombo faulted monocline (Watkeys, 2002; Jourdan et al., 2005; Klausen, 2009). The ~182 Ma old Karoo LIP comprises predominantly continental flood basalts (CFBs) which cover an area of 3×10^6 km^2 in southern Africa (Erlank, 1984). It is contiguous with the Ferrar Province in Antarctica and is associated with precursory extension in the opening of the Indian Ocean as Antarctica split from a position along the eastern edge of southern Africa during the break-up of southern Gondwana (Encarnación et al., 1996; Watkeys, 2002).

It is along this eastern margin that the Lebombo faulted monocline is found. The Lebombo faulted monocline is a linear volcanic margin which extends southwards from south-central Zimbabwe and comprises an east-west (E-W) highly extended terrane characteristic of a volcanic rifted margin (Bristow, 1982; Watkeys, 2002; Klausen, 2009). The Lebombo faulted monocline forms the southern limb of the Karoo triple junction, (Figure 6.1a). The west-northwest (WNW) trending limb comprises the Okavango dyke swarm (ODS) while the east-northeast (ENE) trending limb comprises the Save-Limpopo dyke swarm (SLDS). Dykes of the Lebombo faulted monocline include the Northern Lebombo dyke swarm (NLDS) and the Rooi Rand dyke swarm (RRDS) (Figure 6.1a) (Armstrong et al., 1984; Watkeys, 2002; Jourdan et al., 2004; Jourdan et al., 2007; Klausen, 2009).

The structural and petrological components of the Karoo LIP have been studied in some detail for the last 70 years in order to determine its origin, timing, duration and significance with regard to Gondwana break-up (Du Toit, 1929; Cox et al., 1967; Bristow, 1982; Erlank, 1984; Cox, 1992; Watkeys, 2002; Jourdan et al., 2005; Jourdan et al., 2007; Klausen, 2009). In more recent studies there has been a focus on the dykes associated with the Karoo LIP, particularly the dyke swarms which centre on Mwenezi (formerly Nuanetsi) in south-central Zimbabwe. These dyke swarms have provided significant structural, geochronological and geochemical information regarding the

evolution of the Karoo LIP (Reeves, 1978; Bristow, 1984; Cox, 1989; Le Gall et al., 2002; Jourdan et al., 2004; Le Gall et al., 2005; Jourdan et al., 2006).

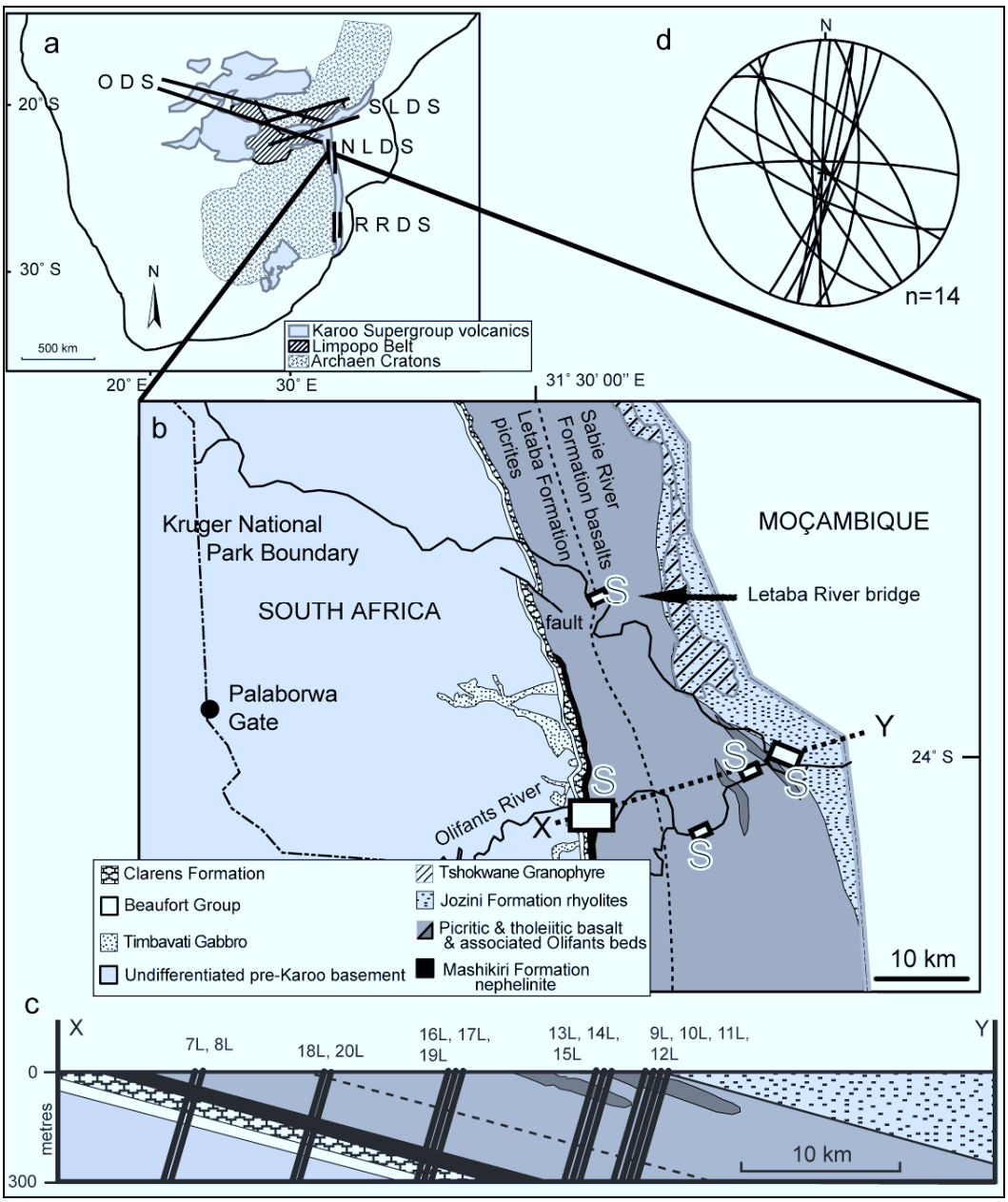

Figure 6.1: (**a**) Schematic map of southern Africa showing the Karoo large igneous province (pale grey) and associated dyke swarms (ODS = Okavango dyke swarm; SLDS = Save-Limpopo dyke swarm; NLDS = Northern Lebombo dyke swarm; RRDS = Rooi Rand dyke swarm) which are bounded by Archaean terranes (after Jourdan et al., 2004) (**b**) Map showing the geology of the northern Lebombo and the sampled regions (marked with "S") of the NLDS in northeast South Africa and the line of section (XY) is marked (modified from Bristow, 1982 and 1984) (**c**) Simplified cross-section XY showing the position of the sampled dykes of the NLDS (modified from Bristow, 1982 and Watkeys, 2002) (**d**) Stereographic projection of the average dyke planes of the 14 sampled dykes from this study.

It is within the context of the Karoo triple junction that this study has been undertaken; in order to find the original flow direction of magma in dykes of the NLDS by measuring and interpreting fabrics pictured using the anisotropy of magnetic susceptibility (AMS) and mineral shape preferred orientation (SPO).

These methods are used because (1) the investigated dykes display no macroscopic evidence of magma flow, (2) AMS measures a large number of grains (>10^6) rapidly and non-destructively and (3) both methods are sensitive to microscopic, weakly anisotropic fabrics. The careful interpretation of AMS fabrics and comparative fabric analysis (mineral SPO) provides a quantitative and reliable picture of the magma flow sense in dykes on a regional scale (Ernst and Baragar, 1992; Ernst and Duncan, 1995; Callot et al., 2001; Aubourg et al., 2008; Kissel et al., 2010). Thus, the need to present an analysis of the 3-dimensional (3D) shape, orientation and intensity of, particularly, the plagioclase petrofabric (additionally to AMS) is emphasised.

Although the measurement and interpretation of data acquired using AMS and mineral SPO can be problematic due to various potential complications (Hastie et al., 2011) its application in regional studies of dyke swarms has already provided significant results within the Karoo LIP. In the ODS, for example, Aubourg et al. (2008) have shown that near-vertical magma flow occurred close to the Karoo triple junction while sub-horizontal flow is in evidence ~400 km west of the triple junction. In addition, a recent study of the southernmost dykes of the Lebombo monocline (the RRDS) indicates that the magnetic fabric and silicate petrofabric are not necessarily coaxial (Hastie et al., 2011).

6.1.2. The Karoo Triple Junction

On the broadest scale, the picture of magma flow within dyke swarms can provide evidence of a potential magma source; as has been shown in East Greenland (Callot et al., 2001) and the ODS for example (Ernst and Duncan, 1995; Aubourg et al., 2008). The origin of the Karoo LIP remains controversial, however, as much evidence has been presented for and against a mantle plume model which originated mainly as a result of

the geometry of the Karoo triple junction (Burke and Dewey, 1973; Campbell and Griffiths, 1990) and the concentrically arranged and compositionally zoned primitive nephelinites and picrites centred on the triple junction (Bristow, 1984; Cox, 1992; White, 1997). There has, therefore, been considerable interest in the ODS, the SLDS and the NLDS (and RRDS) which comprise the main arms of the triple junction (Reeves, 1978; Armstrong et al., 1984; Duncan et al., 1990; Ernst and Duncan, 1995; Reeves, 2000; Watkeys, 2002; Jourdan et al., 2004; Le Gall et al., 2005; Jourdan et al., 2006; Aubourg et al., 2008; Klausen, 2009).

Campbell and Griffiths (1990) suggest that the concentrically arranged, primitive volcanic rocks centred on the triple junction resulted from the relatively "hotter" plume axis which, while ascending, did not interact with the surrounding mantle and/or lithosphere, although this has been disputed by Sm-Nd isotopic studies which suggest otherwise (Ellam and Cox, 1991). Indeed, the mafic Karoo magmas are dominantly tholeiitic in composition (Hawkesworth et al., 1999) and have distinct incompatible trace element geochemistry due to their distribution over either Archaean cratonic terranes (high Ti-Zr) or younger basement (low Ti-Zr) (Sweeney and Watkeys, 1990; Sweeney et al., 1994). This difference is attributed to a contrast in melting, resulting in 30-40% of the incompatible elements in the high Ti-Zr basalts being derived from the lithospheric mantle. However, Sweeney et al. (1994) suggest that more evolved high-Fe basalts in the central region of the Lebombo are compositionally consistent with mantle plume melting.

With regard to the dyke swarms, however, it has been more recently shown that there is clear evidence for the structural inheritance of pre-existing (Proterozoic) fracture and dyke directions in the ODS and SLDS (Le Gall et al., 2002; Le Gall et al., 2005; Jourdan et al., 2006). These authors showed that 87% of the dykes in the ODS are Karoo in age (179±1.2–178.4±1.1 Ma) whilst the remainder are Proterozoic. The structure of the ODS is therefore unlikely to be unique to the Karoo-age dykes, but must pre-date the formation of the triple junction. The geochronology, however, shows that the Karoo-aged dykes of the ODS post-date the volumetric bulk of the flood volcanism by at least 3 Ma (Jourdan et al., 2005). The ENE-trending, 50–100 km wide SLDS extends for 600 km from SE

Botswana to the margins of the Limpopo Belt (Figure 6.1a) where it overlaps with the ODS (Jourdan et al., 2006). Although Karoo ages are indicated for the SLDS (180.4±0.7–178.9±0.8 Ma) (Le Gall et al., 2002; Jourdan et al., 2005), Proterozoic ages have been found in 14 dykes (728±3–1683±18 Ma) which, similarly to the ODS, implicates the role of inheritance of older structures when Karoo-age magmatism began (Jourdan et al., 2006).

It has been shown that the dyke swarms of the Karoo triple junction did not form as part of a singular volcanic feeder system, as the ODS (see ages above) and the RRDS (173.9±0.7 Ma), post-date the main Karoo volcanic event. Furthermore, high-resolution $^{40}Ar/^{39}Ar$ radiometric dating indicates that the duration of Karoo magmatism was ~8 Ma, compared to the more typical 1–2 Ma duration determined for other flood basalt provinces (Jourdan et al., 2005). The south-to-north migration of magmatism evident in the Karoo LIP would also require very rapid migration of the crust over the head of a mantle plume (Le Gall et al., 2002; Jourdan et al., 2007). It seems in general, therefore, that a classical model of rapid and short-lived magmatism driven by an active plume in the genesis of the Karoo LIP is unlikely (Uken and Watkeys, 1997; Jourdan et al., 2004; Jourdan et al., 2006).

In a passive heating model, the development of the Karoo LIP may have started simply due to a lack of cooling related to the incubation of the mantle beneath, rather than active heating by a plume. Anderson et al. (1992) suggest that crustal thinning above non-isothermal, inhomogeneous mantle is responsible for the formation of volcanic ridges and hotspots. Evidently the accumulation and/or generation of heat and subsequent magmatism beneath the supercontinent of Gondwana would have weakened the crust, making continental break-up more likely as opposed to being a direct result of the emplacement of a plume beneath the supercontinent (Storey et al., 1992; White, 1997; Hawkesworth et al., 1999). Further geochemical and structural evidence for passive processes in the Karoo LIP include (1) the Nb-anomaly in the volcanic rocks of the Karoo LIP which is typical of subduction related volcanism (Cox, 1992) and (2) the linear extent of the contemporaneous Ferrar Province in Antarctica which is most likely

beyond the reach of a plume and (3) the siliceous, high-field-strength-element-depleted signature of the Ferrar Province resulting from sedimentary contamination of the mantle source. This is most likely a subduction related process (Hergt et al., 1991; Cox, 1992; Encarnación et al., 1996).

Resolving the active or passive role played by plumes and/or subduction or other processes in the development of CFBs is critical for understanding these large-scale magmatic events. It has been shown that the relative timing of intrusive and eruptive events can be resolved (e.g. Jourdan et al., 2007) and it is within this context that evidence for the regional magma flow direction in the NLDS is presented. The regional pattern of magma flow in the NLDS is therefore potentially significant with respect to magmatism in this region.

6.2. Geological Background

6.2.1. The Lebombo Faulted Monocline

The Lebombo faulted monocline is a 700 km long, N-S trending volcanic rifted-margin which is exposed along the eastern margin of South Africa (Watkeys, 2002, Klausen, 2009). The broad volcanic stratigraphy of the Lebombo faulted monocline comprises the Mashikiri Formation (nephelinites); overlain by the picritic and tholeiitic basalts of the Letaba and Sabie River Formations respectively and finally the Jozini Formation (rhyolites and associated granophyres) (Bristow, 1984; Erlank, 1984; Watkeys 2002). These formations, which collectively form the Lebombo Group, overly older Archaean basement, the Proterozoic Timbavati gabbro and sedimentary rocks of the Mesozoic Clarens Formation and Beaufort Group (Figure 6.1b). Intruding the lowermost units and the basalts themselves are mafic feeder dykes and composite felsic and mafic dykes, all of which comprise the NLDS (Watkeys 2002; Klausen 2009). Magmatism appears to have been preferentially channeled in the Lebombo faulted monocline in the form of the N-S striking NLDS as the dykes are sparsely distributed to the west and north. This is probably because of the position of the Lebombo faulted monocline at the eastern edge of the Kaapvaal craton (Figure 6.1a) (Jourdan et al., 2006; Klausen, 2009).

The monoclinal structure of the Lebombo which characterises its geometry was caused by coast parallel (N-S) faulting during the initial stages of Gondwana break-up along what is now the east coast of South Africa (Watkeys, 2002). This faulting has resulted in the eastward dip of the sedimentary rocks and overlying volcanic successions (Figure 6.1c), indicative of a volcanic rifted margin rather than a classic monocline (Klausen, 2009). It is evident from the predominantly westward dip of the northern Lebombo dykes that they intruded prior to the fault-induced eastward tilting of the Lebombo which began within ±1 Ma of the bulk of the magmatism (~182 Ma) (Riley et al., 2004; Jourdan et al., 2007; Klausen, 2009). There is currently no evidence for structural inheritance (*viz.* ODS, SLDS) in the emplacement history of the NLDS (Jourdan et al., 2006).

6.2.2. The Northern Lebombo Dyke Swarm

Klausen (2009) has tentatively associated 4 generations of dykes with overlying volcanic successions as follows, based on composition and field relationships: dark grey coloured plagioclase-phyric dolerite dykes (D1 generation) which are feeders to the overlying Sabie River Formation basalts; paler D2 dykes which texturally resemble the uppermost amygdaloidal basalts of the Sabie River Formation; a small volume of thin dykes with irregular margins (D3 generation) which are feeders to rhyodacitic units of the Jozini Formation and finally D4 dykes which do not appear to be associated with any volcanics. Dyke generations D1-D3 have consistent N-S strikes, while D4 dykes tend to strike NW-SE. The D1-D3 dykes fed the bulk of the basaltic magmatism during the development of the Lebombo and the D4 dykes intruded concomitantly with the emplacement of the ODS at ~178 Ma (Klausen, 2009).

The main dyking activity in the NLDS therefore most likely pre-dates 178 Ma as the dyke ages are comparable to that of the volcanic rocks within a restricted range, as mentioned previously (Jourdan et al., 2005, 2007). For example, radiometric dating of a D4 dyke (SA-30 of Jourdan et al., 2007 and 9L of this study, see Table 6.1) yielded an age of 178±1 Ma – providing essentially a maximum time interval of 4 Ma (182–178 Ma) during which all the successive dyke generations intruded. In a qualitative sense this is also evident in the field because the volcanic successions which the dykes feed are

conformable and the consistent dip of the dykes (~80° to the west) suggests syn- to post-intrusion tilting of the Lebombo faulted monocline.

6.3. Methodology

6.3.1. Sampling

Five regions were sampled for this study, extending from the Olifants River in the south to the Letaba River Bridge in the north (Figure 6.1b). A total of 224 samples were collected from 14 dykes, as shown in Table 6.1. Each dyke comprises 2 sites (i.e. each margin is 1 sampling site). Note that the data are arranged from the oldest dykes (D1) to youngest (D4) and those with unknown affiliation. Most of the dykes, except 13L, dip steeply (>80°) and strike N-S to NW-SE and E-W (7L) as shown in Table 6.1 and Figure 6.1d. The dykes are well exposed in the field, particularly along the Olifants River where multiple dykes can be seen intruding the host basaltic rocks (Figure 6.2a) and individual dykes may be traced for tens of metres along their length. Field relationships between the dykes and the volcanic rocks are quite clear as, for example, in the Letaba River Bridge section (Figure 6.2b) where picrite basalts are intruded by D3 dykes.

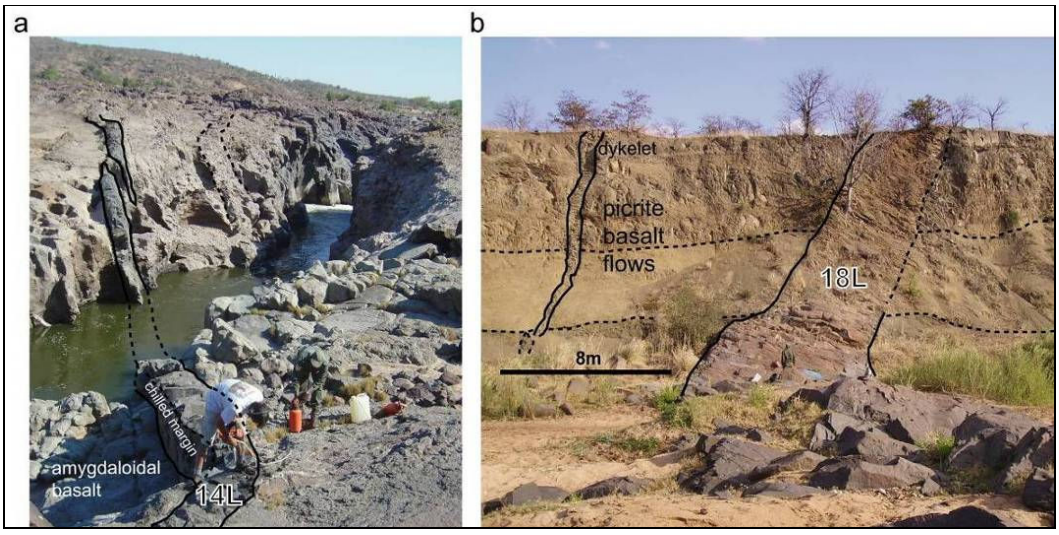

Figure 6.2: Annotated photographs of two field exposures in the sampled region of the NLDS showing (**a**) dyke 14L exposed along the Olifants River and (**b**) dyke 18L exposed along the Letaba River. The direction of view for both photographs is southwards. Dykes are generally well exposed and multiple dykes can be seen in most exposures, although sheeted dykes are uncommon. As is shown in the photographs, dyke 14L (D2) is hosted by amygdaloidal basalts of the Sabie River Formation while the east-dipping dyke 18L (D3) is hosted by older picrite basalts of the Letaba Formation in this exposure.

Table 6.1: Dyke and AMS data for the NLDS. Note that the dykes are shown in order of relative age, from D1 to D4 and opposing margins are discriminated.

Dyke	*Margin*	*Thickness*	*Orientation (dip & strike)*	*Lat. / Long.*	[a]*n*	[b]Km *(10^{-3} SI)*	*K1*	*K2*	*K3*	[c]*P′ [10^{-3} ([d]sd)]*	[e]*T [10^{-3} (sd)]*
19L (D1)	WEST	3m	88°/182°	24°03'30.5" S	9	59.76	30°/343°	35°/096°	41°/223°	1.034(13)	-0.196(34)
	EAST			31°42'41.2" E	8	48.36	05°/010°	19°/102°	71°/267°	1.016(6)	-0.145(38)
16L (D2)	WEST	28m	80°/150°	24°03'02.0" S	8	68.77	02°/145°	19°/054°	71°/240°	1.019(2)	-0.212(49)
	EAST			31°43'53.3" E	8	52.78	15°/322°	67°/193°	17°/057°	1.039(6)	0.532(33)
14L (D2)	WEST	2.3m	88°/192°	24°00'01.3" S	8	84.30	04°/184°	53°/088°	36°/277°	1.020(5)	0.185(37)
	EAST			31°45'07.9" E	8	69.75	02°/308°	05°/218°	85°/057°	1.021(4)	0.040(34)
20L (D3)	WEST	3.5m	82°/178°	23°48'47.2" S	8	64.39	39°/341°	20°/089°	44°/200°	1.018(5)	-0.242(27)
	EAST			31°34'57.1" E	8	64.75	09°/096°	39°/358°	49°/196°	1.054(27)	-0.372(30)
18L (D3)	WEST	7.5m	82°/018°	23°48'48.7" S	8	74.74	20°/123°	37°/017°	47°/253°	1.023(9)	0.149(46)
	EAST			31°34'52.4" E	8	75.41	25°/296°	26°/039°	52°/168°	1.014(5)	-0.284(32)
8L (D4)	WEST	3.5m	85°/183°	24°02'14.0" S	8	20.65	85°/001°	02°/118°	04°/208°	1.050(14)	-0.378(17)
	EAST			31°34'28.8" E	9	31.31	76°/244°	10°/017°	10°/109°	1.050(32)	-0.262(46)
†9L (D4)	WEST	16.8m	88°/325°	23°58'31.0" S	8	28.41	81°/339°	09°/153°	01°/243°	1.029(11)	0.172(49)
	EAST			31°47'37.0" E	8	20.12	71°/321°	19°/145°	01°/055°	1.035(10)	0.197(39)
12L (D4)	WEST	10m	90°/120°	23°58'39.1" S	6	65.22	44°/006°	44°/167°	10°/267°	1.045(6)	0.301(40)
	EAST			31°47'51.5" E	6	53.09	17°/321°	66°/096°	16°/226°	1.027(5)	0.027(26)
13L (D4)	WEST	5.5m	56°/155°	24°00'01.3" S	11	28.11	39°/065°	44°/207°	20°/318°	1.012(5)	-0.234(35)
	EAST			31°45'07.9" E	7	36.91	21°/174°	06°/266°	68°/012°	1.022(5)	-0.188(24)
17L (D4)	WEST	5.2m	82°/168°	24°03'02.2" S	8	81.12	22°/159°	64°/306°	13°/064°	1.022(12)	0.192(36)
	EAST			31°43'52.3" E	8	98.16	12°/183°	68°/303°	19°/089°	1.034(19)	0.421(33)
7L	NORTH	0.55m	83°/271°	24°02'20.1" S	12	5.45	50°/351°	34°/134°	19°/237°	1.032(20)	0.125(42)
	SOUTH			31°34'35.5" E	8	3.26	68°/103°	03°/006°	22°/275°	1.029(19)	0.081(24)
10L	WEST	2m	85°/025°	23°58'39.6" S	8	51.07	55°/204°	35°/031°	03°/299°	1.025(9)	0.267(43)
	EAST			31°47'53.2" E	8	63.23	51°/222°	38°/028°	07°/123°	1.021(8)	0.377(46)
15L	WEST	0.6m	82°/192°	24°00'01.3" S	5	107.53	12°/191°	70°/316°	16°/097°	1.020(10)	0.027(46)
	EAST			31°45'06.3" E	6	90.77	26°/085°	04°/353°	64°/254°	1.023(7)	0.070(20)
11L	WEST	2m	86°/012°	23°58'39.6" S	8	48.69	02°/026°	87°/243°	02°/116°	1.010(3)	0.119(48)
	EAST			31°47'53.2" E	9	35.31	15°/201°	68°/333°	16°/107°	1.013(8)	0.107(29)

[a]*n* =number of specimens

[b]*Km* = (*K1* + *K2* + *K3*)/3

[c]*P′* = degree of anisotropy (Jelinek, 1981)

[d]*sd* = standard deviation

[e]*T* = shape factor (oblate/prolate) (Jelinek, 1981)

† = dyke SA-30 of Jourdan et al., 2007 (178±1 Ma)

Dyke widths are quite variable, from 0.5 m to 10 m, although the D4 dykes tend to be >5m in thickness, with regular margins. The dyke margins are generally well exposed, and as such between 6 and 12 standard cylindrical specimens (22 mm × 25 mm) were collected from opposing margins of an intrusion (Tauxe et al., 1998) using a hand-held petroleum powered drill. Each sample was orientated in the field using a core-orientator with a magnetic compass as there was no noticeable magnetic deviation caused by the dykes.

6.3.2. Anisotropy of Magnetic Susceptibility

Measuring the anisotropy of magnetic susceptibility (AMS) has become a standard tool for the analysis of rock fabrics, notably due to its ability to characterise potentially flow related fabrics in extrusive (e.g. pyroclastics and flows) and intrusive (e.g. dykes and sills) volcanic rocks (Khan, 1962; Ellwood, 1978; Knight and Walker, 1988; Rochette et al., 1991; Tarling and Hrouda, 1993; Poland et al., 2004; Aubourg et al., 2008; Kissel et al., 2010). The source of susceptibility in mafic igneous rocks is typically Fe-bearing minerals such as magnetite and titanomagnetite which may in multi-domain state (MD), pseudo-single domain state (PSD) or single-domain state (SD) (Rochette et al., 1999). The anisotropy of magnetic susceptibility can be shape-controlled (shape anisotropy) for MD grains, as opposed to magneto-crystalline anisotropy found in hematite or pyrrhotite. It may also be controlled by the distribution of magnetic grains (distribution anisotropy, Hargraves et al., 1991) and/or a mixed contribution from a number of susceptible constituent minerals (Borradaile and Gauthier, 2003).

The anisotropy is represented by an ellipsoid of a second order tensor, which is shown stereographically using the three principal susceptibility axes; $K1 > K2 > K3$. For ferromagnetic, MD grains the $K1$ axis is parallel to the long axis of the grain and the $K3$ axis parallel to the short axis. In SD grains these axes may be inverted, resulting in inverse fabric (Potter and Stephenson, 1988; Rochette et al., 1991; Tarling and Hrouda, 1993; Rochette et al., 1999). This is referred to as type-B fabric in this study (Archanjo and Launeau, 2004). This type-B fabric may also originate from a late-stage process

unrelated to the original magma flow direction such that the petrofabric is not necessarily mimicked by AMS, as is the case in the RRDS (Hastie et al., 2011).

Scalar data are also obtained from AMS studies, including the bulk susceptibility (K_m), the corrected degree of anisotropy (P') and the shape parameter (T) (Jelinek 1981). In this study samples were analysed using an AGICO Kappabridge KLY-3 magnetic anisotropy spinner according to the standard 15 position procedure of Jelinek (1978). Recorded data of the principle orientations of the AMS tensor are plotted as lower hemisphere equal area projections in geographic co-ordinates, unless otherwise indicated.

Early AMS studies of flow-related fabrics showed that when a silicate fabric records the flow direction of magma during dyke emplacement – and the magnetic fabric is mimetic – then measuring AMS provides a proxy of the flow fabric. Such fabric is generally termed "normal" because $K1$ is parallel to the long axis of anisotropic grains (Ellwood, 1978; Knight and Walker, 1988; Rochette et al., 1999). This will be termed type-A fabric (Archanjo and Launeau, 2004; Hastie et al., 2011). At the dyke scale, type-A fabric is characterised by the $K1$ axis and the magnetic foliation (to which $K3$ is a pole) being sub-parallel to the magmatic foliation developed from the alignment of mineral grains along the dyke wall. In most studies, the $K1$ axis direction has been used as the magma flow vector, based on the assumption that the long axis of anisotropic grains will be aligned to the direction of magma flow (Ellwood, 1978; Knight and Walker, 1988; Poland et al., 2004; Porreca et al., 2006; Raposo et al., 2007; Soriano et al., 2008; Cañón-Tapia and Herrero-Bervera, 2009; Chadima et al., 2009; Kissel et al., 2010). To find the sense of direction of the magma flow, AMS ellipsoids are usually determined from opposing margins of an intrusion (Figure 6.3) in order to find if the fabric is imbricated relative to the intrusion plane (Aubourg et al., 2002; Geoffroy et al., 2002). Geoffroy et al. (2002) proposed a method for using the imbrication of the magnetic foliation to find the magma flow direction. This is because it has been demonstrated that $K1$ orientations may be parallel to intersection lineations which are entirely unrelated to the magmatic lineation, especially in oblate fabrics ($T > 0$) (Henry, 1997; Launeau and Cruden, 1998; Callot and Guichet, 2003). It is therefore unwise to rely exclusively on the orientation and/or

imbrication of the *K*1 axes, but rather the imbrication of foliations, which are calculated from the *K*3 axes (poles to the foliation) (Figure 6.3).

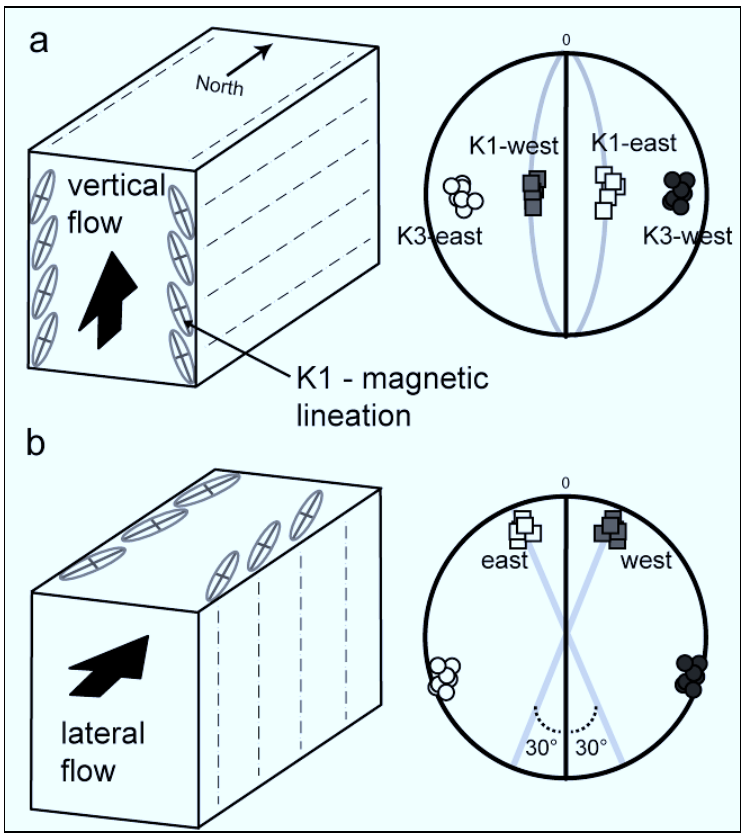

Figure 6.3: Schematic diagrams of a vertical, north-south striking dyke indicating idealised fabric orientation resulting from (**a**) vertical intrusion of magma and the resultant AMS ellipsoid and (**b**) a lateral intrusion of magma and the resultant AMS ellipsoid. The dyke is shown as a north-south black line in the projections, the foliations in grey. Intermediate axes (*K*2) not shown for clarity. Not to scale (modified from Geoffroy et al., 2002 and Gil-Imaz et al., 2006).

6.3.3. Mineral Shape Preferred Orientation

In this study a detailed 3D study of mineral SPO as defined, particularly, by plagioclase in 7 dykes of the NLDS (19L, 16L, 18L, 9L, 17L, 10L, and 15L) is presented. Measuring the 2D ellipse of the mineral fabric and the 3D ellipsoid is achieved using SPO-2003 and Ellipsoid-2003 software packages respectively (Launeau, 2004; Launeau and Robin, 2005). This image analysis software determines grain orientations and fabric intensities on images taken from orientated thin-sections cut from standard AMS cores. An arbitrary *XYZ* co-ordinate system is used (Figure 6.4a) to define the orientations of the sections,

which are digitally filtered to leave only plagioclase in black and white Bitmap images (Figure 6.4b) (see Hastie et al., 2011 – Chapter 4).

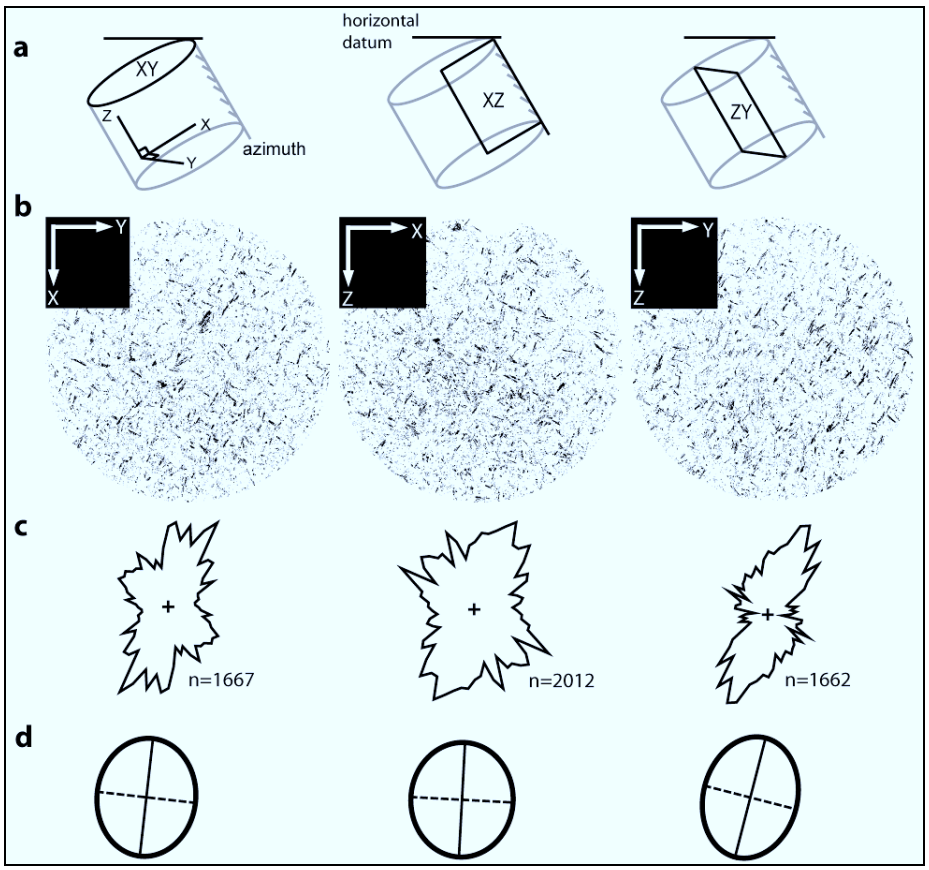

Figure 6.4: Schematic illustration of the methodology employed for studying mineral SPO showing (**a**) the *XYZ* co-ordinate system as applied to a single drill-core sample (17L3) for defining the orientation of the thin-sections (**b**) the *XY*, *XZ* and *ZY* sections of the sample. Circular sections are used in order to reduce any edge effects such as grain-size or orientation distortion (**c**) rose diagrams of grain directions and number of grains (n) determined for each thin-section and (**d**) 2D inertia tensors determined for the same sections (minor axis = dashed line).

The 2D inertia tensors, which are required for finding the 3D ellipsoid, are calculated by indexing grain orientations according to a rose of directions for each section of one sample (Figure 6.4c, d) (Launeau and Robin, 1996; Launeau, 2004; Launeau and Robin, 2005; Launeau et al., 2010). The sensitivity of the SPO program to grain size is essentially dependent on the magnification at which photomicrographs are taken; thus

grains >10 μm could be reliably imaged at a magnification of 20× and the width of the images was consistently kept at 9 mm.

The Ellipsoid-2003 software in particular provides a measure of scalar parameters (*P'* and *T*) as in the case of AMS. Importantly, an incompatibility index ($\sqrt{F}$) provides a measure of the potential misfit between 2D ellipses and the ellipsoid (Launeau and Robin, 2005). A total of 6 thin-sections per margin were analysed for the 7 dykes mentioned above. The nomenclature of the AMS axes *K*1, *K*2 and *K*3 will be termed *L*1, *L*2 and *L*3 respectively for SPO data although the axes symbols remain the same. The calculation of statistical confidence regions for mean SPO principal axes is generally achieved using standard deviations (Launeau and Robin, 2005). However, because it is necessary to compare SPO data to AMS; in which mean principal axes are calculated using the bootstrap method (Tauxe et al., 1998), it is preferred that only the accuracy of the fit of the sectional ellipses to the ellipsoid is constrained. This is achieved using the incompatibility index $\sqrt{F}$ as there is no provision for summation of tensors for each individual SPO sample. Similarly to AMS, it is the orientation and imbrication of the foliations (to which *L*3 is a pole) which is relied upon for magma flow direction determination.

6.4. Results

6.4.1. Petrography

A total of 168 photomicrographs taken from 84 thin-sections were analysed from 7 dykes representing the orientation of thousands of minerals (2×10^5 plagioclase grains and 6×10^4 opaque grains). The thin-sections are dominated by plagioclase and clinopyroxene and contain between 3 and 8% opaque grains. There are, however, some petrographic differences between the dykes which are worth noting. For example, the D1 and D2 dykes appear to have suffered minor alteration; chlorite "patches" are evident, and the plagioclase groundmass and occasional phenocrysts are cloudy with irregular and diffuse grain boundaries (Figure 6.5a, b). The opaque grains vary from small (< 10 μm), equant grains to elongate, acicular and occasionally skeletal in appearance. Dyke 18L (D3) is even-grained, containing abundant elongate and (sub-) equant opaque grains and

relatively fresh, coarse-grained plagioclases (Figure 6.5c). Clinopyroxene is essentially anhedral in all the samples. The youngest dykes (D4) contain anhedral clinopyroxene, ~1% free quartz and > 5% opaque grains which are skeletal to acicular in shape. These dykes tend to be medium- to coarse-grained and contain large plagioclase phenocrysts (Figure 6.5d).

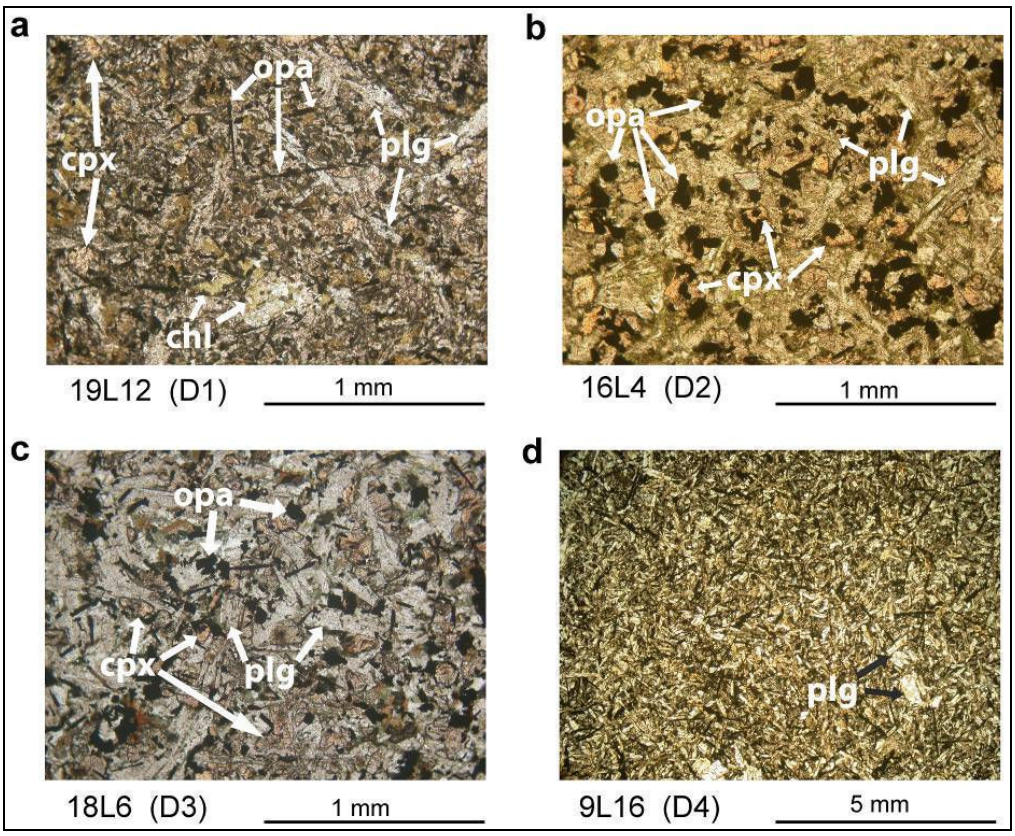

Figure 6.5: Selected thin-section photomicrographs taken under plane-polarised light representing the dyke generations D1 (**a**), D2 (**b**), D3 (**c**) and D4 (**d**). The sample names are indicated beneath each example. Note that the relatively oldest dyke examples (D1 and D2) show patches of chlorite (chl), anhedral clinopyroxene (cpx) and abundant opaque (opa) grains. Plagioclase (plg) in (**a**) and (**b**) are somewhat cloudy in appearance, in contrast to those of (**c**) and (**d**). The D2 dykes lack the acicular opaque grains evident in the other examples. The silicate matrix (plg and cpx) of (**c**) and (**d**) is evidently more coarse-grained than (**a**) and (**b**). The opaque grains of (**d**) are almost exclusively acicular.

6.4.2. Rock Magnetism and Bulk Susceptibility

Thermomagnetic curves which quantify the decay of magnetisation at saturation and magnetic susceptibility (K_m) can be used to infer the unblocking temperature and Curie

temperature (T_c) of the magnetic minerals in a sample respectively. The magnetic mineralogy of samples of the NLDS is revealed by representative thermomagnetic curves in the temperature range 24–700°C. The results of monitoring the magnetic susceptibility with increasing temperature under an argon atmosphere indicate that, for dykes 14L, 9L and 12L (Figure 6.6a-c), the non-reversible curves are most consistent with stoichiometric magnetite with T_c values of 587°C, 556°C and 548°C respectively.

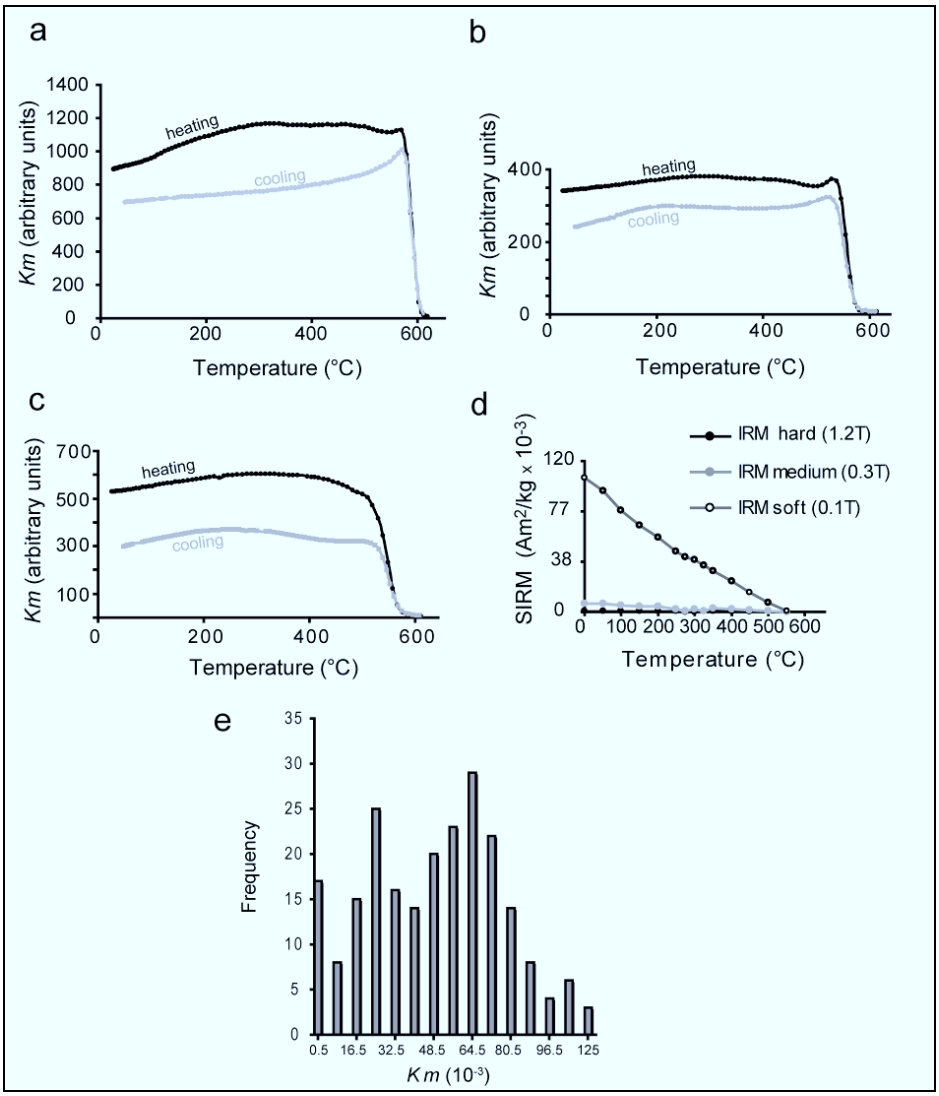

Figure 6.6: Thermomagnetic curve (K_m vs. T) for dyke 14L (**a**), 9L (**b**) and 12L (**c**) and thermal demagnetisation curve of three-component IRM for 12L (**d**). The K_m curves are consistent with the presence of magnetite as Curie temperatures (T_c) are 587°C, 556°C and 548°C respectively. The units of K_m are arbitrary as they are not normalised to the sample mass (*viz.* Bascou et al., 2005). Note the decay of SIRM towards 580°C in (**d**). The frequency distribution of K_m is shown in (**e**). The mean value of K_m is 5.58×10^{-2} SI units.

In dyke 12L, it can be shown that the predominant phase has a maximum unblocking temperature of 580°C (Figure 6.6d) which is also consistent with coarse-grained stoichiometric magnetite (Hopkinson, 1889; Smith and Prevot, 1977; O'Reily, 1984).

A further 3 samples (7L-17, 7L-19, 14L-11) were measured for thermal decay of K_m which provided a range of T_c from 415–587°C (mean: 525°C). A further 5 samples (7L-14, 10L-4, 15L-13, 18L-3, 20L-4) were monitored for decay of isothermal remanence at saturation (SIRM). Values of SIRM range from 0.08–0.42 Am^2/kg with a mean of 0.17 Am^2/kg (a measure of the magnetic field strength per unit area by mass). The bulk susceptibility of the samples is 5.58×10^{-2} ($\pm 0.9 \times 10^{-2}$) SI units as shown in Table 6.1. The frequency distribution of K_m (Figure 6.6e) illustrates a range of susceptibility from relatively low values (0.05×10^{-2} SI units) to values $>10^{-3}$, with a peak value of 6.5×10^{-2} SI units. There is no remarkable variation in K_m according to relative dyke age, dyke thickness or distance of samples from the margin.

Because magnetite is the main contributor to the low-field magnetic susceptibility, it is possible to estimate the volumetric concentration of magnetite. Given that the SIRM value of coarse-grained magnetite is ~ 9 Am^2/kg (Hunt et al., 1995; Gubbins and Herrero-Bervera, 2007), the mean value of 0.17 Am^2/kg in the NLDS indicates a concentration of magnetite of ~0.1%. This is confirmed by the susceptibility measurements, as the initial susceptibility of stoichiometric magnetite is ~1 SI, implying a volumetric concentration of ~0.1 to 1% in the NLDS where K_m values are ~0.05 SI.

6.4.3. Characteristics of the Magnetic Fabric

It is important to first evaluate the shape and intensity of the fabric. Values of anisotropy (*P'*) range from near isotropic (~1.0) to 1.054 (mean: 1.027). The shape parameter (*T*) discriminates oblate ($T > 0$) from prolate ($T < 0$) fabrics; and in the NLDS is 0.027 on average, indicating a triaxial to weakly oblate shape (Figure 6.7). The mean value of *P'* is 1.027 for the magnetic fabric and *T* is > 0 in 64% of the data.

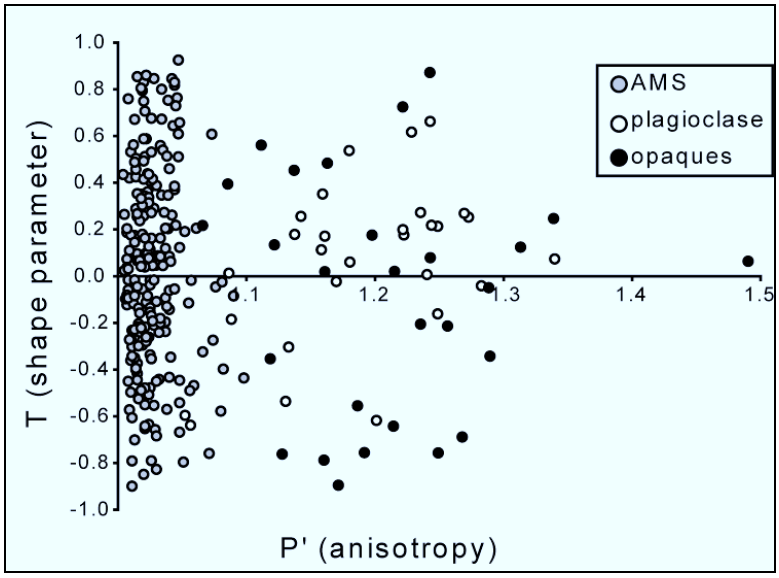

Figure 6.7: Graphical illustration of the fabric shapes of AMS and mineral SPO fabrics in the NLDS as described by the corrected degree of anisotropy (*P'*) and shape parameter (*T*).

The magnetic fabric of all 14 dykes measured for AMS are presented in Figure 6.8 with each dyke discriminated into its two opposing margins. As discussed previously, this is done in order to determine if imbrication of the fabric relative to the average dyke plane exists. When considering the orientation of the AMS ellipsoids and the dispersion of principle axes, it is evident that type-A fabric occurs in ~50% of the sites (e.g. 8L, 9L, 12L, 17L, 10L). Vertical to sub-vertical *K*1 axes are found only in the prolate fabric of dykes 8L and 9L while shallowly plunging *K*1 axes and steeply dipping foliations predominate in other sites (e.g. 19L, 16L, 12L-east, 17L, 10L and 11L). Many sites display scattered fabric. In dykes, such as 14L, 20L, 18L, and 15L, the confidence regions surrounding each principal axis are spread, in many cases overlapping considerably. In some cases (e.g. 16L, 8L and 12L) the fabric is different across the margins, with type-A fabric on one margin and type-B, or apparently a mixture of the two on the other (e.g. 19L, 20L and 7L). Obvious type-B fabric, where *K*1 and *K*3 have interchanged, occurs in sites 20L-east, 18L, 12L-west and 15L-east. There is no evidence for a relationship between the type (or definition) of the fabric and the relative dyke generation because, for example, intermediate or type-B fabric occurs across the range of D1–D4 dykes.

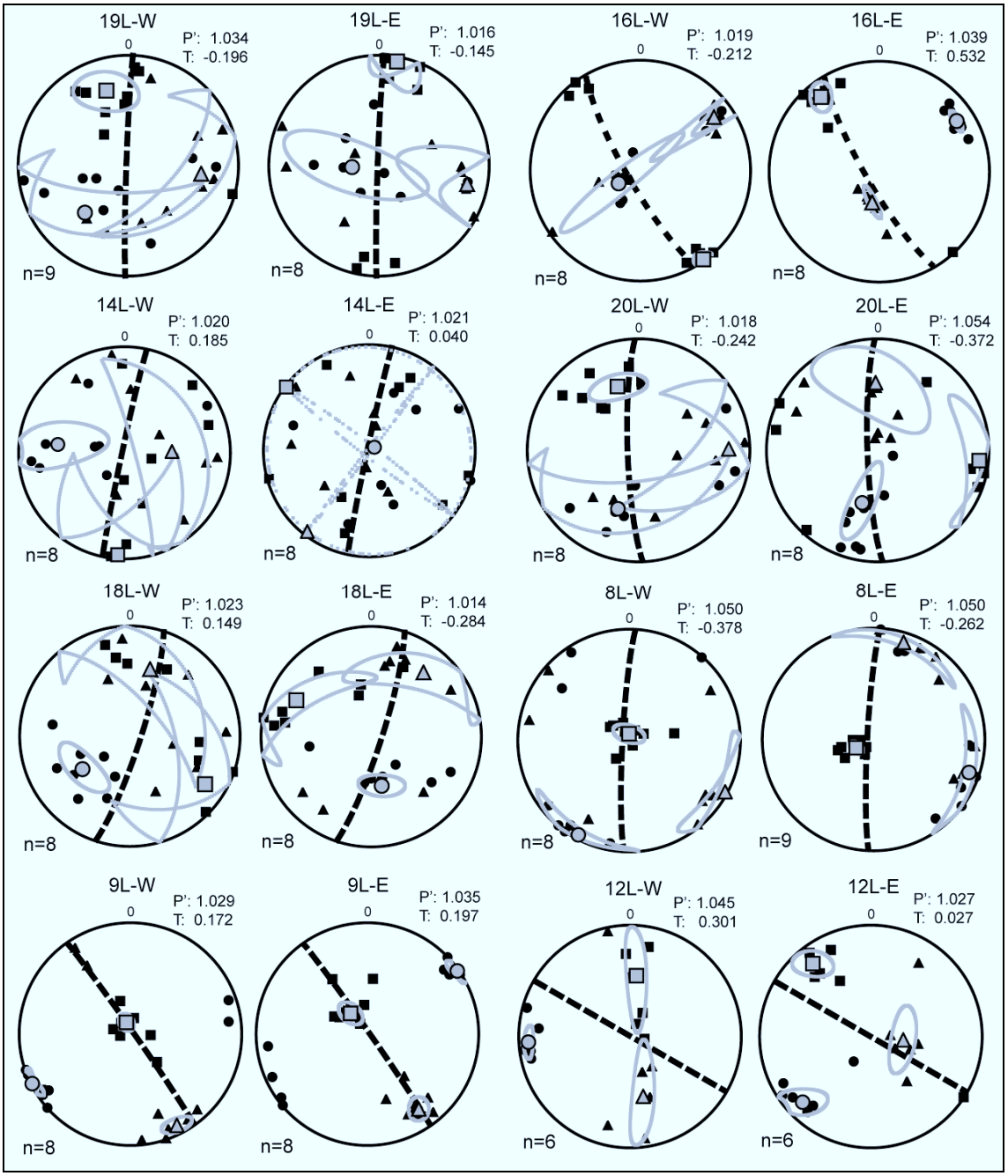

Figure 6.8: Stereographic projections of AMS data from selected dykes of the NLDS. Note that the data are split into west (W) and east (E) margins per dyke in order to better observe any potential imbrication of fabric. The dyke plane is shown as a dashed black line. Ellipses of statistical confidence for each of the principal axes are shown in grey, and calculated using the bootstrap method of Tauxe et al. (1998). Maximum axis ($K1$ = ■); intermediate axis ($K2$ = ▲) and minimum axis ($K3$ = ●) are shown. The number of samples (n); corrected degree of anisotropy (P') and shape (T) are indicated for each margin.

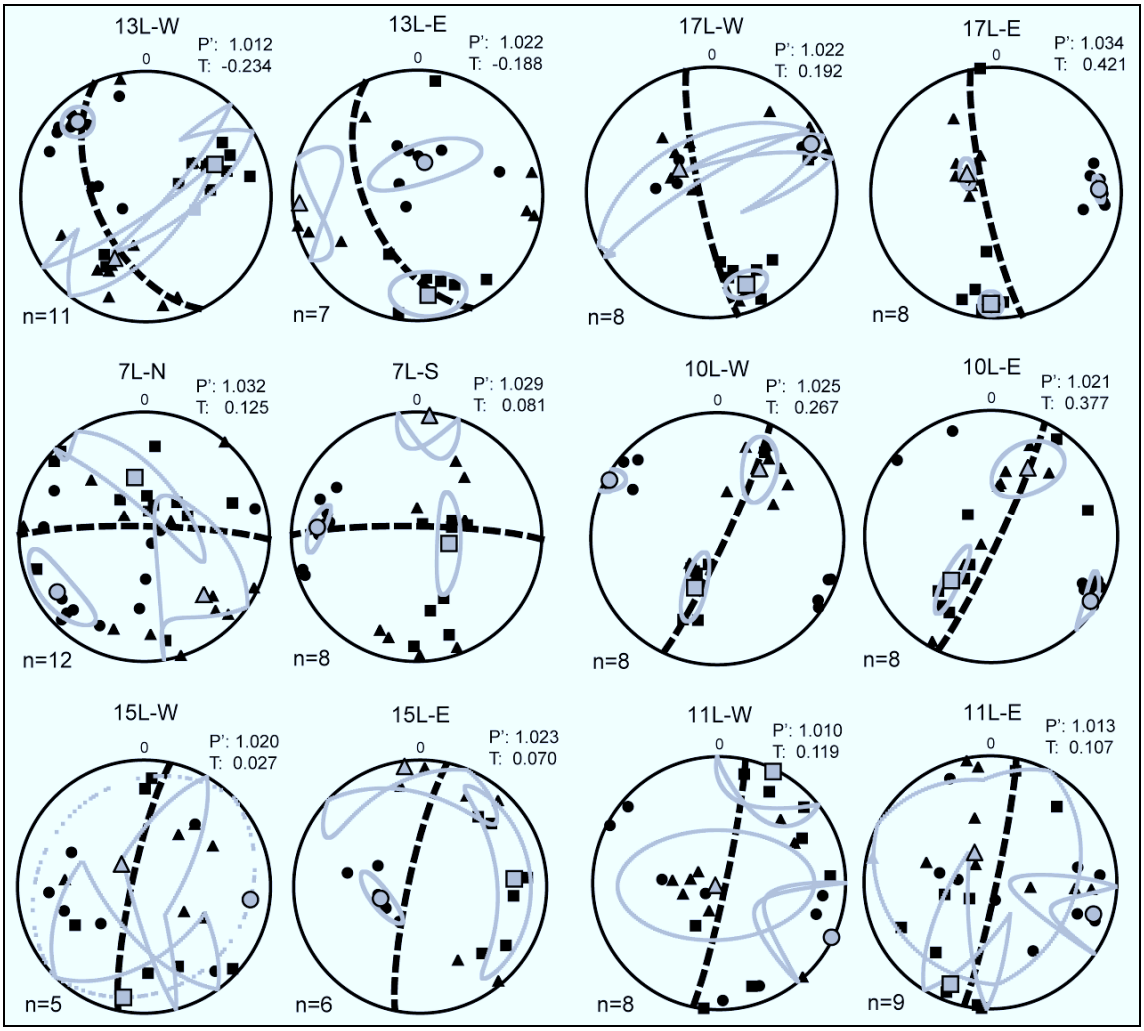

Figure 6.8 cont: Stereographic projections of AMS data from selected dykes of the NLDS.

There does, however, appear to be a relationship between the shape of the fabric ellipsoid and the occurrence of different fabric types. For example, prolate fabrics tend to be intermediate (19L, 16L-west, 20L, 18L-east, 8L) although 14L and 15L are exceptions to this observation as they are neutral to oblate.

No data pertaining to magnetic grain size has been collected and thus explanation of this behaviour would be speculative at best.

6.4.4. Mineral Shape Preferred Orientation

Stereographic projections of the SPO ellipsoids determined from the margins of each dyke are shown in Figure 6.9 in comparison to AMS and the tabulated SPO data are presented in Table 6.2.

The mean maximum axes, $L1$, are typically steeply plunging (> 60°) in 9 of the 14 margins and values of $\sqrt{F}$ are < 10% throughout. The fabric defined by plagioclase is generally type-A, except for 19L-west, 16L-east and 18L-west, and is generally consistent with the overall magnetic fabric orientations shown comparatively by AMS.

The shape of the mineral SPO fabric is predominantly oblate, most notably in the fabric defined by plagioclase (mean $T = 0.042$) (Figure 6.7). The mean T value for the opaque grains is -0.077, which most likely reflects the prolate shape of the needle-like opaque grains in dykes 18L, 9L and 10L. The mean value of P' is 1.208 for the plagioclase SPO fabric. The highest P' values for plagioclase are found in the phenocryst-rich dykes, such as 19L, 16L and 15L (Table 6.2). The least anisotropic opaque grains (mean $P' = 1.14$) are found in the phenocryst-rich dyke 15L.

The mineral SPO fabric is considerably more anisotropic than the AMS fabric, but is similarly oblate in shape. The scatter of the scalar SPO data in Figure 6.7 is greater than that of AMS, perhaps due to the measurement of a greater distribution of grain-sizes across dykes of differing grain texture and phenocryst content, as is evident from the petrography. The frequency distribution of anisotropy in the mineral SPO data is skewed towards higher P' grains which may reflect the occurrence of less abundant, high anisotropy phenocrysts within the matrix.

Interestingly, the type-B fabric orientations of the SPO data are mimicked in the equivalent AMS fabric in 19L-west and 18L-west, similar to fabric found by Hastie et al. (2011). Imbrication of the mineral SPO fabric is found in dykes 19L, 18L, 17L and 10L.

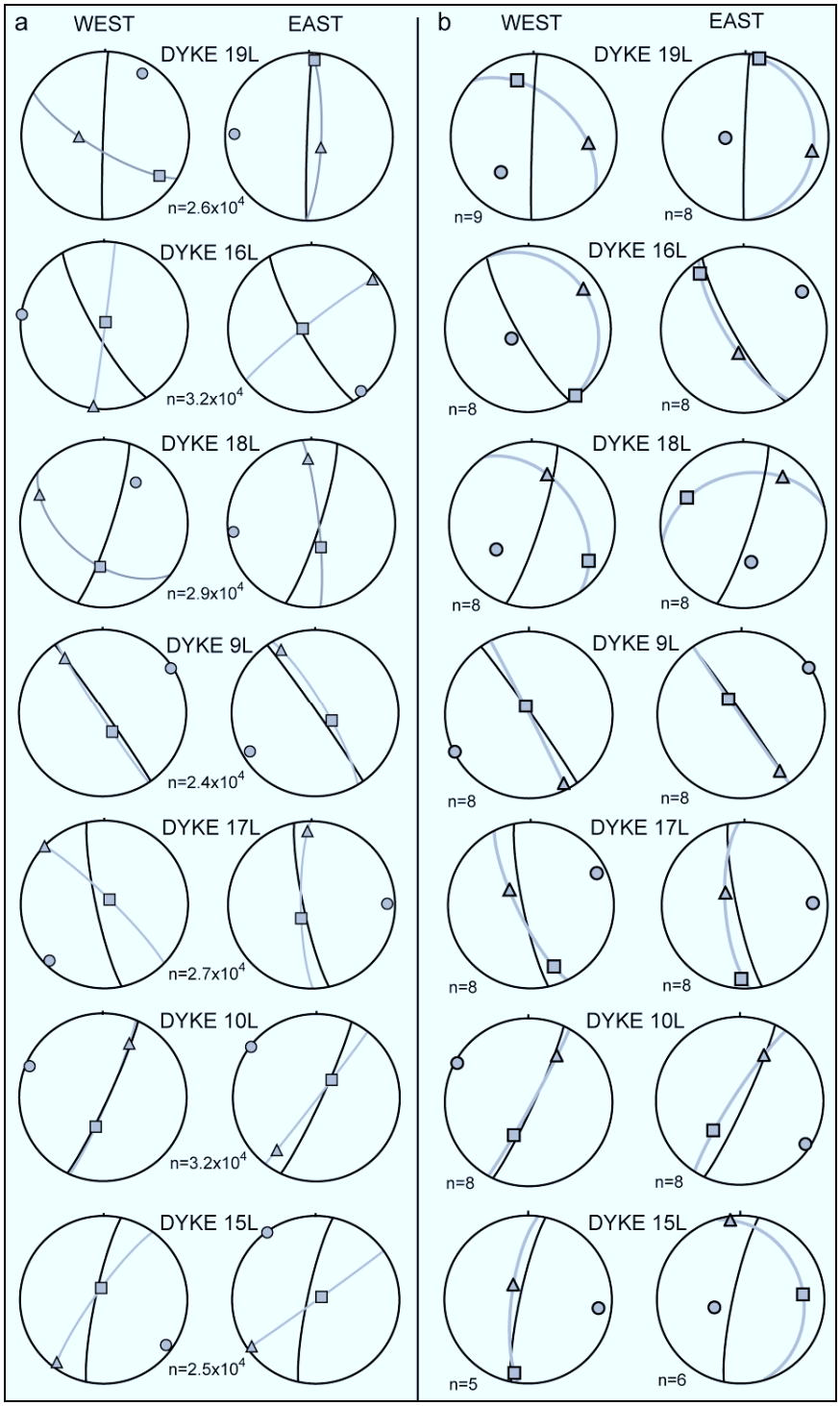

Figure 6.9: Stereographic projections of (**a**) plagioclase SPO for 7 dykes of the NLDS according to the western and eastern dyke margins and (**b**) AMS data for the same dykes, shown for comparative purposes. For SPO data "n" denotes the number of grains analysed and indexed in order to constrain the ellipsoid from 12 thin-sections per dyke. In the interest of clarity, statistical confidence regions are omitted from the figure and only mean principal axes are shown. Foliations are shown as grey lines and the dyke plane in black. For SPO the axes symbolism is as follows: Major axis ($L1$ = ■); intermediate axis ($L2$ = ▲) and minor axis ($L3$ = ●).

Table 6.2: Mineral SPO data discriminated according to the plagioclase and opaque grain fraction and according to opposing dyke margins. See Table 6.1 for key to terminology.

			ellipsoid orientation			angular deviation (sd.)			axial lengths (norm.)					
Dyke	*Margin*	$\sqrt{F}$	*L1*	*L2*	*L3*	*L1*	*L2*	*L3*	*L1*	*L2*	*L3*	*P' [10^{-3} (sd)]*	*T [10^{-2} (sd)]*	*grains*
PLAGIOCLASE														
19L	west	4.72	18°/123°	17°/332°	01°/220°	±34°	±54°	±36°	1.049	0.998	0.955	1.101(30)	-0.065(26)	15448
	east	9.03	11°/354°	56°/041°	09°/270°	±46°	±51°	±35°	1.144	1.004	0.873	1.318(130)	0.057(13)	10891
16L	west	6.40	84°/011°	07°/180°	01°/092°	±13°	±32°	±5°	1.109	1.018	0.887	1.255(50)	0.245(12)	17111
	east	6.39	83°/258°	05°/046°	03°/137°	±12°	±34°	±10°	1.109	1.026	0.879	1.271(30)	0.333(25)	14599
18L	west	3.18	52°/199°	19°/307°	38°/054°	±15°	±21°	±27°	1.051	0.988	0.964	1.094(30)	-0.437(26)	15307
	east	2.86	61°/136°	31°/348°	21°/253°	±4°	±16°	±10°	1.094	0.993	0.921	1.194(50)	-0.088(37)	13794
9L	west	5.65	46°/151°	57°/299°	11°/046°	±29°	±52°	±21°	1.095	1.007	0.909	1.215(104)	-0.080(42)	12494
	east	2.74	75°/081°	05°/331°	14°/239°	±2°	±4°	±3°	1.081	1.012	0.914	1.186(20)	0.227(23)	11938
17L	west	4.70	81°/013°	05°/141°	07°/231°	±23°	±35°	±21°	1.092	0.998	0.918	1.192(20)	-0.03(27)	14381
	east	7.51	62°/221°	30°/029°	02°/126°	±20°	±34°	±15°	1.096	1.008	0.906	1.213(50)	0.153(29)	12452
10L	west	4.76	51°/204°	42°/020°	03°/113°	±18°	±31°	±18°	1.118	0.990	0.905	1.244(100)	-0.178(31)	16037
	east	1.84	66°/040°	24°/218°	01°/308°	±1°	±2°	±1°	1.081	1.043	0.887	1.236(10)	0.637(6)	15824
15L	west	5.28	78°/354°	08°/214°	06°/123°	±5°	±13°	±2°	1.114	1.012	0.887	1.260(50)	0.158(20)	11048
	east	4.33	86°/023°	05°/214°	02°/127°	±11°	±21°	±16°	1.103	0.981	0.924	1.200(20)	-0.344(27)	14022
OPAQUES														
19L	west	7.73	77°/287°	04°/059°	08°/139°	±16°	±42°	±24°	1.099	0.998	0.915	1.217(118)	-0.111(44)	5615
	east	6.25	51°/144°	36°/321°	01°/232°	±24°	±21°	±23°	1.097	1.000	0.913	1.211(70)	0.075(46)	5560
16L	west	6.58	77°/331°	13°/187°	07°/090°	±23°	±48°	±10°	1.118	1.012	0.885	1.270(56)	0.173(36)	3531
	east	7.79	76°/235°	14°/043°	03°/134°	±10°	±35°	±10°	1.199	0.997	0.838	1.442(76)	-0.043(29)	3381
18L	west	5.68	34°/171°	44°/276°	30°/055°	±23°	±40°	±10°	1.063	0.993	0.949	1.125(51)	-0.145(41)	4761
	east	9.51	40°/118°	40°/008°	37°/258°	±26°	±22°	±6°	1.151	0.960	0.905	1.288(61)	-0.505(19)	3747
9L	west	8.88	65°/191°	25°/029°	02°/288°	±8°	±38°	±13°	1.199	0.970	0.865	1.419(185)	-0.218(47)	6056
	east	5.16	82°/128°	06°/306°	01°/036°	±6°	±13°	±2°	1.077	0.998	0.930	1.158(15)	-0.034(8)	5056
17L	west	7.82	77°/303°	07°/150°	01°/214°	±29°	±47°	±22°	1.103	0.994	0.914	1.220(108)	0.036(55)	2799
	east	4.90	71°/218°	21°/069°	12°/319°	±23°	±27°	±30°	1.103	0.973	0.933	1.197(49)	-0.517(42)	3576
10L	west	6.63	49°/201°	39°/001°	09°/099°	±12°	±17°	±10°	1.162	0.997	0.864	1.352(110)	-0.012(21)	4402
	east	6.00	70°/186°	19°/022°	05°/291°	±3°	±12°	±4°	1.105	0.997	0.909	1.230(44)	-0.131(60)	4082
15L	west	3.49	85°/306°	02°/198°	06°/107°	±12°	±11°	±8°	1.058	1.014	0.932	1.141(30)	0.327(35)	4369
	east	5.70	67°/261°	15°/025°	18°/111°	±16°	±53°	±8°	1.084	1.002	0.922	1.182(33)	0.031(43)	2475

Dykes 17L and 10L, in particular, show identical agreement between the imbrication of the SPO foliations and the AMS foliations; both in a southward verging direction. There are examples of northerly directed foliations, such as 15L and 16L but this is evident from only one margin each because intermediate fabric persists and the foliations in these cases are not imbricated.

6.4.5. Bulk AMS and SPO Fabric

Given the varying orientations of the dykes (Table 6.1) it is acceptable to rotate the fabric; particularly *K*1 and *K*3 into a single co-ordinate system; in this case north-south (N–S) vertical dyke co-ordinates (Figure 6.10a). This, in effect, normalises the data into a bulk framework which expresses more clearly the regional trends of the fabric orientation (Rochette et al., 1991; Callot et al., 2001; Aubourg et al., 2008). For example, where dykes strike NW (16L, 9L, 12L, 13L), data are rotated clockwise and counter-clockwise for dykes striking NE (18L, 10L, 11L). The dip of the dykes is also removed by rotating the data about a horizontal, N-S striking axis. Furthermore, the AMS ellipsoids which show scattered principal axes and overlapping, weakly constrained confidence ellipsoids (7L, 11L, 13L, 14L, 15L, 18L, 19L) have been excluded from this bulk data. This allows for a more confident interpretation of the remaining data (n = 115). Using this method, it can be seen that the orientation of the magnetic fabric is relatively well grouped. Note that the girdles shown in Figure 6.10, from which imbrication can be inferred, are computed from the density maximum of each principal axis in each projection (*K*2 is not shown for clarity).

A very slight imbrication is noticeable from the *K*1 distributions; along a NNW-SSE girdle for the western margins and a NNE–SSW girdle for the eastern margins respectively. Indeed this subtle imbrication is evident in the *K*3 axes as well, provided the type-B fabric of the western margins is not considered (NW quadrant of the stereographic projection). A similar imbrication of foliations is also evident in the *L*3 axes of the SPO data, in spite of the sub-vertical *L*1 axes (Figure 6.10b). The orientation of the *L*1 axes would typically be an indication of vertical magma flow.

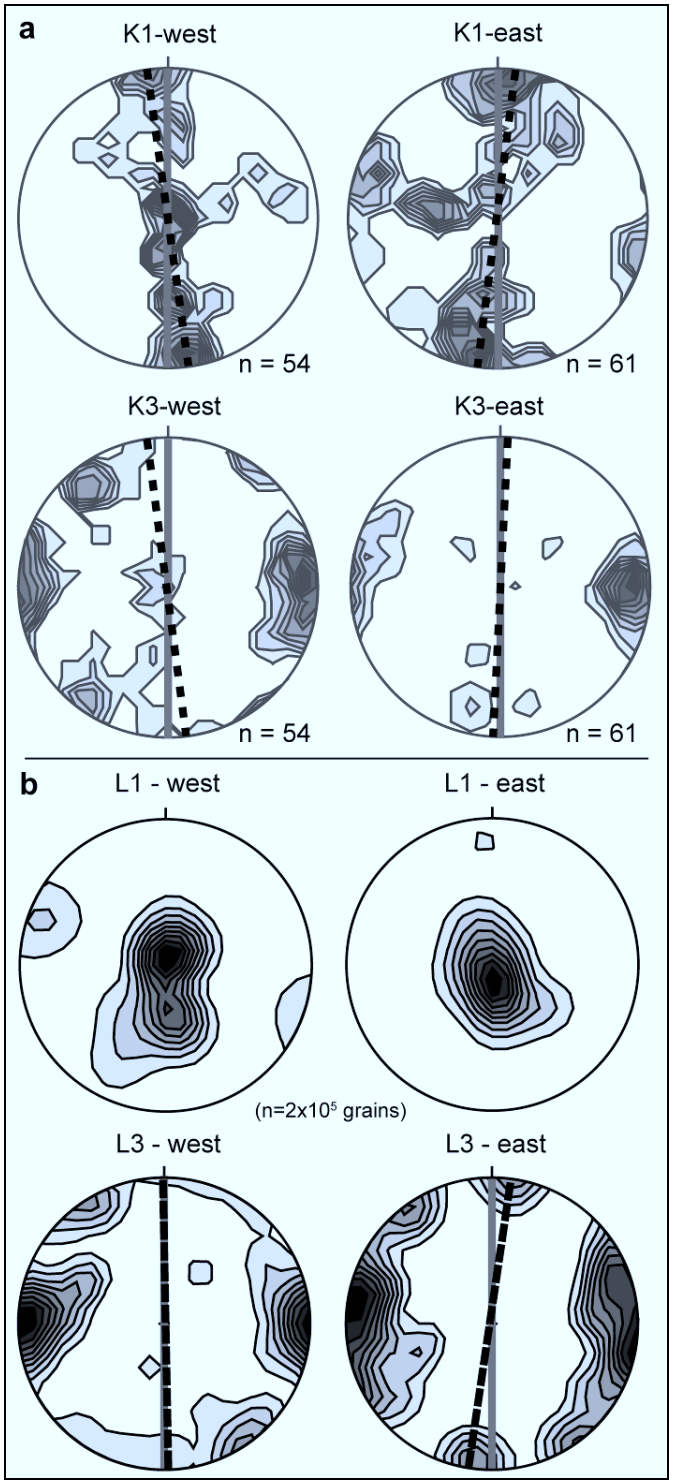

Figure 6.10: Stereographic density diagrams of (**a**) the bulk AMS fabric of the NLDS in north-south (N-S) dyke co-ordinates, with scattered and poorly defined data removed (n = 115) and (**b**) the bulk plagioclase SPO fabric of the NLDS in N-S dyke co-ordinates (28 ellipsoids). Western and eastern margins are discriminated, with only *K*1 (*L*1) and *K*3 (*L*3) axes shown. Note in particular the very subtle imbrication of both the AMS and mineral SPO foliations about the N-S direction (grey lines). The 10 contoured domains are at 1% intervals for both the AMS and mineral SPO diagrams.

However, it has been noted that, in AMS at least, the lineation ($K1$) may represent an intersection, particularly in oblate fabrics ($T > 0$) (Henry, 1997; Launeau and Cruden, 1998; Callot and Guichet, 2003). In this context it is possible to argue that the $L1$ axes determined for the plagioclase SPO may also be misleading. It is evident from Figure 6.10b and Table 6.2 that the $L1$ axes are almost exclusively steeply plunging. Intuitively, this would suggest vertical magma flow. However, Figure 6.3a shows that when vertical magma flow occurs, it is expected that the foliation planes dip at between 20° and 40° with the maximum axis ($K1$ or $L1$) disposed at the same angle from vertical. Such geometry is not evident in the mineral SPO data of Figure 6.10b. There is also no observable imbrication of $L1$ axes in the mineral SPO data of the NLDS, making an assessment of upward or downward vertical flow unclear. Imbrication, albeit weak, is only evident in the $K1$, $K3$ and $L3$ axes of the remaining data. The steeply dipping foliations of the mineral SPO data more closely resemble those shown in Figure 6.3b.

The $L1$ axes are also disproportionately well-grouped compared to the $L3$ axes – considering that the fabric is predominantly oblate. This can occur when the foliations of oblate fabrics intersect which, in the case of steeply dipping, imbricated foliations would result in (sub-) vertical lineations.

At the thin-section scale certain features of the mineral SPO fabric can be scrutinised in more detail. A convenient feature of the *XZ* thin-sections (Figure 6.4) is that these sections are vertically orientated, and it is thus possible in certain cases to show the $L1$-$L2$ planes on these sections (with an estimated error in direction of 10°) (Figure 6.11). Very briefly, it can be observed that in some cases the $L1$ axis direction is parallel to the maximum direction of the plagioclase grains as determined by a rose of directions (Figure 6.11a-c). However, orthogonal to near orthogonal plagioclase orientations which are evidently bisected by the $L1$ axis direction are also observed (Figure 6.11d-f). This suggests that, in these samples at least, the $L1$ direction represents an average orientation in the 2D inertia tensor.

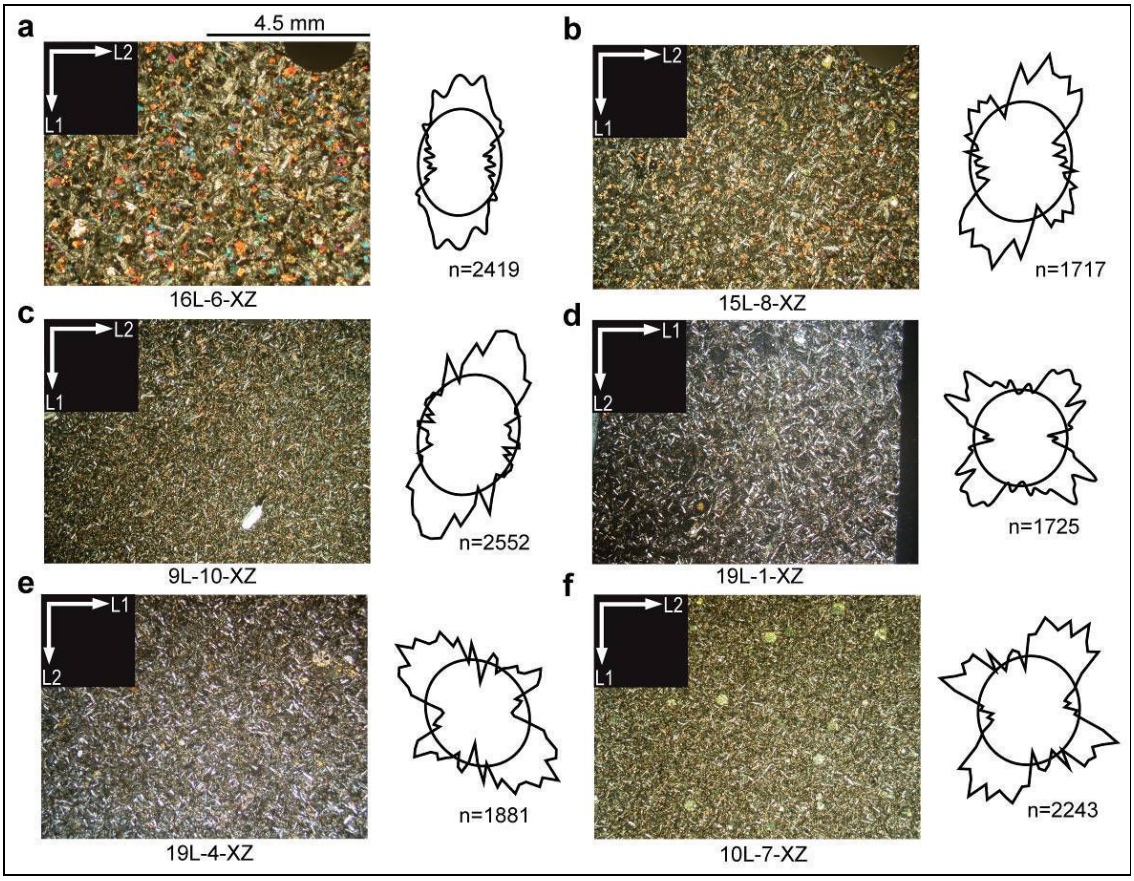

Figure 6.11: Thin-section photomicrographs with *L*1-*L*2 planes indicated (all *XZ* sections, sample numbers indicated). The rose of directions indicated with each section reflects the orientations of the plagioclase grains in each section (measured at 5° intervals) and the average 2D inertia tensor ellipse is also shown. The number of grains (n) indexed for each section is also shown. Sections **a-c** show that *L*1 is coaxial with the maximum plagioclase orientation. Sections **d-f** are examples of apparently competing plagioclase fabric orientations which are not coaxial with the *L*1 direction. All the photomicrographs are at the same scale (each photomicrograph is 9 mm across) and all are taken under crossed-polarisers except (**f**).

This potentially leads to an underestimation of the anisotropy of the tensor and, more importantly, the observation that the *L*1 axes orientations are unlikely to represent a magma flow vector.

These observations cast some doubt on the meaning of the *L*1 axes. It is thus more prudent to focus on the meaning of the foliations and no inference of vertical or sub-vertical magma flow direction is made from the maximum AMS or mineral SPO axes. The similarity in orientation between the bulk AMS and mineral SPO foliations and the

apparent type-A fabric suggests a magmatic origin. The imbrication of the foliations, albeit subtle, hints at southward verging lateral magma flow.

6.5. Discussion

6.5.1. Magnetic and Petrofabric of the NLDS

We have used AMS and mineral SPO to define the characteristics of the petrofabric in 14 dykes of the NLDS in order to constrain the orientation and meaning of any magmatic fabric therein. In general, type-A fabric predominates carried by stoichiometric magnetite which defines a magnetic fabric of relatively low anisotropy ($P' < 1.06$) and triaxial shape. Prolate fabrics tend to be intermediate and have vertical to sub-vertical $K1$ axes. The AMS fabric is remarkably consistent in orientation with the predominantly oblate and higher anisotropy ($P' < 1.40$) mineral SPO fabric. The use of SPO provides constraint on the fabric carried by larger grains, including the plagioclase phenocryst population. With the exception of 3 sites, the SPO results have consistently provided type-A fabric, which is imbricated in 3 dykes. There is also good agreement between the SPO and AMS fabrics in 4 of the 7 dykes tested. The orientation and imbrication of foliations are used as reliable magma flow vector indicators. Steeply dipping, imbricated foliations occur in 5 dykes (e.g. 19L, 18L, 17L, 10L and 11L).

As discussed previously in this paper, type-B and/or intermediate fabrics may result from late-stage fabric acquisition, superimposition of fabrics at different times in the history of the intrusions or complex magnetic interaction, such as distribution anisotropy. With the AMS, however, it is found that a credible interpretation of magma flow is possible after removing the poorly constrained data, and therefore the origin(s) of type-B or intermediate fabric is not discussed any further. Rather, the bulk AMS and SPO fabric form the focus of inferring, where possible, an overall sense of magma flow direction in the NLDS. When assessing the bulk AMS data (in dyke co-ordinates) there is evidence of subtle imbrication which verges southwards. The appearance of a similar imbrication in the bulk mineral SPO data is again consistent with lateral magma flow. The subtlety of the imbrication, however, makes it difficult to confidently provide an absolute flow

sense, although it is possible to speculate that the flow was from north to south, given that this same direction can be demonstrated at the local scale.

6.5.2. Magma Flow in the NLDS

The bulk AMS and SPO of the NLDS appear most consistent with lateral magma flow from a position north of the sampled areas. This provides 2 broad possibilities for the explanation of this result. Firstly, within the Karoo triple junction context, it may be that magma flow was directed from the locus of the triple junction at Mwenezi, or, secondly, that the NLDS was fed from an internal point source within the Lebombo faulted monocline.

In addressing the latter possibility, it is evident that the dykes of the NLDS, particularly D1-D3 dykes along the Olifants River, do not appear to converge on a magmatic centre within the Lebombo itself (Klausen, 2009) as has been found in other similar regions (Sigurdsson and Sparks, 1978; Geoffroy and Aubourg, 1997; Callot et al., 2001).

The NLDS was emplaced during E-W extension from 182–178 Ma with the D4 dykes being emplaced from ~178 Ma, probably concomitant with dykes of the ODS. A NNW-SSE extension was most likely responsible for triggering the emplacement of the ODS at ~178 Ma (Le Gall et al., 2002; Watkeys, 2002; Jourdan et al., 2007; Klausen, 2009). There is clear evidence of Proterozoic dykes in the ODS and SLDS which indicates structural inheritance during later Karoo magmatism (Uken and Watkeys, 1997; Le Gall et al., 2002, Le Gall et al., 2005; Jourdan et al., 2006). However, virtually indistinguishable ages for the ODS and SLDS have been found (179±1.2–178.4±1.1 Ma and 180.4±0.7–178.9±0.8 Ma respectively) (Jourdan et al., 2006, 2007) suggesting synchronous emplacement of these two swarms. This, along with older and overlapping ages in the Lebombo faulted monocline, suggests early development of the NLDS, with slightly later development of the SLDS and ODS – the latter representing the failed rift arm in the triple junction.

Lateral injection of magma into the ODS is favoured due to magnetic fabric evidence (Aubourg et al., 2008) and evidence of the widening of the ODS toward the triple junction caused by relatively greater extension across this proximal part of the rift (Klausen, 2009). Steep flow is in evidence near to the triple junction centre (Ernst and Duncan, 1995; Aubourg at al., 2008). This study has presented evidence in favour of lateral flow of magma in the emplacement of the NLDS. It is reasonable to suggest that the D4 dykes at least, if not the NLDS itself, tapped the same magmatic source (the triple junction?) as the ODS. The lateral intrusion of magma into the extensional environment of the Lebombo may, therefore, be indicative of a pre-Karoo triple junction simply being exploited by upwelling magmas, rather than a point of active rifting induced by mantle plume activity.

It has been suggested that the duration of activity at the triple junction was short (181–178 Ma), ending when Antarctica broke away from the eastern edge of the Lebombo (Jourdan et al., 2007; Klausen, 2009). This may have occurred relatively soon after the emplacement of the asthenosphere-derived, MORB-like RRDS at ~173 Ma, although the earliest movement between Antarctica and southern Africa may have been much later, at ~155 Ma (Watkeys, 2002). It is not the intention of this paper to resolve issues of duration and timing but the evidence of magma flow in the ODS and NLDS study is quite consistent with the geological history outlined above, such that commonality in the genesis of the ODS and NLDS seems likely.

In conclusion, the role of the triple junction as a potential locus of magma supply in this region of the Karoo LIP is emphasised. There is, however, no conclusive evidence in support of the mantle plume hypothesis. This is because the geometry of the triple junction appears to have been primed, since the Proterozoic at least, to accommodate magmatic and tectonic extension rather than being the exclusive product of active, plume-induced rifting during the development of the Karoo LIP (Le Gall et al., 2005; Jourdan et al., 2006).

6.6. Conclusions

- The magnetic fabric in dykes of the NLDS is carried mainly by stoichiometric magnetite with a concentration of ~ 1%.
- Fabrics are type-A in 6 dykes, which is of magmatic origin, and scattered and/or type-B in the remaining dykes.
- The magnetic fabric is of relatively low anisotropy (P' = 1.027±0.02), triaxial to weakly oblate in shape (T = 0.027±0.42).
- The shape preferred orientation fabric defined by plagioclase in the NLDS is of higher anisotropy (P' = 1.208) than the magnetic fabric and also weakly oblate in shape (T = 0.042) while the opaque grain fabric is triaxial to prolate (T = -0.077).
- With the exception of 3 sites the SPO fabric appears to be magmatic in origin (type-A) and furthermore is in agreement with the AMS fabric in 4 of the 7 dykes tested.
- When the bulk magnetic fabric is viewed in dyke co-ordinates on the regional scale a subtle, southward-verging imbrication of both $K1$ and $K3$ principal axes can be observed. A similar imbrication is evident in the $L3$ axes of the plagioclase SPO data plotted in dyke co-ordinates as well.
- The $L1$ axes do not adequately represent a magma flow vector, as orthogonal to near orthogonal plagioclase orientations are bisected by the $L1$ axes. This suggests that the $L1$ direction represents an average orientation in the 2D inertia tensor and may be influenced by the intersection of foliations.
- We suggest that the orientation of the imbricated fabric, although subtle, is most consistent with lateral magma flow, most likely directed from a magmatic source positioned to the north of the dyke swarm.
- It is argued that, similarly to the ODS, lateral magma flow outward from the Karoo triple junction was involved in the emplacement of the NLDS. It cannot be conclusively shown that a mantle plume was involved.

6.7. Acknowledgements

The authors wish to acknowledge the technical staff of the University of Cergy-Pontoise and University of KwaZulu-Natal for assistance with AMS analysis and thin-section

preparation. The authors also acknowledge the NRF-CNRS co-operative “PICS” programme that funded this research and the staff of the Kruger National Park who allowed field work and sample collection during 2006. This work forms part of the Ph.D. research of W. Hastie who acknowledges an NRF Innovation bursary. Massimiliano Porreca and Bernard Le Gall are thanked for thorough and constructive reviews.

6.8. References

Anderson, D.L., Zhang, Y.-S., Tanimoto, T., 1992. Plume heads, continental lithosphere, flood basalts and tomography. In: Storey, B.C., Alabaster, T., Pankhurst, R.J. (Eds.), Magmatism and the Causes of Continental Break-up. Geological Society Special Publication 68, 99–124.

Archanjo, C.J., Launeau, P., 2004. Magma flow inferred from preferred orientations of plagioclase of the Rio Cearf-Mirim dyke swarm (NE Brazil) and its AMS significance. In: Martin-Hernandez, F., Luneburg, C.M., Aubourg C., Jackson, M. (Eds.), Magnetic Fabric: Methods and applications. Geological Society of London Special Publication 238, 285–298.

Armstrong, R.A., Bristow, J.W., Cox, K.G., 1984. The Rooi Rand dyke swarm, southern Lebombo. Geological Society of South Africa Special Publication 13, 77–86.

Aubourg, C., Giordano, G., Mattei, M., Speranza, F., 2002. Magma flow in sub-aqueous rhyolitic dikes inferred from magnetic fabric analysis (Ponza Island, W. Italy). Physics and Chemistry of the Earth 27, 1263–1272.

Aubourg, C., Tshoso, G., Le Gall, B., Bertrand, H., Tiercelin, J.-J., Kampunzu, A.B., Dyment, J., Modisi, M., 2008. Magma flow revealed by magnetic fabric in the Okavango giant dyke swarm, Karoo igneous province, northern Botswana. Journal of Volcanology and Geothermal Research 170, 247–261.

Bascou, J., Camps, P., Dautria, J.M., 2005. Magnetic versus crystallographic fabrics in a basaltic lava flow. Journal of Volcanology and Geothermal Research 145, 119–135.

Borradaile, G.J., Gauthier, D., 2003. Interpreting anomalous magnetic fabrics in ophiolite dikes. Journal of Structural Geology 25, 171–182.

Bristow, J.W., 1982. Geology and structure of Karoo volcanic and sedimentary rocks of the northern and central Lebombo. Transactions of the Geological Society of South Africa 85, 167–178.

Bristow, J.W., 1984. Nephelinites of the north Lebombo and south-east Zimbabwe. Geological Society of South Africa Special Publication 13, 87–104.

Burke, K., Dewey, J.F., 1973. Plume generated triple junctions: key indicators in applying plate tectonics to old rocks. Journal of Geology 81, 406–433.

Callot, J.P., Geoffroy, L., Aubourg, C., Pozzi, J.P., Mege, D., 2001. Magma flow directions of shallow dykes from the East Greenland volcanic margin inferred from magnetic fabric studies. Tectonophysics 335, 313–329.

Callot, J.P., Guichet, X., 2003. Rock texture and magnetic lineation in dykes: a simple analytical model. Tectonophysics 366, 207–222.

Campbell, I.H., Griffiths, R.W., 1990. Implications of mantle plume structure for the evolution of flood basalts. Earth and Planetary Science Letters 99, 79–93.

Cañón-Tapia, E., Herrero-Bervera, E., 2009. Sampling strategies and the anisotropy of magnetic susceptibility of dykes. Tectonophysics 466, 3–17.

Chadima, M., Cajz, V., Týcová, P., 2009. On the interpretation of normal and inverse magnetic fabric in dikes: Examples from the Eger Graben, NW Bohemian Massif. Tectonophysics 466, 47–63.

Cox, K.G., 1989. The role of mantle plumes in the development of continental drainage patterns. Nature 342, 873–877.

Cox, K.G., 1992. Karoo igneous activity, and the early stages of the break-up of Gondwanaland. In: Storey, B.C., Alabaster, T., Pankhurst, R.J. (Eds.), Magmatism and the Causes of Continental Break-up. Geological Society of London Special Publication 68, 137–148.

Cox, K.G., MacDonald, R., Hornung, G., 1967. Geochemical and petrogenetic provinces of in the Karoo basalts of southern Africa. American Mineralogist 52, 1451–1474.

Du Toit, A.L., 1929. The volcanic belt of the Lebombo: a region of tension. Transactions of the Royal Society of South Africa 18, 189–218.

Duncan, A.R., Armstrong, R.A., Erlank, A.J., Marsh, J.S., Watkins, R.T., 1990. MORB-related dolerites associated with the final phases of Karoo flood basalt volcanism in southern Africa. In: Parker, A.J., Rickwood, P.C., Tucker, D.H. (Eds.), Mafic Dykes and Emplacement Mechanisms. Balkema, Rotterdam, 119–129.

Ellam, R.M., Cox, K.G., 1991. An interpretation of Karoo picrite basalts in terms of interaction between asthenospheric magmas and mantle lithosphere. Earth and Planetary Science Letters 105, 330–342.

Ellwood, B.B., 1978. Flow and emplacement direction determined for selected basaltic bodies using magnetic anisotropy measurements. Earth and Planetary Science Letters 41, 254–264.

Encarnación, J., Fleming, T.H., Elliot, D.H., Eales, H.V., 1996. Synchronous emplacement of Ferrar and Karoo dolerites and the early breakup of Gondwana. Geology 24, 535–538.

Erlank, A.J., 1984. Petrogenesis of the volcanic rocks of the Karoo province. Geological Society of South Africa Special Publication 13, 1–26.

Ernst, R.E., Baragar, W.R.A., 1992. Evidence from magnetic fabric for the flow pattern of magma in the Mackenzie giant radiating dyke swarm. Nature 356, 511–513.

Ernst, R.E., Duncan, A.R., 1995. Magma flow in the Giant Botswana dyke swarm from analysis of magnetic fabric (abstract). Third International Dyke Conference, Jerusalem, Israel.

Geoffroy, L., Callot, J.P., Aubourg, C., Moreira, M., 2002. Is the common use of AMS in mafic dykes scientifically correct? Terra Nova 14, 183–190.

Gil-Imaz, A., Pocoví, A., Lago, M., Galé, C., Arranz, E., Rillo C., Guerrero, E., 2006. Magma flow and thermal contraction fabric in tabular intrusions inferred from AMS analysis. A case study in a late-Variscan folded sill of the Albarracín Massif (southeastern Iberian Chain, Spain). Journal of Structural Geology 28, 641–653.

Gubbins, D., Herrero-Bervera, E., 2007. Encyclopedia of Geomagnetism and Paleomagnetism. Springer-Verlag, Berlin, Heidelberg, New York, 1054 pp.

Hargraves, R.B., Johnson, D., Chan, C.Y., 1991. Distribution anisotropy: the cause of AMS in igneous rocks? Geophysical Research Letters 18, 2193–2196.

Hastie, W.W., Aubourg, C., Watkeys, M.K., 2011. When an 'inverse' fabric is not inverse: an integrated AMS-SPO study in MORB-like dykes. Terra Nova 23, 49–55.

Hawkesworth, C., Kelley, S., Turner, S., Le Roex, A., Storey, B.C., 1999. Mantle processes during Gondwana break-up and dispersal. Journal of African Earth Sciences 28, 239–261.

Hergt, J.M., Peate, D.W., Hawkesworth, C.J., 1991. The petrogenesis of Mesozoic Gondwana low-Ti flood basalts. Earth and Planetary Science Letters 105, 134–148.

Henry, B., 1997. The magnetic zone axis: a new element of magnetic fabric for the interpretation of magnetic lineation. Tectonophysics 271, 325–331.

Hopkinson, J., 1889. Magnetic and other physical properties of iron at a high temperature. Philosophical Transactions of the Royal Society of London Series A, 180, 443 pp.

Hunt, C.P., Moskowitz, B.M., Banerjee, S.K., 1995. Magnetic Properties of Rocks and Minerals. In: Ahrens, T.J. (Eds.), Rock physics and phase relations. A Handbook of physical constants. American Geophysical Union, Washington, 189–204.

Jelinek, V., 1978. Statistical processing of anisotropy of magnetic susceptibility measured on groups of specimens and its applications. Studies in Geophysics and Geodynamics 22, 50–62.

Jelinek, V., 1981. Characterization of the magnetic fabric of rocks. Tectonophysics 79, 63–67.

Jourdan, F., Féraud, G., Bertrand, H., Kampunzu, A.B., Tshoso, G., Le Gall, B., Tiercelin, J.-J., Capiez, P., 2004. The Karoo triple junction questioned: evidence from Jurassic and Proterozoic $^{40}Ar/^{39}Ar$ ages and geochemistry of the giant Okavango dyke swarm (Botswana). Earth and Planetary Science Letters 222, 989–1006.

Jourdan, F., Féraud, G., Bertrand, H., Kampunzu, A.B., Tshoso, G., Watkeys, M.K., Le Gall, B., 2005. Karoo large igneous province: Brevity, origin and relation to mass extinction questioned by new $^{40}Ar/^{39}Ar$ age data. Geology 33, 745–748.

Jourdan, F., Féraud, G., Bertrand, H., Watkeys, M.K., Kampunzu, A.B., Le Gall, B., 2006. Basement control on dyke distribution in Large Igneous Provinces: Case study of the Karoo triple junction. Earth and Planetary Science Letters 241, 307–322.

Jourdan, F., Féraud, G., Bertrand, H., Watkeys, M.K., 2007. From flood basalts to the inception of oceanization: Example from the $^{40}Ar/^{39}Ar$ high-resolution picture of the Karoo large igneous province. Geochemistry, Geophysics, Geosystems 8, 1–20.

Khan, M.A., 1962. The anisotropy of magnetic susceptibility of some igneous and metamorphic rocks. Journal of Geophysical Research 67, 2873–2885.

Kissel, C., Laj, C., Sigurdsson, H., Guillou, H., 2010. Emplacement of magma in Eastern Iceland dikes: Insights from magnetic fabric and rock magnetic analyses. Journal of Volcanology and Geothermal Research 191, 79–92.

Klausen, M.B., 2009. The Lebombo monocline and associated feeder dyke swarm: Diagnostic of a successful and highly volcanic rifted margin? Tectonophysics 468, 42–62.

Knight, M.D., Walker, G.P.L., 1988. Magma flow directions in dikes of the Koolau Complex, Oahu, determined from magnetic fabric studies. Journal of Geophysical Research 93, 4301–4319.

Launeau, P., 2004. Mise en évidence des écoulements magmatiques par analyse d'images 2-D des distributions 3-D d'Orientations Préferentielles de Formes. Bulletin of the Geological Society of France 175, 331–350.

Launeau, P., Robin, P.-Y.F., 1996. Fabric analysis using the intercept method. Tectonophysics 267, 91–119.

Launeau, P., Cruden, A.R., 1998. Magmatic fabric acquisition mechanisms in a syenite: Results of a combined anisotropy of magnetic susceptibility and image analysis study. Journal of Geophysical Research 103, 5067–5089.

Launeau, P., Robin, P.-Y.F., 2005. Determination of fabric and strain ellipsoids from measured sectional ellipses - implementation and applications. Journal of Structural Geology 27, 2223–2233.

Launeau, P., Archanjo, C.J., Picard, D., Arbaret, L., Robin, P.-Y.F., 2010. Two- and three-dimensional shape fabric analysis by the intercept method in grey levels. Tectonophysics 492, 230–239.

Le Gall, B., Tshoso, G., Jourdan, F., Féraud, G., Bertrand, H., Tiercelin, J.J., Kampunzu, A.B., Modisi, M.P., Dyment, J., Maia, M., 2002. $^{40}Ar/^{39}Ar$ geochronology and structural data from the giant Okavango and related mafic dyke swarms, Karoo igneous province, northern Botswana. Earth and Planetary Science Letters 202, 595–606.

Le Gall, B., Tshoso, G., Dyment, J., Kampunzu, A.B., Jourdan, F., Féraud, G., Bertrand, H., Aubourg, C., Vétela, W., 2005. The Okavango giant mafic dyke swarm (NE Botswana): its structural significance within the Karoo Large Igneous Province. Journal of Structural Geology 27, 2234–2255.

O'Reilly, W., 1984. Rock and Mineral Magnetism. Blackie & Son, Glasgow, 220 pp.

Poland, M.P., Fink, J.H., Tauxe, L., 2004. Patterns of magma flow in segmented silicic dikes at Summer Coon volcano, Colorado: AMS and thin section analysis. Earth and Planetary Science Letters 219, 155–169.

Porreca, M., Acocella, V., Massimi, E., Mattei, M., Funiciello, R., De Benedetti, A.A., 2006. Geometric and kinematic features of the dike complex at Mt. Somma, Vesuvio (Italy). Earth and Planetary Science Letters 245, 389–407.

Potter, D.K., Stephenson, A., 1988. Single-domain particles in rocks and magnetic fabric analysis. Geophysical Research Letters 15, 1097–1100.

Raposo, M.I.B., D'Agrella-Filho, M.S., Pinese, J.P.P., 2007. Magnetic fabrics and rock magnetism of Archaean and Proterozoic dike swarms in the southern São Francisco Craton, Brazil. Tectonophysics 443, 53–71.

Reeves, C., 1978. A failed Gondwana spreading axis in southern Africa. Nature 273, 222–223.

Reeves, C., 2000. Geophysical mapping of Mesozoic dyke swarms in southern Africa and their origin in the disruption of Gondwana. Journal of African Earth Sciences 30, 499–513.

Riley, T.R., Millar, I.L., Watkeys, M.K., Curtis, M.L., Leat, P.T., Klausen, M.B., Fanning, C.M., 2004. U-Pb zircon (SHRIMP) ages for the Lebombo rhyolites, South Africa. Journal of the Geological Society, London 161, 547–550.

Rochette, P., Jenatton, L., Dupuy, C., Boudier, F., Reuber, I., 1991. Diabase dikes emplacement in the Oman Ophiolite: a magnetic fabric study with reference to geochemistry. In: Peters, T., Nicolas, A., Coleman, R.G. (Eds.), Ophiolite genesis and evolution of the oceanic lithosphere. Ministry of Petroleum and Minerals, Sultanate of Oman, 55–82.

Rochette, P., Aubourg, C., Perrin, M., 1999. Is this magnetic fabric normal? A review and case studies in volcanic formations. Tectonophysics 307, 219–234.

Sigurdsson, H., Sparks, R.S.J., 1978. Lateral magma flow within rifted Icelandic crust. Nature 274, l26–l30.

Smith, B.M., Prévot, M., 1977. Variation of the magnetic properties in a basaltic dyke with concentric cooling zones. Physics of the Earth and Planetary Interiors 14, 120–136.

Soriano, C., Beamud, E., Garcés, M., 2008. Magma flow in dikes from rift zones of the basaltic shield of Tenerife, Canary Islands: Implications for the emplacement of buoyant magma. Journal of Volcanology and Geothermal Research 173, 55–68.

Storey, B.C., Alabaster, T., Hole, M.J., Pankhurst, R.J., Weaver, H.E., 1992. Role of subduction-plate boundary forces during the initial stages of Gondwana break-up: evidence from the proto-Pacific margin of Antarctica. In: Storey, B.C., Alabaster, T., Pankhurst, R.J. (Eds.), Magmatism and the Causes of Continental Break-up 68, 149–163.

Sweeney, R.J., Duncan, A.R., Erlank, A.J., 1994. Geochemistry and petrogenesis of central Lebombo basalts from the Karoo Igneous Province. Journal of Petrology 35, 95–125.

Sweeney, R.J., Watkeys, M.K., 1990. A possible link between Mesozoic lithospheric architecture and Gondwana flood basalts. Journal of African Earth Sciences 10, 707–716.

Tarling, D.H., Hrouda, F., 1993. The Magnetic Anisotropy of Rocks. Chapman & Hall, London, 217 pp.

Tauxe, L., Gee, J.S., Staudigel, H., 1998. Flow directions in dikes from anisotropy of magnetic susceptibility data: The bootstrap way. Journal of Geophysical Research 103, 17775–17790.

Uken, R., Watkeys, M.K., 1997. An interpretation of mafic dyke swarms and their relationship with major mafic magmatic events on the Kaapvaal Craton and Limpopo Belt. South African Journal of Geology 100, 341–349.

Watkeys, M.K., 2002. Development of the Lebombo rifted volcanic margin of southeast Africa. In: Menzies, M.A., Klemperer, S.L., Ebinger, C.J., Baker J. (Eds.), Volcanic Rifted Margins. Geological Society of America Special Paper 362, 27–46.

White, R.S., 1997. Mantle Plume origin for the Karoo and Ventersdorp Flood Basalts, South Africa. South African Journal of Geology 100, 271–283.

- Chapter 7 -

Discussion:

Magma flow in dyke swarms of the Karoo LIP: Implications for the mantle plume hypothesis

Note: The geological background presented in Chapter 3, along with the results, discussion and conclusions of this chapter, are combined in a manuscript in prep. for peer review (Appendix B). In the interest of brevity this chapter has been edited to reduce repetition of background thus far presented. The reference list for this, and the final chapter, is presented at the end of Chapter 8.

7.1. Introduction

Globally, mantle plumes have been implicated in the development of voluminous LIPs (Bryan and Ernst, 2008). Because LIPs represent relatively short-lived (< 5 Ma), high volume magmatism (covering ~10^6 km^2), many of them are believed to have been formed predominantly by mantle plume processes; including the Deccan Traps, Iceland, the Kerguelen Plateau, the Paraná-Etendeka flood basalt province and the ~183 Ma old Karoo LIP (Courtillot and Renne, 2003). Some workers show, however, that LIPs may be related to events of magma drainage (Silver et al., 2006) or processes fundamentally similar to the formation of non-LIPs (Cañón-Tapia, 2010). Indeed, recent work suggests that the development of subduction zones at supercontinent margins can strongly influence thermal convection beneath the lithosphere (O'Neill et al., 2009). Thermal insulation of the mantle by supercontinent assembly has also been proposed as a viable mechanism for the development of thermal, plume-like upwellings (Lenardic, 2005; Coltice et al., 2007).

A mantle plume origin for the Karoo LIP has been favoured for some time, particularly because of the Karoo triple junction (Burke and Dewey, 1973; Campbell and Griffiths, 1990; Cox, 1992; Storey, 1995; Ernst and Buchan, 1997; Storey and Kyle, 1997; White,

1997; Storey et al., 2001). The plume model continues to gain support, particularly in the study of associated magmatism in Antarctica (Elliot and Fleming, 2000; Ferraccioli et al., 2005; Riley et al., 2005; Curtis et al., 2008). The study of magma flow directions in dykes associated with the Karoo LIP also suggest that lateral magma flow from the triple junction has occurred, which may be consistent with a mantle plume (Ernst and Duncan, 1995; Aubourg et al., 2008; Hastie et al., 2011b). There are, however, a number of geochemical (Sweeney and Watkeys, 1990; Sweeney et al., 1994; Jourdan et al., 2007a) and structural features (Le Gall et al., 2005; Klausen, 2009), as well as geochronology, which are inconsistent with a mantle plume (Jourdan et al., 2004, 2005, 2006, 2007b).

Before the reliance on quantitative flow fabrics the existence of a mantle plume was inferred by other means – such as the presence of triple junctions. The basic premise is that, similarly to dykes radiating outward from a volcanic edifice, dyke swarms that converge upon a central point (e.g. the Karoo triple junction, or the CAMP) were intruded laterally from a centralised mantle plume (Ernst and Buchan, 1997). Since the advent of AMS and mineral SPO, however, lateral magma flow in dyke swarms has been used to infer the presence of mantle plumes in a more quantitative way (Ernst and Duncan, 1995; Callot et al., 2001; Chaves and Correia Neves, 2005).

There is little doubt that the eventual dispersion of southern Gondwana at ~139 Ma occurred because of Karoo magmatism (Watkeys, 2002) and the vast network of sills and dykes provide good indicators of stresses in the crust at the time of their formation (Uken and Watkeys, 1997; Le Gall et al., 2005). Relative and/or absolute ages of dykes and magma flow determinations may help in piecing together the tectonic history. In this regard the implications of magma flow direction determined in dykes of the NLDS, ODS and RRDS are explored in the context of the Karoo triple junction. These directions have been determined using AMS and the SPO of plagioclase grains.

In addition, various studies of the Jurassic-age dykes of Dronning Maud Land in Antarctica will be discussed because of their apparently shared history of magmatism with the Karoo LIP (Zhang et al., 2003; Riley et al., 2005; Curtis et al., 2008). This may

provide additional constraint on the cause of magmatism in southern Gondwana as there is overlap in composition and age between magmatism associated with the Karoo triple junction and that of west Dronning Maud Land.

7.2. Aim

This chapter brings together the previously presented data from Chapters 3 and 6 related to (1) the timing and duration of Karoo and associated magmatism, (2) the mantle plume hypothesis for the development of the Karoo LIP and (3) magma flow directions which have been found in dykes of the Karoo LIP and associated magmatic provinces. The aim, therefore, is to constrain magma flow in dykes of the Karoo LIP to the timing of dyke formation in order to more critically assess the mantle plume hypothesis that has been explored in Chapter 3.

7.3. The Dyke Swarms

As discussed in Chapter 3, the Karoo LIP comprises a large number of volcanic and intrusive components which extend across southern Africa, covering ~3×10^6 km^2 (Eales et al., 1984). The bulk of the magmatism occurred between ~183 Ma and ~178 Ma and included the development of an incipient triple rift system occupied by the Save-Limpopo and Lebombo monoclines and the ODS.

The three main dyke swarms associated with the Karoo triple junction include the SLDS, NLDS and ODS (Jourdan et al., 2004), four more isolated swarms (RRDS, UDS, SLeDS, SBDS; Armstrong et al., 1984; Riley et al., 2006; Jourdan et al., 2007a) and at least five dyke swarms in Dronning Maud Land (Curtis et al., 2008).

Dyke swarms for which magma flow determinations have been made include the ODS, NLDS, RRDS, UDS, JDS and SDS (Figure 7.1). Determinations of magma flow in the ODS have been carried out by Ernst and Duncan (1995) and Aubourg et al. (2008). Riley et al. (2006) have studied the UDS and Curtis et al. (2008) have studied the JDS and SDS.

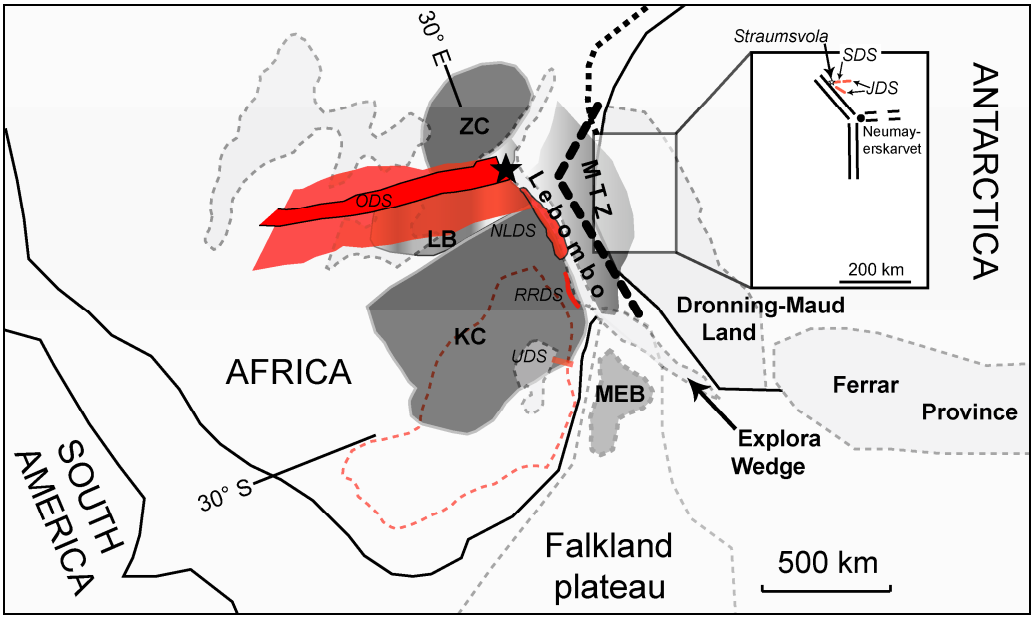

Figure 7.1: Schematic map of southern Gondwana at ~170 Ma showing the broad pre-Karoo crustal structure (solid) with the Karoo and associated volcanic provinces overlaid (in light grey with dashed outline). Only those dyke swarms for which magma flow-related data have been determined are shown. These include the ODS, NLDS, RRDS, SDS, JDS and UDS (all shown in red). The black star shows the position of Mwenezi. The extent of sill intrusion in South Africa (red dashed outline) is also shown. Note the positions (in bold text) of the Lebombo monocline, the Falkland Plateau, the Explora Wedge, Dronning Maud Land, the Ferrar Province, the Kaapvaal Craton (KC), Zimbabwe Craton (ZC), Limpopo Belt (LB), the Mozambique thinned-zone (MTZ) and the Maurice-Ewing Bank (MEB). The incipient rift shown in the MTZ is from Jokat et al. (2003). The triple rift system in Antarctica that converges on Neumayerskarvet is re-drawn from Ferraccioli et al. (2005) (re-drawn from White and McKenzie, 1989; Storey et al., 1992; Encarnación et al., 1996; Storey and Kyle, 1997; Watkeys, 2002; Jourdan et al., 2004; Ferraccioli et al., 2005; Riley et al., 2006; Curtis et al., 2008).

As shown in Chapter 6, magma flow determinations have been made in the NLDS using AMS and the SPO of plagioclase (Hastie et al., 2011b). In this chapter magma flow determinations on the regional scale of the RRDS are presented. This is potentially significant because constraining magma flow direction(s) in the RRDS is important in that it provides insight into the late-stage magma dynamics in the southern Lebombo at ~174 Ma.

The Karoo-age dyke swarms in Dronning Maud Land for which flow-related data are available include the JDS (~205 Ma) and SDS (~178 Ma). The JDS consists predominantly of low-Ti tholeiitic dykes while the SDS is predominantly doleritic in composition. Curtis et al. (2008) have undertaken a study of the form, structure, age and

magma flow characteristics (using AMS) on these dyke swarms. The magma flow data are reviewed here in the context of the evolution of magmatism in the Karoo LIP.

Riley et al. (2006) provide an age of ~176 Ma for the intrusion of the UDS, a dyke swarm derived from sub-lithospheric melts involving some crustal contamination. Although AMS measurements have been undertaken on only three dykes, and therefore the regional significance of the measurements is questionable, they are discussed in the interest of completeness.

7.4. A Brief History of the Karoo Mantle Plume

The proposed mantle plume origin for the Karoo LIP has been discussed in detail in Section 3.6, and will be described only briefly here. The triple junction geometry, geomorphological features and geochemistry of the rocks of the Karoo LIP have all been used as evidence of a starting mantle plume in the Karoo LIP (Burke and Dewey, 1973; Cox, 1989; White, 1997). Still, others have found evidence in mitigation of the mantle plume hypothesis based on lithospheric structural control of the distribution of basalt compositions (Hawkesworth et al., 1984; Sweeney and Watkeys, 1990; Sweeney et al., 1994; Hawkesworth et al., 1999) and structural control of the triple junction (Le Gall et al., 2002; Jourdan et al., 2004; Le Gall et al., 2005).

Indeed, the structure and geochronology of the Karoo LIP shows that the orientation of the SLDS and ODS were inherited from Proterozoic intrusive events. Furthermore, the flood basalt eruptions appear to have been diachronous from south to north and the dyke swarms do not form a singular volcanic feeder system (see Section 3.5.3).

Similar to the Karoo LIP in southern Africa, the Ferrar Province and associated magmatism of west Dronning Maud Land display evidence of subduction related processes (Hergt et al., 1991; Encarnación et al., 1996). However, there is evidence that the Ferrar magmas were emplaced from the Weddell Sea triple junction (Elliot and Fleming, 2000; Leat, 2008), implying a significant degree of lateral magma flow.

The Karoo triple junction and the associated dyke swarms are central to the original mantle plume hypothesis for the Karoo but prior investigation has found a number of characteristics of the dyke swarms which are inconsistent with a mantle plume origin (Watkeys, 2002; Jourdan et al., 2004; Le Gall et al., 2005). Certainly, the Karoo triple junction was an active magmatic centre in the northern Karoo LIP, but lithospheric architecture and its pre-Jurassic past have strongly controlled the distribution of the monoclines and the dyke swarms into which they intrude (Jourdan et al., 2004; Jourdan et al., 2006). Thus, it is necessary to evaluate not only the magma flow directions, but how the flow directions may be related to the age and structure of the dyke swarms on the regional scale.

7.5. Methodology

7.5.1. Inferring Flow Direction

The methodology of measuring AMS has been presented in Section 2.4 and the method of inferring magma flow direction from AMS and SPO data has been discussed in Sections 2.5.2 and 2.10 respectively.

The approach here is to focus on the imbrication of the foliations relative to the dyke plane in predominantly oblate shaped fabric (Aubourg et al., 2002; Geoffroy et al., 2002) while also factoring in the orientation of $K1$ axes (in prolate fabrics) and any field evidence and previous work which may assist in flow determinations. This approach, at the regional scale, works by plotting all the type-A fabric data together in dyke co-ordinates (Figure 2.14). In such a framework it is easiest to observe and interpret the imbrication of the fabric (the bulk foliation as determined by the grouping of $K3$ axes), should it occur.

From the NLDS, RRDS and ODS the regional significance of AMS data determined from a total of 60 dykes is presented. Magnetic fabric data from a further 30 dykes from west Dronning Maud Land are also presented.

7.6. Regional AMS Fabrics

7.6.1. Magnetic Fabric of the NLDS

As discussed in Chapter 6, the magnetic fabric of 14 dykes (224 samples) of the NLDS is carried by stoichiometric magnetite and tends to be normal (type-A) to intermediate. Values of *P'* range from ~1.0 to 1.054 (mean: 1.027). The mean value of *T* in the NLDS is 0.027 with oblate fabric in 64 % of the data.

Magnetic fabric in the youngest (D4) dykes is typically type-A and oblate in shape. Vertical to sub-vertical *K*1 axes are found only in the prolate fabrics and these prolate fabrics tend to be intermediate, although some are neutral to oblate in shape. Four sites display scattered fabric, and another four sites display type-B fabric. Thus six dykes provide a measure of magma flow, including evidence of vertical and lateral flow. The grouped data (Figure 7.2a) reflects these trends and, overall, are consistent with lateral magma flow from the north. Note that the bulk data are split according to western and eastern margins in order to easily see any imbrication of the fabric elements.

7.6.2. Magnetic Fabric of the ODS

Ernst and Duncan (1995) were first to measure the magnetic fabric in the ODS using AMS, focussing their attention on the orientation of the magnetic lineation. These authors interpreted steeply plunging magnetic lineations close to the Karoo triple junction (< 300 km) and shallowly plunging lineations 400 km from the Karoo triple junction to indicate steep (vertical) flow and lateral (sub-horizontal) flow respectively.

The study of Aubourg et al. (2008) focussed on two regions of the ODS, the Thune and Shashe sections in which dykes of the ODS have intrude basement gneisses. The Thune and Shashe sections are 300 km and 400 km west of the Karoo triple junction respectively (inset of Figure 7.2).

The overall magnetic fabric determined by AMS of 23 dykes (386 samples) is type-A. The fabric is carried by ferromagnetic grains. Thermomagnetic measurements indicate that paramagnetic susceptibility is negligible.

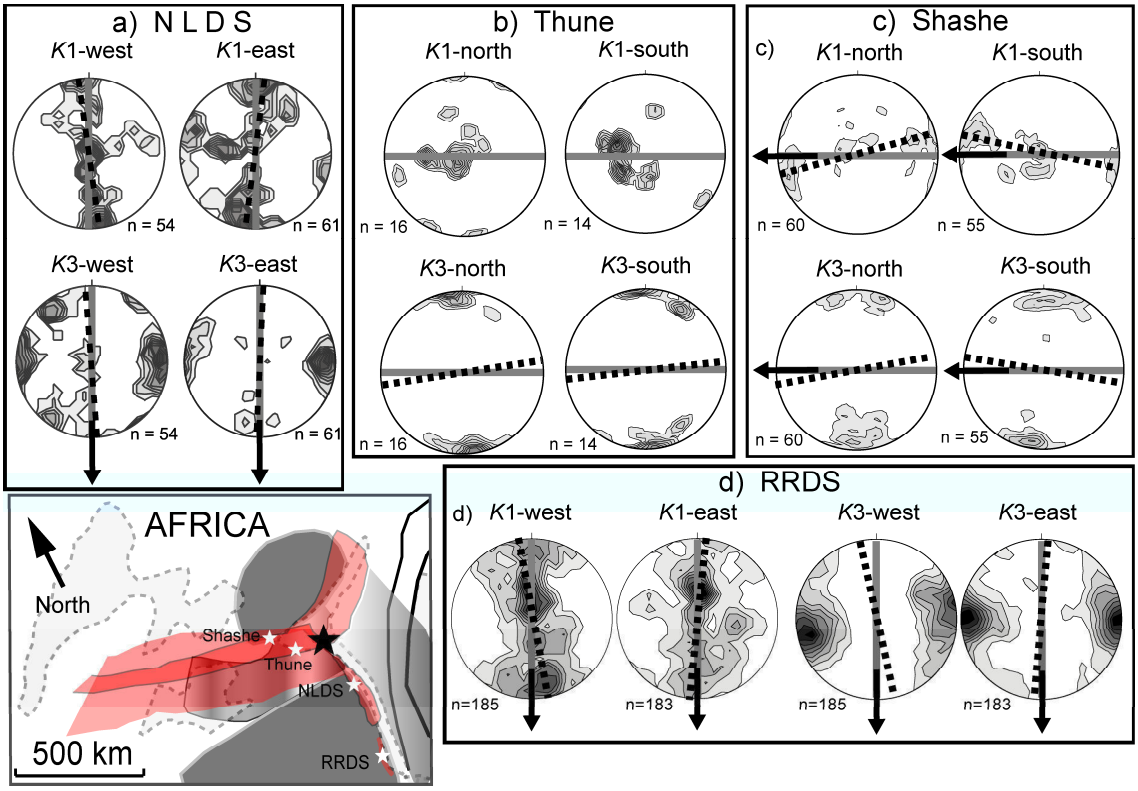

Figure 7.2: Grouped AMS data (type-A fabric only) for (**a**) the NLDS (from Hastie et al., 2011b), (**b**) the Thune section of the ODS (from Aubourg et al., 2008), (**c**) the Shashe section of the ODS (from Aubourg et al., 2008) and (**d**) the RRDS (Hastie et al., 2011a). Inset of the dyke swarms shows the sampled locations. The dyke planes in the stereoplots are shown in grey and the foliations as dashed black lines. Note that the ODS data have been rotated into a common E–W orientation and the NLDS and RRDS data into a common N–S orientation. The data are split according to the west and east margins (for NLDS and RRDS) and north and south (for the ODS) in order to find imbrication of the foliation or *K*1 axes. The number of samples is denoted by "n". Arrows indicate the magma flow direction inferred from the data. Note that the *K*1 axes for the Thune region, and the RRDS, show a degree of sub-vertical flow.

However, Aubourg et al. (2008) showed that the type-B fabric most likely results from strong magnetisation of some samples and the development of planar preferred orientation of ferromagnetic grains orthogonal to the dyke plane.

At the regional scale in the Thune section (Figure 7.2b) there is evidence of sub-vertical magma flow from the *K*1 axes, as well as contrasting lateral flow to the east and west. The magnetic fabric is less well defined in the Shashe section, but the imbrication of the magnetic foliations; in particular, show a more consistent picture of lateral magma flow to the west (Aubourg et al., 2008). Overall, the magnetic fabric in the ODS is well

constrained and imbrication is most consistent with lateral magma flow from east to west (Figure 7.2c).

7.6.3. Magnetic Fabric of the RRDS

Dykes of the RRDS are plagioclase and augite bearing dolerites. As discussed in Chapter 4, the magnetic fabric measured in 23 dykes (368 samples) of the RRDS is predominantly type-A, carried by fine-grained, low-Ti magnetite. The fabric is generally weakly anisotropic (mean P'=1.030) and neutral to oblate in shape (mean T=0.073). Type-B fabric exists in ~30% of the magnetic fabric data (Chapter 4, Hastie et al., 2011a).

The magnetic foliations are generally steeply dipping, and at least three dykes have shallowly plunging $K1$ axes, consistent with lateral magma flow (see Figure 4.6). Field data tend to support steep (60°–80°) emplacement, although inclined, sub-lateral and lateral magma flow is supported by AMS. For example, plots of the regional magnetic fabric show well constrained $K1$ and $K3$ axes, comprising type-A fabric (Figure 7.2d). The $K3$ axes in particular are very tightly grouped and are weakly imbricated. The imbrication is suggestive of inclined to sub-lateral magma flow from the north.

7.6.4. Magnetic Fabric of the JDS & SDS

As discussed already, Curtis et al. (2008) propose two distinct phases of mafic dyke emplacement (the JDS at ~205 Ma and the SDS at ~178–176 Ma) in the H.U. Sverdrupfjella of west Dronning Maud Land. Curtis et al. (2008) conducted AMS studies on 30 dykes, finding that 42% of the magnetic fabric is type-A. The fabric was found to be triaxial to oblate in shape with 1–4% anisotropy. This is very typical of mafic dykes. It is noted that the fabric becomes less well defined from north (48% type-A) to south (32% type-A). Intermediate fabric was found in 8% of the entire sample suite. The magnetic fabric appears to be carried by low-Ti magnetite, with type-A fabric occurring because of multi- and pseudo-single domain magnetite.

These authors use the $K1$ axis as a proxy for the magma flow direction, and find that the magnetic fabric is consistent with steep (sub-vertical) magma flow in the Straumsvola

area (discussed in Section 7.8.4), which is consistent with the orientation of stretched amygdales in one dyke of the SDS. When plotted together in N–S dyke co-ordinates, it is found that 61 of the averaged *K*3 axes (~51% of the data) define a type-B fabric (Figure 7.3a).

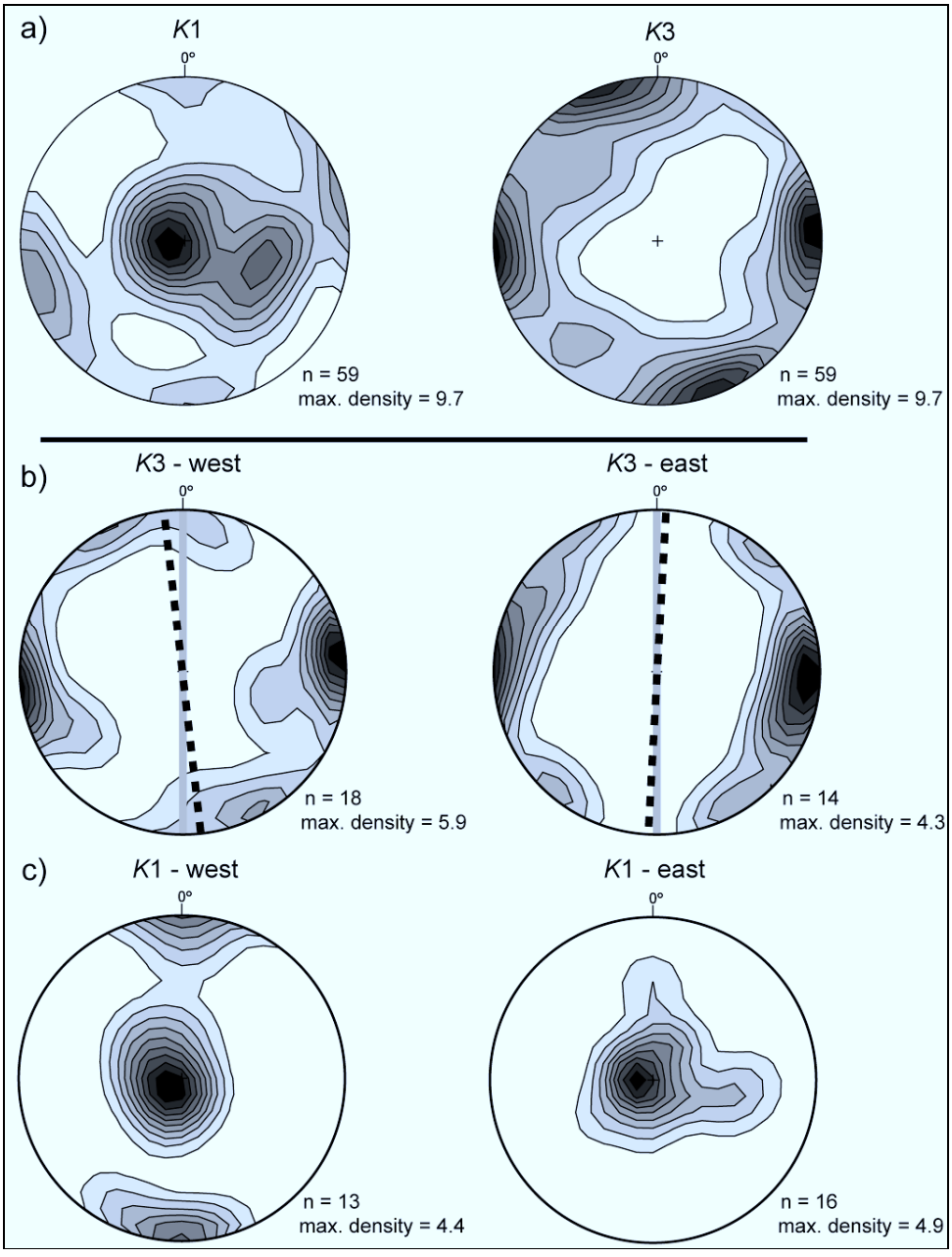

Figure 7.3: Bulk AMS data of the SDS and JDS plotted in (**a**) N-S dyke co-ordinates and separated into (**b**) *K*3 axes (N-S dyke co-ordinates) and (**c**) *K*1 axes (N-S dyke co-ordinates). The axes plotted are the averages from Table 2 of Curtis et al. (2008) (n=59). The N-S dyke plane is shown in grey and the foliation as a dashed black line. The total number of samples measured = 480. See Section 7.6.4 for discussion.

It has been found by a number of workers that mafic dykes tend to contain ~50% type-B magnetic fabric (Baer, 1995; Callot et al., 2001; Aubourg et al., 2008). If this type-B component is removed and the margins are plotted separately it is found that *K*1 axes are consistent with vertical and lateral flow (Figure 7.3c). There is a very slight imbrication of the foliations that suggests lateral flow to the south (Figure 7.3b).

This is consistent with an increasing component of lateral flow ~25 km south of Straumsvola in the Jutulrøra region (Curtis et al., 2008). The lack of shallowly plunging *K*1 axes from the eastern margins is, however, inconsistent with this, as is the arguably weak imbrication, which likely reflects a stronger vertical flow component of the Straumsvola region.

7.7. Regional SPO Results

The overview of the regional mineral SPO fabrics is restricted to the bulk plagioclase fabric for the NLDS and RRDS. In the ODS Aubourg et al. (2008) does indicate that there is generally good agreement between AMS and the orientation of plagioclase grains. There is no mineral SPO data available for the dykes of Dronning Maud Land.

The plagioclase fabric in the NLDS (7 dykes, 28 ellipsoids) is generally type-A, consistent with the magnetic fabric. The plagioclase fabric has a mean *P'* value of 1.208 and is predominantly triaxial to oblate (mean *T*=0.042). The highest *P'* values for plagioclase are found in phenocryst-rich samples. Imbrication of the plagioclase SPO fabric is found in four dykes and southward verging imbrication of foliations in the bulk fabric occurs (Figure 7.4a).

Although the *L*1 axes would be consistent with vertical magma flow, it has been shown that the foliations in this case are more reliable because of the coincidence between intersection lineations and the *L*1 axes (Hastie et al., 2011b). Furthermore, the geological significance of the lineation in a predominantly oblate fabric is debatable.

A total of 41 ellipsoids representative of the plagioclase fabric have been determined for 10 dykes of the RRDS. The fabric is predominantly neutral to oblate in shape (T=0.04) with a mean P' value of 1.19. Approximately 30% of the plagioclase SPO fabric is type-B and prolate in shape (Hastie et al., 2011a). The remaining type-A fabric of 10 dykes is shown in N–S dyke co-ordinates in Figure 7.4b. Similarly to the NLDS, it is the orientation of the foliations that is relied upon to show the magma flow direction.

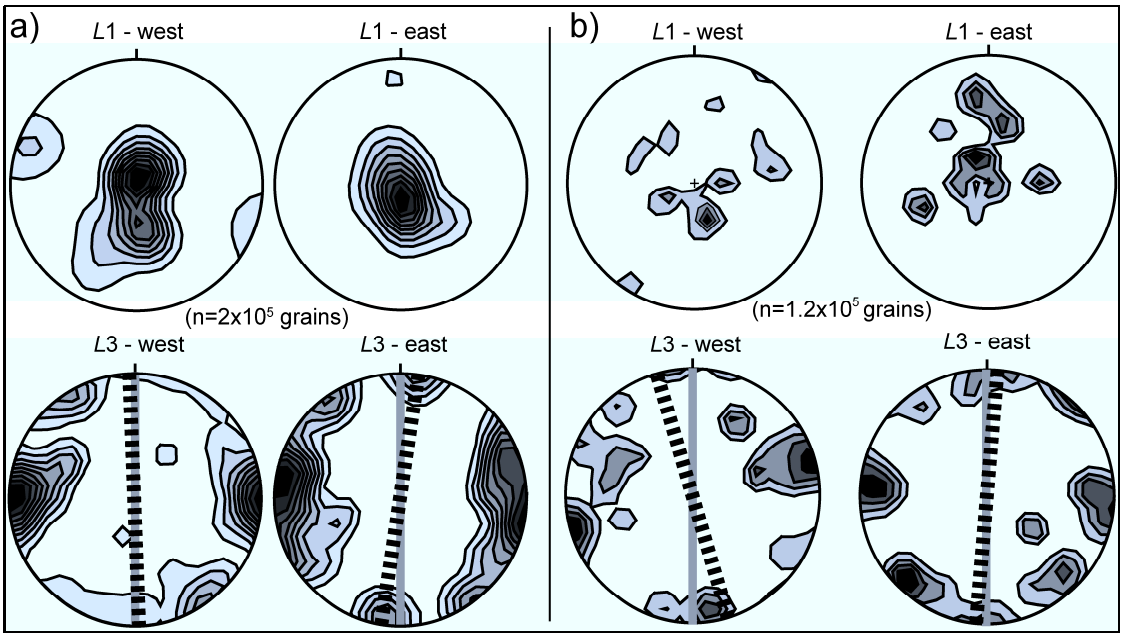

Figure 7.4: Mineral SPO data in N–S dyke co-ordinates for (**a**) the NLDS (from Figure 10 of Hastie et al., 2011b) and (**b**) the RRDS. The average dyke planes are shown in grey, the foliations as dashed black lines. The K1 axes, of the NLDS in particular, suggest vertical flow but the imbrication of the foliations, although slight, is suggestive of lateral magma flow.

The foliation defined by the L3 axes for the western margins is well imbricated with respect to the average dyke orientation, and verges southward. The foliation from the eastern margins appears similar, although the imbrication is arguably not as obvious. Overall, this imbrication is consistent with magma flow directed from north to south. The L1 axes are consistent with flow inclined ~20° from the vertical.

7.8. Magma Flow in the Dyke Swarms

7.8.1. The Northern Lebombo Dyke Swarm

The significance of regional AMS fabric in 90 dykes related to the Karoo LIP has been presented (Aubourg et al., 2008; Curtis et al., 2008; Hastie et al., 2011a, b).

Data for the NLDS are consistent with early vertical flow, followed by lateral flow in the later (D4) dykes. The regional pattern of AMS and SPO are consistent with each other, and subtly suggest a lateral sense of magma flow from north to south. This would be consistent with the Karoo triple junction being a viable magma source.

7.8.2. The Okavango Dyke Swarm

The shallowly plunging $K1$ axes and imbricated foliations of the Shashe region are both consistent with lateral flow from SE to NW, distally to the triple junction. This is consistent with the findings of the NLDS. The predominantly (sub-) vertical $K1$ axes from the Thune section (closer to the triple junction) are consistent with steeper (more vertical) magma flow. The lack of mirrored imbrication of the foliations in the Thune data appears to preclude any significant degree of lateral magma flow.

7.8.3. The Rooi Rand Dyke Swarm

The magnetic and SPO fabric of the RRDS both have imbricated foliations consistent with flow from north to south. Both the $K1$ and $L1$ axes of the eastern dyke margins are consistent with a component of steep, sub-vertical magma flow. Kattenhorn (1994), using the SPO of plagioclase, also found relatively steep flow (23° from the vertical) in a dyke of the RRDS directed from north to south, which is also consistent with field evidence such as steeply plunging broken and rotated bridges along some dyke margins (Nicholson and Pollard, 1985; Bussel, 1989). This suggests that the RRDS was not fed from the Karoo triple junction, as does the fact that the northern end of the RRDS terminates approximately 500 km south of Mwenezi.

Evidence for lateral magma flow in the RRDS is consistent with the findings for the NLDS, but difficult to interpret in light of the RRDS's restricted occurrence and

compositional and age differences. Steep flow coupled with evidence of lateral flow from AMS and SPO is most likely the result of outward flow from a central magmatic source. If the RRDS indeed post-dates the Lebombo rhyolites and is indicative of lithospheric rupturing, it is possible that the RRDS is analogous to a mid-ocean ridge segment (Figure 7.5).

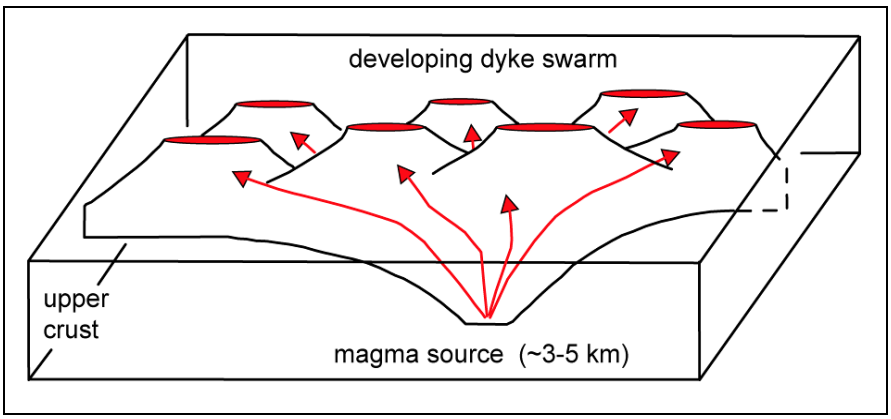

Figure 7.5: Schematic figure illustrating sub-lateral flow in dykes (the RRDS?) forming from a central, vertically fed magma source, analogous to the formation of mid-ocean ridge segments (re-drawn from Archanjo and Launeau, 2004).

In such segments the dominant magma flow direction would become increasingly lateral in dykes distal to the vertically fed central axis. This has been previously demonstrated in such segments by Abelson et al. (2001) and Archanjo and Launeau (2004).

7.8.4. Dyke Swarms of west Dronning Maud Land

The magnetic fabric in the JDS and SDS has two components. There is data consistent with steep (sub-vertical) magma flow in the north (Straumsvola) and with a lateral flow component further south (Jutulrøra) (Curtis et al., 2008). The steep component is particularly evident from the *K*1 axes. The regional pattern of magma flow determined from the type-A fabric in N–S dyke co-ordinates is consistent with this picture of flow from north to south, as can be seen from some of the shallowly plunging *K*1 axes of the western margins and the imbricated foliations.

Curtis et al. (2008) suggest that the JDS (irrespective of the vertically or laterally intruded components) and Group 1 dykes should not be considered contiguous with the Karoo LIP *sensu stricto*. Magma flow data from the ADS and VDS would assist in shedding light on dyke emplacement in this region, because magma flow directed from the previously conjugate Africa-Antarctica margin would be consistent with the plume/melting anomaly position shown in Figure 3.4c (Cox, 1989; White and McKenzie, 1989; Storey et al., 1992; White, 1997; Elliot and Fleming, 2000; Curtis et al., 2008). The north-to-south magma flow direction found in the SDS and JDS is not compatible with the direction expected from the Weddell Sea triple junction (Figure 3.4e).

The flow directions for the dyke swarms under consideration are summarised diagrammatically in Figure 7.6. The overall flow pattern, although somewhat simplified, is consistent with the Karoo triple junction being an important magma source for the NLDS and ODS at least.

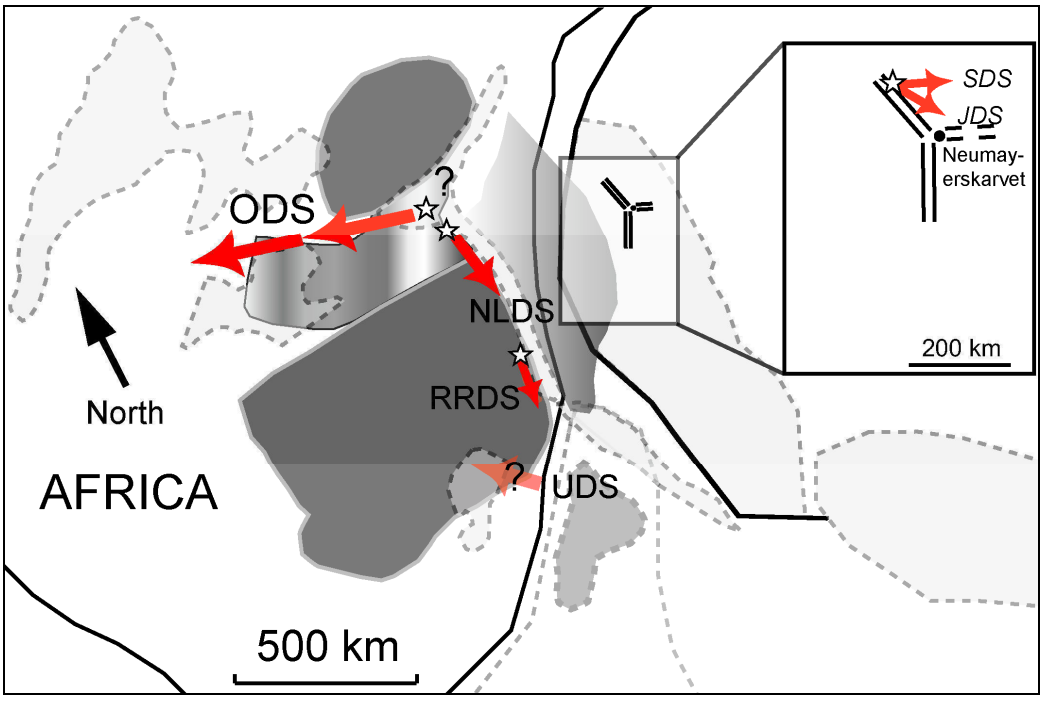

Figure 7.6: Regional schematic map of southern Gondwana between 178–174 Ma with magma flow directions inferred for the ODS, NLDS, RRDS, SDS and JDS. The flow direction of the UDS is uncertain ("?"). See Figure 7.1 and 3.1 for further detail. The red arrows indicate predominantly lateral flow while the stars indicate vertical flow. Note in the ODS, NLDS and RRDS that the edge of the Kaapvaal Craton strongly controls the distribution, and the flow directions, of the dyke swarms.

The flow pattern also highlights the strong role played by the Limpopo Belt and Kaapvaal Craton in controlling the distribution of the Lebombo and Save-Limpopo monoclines and the ODS.

The locus of flow in the JDS and SDS is at least 500 km from the Karoo triple junction, as is the apparent locus for the RRDS. Linked with the field evidence and geochronology that argues for a dyking progression from JDS > NLDS > SDS > ODS > RRDS it seems unlikely that each melt locus could have been a separate mantle plume. Indeed, these loci may be "weak spots" exploited by magma impingement under tensional conditions.

7.8.5. Magnetic Fabric of the UDS

Only three dykes of the UDS have reliable magnetic fabric from which a sense of magma flow direction can be inferred. Dyke SA.18 has magnetic fabric consistent with steeper flow from the northwest (Figure 7.7).

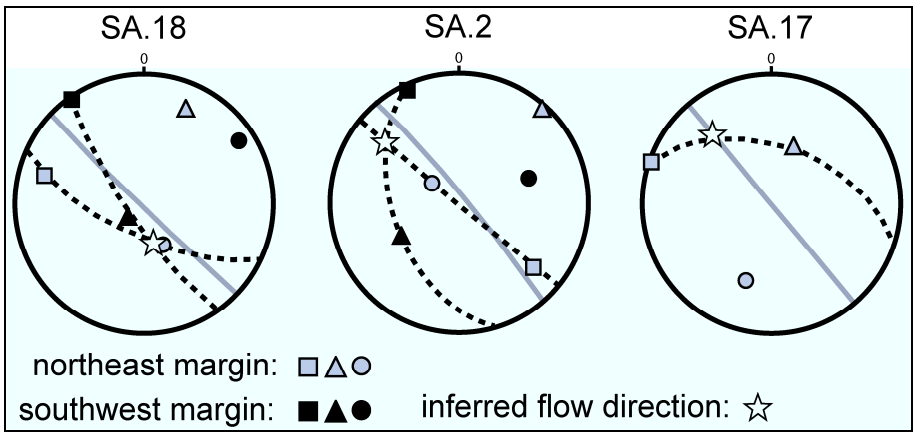

Figure 7.7: AMS data of three dykes from the UDS (re-drawn from Figure 15 of Riley et al., 2006).

However, dykes SA.2 and SA.17 of Riley et al. (2006) both have magnetic fabric consistent with sub-lateral flow from the southeast. This would be compatible with flow from the Weddell Sea triple junction (Figure 3.4e).

7.9. Magma flow & the Plume Hypothesis

Magma flow in the NLDS and ODS suggest that lateral magma flow emanated from the Karoo triple junction. Bearing in mind the evidence for the earliest (nephelinites) and youngest (silicic intrusion of the Mwenezi Igneous Complex) igneous activity at the triple junction, it is reasonable to view the Karoo triple junction as a relatively long-lived (~183–174 Ma) magmatic point source within the region. Still, it remains to be established whether the Karoo triple junction developed as a result of mantle plume activity.

Only three proponents of the original mantle plume models suggest that the plume impinged directly beneath the triple junction (Burke and Dewey, 1973; Campbell and Griffiths, 1990; Storey, 1995). The other models place the mantle plume "head" between Dronning Maud Land and the southern African continent (Figure 3.4c). This position, however, is not consistent with the directions of magma flow found in the dyke swarms of southern Africa.

When the age constraints on the dyke swarms are considered a number of inconsistencies come to light as well (Jourdan et al., 2004). Firstly, the SLDS was the earliest swarm to intrude and, along with the ODS, contains sub-parallel Proterozoic dykes which demonstrate a Jurassic-age exploitation of the older dyke direction. Secondly, dykes of the NLDS mostly pre-date, but also overlap with the ODS. Thirdly, the RRDS is considerably younger (174 Ma) and of asthenosphere-derived, MORB-like composition in comparison to other Karoo magmas (Saggerson et al., 1983; Armstrong et al., 1984; Meth, 1996). If we consider the principal $K1$ axes, and the finding of Kattenhorn (1994), it is evident that some degree of steep flow occurred in the RRDS. Fourthly, the remaining dyke swarms (UDS, SLeDS and SBDS) bear no relation to the triple junction at all. There are currently no ages on the SLeDS and SBDS, although the fact that they have intruded through the basalts, similarly to the UDS, suggests that they may be ~178–176 Ma in age.

The agreement between the magma flow determinations and the triple junction does not exclude the triple junction from being an important magmatic source region, but the timing of the various dyke swarms is evidently a more important factor to consider than the magma flow direction alone. This is apparent in the dykes of west Dronning Maud Land. For example, the ADS, JDS, SDS and Group 1 dykes appear to show a radiating geometry (Figure 3.1) which, along with other compositional and flow characteristics, could be considered indicative of a mantle plume. Indeed, the Straumsvola region has a protracted magmatic history. As discussed, however, magma flow from an igneous centre in the vicinity of Straumsvola at ~205 Ma predates Karoo magmatism by ~15 Ma, while the SDS was emplaced closer to 178 Ma. Thus, the JDS and Group 1 dykes should not be considered to be synchronous with the later Karoo LIP, and the remaining Karoo-aged dykes do not form a radiating pattern that could have resulted from a mantle plume, as first described by Curtis et al. (2008). It also appears highly unlikely that these dykes were fed by lateral intruding melts from the Weddell Sea or Karoo triple junction, but rather from a source coincident with the northeastern edge of the MTZ (Figure 3.1). It would thus appear to be a position between (b) and (c) in Figure 3.4.

Having considered the relevant dyke swarms in relation to the pre-existing crustal architecture and in relation to relative and absolute ages, we can make two basic inferences. Firstly, the Karoo triple junction has been an important magmatic source for the Karoo LIP and, secondly, there is no evidence from the dyke swarms themselves for the influence of a mantle plume. There is a conflict between the magmatic sources amongst the southern African dykes, however. The NLDS and ODS certainly seem to have been fed from a magma source related to the triple junction at Mwenezi, but the UDS may have been fed from the SE and the RRDS intruded at a later stage, possibly after the Jozini Formation rhyolites, and unrelated to a mantle plume. Without magma flow, or any other data, the origin of the SW-1 dyke swarm remains enigmatic. It is apparent that taking into account the triple junction geometry and the magma flow directions is insufficient evidence for proposing a mantle plume origin for the outwardly radiating dyke swarms and associated magmatism.

7.10. Magma Flow & Passive Melting

If a mantle plume did not give rise to the triple junction during the Jurassic, under what conditions did it arise, and how did the distribution of Karoo magmatism occur? Besides the effects of an impacting mantle plume, a triple junction may develop because of tensional stresses in the lithosphere owing to its curved shape because a curved surface responds differently under tension to a flat surface. Indeed, if dykes or dyke swarms exploit regions of lithospheric weakness, which has been demonstrated, it follows that the development of extensional regions on a curved surface would converge in triple junction-type geometry, without necessitating the influence of an upwelling plume from beneath.

In a passive model of magmatism the development of the Karoo LIP may have started because of a lack of cooling rather than active heating by a plume. Anderson et al. (1992) have suggested that crustal thinning above non-isothermal, inhomogeneous mantle is responsible for the formation of volcanic ridges and hotspots. This may be reflected in vertical magma flow in dykes, perhaps with some lateral flow outward from relatively small igneous centres. Evidently the accumulation and/or generation of heat and subsequent magmatism beneath the supercontinent of Gondwana would have weakened the crust, making continental break-up more likely as opposed to being a direct result of the emplacement of a plume beneath the supercontinent (Storey et al., 1992; White, 1997; Hawkesworth et al., 1999).

There has been considerable research into the potential effects of thermal insulation of the sub-continental mantle during times of supercontinent assembly preceding flood basalt formation and continental break-up (Anderson, 1994; Lenardic, 2005; Coltice et al., 2007; O'Neill et al., 2009; Heron and Lowman, 2011). For example, the depleted MORB-like magmas of Dronning Maud Land, generated from an anomalously "hot" source, are interpreted as being consistent with the melting model of Coltice et al. (2009). This potentially implicates internal heating of the upper mantle in Karoo magmatism, as opposed to a mantle plume (Heinonen et al., 2010).

Coltice et al. (2009) have simulated mantle convection beneath a supercontinent in 3-D. The results show that a supercontinent at the Earth's surface can have a significant impact on convection and temperature within the mantle. Their mantle global warming model predicts that (1) heating occurs over an area comparable in size to the overlying supercontinent, (2) melting occurs at modest (≤ 100 °C) temperature increases in the mantle, (3) melt is predominantly sourced from the asthenosphere and the continental lithosphere and (4) tectonic processes control the extraction of melt.

For continental cover > 10% of the Earth's surface, the authors expect the subcontinental mantle to increase in temperature by > 75°C over an area comparable in size to the "insulating" supercontinent. This process of mantle warming, alternatively to mantle plumes, is thus a feasible mechanism for the origin of some CFBs and the authors suggest that the mantle global warming model is becoming a more favourable explanation for the origin of the Karoo LIP. Their model is understandably not valid for all CFB provinces, mainly those that are unrelated to supercontinent dispersion, and for those in which mantle plume signature can be robustly demonstrated.

Indeed, even more recent modelling which incorporates both continental and oceanic plates in a supercontinent-type formation, suggests that this insulating effect is not strong and does not assist in elevating the mantle temperatures (Heron and Lowman, 2011). Instead, the presence of subduction zones surrounding such a supercontinent appears to strongly influence thermal convection beneath the lithosphere (O'Neill et al., 2009) and furthermore, a lack of movement of a supercontinent is a predominant factor in mantle insulation.

In modelling the assembly of a supercontinent Heron and Lowman (2011) have shown that a mantle plume forms beneath the crust at ~150 Ma after the subduction of oceanic crust between the adjoining continental plates. The return mantle flow, therefore, is predisposed to be beneath the supercontinent as the subduction zones are marginal (O'Neill et al., 2009). In the case of southern Africa, this would have occurred ~150 Ma prior to the Pan-African assembly of Gondwana at ~540 Ma (Rino et al., 2008).

However, major expressions of Karoo volcanism did not occur for a further ~360 Ma. From the modelling, it appears that 6 mantle transit times are required to produce continental dispersal (Zhong and Gurnis, 1993; Heron and Lowman, 2011). This is, perhaps fortuitously, equal to 60 Ma for each mantle transition, or 360 Ma. It is after 360 Ma that a plume-like upwelling forms beneath the supercontinent in the model, related to continuing subduction at the supercontinent margins (O'Neill et al., 2009).

Relating the above model directly to Gondwana break-up and the facets of the pre-cursory Karoo LIP is speculative at best. However, it does fit quite well with the time constraints shown above, the structure and the geochemistry of the Karoo LIP that is best explained by a sub-continental lithospheric mantle (SCLM) melt source (Sweeney at al., 1991; Sweeney at al., 1994; Hawkesworth et al., 1999; Jourdan et al., 2007a). Jourdan et al. (2009) have shown that only a slight geochemical evolution has occurred in the enriched, shallow lithospheric mantle beneath southern Africa in the 900 Ma prior to the development of the Karoo LIP. These authors conclude that the SCLM model for the Karoo is well explained by enhanced melting due to subduction processes prior to, and the insulating effects during the formation of Pangaea which broke-up ~200 Ma ago. This is consistent with the model interpretations of Heron and Lowman (2011), who show that subduction related magmatic processes are an important consequence of supercontinent assembly.

- Chapter 8 -

Conclusions

8.1. Petrofabric of the RRDS

- Dykes of the RRDS are plagioclase (55 vol. %) and augite (40 vol. %) bearing and contain magnetite. The dykes can be divided into less common plagioclase-phyric and those with a uniform texture. Plagioclase, which can reach 3-4 mm in length, is typically euhedral to subhedral, while augite is anhedral and stubby.
- Magnetic fabric of the RRDS is dominated by relatively pure, fine-grained, stoichiometric magnetite. The unusually pure and fine-grained magnetite suggests that it is of secondary origin; exsolution or metasomatic processes.
- The SPO of plagioclase determined from 120 thin sections (2.1×10^5 grains) define an anisotropic (P' = 1.19), neutral shaped fabric ($T = 0.04$).
- Plagioclase grains in the 12–13 μm size range with modest shape ratios (1.80–2.20) appear to define type-A fabric. This is comparable to the work of Benn and Allard (1989) who found that imbrication is not common below an r value of 1.50.
- Type-B fabric is associated with small (~8.50 μm) high anisotropy grains.
- The CSD and igneous textures of samples of the RRDS are consistent with heterogeneous nucleation – with phenocrysts having grown early at depth and grains < 80 μm having grown later under conditions of relatively rapid undercooling.
- There is evidence of lateral and inclined magma flow in the 174 Ma old RRDS. Its restricted position in the southern Lebombo monocline, MORB-like composition and possible origin as an MOR-like segment suggests that it was not emplaced as the result of a mantle plume.

8.2. Fabric Types & Acquisition in the RRDS

The grain orientation in both SPO and AMS fabrics yields a type-A fabric sub-parallel to the dyke plane resulting from magmatic flow in 70% the data. This is comparable to a

"steady state" fabric in which anisotropic grains rotate into the shear plane (Ildefonse et al., 1992; Launeau and Cruden., 1998). However, the type-B fabric, which in an AMS study would be interpreted as "inverse", is inconsistent with this steady-state fabric.

Changes in the orientation of thermally altered AMS fabric may occur for a number of reasons, although it is most likely that thermal alteration of the fine-grained magnetite (which dominates the AMS signal during measurement) would lead to oxidation (and decreasing K_m), resulting in the appearance of the type-B fabric. This is consistent with the SPO of the larger opaque grains in the RRDS. Type-B fabric in the opaque grain fraction suggests that large (macroscopic) magnetite grains do not contribute significantly to the generally type-A AMS fabric.

The work presented in Chapter 4 demonstrates that the very fine-grained fraction in dykes of the RRDS define an early-formed type-A fabric and the type-B fabric in the SPO is carried by larger plagioclase and opaque grains in 30% of the data. The type-B fabric in the plagioclase SPO may have resulted from late-stage fluid movement and magmatic pressure drop (Aarnes et al., 2008) occurring towards the dyke margins. The effects of this process on AMS are not clear, however. It can be speculated that the record of type-A fabric is evidence for the finest grains being controlled by an early formed silicate framework, and thus do not mimic the late-stage fabric.

The work presented in Chapter 5 suggests that a different late-stage process may be responsible for type-B fabric in the RRDS. The results demonstrate a correlation between increasing grain shape (r) and type-B fabric [comparable to Dragoni et al. (1997)]. Also, it appears that small grains of high anisotropy ($r > 7$) are likely to have grown at a late stage, perhaps during undercooling caused by upward migration of magma while earlier crystallisation, closer to equilibrium conditions, occurred at depth. This is demonstrated by the "kinked" CSD that reflects two distinct nucleation events (Marsh, 1988).

It was initially suggested that type-B fabric developed as a result of late-stage (high magma viscosity) re-orientation of the fabric caused by the interaction of large grains.

The findings presented in Chapter 5 also suggest late-stage processes, but it seems that rapid nucleation of the plagioclase groundmass at a late-stage has more significantly affected the development of type-B fabric than the process of grain interaction.

8.3. Petrofabric of the NLDS

- Dykes of the NLDS are medium- to coarse-grained dolerites, containing large plagioclase phenocrysts, clinopyroxene and between 3 to 8% opaque grains.
- The D1 and D2 generation dykes appear to have suffered minor alteration and the plagioclase groundmass and occasional phenocrysts are cloudy with irregular and diffuse grain boundaries. Opaque grains vary from small (<10 μm), equant grains to elongate, acicular and occasionally skeletal in the D4 dykes.
- Type-A magnetic fabric is present in 6 dykes of the NLDS and scattered and/or type-B in the remaining dykes.
- The shape preferred orientation fabric defined by plagioclase in the NLDS is of higher anisotropy (P' = 1.208) than the magnetic fabric and also weakly oblate in shape (T = 0.042) while the opaque grain fabric is triaxial to prolate (T = -0.077).
- With the exception of 3 sites the SPO fabric appears to be magmatic in origin (type-A) and furthermore is in agreement with the AMS fabric in 4 of the 7 dykes tested.
- When the bulk magnetic fabric is viewed in dyke co-ordinates on the regional scale a subtle, southward-verging imbrication of both K1 and K3 axes can be seen. Similar imbrication is evident in the L3 axes of the bulk plagioclase SPO data.
- The orientation of the imbricated fabric, although subtle, is most consistent with lateral magma flow, directed from a magma source positioned to the north of the dyke swarm – i.e. the Karoo triple junction.

8.4. The Karoo Mantle Plume

Although magma flow determinations alone are unlikely to provide the ultimate answer to the question of mantle plume influence in the Karoo LIP, a reliable regional picture of magma flow in the NLDS and RRDS has been demonstrated. These results, in the framework of the known structure, field relationships and geochronology related to the Karoo triple junction, are significant. This is because they are superficially consistent

with the pattern of radiating dyke emplacement typically associated with mantle plumes. However, in conjunction with relative ages, high-resolution $^{40}Ar/^{39}Ar$ dating and geochemical and geodynamic considerations it can be concluded that, while the influence of a mantle plume cannot be precluded, it is unlikely that the Karoo triple junction developed solely as the result of a mantle plume and the results themselves do not necessitate a mantle plume for their origin. This is because:

- The only position for a mantle plume that would be consistent with lateral flow in the NLDS and ODS would be one emplaced directly beneath Mwenezi (Figure 3.4a), a position inconsistent with the other dyke swarms and the south-to-north younging of magmatism in the Karoo LIP.
- Magma flow studies in dykes of west Dronning Maud Land show that is highly unlikely that these dykes were fed by lateral intruding melts from the Weddell Sea or Karoo triple junction, but rather from a source coincident with a position between (b) and (c) in Figure 3.4. There is, therefore, inconsistency between magma sources of the southern African and Antarctic dykes of the Karoo LIP.
- Steep flow coupled with evidence of lateral flow from AMS and SPO in the RRDS is most likely the result of outward flow from a magmatic source central to the RRDS itself. The MORB-like composition of the RRDS is also inconsistent with a mantle plume origin.
- The positions and orientations of the ODS, SLDS and Lebombo monocline are a product of the lithospheric structure, most obviously with respect to the ENE-trending structural fabric of the Limpopo Belt and the eastern edge of the Kaapvaal Craton.

It seems too simplistic, therefore, that a single, natural geological process could give rise to the entire Karoo LIP and associated magmatism, over a period of ~10 Ma, across several continents. Certainly, evidence has been presented in favour of a mantle plume, but there can be little doubt that a melt source in the sub-continental lithospheric mantle, which has undergone only slight geochemical evolution in the last ~1.0 Ga (Jourdan et al., 2009), is the most viable bulk melt source for the magmas of the Karoo LIP.

Ideally, more flow-related petrofabric studies in other lesser known dyke swarms are needed to further broaden the understanding of the origin of the Karoo LIP. That is, provided they are linked to rigorous field, structural and geochronological controls.

****

8.5. References

Aarnes, I., Podladchikov, Y.Y., Neumann, E.R., 2008. Post-emplacement melt flow induced by thermal stresses: Implications for differentiation in sills. Earth and Planetary Science Letters 276, 152–166.

Abelson, M., Baer, G., Agnon, A., 2001. Evidence from gabbro of the Troodos ophiolite for lateral magma transport along a slow-spreading mid-ocean ridge. Nature 409, 72–75.

Anderson, D.L., Zhang, Y.S., Tanimoto, T., 1992. Plume heads, continental lithosphere, flood basalts and tomography. In: Alabaster, T., Storey, B.C., Pankhurst, R.J. (Eds.), Magmatism and the Causes of Continental Break-up. Geological Society of London Special Publication 68, 99–124.

Anderson, D.L., 1994. Superplumes or Supercontinents? Geology 22, 39–42.

Archanjo, C.J., Launeau, P. 2004. Magma flow inferred from preferred orientations of plagioclase of the Rio Cearf-Mirim dyke swarm (NE Brazil) and its AMS significance. In: Martin-Hernandez, F., Luneburg, C.M., Aubourg, C., Jackson, M. (Eds.), Magnetic Fabric: Methods and applications. Geological Society of London Special Publication 238, 285–298.

Armstrong, R.A., Bristow, J.W., Cox, K.G., 1984. The Rooi Rand dyke swarm, southern Lebombo. In: Erlank, A.J. (Eds.), Petrogenesis of the volcanic rocks of the Karoo province. Geological Society of South Africa Special Publication 13, 77–86.

Aubourg, C., Giordano, G., Mattei, M., Speranza, F., 2002. Magma flow in sub-aqueous rhyolitic dikes inferred from magnetic fabric analysis (Ponza Island, W. Italy). Physics and Chemistry of the Earth 27, 1263–1272.

Aubourg, C., Tshoso, G., Le Gall, B., Bertrand, H., Tiercelin, J.-J., Kampunzu, A.B., Dyment, J., Modisi, M., 2008. Magma flow revealed by magnetic fabric in the Okavango giant dyke swarm, Karoo igneous province, northern Botswana. Journal of Volcanology and Geothermal Research 170, 247–261.

Baer, G., 1995. Fracture propagation and magma flow in segmented dykes: Field evidence and fabric analyses, Makhtesh Ramon, Israel. In: Baer, G., Heimann, A. (Eds.), Physics and Chemistry of Dykes. A.A. Balkema, Rotterdam, 125–140.

Benn, K., Allard, B., 1989. Preferred mineral orientations related to magmatic flow in ophiolite layered gabbros. Journal of Petrology 30, 925–946.

Bryan, S.E., Ernst, R.E., 2008. Revised definition of Large Igneous Provinces (LIPs). Earth-Science Reviews 86, 175–202.

Burke, K., Dewey, J.F., 1973. Plume generated triple junctions: key indicators in applying plate tectonics to old rocks. Journal of Geology 81, 406–433.

Bussel, M.A., 1989. A simple method for the determination of the dilation direction of intrusive sheets. Journal of Structural Geology 11, 679–687.

Callot, J.P., Geoffroy, L., Aubourg, C., Pozzi, J.P., Mege, D., 2001. Magma flow directions of shallow dykes from the East Greenland volcanic margin inferred from magnetic fabric studies. Tectonophysics 335, 313–329.

Campbell, I.H., Griffiths, R.W., 1990. Implications of mantle plume structure for the evolution of flood basalts. Earth and Planetary Science Letters 99, 79–93.

Cañón-Tapia, E., 2010. Origin of large igneous provinces: The importance of a definition. In: Cañón-Tapia, E., Szakács, A. (Eds), What is a volcano? Geological Society of America Special Paper 470, 77–101.

Chaves, A.O., Correia Neves, J.M., 2005. Magmatism, rifting and sedimentation related to Late Paleoproterozoic mantle plume events of central and southeastern Brazil. Journal of Geodynamics 39, 197–208.

Coltice, N., Phillips, B.R., Bertrand, H., Ricard, Y., Rey, P., 2007. Global warming of the mantle at the origin of flood basalts over supercontinents. Geology 35, 391–394.

Coltice, N., Bertrand, H., Rey, P., Jourdan, F., Phillips, B.R., Ricard, Y., 2009. Global warming of the mantle beneath continents back to the Archaean. Gondwana Research 15, 254–266.

Courtillot, V.E., Renne, P.R., 2003. On the ages of flood basalt events. Comptes Rendus Geosciences 335, 113–140.

Cox, K.G., 1989. The role of mantle plumes in the development of continental drainage patterns. Nature 342, 873–877.

Cox, K.G., 1992. Karoo igneous activity, and the early stages of the break-up of Gondwanaland. In: Storey, B.C., Alabaster, T., Pankhurst R.J. (Eds.), Magmatism and the Causes of Continental Break-up. Geological Society of London Special Publication 68, 37–148.

Curtis, M.L., Riley, T.R., Owens, W.H., Leat, P.T., Duncan, R.A., 2008. The form, distribution and anisotropy of magnetic susceptibility of Jurassic dykes in H.U. Sverdrupfjella, Dronning Maud Land, Antarctica. Implications for dyke swarm emplacement. Journal of Structural Geology 30, 1429–1447.

Dragoni, M., Lanza, R., Tallarico, A., 1997. Magnetic anisotropy produced by magma flow: theoretical model and experimental data from Ferrar dolerite sills (Antarctica). Geophysical Journal International 128, 230–240.

Eales, H.V., Marsh, J.S., Cox, K.G., 1984. The Karoo igneous province: An introduction. In: Erlank, A.J. (Eds.), Petrogenesis of the volcanic rocks of the Karoo province. Geological Society of South Africa Special Publication 13, 1–26.

Elliot, D.H., Fleming, T.H. 2000. Weddell triple junction: The principal focus of Ferrar and Karoo magmatism during initial breakup of Gondwana. Geology 28, 539–542.

Encarnación, J., Fleming, T.H., Elliot, D.H., Eales, H.V., 1996. Synchronous emplacement of Ferrar and Karoo dolerites and the early breakup of Gondwana. Geology 24, 535–538.

Ernst, R.E., Baragar, W.R.A., 1992. Evidence from magnetic fabric for the flow pattern of magma in the Mackenzie giant radiating dyke swarm. Nature 356, 511–513.

Ernst, R.E., Buchan, K.L., 1997. Giant Radiating Swarms: Their Use in Identifying Pre-Mesozoic Large Igneous Provinces and Mantle Plumes. Geophysical Monographs 100, 297–333.

Ernst, R.E., Duncan, A.R., 1995. Magma flow in the Giant Botswana dyke swarm from analysis of magnetic fabric (abstract). In: Agnon, A., Baer, G., (Eds.), Program & Abstracts for the Third International Dyke Conference, September 4-8, Jerusalem, Israel, pp. 30.

Ferraccioli, F., Jones, P.C., Curtis, M.L., Leat, P.T., 2005. Subglacial imprints of early Gondwana break-up as identified from high resolution aerogeophysical data over western Dronning Maud Land, East Antarctica. Terra Nova 17, 573–579.

Geoffroy, L., Aubourg, C., Callot, J.P., Moreira, M., 2002. Is the common use of AMS in mafic dykes scientifically correct? Terra Nova 14, 183–190.

Hastie, W.W., Aubourg, C., Watkeys, M.K., 2011a. When an 'inverse' fabric is not inverse: an integrated AMS-SPO study in MORB-like dykes. Terra Nova 23, 49–55.

Hastie, W.W., Watkeys, M.K., Aubourg, C., 2011b. Significance of magnetic and petrofabric in Karoo-feeder dykes, northern Lebombo. Tectonophysics 513, 96–111.

Hawkesworth, C.J., Kelley, S., Turner, S., Le Roex, A., Storey, B.C., 1999. Mantle processes during Gondwana break-up and dispersal. Journal of African Earth Sciences 28, 239–261.

Hawkesworth, C.J., Marsh, J.S., Duncan, A.R., Erlank, A.J., Norry, M.J., 1984. The role of continental lithosphere in the generation of the Karoo volcanic rocks: evidence from combined Nd- and Sr-isotope studies. In: Erlank, A.J. (Eds.), Petrogenesis of the volcanic rocks of the Karoo province. Geological Society of South Africa Special Publication 13, 341–354.

Heinonen, J.S., Luttinen, A.V., 2010. Mineral chemical evidence for extremely magnesian subalkaline melts from the Antarctic extension of the Karoo large igneous province. Mineralogy and Petrology 99, 201–217.

Heron P.J., Lowman J.P., 2011. The effects of supercontinent size and thermal insulation on the formation of mantle plumes. Tectonophysics 510, 28–38.

Hergt, J.M., Peate, D.W., Hawkesworth, C.J., 1991. The petrogenesis of Mesozoic Gondwana low-Ti flood basalts. Earth and Planetary Science Letters 105, 134–148.

Hopkinson, J., 1889. Magnetic and other physical properties of iron at a high temperature. Philosophical Transactions of the Royal Society of London Series A 180, 443 pp.

Hunt, C.P., Moskowitz, B.M., Banerjee, S.K., 1995. Magnetic Properties of Rocks and Minerals. In: Ahrens, T.J. (Eds.), Rock physics and phase relations. A Handbook of physical constants. American Geophysical Union, Washington, 189–204.

Ildefonse, B.P., Launeau, P., Bouchez, J.L., Fernandez, A., 1992. Effect of mechanical interactions on the development of shape preferred orientations: A two-dimensional experimental approach. Journal of Structural Geology 14, 73–83.

Jokat, W., Boebel, T., König, M., Meyer, U., 2003. Timing and geometry of the early Gondwana breakup. Journal of Geophysical Research. 108, 1–15.

Jourdan, F., Bertrand, H., Féraud, G., Le Gall, B., Watkeys, M.K., 2009. Lithospheric mantle evolution monitored by overlapping large igneous provinces: Case study in southern Africa. Lithos 107, 257–268.

Jourdan, F., Bertrand, H., Sharer, U., Blichert-Toft, J., Féraud, G., Kampunzu, A.B., 2007a. Major and trace element and Sr, Nd, Hf, and Pb isotope compositions of the Karoo large igneous province, Botswana–Zimbabwe: lithosphere vs. mantle plume contribution. Journal of Petrology 48, 1043–1077.

Jourdan, F., Féraud, G., Bertrand, H., Kampunzu, A.B., Tshoso, G., Le Gall, B., Tiercelin, J.J., Capiez, P., 2004. The Karoo triple junction questioned: evidence from Jurassic and Proterozoic $^{40}Ar/^{39}Ar$ ages and geochemistry of the giant Okavango dyke swarm (Botswana). Earth and Planetary Science Letters 222, 989–1006.

Jourdan, F., Féraud, G., Bertrand, H., Kampunzu, A.B., Tshoso, G., Watkeys, M.K., Le Gall, B., 2005. Karoo large igneous province: Brevity, origin and relation to mass extinction questioned by new $^{40}Ar/^{39}Ar$ age data. Geology 33, 745–748.

Jourdan, F., Féraud, G., Bertrand, H., Watkeys, M.K., Kampunzu, A.B., Le Gall, B., 2006. Basement control on dyke distribution in Large Igneous Provinces: Case study of the Karoo triple junction. Earth and Planetary Science Letters 241, 307–322.

Jourdan, F., Féraud, G., Bertrand, H., Watkeys, M.K., 2007b. From flood basalts to the inception of oceanization: Example from the $^{40}Ar/^{39}Ar$ high-resolution picture of the Karoo large igneous province. Geochemistry, Geophysics, Geosystems 8, 989–1006.

Kattenhorn, S.A., 1994. Mechanisms of sill and dyke intrusion (unpubl. MSc. thesis), University of Natal, Durban, South Africa, 149 pp.

Klausen, M.B., 2009. The Lebombo monocline and associated feeder dyke swarm: Diagnostic of a successful and highly volcanic rifted margin? Tectonophysics 468, 42–62.

Launeau, P., Cruden, A.R., 1998. Magmatic fabric acquisition mechanisms in a syenite: Results of a combined anisotropy of magnetic susceptibility and image analysis study. Journal of Geophysical Research 103, 5067–5089.

Leat, P.T., 2008. On the long-distance transport of Ferrar magmas. In: Thomson, K., Petford, N. (Eds.), Structure and Emplacement of High-Level Magmatic Systems. Geological Society of London Special Publication 302, 45–61.

Le Gall, B., Tshoso, G., Dyment, J., Kampunzu, A.B., Jourdan, F., Féraud, G., Bertrand, H., Aubourg, C., Vétela, W., 2005. The Okavango giant mafic dyke swarm (NE Botswana): its structural significance within the Karoo Large Igneous Province. Journal of Structural Geology 27, 2234–2255.

Le Gall, B., Thsoso, G., Jourdan, F., Fe´raud, G., Bertrand, H., Tiercelin, J.J., Kampunzu, A.B., Modisi, M., Dyment, J., Maia, M., 2002. $^{40}Ar–^{39}Ar$ geochronology and structural data from the giant Okavango and related mafic dyke swarms, Karoo igneous province, N Botswana. Earth and Planetary Science Letters 202, 595–606.

Lenardic, A., Moresi, L.-N., Jellinek, A.M., Manga, M., 2005. Continental insulation, mantle cooling, and the surface area of oceans and continents. Earth and Planetary Science Letters 234, 317–333.

Marsh, B.D., 1988. Crystal size distributions (CSD) in rocks and the kinetics and dynamics of crystallization, I, Theory. Contributions to Mineralogy and Petrology 99, 277–291.

Meth, D.L., 1996. The Geology and Geochemistry of the Rooi Rand Dyke Swarm (unpubl. MSc. thesis), University of Natal, Durban, South Africa, 189 pp.

Nicholson, R., Pollard, D.D., 1985. Dilation and linkage of echelon cracks. Journal of Structural Geology 7, 583-590.

O'Neill, C., Lenardic, A., Jellinek, A.M., Moresi, L., 2009. Influence of supercontinents on deep mantle flow. Gondwana Research 15, 276–287.

O'Reilly, W., 1984. Rock and Mineral Magnetism. Blackie & Son, Glasgow, 220 pp.

Riley, T.R., Curtis, M.L., Leat, P.T., Watkeys, M.K., Duncan, R.A., Millar, I.L., Owens, W.H., 2006. Overlap of Karoo and Ferrar magma types in KwaZulu-Natal, South Africa. Journal of Petrology 47, 541–566.

Riley, T.R., Leat, P.T., Curtis, M.L., Millar, L.L., Fazel, A., 2005. Early-Middle Jurassic dolerite dykes from western Dronning Maud Land (Antarctica): identifying mantle sources in the Karoo large igneous province. Journal of Petrology 46, 1489–1524.

Rino, S., Kon, Y., Sato,W., Maruyama, S., Santosh, M., Zhao, D., 2008. The Grenvillian and Pan-African orogens: world's largest orogenies through geologic time, and their implications on the origin of superplume. Gondwana Research 14, 51–72.

Rochette, P., Aubourg, C., Perrin, M., 1999. Is this magnetic fabric normal? A review and case studies in volcanic formations. Tectonophysics 307, 219–234.

Saggerson, E.P., Bristow, J.W., Armstrong, R.A., 1983. The Rooi Rand dyke swarm. South African Journal of Science 79, 365–369.

Silver, P.G., Behn, M.D., Kelley, K., Schmitz, M., Savage, B., 2006, Understanding cratonic flood basalts. Earth and Planetary Science Letters 245, 190–201.

Storey, B.C., 1995. The role of mantle plumes in continental breakup: case histories from Gondwanaland. Nature 377, 301–308.

Storey, B., Alabaster, T., Hole, M.J., Pankhurst, R.J., Wever, H.E., 1992. Role of subduction-plate boundary forces during the initial stages of Gondwana break-up: evidence from the proto-Pacific margin of Antarctica. In: Storey, B.C., Alabaster, T., Pankhurst, R.J. (Eds.), Magmatism and the Causes of Continental Break-up, 149–163.

Storey, B.C., Kyle, P.R., 1997. An active mantle mechanism for Gondwana break-up. South African Journal of Geology 100, 283–290.

Storey, B.C., Leat, P.T., Ferris, J.K., 2001. The location of mantle–plume centers during the initial stages of Gondwana breakup. In: Ernst, R.E., Buchan, K.L. (Eds.), Mantle Plumes: Their identification through time. Geological Society of America Special Paper 352, 71–80.

Sweeney, R.J., Duncan, A.R., Erlank, A.J., 1994. Geochemistry and petrogenesis of central Lebombo basalts from the Karoo Igneous Province. Journal of Petrology 35, 95–125.

Sweeney, R.J., Falloon, T.J., Green, D.H., Tatsumi, Y., 1991. The mantle origins of Karoo picrites. Earth and Planetary Science Letters 107, 256–271.

Sweeney, R.J., Watkeys, M.K., 1990. A possible link between Mesozoic lithospheric architecture and Gondwana flood basalts. Journal of African Earth Sciences 10, 707–716.

Uken, R., Watkeys, M.K., 1997. An interpretation of mafic dyke swarms and their relationship with major mafic magmatic events on the Kaapvaal Craton and Limpopo Belt. South African Journal of Geology 100, 341–349.

Watkeys, M.K., 2002. Development of the Lebombo rifted volcanic margin of southeast Africa. In: Menzies, M.A., Klemperer, S.L., Ebinger, C.J., Baker, J. (Eds.), Volcanic Rifted Margins. Geological Society of America Special Paper 362, 27–46.

White, R.S., 1997. Mantle Plume origin for the Karoo and Ventersdorp Flood Basalts, South Africa. South African Journal of Geology 100, 271–283.

White, R.S., McKenzie, D., 1989. Magmatism at rift zones: The generation of volcanic continental margins and flood basalts. Journal of Geophysical Research 94, 7685–7729.

Zhang, X., Luttinen, A.V., Elliot, D.H., Larsson, K., Foland, K.A., 2003. Early stages of Gondwana breakup: The $^{40}Ar/^{39}Ar$ geochronology of Jurassic basaltic rocks from western Dronning Maud Land, Antarctica, and implications for the timing of magmatic and hydrothermal events. Journal of Geophysical Research 108, 2449.

Zhong, S., Gurnis, M., 1993. Dynamic feedback between a continent like raft and thermal convection. Journal of Geophysical Research 98, 12219–12232.

- Appendix A -

1) Hastie, W.W., Aubourg, C., Watkeys, M.K., 2011. When an “inverse” fabric is not inverse: an integrated AMS-SPO study in MORB-like dykes. Terra Nova 23, 49–55.

2) Hastie, W.W., Watkeys, M.K., Aubourg, C., 2013. Characterisation of grain-size, shape and orientation of plagioclase in the Rooi Rand dyke swarm, South Africa. Tectonophysics 583 145–157.

3) Hastie, W.W., Watkeys, M.K., Aubourg, C., 2011. Significance of magnetic and petrofabric in Karoo-feeder dykes, northern Lebombo. Tectonophysics 513, 96–111.

Terra Nova

doi: 10.1111/j.1365-3121.2010.00983.x

When an 'inverse' fabric is not inverse: an integrated AMS-SPO study in MORB-like dykes

Warwick W. Hastie,[1] Charles Aubourg[2] and Michael K. Watkeys[1]

[1]*School of Geological Sciences, University of KwaZulu-Natal, Building H1, University Road, Westville, Durban, 4001, South Africa;* [2]*Géosciences & Environnement Cergy, University of Cergy Pontoise, 8 Le Campus, 95031 Cergy Cedex, France*

ABSTRACT

Magma flow direction is recorded in the macroscopic mineral petrofabric and magnetic fabric of the MORB-like Rooi Rand dyke swarm. The bulk magnetic fabric is sub-parallel to the dyke plane, resulting from preferred orientation of grains during magma flow. This is referred to as type-A fabric. A study of mineral shape preferred orientation reveals an additional fabric, which is orthogonal to the average dyke orientation in 30% of the data. This fabric is carried by both plagioclase and opaque grains and would typically be interpreted as 'inverse'. It is referred to here as type-B fabric. However, because it is carried by the shape preferred orientation of macroscopic grains and is in most cases not coaxial to the anisotropy of magnetic susceptibility fabric, it is interpreted as having been acquired during increased grain interaction during late-stage magma flow associated with decreasing magma pressure.

Terra Nova, 23, 49–55, 2011

Introduction

Studies of the anisotropy of magnetic susceptibility (AMS) in magmatic rocks focus on flow-related fabrics, which are significant in understanding magma emplacement conditions (Khan, 1962; Ellwood, 1978; Knight and Walker, 1988; Rochette *et al*., 1992; Tarling and Hrouda, 1993; Tauxe *et al*., 1998; Poland *et al*., 2004; Philpotts and Philpotts, 2007; Aubourg *et al*., 2008). AMS is represented as an ellipsoid, the shape and orientation of which are most relevant. In dykes, AMS ellipsoids determined from opposing margins provide constraints on the magma flow orientation if imbrication of the fabric occurs (Tauxe *et al*., 1998; Geoffroy *et al*., 2002). Minerals such as multi-domain (MD) magnetite, pyrrhotite, hematite and phyllosilicates are the most common contributors to magnetic susceptibility; these have a 'normal' magnetic fabric. Conversely, single-domain (SD) magnetite, which is smaller in grain size (< 20 nm), can cause an 'inverse' magnetic fabric (Potter and Stephenson, 1988; Rochette *et al*., 1999). However, few AMS studies of mafic dykes have taken into account the potential complications of turbulence (Cañón-Tapia and Chávez-Álvarez, 2004), grain-size differences (Archanjo and Launeau, 2004) or late-stage fabric (Philpotts and Philpotts, 2007) as possible causes of inverse or anomalous fabrics, which occur frequently in rocks of MORB-like composition (Rochette *et al*., 1991; Cañón-Tapia and Chávez-Álvarez, 2004). The aim of this study was to examine how the magnetic fabric in dykes of the MORB-like Rooi Rand dyke swarm (RRDS) relates to an apparently inverse petrofabric. This work has a bearing on the general interpretation of magnetic fabrics, as it questions whether magnetic grains mimic the silicate or opaque-grain petrofabric.

Correspondence: Warwick W. Hastie, School of Geological Sciences, University of KwaZulu-Natal, Building H1, University Road, Westville, Durban, 4001, South Africa. Tel.: +27 (0) 31 260 1277; fax: +27 (0) 31 260 2280; e-mail: 203505849@ukzn.ac.za and/or warwick.hastie@gmail.com

Geological setting

The RRDS is a north–south trending 200-km long dyke swarm, which extends from the Msunduze River in KwaZulu-Natal (South Africa) northwards into east-central Swaziland (Fig. 1) (Saggerson *et al*., 1983; Armstrong *et al*., 1984; Duncan *et al*., 1990). The RRDS is 10–22 km in width and has intruded sedimentary rocks and basalts of the Karoo Supergroup just to the west of the main Lebombo range, which comprises rhyolites of the Jozini and Mbuluzi Formations (Eales *et al*., 1984). The Lebombo developed during extensive Karoo magmatism from *c*. 184 Ma to *c*. 174 Ma, during which time some 3×10^6 km^3 of basaltic lava covered parts of southern Africa and Antarctica (Eales *et al*., 1984; Encarnación *et al*., 1996). The eastward tilting and domino-style faulting (Fig. 1B) are the result of the separation of Antarctica from the south-east margin of Africa during Gondwana break-up (Eales *et al*., 1984; Watkeys, 2002). The apparent lack of crustal contamination in the RRDS is evidence of rapid emplacement, which occurred between 173.9 and 172.1 Ma (Jourdan *et al*., 2007) and therefore represents the final phase of magmatic activity in the Lebombo prior to sea-floor spreading offshore 33 Ma later (Goodlad *et al*., 1982; Watkeys, 2002).

Methods

The recognition of magmatic flow in rock fabric is usually in the form of a shape preferred orientation (SPO) of inequant grains, such as plagioclase. Such SPO data are useful, as they help corroborate AMS data (Launeau and Robin, 1996; Launeau and Cruden, 1998; Cañón-Tapia and Chávez-Álvarez, 2004; Launeau, 2004).

Standard AMS samples (25 mm × 22 mm) were collected from opposing margins of dykes using a hand-held petroleum-powered drill. Samples were orientated using both a magnetic compass and a sun compass. Forty samples from the same dykes were used for the mineral SPO study and compared with the AMS results. The

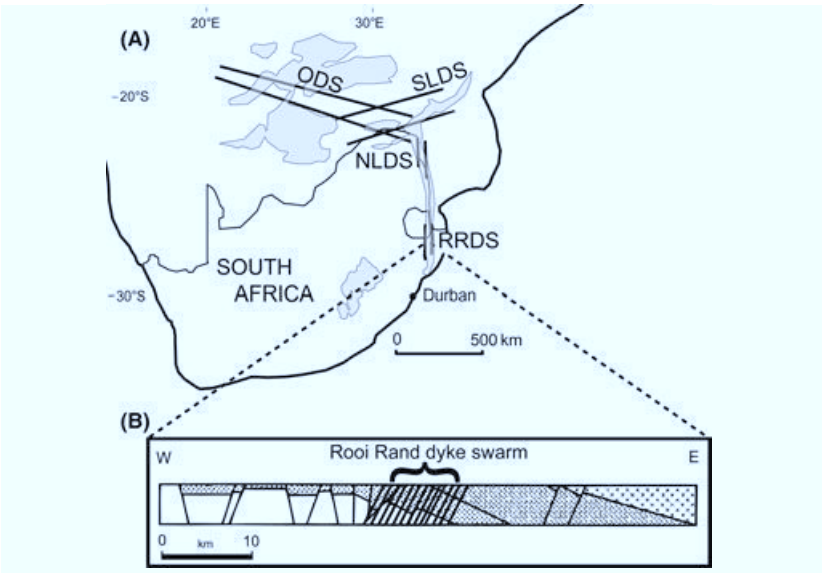

Fig. 1 (A) Southern Africa showing the position and extent of the volcanic remnants of the Karoo large igneous province (shaded). RRDS, Rooi Rand dyke swarm; NLDS, Northern Lebombo dyke swarm; SLDS, Save-Limpopo dyke swarm; ODS, Okavango dyke swarm (modified from Jourdan *et al.*, 2007). (B) Cross-section from west to east through the RRDS showing eastward dipping sedimentary and volcanic (ornamented) rocks of the Karoo Supergroup, which comprise the Lebombo faulted monocline (modified from Watkeys, 2002).

anisotropy of low-field susceptibility was measured using a Kappabridge KLY-3 apparatus at the University of Cergy-Pontoise.

In addition, the magnetic mineralogy of the samples was determined by monitoring susceptibility–temperature curves, which quantify changes in mean susceptibility (K_m) with temperature (Hunt *et al.*, 1995). This involves stepwise thermal demagnetization of powdered samples in an argon atmosphere within a Kappabridge KLY-3 apparatus under low field.

The method of investigating mineral SPO involves digitally filtering grains from photomicrographs of three orthogonal thin sections per sample (Fig. 2) and analysing between 300 and 2800 grains per section to determine the three-dimensional ellipsoid from the two-dimensional SPO inertia ellipses (Launeau, 2004; Launeau and Robin, 2005). This is done by inverting the colours of the image, converting the image to greyscale and then applying a threshold that reduces the image to only black (grains) and white. As the plagioclase grains are larger and darker than the surrounding matrix in these colour-inverted images, applying the threshold effectively removes the finer-grained matrix component. This is achieved using imaging software, such as Adobe® Photoshop® (Adobe Systems Inc., San Jose, California, USA). The results of SPO analysis of images in which individual grains were digitized by hand were found to be the same as those using the method described above.

The potential misfit between the two-dimensional sectional ellipses and the three-dimensional ellipsoid is quantified by an incompatibility index ($\sqrt{F}$), given as a percentage that is analogous to the standard deviation of the population of sectional ellipses (Launeau and Robin, 2005). A total of six thin sections per margin were analysed for 10 dykes, with all ellipsoids yielding $\sqrt{F}$-values $< 13\%$.

Following the work of Park *et al.* (1988), 52 samples were thermally demagnetized to monitor changes in the orientations of the principle AMS axes, especially where poorly grouped data or inverse fabrics were encountered. Park *et al.* (1988) showed that the magnetic fabric of the magnetite-bearing Mealy dyke swarm was irregular and scattered in the natural state, but better grouped after heating samples to 640 °C. The method used in this study involves monitoring changes in magnetic fabric after heating for 1 h in a nil magnetic field, from room temperature to 300 °C and finally to 700 °C. Although the results of this work are discussed (being super-

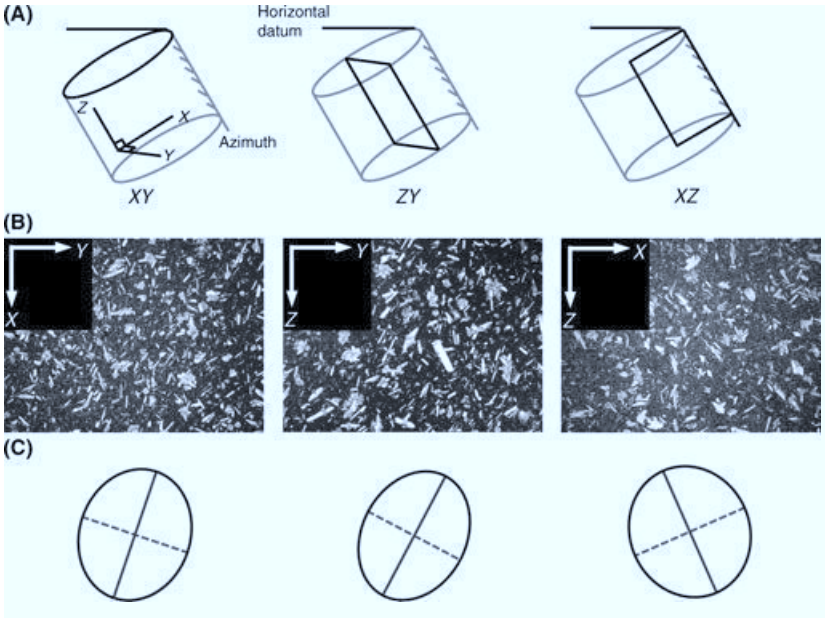

Fig. 2 (A) Schematic diagram illustrating the method employed for producing three orthogonal thin sections from a standard 10 cc drill core sample. Each drill core is cut into three orthogonal sections defined by an *XYZ* co-ordinate system. (B) Examples of greyscale thin-section photomicrographs from dyke WH-07-08 (9 mm in width). (C) Two-dimensional inertia tensors of constituent plagioclase grains are determined from each photomicrograph before being rendered in three dimensions as an ellipsoid.

ficially relevant to the SPO fabric), the interpretation thereof is limited owing to the lack of grain-size and magnetic-domain-state parameters.

Results

Dykes of the RRDS are predominantly plagioclase (55 vol.%) and augite (40 vol.%) bearing and contain magnetite. Olivine may also be present (Meth, 1996). The dykes can be divided into less-common plagioclase phyric (e.g. Fig. 2) and those with a uniform texture. Plagioclase, which can reach 3–4 mm in length, is typically euhedral to subhedral, while augite is anhedral and stubby.

The bulk magnetic fabric (23 dykes, 368 samples) of the RRDS is predominantly normal (Fig. 3A) and carried by low-Ti magnetite – deduced from thermomagnetic curves. The mean value of K_m is $36 \pm 20 \times 10^{-3}$ SI units, which is characteristic of basaltic rocks containing ~1 vol.% magnetite. The shape of the fabric is neutral to oblate and weakly anisotropic (Fig. 3B). Examples of susceptibility–temperature (K–T) curves for the RRDS samples, such as SZ-1, show demagnetization of the dominant phase at ~585 °C in a reversible curve (Fig. 3 C). A Hopkinson peak is also present. In other samples (Fig. 3D), there is evidence of magnetic transitions in the temperature range 180–280 °C.

The magnetic foliation is generally sub-parallel (within 35°) to the north–south-striking dyke; this is referred to as type-A fabric. In contrast, magnetic foliations in ~35% of the magnetic fabric data are orthogonal to the dyke plane. Following the work of Archanjo and Launeau (2004), this fabric will be referred to as type-B.

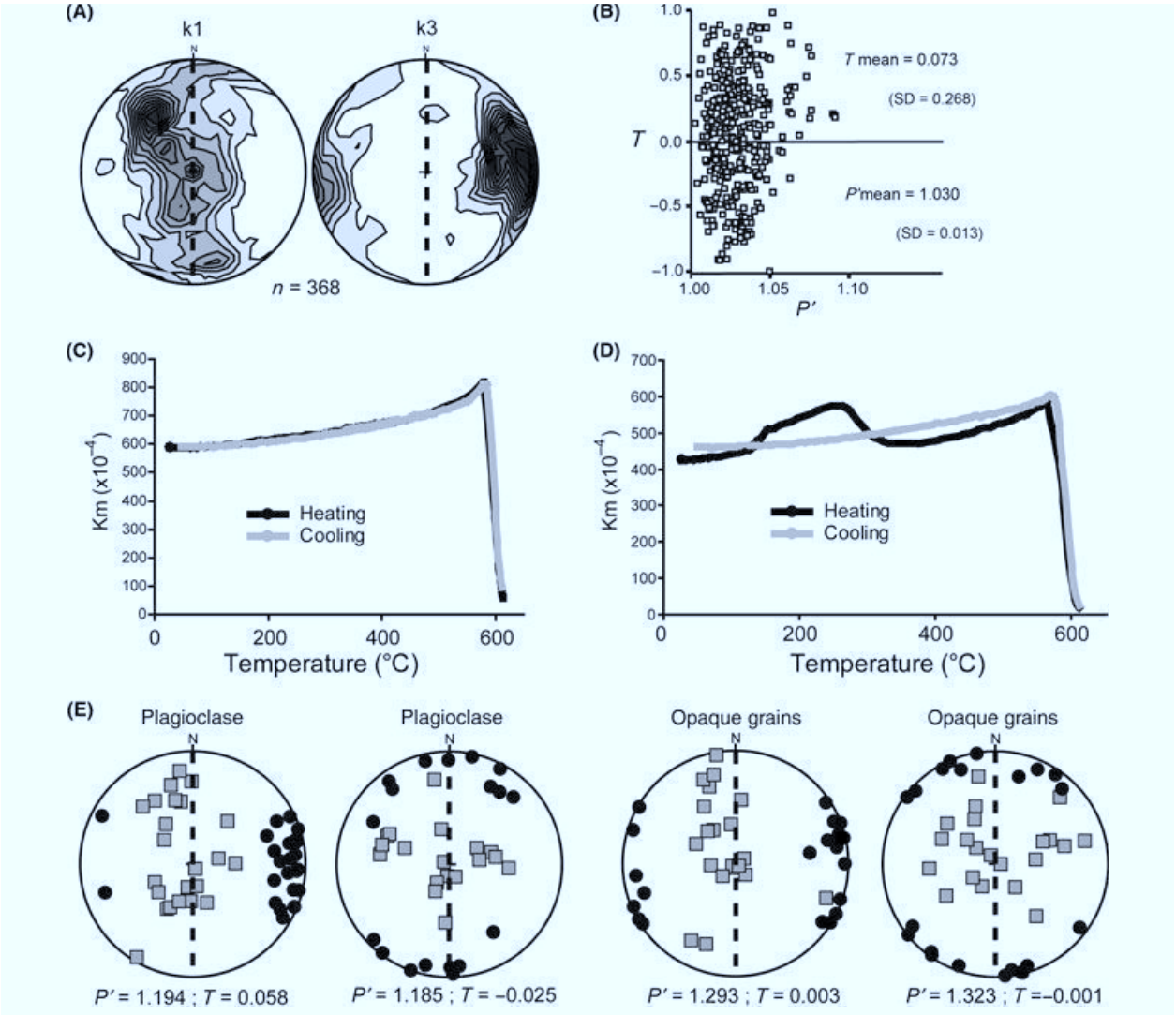

Fig. 3 (A) Density diagrams (k1 and k3) of the bulk AMS fabric for the RRDS in north–south dyke co-ordinates. This fabric is predominantly type-A. (B) P'–T diagram of the AMS fabric, illustrating a neutral to oblate shape and anisotropy < 1.10. (C) Susceptibility–temperature (K–T) curve for dyke SZ-1, illustrating reversibility and a Curie temperature of 580 °C. (D) K–T curve for dyke SZ-10, showing a magnetic transition during heating between 180 and 280 °C. See text for discussion of results. (E) Mineral shape preferred orientation data for both plagioclase and opaque grains in north–south dyke co-ordinates. Note that the type-A and type-B fabrics have been separated.

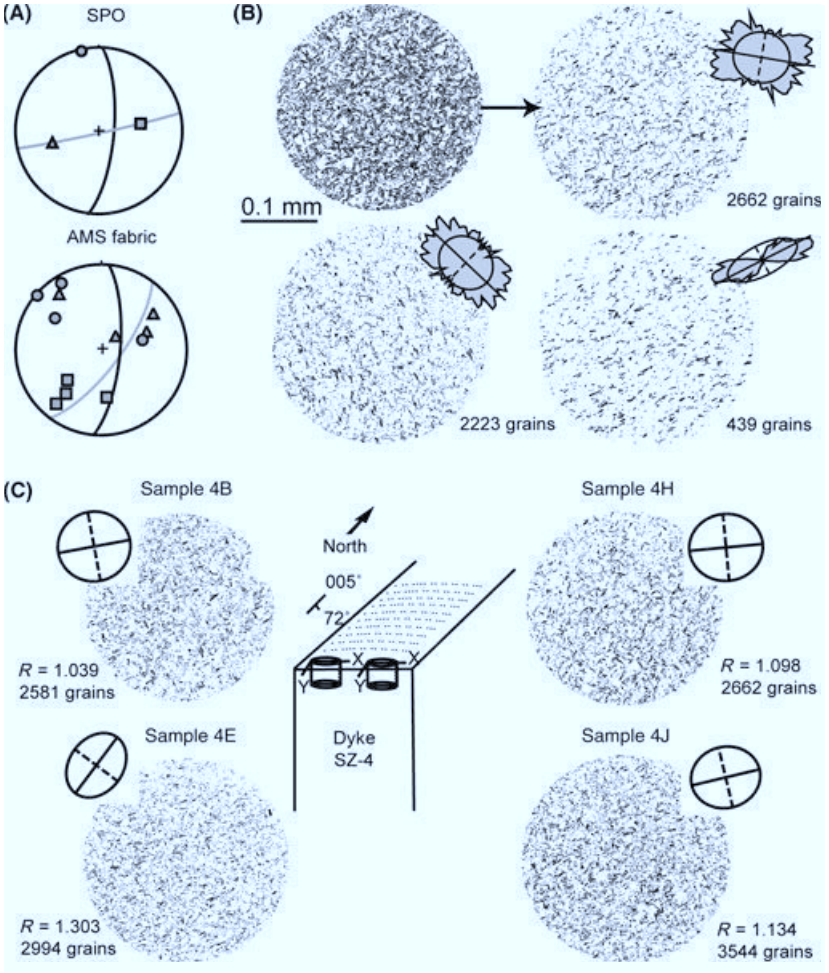

Fig. 4 (A) Stereographic projections of the petrofabric in dyke SZ-4 illustrating the SPO fabric (plagioclase and opaques combined) and AMS fabric (type-A). (B) Grayscale photomicrographs of the *XY* sections of sample 4H illustrating the presence of two plagioclase sub-fabrics (north is to the top of the page). Grain populations of different orientations are differentiated according to a colour-coded rose of directions. In this example, it is evident that two distinct populations of plagioclase coexist: one is shown in grey (magmatic fabric) and the other in black (type-B component). SPO ellipses illustrate the orientation of each population. (C) Plagioclase SPO fabric of all *XY* sections of dyke SZ-4 showing type-B fabric (except sample 4E) as illustrated by the 2-D ellipses (short axis dashed). R = long axis/short axis.

The SPO of plagioclase determined from 120 thin sections (2.1×10^5 grains) defines an anisotropic ($P' = 1.19$) neutral shaped fabric ($T = 0.04$). The opaque-grain fabric ($P' = 1.31$ and $T = 0.00$) is remarkably similar in orientation to the plagioclase fabric and on average is type-A (Fig. 3E). It is coaxial to the AMS fabric in eight dykes. However, like the AMS data, 30% of the SPO data are not comparable because the foliation plane is orthogonal to the dyke plane, i.e. type-B (see Supporting Information). The occurrence of the type-B fabric in the opaque-grain fraction suggests that these macroscopic grains do not necessarily contribute significantly to the generally type-A AMS fabric.

These two fabrics are exemplified by the results of dyke SZ-4; the SPO fabric is type-B, while the AMS fabric is type-A (Fig. 4A). Close inspection of individual greyscale *XY* sections indicates the presence of the two fabrics in question. This was achieved by the 'SPO-2003' program, which differentiates grain populations of different orientations by colour-coding each population according to a rose of directions. Thus, in the example, two distinct populations of plagioclase were found, one of which is type-A fabric (grey grains in Fig. 4B) and the other, type-B (black grains in Fig. 4B). Indeed, the bulk SPO of plagioclase grains can be separated, revealing the presence of the less-common, but significant type-B fabric in all but one *XY* section of dyke SZ-4 (Fig. 4C).

The thermally treated magnetic fabric of SZ-4 appears to be initially type-A, but becomes increasingly type-B after heating to 700 °C, while the bulk thermally altered AMS fabric also reflects this type-B orientation in 28% of the data (Fig. 5). This change is associated with a 45% decrease in bulk susceptibility (K_m).

Discussion

Demagnetization of the dominant phase at ~585 °C in a reversible *K–T* curve indicates the predominance of magnetite, and there is no mineralogical transformation of magnetic minerals (Smith and Prévot, 1977; Henry, 2007). Magnetic transitions in the temperature range 180–280 °C are likely due to the destruction of a sulphide phase during heating (Kontny *et al.*, 2000). The presence of a Hopkinson peak just below the unblocking temperature of the *K–T* curves is consistent with the occurrence of very-fine-grained, stoichiometric magnetite (O'Reilly, 1984; Hopkinson, 1989; Hunt *et al.*, 1995). Magnetite of magmatic origin would typically have a higher Ti content, with a consequently lower Curie temperature. The unusually pure and evidently fine-grained magnetite in some samples suggests that it is of secondary origin, resulting from exsolution or metasomatic processes (Rochette *et al.*, 1999). As a result, residual titanomagnetite remaining after exsolution processes may become overwhelmed in the magnetic signal by the pure magnetite, which has a higher susceptibility (Butler, 1992).

Obliquities may develop between fabrics defined by particles of different aspect ratios owing to the relationship between the amount of shear, governed by the magma flow gradient, and the resulting fabric (Jezek *et al.*, 1994; Cañón-Tapia and Chávez-

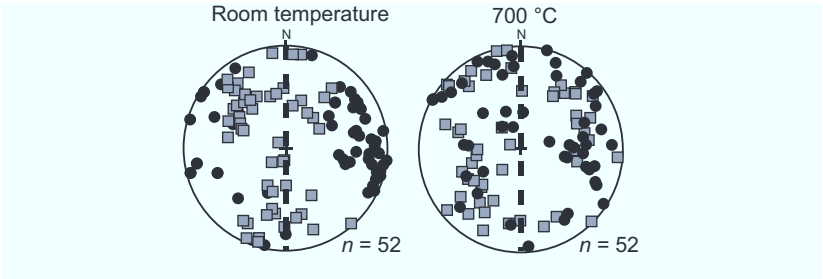

Fig. 5 Magnetic fabric measured at room temperature and after thermal treatment to 700 °C for 52 samples. All data shown are in north–south dyke co-ordinates, as indicated by the dashed black line. The initial fabric is predominantly type-A, but appears type-B after heating; this change is associated with a decrease in susceptibility. Only k1 (grey squares) and k3 (black circles) are shown.

Álvarez, 2004). During continuous grain rotation in a viscous medium, Cañón-Tapia and Chávez-Álvarez (2004) have found that the aspect ratio primarily controls the periodicity of rotation, and oblate particles are more likely to define a type-A fabric. Similarly, Launeau and Cruden (1998) indicate that grain-size differences can be reflected in different fabric orientations. Although SPO and AMS may record fabrics formed by different processes (as SPO is sensitive to grain orientation only), it is evident that the plagioclase grains and the significantly smaller magnetite grains can yield coaxial fabrics. The grain orientation in both SPO and AMS fabrics yields a type-A fabric sub-parallel to the dyke plane, resulting from magmatic flow, in 70% the data. This is comparable to a 'steady-state' fabric in which anisotropic grains rotate into the shear plane (Ildefonse *et al.*, 1992; Launeau and Cruden, 1998). However, the type-B fabric, which in an AMS study would be interpreted as 'inverse', is inconsistent with this steady-state fabric.

Changes in the orientation of a thermally altered AMS fabric must be considered cautiously. If fine-grained magnetite were to dominate the natural AMS signal, it is likely that thermal alteration would lead to oxidation [and a concomitant decrease in K_m (Henry *et al.*, 2003)], allowing the larger grains to contribute more to the AMS signal. This would result in the appearance of the type-B fabric, a result consistent with the SPO of the larger opaque grains. It is possible, however, that complex alteration may occur, resulting in growth of new grains along pre-existing fabrics (Mintsa Mi Nguema *et al.*, 2002; Souque *et al.*, 2002). Additionally, there is no constraint on the absolute grain-size or domain characteristics. Thus, the relationship between the thermally altered magnetic fabric and the type-B SPO fabric remains unresolved at this stage.

Type-B fabric acquisition

Fabric-acquisition models have taken into account cyclical rotation of progressively crystallizing and interacting grains (Cañón-Tapia and Chávez-Álvarez, 2004) or orthogonal fabrics in which prolate grains have evidently rotated about their long axes (Philpotts and Philpotts, 2007). However, type-B fabric in the SPO of plagioclase and opaque grains and the AMS fabric suggest that (1) the very-fine-grained fraction defines an early-formed type-A fabric (measured by AMS) and (2) the type-B fabric in the SPO is carried by larger plagioclase and opaque grains in 30% of the data. In a model of progressive crystallization, it is expected that intermediate fabrics between the type-A and type-B orientations should exist. However, there is no evidence for (sub-)horizontal foliations, fabric axes inversion or scattering of axes in the fabric of the RRDS (*viz*. Fig. 3).

In contrast, a dyke such as SZ-4 contains two distinct fabrics. Assuming that minimal phenocryst crystallization occurs during cooling at a late stage, it is likely that mineral grains in an increasingly more viscous magma could preferentially re-orientate owing to grain interaction, resulting in larger grains developing type-B fabric. Aarnes *et al.* (2008) have shown that significant post-emplacement flow can occur in basaltic melt (viscosity $\sim 10^2$ Pa·s) that is 99% crystallized, with late-stage fluid movement occurring from the intrusion centre towards the margins. This process is driven by a steep pressure drop along the margins caused by cooling and crystallization. The effects of a pressure drop along the dyke margins may be an important characteristic of sheeted dykes, such as the RRDS, which intrude under purely extensional conditions. The late-stage effects on finer grains, which control AMS, are not clear, however. It is possible that the record of type-A fabric is evidence for these grains being controlled by an early-formed silicate framework, but they do not mimic the late-stage fabric.

Acknowledgements

The authors acknowledge the technical staff of the University of Cergy-Pontoise and University of KwaZulu-Natal for assistance during the AMS measurements and thin-section preparation. Patrick Launeau and an anonymous reviewer are thanked for their constructive comments. The authors acknowledge the NRF-CNRS co-operative 'PICS' programme, which funded this research. W. Hastie acknowledges a free-standing NRF Scarce Skills bursary.

References

Aarnes, I., Podladchikov, Y.Y. and Neumann, E.R., 2008. Post-emplacement melt flow induced by thermal stresses: implications for differentiation in sills. *Earth Planet. Sci. Lett.*, **276**, 152–166.

Archanjo, C.J. and Launeau, P., 2004. Magma flow inferred from preferred orientations of plagioclase of the Rio Cearf-Mirim dyke swarm (NE Brazil) and its AMS significance. In: *Magnetic Fabric: Methods and Applications* (F. Martin-Hernandez, C.M. Luneburg, C. Aubourg and M. Jackson, eds). *Geol. Soc. Lond. Spec. Publ.*, **238**, 285–298.

Armstrong, R.A., Bristow, J.W. and Cox, K.G., 1984. The Rooi Rand dyke swarm, southern Lebombo. In: *Petrogenesis of the Volcanic Rocks of the Karoo Province* (A.J. Erlank, ed.). *Geol. Soc. S. Afr. Spec. Publ.*, **13**, 77–86.

Aubourg, C., Tshoso, G., Le Gall, B., Bertrand, H., Tiercelin, J.J., Kampunzu, A.B., Dymente, J. and Modisi, M., 2008. Magma flow revealed by magnetic fabric in the Okavango giant dyke swarm, Karoo igneous province, northern Botswana. *J. Volcanol. Geoth. Res.*, **170**, 247–261.

Butler, R.F., 1992. *Paleomagnetism: Magnetic Domains to Geologic Terranes.*

Blackwell Scientific Publications, Boston, MA.

Cañón-Tapia, E. and Chávez-Álvarez, M.J., 2004. Theoretical aspects of particle movement in flowing magma: implications for the anisotropy of magnetic susceptibility of dykes. In: *Magnetic Fabric: Methods and Applications* (F. Martin-Hernandez, C.M. Luneburg, C. Aubourg and M. Jackson, eds). *Geol. Soc. Lond. Spec. Publ.*, **238**, 227–249.

Duncan, A.R., Armstrong, R.A., Erlank, A.J., Marsh, J.S. and Watkins, R.T., 1990. MORB-related dolerites associated with the final phases of Karoo flood basalt volcanism in southern Africa. In: *Mafic Dykes and Emplacement Mechanisms* (A.J. Parker, P.C. Rickwood and D.H. Tucker, eds), pp. 119–129. Balkema, Rotterdam.

Eales, H.V., Marsh, J.S. and Cox, K.G., 1984. The Karoo igneous province: an introduction. In: *Petrogenesis of the Volcanic Rocks of the Karoo Province* (A.J. Erlank, ed.). *Geol. Soc. S. Afr. Spec. Publ.*, **13**, 1–26.

Ellwood, B.B., 1978. Flow and emplacement direction determined for selected basaltic bodies using magnetic anisotropy measurements. *Earth Planet. Sci. Lett.*, **41**, 254–264.

Encarnación, J., Fleming, T.H., Elliot, D.H. and Eales, H.V., 1996. Synchronous emplacement of Ferrar and Karoo dolerites and the early breakup of Gondwana. *Geology*, **24**, 535–538.

Geoffroy, L., Callot, J.P., Aubourg, C. and Moreira, M., 2002. Divergence between magnetic and plagioclase linear fabrics in dykes: a new approach for defining the flow vector using magnetic foliation. *Terra Nova*, **14**, 183–190.

Goodlad, S.W., Martin, A.K. and Hartnady, C.J.H., 1982. Mesozoic magnetic anomalies in the southern Natal valley. *Nature*, **295**, 686–688.

Henry, B., 2007. Magnetic mineralogy, changes due to heating. In: *Encyclopedia of Geomagnetism and Paleomagnetism* (D. Gubbins and E. Herrero-Bervera, eds), 1054 pp. Springer, Dordrecht.

Henry, B., Jordanova, D., Jordanova, N., Souque, C. and Robion, P., 2003. Anisotropy of magnetic susceptibility of heated rocks. *Tectonophysics*, **366**, 241–258.

Hopkinson, J., 1989. Magnetic and other physical properties of iron at a high temperature. *Phil. Trans. Roy. Soc. London A*, **180**, 443.

Hunt, C.P., Moskowitz, B.M. and Banerjee, S.K., 1995. Magnetic Properties of Rocks and Minerals. In: *Rock Physics and Phase Relations. A Handbook of Physical Constants* (T.J. Ahrens, ed.), pp. 189–204. American Geophysical Union, Washington.

Ildefonse, B.P., Launeau, P., Bouchez, J.L. and Fernandez, A., 1992. Effect of mechanical interactions on the development of shape preferred orientations: a two-dimensional experimental approach. *J. Struct. Geol.*, **14**, 73–83.

Jezek, J.R., Melka, R., Schulman, K. and Venera, Z., 1994. The behavior of rigid triaxial ellipsoidal particles in viscous flows – modeling of fabric evolution in a multiparticle system. *Tectonophysics*, **229**, 165–180.

Jourdan, F., Féraud, G., Bertrand, H. and Watkeys, M.K., 2007. From flood basalts to the inception of oceanization: example from the $^{40}Ar/^{39}Ar$ high-resolution picture of the Karoo large igneous province. *Geochem. Geophys. Geosyst.*, **8**, 1–20.

Khan, M.A., 1962. The anisotropy of magnetic susceptibility of some igneous and metamorphic rocks. *J. Geophys. Res.*, **67**, 2873–2885.

Knight, M.D. and Walker, G.P.L., 1988. Magma flow directions in dikes of the Koolau Complex, Oahu, determined from magnetic fabric studies. *J. Geophys. Res.*, **93**, 4301–4319.

Kontny, A., De Wall, H., Sharp, T.G. and Pósfai, M., 2000. Mineralogy and magnetic behavior of pyrrhotite from a 260 °C section at the KTB drilling site, Germany. *Am. Mineral.*, **85**, 1416–1427.

Launeau, P., 2004. Mise en évidence des écoulements magmatiques par analyse d'images 2-D des distributions 3-D d'Orientations Préferentielles de Formes. *Bull. Geol. Soc. France*, **175**, 331–350.

Launeau, P. and Cruden, A.R., 1998. Magmatic fabric acquisition mechanisms in a syenite: results of a combined anisotropy of magnetic susceptibility and image analysis study. *J. Geophys. Res.*, **103**, 5067–5089.

Launeau, P. and Robin, P.-Y.F., 1996. Fabric analysis using the intercept method. *Tectonophysics*, **267**, 91–119.

Launeau, P. and Robin, P.-Y.F., 2005. Determination of fabric & strain ellipsoids from measured sectional ellipses – implementation and applications. *J. Struct. Geol.*, **27**, 2223–2233.

Meth, D.L., 1996. *The geology and geochemistry of the Rooi Rand dyke swarm*. Unpublished MSc thesis, University of Natal, Durban, 189 pp.

Mintsa Mi Nguema, T., Trindade, R.I.F., Bouchez, J.L. and Launeau, P., 2002. Selective thermal enhancement of magnetic fabrics from the Carnmenellis granite (British Cornwall). *Phys. Chem. Earth*, **27**, 1281–1287.

O'Reilly, W., 1984. *Rock and Mineral Magnetism*. Blackie and Son, Glasgow.

Park, J.K., Tanczyk, E.I. and Desbarats, A., 1988. Magnetic fabric and its significance in the 1400 Ma Mealy diabase dykes of Labrador, Canada. *J. Geophys. Res.*, **93**, 13689–13704.

Philpotts, A.R. and Philpotts, D.E., 2007. Upward and downward flow in a camptonite dike as recorded by deformed vesicles and the anisotropy of magnetic susceptibility (AMS). *J. Volcanol. Geoth. Res.*, **161**, 81–94.

Poland, M.P., Fink, J.H. and Tauxe, L., 2004. Patterns of magma flow in segmented silicic dikes at Summer Coon volcano, Colorado: AMS and thin section analysis. *Earth Planet. Sci. Lett.*, **219**, 155–169.

Potter, D.K. and Stephenson, A., 1988. Single-domain particles in rocks and magnetic fabric analysis. *Geophys. Res. Lett.*, **15**, 1097–1100.

Rochette, P., Jenatton, L., Dupuy, C., Boudier, F. and Reuber, I., 1991. Diabase dikes emplacement in the Oman Ophiolite: a magnetic fabric study with reference to geochemistry. In: *Ophiolite Genesis and Evolution of the Oceanic Lithosphere* (T. Peters, A. Nicolas and R.G. Coleman, eds), Kluwer, Dordrecht, pp. 55–82.

Rochette, P., Jackson, M. and Aubourg, C., 1992. Rock magnetism and the interpretation of anisotropy of magnetic susceptibility. *Rev. Geophys.*, **30**, 209–226.

Rochette, P., Aubourg, C. and Perrin, M., 1999. Is this magnetic fabric normal? A review and case studies in volcanic formations. *Tectonophysics*, **307**, 219–234.

Saggerson, E.P., Bristow, J.W. and Armstrong, R.A., 1983. The Rooi Rand dyke swarm. *S. Afr. J. Sci.*, **79**, 365–369.

Smith, B.M. and Prévot, M., 1977. Variation of the magnetic properties in a basaltic dyke with concentric cooling zones. *Phys. Earth Planet. In.*, **14**, 120–136.

Souque, C., Robion, P. and Frizon de Lamotte, D., 2002. Cryptic magnetic fabric of tectonic origin revealed by heating of sedimentary samples from the Corbières (France). *Phys. Chem. Earth*, **27**, 1253–1262.

Tarling, D.H. and Hrouda, F., 1993. *The Magnetic Anisotropy of Rocks*. Chapman and Hall, London.

Tauxe, L., Gee, J.S. and Staudigel, H., 1998. Flow directions in dikes from anisotropy of magnetic susceptibility data: the bootstrap way. *J. Geophys. Res.*, **103**, 17775–17790.

Watkeys, M.K., 2002. Development of the Lebombo rifted volcanic margin of southeast Africa. In: *Volcanic Rifted Margins* (M.A. Menzies, S.L. Klemperer, C.J. Ebinger and J. Baker, eds). *Geol. Soc. Am. Spec. Pap.*, **362**, 27–46.

Received 13 October 2010; revised version accepted 7 December 2010

Supporting Information

Additional Supporting Information may be found in the online version of this article:

Figure S1. All SPO and AMS data presented stereographically in the lower hemisphere for all 12 dykes studied.

Figure S2. A. Magnetic fabric (AMS) of dyke SZ-4 as pictured after successive heating for 1 h to 300 and 700 °C.

Please note: Wiley-Blackwell are not responsible for the content or functionality of any supporting materials supplied by the authors. Any queries (other than missing material) should be directed to the corresponding author for the article.

Tectonophysics 583 (2013) 145–157

Contents lists available at SciVerse ScienceDirect

Tectonophysics

journal homepage: www.elsevier.com/locate/tecto

Characterisation of grain-size, shape and orientation of plagioclase in the Rooi Rand dyke swarm, South Africa

Warwick William Hastie [a,*], Michael K. Watkeys [a], Charles Aubourg [b]

[a] School of Geological Sciences, Building H1, University of KwaZulu-Natal, University Road, Westville, Durban 4001, South Africa
[b] Laboratoire des Fluides Complexes et Réservoirs, UMR 5150, CNRS, TOTAL, Université de Pau et des Pays de l'Adour, Avenue de l'Université BP 1155, 64013 Pau Cedex, France

ARTICLE INFO

Article history:
Received 25 June 2012
Received in revised form 23 October 2012
Accepted 31 October 2012
Available online 8 November 2012

Keywords:
Magmatic fabric
Shape preferred orientation
Plagioclase
Grain-size

ABSTRACT

Magmatic (type-A) fabric co-exists with dyke-orthogonal (type-B) fabric in both the plagioclase and opaque grain fractions in dykes of the Rooi Rand dyke swarm (RRDS). We present new data from the RRDS pertaining to the size, shape, texture and orientation of plagioclase. Texturally, the samples range from intersertal to sub-ophitic and phenocrystic (plagioclase-phyric). More than 90% of plagioclase grains are <33 μm in size and the modal size is 12.3 μm. The smallest, most abundant grains have modest shape ratios ($1.40<r<1.95$). Larger grains have relatively low shape ratios although grain-size and shape in the RRDS are essentially independent. Additionally, we investigate the angle between individual grains and the respective dyke margins in (sub-) horizontal thin-sections. This apparent imbrication angle, A_i, in conjunction with three dimensional fabric shape tensors and grain-size and shape data, shows that the most common grain-size class, with modest shape ratios (1.80–2.20), is predominantly associated with type-A fabric. The interaction of grains attempting to rotate in even-textured samples appears to have resulted in the lack of correlation between shape and size parameters and the orientation or intensity of the fabric, whilst grains with increasing r values show a tendency towards type-B fabric. Based on textural information and crystal size distribution, we suggest that plagioclase<80 μm in size grew as a result of a late-stage nucleation event, becoming increasingly anisotropic as a result of relatively rapid undercooling. Thus, late-stage, rapid nucleation of the plagioclase groundmass significantly affected the final fabric that developed, and the interaction of large, anisotropic grains has not played as significant a role in the development of type-B fabric as previously thought.

1. Introduction

There have been many studies quantifying fabric development in igneous rocks, whether using anisotropy of magnetic susceptibility (AMS) (Cañón-Tapia, 2004 and references therein) or the shape preferred orientation (SPO) of minerals (Baer, 1995; Blanchard et al., 1979; Blumenfeld and Bouchez, 1988; Cruden, 1990; Ferguson, 1979; Gay, 1966, 1968; Kattenhorn, 1994; Launeau, 2004; Launeau and Cruden, 1998; Launeau and Robin, 1996; Nicolas et al., 1988; Ramsay, 1989; Romeo et al., 2007; Willis, 1977). Lattice preferred orientations (LPO / CPO) and electron back-scattered diffraction (EBSD) studies have also been applied to the study of igneous petrofabrics in gabbro (Benn and Allard, 1989), volcanic flows (Bascou et al., 2005) and dykes (Chadima et al., 2009; Romeo et al., 2007). In the study of dykes these techniques are primarily applied to determine the original flow direction of magma as this has important geodynamic implications, particularly when dealing with a dyke swarm (Aubourg et al., 2008; Callot et al., 2001; Ernst, 1990; Ernst and Baragar, 1992; Ernst and Duncan, 1995; Kissel et al., 2010).

The development of flow-related petrofabrics in mafic dykes follows the general premise that a statistically significant number of grains will become imbricated (tiled) against the dyke walls during magma flow (Blanchard et al., 1979). The recognition of this flow-related fabric is typically based on the angle between the dyke and the tiled grains being in the range ~10–30°. These grains may be phenocrysts or they may be part of the finer grained groundmass in the solidified dyke. The most basic formation of a flow-related magmatic fabric in a dyke occurs under conditions of simple shear in a magma in which constituent grains become tiled against the walls of an intrusion. This would typically develop fabric symmetrical with respect to the dyke plane. Non-symmetrical fabrics may develop for a number of reasons, including but not limited to deformation of the dyke during emplacement and grain interaction (Callot and Guichet, 2003; Correa-Gomes et al., 2001). Oblate shaped AMS fabrics have been shown to develop intersection lineations and S/C type relationships (Callot and Guichet, 2003).

There are, however, many factors which may complicate the acquisition of such an ideal magmatic fabric. This has become evident from petrofabric studies as well as proposed quantitative models

* Corresponding author. Tel.: +27 31 260 1277.
E-mail addresses: warwick.hastie@gmail.com, 203505849@stu.ukzn.ac.za (W.W. Hastie).

0040-1951/$ – see front matter © 2012 Elsevier B.V. All rights reserved.
http://dx.doi.org/10.1016/j.tecto.2012.10.035

which attempt to account for simultaneous grain growth, rotation, interaction and overall magmatic fabric acquisition (Amenta, 2001; Archanjo and Launeau, 2004; Benn and Allard, 1989; Callot and Guichet, 2003; Correa-Gomes et al., 2001; Dragoni et al., 1997; Launeau and Cruden, 1998; Willis, 1977). The study of sub-fabrics and the role of grain shape and rotation is well documented (see citations above and Fernandez et al., 1983; Ildefonse et al., 1992; Jezek et al., 1994). In this paper we present directly observed, two-dimensional (2-D) data pertaining to the size, shape and orientation of plagioclase grains which define the igneous petrofabric in dolerite dykes of the Rooi Rand dyke swarm (RRDS).

In a recent study, the magnetic fabric and the mineral SPO fabric of the RRDS of South Africa was presented (Hastie et al., 2011a). Inverse fabric (referred to as type-B fabric) exists in the mineral SPO of plagioclase grains in ~40% of the data. This is an igneous petrofabric in which the foliation defined by plagioclase (and some opaque grains) is orthogonal to the dyke plane. A model of late-stage fabric acquisition owing to grain interaction has been proposed to explain this fabric orientation. It was also shown that finer grain sizes (<10 μm), particularly those measured by AMS, appeared to preserve the earliest, relict fabric (similarly to Romeo et al., 2007).

From visual inspection alone there seems to be no apparent relationship between the orientation of grains and their morphology (specifically the grain-size and shape ratio) in the RRDS. In one case (Fig. 4b of Hastie et al., 2011a) it was demonstrated that the type-B fabric component could be digitally separated from the type-A (normal) fabric component. The overall fabric comprises a type-A component defined by the majority of the grains and a type-B component defined by the less abundant fraction. It is difficult to judge visually whether particular fabrics are occupied by finer, or coarser grains than the average, or by grains of a particular shape.

2. Grain shape and flow fabric

Benn and Allard (1989) have quantified igneous fabrics in gabbro of the Oman ophiolite using mineral SPO and LPO. These authors found differences in fabric orientation according to grains of different shape ratios. In particular, low shape ratios ($r<1.5$) were less likely to reach an imbricated angle — where r is the ratio of long (L) to short (S) axes. A similar finding has been made by Ildefonse and Fernandez (1988) as well. A study of grain-size and magmatic fabric development in a single dyke of the RRDS by Kattenhorn (1994) revealed that grains of relatively high shape-ratio ($3<r<10$) were found predominantly within 30° of the dyke plane. Furthermore, there is evidence that continued crystallisation (i.e. an increasing number of grains) leads to grain interaction, and therefore a higher degree of grain imbrication is achieved (stable fabric of Ildefonse et al., 1997). Laminar flow also increases the likelihood of grain imbrication. The magnitude of shear (γ) is also important, particularly when considering the magnitude of shear imparted to each of the grain populations with different shape ratios (Launeau and Cruden, 1998).

Dragoni et al. (1997) demonstrated that magma flow typically produces cyclical rotation of grains. Indeed these authors showed that, when considering AMS fabrics, the orientation of the magnetic foliation (the $K1$–$K2$ plane) oscillates between vertical and horizontal positions in mafic sills of the Ferrar Province, Antarctica. Importantly these authors were able to show that these oscillations were dependant on the value of r. For example, as r increased, the greater the time interval $K3$ spent in a vertical position — which essentially defines a type-B fabric. This is contrary to the findings of Ildefonse and Fernandez (1988) and Kattenhorn (1994).

Launeau and Cruden (1998) provide a thorough analysis of grain orientation, fabric intensity and direct measurement of igneous fabric development in the Lebel syenite (Ontario, Canada) using both AMS and mineral SPO. These authors explore the factors involved in the progressive development of the igneous petrofabric in the Lebel syenite. These include free grain rotation, grain interaction and progressive crystallisation. They find that (1) the rate of rotation of grains is proportional to r. Thus, different populations of grains, with differing shape ratios will tend to develop their own preferred orientations provided the grains do not interact. Grains with the smallest r values will have rotated most, (2) fabric anisotropy (P') increases with increasing γ, particularly when there is a component of pure shear (i.e. flattening). Additionally, a pure shear component greatly increases the degree of preferred orientation (Rf_{φ}) for grains of high shape ratio, (3) at high shear magnitudes ($\gamma>6$) preferred orientations begin to show cyclicity; whereby populations of grains with differing values of r have more intense or less intense degrees of preferred orientation. Thus, obliquities between sub-fabrics are a function of their shape ratio and the shear magnitude, (4) progressive simple shear in a nearly crystallised magma (involving grain interaction) will result in anisotropic grains rotating into the shear plane. These grains will most likely maintain a stable orientation irrespective of grain-size and shape and (5) if grain-size is related to time then each grain-size population will have its own range of shape ratios and distribution of preferred orientation. The authors, however, indicate that the distribution of grain sizes in the Lebel syenite appears to be independent of grain shape and preferred orientation. It is thus the product of magmatic, progressive crystallisation, with strong interaction of grains during the final stages of emplacement.

More recently, Cañón-Tapia and Chávez-Álvarez (2004) performed an investigation of simulated grain movement and rotation — primarily in the context of AMS. The orientations of the principal axes of the susceptibility tensor ($K1$, $K2$ and $K3$) were monitored during continuous deformation (in this case grain rotation in a viscous medium). The simulations of particle movement focused on using groups of data with different initial orientations, and increasing shear strain. The results of these simulations showed that (1) the grain shape (r) primarily controls the periodicity of particle rotation, (2) the fabric intensity (anisotropy) fluctuates with particle rotation due to the original orientation and shape (r) of the grains, (3) oblate particles are more likely to be imbricated with $K3$ normal to the dyke plane, which is consistent with the model of Geoffroy et al. (2002) who showed that oblate fabrics tend to be "normally" imbricated, with the foliation being within ~30° of the dyke plane and (4) prolate grains are more likely to produce correctly imbricated, type-A magnetic fabric irrespective of the amount of shear. However, areas of little or no deformation (e.g. the centre of a dyke) yield poorly grouped AMS irrespective of the value of r.

There are number of ways in which the above findings may be applicable to the study of the RRDS. Firstly, one might expect to find that the large, most anisotropic grains will tend to be restricted in their movement owing to their larger size, and later interaction during simple shear. Secondly, there should then be a strong relationship between the grain shape (r) and preferred orientation. Thirdly, the distribution of grain-size may provide, at least qualitatively, an indication of the crystallisation behaviour. The sliding of grains past one another will be important in the shear plane, presumably most evident in the foliation plane. Finally, the fabric studied in the solidified dykes is unlikely to be representative of the early history in the fabric development. Given that the Lebel syenite is of a different composition and not a sheet-like intrusive, however, it is prudent to be cautious about inappropriate comparison. The above brief synthesis suggests that there is a correlation between the orientation of a fabric and its scalar parameters — although it has not been shown previously if this can be directly applied to the grains which constitute the fabric, as we attempt to do here.

3. Aim

We explore the interdependence of grain-size, shape and orientation of plagioclase within the igneous petrofabric of the RRDS in an

attempt to answer the following questions: (1) Is there any correlation between the size and/or shape of plagioclase grains and the angle at which they come to rest against the dyke wall? (2) Is there evidence of an ideal grain-size or grain shape which occur in a "magmatic" orientation (≤30° from the dyke plane)? (3) Is there any correlation between magmatic fabric and the degree of preferred orientation, which is considered independent of grain-size and shape?

We thus continue, in this paper, to investigate the acquisition of petrofabric in the RRDS. However, we turn our attention here to characteristics of the grains themselves, their morphology and any influence or relationship which can be demonstrated between grain morphology, size and the petrofabric orientation. We refrain from comparison between mineral SPO and AMS as it has been carried out previously (Hastie et al., 2011a). The results are interpreted in the context of previously published models which have simulated or demonstrated the relationships between grain-size, shape, rotation and grain interaction (Ildefonse et al., 1997) in the development of preferred orientation (Arbaret et al., 1996; Benn and Allard, 1989; Dragoni et al., 1997; Launeau and Cruden, 1998).

4. Geological background

The Rooi Rand dyke swarm (RRDS) is a 200 km long, 10–20 km wide, N–S trending dyke swarm which crops out between the Msunduze River in northern KwaZulu-Natal (South Africa) and central-eastern Swaziland (Fig. 1). The RRDS is related to the

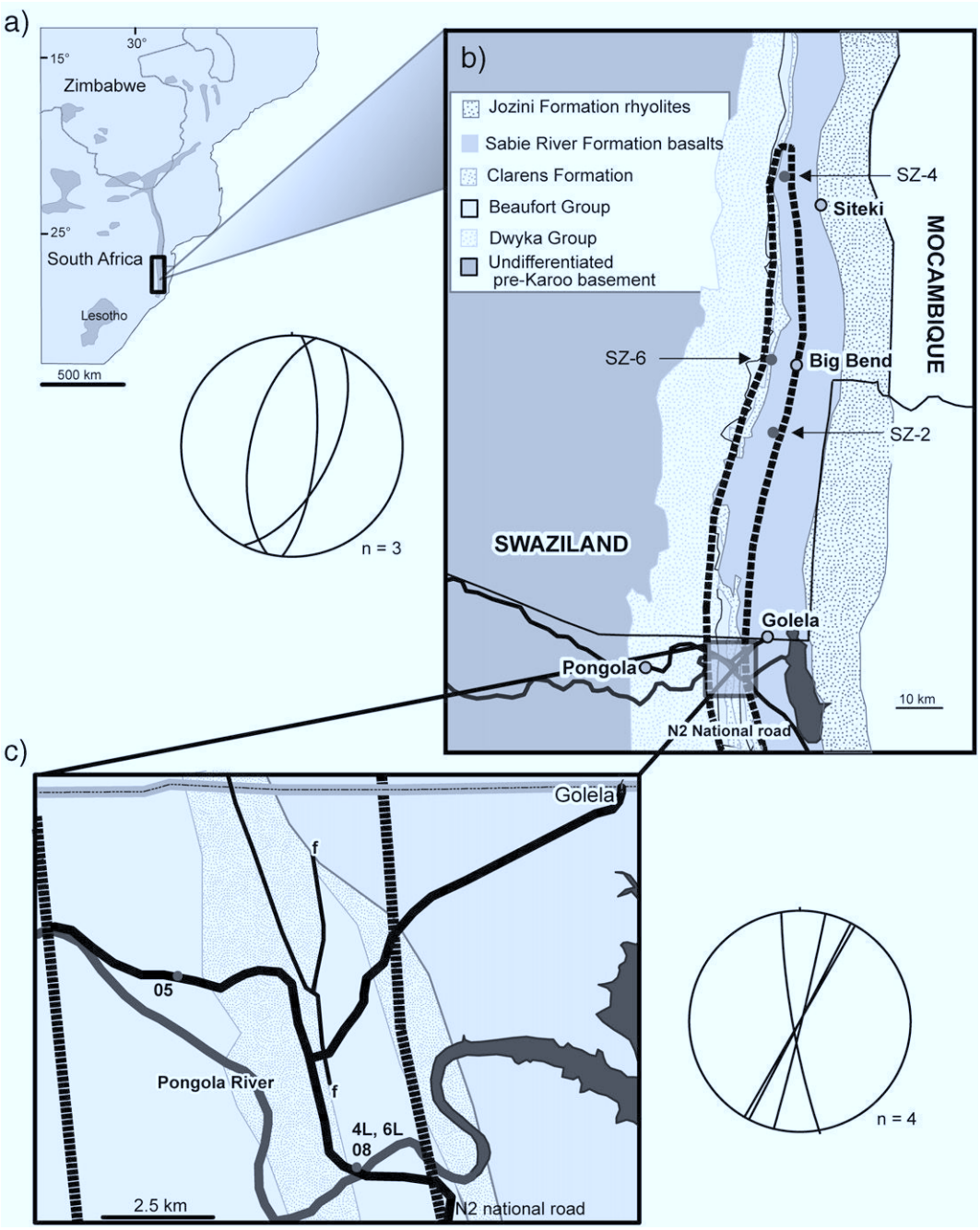

Fig. 1. Sketch maps showing (a) the outcrop pattern of the volcanic rocks of the Karoo LIP in southern Africa, (b) the northern extent of the RRDS (outlined by broad, dashed line) in Swaziland and (c) the central part of the RRDS which is exposed along the Pongola River (dark grey) and N2 National Road (solid black line). Note that only the dykes relevant to this study are shown (SZ-2, SZ-4, SZ-6 and 4L, 6L, 08 and 05). Stereographic projections show the orientations of the dykes (see also Table 1).

~180 Ma old Karoo Large Igneous Province (LIP) and intruded during the final stage in the development of the Lebombo faulted monocline at ~174 Ma (Jourdan et al., 2007). Although strictly dolerites the RRDS has a MORB-like composition, the only such composition known in the Karoo LIP.

The dykes have intruded the Beaufort Group (Permo-Triassic sandstones), Clarens Formation (Triassic sandstones) and Sabie River Formation (basalts). These Formations and Groups form the uppermost part of the Karoo Supergroup. Geochronology suggests that the RRDS is younger than the rhyolites of the Jozini Formation which cap the Lebombo (Armstrong et al., 1984; Riley et al., 2004; Watkeys, 2002).

The steeply dipping (>80°), generally N–S striking dykes of the RRDS in the central area (Fig. 1c) give way to more shallowly dipping (50°–70°) NNE–SSW striking dykes in the north (in Swaziland) (Fig. 1b). The eastward dip of sedimentary strata and basalts (~15°) into which the dykes have intruded suggests that the dykes intruded vertically, and hence their westward dip is the result of this eastward tilting after their intrusion.

Petrological and geochemical evidence indicates that the RRDS originated from the melting of an upwelling asthenosphere, as is typical of MORs (Armstrong et al., 1984; Meth, 1996; Saggerson et al., 1983). The MORB-like composition and intrusion of the RRDS into thinning crust during the earliest phase of break-up in southern Gondwana is consistent with this but this area failed to rift and produce oceanic crust along its present N–S exposure.

5. Methodology

5.1. Sampling and basic parameters

Samples were drilled from the two opposing chilled margins of each dyke. The samples are cylindrical drill-cores which are 22 mm×25 mm in size. In mineral SPO studies a tensor representing the petrofabric is determined from these samples and the principal axes of the tensor are represented by $L1$, $L2$ and $L3$ ($L1>L2>L3$). The tensors are represented stereographically in the lower hemisphere. Scalar quantities are also determined, which quantify the anisotropy (P') and shape (T parameter). Prolate fabrics have $T<0$ and oblate fabrics have $T>0$. In this study the 3-D inertia tensor (see Launeau and Cruden, 1998) is calculated from 2-D ellipses determined from the bulk orientations of plagioclase in three mutually perpendicular thin-sections per sample. This method and the parameters described are discussed in further detail in Section 5.3.

5.2. Finding magmatic fabric

In trying to find the magma flow direction in a dyke using mineral SPO, it is the orientation of the lineation ($L1$) and foliation (the $L1$–$L2$ plane) relative to the dyke plane which is fundamentally important. Magma flow will tend to cause grains, such as plagioclase, to become tiled along the dyke walls (because of simple shear) with the long axes within and along the foliation, both of which become imbricated. If the dyke wall represents the shear plane during magma flow then the angle between the magmatic foliation and the dyke plane can be used to determine the sense of magmatic shear (Fig. 2a) (Aubourg et al., 2002; Benn and Allard, 1989; Blanchard et al., 1979; Callot and Guichet, 2003; Geoffroy et al., 2002).

The angle between the foliations (determined from each, opposing dyke margin) and the respective dyke plane can also be taken as a measure of whether the fabric is reliable as a magma flow indicator. Angles of <30°, or between 30° and 50° are generally accepted as being flow-related (Blanchard et al., 1979; Geoffroy et al., 2002), as opposed to higher angles which are indicative of the presence of sub-fabrics or late-stage fabrics. In this paper a conservative range of 0°–30° will be considered to represent type-A fabric. Mirrored geometry of the foliation planes provide the sense of magma flow, as they converge in the direction of magma flow (Aubourg et al., 2002; Geoffroy et al., 2002). It has been previously shown that the lineation resolved from 3-D tensorial data may be a zone axis — essentially an intersection lineation. This has been demonstrated for oblate shaped AMS fabric (Callot and Guichet, 2003; Geoffroy et al., 2002; Henry, 1997; Launeau and Cruden, 1998) and for plagioclase (Hastie et al., 2011b).

As discussed, however, magmatic fabrics may become complicated by other processes. For example, unexpected and mixed fabrics develop because (1) different grain sub-populations come to rest at different times and (2) grains are likely to interact as they move, rotate and imbricate within a crystallizing magma. It is therefore necessary to consider whether there are any predictors of fabric imbrication, such as grain-size or shape factors and the reasons for the development of sub-fabrics unrelated to that which provides a sense of magma flow direction.

5.3. Shape preferred orientation

Measurement of individual grains or grain populations in 2-D is achieved using the image analysis software SPO-2003 (Launeau, 2004; Launeau and Robin, 1996). The SPO of plagioclase constitutes a direct, quantitative measure of the igneous petrofabric(s) as a whole — and is measured at the scale of individual grains and grain populations. The petrography of the samples and any significant differences between samples is therefore also important.

Most studies carried out to find the 3-D shape ellipsoid or tensor is carried out using Ellipsoid-2003 (Launeau, 2004; Launeau and Robin, 2005; Robin, 2002). The method used here is explained in Launeau and Cruden (1998) and Hastie et al. (2011a). In brief, photomicrographs of thin-sections (of known scale and orientation) are converted to binary (black and white) bitmap images, and analysed using this software. It is generally found that once the images are filtered (colour-inverted binary bitmaps) very few plagioclase grains are in contact with one another. This is ideal, as it prevents the measurement of aggregated grains as single grains. This would evidently introduce bias in terms of grain-size, shape and also orientation. This filtering and inversion does, however, tend to reduce or even remove the smallest grain sizes (<8 μm), a phenomenon which has been noted in previous studies (Launeau and Cruden, 1998).

From SPO-2003 it is possible to export and analyse scalar data of individual grains. This data can also be combined in 3-D using Ellipsoid-2003 to provide the inertia tensor of the petrofabric for an individual sample, or for a dyke margin. The thin-sections used (3 per sample) are mutually perpendicular, cut from standard drill-cores (22 mm×25 mm). The arbitrary co-ordinate system used (XYZ) is based on the geographic orientation of each core. In this scheme, X is parallel to the azimuth and orthogonal to the strike of the core, Y is orthogonal to the azimuth and defines the strike direction and Z is parallel to the azimuth and plunge direction of the core.

Because the grain-size, shape and orientation of many thousands of individual grains are of primary interest here we made these measurements in 2-D sections. This is because the ellipsoid determined in 3-D is a bulk measure of all the grains, and it therefore does not provide any morphological or orientation parameters of individual grains. Our choice of samples is restricted, however, because it is most straightforward to measure the angle between the dyke walls and plagioclase grains in (sub-) horizontal thin-sections from the margins of a vertically orientated dyke with relatively straight margins. Thus, for our analyses we are restricted to XY and some ZY sections through which the dyke plane passes. We have analysed 16 samples from seven dykes of the RRDS. In the investigation of the 3-D SPO tensor, however, four samples (12 thin-sections) per dyke were analysed.

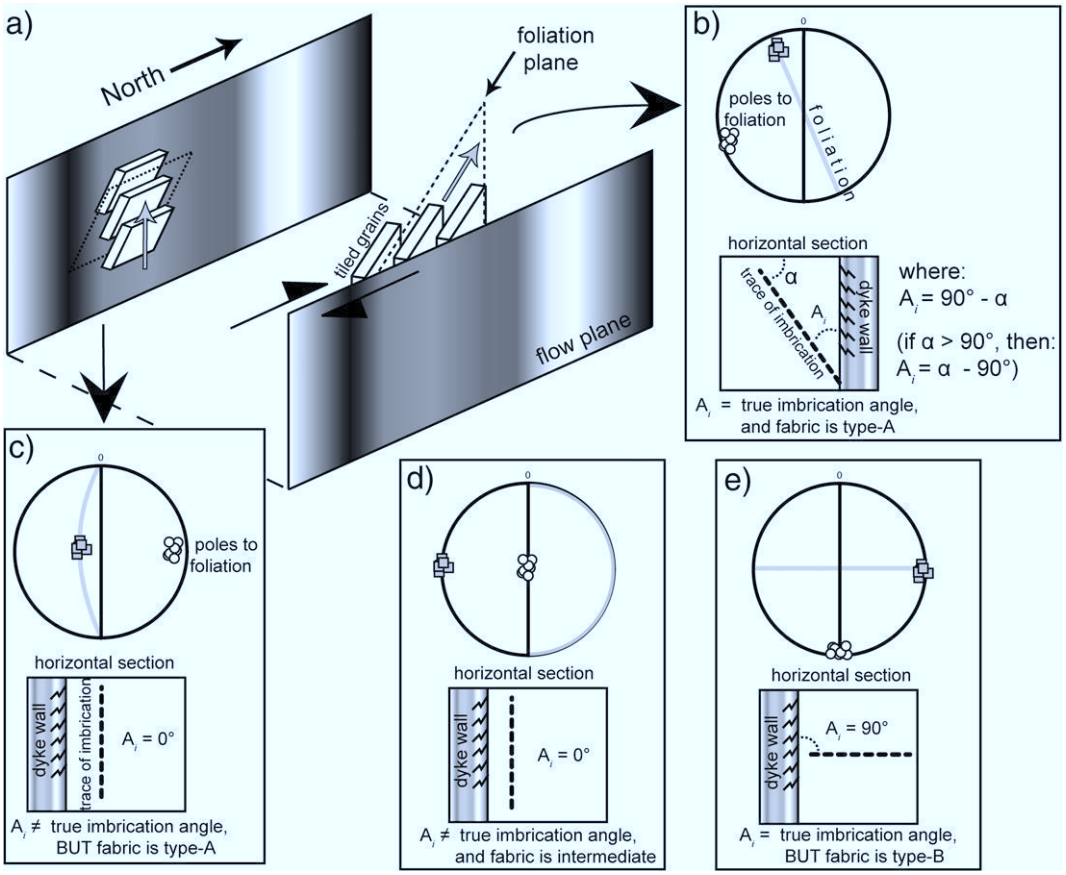

Fig. 2. Schematic diagram summarising the approach used in this study (a) an idealised N–S striking dyke with tiled imbrication (after Blanchard et al., 1979) of grains along the margins (lateral flow on eastern margin and vertical flow on western margin), (b) stereonet showing *L*1 (grey squares) and *L*3 axes (white circles) of the 3-D tensor for lateral flow with the dyke plane (flow plane) and foliation plane (grey line) shown. Below the stereonet is a horizontal section (plan view) showing the trace of imbrication and the method of calculating the apparent imbrication angle (A_i) from angle α (measured in SPO-2003). In this case A_i is coincident with the true imbrication angle, (c) stereonet showing a 3-D tensor for vertical flow and horizontal section illustrating an A_i angle of zero with type-A fabric. End-member geometries of intermediate and type-B fabric are shown in (d) and (e) respectively. These illustrate how comparison of the 2-D measurement of A_i with the 3-D tensor prevents misinterpretation of the A_i angle. See text for further discussion.

Because the angle measured between the plagioclase grains and the dyke margin is in 2-D, it is an apparent angle of imbrication, referred to here as A_i. The angle A_i is calculated by subtracting angle α measured by SPO-2003, which is the angle between the top of a thin-section and the long-axis of each individual grain (Fig. 2b). Within SPO-2003, these orientations are determined according to a rose of directions from 0° to 90° (0° = dyke-parallel; 90° = dyke-orthogonal). We anticipate that orientation measurements in SPO-2003 do not introduce significant errors in calculating A_i, but potential errors are more likely to derive from localised deviations in dyke orientation along the dyke margin. The orientation of thousands of individual grains (10^5) from seven dykes has been measured and it is thus possible to compare and contrast fabric types across different dykes but also maintain a sense of the fabric orientation at the smallest scale.

It must be made clear that, because A_i is an apparent angle, the true measurement of tiled imbrication (as formalised by Blanchard et al., 1979) is not necessarily measured here, except in cases where the elongation of the fabric ellipsoid defined by plagioclase is horizontal (i.e. where lateral flow is evident). This is because the trace of grains in horizontal sections will be coincident with the trace of the foliation (Fig. 2b). This fabric is type-A. There are three other end-member situations which demonstrate how the 3-D tensor can assist in distinguishing between foliation imbrication and A_i which allows us to correctly interpret the fabric type. In the case of vertical flow (Fig. 2a, c) the trace of grains from which A_i is calculated will be <30° (i.e. type-A fabric) despite A_i not being coincident with the true imbrication angle. This is similar to Fig. 2d, except that the 3-D tensor clearly illustrates intermediate fabric, which is not flow related and type-B fabric can be detected from both the 3-D tensor and A_i in horizontal thin-sections (Fig. 2e). There can be intermediate types to those shown here, but these end-member situations demonstrate clearly how the measurement of the angle A_i it must be monitored in conjunction with the 3-D SPO tensor.

5.4. Grain-size

The scalar data (grain-size, shape ratio etc.) can be exported from SPO-2003 and sorted according to any chosen parameter for analysis and comparison. One difficulty encountered with measuring grain-size is that small grains may have similar shape ratios to larger grains, and thus the length of the grain axes are not representative of grain-size. Following the work of Launeau and Cruden (1998) it is reasonable to use the diameter of a circle which is of the same spatial area as each of the grains as a proxy for grain-size.

5.5. Grain shape

The shape ratio (r) for each grain is the ratio of the long axis to the short axis ($r = L/S$). This is measured for plagioclase in 2-D sections. For each of these analyses the angle A_i is critical because it allows us to assess whether the fabric is orientated in a systematic way in each sample based on grain-size and/or shape. In addition we are able to measure the degree of preferred orientation (Rf_φ). This value

provides the intensity of the preferred orientation independently of grain-size and grain shape. For each of these dykes we also present the 3-D SPO tensors.

6. Results

6.1. Igneous textures in the RRDS

Dykes of the RRDS are generally fine to medium-grained, intergranular to plagioclase-phyric dolerites in which plagioclase is the dominant phase (55 vol.%), with the remainder comprising augite (~40%) and opaque oxides such as magnetite. The RRDS has not suffered any late deformation or mineral alteration, and the textures are therefore primary. There are essentially three main igneous textures evident in the dolerite dykes of the RRDS; intergranular, sub-ophitic and phenocrystic (plagioclase-phyric). Intergranular textures are most common, with plagioclase and approximately equal sized augite forming the framework of the fabric (05, 6L15, SZ-4) (Fig. 3). The phenocrystic textures of dyke 08 comprise a fine-grained to aphanitic groundmass with plagioclase phenocrysts while 4L14 does not have an aphanitic groundmass but is nevertheless phenocrystic. Sub-ophitic textures (SZ-2, SZ-6J) are relatively coarse-grained and comprise a framework dominated by plagioclase grains, sometimes partially enclosed within augite. Plagioclase in the phenocrystic samples appears more elongate than plagioclase in the other samples and tends to be sub- to euhedral. Augite is always anhedral and generally granular in shape. As a result, investigation or quantification of fabric defined by augite could not be carried out effectively using SPO-2003.

6.2. Plagioclase SPO

The 3-D tensor data are shown here because the examination of the fabrics/sub-fabrics will proceed in a manner that examines the scalar and orientation parameters of plagioclase in increasingly finer detail. Thus, the 3-D SPO tensor provides an appropriate context in which to gauge the contribution of the textures investigated in 2-D to the full picture of the 3-D fabric. The data are restricted to plagioclase, because (1) plagioclase is the dominant phase, with the remainder comprising anhedral, granular augite and magnetite, (2) it is within this fabric of the RRDS that type-B fabric has been found, (3) a greater number of grains are measured in each thin-section and (4) because a greater variety of grain sizes can be studied according to the different textural types.

The 3-D inertia tensors for each margin of the seven dykes and the orientation of each dyke plane are shown in Fig. 4. Note that two foliations are shown (in grey) per dyke as they are determined from each margin (e.g. western and eastern margin for a N–S striking dyke). The $L1$ axes vary from steeply plunging to sub-horizontal and the foliations generally dip steeply.

The angle between the foliations and the respective dyke planes are shown in Table 1 and it is evident that type-B fabric is found in three dykes (six margins overall). Dykes 6L and 05 do not strictly have type-B fabric, but the foliations fall just outside the 30° criterion and are not imbricated with respect to the dyke plane. Of the seven dykes being considered, only SZ-4 has type-B fabric. The remaining examples carry type-A fabric, but the foliations are only imbricated symmetrically with respect to the dyke plane in 4L. As indicated earlier, the 3-D tensors provide some control on the apparent imbrication angle, because A_i will be significantly different from the true

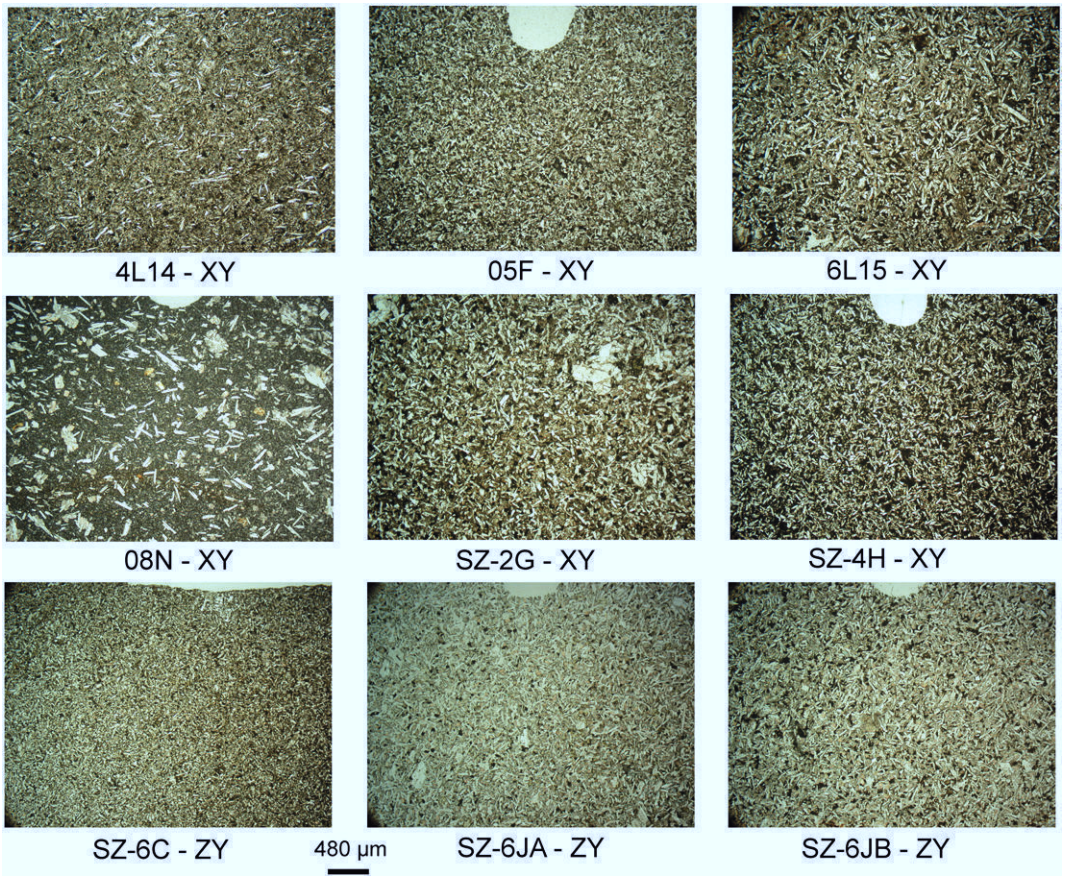

Fig. 3. Thin-section photomicrographs (plane-polarised light) of representative sections of the samples being studied. Note that the scale is the same for all sections (see scale bar). The main textural types are intergranular (05, 6L15, SZ-4) to sub-ophitic (SZ-2, SZ-6J), as well as plagioclase-phyric examples (4L14 and 08N). See Table 1 for thin-section orientations.

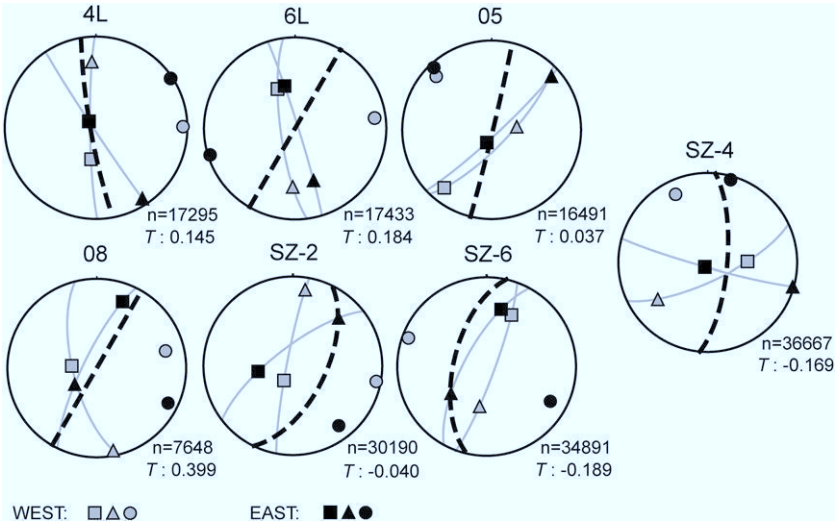

Fig. 4. Stereographic projections of 3-D inertia tensors of the plagioclase SPO for the 7 dykes under consideration (after Fig. 6 of Hastie et al., 2011a). Note that the fabric is split into two respective margins (see key; $L1 = ■$, $L2 = ▲$, $L3 = ●$). Foliations are shown in grey. Dyke plane shown as black dashed line. Note that the fabric in SZ-4 is type-B: the foliations are orthogonal to the dyke plane. The "n" value is the number of plagioclase grains measured for each dyke to construct the inertia tensors. Shape parameters (T) are also shown.

imbrication angle in cases where $L1$ is (sub-) vertical given that we have made 2-D measurements from (sub-) horizontal thin sections. This is acceptable for our use here because we do not make any inference regarding the direction or inclination of magma flow based on the angle A_i.

There is some variation in the shape of the fabrics being considered. The fabric of samples 4L13, 4L14, 05E, 05I, 6L15, 08N, SZ-2B, SZ-2G, SZ-4H and SZ-6JB are oblate in shape (average T: 0.196) (see Table 1) while the remaining six samples are near-neutral to prolate in shape (average T: −0.320). The shape parameters of the 3-D tensors shown in Fig. 4 indicate the slight predominance (57%) of oblate fabric. The percentage anisotropy ($[P' - 1] \times 100$) of the 3-D tensors is in the range 15–24%.

6.3. Apparent imbrication angle (A_i)

Given that type-B fabric exists in the SPO of plagioclase in the RRDS it is worthwhile finding the angle A_i at the scale of individual grains from all 16 samples (Fig. 5). A total of 31% of the grains are <30° from the dyke plane (i.e. type-A fabric) while the remainder show a slight, but noticeable increase in frequency towards a dyke-orthogonal orientation (type-B fabric). From Fig. 4, however, it is evident that the angle A_i in some dykes (4L, SZ-4, 05-east, 08-west) is unlikely to be representative of the true imbrication angle. Thus, we now present grain-size and shape data, while keeping track of the angle A_i across the size and shape classes because we are primarily interested in finding any potential correlation between these parameters and the fabric type.

6.4. Grain-size

The grain-size, shape and orientation of the plagioclase grains have been measured for all individual samples and for the combined data. The distribution of grain sizes is shown in Fig. 6, and those grain-size classes with angle A_i<30° are indicated in black. This is determined by finding the mode of the angle occupied by grains across the population of grains in each size (and shape) class. It is evident that 4L has a bimodal grain-size distribution with peaks at 9–10 μm and 20–21 μm. Dykes 05, SZ-2, SZ-4 and SZ-6 have similar, unimodal distributions that are skewed towards the coarser fraction. Standard deviations are also shown in Fig. 6. Dyke 08 has an unusual grain-size distribution relative to the others that is most likely related to

Table 1
Thin-section, dyke and SPO data for the 16 samples analysed from the RRDS ($L2$ is not shown). Note that the values shown for the 3-D ellipsoids and associated foliations are those calculated for each sample (i.e. inclusive of XY, XZ and ZY sections for each sample).

Sample — section	Dyke orient.	2-D ellipse					3-D ellipsoid							Foliation		
		Strike	Dip	L (μm)	S (μm)	Grains	√F[a]	$L1$-azi.	$L1$-plunge	$L3$-azi.	$L3$-plunge	P'	T	Strike	Dip	Imbrication angle
4L13 — XY	82°/170°	020°	10°	33	30	512	1.6%	142°	86°	002°	03°	1.157	0.07877	92°	87°	05°–15°
4L14 — XY	82°/170°	031°	13°	14	13	825	6.4%	337°	64°	083°	08°	1.200	0.09325	173°	82°	
05E — XY	88°/014°	268°	10°	17	15	1281	4.0%	214°	61°	118°	04°	1.183	0.1401	208°	86°	18°–32°
05F — XY	88°/014°	179°	12°	38	33	244	5.7%	168°	80°	338°	10°	1.296	−0.21875	68°	80°	
05I — XY	88°/014°	264°	21°	7	6	219	0.0%	174°	60°	313°	24°	1.147	0.16988	43°	66°	
6L13 — XY	90°/030°	056°	15°	29	26	676	3.3%	340°	63°	247°	02°	1.201	−0.0410	337°	88°	45°
6L15 — XY	90°/030°	080°	22°	29	24	212	5.9%	349°	33°	255°	06°	1.246	0.2756	345°	84°	
08N — XY	90°/030°	358°	12°	33	28	290	7.3%	237°	68°	093°	18°	1.334	0.50768	183°	72°	0°–24°
SZ-2B — XY	90°/026°	258°	21°	19	17	1900	5.4%	218°	73°	104°	07°	1.209	0.2212	194°	83°	05°–15°
SZ-2F — XY	90°/026°	203°	12°	15	15	1397	1.9%	195°	74°	098°	02°	1.134	−0.2884	188°	88°	
SZ-2G — XY	90°/026°	328°	20°	16	15	1598	1.8%	270°	59°	141°	20°	1.106	0.02215	231°	70°	
SZ-4B — ZY	72°/005°	355°	24°	16	15	1674	3.8%	099°	46°	198°	09°	1.118	−0.55651	288°	81°	70°–88°
SZ-4H — XY	72°/005°	185°	25°	17	16	1781	3.6%	296°	86°	205°	00°	1.135	0.1333	295°	90°	
SZ-6C — ZY	60°/193°	274°	23°	15	13	1126	4.3%	012°	28°	107°	09°	1.173	−0.780795	197°	81°	10°
SZ-6JA — ZY	56°/207°	275°	25°	16	11	1862	9.0%	012°	28°	115°	24°	1.345	−0.03877	205°	66°	
SZ-6JB — ZY	56°/207°	275°	25°	17	15	1736	7.9%	016°	43°	122°	17°	1.31	0.32437	212°	73°	

[a] √F value is a measure of the degree of misfit between 2-D ellipses in the construction of the 3-D ellipsoid (values of <10% are desirable) (Launeau et al., 2010).

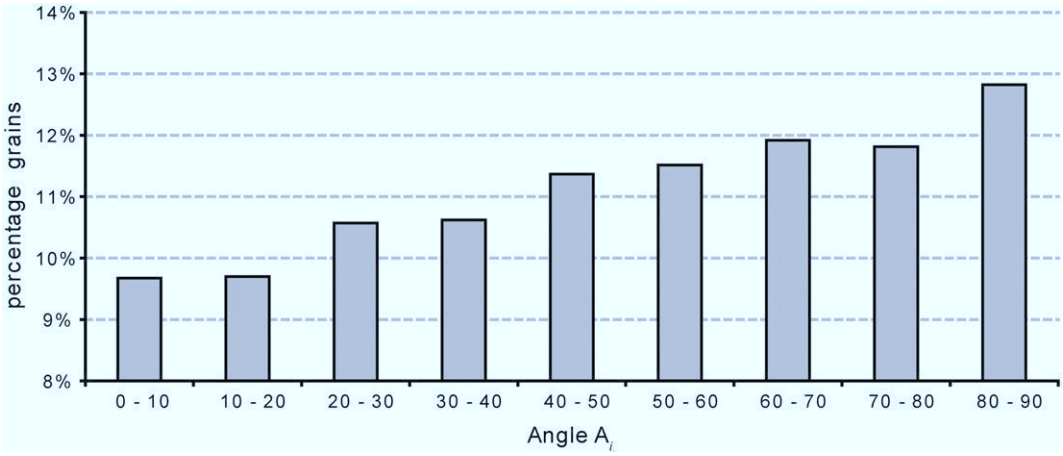

Fig. 5. Graph illustrating the percentage of grains (total = 1.7×10^5) which occupy a particular apparent angle to the respective dyke planes (A_i at 10° intervals). Note the trend of the grains towards increasingly higher angles to the dyke plane (69% of grains > 30° from the dyke plane).

its phenocrystic texture. The apparent peak in the 60–65 μm range is a function of plotting at 5 μm intervals for grains > 60 μm.

When considering all the data it is evident that the majority of grains (90%) are <33 μm in size. Grain sizes range from 8.50 to 254 μm with the most common grain-size being 12.3 μm. The median grain-size is 16.76 μm. In most cases (except 6L, 05 and 08) the grain-size classes 11–12 μm and 12–13 μm have A_i values < 30°. Dykes 6L, 05 and 08 are from the central RRDS (Fig. 1c).

Two observations can be made regarding common trends in the angle A_i within the grain-size populations. Firstly, SZ-4 appears to have a relatively large number of grain sizes with an angle A_i of <30°. Secondly, in samples 4L, 05, SZ-2 and to a lesser extent in SZ-6, regular intervals of grain-size populations have A_i values ≤ 30°.

6.5. Grain shape

Plots of the distribution of grain shapes in the RRDS, with the modal occurrence shown, are presented in Fig. 7. Grain shape classes with angle A_i < 30° from the dyke plane are indicated in black. It was initially found that grains within the shape range 1–5 were most common (91% of all grains) and were thus investigated at 0.05 intervals. Grain shapes, however, reach maximum r values of 17.

It can be seen from the individual dykes that SZ-2 has the highest r value for modal abundance (1.80) and SZ-4 has the lowest (1.22). From the bulk analysis it is evident that the most populated shape classes are in the range 1.40–1.95 (24% of the total grains). It is interesting to note that the shape classes shown in black lie either side of this range in the plot of all the data, and 4L and SZ-2.

The distribution of grain shapes does not match that of the grain-size distribution. Indeed, a plot of grain-size vs. shape (Supplementary material) demonstrates a lack of correlation between the two parameters. The significance of this may be undermined to some extent by the 2-D measurements and consequent sectional effects. Large grain sizes (> 55 μm) do, however, appear to be considerably less anisotropic than the smaller grains. The distribution of grain sizes according to angle A_i is also shown in the Supplementary material. There does not appear to be any correlation between grain-size and A_i or grain shape and A_i.

If the fabric is once again scrutinised in 9 representative examples, bearing in mind the angle A_i and modal grain sizes, we observe type-A fabric in 05F, 6L15 and SZ-4H as demonstrated by the A_i values (Fig. 8). In these examples of type-A fabric the modal grain-size is 27.8 μm, 21.4 μm and 12.3 μm respectively. In samples 05F and 6L15 there seems to be an association between these relatively large grains with relatively high Rf_φ values (~1.3) and type-A fabric. The modal grain-size in the other examples tend to be lower (8.51–11.8 μm), although in the phenocrystic sample 08N the modal grain-size is 27.7 μm, in which the highest value of Rf_φ (1.418) is also found. Values of Rf_φ range from 1.031 to 1.418.

7. Discussion

7.1. Overview

In this study we have assessed factors related to the size, shape and orientation of plagioclase grains which define the igneous petrofabric in the Rooi Rand dyke swarm. Texturally, the samples range from intersertal, even-grained to sub-ophitic and plagioclase-phyric. The modal grain-size is 12.3 μm and 91% of plagioclase grains are <33 μm in size. Some phenocrysts reach > 100 μm in size (max. 250 μm). The distribution of grain sizes is skewed towards the larger fraction, although plagioclase-phyric samples are less common than the sub-ophitic and even-grained samples. The most abundant grain shapes have modest r values; 1.40–1.95, carried by the smallest grain sizes. The larger grains tend to have relatively low shape ratios while the more anisotropic grains (r > 10) are found in the populations of small grain sizes (<55 μm). The modest Rf_φ values throughout (1.031–1.418) suggest that the fabric has not been affected by a component of flattening induced by pure shear (Launeau and Cruden, 1998).

By measuring the modal distribution of angle A_i across plagioclase populations of different size and shape we can show that the most common size class (12–13 μm), with modest shape ratios (1.80–2.20), appears to define the "ideal" type-A fabric (Fig. 7). This is most evident in samples from the northern RRDS in Swaziland. Grains with shape ratios in this range account for 15% of the total plagioclase abundance. In some examples there is type-A fabric carried by slightly larger (20–21 μm), more anisotropic (4.80–4.85) grains but they do not appear in close association in the way the less anisotropic grains do.

However, the 3-D SPO tensors of some dykes and dyke margins (4L, SZ-4, 05-east, 08-west) have steep $L1$ axes, which suggests that the angle A_i may differ significantly from the true angle of tiled imbrication in these dykes. Still, the fabric in dyke 4L is oblate in shape and thus the meaning of the $L1$ tensor axis is debatable because the 3-D SPO tensor shows mirrored imbrication of the foliations with respect to the dyke plane. According to the methodology adopted in this work, therefore, this is most consistent with lateral flow and is not coincident with the lineation, which is essentially vertical.

In samples with shallowly plunging $L1$ axes in the 3-D tensor the apparent imbrication angle will be close, if not coincident, with the true imbrication angle of the long axes of the constituent plagioclase

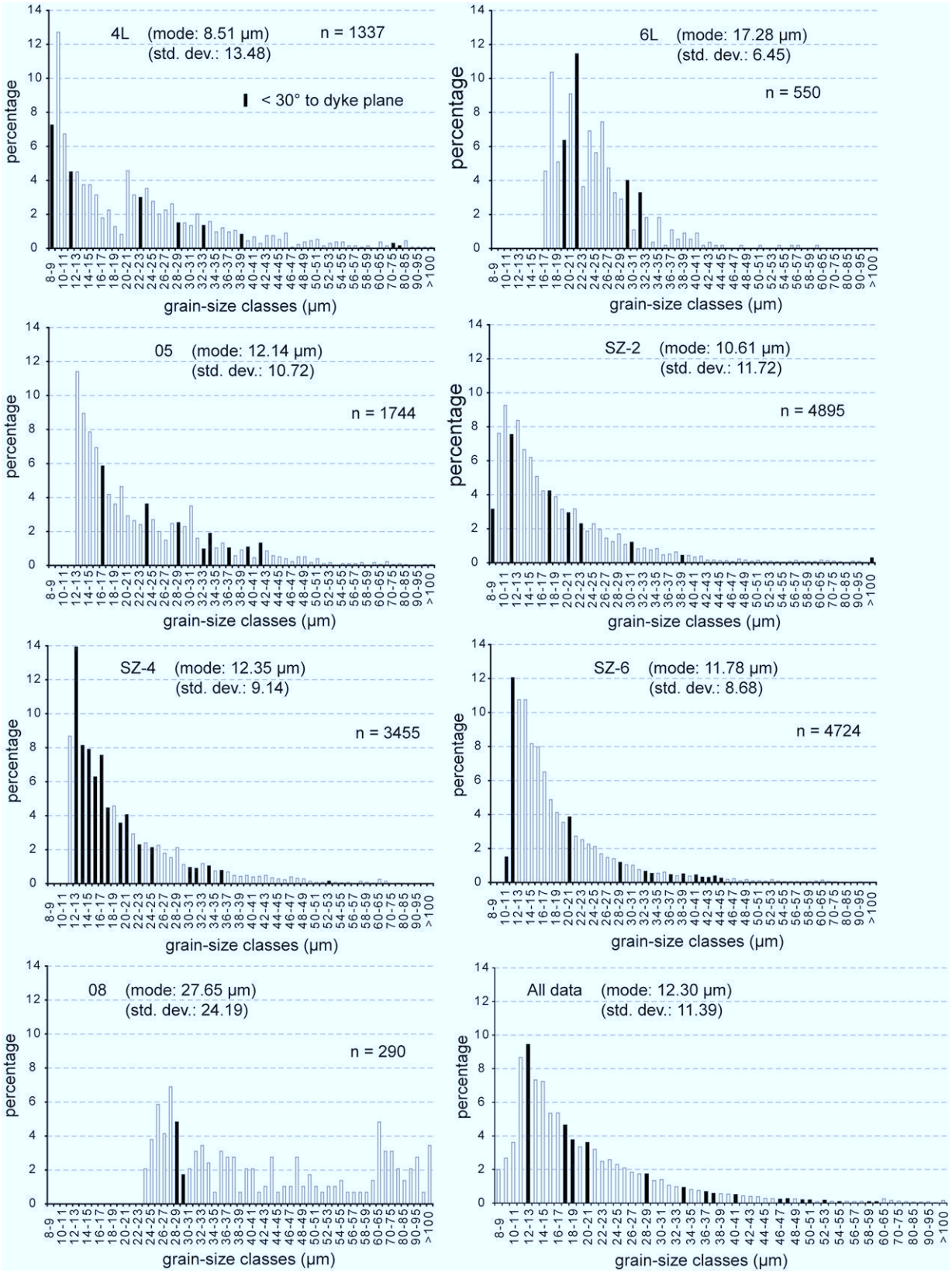

Fig. 6. Grain-size distribution (%) of plagioclase grain sizes in 7 dykes of the RRDS. Note that grain-size classes in which the modal occurrence of angle of A_i is <30° are shown in black. The modal grain-size of all 1.7×10^5 plagioclase grains is 12.30 µm.

grains. This includes dykes SZ-6 and 6L and dyke margins 05-east and 08-east. If discussion is restricted to these dykes and dyke 4L it is evident that grains in the shape ratio range 1.80–2.20 tend to be imbricated within 30° of the dyke plane. Thus, our findings with respect to shape and fabric type are reasonable in these examples, notwithstanding the fact that the angle A_i is not necessarily the true

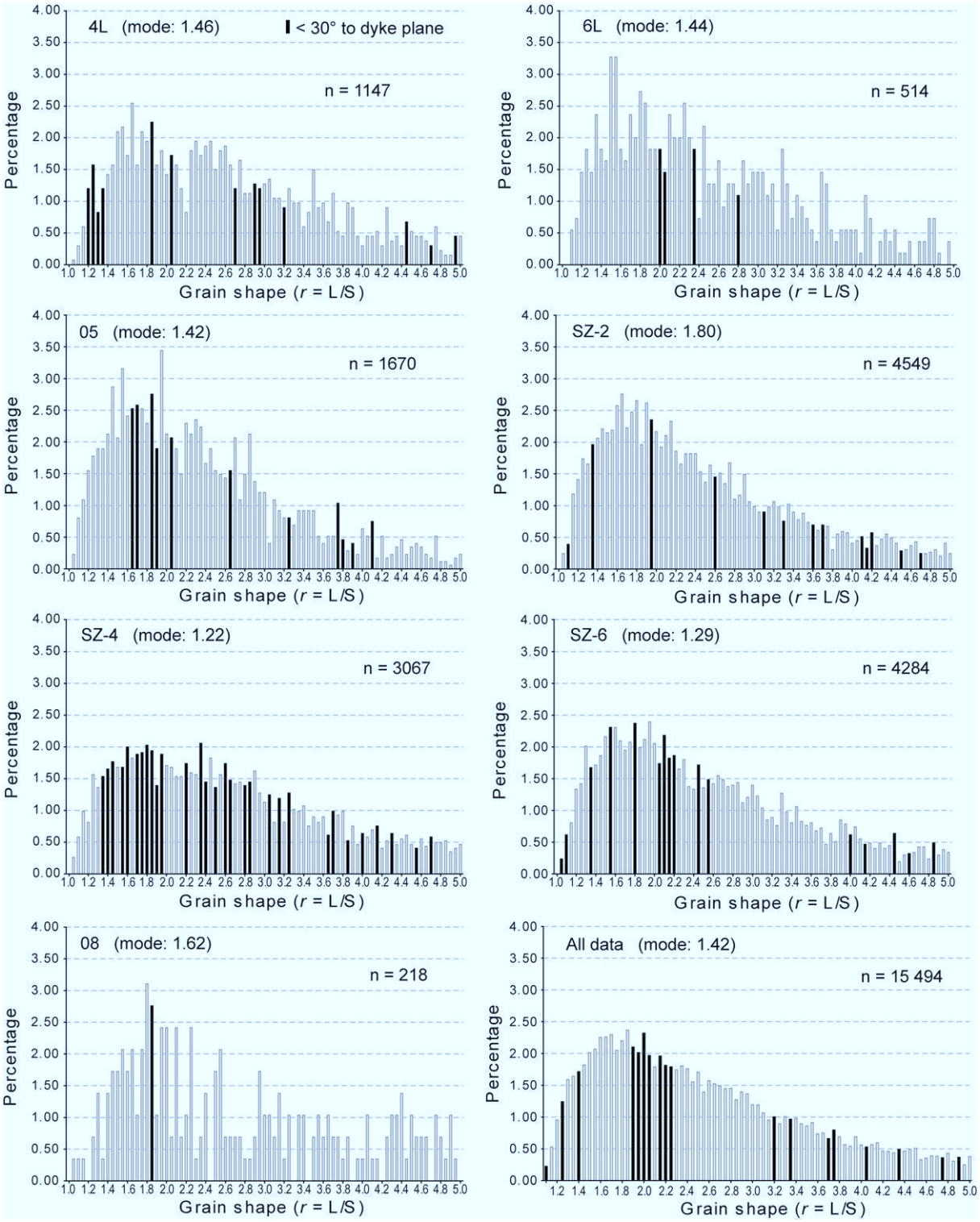

Fig. 7. Graphs showing the distribution (%) of grain shape classes for individual and all samples. Only shape classes up to $r = 5.00$ are shown (note values of "n"). The grain shape classes 1.40–1.95 are the most populated across the entire dataset and account for 24% of the total grains.

imbrication angle of plagioclase. Similarly, in Fig. 8, the tendency towards type-B fabric as r increases in small grains (<8.50 μm) is evident in these same examples.

These results are not consistent with findings of other works which have shown fabric intensity and orientation to be a function of highly anisotropic grains. For example, Kattenhorn (1994) found in the RRDS that the most elongate grains ($3.3 < r < 10$) align within 10–25° of the dyke wall. It has been shown here that these grains constitute only 1/3 of the petrofabric and do not necessarily hold a magmatic fabric orientation.

The phenocrystic sample 08N is interesting because it has the strongest degree of preferred orientation, while displaying an angle of $A_i > 30°$. This may be related to the factors discussed above with regard to the apparent imbrication angle, or it may be indicative of a

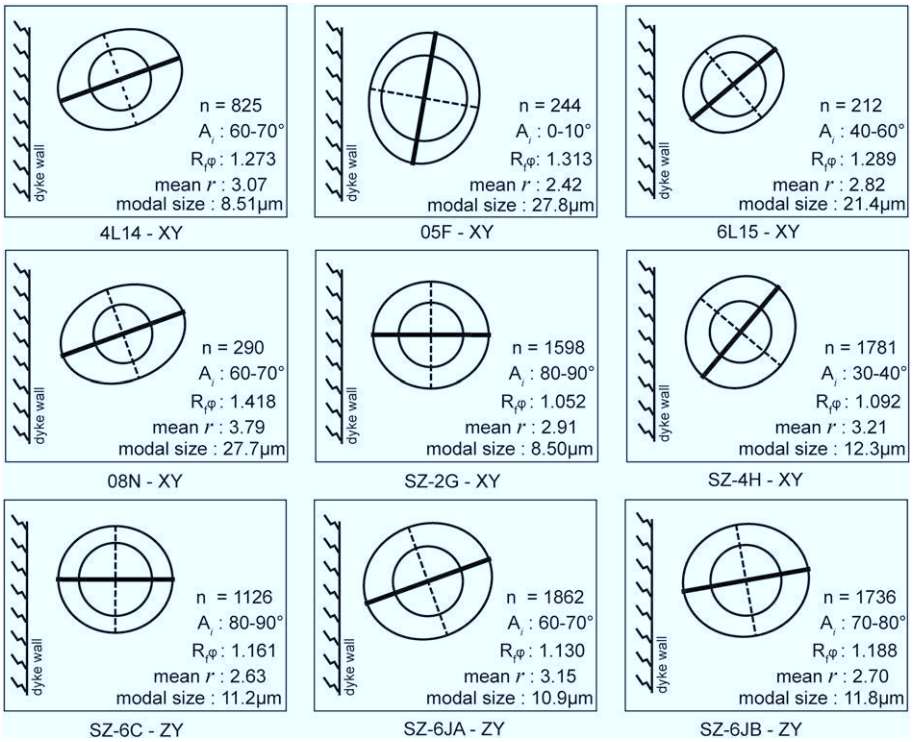

Fig. 8. Schematic representations of selected samples showing the shape tensor (minor axis dashed) and relevant scalar, size and orientation (A_i) data, relative to the dyke wall for each sample. There is no striking correlation, although small grain sizes (~8–12 µm) with high Rf_{φ} values tend to be associated with type-B fabric (4L, SZ-2). Sample SZ-4H is contrary to this observation, however.

lack of grain interaction leading to obliquities developing between different shape classes. In samples in which grains are interconnected (SZ-6) grain interaction during flow of the magma must have played an important role. It is difficult to envision interacting, anisotropic grains rotating preferentially into the magmatic shear plane, particularly as crystallisation is drawing to a close. Thus, grain interaction may indeed increase the stability, but not the type of petrofabric.

It is thus questionable whether placing emphasis on the orientation and characteristics of the most anisotropic, least abundant grains is justified, particularly when comparisons are drawn between fabrics defined by grain populations of significantly different abundance. This is exemplified in dykes in which numerous, widely spaced grain-size classes have $A_i<30°$ (4L, SZ-2, SZ-6). The difference in abundance can be accounted for by nucleation, crystallisation and fractionation processes in the magma. For example, Launeau and Cruden (1998) note that different grain-size populations represent a particular crystallisation event during progressive crystallisation.

7.2. Plagioclase nucleation in the RRDS

Crystal size distribution (CSD) can be used to constrain nucleation and growth rates during crystallisation in igneous rocks — allowing for quantification of the kinetic processes involved (Cashman and Marsh, 1988; Kirkpatrick et al., 1979; Marsh, 1998; Muncill and Lasaga, 1987; Pupier et al., 2008). CSDs are typically shown as plots of the natural logarithm of the population density (vertical axis) as a function of grain-size (horizontal axis) (Higgins, 2000; Marsh, 1988).

While we are not concerned with quantifying crystal growth rates, the CSD in the 16 samples of the RRDS may provide useful information about the nucleation and crystallisation history of these dykes. Dowty (1980) has shown that igneous textures are controlled by the interaction between the pre-cooling history of the melt, the degree of cooling and cooling rate, volatile content of the melt, oxygen fugacity and nucleation kinetics. Nucleation can be homogeneous or heterogeneous; the latter occurring when nucleation begins upon an existing phase in the magma, or along the base of a flow or margins of an intrusive body. Heterogeneous nucleation is also responsible for ophitic/sub-ophitic textures in basaltic rocks (Kirkpatrick, 1977). A relatively uniform distribution of crystal sizes is indicative of continuous nucleation and growth under conditions of constantly decreasing temperature. This tends to depress growth-rates while nucleation is not affected — provided that latent heat of crystallisation is constantly removed (Dowty, 1980; Kirkpatrick, 1977). Uniform lognormal slopes of distribution in the CSD of igneous rocks can thus be explained in essentially two ways. Either the nucleation rate increases exponentially as a function of time (growth rate is constant) or the growth rate increases exponentially as a function of crystal size (nucleation rate is constant) (Hersum and Marsh, 2006; Marsh, 1998).

There are processes which may disturb this uniformity. Sudden undercooling and a resultant burst of nucleation will cause an increase in negative slope at small grain sizes, provided the system does not equilibrate fully. Crystal fractionation will tend to steepen the slope of the correlation line at large grain sizes, while crystal accumulation will tend to develop an upwardly concave CSD curve. Once nucleation has ceased and growth becomes the dominant process the smallest grains tend to be resorbed while larger grains continue to grow (Ostwald ripening). This would cause a downward turn of the CSD curve at the smallest grain sizes (Marsh, 1998). A CSD can become "kinked" if there is crystal agglomeration (Burkhart et al., 1980) or a difference in nucleation rate (Marsh, 1998). Interestingly, in the study of Pupier et al. (2008) it was found that changing the crystal shape of plagioclase in their experiments had essentially no effect on the slope of the CSD. Launeau and Cruden (1998) also showed in their results that CSD was independent of grain shape.

The CSD of the 16 samples of the RRDS is shown in Fig. 9. The distribution shows a break in slope at 80 µm (note the regression lines for the two parts of the CSD) that is consistent with the kinked CSDs described by Marsh (1998). This kinked CSD could be

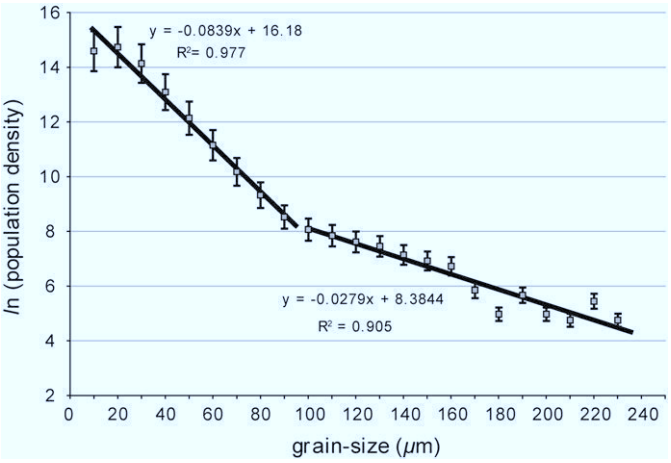

Fig. 9. Crystal size distribution (CSD) of 1.7×10^5 plagioclase grains from 16 samples of the RRDS (error bars at 5%). There is a break in slope at 80 μm (note regression line correlation values) which is probably related to a late-stage nucleation event that gave rise to crystal growth below this grain-size (see Section 7.2.).

interpreted as a function of crystal agglomeration (Burkhart et al., 1980) — a process which tends to cause plagioclase grains to evolve from acicular to blocky shapes because of the coalescence of grains during cooling. However, if crystal agglomeration occurred at a late-stage it would tend to reduce the number of early formed small grains. Furthermore, evidence of textural coarsening (Ostwald ripening), which would also reduce the number of small grains, is not supported by the CSD.

Marsh (1998) indicates that kinked CSDs are related to changes in nucleation rate which may reflect two distinct nucleation events. Marsh (1998) demonstrates that distinct events of heterogeneous nucleation provide the geological explanation for a kinked CSD derived from Makaopuhi lava lake (Hawaii). In thin-sections of samples from this basaltic lava lake there is evidence of co-precipitation of the main phases, with early growth occurring in poorly sorted clusters (heterogeneous nucleation). Larger crystals have "annexed" smaller grains, resulting in a texture comprising large, spatially separate grains which are within a groundmass of smaller grains that grew at a later stage. In phenocrystic samples, this may be a function of different environments of nucleation — phenocrysts nucleate and grow at depth, while the smaller grains grow later, potentially affected by relatively rapid undercooling at a later stage.

Kirkpatrick et al. (1979) and Muncill and Lasaga (1987) have found that the morphology of plagioclase crystals become increasingly skeletal, dendritic and fibrous with increasing undercooling. These crystal shapes are consequently more anisotropic than sub/euhedral crystals grown under equilibrium conditions. This is applicable to the textures and CSD of the RRDS. We have shown that the highest values of anisotropy ($r > 7$) occur in the smallest grains and thus are likely to have grown at a late stage, perhaps during undercooling caused by upward migration of magma while earlier crystallisation, closer to equilibrium conditions, occurred at depth.

8. Conclusions

It is possible to draw the following conclusions based on the results presented:

1. Grain-size and shape in the RRDS are independent, although grains > 55 μm tend to have lower r values than smaller grains.
2. Plagioclase grains in the 12–13 μm size range with modest shape ratios (1.80–2.20) appear to define type-A fabric. This is comparable to the work of Benn and Allard (1989) who found that imbrication is not common below an r value of 1.50.
3. Type-B fabric is more strongly associated with higher anisotropy, small grains (~8.50 μm).
4. The CSD and igneous textures of samples of the RRDS are consistent with heterogeneous nucleation — with phenocrysts having grown early at depth and grains < 80 μm having grown later under conditions of relatively rapid undercooling.
5. Our results are comparable to the findings of Dragoni et al. (1997) given that there is an apparent correlation between increasing grain shape (r) and type-B fabric. We therefore do not favour the strong interaction of grains attempting to rotate as the primary mechanism in the development of type-B fabric.

In our previous work on the SPO fabric of the RRDS we suggested that type-B fabric developed as a result of late-stage (high magma viscosity) re-orientation of the fabric caused by the interaction of large grains. Our findings in this work also suggest late-stage processes, but it seems that rapid nucleation of the plagioclase groundmass at a late-stage has more significantly affected the development of type-B fabric than the process of grain interaction.

Supplementary data to this article can be found online at http://dx.doi.org/10.1016/j.tecto.2012.10.035.

Acknowledgements

The corresponding author would like to acknowledge a freestanding NRF Innovation Scholarship, as this work forms part of his PhD research. Carlos Archanjo and an anonymous reviewer are thanked for their reviews of this paper.

References

Amenta, R.V., 2001. Three-dimensional computer modelling of fabric evolution in igneous rocks. Computers & Geosciences 27, 477–483.
Arbaret, L., Diot, H., Bouchez, J.-L., 1996. Shape fabrics of particles in low concentration suspensions: 2D analogue experiments and application to tiling in magma. Journal of Structural Geology 18, 941–950.
Archanjo, C.J., Launeau, P., 2004. Magma flow inferred from preferred orientations of plagioclase of the Rio Cearf-Mirim dyke swarm (NE Brazil) and its AMS significance. In: Martin-Hernandez, F., Luneburg, C.M., Aubourg, C., Jackson, M. (Eds.), Magnetic Fabric: Methods and Applications: Geological Society of London, Special Publication, 238, pp. 285–298.
Armstrong, R.A., Bristow, J.W., Cox, K.G., Armstrong, R.A., Bristow, J.W., Cox, K.G., 1984. The Rooi Rand dyke swarm, southern Lebombo. In: Erlank, A.J. (Ed.), Petrogenesis of the Volcanic Rocks of the Karoo Province: Geological Society of South Africa, Special Publication, 13, pp. 77–86.
Aubourg, C., Giordano, G., Mattei, M., Speranza, F., 2002. Magma flow in sub-aqueous rhyolitic dikes inferred from magnetic fabric analysis (Ponza Island, W. Italy). Physics and Chemistry of the Earth 27, 1263–1272.
Aubourg, C., Tshoso, G., Le Gall, B., Bertrand, H., Tiercelin, J.-J., Kampunzu, A.B., Dyment, J., Modisi, M., 2008. Magma flow revealed by magnetic fabric in the Okavango giant dyke swarm, Karoo igneous province, northern Botswana. Journal of Geothermal and Volcanic Research 170, 247–261.
Baer, G., 1995. Fracture propagation and magma flow in segmented dykes: Field evidence and fabric analyses, Makhtesh Ramon, Israel. In: Baer, G., Heimann, A. (Eds.), Physics and Chemistry of Dykes. A.A. Balkema, Rotterdam, pp. 125–140.
Bascou, J., Camps, P., Dautria, J.M., 2005. Magnetic versus crystallographic fabrics in a basaltic lava flow. Journal of Volcanology and Geothermal Research 145, 119–135.
Benn, K., Allard, B., 1989. Preferred mineral orientations related to magmatic flow in ophiolite layered gabbros. Journal of Petrology 30, 925–946.
Blanchard, J.-P., Boyer, P., Gagny, C., 1979. Un nouveau critere de sens de mise en place dans une caisse filonienne: Le "pincement" des mineraux aux epontes: orientation des minéraux dans un magma en écoulement. Tectonophysics 53, 1–25.
Blumenfeld, P., Bouchez, J.-L., 1988. Shear criteria in granite and migmatite deformed in the magmatic and solid state. Journal of Structural Geology 10, 361–372.
Burkhart, L.E., Hoyt, R.C., Oolman, T., 1980. Control of particle size distribution and agglomeration in continuous precipitations. In: Kuczynski, G.C. (Ed.), Sintering Processes. Plenum, New York, pp. 23–38.
Callot, J.P., Guichet, X., 2003. Rock texture and magnetic lineation in dykes: a simple analytical model. Tectonophysics 366, 207–222.
Callot, J.P., Geoffroy, L., Aubourg, C., Pozzi, J.P., Mege, D., 2001. Magma flow directions of shallow dykes from the East Greenland volcanic margin inferred from magnetic fabric studies. Tectonophysics 335, 313–329.
Cañón-Tapia, E., 2004. Anisotropy of magnetic susceptibility of lava flows and dykes: an historical account. In: Martín-Hernández, F., Lüneburg, C.M., Aubourg, C., Jackson, M. (Eds.), Magnetic Fabric: Methods and Applications: Geological Society of London, Special Publication, 238, pp. 205–225.

Cañón-Tapia, E., Chávez-Álvarez, M.J., 2004. Theoretical aspects of particle movement in flowing magma: implications for the anisotropy of magnetic susceptibility of dykes. In: Martín-Hernández, F., Lüneburg, C.M., Aubourg, C., Jackson, M. (Eds.), Magnetic Fabric: Methods and Applications: Geological Society of London, Special Publication, 238, pp. 227–249.
Cashman, K.V., Marsh, B.D., 1988. Crystal size distribution (CSD) in rocks and the kinetics and dynamics of crystallization—II: Makaopuhi lava lake. Contributions to Mineralogy and Petrology 99, 292–305.
Chadima, M., Cajz, V., Týcová, P., 2009. On the interpretation of normal and inverse magnetic fabric in dikes: examples from the Eger Graben, NW Bohemian Massif. Tectonophysics 466, 47–63.
Correa-Gomes, L.C., Souza Filho, C.R., Martins, C.J.F.N., Oliveira, E.P., 2001. Development of symmetrical and asymmetrical fabrics in sheet-like igneous bodies: the role of magma flow and wall-rock displacements in theoretical and natural cases. Journal of Structural Geology 23, 1415–1428.
Cruden, A.R., 1990. Flow and fabric development during the diapiric rise of magma. Journal of Geology 98, 681–698.
Dowty, R., 1980. Crystal growth and nucleation theory and the numerical simulation of igneous crystallization. In: Hargraves, R.B. (Ed.), Physics of Magmatic Processes. Princeton University Press, Princeton, New Jersey, pp. 419–485.
Dragoni, M., Lanza, R., Tallarico, A., 1997. Magnetic anisotropy produced by magma flow: theoretical model and experimental data from Ferrar dolerite sills (Antarctica). Geophysical Journal International 128, 230–240.
Ernst, R.E., 1990. Magma flow directions in two mafic Proterozoic dyke swarms of the Canadian Shield: as estimated using anisotropy of magnetic susceptibility data. In: Parker, A.J., Rickwood, P.C., Tucker, D.H. (Eds.), Mafic Dykes and Emplacement Mechanisms. A.A. Balkema, Rotterdam, pp. 231–235.
Ernst, R.E., Baragar, W.R.A., 1992. Evidence from magnetic fabric for the flow pattern of magma in the MacKenzie giant radiating dyke swarm. Nature 356, 511–513.
Ernst, R.E., Duncan, A.R., 1995. Magma flow in the Giant Botswana dyke swarm from analysis of magnetic fabric (abstract). Third International Dyke Conference (Jerusalem, Israel).
Ferguson, C.C., 1979. Rotations of elongate rigid particles in slow non-Newtonian fluids. Tectonophysics 60, 247–262.
Fernandez, A., Feybesse, J.-L., Mezure, J.-F., 1983. Theoretical and experimental study of fabrics developed by different shaped markers in two-dimensional simple shear. Bulletin of the Geological Society of France 25, 319–326.
Gay, N.C., 1966. Orientation of mineral lineation along the flow direction in rocks: a discussion. Tectonophysics 3, 559–564.
Gay, N.C., 1968. The motion of rigid particles embedded in a viscous fluid during pure shear deformation of the fluid. Tectonophysics 5, 81–88.
Geoffroy, L., Callot, J.P., Aubourg, C., Moreira, M., 2002. Divergence between magnetic and plagioclase linear fabrics in dykes: a new approach for defining the flow vector using magnetic foliation. Terra Nova 14, 183–190.
Hastie, W.W., Aubourg, C., Watkeys, M.K., 2011a. When an 'inverse' fabric is not inverse: an integrated AMS-SPO study in MORB-like dykes. Terra Nova 23, 49–55.
Hastie, W.W., Watkeys, M.K., Aubourg, C., 2011b. Significance of magnetic and petrofabric in Karoo-feeder dykes, northern Lebombo. Tectonophysics 513, 96–111.
Henry, B., 1997. The magnetic zone axis: a new element of magnetic fabric for the interpretation of the magnetic lineation. Tectonophysics 271, 325–356.
Hersum, T.G., Marsh, B.D., 2006. Igneous microstructures from kinetic models of crystallization. Journal of Volcanology and Geothermal Research 154, 34–47.
Higgins, M.D., 2000. Measurement of crystal size distributions. American Mineralogist 85, 1105–1116.
Ildefonse, B., Fernandez, A., 1988. Influence of the concentration of rigid markers in a viscous medium on the production of preferred orientations. An experimental contribution, 1. Non-coaxial strain. Geological Kinematics and Dynamics (in Honor of the 70th Birthday of Hans Ramberg): Bulletin of the Geological Institute University Uppsala, 14, pp. 55–60.
Ildefonse, B., Launeau, P., Bouchez, J.L., Fernandez, A., 1992. Effect of mechanical interactions on the development of shape preferred orientation: a two-dimensional experimental approach. Journal of Structural Geology 14, 73–83.
Ildefonse, B., Arbaret, L., Diot, H., 1997. Rigid particles in simple shear flow: is their preferred orientation periodic or steady-state? In: Bouchez, J.L., Hutton, D.H.W., Stephens, W.E. (Eds.), Granite: From Segregation of Melt to Emplacement Fabrics. Kluwer academic publishers, Dordrecht, pp. l77–l185.
Jezek, J.R., Melka, R., Schulman, K., Venera, Z., 1994. The behavior of rigid triaxial ellipsoidal particles in viscous flows — modeling of fabric evolution in a multiparticle system. Tectonophysics 229, 165–180.
Jourdan, F., Féraud, G., Bertrand, H., Watkeys, M.K., 2007. From flood basalts to the inception of oceanization: Example from the $^{40}Ar/^{39}Ar$ high-resolution picture of the Karoo large igneous province. Geochemistry, Geophysics, Geosystems 8, 1–20.
Kattenhorn, S.A., 1994. Mechanisms of sill and dyke intrusion. (unpubl. MSc thesis). University of Natal (Durban) pp. 149.
Kirkpatrick, R.J., 1977. Nucleation and growth of plagioclase, Makapuhi and Alae lava lakes, Kilauea Volcano, Hawaii. Geological Society of America Bulletin 88, 78–84.
Kirkpatrick, R.J., Klein, L., Uhlmann, D.R., Hays, J.F., 1979. Rates and processes of crystal growth in the system anorthite-albite. Journal of Geophysical Research 84, 3671–3676.
Kissel, C., Laj, C., Sigurdsson, H., Guillou, H., 2010. Emplacement of magma in Eastern Iceland dikes: insights from magnetic fabric and rock magnetic analyses. Journal of Volcanology and Geothermal Research 191, 79–92.
Launeau, P., 2004. Mise en évidence des écoulements magmatiques par analyse d'images 2-D des distributions 3-D d'orientations préferentielles de formes. Bulletin of the Geological Society of France 175, 331–350.
Launeau, P., Cruden, A.R., 1998. Magmatic fabric acquisition mechanisms in a syenite: results of a combined anisotropy of magnetic susceptibility and image analysis study. Journal of Geophysical Research 103, 5067–5089.
Launeau, P., Robin, P.-Y.F., 1996. Fabric analysis using the intercept method. Tectonophysics 267, 91–119.
Launeau, P., Robin, P.-Y.F., 2005. Determination of fabric & strain ellipsoids from measured sectional ellipses — implementation and applications. Journal of Structural Geology 27, 2223–2233.
Launeau, P., Archanjo, C.J., Picard, D., Arbaret, L., Robin, P.-Y., 2010. Two- and three-dimensional shape fabric analysis by the intercept method in grey levels. Tectonophysics 492, 230–239.
Marsh, B.D., 1988. Crystal size distributions (CSD) in rocks and the kinetics and dynamics of crystallization, I, theory. Contributions to Mineralogy and Petrology 99, 277–291.
Marsh, B.D., 1998. On the interpretation of crystal size distributions in magmatic systems. Journal of Petrology 39, 553–599.
Meth, D.L., 1996. The Geology and Geochemistry of the Rooi Rand Dyke Swarm. (unpubl. MSc. thesis). University of Natal (Durban), pp. 189.
Muncill, G.E., Lasaga, A.C., 1987. Crystal-growth kinetics of plagioclase in igneous systems: one-atmosphere experiments and application of a simplified growth model. American Mineralogist 72, 299–311.
Nicolas, A., Reuber, L., Benn, K., 1988. A new magma chamber model based on structural studies in the Oman ophiolite. Tectonophysics 151, 87–105.
Pupier, E., Duchene, S., Toplis, M.J., 2008. Experimental quantification of plagioclase crystal size distribution during cooling of a basaltic liquid. Contributions to Mineralogy and Petrology 155, 555–570.
Ramsay, J.G., 1989. Emplacement kinematics of a granite diapir: the Chindamora batholith, Zimbabwe. Journal of Structural Geology 11, 191–209.
Riley, T.R., Millar, I.L., Watkeys, M.K., Curtis, M.L., Leat, P.T., Klausen, M.B., Fanning, C.M., 2004. U–Pb zircon (SHRIMP) ages for the Lebombo rhyolites, South Africa. Journal of the Geological Society of London 161, 547–550.
Robin, P.-Y.F., 2002. Determination of fabric and strain ellipsoids from measured sectional ellipses — theory. Journal of Structural Geology 24, 531–544.
Romeo, I., Capote, R., Lunar, R., Cayzer, N., 2007. Polymineralic orientation analysis of magmatic rocks using electron back-scatter diffraction: implications for igneous fabric origin and evolution. Tectonophysics 444, 45–62.
Saggerson, E.P., Bristow, J.W., Armstrong, R.A., 1983. The Rooi Rand dyke swarm. South African Journal of Science 79, 365–369.
Watkeys, M.K., 2002. Development of the Lebombo rifted volcanic margin of southeast Africa. In: Menzies, M.A., Klemperer, S.L., Ebinger, C.J., Baker, J. (Eds.), Volcanic Rifted Margins: Geological Society of America Special Paper, 362, pp. 27–46.
Willis, D.G., 1977. A kinematic model of preferred orientation. Geological Society of America Bulletin 88, 883–894.

Tectonophysics 513 (2011) 96–111

Contents lists available at SciVerse ScienceDirect

Tectonophysics

journal homepage: www.elsevier.com/locate/tecto

Significance of magnetic and petrofabric in Karoo-feeder dykes, northern Lebombo

Warwick W. Hastie [a,*], Michael K. Watkeys [a], Charles Aubourg [b]

[a] School of Geological Sciences, Building H1, University of KwaZulu-Natal, University Road, Westville, Durban 4001, South Africa
[b] Laboratoire des Fluides Complexes et Réservoirs, UMR 5150, CNRS, TOTAL, Université de Pau et des Pays de l'Adour, Avenue de l'Université BP 1155, 64013 Pau Cedex, France

ARTICLE INFO

Article history:
Received 12 July 2011
Received in revised form 6 October 2011
Accepted 8 October 2011
Available online 15 October 2011

Keywords:
Anisotropy of magnetic susceptibility
Karoo feeder dykes
Magma flow
Northern Lebombo dyke swarm

ABSTRACT

The orientation of magnetic and petrofabric in 14 mafic dykes of the Northern Lebombo dyke swarm (NLDS) has been determined using the anisotropy of magnetic susceptibility (AMS) and mineral shape preferred orientation (SPO) in order to constrain the magma flow direction during dyke emplacement. The N–S striking NLDS intruded the N–S trending; 700 km long Lebombo faulted monocline between 182 and 178 Ma. The Lebombo faulted monocline, which forms the eastern-most sub-province of the Karoo large igneous province (LIP), is essentially a volcanic rifted margin with a protracted magmatic and tectonic history related to the break-up of southern Gondwana. It also forms the southern limb of the Karoo triple-rift system which has been hypothesised to have formed by a mantle plume centred on the triple junction locus. The other two arms of the rift which converge on the triple junction are the WNW trending Okavango dyke swarm (ODS) and NE trending Save-Limpopo dyke swarm (SLDS). In the NLDS it is found that the magnetic fabric, which is of magmatic origin in ~50% of the samples, is carried predominantly by stoichiometric magnetite. There is remarkable agreement between the orientations of the AMS and SPO fabrics and at least two dykes show coaxial AMS and mineral SPO fabric consistent with lateral magma flow from the north. This direction is supported by the imbrication of the foliations of the well-defined bulk AMS and plagioclase SPO fabric when viewed in a dyke co-ordinate system. Although steeply plunging maximum axes occur in the SPO fabric, their possible use as magma flow vectors is questioned because they do not necessarily mimic the elongation of plagioclase grains visible in orientated thin sections. The magnetic and petrofabric of the NLDS is interpreted to have developed during lateral magma flow from the locus of the Karoo triple junction.

1. Introduction

1.1. The Karoo large igneous province

Dykes of the northern Lebombo in northeast South Africa have been directly linked to basaltic volcanism of the Karoo large igneous province (LIP) along the Lebombo faulted monocline (Jourdan et al., 2005; Klausen, 2009; Watkeys, 2002). The ~182 Ma old Karoo LIP comprises predominantly continental flood basalts (CFBs) which cover an area of 3×10^6 km^2 in southern Africa (Erlank, 1984). It is contiguous with the Ferrar Province in Antarctica and is associated with precursory extension in the opening of the Indian Ocean as Antarctica split from a position along the eastern edge of southern Africa during the break-up of southern Gondwana (Encarnación et al., 1996; Watkeys, 2002).

It is along this eastern margin that the Lebombo faulted monocline is found. The Lebombo faulted monocline is a linear volcanic margin which extends southwards from south-central Zimbabwe and comprises an east–west (E–W) highly extended terrane characteristic of a volcanic rifted margin (Bristow, 1982; Klausen, 2009; Watkeys, 2002). The Lebombo faulted monocline forms the southern limb of the Karoo triple junction, (Fig. 1a). The west-northwest (WNW) trending limb comprises the Okavango dyke swarm (ODS) while the east-northeast (ENE) trending limb comprises the Save-Limpopo dyke swarm (SLDS). Dykes of the Lebombo faulted monocline include the Northern Lebombo dyke swarm (NLDS) and the Rooi Rand dyke swarm (RRDS) (Fig. 1a) (Armstrong et al., 1984; Jourdan et al., 2004, 2007; Klausen, 2009; Watkeys, 2002).

The structural and petrological components of the Karoo LIP have been studied in some detail for the last 70 years in order to determine its origin, timing, duration and significance with regard to Gondwana break-up (Bristow, 1982; Cox, 1992; Cox et al., 1967; Du Toit, 1929; Erlank, 1984; Jourdan et al., 2005, 2007; Klausen, 2009; Watkeys, 2002). In more recent studies there has been a focus on the dykes associated with the Karoo LIP, particularly the dyke swarms which centre on Mwenezi (formerly Nuanetsi) in south-central Zimbabwe. These dyke swarms have provided significant structural, geochronological and geochemical information regarding the evolution of the Karoo LIP (Bristow, 1984; Cox, 1989; Jourdan et al., 2004, 2006; Le Gall et al., 2002, 2005; Reeves, 1978).

* Corresponding author. Tel.: +27 31 260 1277.
E-mail addresses: 203505849@ukzn.ac.za, warwick.hastie@gmail.com (W.W. Hastie).

0040-1951/$ – see front matter © 2011 Elsevier B.V. All rights reserved.
doi:10.1016/j.tecto.2011.10.008

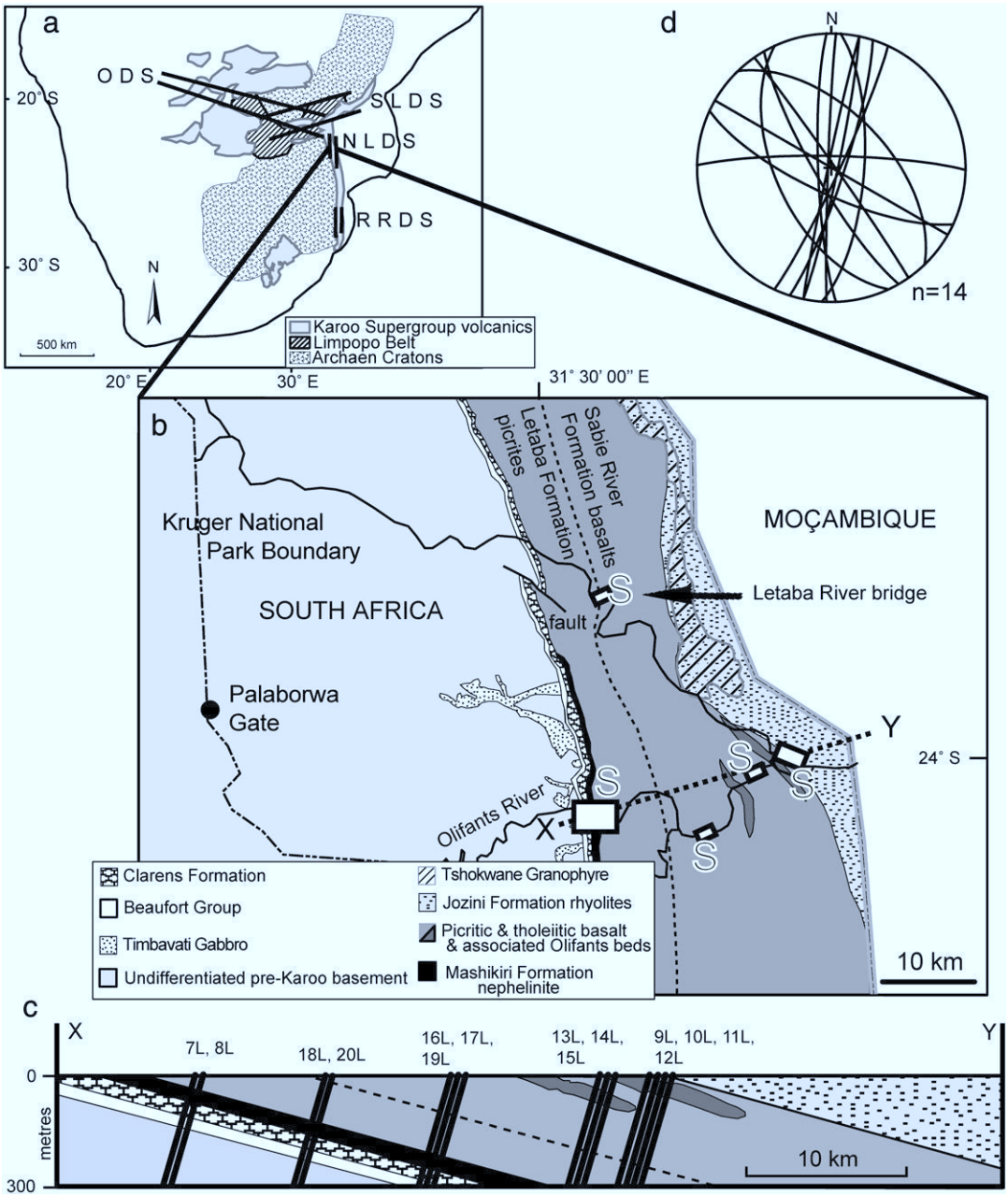

Fig. 1. (a) Schematic map of southern Africa showing the Karoo large igneous province (pale grey) and associated dyke swarms (ODS = Okavango dyke swarm; SLDS = Save-Limpopo dyke swarm; NLDS = Northern Lebombo dyke swarm; RRDS = Rooi Rand dyke swarm) which are bounded by Archaean terranes (after Jourdan et al., 2004) (b) Map showing the geology of the northern Lebombo and the sampled regions (marked with "S") of the NLDS in northeast South Africa and the line of section (XY) is marked (modified from Bristow, 1982, 1984) (c) Simplified cross-section XY showing the position of the sampled dykes of the NLDS (modified from Bristow, 1982 and Watkeys, 2002) (d) Stereographic projection of the average dyke planes of the 14 sampled dykes from this study.

It is within the context of the Karoo triple junction that we have attempted to find the original flow direction of magma in dykes of the NLDS by measuring and interpreting fabrics pictured using the anisotropy of magnetic susceptibility (AMS) and mineral shape preferred orientation (SPO). These methods are used because (1) the investigated dykes display no macroscopic evidence of magma flow, (2) AMS measures a large number of grains ($>10^6$) rapidly and non-destructively and (3) both methods are sensitive to microscopic, weakly anisotropic fabrics. The careful interpretation of AMS fabrics and comparative fabric analysis (mineral SPO) provides a quantitative and reliable picture of the magma flow sense in dykes on a regional scale (Aubourg et al., 2008; Callot et al., 2001; Ernst and Baragar, 1992; Ernst and Duncan, 1995; Kissel et al., 2010). Thus we emphasise the need, additionally to AMS, to present an analysis of the 3-dimensional (3D) shape, orientation and intensity of, particularly, the plagioclase petrofabric.

Although the measurement and interpretation of data acquired using AMS and mineral SPO can be problematic due to various potential complications (discussed in Section 3, Methodology) its application in regional studies of dyke swarms has already provided significant results within the Karoo LIP. In the ODS, for example, Aubourg et al. (2008) have shown that near-vertical magma flow occurred close to the Karoo triple junction while sub-horizontal flow is in evidence ~400 km west of the triple junction. In addition, a recent study of the southernmost dykes of the Lebombo monocline (the RRDS) indicates that the magnetic fabric and silicate petrofabric are

not necessarily coaxial (Hastie et al., 2011). These authors show that there is no strong indication of magma flow sense in the petrofabric of the RRDS.

1.2. The Karoo triple junction

On the broadest scale, the picture of magma flow within dyke swarms can provide evidence of a potential magma source; as has been shown in East Greenland (Callot et al., 2001) and the ODS for example (Aubourg et al., 2008; Ernst and Duncan, 1995). The origin of the Karoo LIP remains controversial, however, as much evidence has been presented for and against a mantle plume model which originated mainly as a result of the geometry of the Karoo triple junction (Burke and Dewey, 1973; Campbell and Griffiths, 1990) and the concentrically arranged and compositionally zoned primitive nephelinites and picrites centred on the triple junction (Bristow, 1984; Cox, 1992; White, 1997). There has, therefore, been considerable interest in the ODS, the SLDS and the NLDS (and RRDS) which comprise the main arms of the triple junction (Armstrong et al., 1984; Aubourg et al., 2008; Duncan et al., 1990; Ernst and Duncan, 1995; Jourdan et al., 2004, 2006; Klausen, 2009; Le Gall et al., 2005; Reeves, 1978, 2000; Watkeys, 2002).

Campbell and Griffiths (1990) suggest that the concentrically arranged, primitive volcanic rocks centred on the triple junction resulted from the relatively "hotter" plume axis which, while ascending, did not interact with the surrounding mantle and/or lithosphere, although this has been disputed by Sm–Nd isotopic studies which suggest otherwise (Ellam and Cox, 1991). Indeed, the mafic Karoo magmas are dominantly tholeiitic in composition (Hawkesworth et al., 1999) and have distinct incompatible trace element geochemistry due to their distribution over either Archaean cratonic terranes (high Ti–Zr) or younger basement (low Ti–Zr) (Sweeney and Watkeys, 1990; Sweeney et al., 1994). This difference is attributed to a contrast in melting, resulting in 30–40% of the incompatible elements in the high Ti–Zr basalts being derived from the lithospheric mantle. However, Sweeney et al. (1994) suggest that more evolved high-Fe basalts in the central region of the Lebombo are compositionally consistent with mantle plume melting.

With regard to the dyke swarms, however, it has been more recently shown that there is clear evidence for the structural inheritance of pre-existing (Proterozoic) fracture and dyke directions in the ODS and SLDS (Jourdan et al., 2006; Le Gall et al., 2002, 2005). These authors showed that 87% of the dykes in the ODS are Karoo in age (179 ± 1.2–178.4 ± 1.1 Ma) whilst the remainder are Proterozoic. The structure of the ODS is therefore unlikely to be unique to the Karoo-age dykes, but must pre-date the formation of the triple junction. The geochronology, however, shows that the Karoo-aged dykes of the ODS post-date the volumetric bulk of the flood volcanism by at least 3 Ma (Jourdan et al., 2005). The ENE-trending, 50–100 km wide SLDS extends for 600 km from SE Botswana to the margins of the Limpopo belt (Fig. 1a) where it overlaps with the ODS (Jourdan et al., 2006). Although Karoo ages are indicated for the SLDS (180.4 ± 0.7–178.9 ± 0.8 Ma) (Jourdan et al., 2005; Le Gall et al., 2002), Proterozoic ages have been found in 14 dykes (728 ± 3–1683 ± 18 Ma) which, similarly to the ODS, implicates the role of inheritance of older structures when Karoo-age magmatism began (Jourdan et al., 2006).

It has been shown that the dyke swarms of the Karoo triple junction did not form as part of a singular volcanic feeder system, as the ODS (see ages above) and the RRDS (173.9 ± 0.7 Ma), post-date the main Karoo volcanic event. Furthermore, high-resolution $^{40}Ar/^{39}Ar$ radiometric dating indicate that the duration of Karoo magmatism was ~8 Ma, compared to the more typical 1–2 Ma duration determined for other flood basalt provinces (Jourdan et al., 2005). The south-to-north migration of magmatism evident in the Karoo LIP would also require very rapid migration of the crust over the head of a mantle plume (Jourdan et al., 2007; Le Gall et al., 2002). It seems in general, therefore, that a classical model of rapid and short-lived magmatism driven by an active plume in the genesis of the Karoo LIP is unlikely (Jourdan et al., 2004, 2006; Uken and Watkeys, 1997).

In a passive heating model, the development of the Karoo LIP may have started simply due to a lack of cooling related to the incubation of the mantle beneath, rather than active heating by a plume. Anderson et al. (1992) suggest that crustal thinning above non-isothermal, inhomogeneous mantle is responsible for the formation of volcanic ridges and hotspots. Evidently the accumulation and/or generation of heat and subsequent magmatism beneath the supercontinent of Gondwana would have weakened the crust, making continental break-up more likely as opposed to being a direct result of the emplacement of a plume beneath the supercontinent (Hawkesworth et al., 1999; Storey et al., 1992; White, 1997). Further geochemical and structural evidence for passive processes in the Karoo LIP include (1) the Nb-anomaly in the volcanic rocks of the Karoo LIP which is typical of subduction related volcanism (Cox, 1992) and (2) the linear extent of the contemporaneous Ferrar Province in Antarctica which is most likely beyond the reach of a plume and (3) the siliceous, high-field-strength-element-depleted signature of the Ferrar Province resulting from sedimentary contamination of the mantle source. This is most likely a subduction related process (Cox, 1992; Encarnación et al., 1996; Hergt et al., 1991).

Resolving the active or passive role played by plumes and/or subduction or other processes in the development of CFBs is critical for understanding these large-scale magmatic events. It has been shown that the relative timing of intrusive and eruptive events can be resolved (e.g. Jourdan et al., 2007) and it is within this context that we present evidence for the regional magma flow direction in the NLDS. The regional pattern of magma flow in the NLDS is therefore potentially significant with respect to magmatism in this region.

2. Geological background

2.1. The Lebombo faulted monocline

The Lebombo faulted monocline is a 700 km long, N–S trending volcanic rifted-margin which is exposed along the eastern margin of South Africa (Klausen, 2009; Watkeys, 2002). The broad volcanic stratigraphy of the Lebombo faulted monocline comprises the Mashikiri Formation (nephelinites); overlain by the picritic and tholeiitic basalts of the Letaba and Sabie River Formations respectively and finally the Jozini Formation (rhyolites and associated granophyres) (Bristow, 1984; Erlank, 1984; Watkeys, 2002). These formations, which collectively form the Lebombo Group, overly older Archaean basement, the Proterozoic Timbavati gabbro and sedimentary rocks of the Mesozoic Clarens Formation and Beaufort Group (Fig. 1b). Intruding the lowermost units and the basalts themselves are mafic feeder dykes and composite felsic and mafic dykes, all of which comprise the NLDS (Klausen, 2009; Watkeys, 2002). Magmatism appears to have been preferentially channelled in the Lebombo faulted monocline in the form of the N–S striking NLDS as the dykes are sparsely distributed to the west and north. This is probably because of the position of the Lebombo faulted monocline at the eastern edge of the Kaapvaal craton (Fig. 1a) (Jourdan et al., 2006; Klausen, 2009).

The monoclinal structure of the Lebombo which characterises its geometry was caused by coast parallel (N–S) faulting during the initial stages of Gondwana break-up along what is now the east coast of South Africa (Watkeys, 2002). This faulting has resulted in the eastward dip of the sedimentary rocks and overlying volcanic successions (Fig. 1c), indicative of a volcanic rifted margin rather than a classic monocline (Klausen, 2009). It is evident from the predominantly westward dip of the northern Lebombo dykes that they intruded prior to the fault-induced eastward tilting of the Lebombo which

began within ±1 Ma of the bulk of the magmatism (182 Ma) (Jourdan et al., 2007; Klausen, 2009; Riley et al., 2004). There is currently no evidence for structural inheritance (viz. ODS, SLDS) in the emplacement history of the NLDS (Jourdan et al., 2006).

2.2. The Northern Lebombo dyke swarm

Klausen (2009) has tentatively associated 4 generations of dykes with overlying volcanic successions as follows, based on composition and field relationships: dark grey coloured plagioclase-phyric dolerite dykes (D1 generation) which are feeders to the overlying Sabie River Formation basalts; paler D2 dykes which texturally resemble the uppermost amygdaloidal basalts of the Sabie River Formation; a small volume of thin dykes with irregular margins (D3 generation) which are feeders to rhyodacitic units of the Jozini Formation and finally D4 dykes which do not appear to be associated with any volcanics. Dyke generations D1–D3 have consistent N–S strikes, while D4 dykes tend to strike NW–SE. The D1–D3 dykes fed the bulk of the basaltic magmatism during the development of the Lebombo and the D4 dykes intruded concomitantly with the emplacement of the ODS at ~178 Ma (Klausen, 2009).

The main dyking activity in the NLDS therefore most likely predates 178 Ma as the dyke ages are comparable to that of the volcanic rocks within a restricted range, as mentioned previously (Jourdan et al., 2005, 2007). For example, radiometric dating of a D4 dyke (SA-30 of Jourdan et al., 2007 and 9L of this study, see Table 1) yielded an age of 178 ± 1 Ma—providing essentially a maximum time interval of 4 Ma (182–178 Ma) during which all the successive dyke generations intruded. In a qualitative sense this is also evident in the field because the volcanic successions which the dykes feed are conformable and the consistent dip of the dykes (~80° to the west) suggests syn- to post-intrusion tilting of the Lebombo faulted monocline. Readers are referred to Klausen (2009) for more in-depth analysis of the field, geochemical and tectonic aspects of the NLDS and associated volcanic successions.

3. Methodology

3.1. Sampling

Five regions were sampled for this study, extending from the Olifants River in the south to the Letaba River Bridge in the north (Fig. 1b). A total of 224 samples were collected from 14 dykes, as shown in Table 1. Each dyke comprises 2 sites (i.e. each margin is 1 sampling site). Note that the data are arranged from the oldest dykes (D1) to youngest (D4) and those with unknown affiliation. Most of the dykes, except 13L, dip steeply (>80°) and strike N–S to NW–SE and E–W (7L) as shown in Table 1 and Fig. 1d. The dykes are well exposed in the field, particularly along the Olifants River where multiple dykes can be seen intruding the host basaltic rocks (Fig. 2a) and individual dykes may be traced for tens of metres along their length. Field relationships between the dykes and the volcanic rocks are quite clear as, for example, in the Letaba River Bridge section (Fig. 2b) where picrite basalts are intruded by D3 dykes. Dyke widths are quite variable, from 0.5 m to 10 m, although the D4 dykes tend to be >5 m in thickness, with regular margins. The dyke margins are generally well exposed, and as such between 6 and 12 standard cylindrical specimens (22 mm×25 mm) were collected from opposing margins of an intrusion (Tauxe et al., 1998) using a hand-held petroleum powered drill. Each sample was orientated in the field using a core-orientator with a magnetic compass as there was no noticeable magnetic deviation caused by the dykes.

Table 1
Dyke and AMS data for the NLDS. Note that the dykes are shown in order of relative age, from D1 to D4 and opposing margins are discriminated.

Dyke	Margin	Thickness	Orientation (dip and strike)	Lat./Long.	[a]n	[b]Km (10^{-3} SI)	K1	K2	K3	[c]P′ [10^{-3} ([d]sd)]	[e]T [10^{-3} (sd)]
19L (D1)	West	3 m	88°/182°	24°03′30.5″ S	9	59.76	30°/343°	35°/096°	41°/223°	1.034(13)	−0.196(34)
	East			31°42′41.2″ E	8	48.36	05°/010°	19°/102°	71°/267°	1.016(6)	−0.145(38)
16L (D2)	West	28 m	80°/150°	24°03′02.0″ S	8	68.77	02°/145°	19°/054°	71°/240°	1.019(2)	−0.212(49)
	East			31°43′53.3″ E	8	52.78	15°/322°	67°/193°	17°/057°	1.039(6)	0.532(33)
14L (D2)	West	2.3 m	88°/192°	24°00′01.3″ S	8	84.30	04°/184°	53°/088°	36°/277°	1.020(5)	0.185(37)
	East			31°45′07.9″ E	8	69.75	02°/308°	05°/218°	85°/057°	1.021(4)	0.040(34)
20L (D3)	West	3.5 m	82°/178°	23°48′47.2″ S	8	64.39	39°/341°	20°/089°	44°/200°	1.018(5)	−0.242(27)
	East			31°34′57.1″ E	8	64.75	09°/096°	39°/358°	49°/196°	1.054(27)	−0.372(30)
18L (D3)	West	7.5 m	82°/018°	23°48′48.7″ S	8	74.74	20°/123°	37°/017°	47°/253°	1.023(9)	0.149(46)
	East			31°34′52.4″ E	8	75.41	25°/296°	26°/039°	52°/168°	1.014(5)	−0.284(32)
8L (D4)	West	3.5 m	85°/183°	24°02′14.0″ S	8	20.65	85°/001°	02°/118°	04°/208°	1.050(14)	−0.378(17)
	East			31°34′28.8″ E	9	31.31	76°/244°	10°/017°	10°/109°	1.050(32)	−0.262(46)
†9L (D4)	West	16.8 m	88°/325°	23°58′31.0″ S	8	28.41	81°/339°	09°/153°	01°/243°	1.029(11)	0.172(49)
	East			31°47′37.0″ E	8	20.12	71°/321°	19°/145°	01°/055°	1.035(10)	0.197(39)
12L (D4)	West	10 m	90°/120°	23°58′39.1″ S	6	65.22	44°/006°	44°/167°	10°/267°	1.045(6)	0.301(40)
	East			31°47′51.5″ E	6	53.09	17°/321°	66°/096°	16°/226°	1.027(5)	0.027(26)
13L (D4)	West	5.5 m	56°/155°	24°00′01.3″ S	11	28.11	39°/065°	44°/207°	20°/318°	1.012(5)	−0.234(35)
	East			31°45′07.9″ E	7	36.91	21°/174°	06°/266°	68°/012°	1.022(5)	−0.188(24)
17L (D4)	West	5.2 m	82°/168°	24°03′02.2″ S	8	81.12	22°/159°	64°/306°	13°/064°	1.022(12)	0.192(36)
	East			31°43′52.3″ E	8	98.16	12°/183°	68°/303°	19°/089°	1.034(19)	0.421(33)
7L	North	0.55 m	83°/271°	24°02′20.1″ S	12	5.45	50°/351°	34°/134°	19°/237°	1.032(20)	0.125(42)
	South			31°34′35.5″ E	8	3.26	68°/103°	03°/006°	22°/275°	1.029(19)	0.081(24)
10L	West	2 m	85°/025°	23°58′39.6″ S	8	51.07	55°/204°	35°/031°	03°/299°	1.025(9)	0.267(43)
	East			31°47′53.2″ E	8	63.23	51°/222°	38°/028°	07°/123°	1.021(8)	0.377(46)
15L	West	0.6 m	82°/192°	24°00′01.3″ S	5	107.53	12°/191°	70°/316°	16°/097°	1.020(10)	0.027(46)
	East			31°45′06.3″ E	6	90.77	26°/085°	04°/353°	64°/254°	1.023(7)	0.070(20)
11L	West	2 m	86°/012°	23°58′39.6″ S	8	48.69	02°/026°	87°/243°	02°/116°	1.010(3)	0.119(48)
	East			31°47′53.2″ E	9	35.31	15°/201°	68°/333°	16°/107°	1.013(8)	0.107(29)

a n = number of specimens.
b $K_m = (K1 + K2 + K3)/3$.
c P' = degree of anisotropy (Jelinek, 1981).
d sd = standard deviation.
e T = shape factor (oblate/prolate) (Jelinek, 1981).
† Dyke SA-30 of Jourdan et al., 2007 (178 ± 1 Ma).

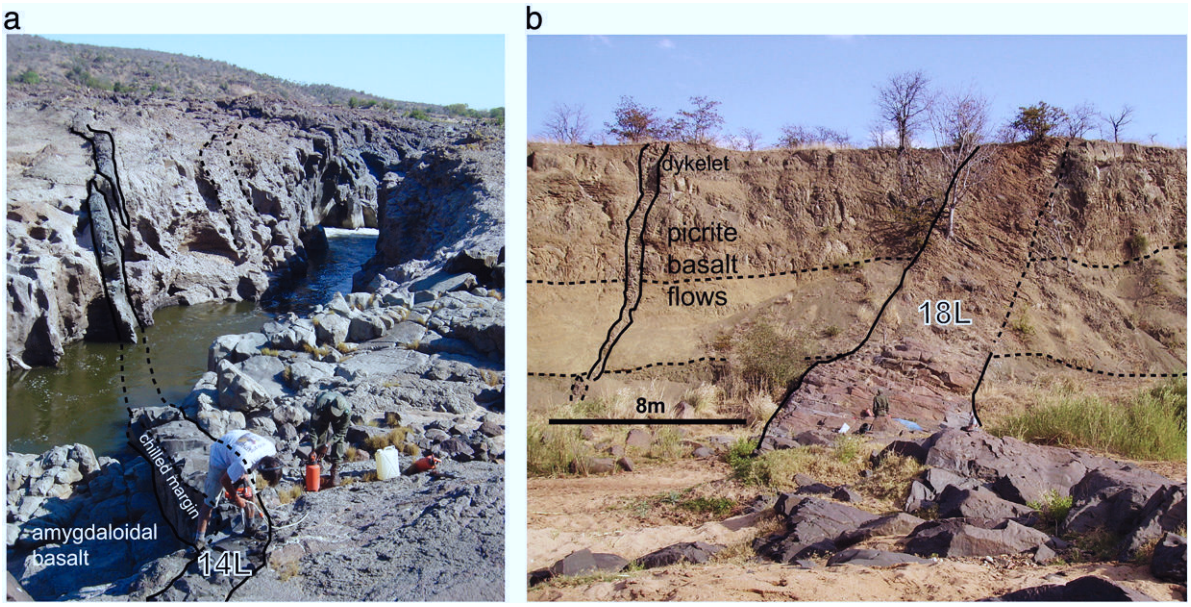

Fig. 2. Annotated photographs of two field exposures in the sampled region of the NLDS showing (a) dyke 14L exposed along the Olifants River and (b) dyke 18L exposed along the Letaba River. The direction of view for both photographs is southwards. Dykes are generally well exposed and multiple dykes can be seen in most exposures, although sheeted dykes are uncommon. As is shown in the photographs, dyke 14L (D2) is hosted by amygdaloidal basalts of the Sabie River Formation while the east-dipping dyke 18L (D3) is hosted by older picrite basalts of the Letaba Formation in this exposure.

3.2. Anisotropy of magnetic susceptibility

Measuring the anisotropy of magnetic susceptibility (AMS) has become a standard tool for the analysis of rock fabrics, notably due to its ability to characterise potentially flow related fabrics in extrusive (e.g. pyroclastics and flows) and intrusive (e.g. dykes and sills) volcanic rocks (Aubourg et al., 2008; Ellwood, 1978; Khan, 1962; Kissel et al., 2010; Knight and Walker, 1988; Poland et al., 2004; Rochette et al., 1991; Tarling and Hrouda, 1993). The source of susceptibility in mafic igneous rocks is typically Fe-bearing minerals such as magnetite and titanomagnetite which may in multi-domain state (MD), pseudo-single domain state (PSD) or single-domain state (SD) (Rochette et al., 1999). The anisotropy of magnetic susceptibility can be shape-controlled (shape anisotropy) for MD grains, as opposed to magneto-crystalline anisotropy found in hematite or pyrrhotite. It may also be controlled by the distribution of magnetic grains (distribution anisotropy, Hargraves et al., 1991) and/or a mixed contribution from a number of susceptible constituent minerals (Borradaile and Gauthier, 2003).

The anisotropy is represented by an ellipsoid of a second order tensor, which is shown stereographically using the three principal susceptibility axes; $K1 > K2 > K3$. For ferromagnetic, MD grains the $K1$ axis is parallel to the long axis of the grain and the $K3$ axis parallel to the short axis. In SD grains these axes may be inverted, resulting in inverse fabric (Potter and Stephenson, 1988; Rochette et al., 1991, 1999; Tarling and Hrouda, 1993). This is referred to as type-B fabric in this study (Archanjo and Launeau, 2004; Hastie et al., 2011). This type-B fabric may also originate from a late-stage process unrelated to the original magma flow direction such that the petrofabric is not necessarily mimicked by AMS, as is the case in the RRDS (Hastie et al., 2011).

Scalar data are also obtained from AMS studies, including the bulk susceptibility (K_m), the corrected degree of anisotropy (P') and the shape parameter (T) (Jelinek, 1981). In this study samples were analysed using an AGICO Kappabridge KLY-3 magnetic anisotropy spinner according to the standard 15 position procedure of Jelinek (1978) (in the manual mode). Recorded data of the principle orientations of the AMS tensor are plotted as lower hemisphere equal area projections in geographic co-ordinates, unless otherwise indicated.

Early AMS studies of flow-related fabrics showed that when a silicate fabric records the flow direction of magma during dyke emplacement—and the magnetic fabric is mimetic—then measuring AMS provides a proxy of the flow fabric. Such fabric is generally termed "normal" because $K1$ is parallel to the long axis of anisotropic grains (Ellwood, 1978; Knight and Walker, 1988; Rochette et al., 1999). This will be termed type-A fabric (Archanjo and Launeau, 2004; Hastie et al., 2011). At the dyke scale, type-A fabric is characterised by the $K1$ axis and the magnetic foliation (to which $K3$ is a pole) being sub-parallel to

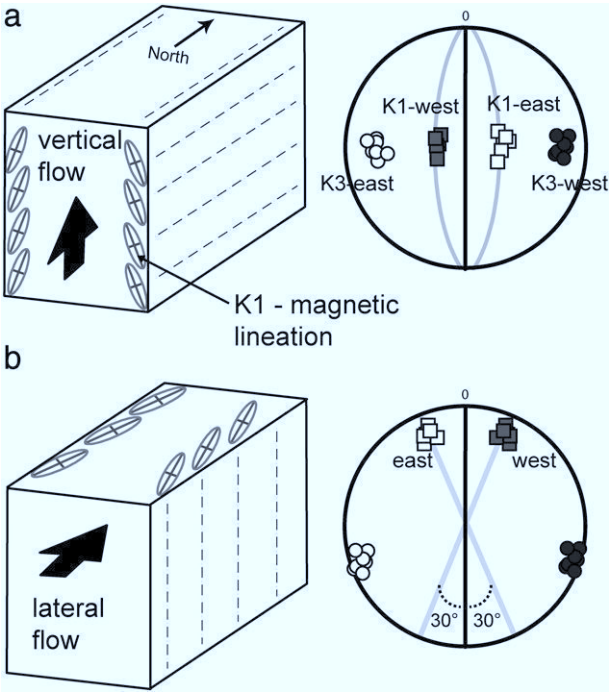

Fig. 3. Schematic diagrams of a vertical, north–south striking dyke indicating idealised fabric orientation resulting from (a) vertical intrusion of magma and the resultant AMS ellipsoid and (b) a lateral intrusion of magma and the resultant AMS ellipsoid. The dyke is shown as a north–south black line in the projections, the foliations in grey. Intermediate axes ($K2$) not shown for clarity. Not to scale (modified from Geoffroy et al., 2002 and Gil-Imaz et al., 2006).

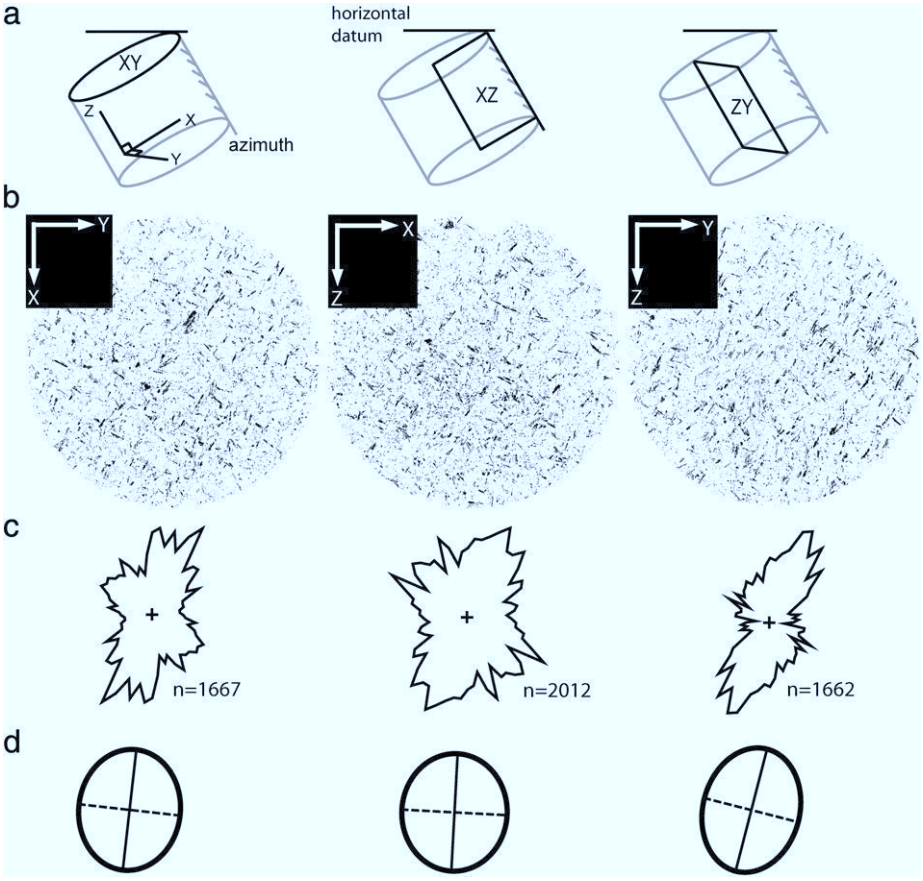

Fig. 4. Schematic illustration of the methodology employed for studying mineral SPO showing (a) the *XYZ* co-ordinate system as applied to a single drill-core sample (17L3) for defining the orientation of the thin-sections (b) the *XY*, *XZ* and *ZY* sections of the sample. Circular sections are used in order to reduce any edge effects such as grain-size or orientation distortion (c) rose diagrams of grain directions and number of grains (n) determined for each thin-section and (d) 2D inertia tensors determined for the same sections (minor axis = dashed line).

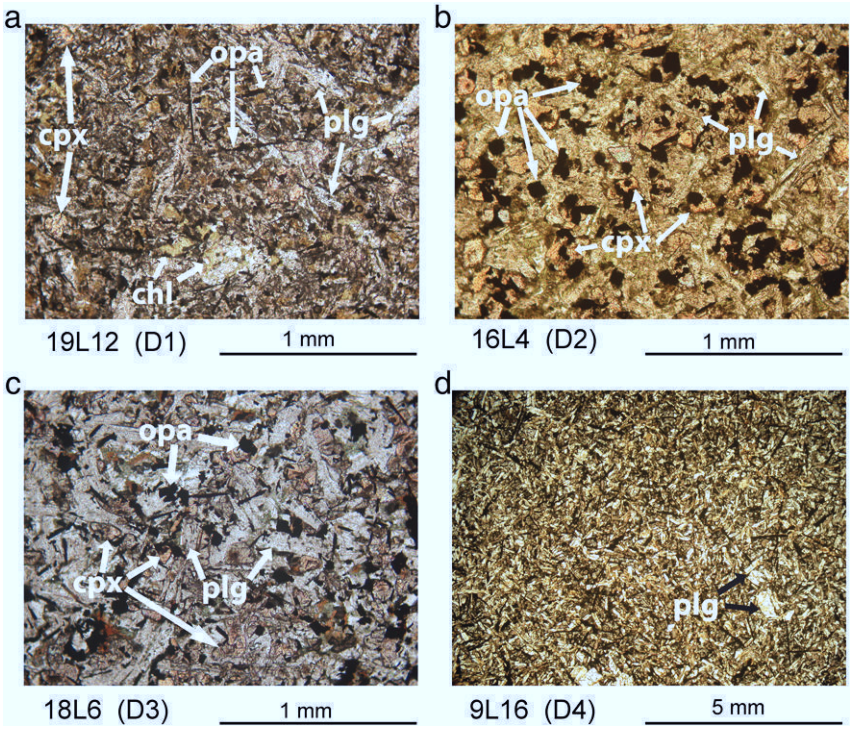

Fig. 5. Selected thin-section photomicrographs taken under plane-polarised light representing the dyke generations D1 (a), D2 (b), D3 (c) and D4 (d). The sample names are indicated beneath each example. Note that the relatively oldest dyke examples (D1 and D2) show patches of chlorite (chl), anhedral clinopyroxene (cpx) and abundant opaque (opa) grains. Plagioclases (plg) in (a) and (b) are somewhat cloudy in appearance, in contrast to those of (c) and (d). The D2 dykes lack the acicular opaque grains evident in the other examples. The silicate matrix (plg and cpx) of (c) and (d) is evidently more coarse-grained than (a) and (b). The opaque grains of (d) are almost exclusively acicular.

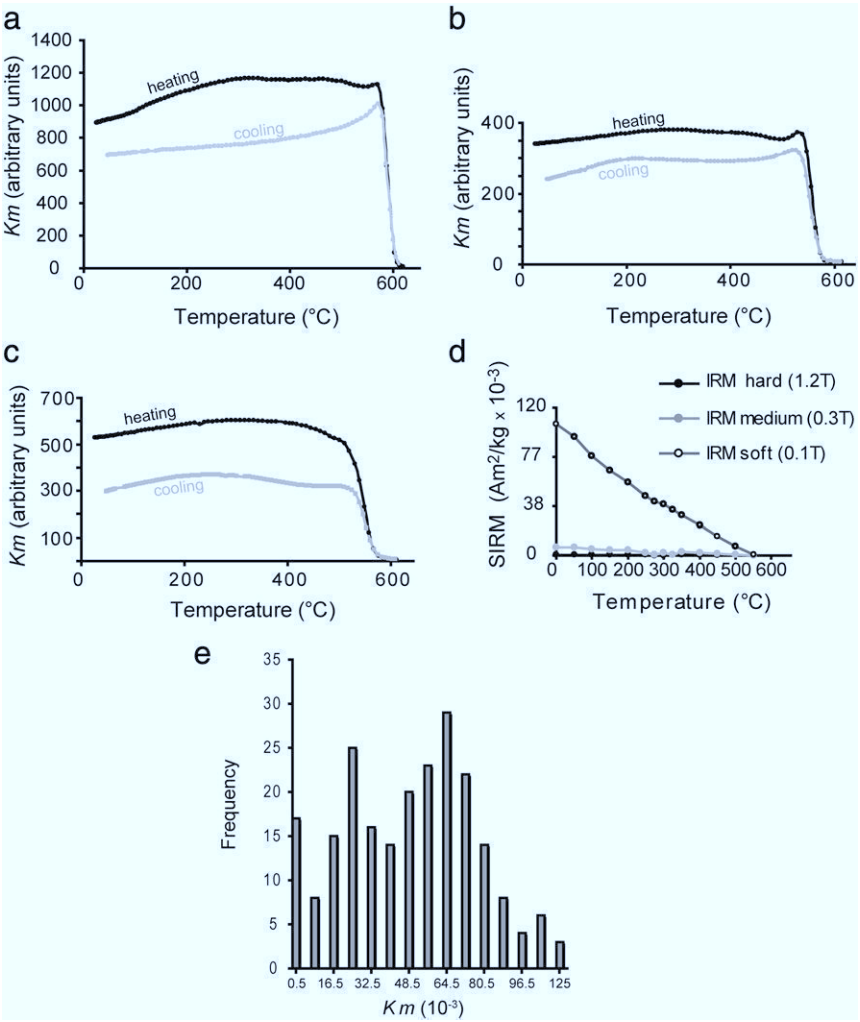

Fig. 6. Thermomagnetic curve (K_m vs. T) for dyke 14 L (a), 9 L (b) and 12 L (c) and thermal demagnetization curve of three-component IRM for 12 L (d). The K_m curves are consistent with the presence of magnetite as Curie temperatures (T_c) are 587 °C, 556 °C and 548 °C respectively. The units of K_m are arbitrary as they are not normalised to the sample mass (viz. Bascou et al., 2005). Note the decay of SIRM towards 580 °C in (d). The frequency distribution of K_m is shown in (e). The mean value of K_m is 5.58×10^{-2} SI units.

the magmatic foliation developed from the alignment of mineral grains along the dyke wall. In most studies, the *K1* axis direction has been used as the magma flow vector, based on the assumption that the long axis of anisotropic grains will be aligned to the direction of magma flow (Cañón-Tapia and Herrero-Bervera, 2009; Chadima et al., 2009; Ellwood, 1978; Kissel et al., 2010; Knight and Walker, 1988; Poland et al., 2004; Porreca et al., 2006; Raposo et al., 2007; Soriano et al., 2008). To find the sense of direction of the magma flow, AMS ellipsoids are usually determined from opposing margins of an intrusion (Fig. 3) in order to find if the fabric is imbricated relative to the intrusion plane (Aubourg et al., 2002; Geoffroy et al., 2002). Geoffroy et al. (2002) proposed a method for using the imbrication of the magnetic foliation to find the magma flow direction. This is because it has been demonstrated that *K1* orientations may be parallel to intersection lineations which are entirely unrelated to the magmatic lineation, especially in oblate fabrics ($T>0$) (Callot and Guichet, 2003; Henry, 1997; Launeau and Cruden, 1998). We therefore do not rely exclusively on the orientation and/or imbrication of the *K1* axes, but rather the imbrication of foliations, which are calculated from the *K3* axes (poles to the foliation) (Fig. 3).

3.3. Mineral shape preferred orientation

In this study we present a detailed 3D study of mineral SPO as defined, particularly, by plagioclase in 7 dykes of the NLDS (19L, 16L, 18L, 9L, 17L, 10L, and 15L). Measuring the 2D ellipse of the mineral fabric and the 3D ellipsoid is achieved using SPO-2003 and Ellipsoid-2003 software packages respectively (Launeau, 2004; Launeau and Robin, 2005). This image analysis software determines grain orientations and fabric

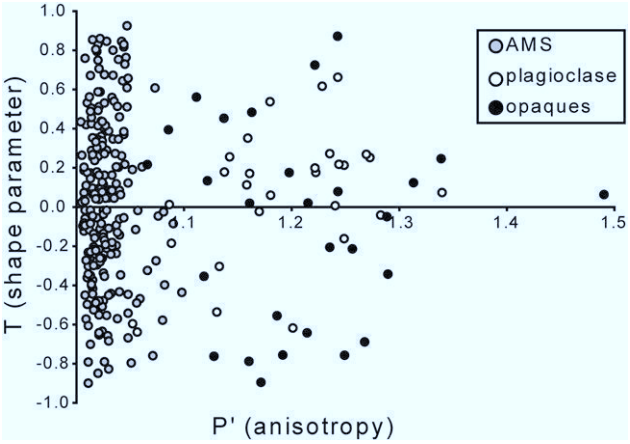

Fig. 7. Graphical illustration of the fabric shapes of AMS and mineral SPO fabrics in the NLDS as described by the corrected degree of anisotropy (P') and shape parameter (T).

intensities on images taken from orientated thin-sections cut from standard AMS cores. An arbitrary *XYZ* co-ordinate system is used (Fig. 4a) to define the orientations of the sections, which are digitally filtered to leave only plagioclase in black and white Bitmap images (Fig. 4b) (see Hastie et al., 2011). The 2D inertia tensors, which are required for finding the 3D ellipsoid, are calculated by indexing grain orientations according to a rose of directions for each section of one sample (Fig. 4c and d) (Launeau, 2004; Launeau and Robin, 1996, 2005; Launeau et al., 2010). The sensitivity of the SPO programme to grain size is essentially dependent on the magnification at which photomicrographs are taken; thus

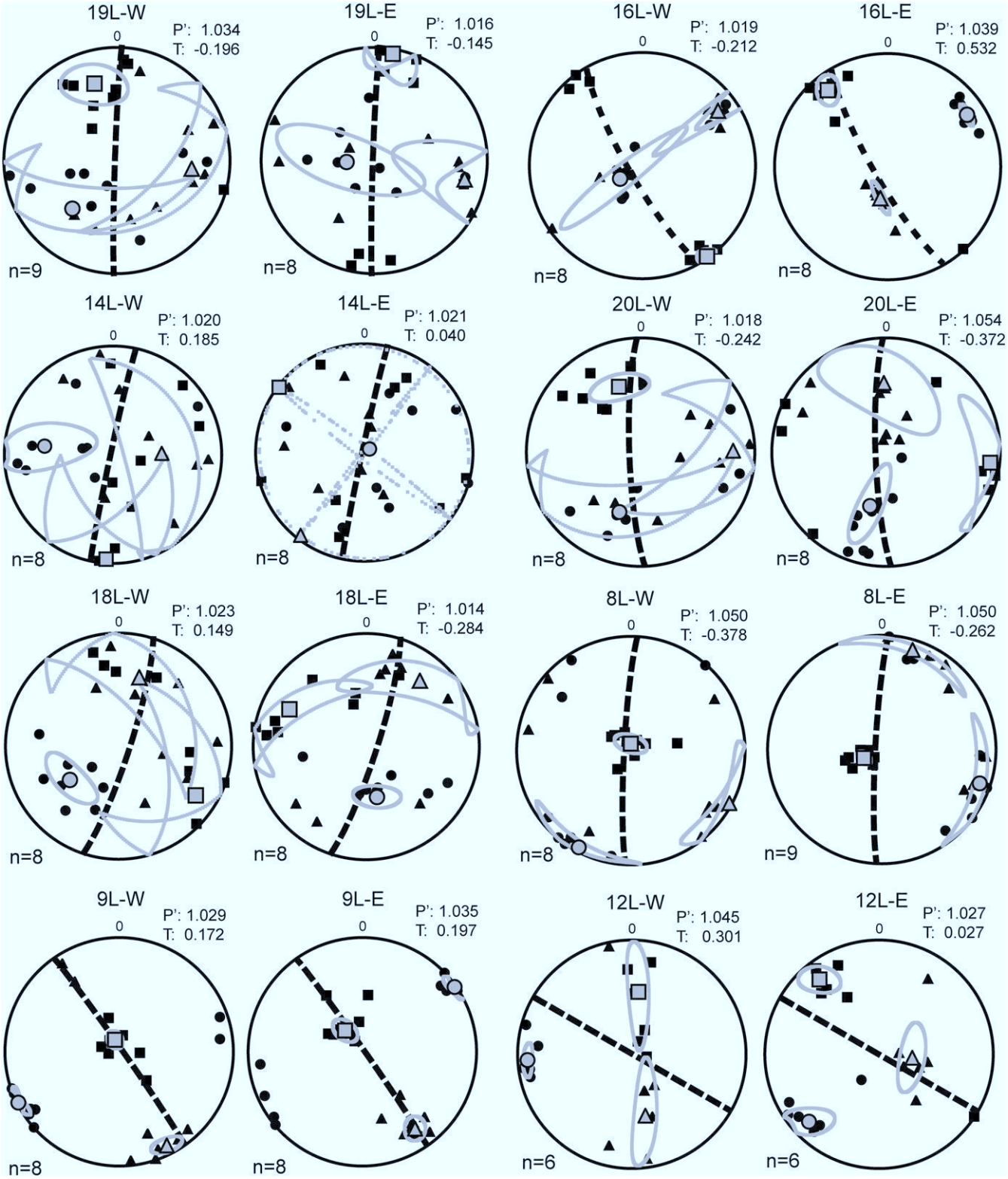

Fig. 8. Stereographic projections of AMS data from selected dykes of the NLDS. Note that the data are split into west (W) and east (E) margins per dyke in order to better observe any potential imbrication of fabric. The dyke plane is shown as a dashed black line. Ellipses of statistical confidence for each of the principal axes are shown in grey, and calculated using the bootstrap method of Tauxe et al. (1998). Maximum axis (*K1* = ■); intermediate axis (*K2* = ▲) and minimum axis (*K3* = ●) are shown. The number of samples (n); corrected degree of anisotropy (*P'*) and shape (*T*) are indicated for each margin. Stereographic projections of AMS data from selected dykes of the NLDS. See Fig. 8 for explanation and key to symbols.

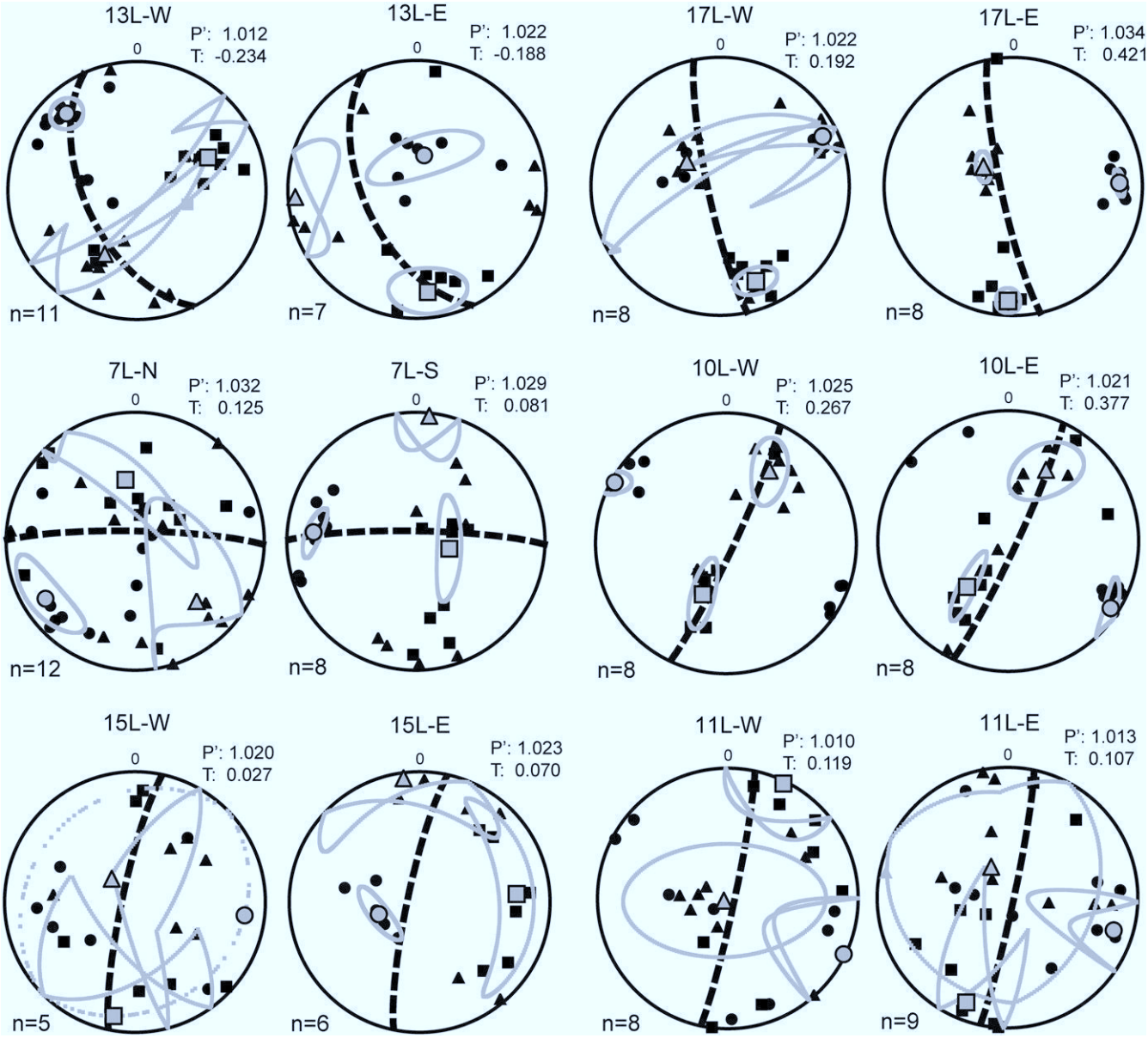

Fig. 8 (*continued*).

grains >10 μm could be reliably imaged at a magnification of 20× and the width of the images was consistently kept at 9 mm.

The Ellipsoid-2003 software in particular provides a measure of scalar parameters (P' and T) as in the case of AMS. Importantly, an incompatibility index ($\sqrt{F}$) provides a measure of the potential misfit between 2D ellipses and the ellipsoid (Launeau and Robin, 2005). A total of 6 thin-sections per margin were analysed for the 7 dykes mentioned above. The nomenclature of the AMS axes *K1*, *K2* and *K3* will be termed *L1*, *L2* and *L3* respectively for SPO data although the axes symbols remain the same. The calculation of statistical confidence regions for mean SPO principal axes is generally achieved using standard deviations (Launeau and Robin, 2005). However, because it is necessary to compare SPO data to AMS; in which mean principal axes are calculated using the bootstrap method (Tauxe et al., 1998), we prefer here to constrain only the accuracy of the fit of the sectional ellipses to the ellipsoid. This is achieved using the incompatibility index $\sqrt{F}$ as there is no provision for summation of tensors for each individual SPO sample. Similarly to AMS, we rely on the orientation and imbrication of the foliations (to which *L3* is a pole).

4. Results

4.1. Petrography

A total of 168 photomicrographs taken from 84 thin-sections were analysed from 7 dykes representing the orientation of thousands of minerals (2×10^5 plagioclase grains and 6×10^4 opaque grains). The thin-sections are dominated by plagioclase and clinopyroxene and contain between 3 and 8% opaque grains. There are, however, some petrographic differences between the dykes which are worth noting. For

Fig. 9. Stereographic projections of (a) plagioclase SPO for 7 dykes of the NLDS according to the western and eastern dyke margins and (b) AMS data for the same dykes, shown for comparative purposes. For SPO data "n" denotes the number of grains analysed and indexed in order to constrain the ellipsoid from 12 thin-sections per dyke. In the interest of clarity, statistical confidence regions are omitted from the figure and only mean principal axes are shown. Foliations are shown as grey lines and the dyke plane in black. For SPO the axes symbolism is as follows: Major axis (*L1* = ■); intermediate axis (*L2* = ▲) and minor axis (*L3* = ●).

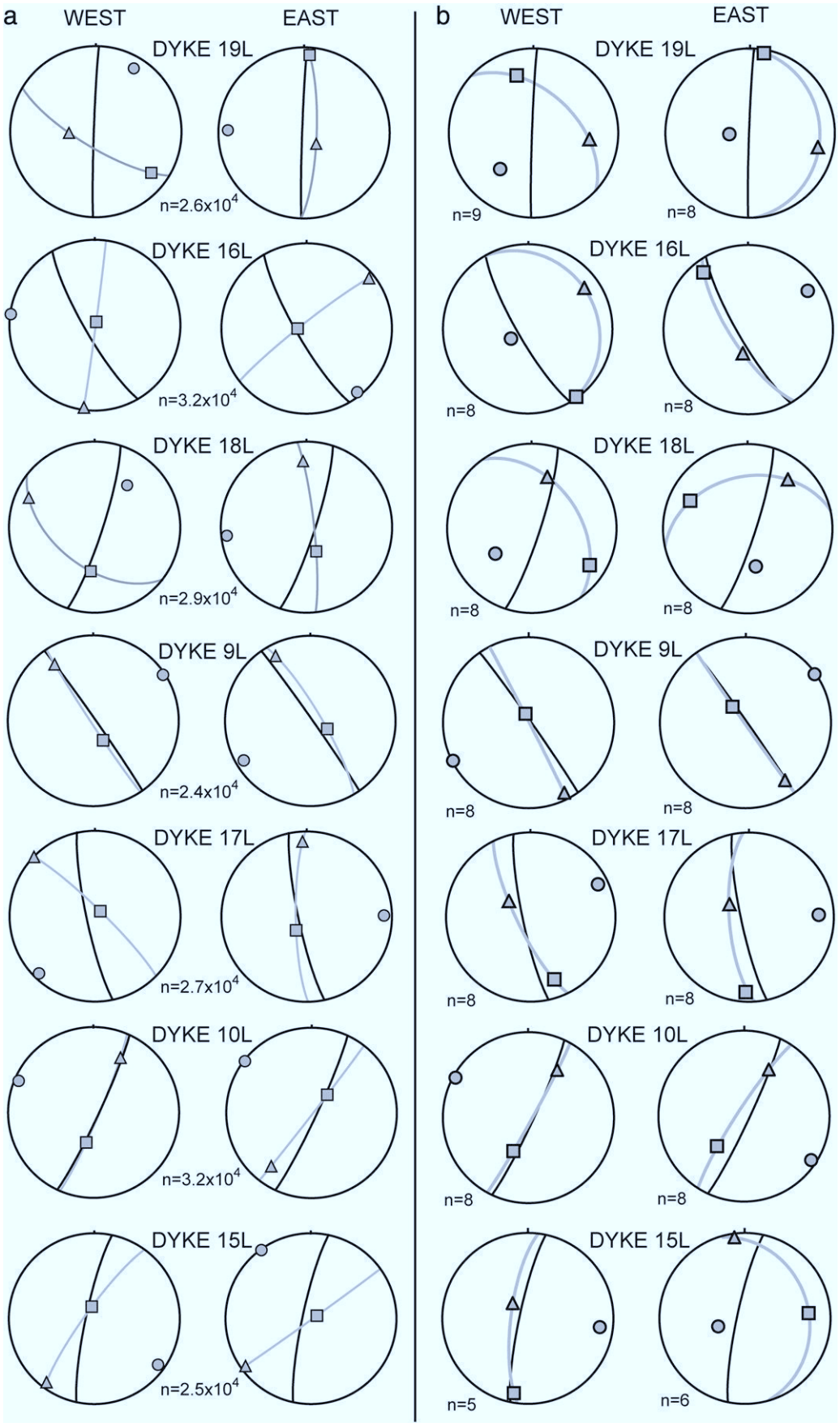

Table 2
Mineral SPO data discriminated according to the plagioclase and opaque grain fraction and according to opposing dyke margins. See Table 1 for key to terminology.

Dyke	Margin	√F	Plagioclase									P' [10^{-3} (sd)]	T [10^{-2} (sd)]	Grains
			Ellipsoid orientation			Angular deviation (sd.)			Axial lengths (norm.)					
			L1	*L2*	*L3*	*L1*	*L2*	*L3*	*L1*	*L2*	*L3*			
19L	West	4.72	18°/123°	17°/332°	01°/220°	±34°	±54°	±36°	1.049	0.998	0.955	1.101(30)	−0.065(26)	15,448
	East	9.03	11°/354°	56°/041°	09°/270°	±46°	±51°	±35°	1.144	1.004	0.873	1.318(130)	0.057(13)	10,891
16L	West	6.40	84°/011°	07°/180°	01°/092°	±13°	±32°	±5°	1.109	1.018	0.887	1.255(50)	0.245(12)	17,111
	East	6.39	83°/258°	05°/046°	03°/137°	±12°	±34°	±10°	1.109	1.026	0.879	1.271(30)	0.333(25)	14,599
18L	West	3.18	52°/199°	19°/307°	38°/054°	±15°	±21°	±27°	1.051	0.988	0.964	1.094(30)	−0.437(26)	15,307
	East	2.86	61°/136°	31°/348°	21°/253°	±4°	±16°	±10°	1.094	0.993	0.921	1.194(50)	−0.088(37)	13,794
9L	West	5.65	46°/151°	57°/299°	11°/046°	±29°	±52°	±21°	1.095	1.007	0.909	1.215(104)	−0.080(42)	12,494
	East	2.74	75°/081°	05°/331°	14°/239°	±2°	±4°	±3°	1.081	1.012	0.914	1.186(20)	0.227(23)	11,938
17L	West	4.70	81°/013°	05°/141°	07°/231°	±23°	±35°	±21°	1.092	0.998	0.918	1.192(20)	−0.03(27)	14,381
	East	7.51	62°/221°	30°/029°	02°/126°	±20°	±34°	±15°	1.096	1.008	0.906	1.213(50)	0.153(29)	12,452
10L	West	4.76	51°/204°	42°/020°	03°/113°	±18°	±31°	±18°	1.118	0.990	0.905	1.244(100)	−0.178(31)	16,037
	East	1.84	66°/040°	24°/218°	01°/308°	±1°	±2°	±1°	1.081	1.043	0.887	1.236(10)	0.637(6)	15,824
15L	West	5.28	78°/354°	08°/214°	06°/123°	±5°	±13°	±2°	1.114	1.012	0.887	1.260(50)	0.158(20)	11,048
	East	4.33	86°/023°	05°/214°	02°/127°	±11°	±21°	±16°	1.103	0.981	0.924	1.200(20)	−0.344(27)	14,022
Opaques														
19L	West	7.73	77°/287°	04°/059°	08°/139°	±16°	±42°	±24°	1.099	0.998	0.915	1.217(118)	−0.111(44)	5615
	East	6.25	51°/144°	36°/321°	01°/232°	±24°	±21°	±23°	1.097	1.000	0.913	1.211(70)	0.075(46)	5560
16L	West	6.58	77°/331°	13°/187°	07°/090°	±23°	±48°	±10°	1.118	1.012	0.885	1.270(56)	0.173(36)	3531
	East	7.79	76°/235°	14°/043°	03°/134°	±10°	±35°	±10°	1.199	0.997	0.838	1.442(76)	−0.043(29)	3381
18L	West	5.68	34°/171°	44°/276°	30°/055°	±23°	±40°	±10°	1.063	0.993	0.949	1.125(51)	−0.145(41)	4761
	East	9.51	40°/118°	40°/008°	37°/258°	±26°	±22°	±6°	1.151	0.960	0.905	1.288(61)	−0.505(19)	3747
9L	West	8.88	65°/191°	25°/029°	02°/288°	±8°	±38°	±13°	1.199	0.970	0.865	1.419(185)	−0.218(47)	6056
	East	5.16	82°/128°	06°/306°	01°/036°	±6°	±13°	±2°	1.077	0.998	0.930	1.158(15)	−0.034(8)	5056
17L	West	7.82	77°/303°	07°/150°	01°/214°	±29°	±47°	±22°	1.103	0.994	0.914	1.220(108)	0.036(55)	2799
	East	4.90	71°/218°	21°/069°	12°/319°	±23°	±27°	±30°	1.103	0.973	0.933	1.197(49)	−0.517(42)	3576
10L	West	6.63	49°/201°	39°/001°	09°/099°	±12°	±17°	±10°	1.162	0.997	0.864	1.352(110)	−0.012(21)	4402
	East	6.00	70°/186°	19°/022°	05°/291°	±3°	±12°	±4°	1.105	0.997	0.909	1.230(44)	−0.131(60)	4082
15L	West	3.49	85°/306°	02°/198°	06°/107°	±12°	±11°	±8°	1.058	1.014	0.932	1.141(30)	0.327(35)	4369
	East	5.70	67°/261°	15°/025°	18°/111°	±16°	±53°	±8°	1.084	1.002	0.922	1.182(33)	0.031(43)	2475

example, the D1 and D2 dykes appear to have suffered minor alteration; chlorite "patches" are evident, and the plagioclase groundmass and occasional phenocrysts are cloudy with irregular and diffuse grain boundaries (Fig. 5a and b). The opaque grains vary from small (<10 μm), equant grains to elongate, acicular and occasionally skeletal in appearance. Dyke 18 L (D3) is even-grained, containing abundant elongate and (sub-) equant opaque grains and relatively fresh, coarse-grained plagioclases (Fig. 5c). Clinopyroxene is essentially anhedral in all the samples. The youngest dykes (D4) contain anhedral clinopyroxene, ~1% free quartz and >5% opaque grains which are skeletal to acicular in shape. These dykes tend to be medium- to coarse-grained and contain large plagioclase phenocrysts (Fig. 5d).

4.2. Rock magnetism and bulk susceptibility

Thermomagnetic curves which quantify the decay of magnetization at saturation and magnetic susceptibility (K_m) can be used to infer the unblocking temperature and Curie temperature (T_c) of the magnetic minerals in a sample respectively. The magnetic mineralogy of samples of the NLDS is revealed by representative thermomagnetic curves in the temperature range of 24–700 °C. The results of monitoring the magnetic susceptibility with increasing temperature under an argon atmosphere indicate that, for dykes 14L, 9L and 12L (Fig. 6a–c), the non-reversible curves are most consistent with stoichiometric magnetite with T_c values of 587 °C, 556 °C and 548 °C respectively. In dyke 12L, it can be shown that the predominant phase has a maximum unblocking temperature of 580 °C (Fig. 6d) which is also consistent with coarse-grained stoichiometric magnetite (Hopkinson, 1989; O'Reilly, 1984; Smith and Prévot, 1977).

A further 3 samples (7L-17, 7L-19, 14L-11) were measured for thermal decay of K_m which provided a range of T_c from 415 to 587 °C (mean: 525 °C). A further 5 samples (7L-14, 10L-4, 15L-13, 18L-3, 20L-4) were monitored for decay of isothermal remanence at saturation (SIRM). Values of SIRM range from 0.08 to 0.42 Am^2/kg with a mean of 0.17 Am^2/kg (a measure of the magnetic field strength per unit area by mass). The bulk susceptibility of the samples is 5.58×10^{-2} ($\pm0.9\times10^{-2}$) SI units as shown in Table 1. The frequency distribution of K_m (Fig. 6e) illustrates a range of susceptibility from relatively low values (0.05×10^{-2} SI units) to values $>10^{-3}$, with a peak value of 6.5×10^{-2} SI units. There is no remarkable variation in K_m according to relative dyke age, dyke thickness or distance of samples from the margin.

Because magnetite is the main contributor to the low-field magnetic susceptibility, it is possible to estimate the volumetric concentration of magnetite. Given that the SIRM value of coarse-grained magnetite is ~9 Am^2/kg (Gubbins and Herrero-Bervera, 2007; Hunt et al., 1995), the mean value of 0.17 Am^2/kg in the NLDS indicates a concentration of magnetite of ~0.1%. This is confirmed by the susceptibility measurements, as the initial susceptibility of stoichiometric magnetite is ~1 SI, implying a volumetric concentration of ~0.1 to 1% in the NLDS where K_m values are ~0.05 SI.

4.3. Characteristics of the magnetic fabric

It is important to first evaluate the shape and intensity of the fabric. Values of anisotropy (P') range from near isotropic (~1.0) to 1.054 (mean: 1.027). The shape parameter (T) discriminates oblate ($T>0$) from prolate ($T<0$) fabrics; and in the NLDS is 0.027 on average, indicating a triaxial to weakly oblate shape (Fig. 7). The mean value of P' is 1.027 for the magnetic fabric and T is >0 in 64% of the data.

The magnetic fabric of all 14 dykes measured for AMS are presented in Fig. 8 with each dyke discriminated into its two opposing margins. As discussed previously, this is done in order to determine if imbrication of the fabric relative to the average dyke plane exists. When considering the orientation of the AMS ellipsoids and the dispersion of principle axes, it is evident that type-A fabric occurs in ~50% of the sites (e.g. 8L,

9L, 12L, 17L, 10L). Vertical to sub-vertical *K1* axes are found only in the prolate fabric of dykes 8L and 9L while shallowly plunging *K1* axes and steeply dipping foliations predominate in other sites (e.g. 19L, 16L, 12L-east, 17L, 10L and 11L). Many sites display scattered fabric. In dykes, such as 14L, 20L, 18L, and 15L, the confidence regions surrounding each principal axis are spread, in many cases overlapping considerably. In some cases (e.g. 16L, 8L and 12L) the fabric is different across the margins, with type-A fabric on one margin and type-B, or apparently a mixture of the two on the other (e.g. 19L, 20L and 7L). Obvious type-B fabric, where *K1* and *K3* have interchanged, occurs in sites 20L-east, 18L, 12L-west and 15L-east. There is no evidence for a relationship between the type (or definition) of the fabric and the relative dyke generation because, for example, intermediate or type-B fabric occurs across the range of D1–D4 dykes. There does, however, appear to be a relationship between the shape of the fabric ellipsoid and the occurrence of different fabric types. For example, prolate fabrics tend to be intermediate (19L, 16L-west, 20L, 18L-east, 8L) although 14L and 15L are exceptions to this observation as they are neutral to oblate. We do not have data pertaining to magnetic grain size and thus explanation of this behaviour would be speculative at best.

4.4. Mineral shape preferred orientation

Stereographic projections of the SPO ellipsoids determined from the margins of each dyke are shown in Fig. 9 in comparison to AMS and the tabulated SPO data are presented in Table 2. The mean maximum axes, *L1*, are typically steeply plunging ($>60°$) in 9 of the 14 margins and values of $\sqrt{F}$ are <10% throughout. The fabric defined by plagioclase is generally type-A, except for 19L-west, 16L-east and 18L-west, and is generally consistent with the overall magnetic fabric orientations shown comparatively by AMS.

The shape of the mineral SPO fabric is predominantly oblate, most notably in the fabric defined by plagioclase (mean $T=0.042$) (Fig. 7). The mean T value for the opaque grains is -0.077, which most likely reflects the prolate shape of the needle-like opaque grains in dykes 18L, 9L and 10L. The mean value of P' is 1.208 for the plagioclase SPO fabric. The highest P' values for plagioclase are found in the phenocryst-rich dykes, such as 19L, 16L and 15L (Table 2). The least anisotropic opaque grains (mean $P'=1.14$) are found in the phenocryst-rich dyke 15L. The mineral SPO fabric is considerably more anisotropic than the AMS fabric, but is similarly oblate in shape. The scatter of the scalar SPO data in Fig. 7 is greater than that of AMS, perhaps due to the measurement of a greater distribution of grain-sizes across dykes of differing grain texture and phenocryst content, as is evident from the petrography. The frequency distribution of anisotropy in the mineral SPO data is skewed towards higher P' grains which may reflect the occurrence of less abundant, high anisotropy phenocrysts within the matrix.

Interestingly, the type-B fabric orientations of the SPO data are mimicked in the equivalent AMS fabric in 19L-west and 18L-west, similar to fabric found by Hastie et al. (2011). Imbrication of the mineral SPO fabric is found in dykes 19L, 18L, 17L and 10L. Dykes 17L and 10L, in particular, show identical agreement between the imbrication of the SPO foliations and the AMS foliations; both in a southward verging direction. There are examples of northerly directed foliations, such as 15L and 16L but this is evident from only one margin each because intermediate fabric persists and the foliations in these cases are not imbricated.

4.5. Bulk AMS and SPO fabric

Given the varying orientations of the dykes (Table 1) it is acceptable to rotate the fabric; particularly *K1* and *K3* into a single co-ordinate system; in this case north–south (N–S) vertical dyke co-ordinates (Fig. 10a). This, in effect, normalises the data into a bulk framework which expresses more clearly the regional trends of the fabric orientation (Aubourg et al., 2008; Callot et al., 2001; Rochette et al., 1991). For example, where dykes strike NW (16L, 9L, 12L, 13L), data are rotated clockwise and counter-clockwise for dykes striking NE (18L, 10L, 11L). The dip of the dykes is also removed by rotating the data about a horizontal, N–S striking axis. Furthermore, the AMS ellipsoids which show scattered principal axes and overlapping, weakly constrained confidence ellipsoids (7L, 11L, 13L, 14L, 15L, 18L, 19L) have been excluded from this bulk data. This allows for a

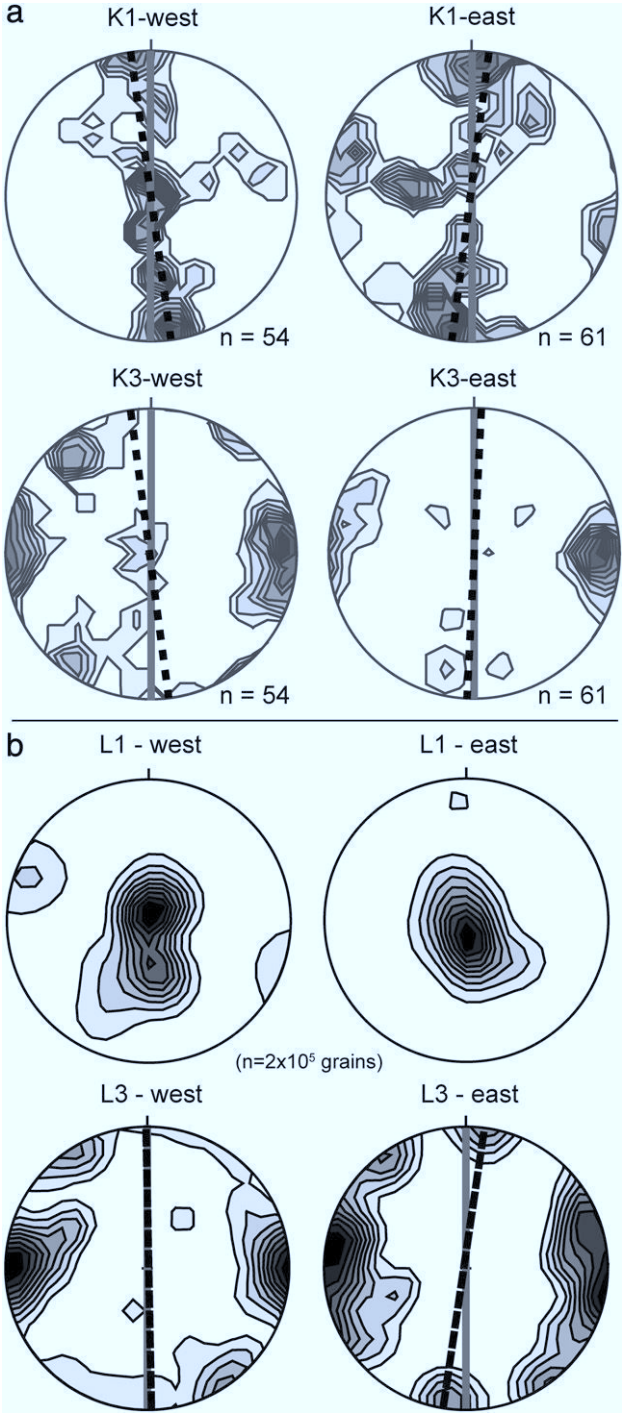

Fig. 10. Stereographic density diagrams of (a) the bulk AMS fabric of the NLDS in north–south (N–S) dyke co-ordinates, with scattered and poorly defined data removed (n = 115) and (b) the bulk plagioclase SPO fabric of the NLDS in N–S dyke co-ordinates (28 ellipsoids). Western and eastern margins are discriminated, with only *K1* (*L1*) and *K3* (*L3*) axes shown. Note in particular the very subtle imbrication of both the AMS and mineral SPO foliations about the N–S direction (grey lines). The 10 contoured domains are at 1% intervals for both the AMS and mineral SPO diagrams.

more confident interpretation of the remaining data (n = 115). Using this method, it can be seen that the orientation of the magnetic fabric is relatively well grouped. Note that the girdles shown in Fig. 10, from which imbrication can be inferred, are computed from the density maximum of each principal axis in each projection (*K2* is not shown for clarity).

A very slight imbrication is noticeable from the *K1* distributions; along a NNW–SSE girdle for the western margins and a NNE–SSW girdle for the eastern margins respectively. Indeed this subtle imbrication is evident in the *K3* axes as well, provided the type-B fabric of the western margins is not considered (NW quadrant of the stereographic projection). A similar imbrication of foliations is also evident in the *L3* axes of the SPO data, in spite of the sub-vertical *L1* axes (Fig. 10b). The orientation of the *L1* axes would typically be an indication of vertical magma flow. However, it has been noted that, in AMS at least, the lineation (*K1*) may represent an intersection, particularly in oblate fabrics ($T>0$) (Callot and Guichet, 2003; Henry, 1997; Launeau and Cruden, 1998). In this context it is possible to argue that the *L1* axes determined for the plagioclase SPO may also be misleading. It is evident from Fig. 10b and Table 2 that the *L1* axes are almost exclusively steeply plunging. Intuitively, this would suggest vertical magma flow. However, Fig. 3a shows that when vertical magma flow occurs, it is expected that the foliation planes dip at between 20° and 40° with the maximum axis (*K1* or *L1*) disposed at the same angle from vertical. Such geometry is not evident in the mineral SPO data of Fig. 10b. There is also no observable imbrication of *L1* axes in the mineral SPO data of the NLDS, making an assessment of upward or downward vertical flow unclear. Imbrication, albeit weak, is only evident in the *K1*, *K3* and *L3* axes of the remaining data. The steeply dipping foliations of the mineral SPO data more closely resemble those shown in Fig. 3b.

The *L1* axes are also disproportionately well-grouped compared to the *L3* axes—considering that the fabric is predominantly oblate. This can occur when the foliations of oblate fabrics intersect which, in the case of steeply dipping, imbricated foliations would result in (sub-) vertical lineations.

At the thin-section scale certain features of the mineral SPO fabric can be scrutinised in more detail. A convenient feature of the *XZ* thin-sections (Fig. 4) is that these sections are vertically orientated, and it is thus possible in certain cases to show the *L1–L2* planes on these sections (with an estimated error in direction of 10°) (Fig. 11). Very briefly, we observe that in some cases the *L1* axis direction is parallel to the maximum direction of the plagioclase grains as determined by a rose of directions (Fig. 11a–c). However, we also observe orthogonal to near orthogonal plagioclase orientations which are evidently bisected by the *L1* axis direction (Fig. 11d–f). This suggests that, in these samples at least, the *L1* direction represents an average orientation in the 2D inertia tensor. This potentially leads to an underestimation of the anisotropy of the tensor and, more importantly, the observation that the *L1* axes orientations are unlikely to represent a magma flow vector.

These observations cast some doubt on the meaning of the *L1* axes. We thus focus on the meaning of the foliations and therefore do not infer a vertical or sub-vertical sense of magma flow from the maximum AMS or mineral SPO axes. The similarity in orientation between the bulk AMS and mineral SPO foliations and the apparent type-A fabric suggests a magmatic origin. The imbrication of the foliations, albeit subtle, hints at southward verging lateral magma flow.

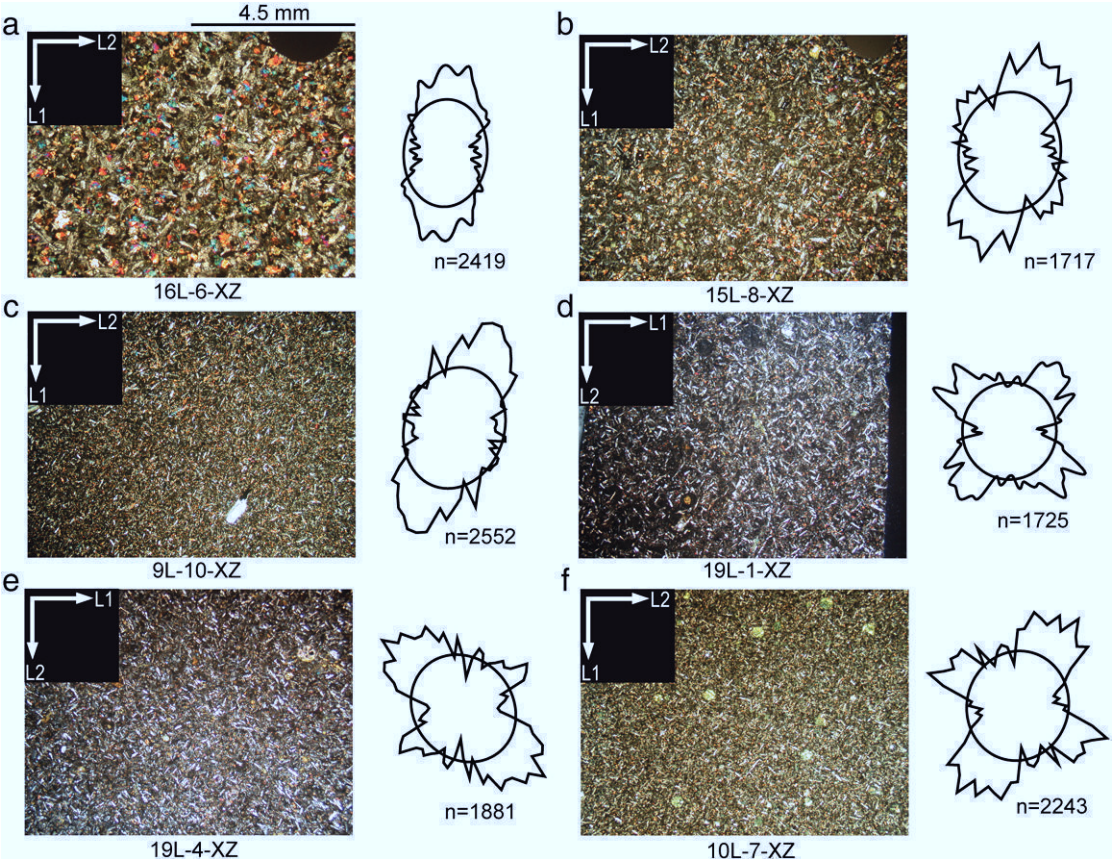

Fig. 11. Thin-section photomicrographs with *L1–L2* planes indicated (all *XZ* sections, sample numbers indicated). The rose of directions indicated with each section reflects the orientations of the plagioclase grains in each section (measured at 5° intervals) and the average 2D inertia tensor ellipse is also shown. The number of grains (n) indexed for each section is also shown. Sections a–c show that *L1* is coaxial with the maximum plagioclase orientation. Sections d–f are examples of apparently competing plagioclase fabric orientations which are not coaxial with the *L1* direction. All the photomicrographs are at the same scale (each photomicrograph is 9 mm across) and all are taken under crossed-polarizers except (f).

5. Discussion

5.1. Magnetic and petrofabric of the NLDS

We have used AMS and mineral SPO to define the characteristics of the petrofabric in 14 dykes of the NLDS in order to constrain the orientation and meaning of any magmatic fabric therein. In general, type-A fabric predominates carried by stoichiometric magnetite which defines a magnetic fabric of relatively low anisotropy ($P'<1.06$) and triaxial shape. Prolate fabrics tend to be intermediate and have vertical to sub-vertical *K1* axes. The AMS fabric is remarkably consistent in orientation with the predominantly oblate and higher anisotropy ($P'<1.40$) mineral SPO fabric. The use of SPO provides constraint on the fabric carried by larger grains, including the plagioclase phenocryst population. With the exception of 3 sites, the SPO results have consistently provided type-A fabric, which is imbricated in 3 dykes. There is also good agreement between the SPO and AMS fabrics in 4 of the 7 dykes tested. To find a magma flow vector we do not make use of the magnetic or mineral lineation (*K1*, *L1* respectively) but focus on the orientation and imbrication of foliations to reliably find the flow direction. Steeply dipping, imbricated foliations occur in 5 dykes (e.g. 19L, 18L, 17L, 10L and 11L).

As discussed previously in this paper, type-B and/or intermediate fabrics may result from late-stage fabric acquisition, superimposition of fabrics at different times in the history of the intrusions or complex magnetic interaction, such as distribution anisotropy. With the AMS, however, we find that a credible interpretation of magma flow is possible after removing the poorly constrained data, and therefore do not discuss the origin(s) of type-B or intermediate fabric any further. Rather, the bulk AMS and SPO fabric form the focus of inferring, where possible, an overall sense of magma flow direction in the NLDS. When assessing the bulk AMS data (in dyke co-ordinates) there is evidence of subtle imbrication which verges southwards. The appearance of a similar imbrication in the bulk mineral SPO data is again consistent with lateral magma flow. The subtlety of the imbrication, however, makes it difficult to confidently provide an absolute flow sense, although we can speculate that the flow was from north to south, given that this same direction can be demonstrated at the local scale.

5.2. Magma flow in the NLDS

The bulk AMS and SPO of the NLDS appear most consistent with lateral magma flow from a position north of the sampled areas. This provides 2 broad possibilities for the explanation of this result. Firstly, within the Karoo triple junction context, it may be that magma flow was directed from the locus of the triple junction at Mwenezi, or, secondly, that the NLDS was fed from an internal point source within the Lebombo faulted monocline.

In addressing the latter possibility, it is evident that the dykes of the NLDS, particularly D1–D3 dykes along the Olifants River, do not appear to converge on a magmatic centre within the Lebombo itself (Klausen, 2009) as has been found in other similar regions (Sigurdsson and Sparks, 1978; Callot et al., 2001).

The NLDS was emplaced during E–W extension from 182 to 178 Ma with the D4 dykes being emplaced from ~178 Ma, probably concomitant with dykes of the ODS. A NNW–SSE extension was most likely responsible for triggering the emplacement of the ODS at ~178 Ma (Jourdan et al., 2007; Klausen, 2009; Le Gall et al., 2002; Watkeys, 2002). There is clear evidence of Proterozoic dykes in the ODS and SLDS which indicates structural inheritance during later Karoo magmatism (Jourdan et al., 2006; Le Gall et al., 2002, 2005; Uken and Watkeys, 1997). However, virtually indistinguishable ages for the ODS and SLDS have been found (179 ± 1.2–178.4 ± 1.1 Ma and 180.4 ± 0.7–178.9 ± 0.8 Ma respectively) (Jourdan et al., 2006, 2007) suggesting synchronous emplacement of these two swarms. This, along with older and overlapping ages in the Lebombo faulted monocline, suggests early development of the NLDS, with slightly later development of the SLDS and ODS—the latter representing the failed rift arm in the triple junction.

Lateral injection of magma into the ODS is favoured due to magnetic fabric evidence (Aubourg et al., 2008) and evidence of the widening of the ODS toward the triple junction caused by relatively greater extension across this proximal part of the rift (Klausen, 2009). Steep flow is in evidence near to the triple junction centre (Aubourg et al., 2008; Ernst and Duncan, 1995). This study has presented evidence in favour of lateral flow of magma in the emplacement of the NLDS. It is reasonable to suggest that the D4 dykes at least, if not the NLDS itself, tapped the same magmatic source (the triple junction?) as the ODS. The lateral intrusion of magma into the extensional environment of the Lebombo may, therefore, be indicative of a pre-Karoo triple junction simply being exploited by upwelling magmas, rather than a point of active rifting induced by mantle plume activity.

It has been suggested that the duration of the triple junction was short, from 181 to 178 Ma, ending when Antarctica broke away from the eastern edge of the Lebombo (Jourdan et al., 2007; Klausen, 2009). This may have occurred relatively soon after the emplacement of the asthenosphere-derived, MORB-like RRDS at ~173 Ma, although the earliest movement between Antarctica and southern Africa may have been much later, at ~155 Ma (Watkeys, 2002). It is not the intention of this paper to resolve issues of duration and timing but the evidence of magma flow in the ODS and NLDS study is quite consistent with the geological history outlined above, such that commonality in the genesis of the ODS and NLDS seems likely. In conclusion we thus emphasise the role of the triple junction as a potential locus of magma supply in this region of the Karoo LIP. We do not, however, find evidence in support of the mantle plume hypothesis. This is because the geometry of the triple junction appears to have been primed, since the Proterozoic at least, to accommodate magmatic and tectonic extension rather than being the exclusive product of active, plume-induced rifting during the development of the Karoo LIP (Jourdan et al., 2006; Le Gall et al., 2005).

6. Conclusions

- The magnetic fabric in dykes of the NLDS is carried mainly by stoichiometric magnetite with a concentration of ~1%.
- Fabrics are type-A in 6 dykes, which is of magmatic origin, and scattered and/or type-B in the remaining dykes.
- The magnetic fabric is of relatively low anisotropy ($P'=1.027\pm0.02$), triaxial to weakly oblate in shape ($T=0.027\pm0.42$).
- The shape preferred orientation fabric defined by plagioclase in the NLDS is of higher anisotropy ($P'=1.208$) than the magnetic fabric and also weakly oblate in shape ($T=0.042$) while the opaque grain fabric is triaxial to prolate ($T=-0.077$).
- With the exception of 3 sites the SPO fabric appears to be magmatic in origin (type-A) and furthermore is in agreement with the AMS fabric in 4 of the 7 dykes tested.
- When the bulk magnetic fabric is viewed in dyke co-ordinates on the regional scale a subtle, southward-verging imbrication of both *K1* and *K3* principal axes can be observed. A similar imbrication is evident in the *L3* axes of the plagioclase SPO data plotted in dyke co-ordinates as well.
- The *L1* axes do not adequately represent a magma flow vector, as orthogonal to near orthogonal plagioclase orientations are bisected by the *L1* axes. This suggests that the *L1* direction represents an average orientation in the 2D inertia tensor and may be influenced by the intersection of foliations.
- We suggest that the orientation of the imbricated fabric, although subtle, is most consistent with lateral magma flow, most likely

directed from a magmatic source positioned to the north of the dyke swarm.
- It is argued that, similarly to the ODS, lateral magma flow outward from the Karoo triple junction was involved in the emplacement of the NLDS. It cannot be conclusively shown that a mantle plume was involved.

Acknowledgements

The authors wish to acknowledge the technical staff of the University of Cergy-Pontoise and University of KwaZulu-Natal for assistance with AMS analysis and thin-section preparation. The authors also acknowledge the NRF–CNRS co-operative "PICS" programme that funded this research and the staff of the Kruger National Park who allowed field work and sample collection during 2006. This work forms part of the Ph.D. research of W. Hastie who acknowledges an NRF Innovation bursary. Massimiliano Porreca and Bernard Le Gall are thanked for thorough and constructive reviews.

References

Anderson, D.L., Zhang, Y.-S., Tanimoto, T., 1992. Plume heads, continental lithosphere, flood basalts and tomography. In: Storey, B.C., Alabaster, T., Pankhurst, R.J. (Eds.), Magmatism and the Causes of Continental Break-up. Geological Society Special Publication, pp. 99–124.

Archanjo, C.J., Launeau, P., 2004. Magma flow inferred from preferred orientations of plagioclase of the Rio Cearf-Mirim dyke swarm (NE Brazil) and its AMS significance. In: Martin-Hernandez, F., Luneburg, C.M., Aubourg, C., Jackson, M. (Eds.), Magnetic Fabric: Methods and applications, 238. Geological Society of London, Special Publication, pp. 285–298.

Armstrong, R.A., Bristow, J.W., Cox, K.G., 1984. The Rooi Rand dyke swarm, southern Lebombo. Geological Society of South Africa, Special Publication 13, 77–86.

Aubourg, C., Giordano, G., Mattei, M., Speranza, F., 2002. Magma flow in sub-aqueous rhyolitic dikes inferred from magnetic fabric analysis (Ponza Island, W. Italy). Physics and Chemistry of the Earth 27, 1263–1272.

Aubourg, C., Tshoso, G., Le Gall, B., Bertrand, H., Tiercelin, J.-J., Kampunzu, A.B., Dyment, J., Modisi, M., 2008. Magma flow revealed by magnetic fabric in the Okavango giant dyke swarm, Karoo igneous province, northern Botswana. Journal of Volcanology and Geothermal Research 170, 247–261.

Bascou, J., Camps, P., Dautria, J.M., 2005. Magnetic versus crystallographic fabrics in a basaltic lava flow. Journal of Volcanology and Geothermal Research 145, 119–135.

Borradaile, G.J., Gauthier, D., 2003. Interpreting anomalous magnetic fabrics in ophiolite dikes. Journal of Structural Geology 25, 171–182.

Bristow, J.W., 1982. Geology and structure of Karoo volcanic and sedimentary rocks of the northern and central Lebombo. Transactions of the Geological Society of South Africa. 85, 167–178.

Bristow, J.W., 1984. Nephelinites of the north Lebombo and south–east Zimbabwe. Geological Society of South Africa, Special Publication 13, 87–104.

Burke, K., Dewey, J.F., 1973. Plume generated triple junctions: key indicators in applying plate tectonics to old rocks. Journal of Geology 81, 406–433.

Callot, J.P., Guichet, X., 2003. Rock texture and magnetic lineation in dykes: a simple analytical model. Tectonophysics 366, 207–222.

Callot, J.P., Geoffroy, L., Aubourg, C., Pozzi, J.P., Mege, D., 2001. Magma flow directions of shallow dykes from the East Greenland volcanic margin inferred from magnetic fabric studies. Tectonophysics 335, 313–329.

Campbell, I.H., Griffiths, R.W., 1990. Implications of mantle plume structure for the evolution of flood basalts. Earth and Planetary Science Letters 99, 79–93.

Cañón-Tapia, E., Herrero-Bervera, E., 2009. Sampling strategies and the anisotropy of magnetic susceptibility of dykes. Tectonophysics 466, 3–17.

Chadima, M., Cajz, V., Týcová, P., 2009. On the interpretation of normal and inverse magnetic fabric in dikes: examples from the Eger Graben, NW Bohemian Massif. Tectonophysics 466, 47–63.

Cox, K.G., 1989. The role of mantle plumes in the development of continental drainage patterns. Nature 342, 873–877.

Cox, K.G., 1992. Karoo igneous activity, and the early stages of the break-up of Gondwanaland. In: Storey, B.C., Alabaster, T., Pankhurst, R.J. (Eds.), Magmatism and the Causes of Continental Break-up. Geological Society of London, Special Publication, pp. 37–148.

Cox, K.G., MacDonald, R., Hornung, G., 1967. Geochemical and petrogenetic provinces of in the Karoo basalts of southern Africa. American Mineralogist 52, 1451–1474.

Du Toit, A.L., 1929. The volcanic belt of the Lebombo: a region of tension. Transactions of the Royal Society of South Africa 18, 189–218.

Duncan, A.R., Armstrong, R.A., Erlank, A.J., Marsh, J.S., Watkins, R.T., 1990. MORB-related dolerites associated with the final phases of Karoo flood basalt volcanism in southern Africa. In: Parker, A.J., Rickwood, P.C., Tucker, D.H. (Eds.), Mafic Dykes and Emplacement Mechanisms. Balkema, Rotterdam, pp. 119–129.

Ellam, R.M., Cox, K.G., 1991. An interpretation of Karoo picrite basalts in terms of interaction between asthenospheric magmas and mantle lithosphere. Earth and Planetary Science Letters 105, 330–342.

Ellwood, B.B., 1978. Flow and emplacement direction determined for selected basaltic bodies using magnetic anisotropy measurements. Earth and Planetary Science Letters 41, 254–264.

Encarnación, J., Fleming, T.H., Elliot, D.H., Eales, H.V., 1996. Synchronous emplacement of Ferrar and Karoo dolerites and the early breakup of Gondwana. Geology 24, 535–538.

Erlank, A.J., 1984. Petrogenesis of the volcanic rocks of the Karoo province. Geological Society of South Africa, Special Publication 13, 1–26.

Ernst, R.E., Baragar, W.R.A., 1992. Evidence from magnetic fabric for the flow pattern of magma in the Mackenzie giant radiating dyke swarm. Nature 356, 511–513.

Ernst, R.E., Duncan, A.R., 1995. Magma flow in the Giant Botswana dyke swarm from analysis of magnetic fabric (abstract). Third International Dyke Conference, Jerusalem, Israel.

Geoffroy, L., Callot, J.P., Aubourg, C., Moreira, M., 2002. Is the common use of AMS in mafic dykes scientifically correct? Terra Nova 14, 183–190.

Gil-Imaz, A., Pocoví, A., Lago, M., Galé, C., Arranz, E., Rillo, C., Guerrero, E., 2006. Magma flow and thermal contraction fabric in tabular intrusions inferred from AMS analysis. A case study in a late-Variscan folded sill of the Albarraci'n Massif (southeastern Iberian Chain, Spain). Journal of Structural Geology 28, 641–653.

Gubbins, D., Herrero-Bervera, E., 2007. Encyclopedia of Geomagnetism and Paleomagnetism. Springer-Verlag, Berlin, Heidelberg, New York, p. 1054.

Hargraves, R.B., Johnson, D., Chan, C.Y., 1991. Distribution anisotropy: the cause of AMS in igneous rocks? Geophysical Research Letters 18, 2193–2196.

Hastie, W.W., Aubourg, C., Watkeys, M.K., 2011. When an 'inverse' fabric is not inverse: an integrated AMS-SPO study in MORB-like dykes. Terra Nova 23, 49–55.

Hawkesworth, C., Kelley, S., Turner, S., Le Roex, A., Storey, B., 1999. Mantle processes during Gondwana break-up and dispersal. Journal of African Earth Sciences 28, 239–261.

Henry, B., 1997. The magnetic zone axis: a new element of magnetic fabric for the interpretation of magnetic lineation. Tectonophysics 271, 325–331.

Hergt, J.M., Peate, D.W., Hawkesworth, C.J., 1991. The petrogenesis of Mesozoic Gondwana low-Ti flood basalts. Earth and Planetary Science Letters 105, 134–148.

Hopkinson, J., 1989. Magnetic and other physical properties of iron at a high temperature. Philosophical Transactions of the Royal Society of London. Series A 180, 443.

Hunt, C.P., Moskowitz, B.M., Banerjee, S.K., 1995. Magnetic Properties of Rocks and Minerals. In: Ahrens, T.J. (Ed.), Rock Physics and Phase Relations. A Handbook of physical constants. American Geophysical Union, Washington, pp. 189–204.

Jelinek, V., 1978. Statistical processing of anisotropy of magnetic susceptibility measured on group of specimens and its applications. Studies in Geophysics and Geodynamics 22, 50–62.

Jelinek, V., 1981. Characterization of the magnetic fabric of rocks. Tectonophysics 79, 63–67.

Jourdan, F., Féraud, G., Bertrand, H., Kampunzu, A.B., Tshoso, G., Le Gall, B., Tiercelin, J.-J., Capiez, P., 2004. The Karoo triple junction questioned: evidence from Jurassic and Proterozoic $^{40}Ar/^{39}Ar$ ages and geochemistry of the giant Okavango dyke swarm (Botswana). Earth and Planetary Science Letters 222, 989–1006.

Jourdan, F., Féraud, G., Bertrand, H., Kampunzu, A.B., Tshoso, G., Watkeys, M.K., Le Gall, B., 2005. Karoo large igneous province: brevity, origin and relation to mass extinction questioned by new $^{40}Ar/^{39}Ar$ age data. Geology 33, 745–748.

Jourdan, F., Féraud, G., Bertrand, H., Watkeys, M.K., Kampunzu, A.B., Le Gall, B., 2006. Basement control on dyke distribution in Large Igneous Provinces: case study of the Karoo triple junction. Earth and Planetary Science Letters 241, 307–322.

Jourdan, F., Féraud, G., Bertrand, H., Watkeys, M.K., 2007. From flood basalts to the inception of oceanization: example from the $^{40}Ar/^{39}Ar$ high-resolution picture of the Karoo large igneous province. Geochemistry, Geophysics, Geosystems 8, 1–20.

Khan, M.A., 1962. The anisotropy of magnetic susceptibility of some igneous and metamorphic rocks. Journal of Geophysical Research 67, 2873–2885.

Kissel, C., Laj, C., Sigurdsson, H., Guillou, H., 2010. Emplacement of magma in Eastern Iceland dikes: insights from magnetic fabric and rock magnetic analyses. Journal of Volcanology and Geothermal Research 191, 79–92.

Klausen, M.B., 2009. The Lebombo monocline and associated feeder dyke swarm: diagnostic of a successful and highly volcanic rifted margin? Tectonophysics 468, 42–62.

Knight, M.D., Walker, G.P.L., 1988. Magma flow directions in dikes of the Koolau Complex, Oahu, determined from magnetic fabric studies. Journal of Geophysical Research 93, 4301–4319.

Launeau, P., 2004. Mise en évidence des écoulements magmatiques par analyse d'images 2-D des distributions 3-D d'Orientations Préferentielles de Formes. Bulletin of the Geological Society of France 175, 331–350.

Launeau, P., Cruden, A.R., 1998. Magmatic fabric acquisition mechanisms in a syenite: results of a combined anisotropy of magnetic susceptibility and image analysis study. Journal of Geophysical Research 103, 5067–5089.

Launeau, P., Robin, P.-Y.F., 1996. Fabric analysis using the intercept method. Tectonophysics 267, 91–119.

Launeau, P., Robin, P.-Y.F., 2005. Determination of fabric and strain ellipsoids from measured sectional ellipses—implementation and applications. Journal of Structural Geology 27, 2223–2233.

Launeau, P., Archanjo, C.J., Picard, D., Arbaret, L., Robin, P.-Y.F., 2010. Two- and three-dimensional shape fabric analysis by the intercept method in grey levels. Tectonophysics 492, 230–239.

Le Gall, B., Tshoso, G., Jourdan, F., Féraud, G., Bertrand, H., Tiercelin, J.J., Kampunzu, A.B., Modisi, M.P., Dyment, J., Maia, M., 2002. $^{40}Ar/^{39}Ar$ geochronology and structural data from the giant Okavango and related mafic dyke swarms, Karoo igneous province, northern Botswana. Earth and Planetary Science Letters 202, 595–606.

Le Gall, B., Tshoso, G., Dyment, J., Kampunzu, A.B., Jourdan, F., Féraud, G., Bertrand, H., Aubourg, C., Vétela, W., 2005. The Okavango giant mafic dyke swarm (NE Botswana): its structural significance within the Karoo Large Igneous Province. Journal of Structural Geology 27, 2234–2255.

O'Reilly, W., 1984. Rock and Mineral Magnetism. Blackie & Son, Glasgow, p. 220.
Poland, M.P., Fink, J.H., Tauxe, L., 2004. Patterns of magma flow in segmented silicic dikes at Summer Coon volcano, Colorado: AMS and thin section analysis. Earth and Planetary Science Letters 219, 155–169.
Porreca, M., Acocella, V., Massimi, E., Mattei, M., Funiciello, R., De Benedetti, A.A., 2006. Geometric and kinematic features of the dike complex at Mt. Somma, Vesuvio (Italy). Earth and Planetary Science Letters 245, 389–407.
Potter, D.K., Stephenson, A., 1988. Single-domain particles in rocks and magnetic fabric analysis. Geophysical Research Letters 15, 1097–1100.
Raposo, M.I.B., D'Agrella-Filho, M.S., Pinese, J.P.P., 2007. Magnetic fabrics and rock magnetism of Archaean and Proterozoic dike swarms in the southern São Francisco Craton, Brazil. Tectonophysics 443, 53–71.
Reeves, C., 1978. A failed Gondwana spreading axis in southern Africa. Nature 273, 222–223.
Reeves, C., 2000. Geophysical mapping of Mesozoic dyke swarms in southern Africa and their origin in the disruption of Gondwana. Journal of African Earth Sciences 30, 499–513.
Riley, T.R., Millar, I.L., Watkeys, M.K., Curtis, M.L., Leat, P.T., Klausen, M.B., Fanning, C.M., 2004. U–Pb zircon (SHRIM, P) ages for the Lebombo rhyolites, South Africa. Journal of the Geological Society of London 161, 547–550.
Rochette, P., Jenatton, L., Dupuy, C., Boudier, F., Reuber, I., 1991. Diabase dikes emplacement in the Oman Ophiolite: a magnetic fabric study with reference to geochemistry. In: Peters, T., Nicolas, A., Coleman, R.G. (Eds.), Ophiolite Genesis and Evolution of the Oceanic Lithosphere. Ministry of petroleum and minerals, Sultanate of Oman, pp. 55–82.
Rochette, P., Aubourg, C., Perrin, M., 1999. Is this magnetic fabric normal? A review and case studies in volcanic formations. Tectonophysics 307, 219–234.
Sigurdsson, H., Sparks, R.S.J., 1978. Lateral magma flow within rifted Icelandic crust. Nature 274, l26–I30.
Smith, B.M., Prévot, M., 1977. Variation of the magnetic properties in a basaltic dyke with concentric cooling zones. Physics of the Earth and Planetary Interiors 14, 120–136.
Soriano, C., Beamud, E., Garcés, M., 2008. Magma flow in dikes from rift zones of the basaltic shield of Tenerife, Canary Islands: implications for the emplacement of buoyant magma. Journal of Volcanology and Geothermal Research 173, 55–68.
Storey, B., Alabaster, T., Hole, M.J., Pankhurst, R.J., Weaver, H.E., 1992. Role of subduction-plate boundary forces during the initial stages of Gondwana break-up: evidence from the proto-Pacific margin of Antarctica. In: Storey, B.C., Alabaster, T., Pankhurst, R.J. (Eds.), Magmatism and the Causes of Continental Break-up, pp. 149–163.
Sweeney, R.J., Watkeys, M.K., 1990. A possible link between Mesozoic lithospheric architecture and Gondwana flood basalts. Journal of African Earth Sciences 10, 707–716.
Sweeney, R.J., Duncan, A.R., Erlank, A.J., 1994. Geochemistry and petrogenesis of central Lebombo basalts from the Karoo Igneous Province. Journal of Petrology 35, 95–125.
Tarling, D.H., Hrouda, F., 1993. The Magnetic Anisotropy of Rocks. Chapman & Hall, London, p. 217.
Tauxe, L., Gee, J.S., Staudigel, H., 1998. Flow directions in dikes from anisotropy of magnetic susceptibility data: the bootstrap way. Journal of Geophysical Research 103, 17775–17790.
Uken, R., Watkeys, M.K., 1997. An interpretation of mafic dyke swarms and their relationship with major mafic magmatic events on the Kaapvaal Craton and Limpopo Belt. South African Journal of Geology 100, 341–349.
Watkeys, M.K., 2002. Development of the Lebombo rifted volcanic margin of southeast Africa. In: Menzies, M.A., Klemperer, S.L., Ebinger, C.J., Baker, J. (Eds.), Volcanic Rifted Margins: Geological Society of America Special Paper, pp. 27–46.
White, R.S., 1997. Mantle plume origin for the Karoo and Ventersdorp Flood Basalts, South Africa. South African Journal of Geology 100, 271–283.

- Appendix B -

Hastie, W.W., Watkeys, M.K., Aubourg, C. Magma flow in dykes of the Karoo LIP: Implications for the mantle plume model (*manuscript in preparation*).

Magma flow in dyke swarms of the Karoo LIP: Implications for the mantle plume hypothesis

WARWICK W. HASTIE [1]*

[1] School of Geological Sciences, Building H1, University of KwaZulu-Natal, University Road, Westville, Durban 4001, South Africa

MICHAEL K. WATKEYS [1]

[1] School of Geological Sciences, Building H1, University of KwaZulu-Natal, University Road, Westville, Durban 4001, South Africa

CHARLES AUBOURG [2]

[2] Laboratoire des Fluides Complexes et Réservoirs. UMR 5150. CNRS. TOTAL. Université de Pau et des Pays de l'Adour. Avenue de l'Université BP 1155, 64013 Pau Cedex, France

*Corresponding author

(e-mail: warwick.hastie@gmail.com / 203505849@stu.ukzn.ac.za)

Abstract

The ~183 Ma old Karoo Large Igneous Province is a predominantly flood basalt province that extends across southern Africa and is represented by related magmatism in Antarctica (west Dronning Maud Land and Transantarctic Mountains) and parts of Australasia. Intrusive events, including the emplacement of at least ten dyke swarms, occurred between ~183 Ma and ~174 Ma. Magma flow-related magnetic fabric in 90 dykes from five of these swarms is reviewed; as well the mineral shape-preferred orientation of plagioclase in the northern Lebombo and Rooi Rand dyke swarms. These two dyke swarms form an integral part of the Lebombo monocline, which converges upon the Karoo "triple junction" at Mwenezi, southern Zimbabwe. Dykes of the Northern Lebombo dyke swarm (182–178 Ma) appear to have initially intruded vertically, followed later by lateral flow in the youngest dykes. In dykes of the Okavango dyke swarm (178 Ma) there is evidence of steep magma flow proximal to the triple junction, and lateral flow from the southeast to the northwest in the distal regions. This is consistent with the Karoo triple junction being a viable magma source for both these dyke swarms. In the Rooi Rand dyke swarm (174 Ma), situated in the southernmost Lebombo, there is also evidence of inclined magma flow from north to south. This flow direction cannot be reconciled with the Karoo triple junction, as the northern termination of the Rooi Rand dyke swarm is in east-central Swaziland. The magnetic fabric in the Jutulrøra and Straumsvola dyke swarms of Dronning Maud Land, Antarctica has two components. There is evidence of sub-vertical magma flow in the north (Straumsvola) and evidence of lateral flow further south (Jutulrøra). The regional pattern of magma flow is consistent with this picture of flow from north to south, and is therefore not compatible with magma flow that would be expected from the Weddell Sea triple junction. The overall flow pattern in the Karoo dykes is consistent with the Karoo triple junction being an important magma source. However, the Limpopo Belt and Kaapvaal Craton have significantly controlled the distribution of the Lebombo and Save-Limpopo monoclines and the Okavango dyke swarm. The locus of flow in the dykes of Dronning Maud Land is at least 500 km from the Karoo triple junction, as is the apparent locus for the Rooi Rand dyke swarm. Linked with field evidence and geochronology we suggest that it is unlikely that each melt locus was a separate mantle plume but may have been "weak spots" exploited by magma impingement.

1. Introduction

Globally, mantle plumes have been implicated in the development of voluminous large igneous provinces (LIPs) (Bryan and Ernst, 2008). Because LIPs represent relatively short-lived (< 5 Ma), high volume magmatism (covering ~10^6 km^2), many of them are believed to have been formed predominantly by mantle plume processes; including the Deccan Traps, Iceland, the Kerguelen Plateau, the Paraná-Etendeka flood basalt province and the ~183 Ma old Karoo LIP (Courtillot and Renne, 2003). Some workers show, however, that LIPs may be related to events of magma drainage (Silver et al., 2006) or processes fundamentally similar to the formation of non-LIPs (Cañón-Tapia, 2010). Indeed, recent work suggests that the development of subduction zones at supercontinent margins can strongly influence thermal convection beneath the lithosphere (O'Neill et al., 2009). Thermal insulation of the mantle by supercontinent assembly has also been proposed as a viable mechanism for the development of thermal upwellings; plumes (Lenardic, 2005; Coltice et al., 2007).

A mantle plume origin for the Karoo LIP has been favoured for some time, particularly because of the Karoo triple junction (Burke and Dewey, 1973; Campbell and Griffiths, 1990; Cox, 1992; Storey, 1995; Ernst and Buchan, 1997; Storey and Kyle, 1997; White, 1997; Storey et al., 2001). The plume model continues to gain support, particularly in the study of associated magmatism in Antarctica (Elliot and Fleming, 2000; Ferraccioli et al., 2005; Riley et al., 2005; Curtis et al., 2008). The study of magma flow directions in dykes associated with the Karoo triple junction also suggest that lateral magma flow from the triple junction has occurred, which may be consistent with a mantle plume (Ernst and Duncan, 1995; Aubourg et al., 2008; Hastie et al., 2011b). There are, however, a number of geochemical (Sweeney and Watkeys, 1990; Sweeney et al., 1994; Jourdan et al., 2007a) and structural features (Le Gall et al., 2005; Klausen, 2009), as well as geochronology, which are inconsistent with a mantle plume (Jourdan et al., 2004, 2005, 2006, 2007b).

Lateral magma flow in dyke swarms has been used to infer the presence of mantle plumes (Ernst and Baragar, 1992; Ernst and Duncan, 1995; Ernst and Buchan, 1997; Callot et al.,

2001; Chaves and Correia Neves, 2005). Before the reliance on quantitative flow fabrics measured using anisotropy of magnetic susceptibility (AMS) and mineral shape-preferred orientation (SPO), the existence of a mantle plume was inferred by other means – such as the presence of triple junctions. The basic premise is that, similarly to dykes radiating outward from a volcanic edifice, dyke swarms that converge upon a central point (e.g. the Karoo triple junction, or the Central Atlantic magmatic province [CAMP]) were intruded laterally from a centralized mantle plume (Ernst and Baragar, 1992; Ernst et al., 1995; Ernst and Buchan, 1997).

There is little doubt that the eventual dispersion of southern Gondwana at ~139 Ma occurred because of Karoo magmatism (Watkeys, 2002). The vast network of sills and dykes provide good indicators of stresses in the crust at the time of their formation (Uken and Watkeys, 1997; Le Gall et al., 2005). Relative and/or absolute ages of dykes and magma flow determinations may help in piecing together the tectonic history. In this regard we explore the implications of magma flow direction determined in dykes of the Northern Lebombo dyke swarm (NLDS), Okavango dyke swarm (ODS) and Rooi Rand dyke swarm (RRDS) in the context of the Karoo triple junction (Aubourg et al., 2008; Hastie et al., 2011b and previously unpublished data). These directions have been determined using AMS and the SPO of plagioclase grains.

In addition, various studies of the Jurassic-age dykes of Dronning Maud Land in Antarctica will be discussed because of their apparently shared history of magmatism with the Karoo LIP (Zhang et al., 2003; Riley et al., 2005; Curtis et al., 2008). This may provide additional constraint on the cause of magmatism in southern Gondwana as there is overlap in composition and age between magmatism associated with the Karoo triple junction and dyke swarms that occur in Dronning Maud Land.

We attempt to bring together the existing data related to (1) the timing and duration of Karoo and associated magmatism, (2) the mantle plume hypothesis for the development of the Karoo LIP and (3) magma flow directions which have been found in dykes of the Karoo LIP and associated magmatic provinces. We aim, therefore, to constrain magma

flow in dykes of the Karoo LIP to the timing of dyke formation in order to critically assess the mantle plume hypothesis.

2. The Karoo Large Igneous Province

In this section we discuss the Karoo LIP and associated magmatism within Gondwana, turning our attention to the distribution and compositional types of magma in the Karoo LIP. We also consider the distribution and relative age of intrusive components of southern Africa and Dronning Maud Land, as well as the Karoo triple junction. Finally, we present a synopsis of relevant geochronology which contextualizes the dyke swarms with respect to the bulk of the magmatism.

2.1. Regional distribution

The Karoo LIP comprises a large number of volcanic and intrusive components, which in South Africa alone have been studied for more than 80 years (e.g. Du Toit, 1929; Cox et al., 1967; Duncan et al., 1984; Ellam et al., 1992; Jourdan et al., 2009). There has not been a collation of the existing and more recent work on the Karoo LIP since Erlank, (1984), but readers are referred to Jourdan et al. (2009) who provide an updated synthesis of the current understanding of Karoo magmatism.

The Karoo LIP extends across southern Africa, covering ~3×10^6 km^2 (Eales et al, 1984). The Karoo LIP is contemporaneous with other igneous provinces, including the Ferrar Province of Antarctica (Fig. 1) (Kyle et al., 1981; Encarnación et al., 1996; Zhang et al., 2003), the associated Kirkpatrick basalts and various intrusive components of west Dronning Maud Land and the Tasman dolerites of Australasia (Elliot, 1975; Fleming et al., 1995).

Geochronology indicates that the bulk of the magmatism occurred between ~183 Ma and ~178 Ma, but continued up to ~174 Ma with the intrusion of the RRDS in the southern Lebombo "monocline" (Duncan et al., 1997; Jourdan et al., 2005; Jourdan et al., 2007b, c). The Lebombo is in fact a N–S striking, easterly dipping structure comprising a highly magmatic and rifted volcanic margin (Watkeys, 2002; Klausen, 2009).

The voluminous, low-Ti, tholeiitic magmas which characterise much of the Karoo LIP erupted within 3–4.5 Ma as continental flood basalts (CFBs) now preserved mainly in Lesotho and western Botswana (Jourdan et al., 2007a, c). The volcanic sequences of the Lebombo reach a thickness of 1.5–12 km and overlie the uppermost arenaceous rocks of the Karoo Supergroup (Clarens Formation) (Eales et al., 1984; Watkeys, 2002). There is also an associated network of dolerite sills extending throughout the Karoo basin of South Africa (Fig. 1).

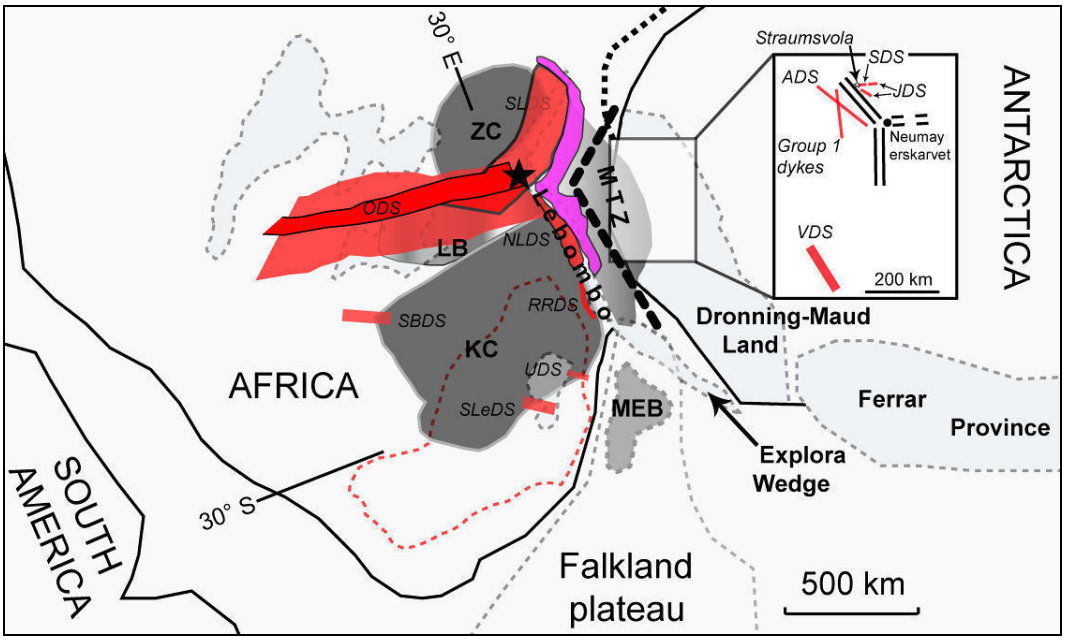

Figure 1: Schematic map of southern Gondwana at ~170 Ma showing the broad pre-Karoo crustal structure (solid) with the Karoo and associated volcanic provinces overlaid (in light grey with dashed outline). Note the positions (in bold text) of the Lebombo monocline, the Falkland Plateau, the Explora Wedge, Dronning Maud Land, the Ferrar Province, the Kaapvaal Craton (KC), Zimbabwe Craton (ZC), Limpopo Belt (LB), the Mozambique thinned-zone (MTZ) and the Maurice-Ewing Bank (MEB). The Jurassic dyke swarms are shown in red (ODS=Okavango dyke swarm, SLDS=Save-Limpopo dyke swarm, NLDS=Northern Lebombo dyke swarm, RRDS=Rooi Rand dyke swarm, UDS=Underberg dyke swarm, SBDS=Southern Botswana dyke swarm, SLeDS=Southern Lesotho dyke swarm). The SW-1 dyke swarm of Mozambique is shown in pink (see Section 2.3). The incipient rift shown in the MTZ is from Jokat et al. (2003). Inset over Antarctica shows the two regions of the Jutulrøra dyke swarm (JDS), the Straumsvola dyke swarm (SDS), the Alhmannryggen dyke swarm (ADS), the Vestfjella dyke swarm (VDS) and the Group 1 dyke swarm. Note the triple rift system in Antarctica that converges on Neumayerskarvet (Ferraccioli et al., 2005). The black star at the convergence of the ODS and SLDS shows the position of Mwenezi. The full extent of the ODS is illustrated as it comprises a heavily intruded zone (darker) bounded by regions of decreasing dyke density, reaching > 300 km in width. Note the overlap of the SLDS with the ODS, and the overlap of the ODS with the NLDS. The extent of sill intrusion in South Africa (red dashed outline) is also shown. The present coastline of Mozambique is shown as a heavy dashed black line to the north of the MTZ (re-drawn from White and McKenzie, 1989; Storey et al., 1992; Encarnación et al., 1996; Storey and Kyle, 1997; Watkeys, 2002; Jourdan et al., 2004; Ferraccioli et al., 2005; Riley et al., 2006; Curtis et al., 2008).

186 The dyke swarms associated with the Karoo LIP have become increasingly studied as
187 they provide structural, geochemical and geochronological information about their own
188 development, and that of the entire Karoo. These include, but are not limited to, the ODS
189 (Reeves, 1978; Elburg and Goldberg, 2000; Reeves, 2000; Le Gall et al., 2002, 2005;
190 Jourdan et al., 2004; Aubourg et al., 2008) and the NLDS and RRDS of the Lebombo
191 monocline (Saggerson et al., 1983; Armstrong et al., 1984; Watkeys, 2002; Jourdan et al.,
192 2006; Klausen, 2009; Hastie et al., 2011a, b) (Fig. 1). The dyke swarms and Karoo triple
193 junction are discussed in further detail in Section 2.3.
194
195 Along with the ODS and Lebombo monocline, another dyke swarm, the Save-Limpopo
196 dyke swarm (SLDS) (Jourdan et al., 2006) converges on Mwenezi (formerly Nuanetsi) in
197 southern Zimbabwe (Fig. 1). The SLDS is found primarily within the Sabi monocline (or
198 Save-Limpopo monocline) which developed during normal faulting in the Permian
199 (Watkeys, 2002). The intersection of the monoclines and the ODS produces a
200 conspicuous triple junction. This geometry has been used (other than compositional and
201 geochemical data) as evidence for the role played by a mantle plume in its formation
202 (Burke and Dewey, 1973; White and McKenzie, 1989; Campbell and Griffiths, 1990;
203 Cox, 1992; Ernst and Buchan, 1997; Storey and Kyle, 1997; White, 1997). Before further
204 discussion of the timing and duration of the eruptive and intrusive phases it is necessary
205 to examine the distribution and relevant petrology of the rock types within the Karoo LIP.
206
207 *2.2. Igneous stratigraphy and petrology*
208 Volcanic rocks of Karoo LIP range from earliest nephelinites and picrites to continental
209 tholeiites and rhyolites (Eales et al., 1984). There has been much geochemical study
210 performed on the compositionally diverse igneous rocks of the Karoo LIP (Cox et al.,
211 1967; Duncan et al., 1984; Sweeney and Watkeys, 1990; Hergt et al., 1991; Ellam et al.,
212 1992; Sweeney et al., 1994; Riley et al., 2006). These findings have a significant bearing
213 on the mantle plume model for the Karoo LIP, and are summarised below.
214
215 The most primitive rock types are centred on the Karoo triple junction (Fig. 2) and
216 consist of the incompatible element enriched Mashikiri Formation nephelinites and the

Letaba Formation picrites (Bristow, 1982; Bristow and Cox, 1984). The triple junction, at the northern termination (Mwenezi) of the Lebombo monocline, is within the Limpopo Belt (discussed further in Section 2.3) while the remainder of the N–S trending structure occupies a position along the eastern edge of the Archaean Kaapvaal Craton (Fig. 1).

The Mashikiri Formation overlies the arenaceous Clarens Formation, which in the northern Lebombo directly overlies Precambrian basement. The Mashikiri Formation is not as laterally extensive north-to-south as the overlying volcanics of the Lebombo Group, which include the Letaba Formation picrites (~4 km thick), Sabie River Formation basalts (4–5 km thick) and finally the Jozini and Mbuluzi Formation rhyolites which together are ~5 km in thickness (Watkeys 2002; Klausen 2009).

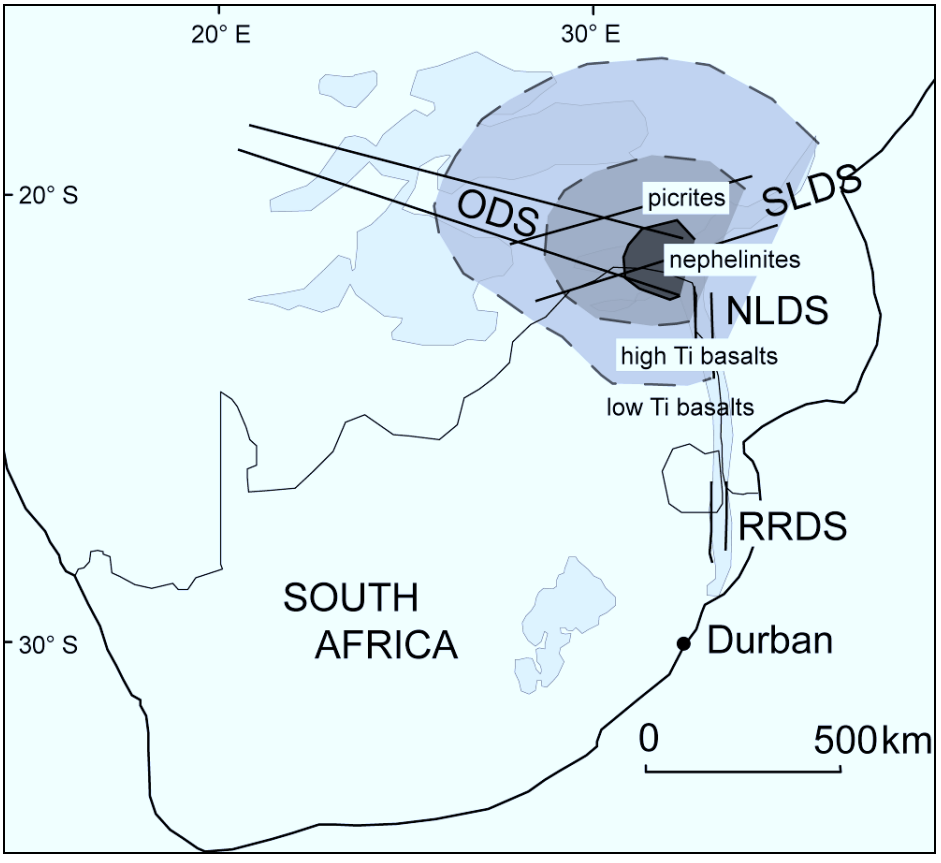

Figure 2: Schematic map of the outcrop of the Karoo LIP (lightest grey) in southern Africa, illustrating the concentric distribution of nephelinites, picrites and high- and low-Ti basalts with respect to the Karoo triple junction centred on Mwenezi, southern Zimbabwe (re-drawn from Jourdan et al., 2004; Klausen, 2009).

234 The Mashikiri nephelinites display enrichment of incompatible trace elements which
235 reflect melting of an ancient, metasomatically-enriched sub-continental lithospheric
236 mantle (SCLM) (Ellam and Cox, 1989; Hawkesworth et al., 1999; Jourdan et al., 2007a).
237 There are units of rhyolites (flows and intrusions) within the basalts of the Sabie River
238 Formation known as the Olifants Beds (Bristow, 1982; Riley et al., 2004).
239
240 The Letaba Formation picrites (MgO 10–24%) of the northern Lebombo monocline are
241 more voluminous than the nephelinites and reach a maximum thickness of 4 km. They
242 may have been derived from the SCLM (Bristow et al., 1984; Ellam and Cox, 1989) or
243 from mixing between asthenospheric mantle and SCLM (Ellam and Cox, 1991; Sweeney
244 et al., 1991) or from a heterogeneous source (Ellam, 2006).
245
246 The voluminous continental flood basalts and associated dykes and sills which followed
247 the primitive volcanics at ~182 Ma are low in MgO (2% < MgO < 9%) and possess a
248 variation in Ti and Zr across southern Africa. Specifically, basalts in the northern
249 Lebombo and further north into Zimbabwe are high-Ti (TiO_2 > 2%), whilst basalts of the
250 southern Lebombo, Lesotho, central Botswana and central Namibia are low-Ti (Fig. 2)
251 (Cox et al., 1967; Duncan et al., 1984; Jourdan et al., 2007a) and those of the Lebombo
252 have calc-alkaline affinities (low-K tholeiites) (Duncan, 1987). This distinction is
253 attributed to differences in melting, resulting in 30–40% of the incompatible elements in
254 the high-Ti basalts being derived from the lithospheric mantle (Sweeney and Watkeys,
255 1990; Sweeney et al., 1994). Indeed Ellam and Cox (1989) have shown, using Sm-Nd
256 systematics that the Karoo yields a Proterozoic eruption “isochron” which demonstrates
257 mixing in the melt source region. This is also evident from the background levels of
258 crustal contamination and generally MORB-like signature of incompatible elements (Cox
259 and Bristow, 1984; Hawkesworth et al., 1984). Bristow et al. (1984) also find evidence
260 for a heterogeneous mantle source for the bulk of the Karoo basalts in the $^{87}Sr/^{86}Sr$ ratios,
261 although these authors find no convincing evidence for interaction of the melts with
262 crustal material. The low-Ti basalts were possibly derived from an asthenospheric source
263 which equilibrated with refractory lithospheric mantle (Sweeney et al., 1991). The
264 voluminous basaltic volcanism was followed by the eruption of the Jozini and Mbuluzi

Formation rhyolites which cap the Karoo volcanics of the Lebombo monocline (Bristow, 1982). This was followed by the intrusion of the RRDS in the southernmost region of the Lebombo (Armstrong et al., 1984).

The Ferrar Province is exposed along the length of the Transantarctic Mountains and comprises the Dufek intrusion as well as massive, laterally extensive dolerite sills (Elliot et al., 1999) and pyroclastics capped by the Kirkpatrick basalts (Kyle et al., 1981; Elliot and Fleming, 2000). The Ferrar Province is dominated by low-Ti tholeiitic basalts which were most likely derived from a lithospheric mantle source (Hergt et al., 1991). The extensional rift-like structure along which the Ferrar magmas intruded has been suggested as the reason for its linear extent (Storey et al., 1992) (Fig. 1). It has also been suggested that the Ferrar is indicative of a linear melting anomaly caused by a long-lived subduction zone on the southern margin of Gondwana (Cox, 1992; Storey, 1995). However, some workers argue that the Ferrar and related magmas were emplaced from the Weddell Sea triple junction (Elliot and Fleming, 2000, 2004; Leat, 2008; Luttinen et al., 2010). This is discussed in further detail in Section 4.

The basic rocks of Dronning Maud Land are comparable to those in southern Africa with two varieties, DM1 and CT1 (Riley et al., 2005 and Luttinen et al., 1998 respectively) being similar to the low-Ti compositions of southern Africa. Luttinen et al., (1998) provide general geochemical and isotopic data from the basalts and dykes of Vestfjella, in Dronning Maud Land. Using Sr and Nd isotopes, they differentiate 4 magma types (CT1–CT4) which can be identified in related lavas and dykes. Dolerite dykes belonging to the CT4 magma type are the only OIB-like magmas known from Karoo-age magmatism. The CT1 magma type is tholeiitic, most likely derived from an Archaean, sub-lithospheric mantle source. The CT2 and DM2 magma types have MORB affinities similar to the RRDS and most likely derive from an asthenospheric source. There is also a high-Ti basalt composition (Group 4 of Riley et al., 2005). The ferro-picrite CT3 magma type does not have a comparable composition within the Karoo LIP of southern Africa and is thought to be derived from early mantle plume melts (Riley et al., 2005).

296 The evidence for structural control on the distribution of basaltic compositions in
297 southern Africa is found in compositional changes (e.g. low-Ti to high-Ti) that occur
298 across basement boundaries through which the basalts erupted (Proterozoic mobile belts
299 vs. Archaean cratons) (Cox et al., 1967; Duncan et al., 1984; Watkeys, 2002; Jourdan et
300 al., 2004, 2006). Field relationships and geochronology show that the lithospheric
301 architecture has also controlled the development of the Karoo triple junction and
302 associated dyke swarms (Watkeys, 2002; Jourdan et al., 2004; Le Gall et al., 2005).
303
304 This has also been shown in Dronning Maud Land by Luttinen et al., (2010) who identify
305 Grunehogna province magmas and Maud province magmas on the basis of geochemistry
306 and Nd and Sr isotope data. In brief, the authors indicate that the Grunehogna magma
307 type shows evidence of recycled oceanic crust in the parent magma, and that the magmas
308 most likely derived from the partial melting of eclogite-bearing asthenospheric mantle.
309 Contamination has occurred, with high-Ti types showing evidence of lithospheric mantle
310 contamination and low-Ti types showing evidence of crustal contamination. The Maud
311 province magma type, however, derived from relatively low-pressure partial melting of
312 lithospheric mantle associated with rifting in the region of the Weddell Sea triple
313 junction. This is a broadly similar pattern to the distribution of magma types across the
314 southern African cratonic regions (high-Ti) and the central (Lesotho) Karoo and
315 Botswana areas (low-Ti).
316
317 *2.3. Dykes of the Karoo and associated LIP's*
318 There are three main dyke swarms associated with the Karoo triple junction (SLDS,
319 NLDS, ODS; Jourdan et al., 2004), four more isolated swarms (RRDS, UDS, SLeDS,
320 SBDS; Armstrong et al., 1984; Riley et al., 2006; Jourdan et al., 2007a) and at least five
321 dyke swarms in Dronning Maud Land (Curtis et al., 2008) (Fig. 1).
322
323 The Karoo triple junction at Mwenezi is situated within the Limpopo Belt and comprises
324 both the earliest (nephelinites, picrites) and latest (Mwenezi igneous complex)
325 manifestations of Karoo magmatism. The Limpopo Belt comprises poly-metamorphosed
326 rocks that represent an Archaean collision between the Kaapvaal and Zimbabwe Cratons.

These deformed cratonic and volcano-sedimentary rocks have a strong ENE-trending fabric which has been exploited by both faulting (Watkeys, 2002) and dyking (Uken and Watkeys, 1997; Jourdan et al., 2004) since the Proterozoic.

The ENE-trending SLDS comprises predominantly fine to medium grained dolerite dykes emplaced within the central and northeastern regions of the Limpopo Belt, extending for ~600 km from SE Botswana (the Tuli basin) to the NE of the Limpopo Belt. The SLDS is 50–100 km wide and comprises vertical to sub-vertically dipping dykes. These dykes have been dated to 180.4±0.7–178.9±0.8 Ma although a significant proportion of the dykes are Proterozoic in age (Le Gall et al., 2002; Jourdan et al., 2005, 2006). Field relationships indicate that this dyke orientation (ENE to NE) predate dykes of the NLDS and ODS, particularly evident from the picritic dykes of the Mwenezi region having intruded in this orientation (Watkeys, 2002).

The NLDS is hosted by the basaltic and other volcanic units, as well as the Clarens Formation, of the Lebombo. Dykes of the N–S trending NLDS comprise several generations of feeder dykes which can be directly correlated with volcanic units of the Sabie River Formation basalts (D1 and D2 generation), the Jozini Formation (D3 generation) and possibly the Movene Formation basalts (D4 dykes) within the Lebombo monocline (Klausen, 2009). In other areas, such as the ODS and RRDS, the dykes intrude the basalts of the Karoo, and have no known extrusive equivalents. The D1 to D4 nomenclature is indicative of relative dyke ages, such that D4 dykes are the youngest, and tend to strike NW, similar to the ODS. Two radiogenic ages of 181.4±0.7 and 182.3±1.7 Ma have been found for the NLDS (Jourdan et al., 2005). As yet, no Proterozoic age dykes have been recognised in the NLDS, suggesting that the N–S dyke trend developed in the Lebombo monocline during the Jurassic in response to E–W extension (Watkeys, 2002).

The WNW-trending ODS is ~1500 km in length, reaching ~300 km in width, where it overlaps with the northernmost Lebombo and the SLDS (Jourdan et al., 2006) (Fig. 1). It converges with the Lebombo monocline and SLDS at Mwenezi (Jourdan et al., 2004).

Dykes of the ODS have intruded Precambrian basement (central and northwestern regions of the Limpopo Belt) and sedimentary and volcanic rocks of the Karoo Supergroup within the Tuli basin (Smith, 1984; Elburg and Goldberg, 2000; Le Gall et al., 2005; Aubourg et al., 2008). The orientation of the ODS has been recognised as essentially a reactivation of an older structural trend evident in both the Kaapvaal and Zimbabwe Cratons (Watkeys, 2002). From field evidence, Le Gall et al., (2005) inferred a NNW-SSE dilation direction for the dykes, a similar direction to that inferred for the SLDS.

The ODS was first described as a post-Karoo (Cretaceous) dyke swarm associated with a failed rift axis (Reeves, 1978, 2000), i.e. an aulacogen. Uken and Watkeys, (1997) considered the ODS to be Karoo in age. Indeed, subsequent work has shown a predominantly Karoo-age with ~13% of the dykes being Proterozoic in age (Elburg and Goldberg, 2000; Le Gall et al., 2002, 2005). Dykes of the ODS have been dated to 179±1.2–178.4±1.1 Ma, with the Proterozoic component providing ages of 851±6–1672±7 Ma (Jourdan et al., 2004). The dykes are doleritic in composition; dominated by plagioclase (35–45 %), clinopyroxene (20–35 %) and Fe-Ti oxides. Both high-Ti and low-Ti varieties occur (Elburg and Goldberg, 2000; Aubourg et al., 2008).

The youngest dyke swarm in the Karoo LIP is the RRDS (173.9±0.7 Ma) which post-dates the main Karoo flood basalts (Jourdan et al., 2007b, c). The MORB-like RRDS is a N–S trending dyke swarm found in the southern Lebombo monocline, extending ~180 km from the Msunduze River in KwaZulu-Natal northwards to central Swaziland. The 10–22 km thick swarm intruded the Sabie River Formation and Beaufort Group, just to the west of the Lebombo monocline (Marsh, 1987; Marsh, 2002; Watkeys, 2002). The steeply dipping (> 80°), generally N–S striking dykes of the RRDS in the central area give way to more shallowly dipping (50°–70°) NNE–SSW striking dykes in the north (in Swaziland). The RRDS most likely originated from the melting of an upwelling asthenosphere, as is typical during lithospheric rupture during the early stages of continental break-up (Armstrong et al., 1984; Meth, 1996; Saggerson et al., 1983). The Explora Wedge probably developed at this time (Cox, 1992; Leinweber and Jokat, 2012)

(Fig. 1). As previously mentioned, the CT2 and DM2 magma types of Dronning Maud Land have MORB affinities similar to the RRDS (Luttinen et al., 1998) which is consistent with the coeval development of the Lebombo monocline and Explora Wedge.

There are additional dyke swarms in southern Africa which require introduction, as they are relevant to the tectonomagmatic characteristics of the Karoo LIP. These are the southern Botswana and southern Lesotho dyke swarms (SBDS and SLeDS respectively) and the NW–SE striking Underberg dyke swarm (UDS) (Jourdan et al., 2004) (Fig. 1). The SBDS and SLeDS are shown only in the interest of completeness, because magma flow and geochronological studies have not been conducted on these swarms.

Dykes of the UDS are fine- to medium-grained dolerites with intergranular and/or sub-ophitic textures. The UDS intruded sedimentary sequences of the Triassic Beaufort Group and the overlying Molteno, Elliot and Clarens Formations. The UDS is geochemically similar to the low-Ti basalts of Lesotho (and the SLeDS); although field relationships and geochronology confirm that the dykes are younger than the Lesotho basalts. Riley et al. (2006) provide an age of ~176 Ma for the intrusion of the UDS. These authors have found that the strike of the dykes is remarkably uniform (130°–140°), which differs slightly from the ODS and SBDS (110°–120°). The UDS was derived from sub-lithospheric melts involving some crustal contamination (Riley et al., 2006). AMS measurements have been undertaken on only three dykes, and therefore we remain sceptical of the regional significance of the measurements.

In addition, there is the Olifants River dyke swarm (ORDS, not shown) which was once thought to be related to the Karoo LIP, but has been shown to be older than ~800 Ma (Marsh, 2002; Jourdan et al., 2006). The ORDS extends south-westward from the Lebombo monocline following an Archaean/Proterozoic dyking direction (Uken and Watkeys, 1997; Watkeys, 2002). It is common to find that NE–SW striking dykes are truncated by NW–SE striking dykes – which is the orientation of the ODS. For example, the SLDS (Fig. 1) overlaps with the ODS and has been dated to 180.4±0.7–178.9±0.8 Ma (Le Gall et al., 2002; Jourdan et al., 2005, 2006) although Proterozoic ages have been

found (728±3–1683±18 Ma, n=14). Karoo dykes generally don't occur in the 0°–40° orientation, which is best explained by the SW–NE strike of the Proterozoic age dykes of the SLDS. The geochronology of the Karoo-age dykes is considered in further detail in Section 3.

Karoo-age dyke swarms in Dronning Maud Land include the Alhmannryggen (178 Ma), Straumsvola (178–176 Ma) and Vestfjella (177 Ma) dyke swarms (ADS, SDS and VDS respectively). There are two older dyke swarms, the Group 1 dykes of the Alhmannryggen region (~190 Ma) (Riley et al., 2005) and the Jutulrøra dyke swarm (JDS) (~205 Ma). The JDS consists predominantly of low-Ti tholeiitic dykes that trend NNW–SSE (Fig. 1). The SDS, which is mainly restricted to the Straumsvola area (Fig. 1), is predominantly doleritic in composition and was emplaced between 178.5 Ma and 174.8 Ma (concordant $^{40}Ar/^{39}Ar$ isochron age of 174.8±2.0 Ma). Heinonen et al., (2010) have shown that the VDS comprises two geochemically distinct suites – an enriched, OIB-like type and a depleted, MORB-like type.

The youngest dyke phase of the SDS yielded an age of 170.9±1.7 Ma (younger than the Lebombo rhyolites). These younger dykes, including phonolitic and lamprophyric compositions, cross-cut the dolerite dykes. Curtis et al. (2008) propose two distinct phases of mafic dyke emplacement rather than a protracted magmatic history. From field, structural and AMS data these authors assert that the dykes were sourced locally. For example, power-law distribution of the dyke thicknesses and spacing indicates that the dykes generally become more widely spaced ~25 km south of Straumsvola. This may reflect a spatial variation in magma pressure, such that the SDS was emplaced under higher magmatic pressure than the JDS; the restricted orientations thereof indicating that the JDS was bound to the stress field of the host rock and not the magma pressure driving emplacement.

Despite attributing the origin of these dykes to a mantle plume (Curtis et al., 2008), it is evident that the majority of these dykes are low-Ti tholeiites, similar to the bulk of the Karoo mafic dykes and lava flows. Interestingly, these compositions are also found off-

craton in Antarctica in the same manner as the Grunehogna magma type (Luttinen et al., 2010) and the low-Ti tholeiites of the Karoo LIP (Cox et al., 1967).

An important structural feature of this region of Dronning Maud Land is un-named triple rift system first described by Ferraccioli et al. (2005). It was discovered beneath the Antarctic ice sheet in west Dronning Maud Land and converges on Neumayerskarvet, which is near the southern termination of the ADS (Fig. 1). The convergent rifts of this triple junction are occupied by Jurassic-age volcanic rocks and alkaline and tholeiitic intrusions (Ferraccioli et al., 2005; Curtis et al., 2008). Riley et al., (2005) observed in the Ahlmannryggen region that initial crustal dilation due to dyking was N–S oriented (190 Ma) followed at 178 Ma by regional NW–SE oriented dilation. Ferraccioli et al., (2005) demonstrate, however, that extension in these rifts cannot be accounted for by dyke dilation alone, and suggest considerable crustal thinning prior to, or post-dyking. These authors also argue that the triple junction geometry and the ferro-picrite composition of certain dykes are consistent with derivation from an early mantle plume (~190 Ma?), although the Jurassic dyke swarms described above do not coincide geometrically with these rifts (Fig. 1). The same is clear in the dyke swarms of the Karoo LIP (e.g. the RRDS, SLeDS and UDS).

There is a "new" dyke swarm that has been recognised geophysically within the Mozambique thinned-zone (MTZ) (Fig. 1) that is known as the SW-1 dyke swarm (or Mozambique dyke swarm) (Mekonnen, 2004). There is virtually nothing known about or published regarding these dykes. However, its prominent NNE strike direction and presence within the MTZ suggests that it intruded later (~170 Ma) than the Karoo LIP in response to extension between SE Africa and Antarctica (Jokat et al., 2003; Mekonnen, 2004).

3. Geochronology of the Karoo LIP

3.1. Overview

As illustrated already, the Karoo LIP comprises many components; volcanic and intrusive, with contemporaneous and overlapping volcanism spread across southern

Africa and Antarctica. Handling the observed and resolved field relationships and the radiogenic age-data can therefore be somewhat cumbersome. Thus, an overview of the salient and reliable dates from the growing number of data on the Karoo is provided, which better constrain the ages of particular lithologies and events (and the duration of Karoo magmatism).

Although Jourdan et al., (2007b) provide a thorough analysis and review of the development of the Karoo LIP based on $^{40}Ar/^{39}Ar$ geochronology, there are new data (Curtis et al., 2008) and previously determined ages on the Antarctic components of the Karoo LIP which have not been discussed (Heimann et al., 1994; Zhang et al., 2003; Riley et al., 2005). Thus, a concise chronostratigraphy of the major components of the Karoo LIP is presented (Fig. 3). The source references for the ages are shown below the key in Figure 3. The assembly of ages shown is not exhaustive, but is restricted to ages determined by the $^{40}Ar/^{39}Ar$ and U-Pb methods on single plagioclase and zircon grains respectively (i.e. no bulk sample / bulk rock / groundmass ages). A synopsis of the reliability of these ages, and the omission of others, is presented below because this impacts on what geologically significant conclusions can be drawn from this chronostratigraphy.

3.2. Reliability of ages

Firstly, whole-rock ages (including those determined using K/Ar and Rb/Sr) are excluded because their meaning is highly debatable (Jourdan et al., 2005). Also, only Jurassic ages are shown for dyke swarms in which Proterozoic ages have also been found (the SLDS and ODS).

There is some concern about the ages found by Riley et al. (2005) for the Group 1 dykes and the ADS. These authors indicate that the criteria necessary to define an age plateau during step-heating in the $^{40}Ar/^{39}Ar$ method were generally not met and the effects of alteration and/or excess ^{40}Ar make distinguishing any age differences uncertain.

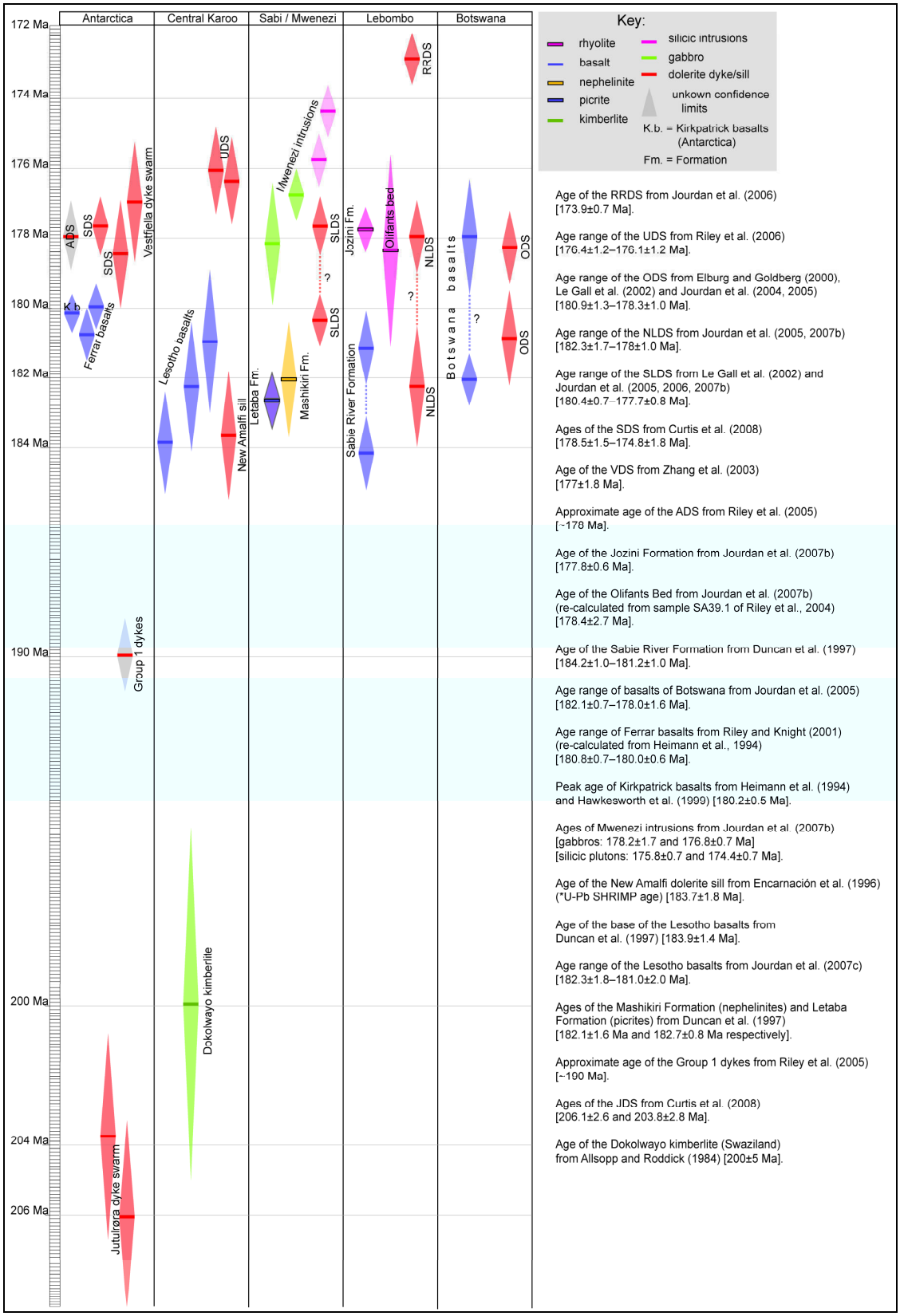

Figure 3: Chronostratigraphy of the major regions of the Karoo LIP and associated igneous provinces. Note that ages are shown in solid colours with lighter shaded error bars. The smallest age increments are 0.1 Ma. RRDS=Rooi rand dyke swarm, UDS=Underberg dyke swarm, ODS=Okavango dyke swarm, SLDS=Save-Limpopo dyke swarm, NLDS=Northern Lebombo dyke swarm, SDS=Straumsvola dyke swarm, VDS=Vestfjella dyke swarm, ADS=Alhmannryggen dyke swarm, JDS=Jutulrøra dyke swarm. See Section 3.2 for discussion of age reliability.

These criteria are: [1] at least 70% of the ^{39}Ar must be released, [2] a minimum of three successive steps in the age plateau must be evident and [3] the integrated age of the plateau should (within 2σ confidence limits) agree with each apparent age increment of the plateau (Jourdan et al., 2007b).

This probably relates to making age determinations on the groundmass of 2 samples which can be problematic because of mineralogical alteration (Jourdan et al., 2007c). These ages have, therefore, only been included in the interest of completeness and they are shown with "unknown" confidence limits.

The age of 180.2±2.7 Ma found for the lowermost Olifants Bed (rhyolite flow within the Sabie River Formation basalt) is a reliable regression age (Figure 3a of Riley et al., 2004). The other ages determined (U-Pb zircon ages) are discordant. Unfortunately, this includes the ages determined for the Jozini Formation rhyolites, which also have provided older ages (182.1±2.9 Ma) than the rhyolites stratigraphically beneath them. Thus, these ages are not included here.

Jourdan et al. (2007b) re-calculated the U-Pb age of Riley et al. (2004) in order to compare it to $^{40}Ar/^{39}Ar$ ages, and found the age to be 178.4±2.7 Ma. This is essentially indistinguishable from the age of 177.8±0.6 Ma found for the Jozini Formation rhyolites (Jourdan et al., 2007b), although these evidently overlie the rhyolite flow within the Sabie River Formation. Duncan et al. (1997) determined $^{40}Ar/^{39}Ar$ ages of the Jozini rhyolites, but these may represent cooling ages (Riley et al., 2004) and are therefore not considered here.

The re-calculation of ages by Riley and Knight (2001) on the basalts of the Ferrar Province was done because ages calibrated to older standards (e.g. McClure Mountain Hornblende, MMhb-1 at 523.1±2.6 Ma) cannot be compared reliably to those calibrated to newer standards (e.g. Hb3gr hornblende at 1072 Ma). See Jourdan et al. (2007c) for further discussion about the intercalibration of radiometric ages within the Karoo LIP.

3.3. Progression & duration of the Karoo LIP

If the oldest (~184 Ma) and youngest (~174 Ma) ages are considered as reliable, there is an approximate duration of 10 Ma for the Karoo LIP *sensu stricto*. The older age (~205 Ma) for the JDS is most likely a legitimate pre-Karoo LIP age. However, there is evidence of older volcanism in southern Africa from this time. For example, there is evidence of small volumes of volcaniclastic material associated with diatreme-like vents within the Molteno, Elliot and Clarens Formations and andesitic to dacitic dome complexes (McClintock et al., 2008). Although no absolute ages are known, the field relationships do suggest that they pre-date the earliest mafic eruptions of Karoo LIP proper. Furthermore, it has been shown that the Dokolwayo kimberlite (Swaziland) intruded during the deposition of the Karoo Supergroup, but is older than the uppermost sedimentary units (Molteno and Clarens Formations). Dokolwayo has been dated to 200±5 Ma ($^{40}Ar/^{39}Ar$ age on phlogopite) (Allsopp and Roddick, 1984).

It is clear from Figure 3 that there was an overlap of basalt eruption (Lesotho and Lebombo) and sill intrusion with volcanic and intrusive activity in the northern Lebombo (NLDS). If the dyking activity in the northern Lebombo is assumed to have been continuous, it overlaps consistently with the age ranges of both the SLDS and ODS. The voluminous outpourings of flood basalts in northern Botswana occurred over this time, from ~182–178 Ma, while those of southern Botswana erupted from ~185–181 Ma (Jourdan et al., 2005).

At approximately the same time volcanic activity that gave rise to the Ferrar Province began in Antarctica, with clearly later dyking of the VDS and SDS (Zhang et al., 2003; Curtis et al., 2008) and a remarkable lack of concomitant basalt eruption. This is consistent with the earlier findings of Riley and Knight (2001), who showed that the bulk of Ferrar magmatism occurred at ~180 Ma, approximately 3 Ma after the bulk of Karoo magmatism in southern Africa.

There is a dearth of ages for the Sabie River Formation which, on the basis of the interbedded Olifants Bed, suggests that it may have erupted until ~178 Ma, although Jourdan et al. (2007b) suggests that it may have only erupted over a 2–3 Ma period. The Sabie River Formation was fed from the D2 dyke generation of the NLDS (Klausen, 2009).

585 By this time in the Lebombo volcanism had progressed to more rhyolitic outpourings
586 and intrusive activity in the Sabi/Mwenezi region, culminating in the youngest
587 intrusive activity (silicic and syenite intrusions) of the northern Karoo LIP. This was
588 likely contemporaneous with the intrusion of the ODS and SLDS (Jourdan et al.,
589 2007b). The ~176 Ma old UDS intruded at this time in the central Karoo region,
590 cross-cutting the basalts of Lesotho, while the youngest Karoo LIP-related
591 magmatism is represented in the southern Lebombo by the intrusion of the RRDS at
592 ~174 Ma.
593
594 Besides the D2 dyke generation of the NLDS, there is little evidence to suggest that
595 the dykes were feeders flowing from the Karoo triple junction to the now preserved
596 basaltic volcanic pile. While many of the sills may be comparable in age to the basalts
597 (see Jourdan et al., 2007c), the dyke swarms are not. For example, to the southeast of
598 the main Lesotho basalts is the UDS which is ~176 Ma in age compared to ~183 Ma
599 for the basalts. The same is true of the ADS and VDS in Antarctica, and SLDS and
600 RRDS.
601
602 There is also evidence of diachronous magmatism in field evidence (Watkeys, 2002)
603 and the broad geochronological data (Jourdan et al., 2004). Early primitive melts
604 erupted at the Karoo triple junction, followed by volcanism and early dykes (earliest
605 dykes of the NLDS) in the south and central (Lesotho basalts) regions, followed by
606 further dyking in the north (ODS) and Antarctica (early SDS), rhyolitic volcanism in
607 the Lebombo virtually synchronous with Antarctic magmatism and finally an apparent
608 return to activity in the south (UDS and RRDS). Magmatism of the Mwenezi Igneous
609 Complex appears to span this period of late dyking (178–174 Ma).
610
611 **4. Mantle plume origin for the Karoo LIP**
612 Burke and Dewey, (1973) were the first to postulate a link between mantle plumes
613 and the Karoo triple junction. To account for the geometry of the triple junction, and
614 volcanism further to the northeast, they proposed two possible mantle plume
615 positions: one at the triple junction (Fig. 4a) and one in the lower Zambezi valley
616 (Fig. 4b). White and McKenzie (1989), however, proposed a much broader (~2000
617 km diameter) plume situated at the juncture between Antarctica and the Lebombo

(~450 km ENE of Maputo) to account for the contiguous magmatism of Dronning Maud Land and the Karoo (Fig. 4c).

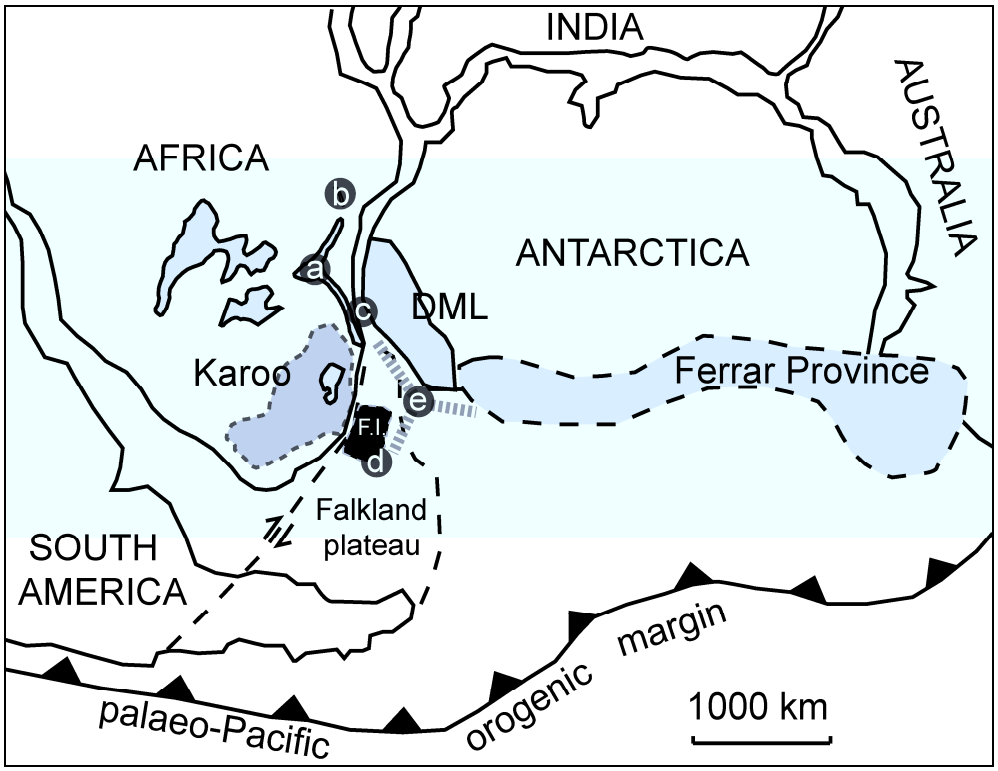

Figure 3: Regional schematic map of the Karoo LIP and associated magmatic provinces (shown in grey). Area of major sill intrusion in South Africa is shown in darker grey with a dashed outline. DML=Dronning Maud Land. The plume positions shown (a–d) are from (a) Burke and Dewey (1973); Storey (1995), (b) Burke and Dewey (1973), (c) Cox (1989); White and McKenzie (1989); Storey et al., (1992); White (1997); Curtis et al., (2008), (d) "megaplume" of Storey and Kyle (1997), (e) Weddell Sea triple junction of Elliot and Fleming, (2000) (F.I.=Falkland Islands) (regional map modified from Cox, 1992 and Riley et al., 2006).

Campbell and Griffiths, (1990) and Storey, (1995) upheld the idea of a plume head impacting directly beneath the triple junction itself, to account for its geometry and the composition and distribution of the nephelinites and picrites (Fig. 2). Cox (1989) showed that drainage patterns of rivers of the northern Lebombo break along an arc that coincides with the circumference of the plume position proposed by White and McKenzie, (1989). This area may have been underplated by a hot, low density upwelling from the mantle, an idea upheld by White (1997) who also suggest that uplift across an area of up to 2000 km in diameter occurred above the plume head. It is difficult, however, to infer uplift caused by a mantle plume in the Mwenezi region because it has been a long-lived palaeo-high (a horst-like structure) since the Permo-Carboniferous (Watkeys, 2002).

642 It has also been suggested that the axis of the proposed plume was not necessarily
643 responsible for the primitive rocks centred on Mwenezi (Cox, 1992). The ENE-
644 striking fabric and relative structural weakness of the Limpopo Belt has influenced the
645 position of the primitive lithologies, an idea upheld later by specific geochronological
646 and structural studies (Le Gall et al., 2002; Watkeys, 2002; Jourdan et al., 2004; Le
647 Gall et al., 2005).
648
649 The mantle plume origin for the Karoo LIP suggested by White (1997) is a modified
650 version – with stretching of the lithosphere from ~150 km to 50–60 km depth. This
651 would have allowed for decompression melting brought about by an upwelling mantle
652 plume to occur. White (1997) favours a plume centred off the Kaapvaal Craton
653 because a plume would have thermally perturbed the sub-continental lithosphere; an
654 unlikely scenario given the eruption of Proterozoic and older diamonds through the
655 Craton during the emplacement of Jurassic and Cretaceous-age kimberlites. Storey
656 and Kyle (1997) suggest that a "megaplume" (≥ 2000 km diameter) positioned on the
657 pre-break up position of the Falkland Plateau (Fig. 4d) can account best for the
658 contiguous magmatism across the region.
659
660 There are also compositional factors of the Karoo LIP that are consistent with mantle
661 plume melting. The earliest magmatism in the Karoo is composed of picrites and
662 nephelinites (Bristow, 1984) which are geochemically compatible with
663 uncontaminated plume-derived melt (White, 1997). Furthermore, Sweeney et al.
664 (1994) have suggested that the more evolved high-Fe basalts in the central region of
665 the Lebombo are consistent with mantle plume melting. This is echoed by Riley et al.,
666 (2005) who suggest that the ferro-picrite CT3 magma type is derived from a mantle
667 plume melt.
668
669 Indeed, the early nephelinites and picrites which centre on the Karoo triple junction
670 may be accounted for in this fashion. There are few OIB-like compositions in the
671 Karoo (except the CT4 magma type of Luttinen et al., 1998), a melt composition
672 generally regarded as being plume-derived. It is only igneous provinces younger than
673 the Karoo, such as the Paraná, Etendeka and the Deccan Traps that display isotopic
674 and major and trace element signatures comparable to OIB (Hawkesworth et al.,

675 1999). Regardless, some models suggest that ocean-island basalt (OIB) can originate
676 from sub-lithospheric fractionation (Anderson, 1985).
677
678 The vast majority of the Karoo magmas are low-Ti tholeiites (Hawkesworth et al.,
679 1999) and it is quite consistent with a mantle plume that a progression from primitive
680 to tholeiitic compositions exists. Although high-Ti compositions are indeed
681 widespread in the Karoo, there is the conspicuous link between crustal architecture
682 and the occurrence of these compositions: low-Ti compositions tend to occur over
683 mobile belts, while high-Ti compositions occur over cratonic basement (Cox et al.,
684 1967). This has been attributed to sub-continental lithospheric mantle (SCLM) control
685 on the melts produced (Sweeney and Watkeys, 1990; Sweeney et al., 1994).
686
687 The siliceous, high field strength element-depleted signature in the Ferrar Province is
688 believed to be the result of sedimentary contamination of the mantle source, most
689 likely because of subduction (Hergt et al., 1991). Cox (1992) also indicates that the
690 linear extent of the Ferrar Province in Antarctica is most likely beyond the extent of a
691 proposed mantle plume(s). Encarnación (1996) provided the first evidence for the
692 geochronological link between the Ferrar Province and the Karoo LIP, indicating a
693 subduction related process to account for the linear extent and geochemistry of the
694 basalts. The suggestions that a plume may be more linear in extent (Storey and Kyle,
695 1997; White, 1997), or that a number of non-interacting plumes operated
696 simultaneously in different regions (Storey and Kyle, 1997) seems possible, but
697 speculative in light of other evidence. Some workers suggest that the Ferrar magmas
698 were emplaced from the Weddell Sea triple junction (Elliot and Fleming, 2000) (Fig.
699 4e) and Leat (2008) also suggests that the magma source for the laterally emplaced
700 Ferrar magmas was in the rift between SE Africa and Antarctica.
701
702 Central to the plume hypothesis are the Karoo triple junction and associated dyke
703 swarms. Previous work has shown that there are a number of characteristics of the
704 dyke swarms which strongly question the validity of a mantle plume origin for the
705 Karoo LIP. The Karoo triple junction was undoubtedly an active feature of the Karoo
706 LIP, but its history is linked firmly to lithospheric architecture and its pre-Jurassic
707 past (Jourdan et al., 2004). For example, the Lebombo monocline occupies the eastern
708 edge of the Kaapvaal Craton and the structural trend of the Limpopo Belt has been

709 exploited by the SLDS (Jourdan et al., 2006). Indeed, the area of maximum basalt
710 thickness in Lesotho lies conspicuously on the southern boundary of the Kaapvaal
711 Craton where it is adjacent to granite-gneiss terranes of the Proterozoic Namaqua-
712 Natal metamorphic province.
713
714 Furthermore, geochronology shows two important features of the radiating dyke
715 swarms of the Karoo triple junction. Firstly, there are many dykes in the ODS and
716 SLDS that are Proterozoic in age, suggesting that the orientation of these two swarms
717 was determined prior to Karoo magmatism (Uken and Watkeys, 1997; Watkeys,
718 2002; Le Gall et al., 2002, 2005; Jourdan et al., 2004). Secondly, dating of basalts
719 quite clearly shows a progression in age from south to north (Fig. 3) while the
720 intrusion of Jurassic dykes appears to have progressed from the Lebombo (NLDS) to
721 the northern (ODS) and central regions (UDS), Antarctica (SDS and VDS) and finally
722 to the RRDS (Watkeys, 2002).
723
724 The dyke swarms of the Karoo LIP around southern Africa do not form part of a
725 singular volcanic feeder system, as most of the dyke swarms (ODS, RRDS, SLeDS,
726 UDS) cross-cut the basalts. This is reflected in the geochronology which shows that
727 the ODS and RRDS post-date the main Karoo volcanic event by at least 3 Ma. This
728 seems counterintuitive given the classic model of radial injection of dykes from a
729 triple junction (Ernst and Baragar, 1992), simultaneously feeding overlying volcanics.
730 Furthermore, short-lived (~2–5 Ma), high volume magmatism is not strictly
731 applicable to the Karoo LIP; although the volumetrically significant tholeiitic, CFB
732 component did erupt relatively rapidly (Jourdan et al., 2005).
733
734 Taking the entire igneous component of the Karoo into consideration it is evident that
735 magmatism extended over the period 183–174 Ma, almost twice the duration that has
736 been suggested for other LIP's and is atypical of the classical model of short lived,
737 rapid magmatism driven by an active plume (Jourdan et al., 2004, 2006). This
738 relatively long duration is suggestive of long-term magma storage and a lack of
739 preservation of primitive melt compositions. The south-to-north migration of
740 magmatism also appears to have been too rapid for it to have occurred as a result of
741 the crust migrating over a plume head (Jourdan et al., 2007b). Magmatism at
742 Mwenezi and in the Lebombo monocline appears to be the longest-lived (183–174

743 Ma) compared to the other arms of the triple junction (Watkeys, 2002; Jourdan et al.,
744 2007b). The 174 Ma old RRDS most likely represents an isolated dyking event, given
745 its restricted occurrence, age and unique MORB-like composition. The youngest
746 Karoo volcanic activity is preserved as the predominantly felsic Mwenezi igneous
747 complex which intrudes rhyolites in the Mwenezi trough (Watkeys, 2002). Such
748 diversity in distribution and age is difficult to reconcile with a mantle plume.
749
750 It has been asserted that vigorous output of large volumes of magma is linked to
751 active crustal extension caused by mantle plumes (Richards et al., 1989; White, 1997).
752 This would suggest, in the case of the Karoo, a relatively short period of magmatism
753 followed rapidly by continental break-up, i.e. within ~10 Ma as is typical of other
754 LIPs. Jourdan et al. (2005) indicate that the bulk of Karoo magmatism occurred over
755 ~6 Ma, resulting in calculated eruption volumes of ~0.3 $km^3.yr^{-1}$, approximately a
756 third of the rate for the CAMP (Marzoli et al., 1999). If, for example, full oceanization
757 occurred at this time (consistent with rapid rifting caused by a plume), it would still
758 imply a long-lived thermal incubation of at least 10 Ma, which is odds with a mantle
759 plume. In addition, the first sea-floor anomalies of southern Gondwana are ~155 Ma
760 old (Goodlad et al., 1982). This puts ~28 Ma between the onset of magmatism and
761 oceanisation, which seems too protracted a time for a plume to have heated the
762 lithosphere without it rupturing (Storey et al., 1992). However, if we consider new
763 sea-floor magnetic data (Leinweber and Jokat, 2012), which puts the earliest sea-floor
764 spreading at 166 Ma, there is a shorter period of 8 Ma following the intrusion of the
765 RRDS before sea-floor spreading initiated.
766
767 Workers generally agree that, whichever mechanism operated, there was clearly a
768 temperature elevation in the mantle that gave rise to melting (Cox, 1989; White and
769 McKenzie, 1989; Sweeney et al., 1994). Indeed, Cox (1992) suggests that there may
770 have been interplay between a hinterland plume (Karoo) and more distal subduction
771 along the Pacific margin of southern Gondwana (Ferrar, Antarctica). A similar idea is
772 echoed by Jourdan et al., (2007a), who indicate that the isotope and trace element
773 geochemistry of the Karoo magmas are compatible with a combination of isolation of
774 mantle source regions and enrichment processes that may have involved a mixed
775 mantle plume contribution. Cox (1992) also speculated that the slightly earlier

776 beginning of subduction may have triggered the upwelling of a mantle plume, an idea
777 which is explored later in Section 7 (O'Neill et al., 2009).
778
779 It is of interest, therefore, to investigate whether the dyke swarms of the Karoo LIP
780 and those of Dronning Maud Land can provide any convincing evidence for lateral
781 intrusion from a point source. A scenario involving lateral magma flow from the
782 Karoo triple junction would be expected under the influence of an active mantle
783 plume – an idea explored in the next section of this paper. An overview of magma
784 flow data illustrates the most likely magma supply scenario for these dyke swarms.
785
786 **5. Methodology**
787 *5.1. Introduction*
788 Measuring the AMS of samples from mafic dykes has become a standard method of
789 quantifying flow-related petrofabric (Khan, 1962; Ellwood, 1978; Knight and Walker,
790 1988; Ernst and Baragar, 1992; Poland et al., 2004; Kissel et al., 2010). The
791 susceptibility of mafic igneous rocks derives from Fe-bearing minerals such as
792 magnetite and titanomagnetite. The anisotropy may be controlled by the distribution
793 of grains within the rock (distribution anisotropy, Hargraves et al., 1991) or by
794 magnetocrystalline anisotropy (e.g. hematite or pyrrhotite). For multidomain
795 magnetite, however, it is more typically shape controlled (shape anisotropy) and AMS
796 can therefore be representative of the shape and orientation of the petrofabric
797 (Rochette et al., 1999).
798
799 Measurements are typically made on cylindrical drill-core samples (22 mm × 25 mm)
800 collected along opposing chilled margins of a dyke in order to determine if any
801 imbrication of the fabric elements (lineation and/or foliation) can be found (Tauxe et
802 al., 1998; Aubourg et al., 2002; Geoffroy et al., 2002). This is regarded as local scale
803 because data are determined per margin, and per dyke. In the case of a dyke swarm it
804 is useful to view the "bulk" fabric however. This approach is explained further in
805 Section 5.2.
806
807 AMS is represented by an ellipsoid with principal axes $K1$, $K2$ and $K3$ (where $K1 >$
808 $K2 > K3$). The magnetic lineation ($K1$) and foliation (to which $K3$ is a pole) are most
809 important for our purposes, and are typically shown stereographically – either for a

single dyke (usually shown as separate margins), or grouped in order to visualise the bulk fabric. The ellipsoid is further described by the degree of anisotropy (*P'*) and the shape of the ellipsoid is indicated by the factor *T* (where oblate fabrics have $T > 0$ and prolate fabrics have $T < 0$).

There are essentially three types of magnetic fabric (Rochette et al., 1999). Type-A fabric is characterised by the *K*3 axes clustering perpendicular to the dyke wall, with *K*1 and *K*2 lying along the magnetic foliation (sub-) parallel to the dyke plane. This is often referred to as "normal" fabric, and is considered to form by magma flow (Ellwood, 1978; Knight and Walker, 1988; Rochette et al., 1999; Cañón-Tapia, 2004). Type-B, or "inverse", fabric is characterised by the interchange of *K*1 for *K*3 axes, with clustering of *K*1 axes perpendicular to the dyke plane (Potter and Stephenson, 1988; Tarling and Hrouda, 1993; Rochette et al., 1999). The third type of magnetic fabric is known as "intermediate", with *K*2 interchanged with the expected orientation of *K*3 in type-A fabric. Intermediate fabric is most commonly attributed to the mixing of fabric types (Rochette et al., 1999) and/or the effects of late-stage compaction (Park et al., 1988; Philpotts and Philpotts, 2007). In addition, AMS fabrics can be highly scattered or fabrics may bear no relation to the intrusion plane at all. The use of type-B fabrics in determining magma flow direction has been well illustrated by Callot et al., (2001) and Aubourg et al., (2008) where inverse *K*1 axes are treated as *K*3 axes in density stereoplots of the bulk AMS fabric.

It must be noted here that the AMS and SPO data and interpretations pertaining to the NLDS are from Hastie et al., (2011b) and data for the ODS are from Aubourg et al., (2008). Magnetic fabric data for dykes of Dronning Maud Land are from Curtis et al., (2008) and we present previously unpublished data from the RRDS in conjunction with the prior work of Hastie et al., (2011a).

5.2. Inferring flow direction

While many studies continue to use the magnetic lineation as an indicator of flow direction Henry (1997) has shown that the lineation may be meaningless if the intersection of magnetic foliations is correlative with the magnetic lineation. This has been demonstrated in further studies as well (e.g. Dragoni et al., 1997; Callot and Guichet, 2003; Hastie et al., 2011b) where the *K*1 axis can be at right angles to the

flow direction. Our approach here is to focus on the imbrication of the foliations relative to the dyke plane in predominantly oblate shaped fabric (Aubourg et al., 2002; Geoffroy et al., 2002) while also factoring in the orientation of *K*1 axes (in prolate fabrics) and any field evidence which may assist in flow determinations.

This approach, at the scale of a single dyke, works by plotting the principal AMS axes for each margin (thus two stereoplots per dyke) which when compared may reveal mirrored imbrication of foliations and/or lineations (Fig. 5). The finding of vertical flow (Fig. 5a) and lateral flow (Fig. 5b) across a suite of dykes or a dyke swarm is, however, generally interpreted in a regional sense.

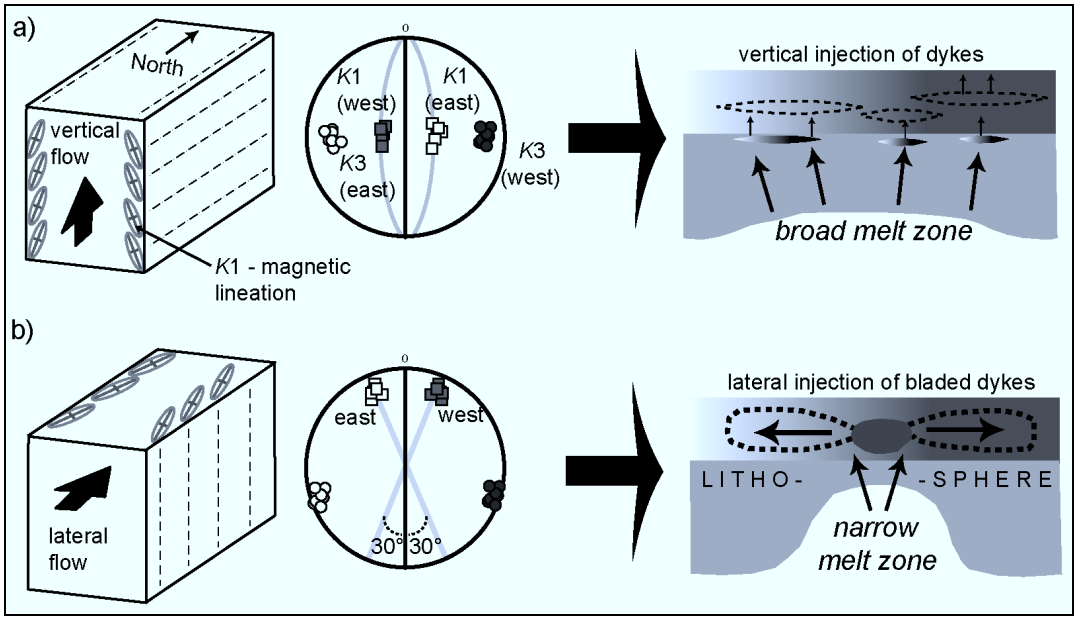

Figure 4: Schematic diagrams of a vertical, N–S striking dyke indicating idealised AMS fabric orientation resulting from (a) vertical intrusion of magma and (b) lateral intrusion of magma. Dyke plane is shown as N-S striking black line and the magnetic foliations in grey. Intermediate axes (*K*2) have been omitted for clarity. Not to scale (modified from Geoffroy et al., 2002 and Gil-Imaz et al., 2006). The application of AMS in determining the mode of dyke emplacement is illustrated by the simplified sketches on the right of each end-member of flow type (re-drawn from Callot et al., 2001). Lateral injection of bladed dykes is commonly associated with mantle plumes.

This is because the flow history is strongly controlled by the disposition of the melt source (e.g. broad vs. narrow melt zone, see Fig. 5), the characteristics of the crust (e.g. nature and orientation of stress) and the magma (e.g. overpressure, viscosity, neutral buoyancy level and volatile content). If a mantle plume is involved in the

injection of dykes from a local, narrow melt zone, it is expected that flow will be lateral (Ernst and Baragar, 1992; Fialko and Rubin, 1999) (Fig. 6).

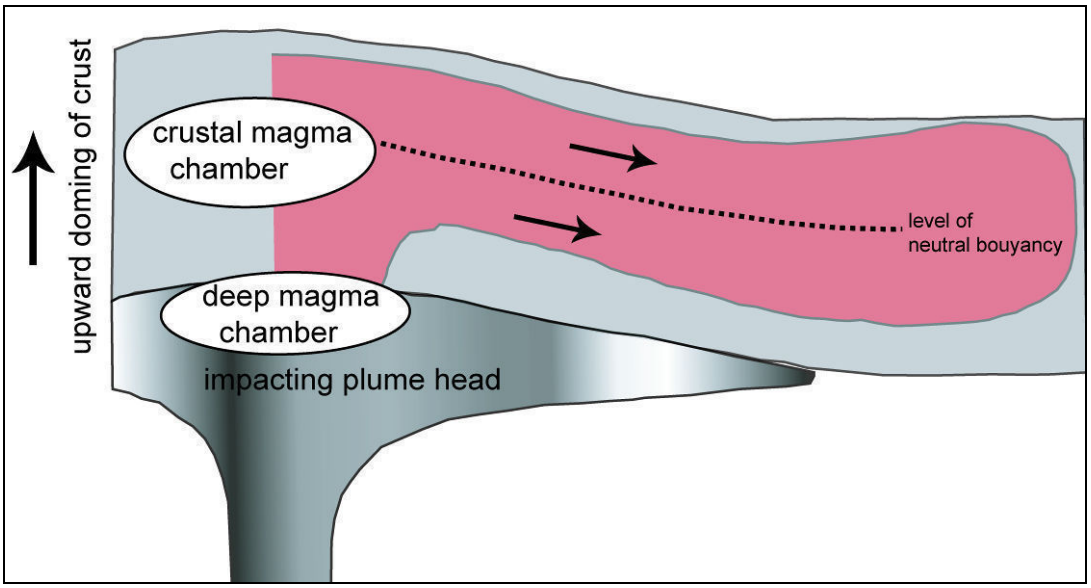

Figure 5: Schematic figure showing proposed lateral flow (arrows) of a dyke along the level of neutral magma buoyancy in the crust (not to scale). Note the doming caused by plume-related uplift (re-drawn from Fialko and Rubin, 1999).

It is important to note that AMS fabric may not be directly related to the original flow-fabric. For example, late-stage settling can cause compaction fabric, and even back-flow (downward flow) can occur in dykes (Aubourg et al., 2002; Philpotts and Philpotts, 2007).

Indeed late-stage flow may result in more complex or mixed fabrics resulting from significant grain interaction, as has been found in the RRDS (Hastie et al., 2011a). It is thus imperative to view the bulk AMS (and mineral SPO) data to provide a sense of the regional flow-fabric. This is done by plotting all the data together in order to observe and interpret the AMS, or other petrofabric, on a regional scale (Rochette et al., 1991; Tamrat and Ernesto, 1999; Callot et al., 2001; Aubourg et al., 2002; Archanjo and Launeau, 2004).

This can only be achieved, however, if a relatively large number of dykes (> 20) are studied across a region (Ernst and Baragar, 1992). From the NLDS, RRDS and ODS we discuss the regional significance of AMS data determined from a total of 60

894 dykes. We show AMS data plotted in a regional manner from a further 30 dykes from
895 west Dronning Maud Land.
896
897 This regional AMS fabric is shown in dyke co-ordinates, where data have been
898 rotated in accordance with the orientations of the dykes from which data was
899 collected. This essentially "normalizes" the data for ease of viewing and interpretation
900 (Rochette et al., 1991; Callot et al., 2001; Aubourg et al., 2008). In such a framework
901 it is easiest to observe and interpret the imbrication of the fabric (the bulk foliation as
902 determined by the grouping of *K*3 axes), should it occur. The "normalized" regional
903 data presented in the following sections is contoured on an equal area stereonet and
904 type-B fabric has been omitted.
905
906 *5.3. Mineral SPO*
907 The method of quantifying mineral SPO, as applied to the NLDS and RRDS, begins
908 by cutting three orthogonal thin sections per AMS sample. From these, between 300
909 and 2800 plagioclase grains per section are digitally imaged and analysed to
910 determine an inertia tensor from the 2-D SPO inertia ellipses (Launeau and Robin,
911 2005 and references therein). This ellipsoid, similarly to AMS, is defined by three
912 orthogonal principal axes ($L1 > L2 > L3$). We infer a sense of magma flow in the
913 same way as AMS – imbrication of the foliation defined by the principal ellipsoid
914 axes with respect to the dyke plane. The methodology of SPO study applied to the
915 RRDS and NLDS is covered in more detail by Hastie et al., (2011a).
916
917 **6. Results**
918 *6.1. Magnetic fabric of the NLDS*
919 Magnetic fabric has been studied in 14 dykes (224 samples) of the NLDS (Hastie et
920 al., 2011b). In the NLDS, magnetic fabric is carried by stoichiometric magnetite and
921 tends to be normal (type-A) to intermediate. Values of P' range from ~1.0 to 1.054
922 (mean: 1.027). The mean value of T in the NLDS is 0.027 with oblate fabric in 64 %
923 of the data.
924
925 Magnetic fabric in the youngest (D4) dykes is typically type-A and oblate in shape.
926 Vertical to sub-vertical *K*1 axes are found only in the prolate fabrics and these prolate
927 fabrics tend to be intermediate, although some are neutral to oblate in shape. Four

sites display scattered fabric, and another four sites display type-B fabric. Thus six dykes provide a measure of magma flow, including evidence of vertical and lateral flow. The grouped data (Fig. 7a) reflects these trends and, overall, is consistent with lateral magma flow from the north. Note that the bulk data are split according to western and eastern margins in order to easily see any imbrication of the fabric elements.

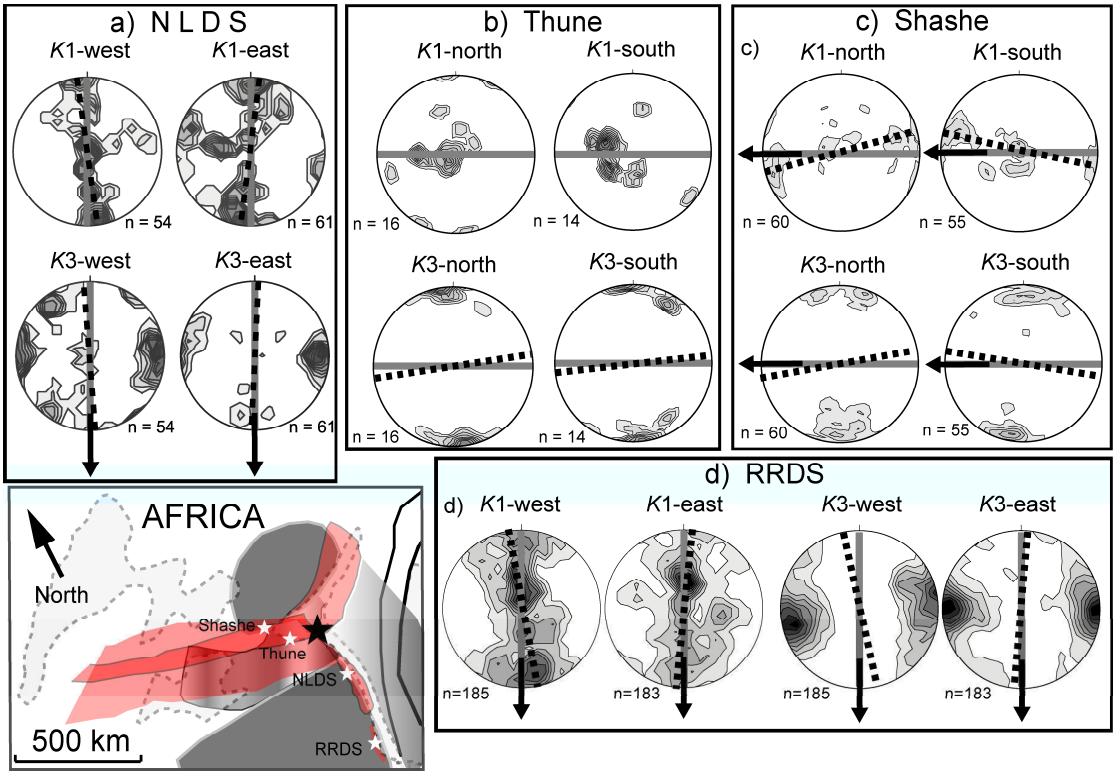

Figure 6: Grouped AMS data (type-A fabric only) for (a) the NLDS (from Hastie et al., 2011b), (b) the Thune section of the ODS (from Aubourg et al., 2008), (c) the Shashe section of the ODS (from Aubourg et al., 2008) and (d) the RRDS (Hastie et al., 2011a). Inset of the dyke swarms shows the sampled locations. The dyke planes in the stereoplots are shown in grey and the foliations as dashed black lines. Note that the ODS data have been rotated into a common E–W orientation and the NLDS and RRDS data into a common N–S orientation. The data are split according to the west and east margins (for NLDS and RRDS) and north and south (for the ODS) in order to find imbrication of the foliation or *K*1 axes. The number of samples is denoted by "n". Arrows indicate the magma flow direction inferred from the data. Note that the *K*1 axes for the Thune region, and the RRDS, show a degree of sub-vertical flow.

6.2. The Okavango dyke swarm

Ernst and Duncan (1995) were first to measure the magnetic fabric in the ODS using AMS, focussing their attention on the orientation of the magnetic lineation. These authors interpreted steeply plunging magnetic lineations close to the triple junction (<

300 km) and shallowly plunging lineations 400 km from the triple junction to indicate steep (vertical) flow and lateral (sub-horizontal) flow respectively.

The study of Aubourg et al. (2008) focussed on two regions of the ODS, the Thune and Shashe sections in which dykes of the ODS have intrude basement gneisses. The Thune and Shashe sections are 300 km and 400 km west of the Karoo triple junction respectively (Fig. 7). The overall magnetic fabric determined by AMS of 23 dykes (386 samples) is type-A. The fabric is carried by ferromagnetic grains. Thermomagnetic measurements indicate that paramagnetic susceptibility is negligible. However, Aubourg et al., (2008) showed that the type-B fabric most likely results from strong magnetization of some samples and the development of planar preferred orientation of ferromagnetic grains orthogonal to the dyke plane.

At the dyke scale in the Thune section (Fig. 6b) there is evidence of sub-vertical magma flow in the ODS, as well as lateral flow to the east and west. The magnetic fabric is less well defined in the Shashe section, although the imbrication of the magnetic foliations, in particular, is consistent with magma flow to the west (Aubourg et al., 2008). On the regional scale, the magnetic fabric in the ODS is well constrained and imbrication is most consistent with lateral magma flow from east to west (Fig. 7c).

6.3. The Rooi Rand dyke swarm

Dykes of the RRDS are plagioclase and augite bearing dolerites. Magnetic fabric measured in 23 dykes (368 samples) of the RRDS is predominantly type-A, carried by fine-grained, low-Ti magnetite. The fabric is generally weakly anisotropic (mean P'=1.030) and neutral to oblate in shape (mean T=0.073). In ~30% of the magnetic fabric data we found that the magnetic foliation or lineation was orthogonal to the dyke plane; this is type-B fabric (Hastie et al., 2011a).

The magnetic foliations are generally steeply dipping, and two dykes have shallowly plunging $K1$ axes, consistent with lateral magma flow. Field data tend to support steep (60°–80°) emplacement, although in 12 of the 23 dykes, inclined, sub-lateral and lateral magma flow is supported by AMS. The density plots of $K1$ and $K3$ axes for the RRDS are well constrained, comprising type-A fabric and the $K3$ axes in particular

are very tightly grouped and are weakly imbricated (Fig. 7d). The imbrication is suggestive of inclined to sub-lateral magma flow from the north.

6.4. Dykes of west Dronning Maud Land

As discussed already, Curtis et al. (2008) propose two distinct phases of mafic dyke emplacement (the JDS, then the SDS at 170.9±1.7 Ma) in the H.U. Sverdrupfjella of west Dronning Maud Land. Curtis et al. (2008) conducted AMS studies on 30 dykes, finding that 42% of the magnetic fabric is type-A. Furthermore, the fabric was found to be triaxial to oblate in shape with 1–4% anisotropy. This is very typical of mafic dykes. It is noted that the fabric becomes less well defined from north (48% type-A) to south (32% type-A). Intermediate fabric was found in 8% of the entire sample suite. The magnetic fabric appears to be carried by low-Ti magnetite, with type-A fabric arising from multi- and pseudo-single domain magnetite.

These authors use the *K*1 axis as a proxy for the magma flow direction, and find that the magnetic fabric is consistent with steep (sub-vertical) magma flow in the Straumsvola area (Fig. 8a), which is consistent with the orientation of stretched amygdales in one dyke of the SDS. When plotted together in N-S dyke co-ordinates, it is found that 61 of the averaged *K*3 axes (~51% of the data) are inverse (type-B fabric) (Fig. 8a). It has been found by numerous workers in AMS that mafic dykes tend to contain ~50% type-B fabric (Baer, 1995; Callot et al., 2001; Aubourg et al., 2008).

If this type-B component is removed and the margins are plotted separately we find *K*1 consistent with vertical and lateral flow (Fig. 8c). There is a very slight imbrication of the foliations that suggests lateral flow to the south (Fig. 8b). This is consistent with an increasing component of lateral flow ~25 km south of Straumsvola in the Jutulrøra region (Curtis et al., 2008). The lack of shallowly plunging *K*1 axes from the eastern margins is, however, inconsistent with this, as is the arguably weak imbrication, which likely reflects the vertical flow component of the Straumsvola region.

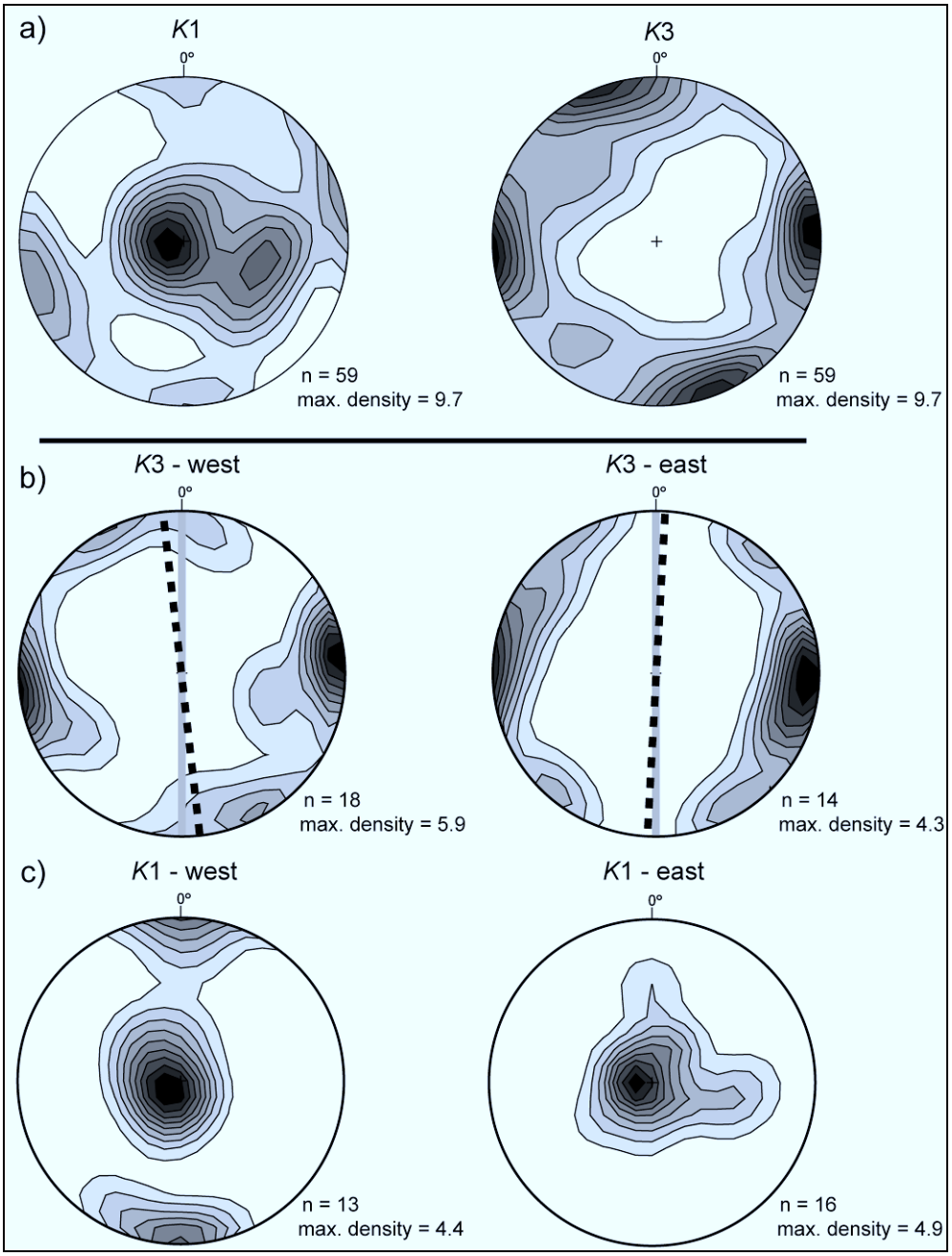

Figure 7: Bulk AMS data of the SDS and JDS from Curtis et al., (2008) plotted in a) N-S dyke co-ordinates and separated into b) *K*3 axes (N-S dyke co-ordinates) and c) *K*1 axes (N-S dyke co-ordinates). The N-S dyke plane is shown in grey and the foliation as a dashed black line. Note the slight imbrication of the foliations, which is consistent with the shallow plunging *K*1 axes from the western dyke margins in c). The (sub-) vertical *K*1 axes in c) are consistent with a component of steep, upward flow. The axes plotted are the averages from Table 2 of Curtis et al., (2008) (i.e. n = 59). The total number of samples measured = 480.

6.5. Mineral Shape Preferred Orientation

The results of the mineral SPO study are restricted to the bulk plagioclase fabric for the NLDS and RRDS. In the ODS Aubourg et al. (2008) does indicate that there is

generally good agreement between AMS and the orientation of plagioclase grains. There are no mineral SPO data available for the dykes of Dronning Maud Land.

The plagioclase fabric in the NLDS (7 dykes, 28 ellipsoids) is generally type-A, consistent with the magnetic fabric. The plagioclase fabric has a mean *P'* value of 1.208 and is predominantly triaxial to oblate (mean $T = 0.042$). The highest *P'* values for plagioclase are found in phenocryst-rich samples. Imbrication of the plagioclase SPO fabric is found in four dykes and southward verging imbrication of foliations in the bulk fabric occurs (Fig. 9a).

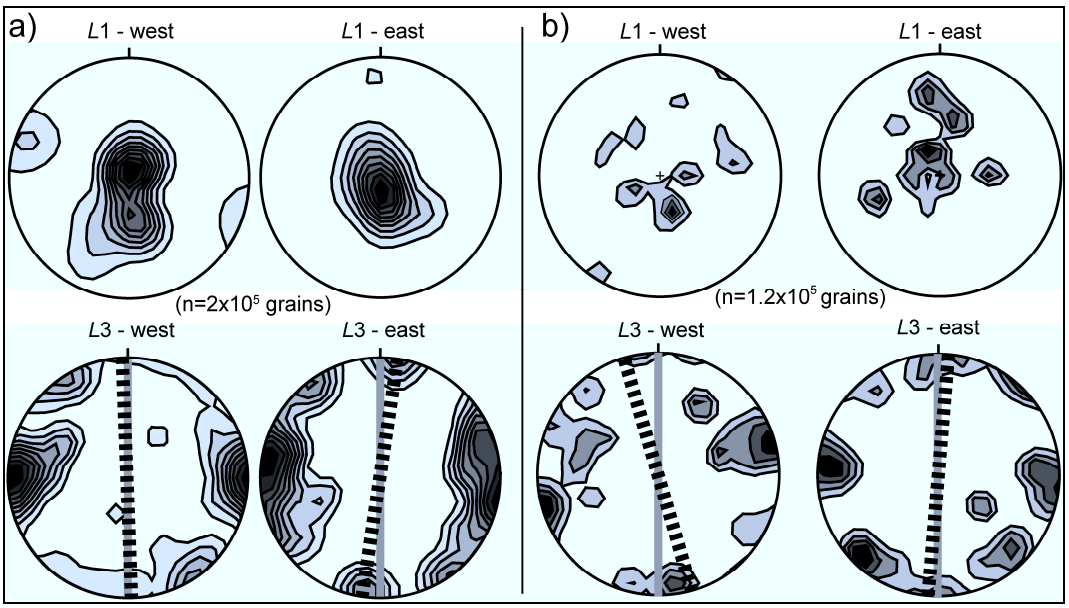

Figure 8: Mineral SPO data in N–S dyke co-ordinates for (a) the NLDS (from Fig. 10 of Hastie et al., 2011b) and (b) the RRDS. The average dyke planes are shown in grey, the foliations as dashed black lines. The *K*1 axes, of the NLDS in particular, suggest vertical flow but the imbrication of the foliations, although slight, is suggestive of lateral magma flow.

Although the *L*1 axes would be consistent with vertical magma flow, it has been shown that the foliations in this case are more reliable because of the coincidence between intersection lineations and the *L*1 axes (Hastie et al., 2011b). Furthermore, the geological significance of the lineation in a predominantly oblate fabric is debatable.

A total of 41 ellipsoids representative of the plagioclase fabric have been determined for 10 dykes of the RRDS. The fabric is predominantly neutral to oblate in shape ($T =$

0.04) with a mean *P'* value of 1.19. Approximately 30% of the plagioclase SPO fabric is type-B and prolate in shape (Hastie et al., 2011a). The remaining type-A fabric of 10 dykes is shown in N–S dyke co-ordinates in Figure 9b. Similarly to the NLDS we rely upon the orientation of the foliations to show the magma flow direction.

The foliation defined by the *L*3 axes for the western margins is well imbricated with respect to the average dyke orientation, and verges southward. The foliation from the eastern margins appears similar, although the imbrication is arguably not as obvious. Overall, this imbrication is consistent with magma flow directed from north to south. The *L*1 axes are consistent with flow inclined ~20° from the vertical.

7. Discussion

7.1. Magma flow in the dyke swarms

The significance of AMS fabric in 90 dykes related to the Karoo LIP has been presented (Riley et al., 2006; Aubourg et al., 2008; Curtis et al., 2008; Hastie et al., 2011a, b). Data for the NLDS are consistent with early vertical flow, followed by lateral flow in the later (D4) dykes. The regional pattern of AMS and SPO are consistent with each other, and subtly suggest a lateral sense of magma flow from north to south. This would be consistent with the Karoo triple junction being a viable magma source.

This is also reflected in the AMS data of the ODS. The shallowly plunging *K*1 axes and imbricated foliations of the Shashe region are both consistent with lateral flow from SE to NW, distally to the triple junction. The predominantly (sub-) vertical *K*1 axes from the Thune section (closer to the triple junction) are consistent with steeper (more vertical) magma flow. The lack of mirrored imbrication of the foliations in the Thune data also appears to preclude any significant degree of lateral magma flow. The magnetic and SPO fabric of the RRDS both have imbricated foliations consistent with flow from north to south. Both the *K*1 and *L*1 axes of the eastern dyke margins are consistent with a component of steep, sub-vertical magma flow. Kattenhorn (1994), using the SPO of plagioclase, also found relatively steep flow (23° from the vertical) in a dyke of the RRDS directed from north to south, which is also consistent with field evidence such as steeply plunging broken and rotated bridges along some dyke margins (Nicholson and Pollard, 1985; Bussel, 1989). This suggests that the RRDS

was not fed from the Karoo triple junction, as does the fact that the northern end of the RRDS terminates approximately 500 km south of Mwenezi.

If the RRDS indeed post-dates the Lebombo rhyolites and is indicative of lithospheric rupturing, it may be that the RRDS is analogous to a mid-ocean ridge segment. In such segments the dominant flow direction would be lateral in dykes distal to the vertically fed central axis. This has been previously demonstrated in such segments by Abelson et al., (2001) and Archanjo and Launeau, (2004) (Fig. 10).

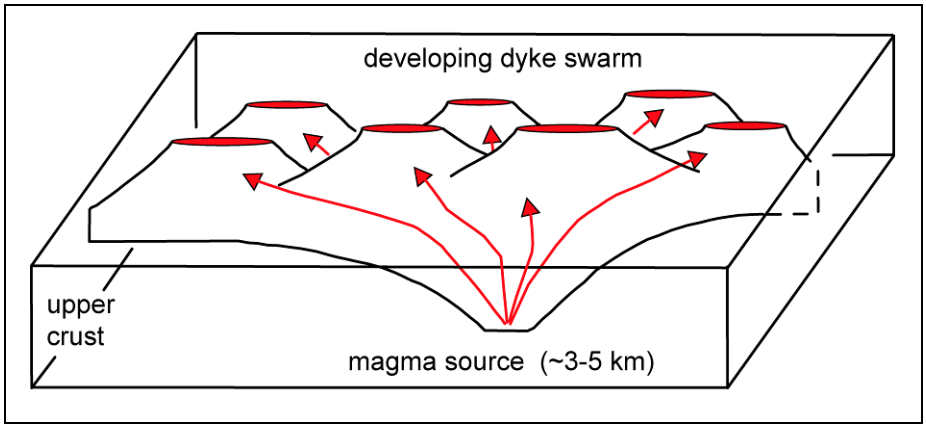

Figure 9: Schematic figure illustrating sub-lateral flow in dykes (the RRDS?) forming from a central, vertically fed magma source, analogous to the formation of mid-ocean ridge segments (re-drawn from Archanjo and Launeau, 2004).

The magnetic fabric in the JDS and SDS has two components. There is data consistent with steep (sub-vertical) magma flow in the north (Straumsvola) and with a lateral flow component further south (Jutulrøra) (Curtis et al., 2008). The steep omcponent is particularly evident from the *K*1 axes. The regional pattern of magma flow determined from the type-A fabric in N–S co-ordinates are consistent with this picture of flow from north to south, as can be seen from some of the shallowly plunging *K*1 axes of the western margins and the imbricated foliations. The flow directions for the dyke swarms under consideration are summarized diagrammatically in Figure 11. The flow direction determined from the UDS is included, but we do not speculate further on its significance because only three dykes showed reliable flow directions.

Curtis et al., (2008) suggest that the JDS (irrespective of the vertically or laterally intruded components) and Group 1 dykes should not be considered contiguous with the later Karoo LIP.

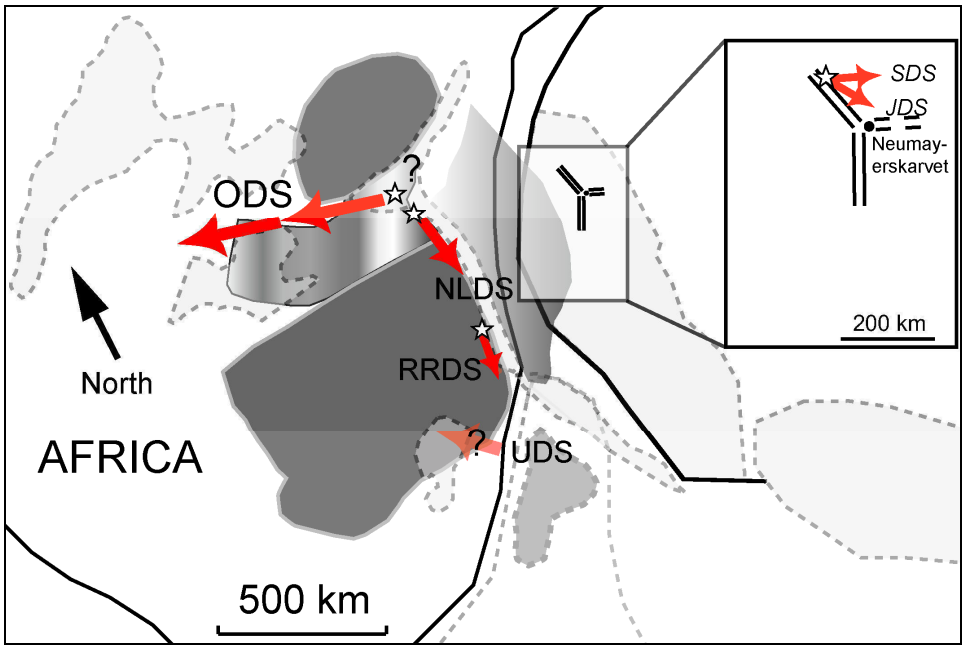

Figure 10: Regional schematic map of southern Gondwana between 178–174 Ma with magma flow directions inferred for the ODS, NLDS, RRDS, SDS and JDS. The flow direction of the UDS is uncertain ("?"). The red arrows indicate predominantly lateral flow while the stars indicate vertical flow. Note in the ODS, NLDS and RRDS that the edge of the Kaapvaal Craton strongly controls the distribution, and the flow directions, of the dyke swarms (base map re-drawn from White and McKenzie, 1989; Storey et al., 1992; Encarnación et al., 1996; Storey and Kyle, 1997; Watkeys, 2002; Jourdan et al., 2004; Ferraccioli et al., 2005; Riley et al., 2006; Curtis et al., 2008).

Magma flow data from the ADS and VDS would assist in shedding light on dyke emplacement in this region, because flow directed from the previously conjugate Africa-Antarctica margin would be consistent with the plume/melting anomaly position shown in Figure 4c (Cox, 1989; White and McKenzie, 1989; Storey et al., 1992; White, 1997; Elliot and Fleming, 2000; Curtis et al., 2008). The north-to-south flow direction found in the SDS and JDS is not compatible with the flow direction that would be expected from the Weddell Sea triple junction (Fig. 4e).

The overall flow pattern, although somewhat simplified, is consistent with the Karoo triple junction being an important magma source for the NLDS and ODS at least. It furthermore highlights the strong role played by the Limpopo Belt and Kaapvaal Craton in controlling the distribution of the Lebombo and Save-Limpopo monoclines

and the ODS. The locus of flow in the JDS and SDS is at least 500 km from the Karoo triple junction, as is the apparent locus for the RRDS. Linked with the field evidence and geochronology that argues for a dyking progression from JDS > NLDS > SDS > ODS > RRDS it seems unlikely that each melt locus could have been a separate mantle plume. Indeed, these loci may be "weak spots" exploited by magma impingement under tensional conditions.

7.2. Magma flow and the plume hypothesis

Magma flow in the NLDS and ODS suggest that lateral magma flow emanated from the Karoo triple junction. Bearing in mind the evidence for the earliest (nephelinites) and youngest (Mwenezi intrusions) igneous activity at the triple junction, it is reasonable to view the Karoo triple junction as a relatively long-lived (~183–174 Ma) magmatic point source within the region. Still, it remains to be established whether the Karoo triple junction developed as a result of mantle plume activity.

Only three proponents of the original mantle plume models suggest that the plume impinged directly beneath the triple junction (Burke and Dewey, 1973; Campbell and Griffiths, 1990; Storey, 1995). The other models place the mantle plume "head" between Dronning Maud Land and the southern African continent (Fig. 4c). This position, however, is not consistent with the directions of magma flow found in the dyke swarms of southern Africa.

It is apparent, therefore, that taking into account the triple junction geometry and the magma flow directions is insufficient evidence for proposing a mantle plume origin for the outwardly radiating dyke swarms and associated magmatism. When the age constraints on the dyke swarms are considered a number of inconsistencies come to light as well (Jourdan et al., 2004). Firstly, the SLDS was the earliest swarm to intrude and, along with the ODS, contains sub-parallel Proterozoic dykes which demonstrate a Jurassic-age exploitation of the older dyke direction. Secondly, dykes of the NLDS mostly pre-date, but also overlap with the ODS. Thirdly, the RRDS is considerably younger (174 Ma) and of asthenosphere-derived, MORB-like composition in comparison to other Karoo magmas (Saggerson et al., 1983; Armstrong et al., 1984; Meth, 1996). If we consider the principal $K1$ axes, and the finding of Kattenhorn (1994), it is evident that some degree of steep flow occurred in

the RRDS. Fourthly, the remaining dyke swarms (UDS, SLeDS and SBDS) bear no relation to the triple junction at all. There are currently no ages on the SLeDS and SBDS, although the fact that they have intruded through the basalts, similarly to the UDS, suggests that they may be ~178–176 Ma in age.

The agreement between the magma flow determinations and the triple junction does not exclude the triple junction from being an important magmatic source region, but the timing of the various dyke swarms is evidently a more important factor to consider than the magma flow direction alone. This is apparent in the dykes of west Dronning Maud Land. For example, the ADS, JDS, SDS and Group 1 dykes appear to show a radiating geometry (Fig. 1) which, along with other compositional and flow characteristics, could be considered indicative of a mantle plume. Indeed, the Straumsvola region has a protracted magmatic history. As discussed, however, magma flow from an igneous centre in the vicinity of Straumsvola at ~205 Ma predates Karoo magmatism by ~15 Ma, while the SDS was emplaced closer to 178 Ma. Thus, the JDS and Group 1 dykes should not be considered to be synchronous with the later Karoo LIP, and the remaining Karoo-aged dykes do not form a radiating pattern that could have resulted from a mantle plume, as first described by Curtis et al., (2008). It also appears highly unlikely that these dykes were fed by lateral intruding melts from the Weddell Sea or Karoo triple junction, but rather from a source coincident with the northeastern edge of the MTZ (Fig. 1). It would thus appear to be a position between (b) and (c) in Figure 4.

Having considered the relevant dyke swarms in relation to the pre-existing crustal architecture and in relation to relative and absolute ages, we can make two basic inferences. Firstly, the Karoo triple junction has been an important magmatic source for the Karoo LIP and, secondly, there is no evidence from the dyke swarms themselves for the influence of a mantle plume. There is a conflict between the magmatic sources amongst the southern African dykes, however. The NLDS and ODS certainly seem to have been fed from a magma source related to the triple junction at Mwenezi, but the UDS may have been fed from the SE and the RRDS intruded at a later stage, possibly after the Jozini rhyolites, and unrelated to a mantle plume. Without magma flow or any other data the origin of the SW-1 dyke swarm

remains enigmatic. It is most likely related to E–W extension between SE Africa and Antarctica and the consequent development of the MTZ.

7.3. Magma flow and passive melting

If a mantle plume did not give rise to the triple junction during the Jurassic, under what conditions did it arise, and how did the distribution of Karoo magmatism occur? Besides the effects of an impacting mantle plume, a triple junction may develop because of tensional stresses in the lithosphere owing to its curved shape because a curved surface responds differently under tension to a flat surface. Indeed, if dykes or dyke swarms exploit regions of lithospheric weakness, which has been demonstrated, it follows that the development of extensional regions on a curved surface would converge in triple junction-type geometry, without necessitating the influence of an upwelling plume from beneath.

In a passive model of magmatism the development of the Karoo LIP may have started because of a lack of cooling rather than active heating by a plume. Anderson et al. (1992) have suggested that crustal thinning above non-isothermal, inhomogeneous mantle is responsible for the formation of volcanic ridges and hotspots. This may be reflected in vertical magma flow in dykes, perhaps with some lateral flow outward from relatively small igneous centres. Evidently the accumulation and/or generation of heat and subsequent magmatism beneath the supercontinent of Gondwana would have weakened the crust, making continental break-up more likely as opposed to being a direct result of the emplacement of a plume beneath the supercontinent (Storey et al., 1992; White, 1997; Hawkesworth et al., 1999).

There has been considerable research into the potential effects of thermal insulation of the sub-continental mantle during times of supercontinent assembly preceding flood basalt formation and continental break-up (Anderson, 1994; Lenardic, 2005; Coltice et al., 2007; O'Neill et al., 2009; Heron and Lowman, 2011). For example, the depleted MORB-like magmas of Dronning Maud Land, generated from an anomalously "hot" source, are interpreted as being consistent with the melting model of Coltice et al. (2009). This potentially implicates internal heating of the upper mantle in Karoo magmatism, as opposed to a mantle plume (Heinonen et al., 2010).

Coltice et al. (2009) have simulated mantle convection beneath a supercontinent in 3-D. The results show that a supercontinent at the Earth's surface can have a significant impact on convection and temperature within the mantle. Their mantle global warming model predicts that (1) heating occurs over an area comparable in size to the overlying supercontinent, (2) melting occurs at modest (≤ 100 °C) temperature increases in the mantle, (3) melt is predominantly sourced from the asthenosphere and the continental lithosphere and (4) tectonic processes control the extraction of melt.

For continental cover >10% of the Earth's surface, the authors expect the subcontinental mantle to increase in temperature by > 75 °C over an area comparable in size to the "insulating" supercontinent. This process of mantle warming, alternatively to mantle plumes, is thus a feasible mechanism for the origin of some CFBs and the authors suggest that the mantle global warming model is becoming a more favourable explanation for the origin of the Karoo LIP. Their model is understandably not valid for all CFB provinces, mainly those that are unrelated to supercontinent dispersion, and for those in which mantle plume signature can be robustly demonstrated.

Indeed, even more recent modelling which incorporates both continental and oceanic plates in a supercontinent-type formation, suggests that this insulating effect is not strong and does not assist in elevating the mantle temperatures (Heron and Lowman, 2011). Instead, the presence of subduction zones surrounding such a supercontinent appears to strongly influence thermal convection beneath the lithosphere (O'Neill et al., 2009) and furthermore, a lack of movement of a supercontinent is a predominant factor in mantle insulation.

In modelling the assembly of a supercontinent Heron and Lowman (2011) have shown that a mantle plume forms beneath the crust at ~150 Ma after the subduction of oceanic crust between the adjoining continental plates. The return mantle flow, therefore, is predisposed to be beneath the supercontinent as the subduction zones are marginal (O'Neill et al., 2009). In the case of southern Africa, this would have occurred ~150 Ma prior to the Pan-African assembly of Gondwana at ~540 Ma (Rino et al., 2008). However, major expressions of Karoo volcanism did not occur for a further ~360 Ma. From the modelling, it appears that 6 mantle transit times are

required to produce continental dispersal (Zhong and Gurnis, 1993; Heron and Lowman, 2011). This is, perhaps fortuitously, equal to 60 Ma for each mantle transition, or 360 Ma. It is after 360 Ma that a plume-like upwelling forms beneath a supercontinent in the model, and is related to continuing subduction at the supercontinent margins (O'Neill et al., 2009).

Relating the above model directly to Gondwana break-up and the facets of the pre-cursory Karoo LIP in which we are interested in is speculative at best. However, it does fit quite well with the time constraints shown above, the structure and the geochemistry of the Karoo LIP that is best explained by a sub-continental lithospheric mantle (SCLM) melt source (Sweeney at al., 1994; Hawkesworth et al., 1999; Jourdan et al., 2007a). Jourdan et al. (2009) have shown that only a slight geochemical evolution has occurred in the enriched, shallow lithospheric mantle beneath southern Africa in the 900 Ma prior to the development of the Karoo LIP. These authors conclude that the SCLM model for the Karoo is well explained by enhanced melting due to subduction processes prior to, and the insulating effects during the formation of Pangaea which broke-up ~200 Ma ago. This is consistent with the model interpretations of Heron and Lowman (2011), who show that subduction related magmatic processes are an important consequence of supercontinent assembly.

8. Conclusions

We have briefly reviewed the geological setting, field relationships, petrology and geochronology of the Karoo LIP, focussing on magma flow determinations in dyke swarms for which there are data. We can conclude that:

1. Evidence for vertical and lateral flow exists in the magnetic and plagioclase SPO fabric of the NLDS, ODS and RRDS.
2. Lateral flow predominates in the ODS and the youngest dykes of the NLDS. This is consistent with the Karoo triple junction being a viable magma source for these swarms.
3. The only position for a mantle plume that would be consistent with this finding would be one emplaced directly beneath Mwenezi (Fig. 4a).
4. Evidence for lateral magma flow in the RRDS is consistent with the findings for the NLDS, but difficult to interpret in light of its restricted occurrence and

compositional and age differences. Steep flow coupled with evidence of lateral flow from AMS and SPO is most likely the result of outward flow from a central magmatic source.

5. The positions and orientations of the ODS, SLDS and Lebombo monocline are a product of the lithospheric structure, most obviously with respect to the ENE-trending structural fabric of the Limpopo Belt and the eastern edge of the Kaapvaal Craton.
6. Dykes of west Dronning Maud Land show a more protracted history (~205 Ma to ~175 Ma) than those of the Karoo LIP. The age and progression of magma flow characteristics is similar to the Karoo dyke swarms, however. Magma flow in the SDS and JDS is similar to that in the NLDS and ODS. Dykes close to Straumsvola have been fed (sub-) vertically and emplaced under high magmatic pressure.
7. Thus, it is highly unlikely that these dykes were fed by lateral intruding melts from the Weddell Sea or Karoo triple junction, but rather from a source coincident with a position between (b) and (c) in Figure 4. There is, therefore, inconsistency between magma sources of the southern African and Antarctic dykes of the Karoo LIP.
8. The influence of a mantle plume cannot be precluded but it is unlikely that the Karoo triple junction developed solely as the result of a mantle plume.
9. These results, in the framework of the known structure, field relationships and geochronology related to the Karoo triple junction, are significant. This is because they are superficially consistent with the pattern of radiating dyke emplacement typically associated with mantle plumes. However, in conjunction with high-resolution $^{40}Ar/^{39}Ar$ dating, relative timing of dyking events and geochemical and geodynamic considerations, the results do not necessitate a mantle plume for their origin.

Acknowledgements

This work forms part of the PhD research of W. Hastie, who gratefully acknowledges a NRF Innovation Scholarship. This work forms part of the PICS co-operative research program between the CNRS (France) and the NRF (South Africa).

References

Abelson, M., Baer, G., Agnon, A., 2001. Evidence from gabbro of the Troodos ophiolite for lateral magma transport along a slow-spreading mid-ocean ridge. Nature 409, 72–75.

Allsopp, H.L., Roddick, J.C., 1984. Rb-Sr and ^{40}Ar-^{39}Ar age determinations on phlogopite micas from the pre-Lebombo Group Dokolwayo kimberlite pipe. Geological Society of South Africa Special Publication 13, 267–272.

Anderson, D.L., 1985. Hotspot magmas can form by fractionation and contamination of MORB. Nature 318, 145–149.

Anderson, D.L., 1994. Superplumes or Supercontinents? Geology 22, 39–42.

Anderson, D.L., Zhang, Y.S., Tanimoto, T., 1992. Plume heads, continental lithosphere, flood basalts and tomography. In: Alabaster, T., Storey, B.C., Pankhurst, R.J. (Eds.), Magmatism and the Causes of Continental Break-up. Geological Society of London Special Publication 68, 99–124.

Archanjo, C.J., Launeau, P. 2004. Magma flow inferred from preferred orientations of plagioclase of the Rio Cearf-Mirim dyke swarm (NE Brazil) and its AMS significance. In: Martin-Hernandez, F., Luneburg, C.M., Aubourg, C., Jackson, M. (Eds.), Magnetic Fabric: Methods and applications. Geological Society of London Special Publication 238, 285–298.

Armstrong, R.A., Bristow, J.W., Cox, K.G., 1984. The Rooi Rand dyke swarm, southern Lebombo. In: Erlank, A.J. (Ed.), Petrogenesis of the volcanic rocks of the Karoo province. Geological Society of South Africa Special Publication 13, 77–86.

Aubourg, C., Giordano, G., Mattei, M., Speranza, F., 2002. Magma flow in sub-aqueous rhyolitic dikes inferred from magnetic fabric analysis (Ponza Island, W. Italy). Physics and Chemistry of the Earth 27, 1263–1272.

Aubourg, C., Tshoso, G., Le Gall, B., Bertrand, H., Tiercelin, J.-J., Kampunzu, A.B., Dyment, J., Modisi, M., 2008. Magma flow revealed by magnetic fabric in the Okavango giant dyke swarm, Karoo igneous province, northern Botswana. Journal of Volcanology and Geothermal Research 170, 247–261.

Baer, G., 1995. Fracture propagation and magma flow in segmented dykes: Field evidence and fabric analyses, Makhtesh Ramon, Israel. In: Baer, G., Heimann, A. (Eds.), Physics and Chemistry of Dykes. Balkema, Rotterdam, 125–140.

Bristow, J.W., 1982. Geology and structure of Karoo volcanic and sedimentary rocks of the northern and central Lebombo. Transactions of the Geological Society of South Africa 85, 167–178.

Bristow, J.W., 1984. Nephelinites of the north Lebombo and south-east Zimbabwe. In: Erlank, A.J. (Ed.), Petrogenesis of the volcanic rocks of the Karoo province. Geological Society of South Africa Special Publication 13, 87–104.

Bristow, J.W., Allsopp, H.L., Erlank, A.J., Marsh, J.S., Armstrong, R.A., 1984. Strontium isotope characterization of Karoo volcanic rocks. In: Erlank, A.J. (Ed.), Petrogenesis of the volcanic rocks of the Karoo province. Geological Society of South
Africa Special Publication 13, 295–329.

Bryan, S.E., Ernst, R.E., 2008. Revised definition of Large Igneous Provinces (LIPs). Earth-Science Reviews 86, 175–202.

Burke, K., Dewey, J.F., 1973. Plume generated triple junctions: key indicators in applying plate tectonics to old rocks. Journal of Geology 81, 406–433.

Bussel, M.A., 1989. A simple method for the determination of the dilation direction of intrusive sheets. Journal of Structural Geology 11, 679–687.

Callot, J.P., Geoffroy, L., Aubourg, C., Pozzi, J.P., Mege, D., 2001. Magma flow directions of shallow dykes from the East Greenland volcanic margin inferred from magnetic fabric studies. Tectonophysics 335, 313–329.

Campbell, I.H., Griffiths, R.W., 1990. Implications of mantle plume structure for the evolution of flood basalts. Earth and Planetary Science Letters 99, 79–93.

Cañón-Tapia, E., 2004. Anisotropy of magnetic susceptibility of lava flows and dykes: an historical account. In: Martín-Hernández, F., Lüneburg, C.M., Aubourg, C., Jackson, M. (Eds.), Magnetic Fabric: Methods and Applications. Geological Society of London Special Publication 238, 205–225.

Cañón-Tapia, E., 2010. Origin of large igneous provinces: The importance of a definition. In: Cañón-Tapia, E., Szakács, A. (Eds), What is a volcano? Geological Society of America Special Paper 470, 77–101.

Chaves, A.O., Correia Neves, J.M., 2005. Magmatism, rifting and sedimentation related to Late Paleoproterozoic mantle plume events of central and southeastern Brazil. Journal of Geodynamics 39, 197–208.

Coltice, N., Phillips, B.R., Bertrand, H., Ricard, Y., Rey, P., 2007. Global warming of the mantle at the origin of flood basalts over supercontinents. Geology 35, 391–394.

Coltice, N., Bertrand, H., Rey, P., Jourdan, F., Phillips, B.R., Ricard, Y., 2009. Global warming of the mantle beneath continents back to the Archaean. Gondwana Research 15, 254–266.

Courtillot, V.E., Renne, P.R., 2003. On the ages of flood basalt events. Comptes Rendus Geosciences 335, 113–140.

Cox, K.G., 1989. The role of mantle plumes in the development of continental drainage patterns. Nature 342, 873–877.

Cox, K.G., 1992. Karoo igneous activity, and the early stages of the break-up of Gondwanaland. In: Storey, B.C., Alabaster, T., Pankhurst R.J. (Eds.), Magmatism and the Causes of Continental Break-up. Geological Society of London Special Publication 68, 37–148.

Cox, K.G., Bristow, J.W., 1984. The Sabie river basalt Formation of the Lebombo monocline and south-east Zimbabwe. In: Erlank, A.J. (Ed.), Petrogenesis of the volcanic rocks of the Karoo province. Geological Society of South Africa Special Publication 13, 125–147.

Cox, K.G., Duncan, A.R., Bristow, J.W., Taylor, S.R., Erlank, A.J., 1984. Petrogenesis of the basic rocks of the Lebombo. In: Erlank, A.J. (Ed.), Petrogenesis of the volcanic rocks of the Karoo province. Geological Society of South Africa Special Publication 13, 149–169.

Cox, K.G., MacDonald, R., Hornung, G., 1967. Geochemical and petrogenetic provinces in the Karoo basalts of southern Africa. American Mineralogist 52, 1451–1474.

Curtis, M.L., Riley, T.R., Owens, W.H., Leat, P.T., Duncan, R.A., 2008. The form, distribution and anisotropy of magnetic susceptibility of Jurassic dykes in H.U. Sverdrupfjella, Dronning Maud Land, Antarctica. Implications for dyke swarm emplacement. Journal of Structural Geology 30, 1429–1447.

Du Toit, A.L., 1929. The volcanic belt of the Lebombo: a region of tension. Transactions of the Royal Society of South Africa 18, 189–218.

Duncan, A.R., 1987. The Karoo igneous province - a problem area for inferring tectonic setting from basalt geochemistry. Journal of Volcanology and Geothermal Research 32, 13–34.

Duncan, A.R., Erlank, A.J., Marsh, J.S., 1984. Regional geochemistry of the Karoo igneous province. In: Erlank, A.J. (Ed.), Petrogenesis of the Volcanic Rocks of the Karoo Province. Geological Society of South Africa Special Publication 13, 355–388.

Duncan, R.A., Hooper, P.R., Rehacek, J., Marsh, J.S., Duncan, A.R., 1997. The timing and duration of the Karoo igneous event, southern Gondwanaland. Journal of Geophysical Research 102, 18127–18138.

Eales, H.V., Marsh, J.S., Cox, K.G., 1984. The Karoo igneous province: An introduction. In: Erlank, A.J. (Ed.), Petrogenesis of the volcanic rocks of the Karoo province. Geological Society of South Africa Special Publication 13, 1–26.

Elburg, M., Goldberg, A., 2000. Age and geochemistry of Karoo dolerite dykes from northeast Botswana. Journal of African Earth Sciences 31, 539–554.

Ellam, R.M., 2006. New constraints on the petrogenesis of the Nuanetsi picrite basalts from Pb and Hf isotope data. Earth and Planetary Science Letters 245, 153–161.

Ellam, R.M., Carlson, R.W., Shirley, S.B., 1992. Evidence from Re–Os isotopes for plume–lithosphere mixing in Karoo flood basalt genesis. Nature 359, 718–721.

Ellam, R.M., Cox, K.G., 1989. A Proterozoic lithospheric source for Karoo magmatism: evidence from the Nuanetsi picrites. Earth and Planetary Science Letters 92, 207–218.

Ellam, R.M., Cox, K.G., 1991. An interpretation of Karoo picrite basalts in terms of interaction between asthenospheric magmas and mantle lithosphere. Earth and Planetary Science Letters 105, 330–342.

Elliot, D.H., 1975. Tectonics of Antarctica: a review. American Journal of Science 275, 45–106.

Elliot, D.H., Fleming, T.H. 2000. Weddell triple junction: The principal focus of Ferrar and Karoo magmatism during initial breakup of Gondwana. Geology 28, 539–542.

Elliot, D.H., Fleming, T.H., 2004. Occurrence and Dispersal of Magmas in the Jurassic Ferrar Large Igneous Province, Antarctica. Gondwana Research 7, 223–237.

Elliot, D.H., Fleming, T.H., Kyle, P.R., Foland, K.A., 1999. Long-distance transportation of magmas in the Jurassic Ferrar Large Igneous Province, Antarctica. Earth and Planetary Science Letters 167, 89–104.

Encarnación, J., Fleming, T.H., Elliot, D.H., Eales, H.V., 1996. Synchronous emplacement of Ferrar and Karoo dolerites and the early breakup of Gondwana. Geology 24, 535–538.

Erlank, A.J., 1984. Petrogenesis of the volcanic rocks of the Karoo province, Geological Society of South Africa Special Publication 13, 395 pp.

Ernst, R.E., Baragar, W.R.A., 1992. Evidence from magnetic fabric for the flow pattern of magma in the Mackenzie giant radiating dyke swarm. Nature 356, 511–513.

Ernst, R.E., Buchan, K.L., 1997. Giant Radiating Swarms: Their Use in Identifying Pre-Mesozoic Large Igneous Provinces and Mantle Plumes. Geophysical Monographs 100, 297–333.

Ernst, R.E., Duncan, A.R., 1995. Magma flow in the Giant Botswana dyke swarm from analysis of magnetic fabric (abstract). In: Agnon, A., Baer, G., (Eds.), Program & Abstracts for the Third International Dyke Conference, September 4-8, Jerusalem, Israel, pp. 30.

Ferraccioli, F., Jones, P.C., Curtis, M.L., Leat, P.T., 2005. Subglacial imprints of early Gondwana break-up as identified from high resolution aerogeophysical data over western Dronning Maud Land, East Antarctica. Terra Nova 17, 573–579.

Fialko, Y.A., Rubin, A.M., 1999. Thermal and mechanical aspects of magma emplacement in giant dike swarms. Journal of Geophysical Research 104, 23033–23049.

Fleming, T.H., Poland, K.A., Elliot, D.H., 1995. Isotopic and chemical constraints on the crustal evolution and source signature of Ferrar magmas, north Victoria Land, Antarctica. Contributions to Mineralogy and Petrology 121, 217–236.

Geoffroy, L., Aubourg, C., Callot, J.P., Moreira, M., 2002. Is the common use of AMS in mafic dykes scientifically correct? Terra Nova 14, 183–190.

Gil-Imaz, A., Pocoví, A., Lago, M., Galé, C., Arranz, E., Rillo, C., Guerrero, E., 2006. Magma flow and thermal contraction fabric in tabular intrusions inferred from AMS analysis. A case study in a late-Variscan folded sill of the Albarracı´n Massif (southeastern Iberian Chain, Spain). Journal of Structural Geology 28, 641–653.

Goodlad, S.W., Martin, A.K., Hartnady, C.J.H., 1982. Mesozoic magnetic anomalies in the southern Natal valley. Nature 295, 686–688.

Hastie, W.W., Aubourg, C., Watkeys, M.K., 2011a. When an 'inverse' fabric is not inverse: an integrated AMS-SPO study in MORB-like dykes. Terra Nova 23, 49–55.

Hastie, W.W., Watkeys, M.K., Aubourg, C., 2011b. Significance of magnetic and petrofabric in Karoo-feeder dykes, northern Lebombo. Tectonophysics 513, 96–111.

Hawkesworth, C.J., Kelley, S., Turner, S., Le Roex, A., Storey, B.C., 1999. Mantle processes during Gondwana break-up and dispersal. Journal of African Earth Sciences 28, 239–261.

Hawkesworth, C.J., Marsh, J.S., Duncan, A.R., Erlank, A.J., Norry, M.J., 1984. The role of continental lithosphere in the generation of the Karoo volcanic rocks: evidence from combined Nd- and Sr-isotope studies. In: Erlank, A.J. (Ed.), Petrogenesis of the volcanic rocks of the Karoo province. Geological Society of South Africa Special Publication 13, 341–354.

Heimann, A., Fleming, T.H., Elliot, D.H., Foland, K.A., 1994. A short interval of Jurassic continental flood basalt volcanism in Antarctica as demonstrated by $^{40}Ar/^{39}Ar$ geochronology. Earth and Planetary Science Letters 121, 19–41.

Heinonen, J.S., Luttinen, A.V., 2010. Mineral chemical evidence for extremely magnesian subalkaline melts from the Antarctic extension of the Karoo large igneous province. Mineralogy and Petrology 99, 201–217.

Heron P.J., Lowman J.P., 2011. The effects of supercontinent size and thermal insulation on the formation of mantle plumes. Tectonophysics 510, 28–38.

Henry, B., 1997. The magnetic zone axis: a new element of magnetic fabric for the interpretation of the magnetic lineation. Tectonophysics 271, 325–356.

Hergt, J.M., Peate, D.W., Hawkesworth, C.J., 1991. The petrogenesis of Mesozoic Gondwana low-Ti flood basalts. Earth and Planetary Science Letters 105, 134–148.

Jokat, W., Boebel, T., König, M., Meyer, U., 2003. Timing and geometry of the early Gondwana breakup. Journal of Geophysical Research. 108, 1–15.

Jourdan, F., Bertrand, H., Féraud, G., Le Gall, B., Watkeys, M.K., 2009. Lithospheric mantle evolution monitored by overlapping large igneous provinces: Case study in southern Africa. Lithos 107, 257–268.

Jourdan, F., Bertrand, H., Sharer, U., Blichert-Toft, J., Féraud, G., Kampunzu, A.B., 2007a. Major and trace element and Sr, Nd, Hf, and Pb isotope compositions of the Karoo large igneous province, Botswana–Zimbabwe: lithosphere vs. mantle plume contribution. Journal of Petrology 48, 1043–1077.

Jourdan, F., Féraud, G., Bertrand, H., Kampunzu, A.B., Tshoso, G., Le Gall, B., Tiercelin, J.J., Capiez, P., 2004. The Karoo triple junction questioned: evidence from Jurassic and Proterozoic $^{40}Ar/^{39}Ar$ ages and geochemistry of the giant Okavango dyke swarm (Botswana). Earth and Planetary Science Letters 222, 989–1006.

Jourdan, F., Féraud, G., Bertrand, H., Kampunzu, A.B., Tshoso, G., Watkeys, M.K., Le Gall, B., 2005. Karoo large igneous province: Brevity, origin and relation to mass extinction questioned by new $^{40}Ar/^{39}Ar$ age data. Geology 33, 745–748.

Jourdan, F., Féraud, G., Bertrand, H., Watkeys, M.K., Kampunzu, A.B., Le Gall, B., 2006. Basement control on dyke distribution in Large Igneous Provinces: Case study of the Karoo triple junction. Earth and Planetary Science Letters 241, 307–322.

Jourdan, F., Féraud, G., Bertrand, H., Watkeys, M.K., 2007b. From flood basalts to the inception of oceanization: Example from the $^{40}Ar/^{39}Ar$ high-resolution picture of the Karoo large igneous province. Geochemistry, Geophysics, Geosystems 8, 989–1006.

Jourdan, F., Féraud, G., Bertrand, H., Watkeys, M.K., Renne, P.R., 2007c. Distinct brief major events in the Karoo large igneous province clarified by new $^{40}Ar/^{39}Ar$ ages on the Lesotho basalts. Lithos 98, 195–209.

Kattenhorn, S.A., 1994. Mechanisms of sill and dyke intrusion (unpubl. MSc. thesis), University of Natal, Durban, South Africa 149 pp.

Klausen, M.B., 2009. The Lebombo monocline and associated feeder dyke swarm: Diagnostic of a successful and highly volcanic rifted margin? Tectonophysics 468, 42–62.

Kyle, P.R., Elliot, D.H., Sutter, J.P., 1981. Jurassic Ferrar Supergroup tholeiites from the Transantarctic Mountains, Antarctica, and their relationship to the initial fragmentation of Gondwana. In: Cresswell, M.M., Vella, P. (Eds.), Gondwana Five. A.A. Balkema, Rotterdam, 283–287.

Leat, P.T., 2008. On the long-distance transport of Ferrar magmas. In: Thomson, K., Petford, N. (Eds.), Structure and Emplacement of High-Level Magmatic Systems. Geological Society of London Special Publication 302, 45–61.

Le Gall, B., Tshoso, G., Dyment, J., Kampunzu, A.B., Jourdan, F., Féraud, G., Bertrand, H., Aubourg, C., Vétela, W., 2005. The Okavango giant mafic dyke swarm (NE Botswana): its structural significance within the Karoo Large Igneous Province. Journal of Structural Geology 27, 2234–2255.

Le Gall, B., Thsoso, G., Jourdan, F., Fe´raud, G., Bertrand, H., Tiercelin, J.J., Kampunzu, A.B., Modisi, M., Dyment, J., Maia, M., 2002. $^{40}Ar–^{39}Ar$ geochronology and structural data from the giant Okavango and related mafic dyke swarms, Karoo igneous province, N Botswana. Earth and Planetary Science Letters 202, 595–606.

Leinweber, V.T., Jokat, W., 2012. The Jurassic history of the Africa-Antarctica Corridor - new constraints from magnetic data on the conjugate continental margins. Tectonophysics 530–531, 87–101.

Lenardic, A., Moresi, L.-N., Jellinek, A.M., Manga, M., 2005. Continental insulation, mantle cooling, and the surface area of oceans and continents. Earth and Planetary Science Letters 234, 317–333.

Luttinen, A.V., Leat, P.T., Furnes, H., 2010. Björnnutane and Sembberget basalt lavas and the geochemical provinciality of Karoo magmatism in western Dronning Maud Land, Antarctica. Journal of Volcanology and Geothermal Research 198, 1–18.

Luttinen, A.V., Rämö, O.T., Huhma, H., 1998. Neodymium and strontium isotopic and trace element composition of a Mesozoic CFB suite from Dronning Maud Land, Antarctica: Implications for lithosphere and asthenosphere contributions to Karoo magmatism. Geochimica et Cosmochimica Acta 62, 2701–2714.

Marsh, J.S., 1987. Basalt geochemistry and tectonic discrimination within continental flood basalt provinces. Journal of Volcanology and Geothermal Research 32, 35–49.

Marsh, J.S., 2002. Discussion: ‘‘The geophysical mapping of Mesozoic dyke swarms in southern Africa and their origin in the disruption of Gondwana’’ [J. Afr. Earth Sci. 30 (2000) 499–513]. Journal of African Earth Sciences 35, 525–527.

Martin, A.K., Hartnady, C.J.H., 1986. Plate tectonic development of the South West Inidian Ocean: a revised reconstruction of East Antarctica and Africa. Journal of Geophysical Research 91, 4767–4786.

McClintock, M., White, J.D.L., Houghton, B.F., Skilling, I.P., 2008. Physical volcanology of a large crater-complex formed during the initial stages of Karoo flood basalt volcanism, Sterkspruit, Eastern Cape, South Africa. Journal of Volcanology and Geothermal Research 172, 93–111.

Mekonnen, T.K., 2004. Interpretation & Geodatabase of Dykes Using Aeromagnetic Data of Zimbabwe and Mozambique (unpubl. MSc. thesis), International Institute for Geoinformation Science and Earth Observation, Enschede, The Netherlands, 72 pp.

Meth, D.L., 1996. The Geology and Geochemistry of the Rooi Rand Dyke Swarm (unpubl. MSc. thesis), University of Natal, South Africa, 189 pp.

Nicholson, R., Pollard, D.D., 1985. Dilation and linkage of echelon cracks. Journal of Structural Geology 7, 583-590.

O'Neill, C., Lenardic, A., Jellinek, A.M., Moresi, L., 2009. Influence of supercontinents on deep mantle flow. Gondwana Research 15, 276–287.

Reeves, C., 1978. A failed Gondwana spreading axis in southern Africa. Nature 273, 222–223.

Reeves, C.V., 2000. The geophysical mapping of Mesozoic dyke swarms in southern Africa and their origin in the disruption of Gondwana. Journal of African Earth Sciences 30, 499–513.

Riley, T.R., Curtis, M.L., Leat, P.T., Watkeys, M.K., Duncan, R.A., Millar, I.L., Owens, W.H., 2006. Overlap of Karoo and Ferrar magma types in KwaZulu-Natal, South Africa. Journal of Petrology 47, 541–566.

Riley, T.R., Knight, K.B., 2001. Age of pre-break-up Gondwana magmatism: a review. Antarctic Science 13, 99–110.

Riley, T.R., Leat, P.T., Curtis, M.L., Millar, L.L., Fazel, A., 2005. Early-Middle Jurassic dolerite dykes from western Dronning Maud Land (Antarctica): identifying mantle sources in the Karoo large igneous province. Journal of Petrology 46, 1489–1524.

Riley, T.R., Millar, L.L., Watkeys, M.K., Curtis, M.L., Leat, P.T., Klausen, M.B., Fanning, C.M., 2004. U-Pb zircon (SHRIMP) ages for the Lebombo rhyolites, South Africa: refining the duration of Karoo volcanism. Journal of the Geological Society of London 161, 547–550.

Rino, S., Kon, Y., Sato,W., Maruyama, S., Santosh, M., Zhao, D., 2008. The Grenvillian and Pan-African orogens: world's largest orogenies through geologic time, and their implications on the origin of superplume. Gondwana Research 14, 51–72.

Rochette, P., Aubourg, C., Perrin, M., 1999. Is this magnetic fabric normal? A review and case studies in volcanic formations. Tectonophysics 307, 219–234.

Rochette, P., Jenatton, L., Dupuy, C., Boudier, F., Reuber, I., 1991. Diabase dyke emplacement in the Oman ophiolite: a magnetic fabric study with reference to geochemistry. In: Peters, T., Nicolas, A., Coleman, R.G. (Eds.), Ophiolite genesis and evolution of the oceanic lithosphere. Ministry of Petroleum and Minerals, Sultanate of Oman. 55–82.

Saggerson, E.P., Bristow, J.W., Armstrong, R.A., 1983. The Rooi Rand dyke swarm. South African Journal of Science 79, 365–369.

Silver, P.G., Behn, M.D., Kelley, K., Schmitz, M., Savage, B., 2006, Understanding cratonic flood basalts. Earth and Planetary Science Letters 245, 190–201.

Smith, R.A., 1984. The lithostratigraphy of the Karoo Supergroup in Botswana. Bulletin of the Geological Survey of Botswana 26, 239.

Storey, B.C., 1995. The role of mantle plumes in continental breakup: case histories from Gondwanaland. Nature 377, 301–308.

Storey, B., Alabaster, T., Hole, M.J., Pankhurst, R.J., Wever, H.E., 1992. Role of subduction-plate boundary forces during the initial stages of Gondwana break-up: evidence from the proto-Pacific margin of Antarctica. In: Storey, B.C., Alabaster, T., Pankhurst, R.J. (Eds.), Magmatism and the Causes of Continental Break-up 68, 149–163.

Storey, B.C., Kyle, P.R., 1997. An active mantle mechanism for Gondwana break-up. South African Journal of Geology 100, 283–290.

Storey, B.C., Leat, P.T., Ferris, J.K., 2001. The location of mantle–plume centers during the initial stages of Gondwana breakup. In: Ernst, R.E., Buchan, K.L. (Eds.), Mantle Plumes: Their identification through time. Geological Society of America Special Paper 352, 71–80.

Sweeney, R.J., Duncan, A.R., Erlank, A.J., 1994. Geochemistry and petrogenesis of central Lebombo basalts from the Karoo Igneous Province. Journal of Petrology 35, 95–125.

Sweeney, R.J., Falloon, T.J., Green, D.H., Tatsumi, Y., 1991. The mantle origins of Karoo picrites. Earth and Planetary Science Letters 107, 256–271.

Sweeney, R.J., Watkeys, M.K., 1990. A possible link between Mesozoic lithospheric architecture and Gondwana flood basalts. Journal of African Earth Sciences 10, 707–716.

Tamrat, E., Ernesto, M., 1999. Magnetic fabric and rock-magnetic character of the Mesozoic flood basalts of the Paranâ Basin, Brazil. Journal of Geodynamics 28, 419–437.

Uken, R., Watkeys, M.K., 1997. An interpretation of mafic dyke swarms and their relationship with major mafic magmatic events on the Kaapvaal Craton and Limpopo Belt. South African Journal of Geology 100, 341–349.

Watkeys, M.K., 2002. Development of the Lebombo rifted volcanic margin of southeast Africa. In: Menzies, M.A., Klemperer, S.L., Ebinger, C.J., Baker, J. (Eds.), Volcanic Rifted Margins. Geological Society of America Special Paper 362, 27–46.

White, R.S., 1997. Mantle Plume origin for the Karoo and Ventersdorp Flood Basalts, South Africa. South African Journal of Geology 100, 271–283.

White, R.S., McKenzie, D., 1989. Magmatism at rift zones: The generation of volcanic continental margins and flood basalts. Journal of Geophysical Research 94, 7685–7729.

Zhang, X., Luttinen, A.V., Elliot, D.H., Larsson, K., Foland, K.A., 2003. Early stages of Gondwana breakup: The $^{40}Ar/^{39}Ar$ geochronology of Jurassic basaltic rocks from western Dronning Maud Land, Antarctica, and implications for the timing of magmatic and hydrothermal events. Journal of Geophysical Research 108, 2449.

Zhong, S., Gurnis, M., 1993. Dynamic feedback between a continent like raft and thermal convection. Journal of Geophysical Research 98, 12219–12232.

- Appendix C -

Conference Proceedings

1. Hastie, W.W., Aubourg, C., Watkeys, M.K., 2009. Orthogonal AMS and SPO fabrics in the MORB-like Rooi-Rand dyke swarm of South Africa and Swaziland. Abstracts, 11th biennial conference and exhibition of the South African Geophysical Association (SAGA). Mbabane, Swaziland, pp. 66.

2. Hastie, W.W., Watkeys, M.K., Aubourg, C., 2011. Problems associated with interpreting magmatic fabrics. 23rd Colloquium for African Geology (CAG-23). Abstracts, University of Johannesburg, South Africa, pp. 180.

Orthogonal AMS and SPO fabrics in the MORB-like Rooi-Rand dyke swarm of South Africa and Swaziland

Warwick Hastie[1], C. Aubourg[2], M. K. Watkeys[3]

1. School of Geological Sciences, University of KwaZulu-Natal, South Africa, 203505849@ukzn.ac.za
2. University of Cergy Pontoise, Cergy, France, charly.aubourg@u-cergy.fr
3. School of Geological Sciences, University of KwaZulu-Natal, South Africa, watkeys@ukzn.ac.za

ABSTRACT

The cause of the ca. 185-175 Ma Karoo volcanism in southern Africa has been ascribed to the presence of a mantle plume centred on the Nuanetsi (now Mwenezi) Igneous Province, southern Zimbabwe. In the mantle plume model, this area is considered to represent a triple junction between the WNW-trending Okavango Dyke Swarm (ODS), the ENE-trending Sabi monocline and the N-S trending Lebombo monocline. The plume model predicts that magma flow in Karoo dykes of the Lebombo monocline should be away from the plume head and should be sub-horizontal in the distal regions. A brief study of the anisotropy of magnetic susceptibility (AMS) of 23 dykes in the MORB-like Rooi-Rand dyke swarm (RRDS) is presented. The AMS in the samples results from fine-grained, Ti-poor magnetite which in 20 dykes defines fabric sub-parallel to the dyke plane, consistent with the plume model. The magnetite defines a weakly anisotropic and dominantly oblate fabric. From a total of 10 dykes studied for plagioclase mineral shape preferred orientation (SPO), 8 have a dyke-parallel foliation most consistent with vertical magma flow. The plagioclase grains define a weakly anisotropic, oblate fabric, which is magmatic in origin. In 8 dykes this fabric is coaxial with the AMS fabric. However, in 40% of the dykes, the fabric defined by the SPO of opaque grains is non-coaxial with AMS and is at a high angle to the dyke plane and dips steeply. The non-coaxial AMS and SPO fabric, coupled with the orthogonal SPO fabrics suggests that late-stage lateral flow of relatively high viscosity magma has occurred. This results in a fabric which most workers would regard as "inverse" and/or non-magmatic, and, therefore, would misinterpret.

Key words: Lebombo monocline, Karoo mantle plume, AMS, magma flow

INTRODUCTION

Studies of the anisotropy of magnetic susceptibility (AMS) in magmatic rocks tend to focus on results which reveal flow-related fabrics, and are therefore geodynamically significant in terms of magmatic emplacement directions and conditions (Knight & Walker, 1988 ; Aubourg *et al*., 2008). This study began as such, focusing on the magnetic fabrics of MORB-like dolerite dykes of the Rooi-Rand dyke swarm (RRDS). However, the appearance of significant "inverse" and irregular magnetic fabrics allowed a shift in focus of the study. Inverse magnetic fabrics are generally attributed to the appearance of very fine-grained single domain (SD) magnetite grains (Rochette *et al*., 1999). The results of this study, however, show that the magnetic fabric, when compared to the silicate fabric (mineral shape preferred orientation [SPO]), suggests that both the AMS and SPO fabrics are the result of very late-stage flow of highly viscous magma.

The RRDS is a north-south (N-S) trending dyke swarm, approximately 200km long, extending from the Msunduze River in KwaZulu-Natal northwards into east-central Swaziland (Saggerson *et al.*, 1983 ; Duncan *et al.*, 1990 ; Meth, 1996) (Figure 1). The swarm is 10-22km thick and intruded basalts and sedimentary rocks of the Karoo Supergroup just to the west of the main Lebombo range, which comprises mostly rhyolites (Eales *et al.*, 1984). The Lebombo faulted monocline developed during extensive Karoo magmatism from ~184 Ma to ~174 Ma, during which some $3x10^6$ km^2 of basaltic lava covered parts of Southern Africa and Antarctica (Eales *et al.*, 1984 ; Encarnación *et al.*, 1996). The eastward tilting and domino-style faulting has resulted in a monocline-type appearance – owing to the separation of Antarctica from what is now the northeast coast of South Africa during the break-up of Gondwana (Eales *et al.*, 1984 ; Watkeys, 2002).

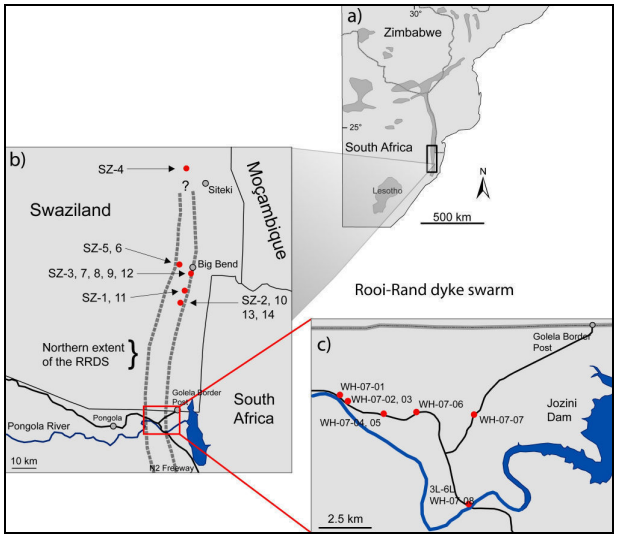

Figure 1: Locality maps of the Rooi-Rand dyke swarm showing a) the sampled area of the Lebombo monocline (dark grey) (re-drawn from Cox, 1992), b) south eastern Swaziland and the sampling sites of the northern RRDS and c) sampling sites of the central RRDS along the Pongola River in northern KwaZulu-Natal province, South Africa.

METHODOLOGY

Sampling

Core samples 25mm in diameter and 40-200mm in length were taken from opposing margins of a single dyke using a hand-held petroleum powered drill. Each sample is orientated using both a core-orientator magnetic compass and sun compass. For this study in particular, 12 samples from the central RRDS were used and 48 samples from the northern RRDS, representing a total of 7 dykes (see Figure 1).

Anisotropy of Magnetic Susceptibility

Anisotropy of magnetic susceptibility (AMS) has become a standard tool for the analysis of rock fabrics, most notably characterizing possible flow related fabrics in volcanic and intrusive rocks (Khan, 1962 ; Ellwood, 1978 ; Knight & Walker, 1988 ; Rochette *et al.*, 1992 ; Dragoni *et al.*, 1997). AMS is represented as an ellipsoid, the shape and orientation of which is most commonly described. The magnetic lineation is referred to as k1 and the pole to magnetic foliation as k3. In dykes, AMS ellipsoids are determined from opposing margins of an intrusion, which provide constraint on the original magma flow orientation because it is possible to recognize imbrication of either the magnetic foliation, lineation or both which may provide the magma flow sense (Geoffroy *et al.*, 2002). Minerals such as multi-domain (MD) magnetite, pyrrhotite, hematite and phyllosilicates are the most common carriers of magnetic susceptibility which have a normal magnetic fabric although single domain (SD) magnetite is commonly inverse (Potter and Stephenson, 1988 ; Rochette *et al.*, 1999). With increasing use of AMS it has become evident that complications arise during the interpretation of AMS data, mostly regarding the shape of the fabric, its relation to the rock fabric/orientation (e.g. the dyke plane in this case) and also the relationship between the magnetic minerals and the fabric which they produce (e.g. Launeau and Cruden, 1998). Thus, the aim here is to possibly unravel some causes of such complications through quantitative thermal experiments and the relationship between rock fabric and magnetic fabric is examined using the shape preferred orientation (SPO) of both opaque mineralogy and plagioclase grains.

Mineral Shape Preferred Orientation

Magmatic flow in intrusions results in rigid body rotation and movement of crystals in the magma (Cañón-Tapia and Chávez-Álvarez, 2004). As a result, the recognition of magmatic flow in the rock fabric is usually in the form of a shape preferred orientation (SPO) of inequant grains, such as plagioclase. Such data is therefore useful as it supplements AMS data for the purpose of determining magma flow direction. The work presented provides a detailed account of the mineral SPO in the RRDS, in which the ratio of AMS samples to SPO samples will be ~4:1, as opposed to ~9:1 (Callot *et al.*, 2001). Most of the pioneering work in studying mineral SPO's has arisen from the research of Patrick Launeau into methods of comparing SPO's with AMS, and evidently the determination of magma flow from such data (Launeau and Robin, 1996 ; Launeau and Cruden, 1998 ; Launeau, 2004). Some deviation in the orientation of the petro-fabric from the magnetic fabric is, however, to be expected (Archanjo and Launeau, 2004). The method employed in this work involves digitally filtering plagioclase and opaque grains from photomicrographs using Adobe® Photoshop®. The resulting Bitmap images are then analyzed using the program "SPO 2003" (Launeau and Cruden, 1998). Between 300 and 2800 grains are indexed per thin section. Each photomicrograph is analyzed using the inertia tensor method, as it is directly comparable to the AMS tensor. From such data the 3-D shape preferred orientation (SPO) of grains is determined (Launeau, 2004).

Thermal AMS Monitoring

It has been shown that thermally treating AMS samples can change and/or improve the magnetic fabric by: [1] oxidizing magnetite, leading to a decrease in susceptibility (Henry *et al.*, 2003), [2] growing new grains along pre-existing fabrics (Mintsa Mi Nguema *et al.*, 2002) and [3] revealing pre-existing tectonic fabrics (Souque *et al.*, 2002). Whether thermal stress (up to ~700°C) is a valuable test of normal magnetic fabric in dolerite remains to be established. However, it is expected that growth and/or destruction of magnetic minerals will occur. The method used in this study involves monitoring changes in magnetic fabric at 100°C intervals for 2 dykes (central RRDS) from room temperature to 700°C. A second experiment, carried out on 48 samples of the northern RRDS involves three

steps in heating: room temperature, 300°C and 700°C. Furthermore, for these samples it is possible to calculate the orientation and intensity of the difference tensor between thermal steps, allowing a more detailed analysis of fabrics which have been removed or added. The AMS measurements were carried out on a Kappabridge KLY-3 anisotropy magnetometer. The principle AMS axes are represented as lower hemisphere equal area projections.

RESULTS

Magnetic Fabric

Results of an anisotropy of magnetic susceptibility (AMS) study of 23 dykes from the RRDS reveals a predominantly normal fabric (60% of total data) carried by relatively pure magnetite. The magnetic foliation, on average, is congruent with the average north-south dyke planes. The imbrication of the magnetic foliation is consistent with lateral magma flow from the north. This is consistent with the Karoo mantle plume model. However, the initial AMS assessment of the magnetic fabric of the RRDS also shows that 30% of the samples have "inverse" or irregular magnetic fabric in the natural state. Park *et al.* (1988) conducted one of the few thermal AMS treatment studies on the Mealy diabase dykes of Labrador, Canada. Essentially, they showed, similarly, that the magnetic fabric of the magnetite-bearing dykes was irregular and scattered in the natural state, as opposed to a better grouped and significant AMS fabric after heating to 640°C.

Thermal AMS Monitoring

The magnetic fabric, in general, appears to be initially flow related, but the fabric becomes increasingly poorly defined with increasing thermal treatment. Thermal demagnetization of samples reveals a pattern of "inverse" fabric, even after heating to 700°C. It is found that 28% of the total of 60 samples has a magnetic foliation which is orthogonal to the dyke plane of the respective dyke. The appearance of this fabric is associated with a decrease in bulk susceptibility (*Km*), evidently resulting from the loss of signal of a fine-grained magnetic phase (Henry *et al.*, 2003). Although this may be dismissed as inverse magnetic fabric, what cannot be ignored is the appearance of a similarly orientated fabric in the SPO results, as discussed above. The decrease of *Km* with heating, with an associated change in orientation in principle axes, indicates that minerals of the primary fabric are lost, and not replaced by a similar fabric. It is for this reason that it cannot be assumed that the enhancement of primary magnetic fabric can be achieved simply by heating samples (Mintsa Mi Nguema *et al.*, 2002).

Mineral Shape Preferred Orientation

A study of plagioclase and opaque grain orientations is consistent with AMS results. The plagioclase grains measured ($n=2.1x10^5$) define a weakly anisotropic, oblate fabric. This fabric is indicative of being magmatic in origin and in 8 dykes is coaxial with the AMS fabric. However, 40% of the data are not comparable because the foliation plane is orthogonal to the dyke plane. This unexpected fabric is most pronounced in the opaque grain fraction suggesting that macroscopic opaque (magnetite) grains are not necessarily controlling the magnetic signal of AMS.

CONCLUSIONS

The heating of samples has an effect on *Km* due to changes (e.g. oxidation) in the magnetic carriers (e.g. magnetite or sulphides). Correctly interpreting these changes in terms of AMS is important, because the AMS fabric inversion still persists in some sites and in others increases with increasing temperature (Souque *et al.*, 2002). It appears; firstly, that fine-grained magnetite in certain samples dominates the AMS signal, until they are demagnetized. This results in SD grains dominating the AMS signal after heating and the orientation of this fabric in essentially "inverse". This can be demonstrated by the orthogonal relationship between the magnetic foliation and dyke plane. Secondly, the results suggest that the measured AMS not only measures the grain shape, but also a change in orientation and/or distribution of the new magnetic phases. This provides a useful comparison to the orientation of SPO ellipsoids, which provide constraint on the true silicate petro-fabric. In summary, the results suggest that it is possible for secondary fabrics, whatever their cause, to mimic the primary silicate fabric. Aarnes *et al.* (2008) have found that a melt of basaltic viscosity can undergo significant post-emplacement flow, even if the matrix has 99% crystallized. This flow is strongly influenced by the crystal percentage and the cooling profile, which in dykes is controlled by internal magma pressure and the dyke width. The effect this may have on both AMS and SPO studies is clearly related to potentially picturing only the very late stage magma flow, which may provide little insight into the overall flow direction of the dyke as a whole. Thus, this work suggests that [1] unexpected fabrics may be preserved in the SPO of plagioclase and more commonly, by opaque grains, and thermally demagnetized AMS, [2] natural AMS is not strictly linked with the silicate (SPO) fabric, whether AMS is "inverse" or not and [3] the origin of the orthogonal SPO fabric may be related to late stage flow (post-emplacement) of viscous magma, resulting in grains "rolling" through the silicate mush, rather than imbricating against the dyke margin in the expected manner.

REFERENCES

Aarnes I., Podladchikov Y. Y. and Neumann E.-R., 2008, Post-emplacement melt flow induced by thermal stresses: Implications for differentiation in sills: Earth and Planetary Science Letters, 276, 152-166.

Archanjo C. J. and Launeau P., 2004, Magma flow inferred from preferred orientations of plagioclase of the Rio Cearf-Mirim dyke swarm (NE Brazil) and its AMS significance. In: Martin-Hernandez F., Luneburg, C. M., Aubourg, C. and Jackson, M. (eds.). Magnetic Fabric: Methods and

applications, Geological Society of London, Special Publication, 238, 285-298.

Callot J. P., Geoffroy L., Aubourg C., Pozzi J. P. and Mege D., 2001, Magma flow directions of shallow dykes from the East Greenland volcanic margin inferred from magnetic fabric studies: Tectonophysics, 335, 313-329.

Cañón-Tapia E. and Chávez-Álvarez M. J., 2004, Theoretical aspects of particle movement in flowing magma: implications for the anisotropy of magnetic susceptibility of dykes. In: Martin-Hernandez F., Luneburg, C. M., Aubourg, C. and Jackson, M. (eds.). Magnetic Fabric: Methods and Applications, Geological Society of London, Special Publication, 238, 227-249.

Dragoni M., Lanza R. and Tallarico A., 1997, Magnetic anisotropy produced by magma flow: theoretical model and experimental data from Ferrar dolerite sills (Antarctica): Geophysical Journal International, 128, 230-240.

Ellwood B. B., 1978, Flow and emplacement direction determined for selected basaltic bodies using magnetic anisotropy measurements: Earth and Planetary Science Letters, 41, 254–264.

Geoffroy L., Callot J. P., Aubourg C. and Moreira M., 2002, Divergence between magnetic and plagioclase linear fabrics in dykes: a new approach for defining the flow vector using magnetic foliation: Terra Nova, 14, 183-190.

Henry B., Jordanova D., Jordanova N., Souque C. and Robion P., 2003, Anisotropy of magnetic susceptibility of heated rocks: Tectonophysics, 366, 241-258.

Khan M. A, 1962., The anisotropy of magnetic susceptibility of some igneous and metamorphic rocks: Journal of Geophysical Research, 67, 2873-2885.

Knight M. D. and Walker G. P. L., 1988, Magma flow directions in dikes of the Koolau Complex, Oahu, determined from magnetic fabric studies: Journal of Geophysical Research, 93, 4301-4319.

Launeau P., 2004, Mise en évidence des écoulements magmatiques par analyse d'images 2-D des distributions 3-D d'Orientations Préferentielles de Formes: Bulletin of the Geological Society of France, 175, 331-350.

Launeau P. and Cruden A. R., 1998, Magmatic fabric acquisition mechanisms in a syenite: Results of a combined anisotropy of magnetic susceptibility and image analysis study: Journal of Geophysical Research, 103, 5067-5089.

Launeau P. and Robin P.-Y. F., 1996, Fabric analysis using the intercept method: Tectonophysics, 267, 91-119.

Mintsa Mi Nguema T., Trindade R. I. F., Bouchez J.-L. & Launeau P., 2002, Selective thermal enhancement of magnetic fabrics from the Carnmenellis granite (British Cornwall): Physics and Chemistry of the Earth, 27, 1281-1287.

Park J. K., Tanczyk E. I. and Desbarats A., 1988, Magnetic fabric and its significance in the 1400 Ma Mealy diabase dykes of Labrador, Canada: Journal of Geophysical Research, 93, 13689-13704.

Potter D. K. and Stephenson A., 1988, Single-domain particles in rocks and magnetic fabric analysis: Geophysical Research Letters, 15, 1097-1100.

Rochette P., Aubourg C. and Perrin M., 1999, Is this magnetic fabric normal? A review and case studies in volcanic formations: Tectonophysics, 307, 219-234.

Rochette P., Jackson M. and Aubourg C., 1992, Rock magnetism and the interpretation of anisotropy of magnetic susceptibility: Reviews of Geophysics, 30, 209-226.

Souque C., Robion P. and Frizon de Lamotte D., 2002, Cryptic magnetic fabric of tectonic origin revealed by heating of sedimentary samples from the Corbières (France): Physics and Chemistry of the Earth, 27, 1253-1262.

PROBLEMS ASSOCIATED WITH INTERPRETING MAGMATIC FABRICS

Hastie, W.W.[1], Watkeys, M.K.[1] & Aubourg C.[2]

[1] School of Geological Sciences, University of KwaZulu-Natal, South Africa; 203505849@ukzn.ac.za

[2] Department of Geosciences & Environment, University of Cergy-Pontoise, France.

Keywords: AMS, dykes, magma flow, shape preferred orientation

Dykes and dyke swarms are fundamental components of large igneous provinces (LIPs) (Jourdan et al. 2004). They can be used as indicators of stress conditions and crustal extension during continental break-up, and increasingly are being studied in order to constrain magma movement through the crust (Ernst 1990, Ernst & Duncan 1995; Aubourg et al., 2008). However, common methods of measuring and interpreting any fabric acquired during magmatic flow remain contentious, especially with regards to magmatic flow in large dyke swarms. The methods are typically restricted to (1) quantifying relevant dyke morphology in the field, (2) measuring the 3-dimensional orientation of silicates which become tiled along the margin of an intrusion and (3) comparable geophysical measurements such as the anisotropy of magnetic susceptibility (AMS). Difficulties in interpretation however, arise from the dyke morphology often being neglected and reasonable geological explanations for unusual magnetic susceptibility fabrics not being made (Philpotts & Philpotts 2007). Recent studies of dolerite dykes of the Lebombo faulted monocline, which forms part of the ~182 Ma-old Karoo LIP in southern Africa has yielded some surprising results. Besides clearly flow-related magmatic fabrics, 4 distinct phenomena can be illustrated from this study: contradictory field and geophysical data, evidence for backflow in dykes (i.e. downward flow), sub-horizontal fabrics which may be due to late-stage magma compaction and dyke-orthogonal fabrics resulting from significant degrees of grain interaction during late-stage flow.

Aubourg, C., Tshoso, G., Le Gall, B., Bertrand, H., Tiercelin, J.-J., Kampunzu, A. B., Dymente, J. & Modisi, M., 2008. Magma flow revealed by magnetic fabric in the Okavango giant dyke swarm, Karoo igneous province, northern Botswana. *Journal of Volcanology and Geothermal Research* **170,** 247-261.

Ernst, R. E., 1990. Magma flow directions in two mafic Proterozoic dyke swarms of the Canadian Shield: As estimated using anisotropy of magnetic susceptibility data. In: *Mafic Dykes and Emplacement Mechanisms* (Parker, A. J., Rickwood, P. C. & Tucker, D. H. eds.). Balkema, Rotterdam, 231-235.

Ernst, R. E. & Duncan, A. R., 1995. Magma flow in the Giant Botswana dyke swarm from analysis of magnetic fabric (abstract). *Third International Dyke Conference*, Jerusalem, Israel.

Jourdan, F., Féraud, G., Bertrand, H., Kampunzu, A. B., Tshoso, G., Le Gall, B., Tiercelin, J. J. & Capiez, P., 2004. The Karoo triple junction questioned: evidence from Jurassic and Proterozoic 40Ar/39Ar ages and geochemistry of the giant Okavango dyke swarm (Botswana). *Earth and Planetary Science Letters* **222,** 989-1006.

Philpotts, A. R. & Philpotts, D. E., 2007. Upward and downward flow in a camptonite dike as recorded by deformed vesicles and the anisotropy of magnetic susceptibility (AMS). *Journal of Volcanology and Geothermal Research* **161,** 81-94.

- Appendix D -

MINERAL SHAPE PREFERRED ORIENTATION

A guide to using "SPO-2003" and "Ellipsoid-2003" software

This manual is now available to graduate and post-graduate students in the Department of Geology, University of KwaZulu-Natal. Accompanying the manual is a CD containing "SPO-2003", "Ellipsoid-2003", ArcSoft® Photostudio®, test sections, a Microsoft® Excel® spreadsheet template, PDF copies of useful journal articles and a copy of this manual. This material is not supplied with this thesis.

MINERAL SHAPE PREFERRED ORIENTATION

A guide to using “SPO-2003” and “Ellipsoid-2003” software

Warwick W. Hastie

Discipline of Geological Sciences

School of Agriculture, Earth and Environmental Sciences
College of Agriculture, Engineering and Science
University of KwaZulu-Natal
Westville
South Africa

2012

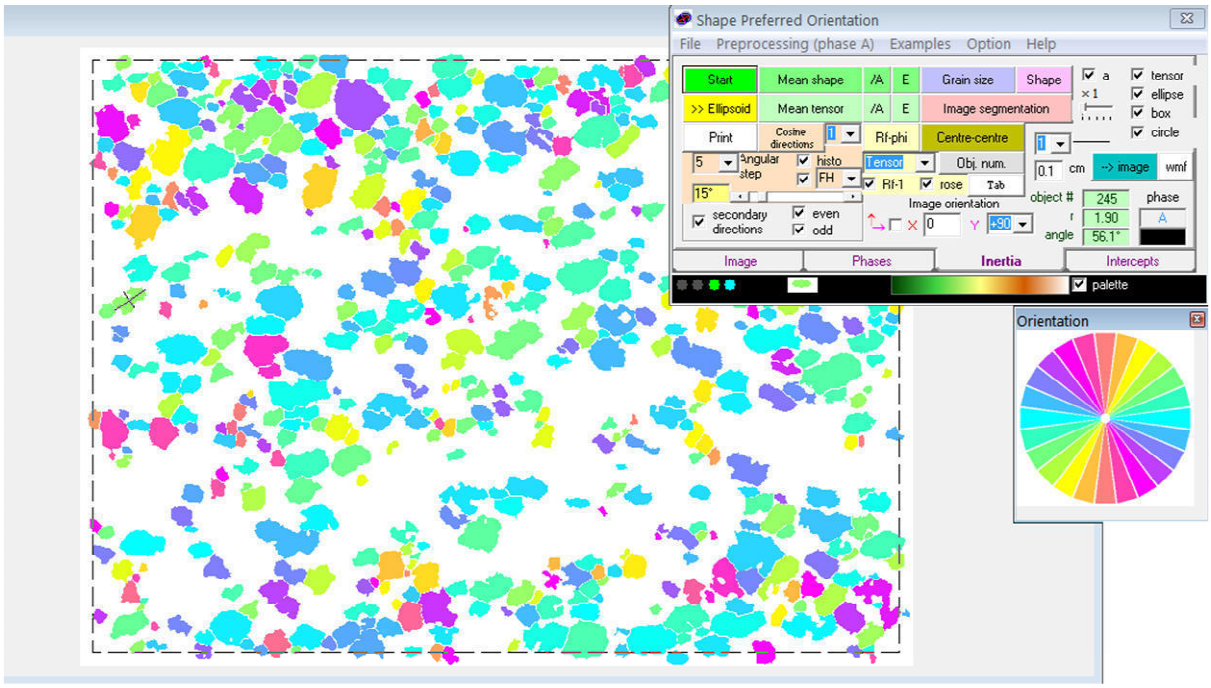

- Table of Contents -

page

1. Introduction

1.1. Mineral Shape Preferred Orientation

Mineral shape preferred orientation (SPO) is a useful means of quantifying the shape, orientation and intensity of a fabric in a rock. Specifically it can be used to quantify both linear and planar fabrics in metamorphic rocks, and is sensitive to even weakly developed fabrics in unstrained igneous rocks. It can also be applied to sedimentary rocks in order to study grain alignment induced by fluid flow and/or the shape and orientation of porosity and grain or crystal size distribution. This manual is by no means authoritative or exhaustive, but is a simple guide for "getting to grips" with the processes and software necessary to measure any kind of SPO in a geological sample. Both SPO-2003 and Ellipsoid-2003 have "help" functions, and worked examples which may be very useful in conjunction with this manual.

The technique requires the following:

1) ORIENTATED field samples: block sample or drill core.
2) Thin sections (of known orientation) cut from the above samples.
3) Field control: this includes measurement of the fabric from the field (if present) and/or the orientation of the structure to which the fabric relates; i.e. the orientation of bedding/layering/intrusion margin etc.

From the above it is possible to relate the measured fabric to the field data, allowing a geologically sensible interpretation of the origin of the fabric to be made. It is important to note that SPO is not sensitive to alignment (e.g. aligned circles will give an isotropic result). It is sensitive to orientation of anisotropic elements and fabric intensity only.

Most of the pioneering work and software development in studying SPO has arisen from the research of Patrick Launeau into methods of comparing mineral SPO to AMS (anisotropy of magnetic susceptibility), and evidently the determination of magma flow from such data (Launeau & Robin, 1996; Launeau & Cruden, 1998; Launeau, 2004;

Launeau & Robin 2005). Much of what is written here is based on these works, but is not cited *ad nauseam* in the text, as it will make the reading of this manual too clumsy.

1.2. Nomenclature used in this manual

SPO: shape preferred orientation (generally refers to minerals, but may be applied to clasts, vesicles, amygdales, pores or other orientated elements in a rock).

Plunge: the maximum angle (00°–90°) measured of an inclined linear feature as measured from the horizontal.

Plunge direction: the geographically defined direction (000°–359°) towards which a linear feature plunges (synonymous with "azimuth" and "trend").

Dip: the maximum angle (00°–90°) measured of an inclined planar feature as measured from the horizontal (synonymous with "inclination").

Strike: the geographically defined direction (000°–359°) of zero dip of a planar feature, as measured using the right-hand rule (synonymous with "declination").

Sample: one drill-core or block sample from which three thin-sections must be cut, in order to quantify the fabric.

Thin section: one ~30 μm thick rock slice which, in the context of SPO, must have a known orientation and known relation to two other sections of the same sample.

Linear fabric: fabric with no planar element, e.g. alignment of elongate minerals such as pyroxene or amphibole.

Planar fabric: fabric produced by preferred orientation of non-linear minerals, such as mica's (and plagioclase).

L1: maximum principal axis of 3-D SPO ellipsoid

L2: intermediate principal axis of 3-D ellipsoid

L3: minimum principal axis of 3-D ellipsoid

Lineation: the overall linear element from a set of data, which has a known orientation measured as plunge and plunge direction. The principal axes described above are all lineations.

Foliation: the overall planar element from a set of data, which has a known orientation measured as a dip and strike (L3 or K3 is always taken as the pole to a foliation).

Note: The distinction between planar and linear fabrics is important, as the software ALWAYS produces a measure of linear and planar elements (Figure 1.1), even if no such element is present.

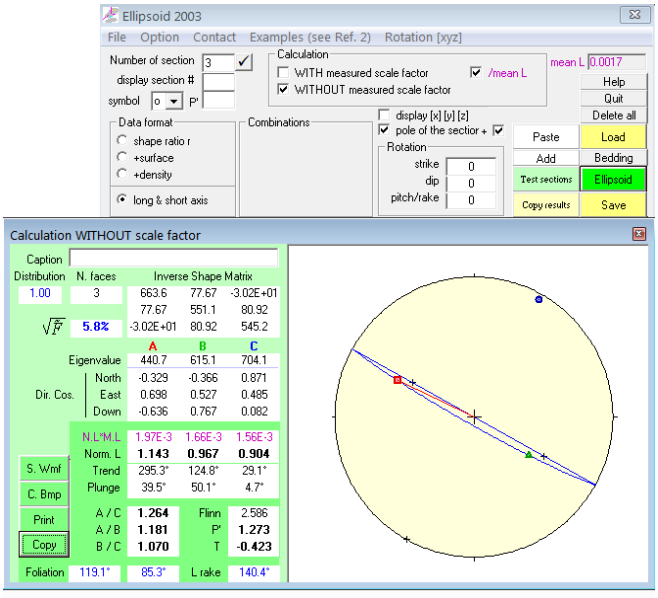

Figure 1.1: Example of a sample analysed by "Ellipsoid-2003". Note the principal axes (L1 = red, L2 = green and L3 = blue). The L1 axis defines the linear component of the fabric, while the plane delineated in blue (to which L3 is a pole) defines the planar component (the "foliation").

2. Sample Processing

In this section the correct manipulation of samples and subsequent processing of orientated thin sections will be demonstrated. The processing of drill-core samples and block samples will be illustrated. As will become clear, the processing of drill-cores is far easier and less likely to result in errors.

2.1. Drill-core samples

For the case of a drill core sample, it is ideal that each thin section corresponds to a plane of the drill core (of which the orientation MUST be known, preferably as plunge and plunge direction of the core). Thus sections XY, XZ and ZY are produced; with XY being parallel to the top of the core; XZ is a vertical section parallel to the plunge direction of the core and ZY at right angles to XY and XZ (Figure 2.1). The XYZ co-ordinate system is NOT geographic, but simply a construct which applies to the method of analysis used in SPO-2003.

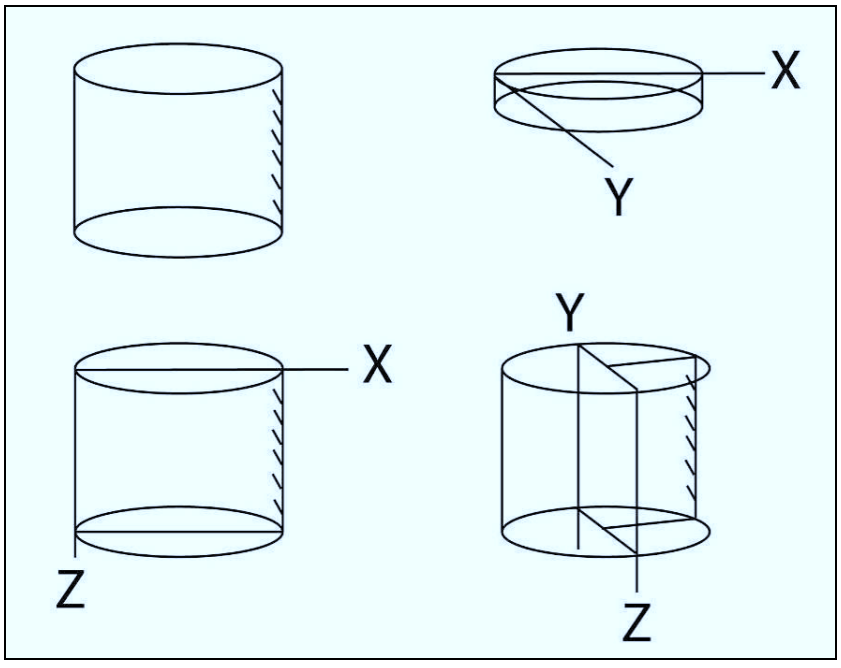

Figure 2.1: Illustration showing the three relevant planes (XZ, XY, ZY) exploited for making three orthogonal thin sections from a drill core. Each core is ~22 mm in height and 25 mm in diameter. The tick marks shown verge downwards along the plunge of the core (adapted from Archanjo & Launeau, 2004).

Defining the orientation of the thin sections is rigorous: the dip of the XY plane (top of the core) is equal to [90° – plunge angle (α)] of the core and the strike using the right-hand rule (RHR) is [azimuth of the core + 90°] (Figures 2.2 and 2.3).

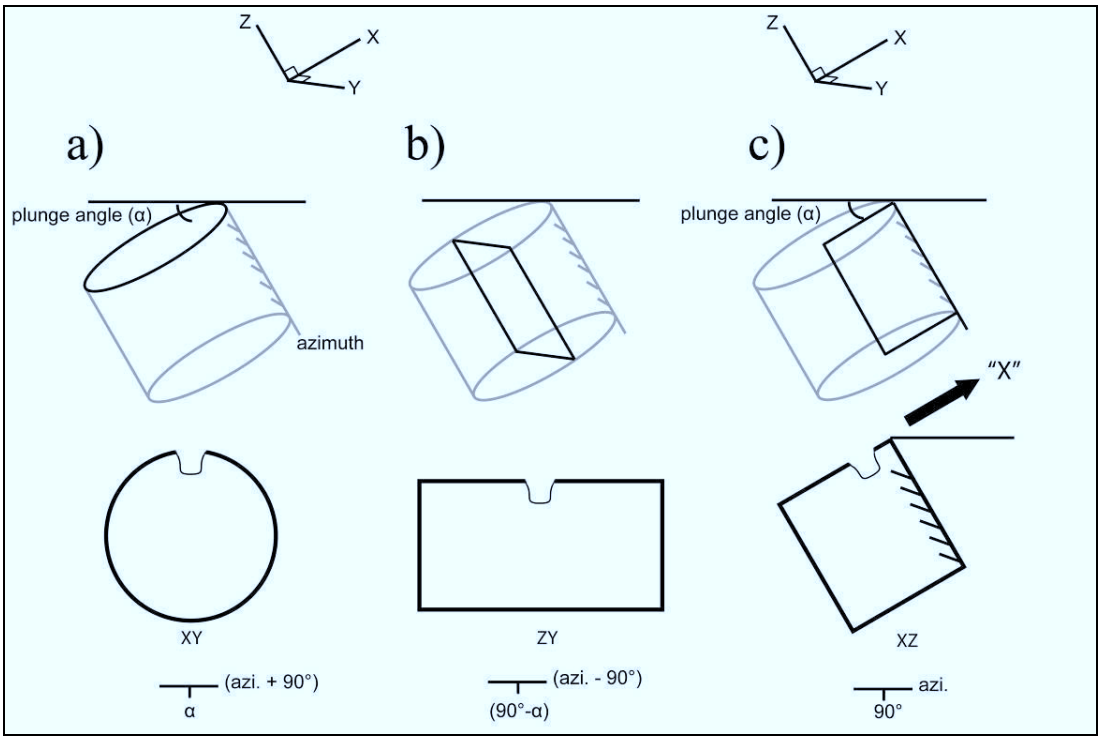

Figure 2.2: Schematic diagram of AMS cores showing XYZ sections used for mineral SPO analysis: a) Section XY; dip and strike = [90°-α], [azimuth + 90°], b) Section ZY; dip and strike = [α°], [azimuth – 90°], c) Section XZ; dip and strike = [90°], [azimuth]. The apparent "X" direction for XZ, however, is (90°+α). The U-shaped notches cut into the thin-section edges provide constraint on the "way-up". For example, the notch in the XY section points in the down-plunge direction, the notch in the XY section points "up" (i.e. into the underside of the XY section). The same is true of the XZ section.

By way of geometry, the XZ section always has a dip of 90°, and the strike is equal to the azimuth direction of the core. The ZY section has a dip equal to the amount of plunge of the core, and the strike is [azimuth – 90°].

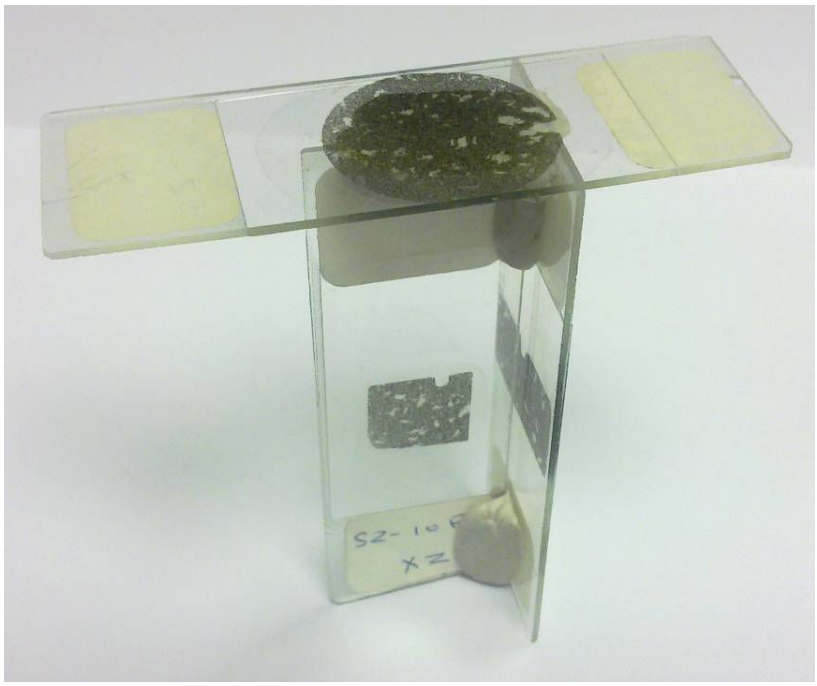

Figure 2.3: Photograph of three orientated thin sections cut from a drill-core sample of plagioclase-phyric dolerite, illustrating how the thin sections relate in three dimensions. Note that the top section is XY. Section XZ (facing section) has a notch on the upper side, and the far right thin section is the ZY section. Note in the XZ section that the notch is cut slightly asymmetrically, being closer towards the down-plunge side of the sample. This prevents lateral inversion of the thin section when viewing it under the microscope.

2.2. The "X" direction (see sections 3.1 and 5.1)

This is extremely critical, as major errors can result from a misunderstanding of this convention. For the purposes of analysis, it is necessary to define the "X" direction for each thin section, if it is assumed that each image is defined by a left-hand line (X) and a lower line (Y). These directions are INDEPENDENT of the XY/XZ/ZY system. It is a convention of SPO-2003 which, unfortunately, uses the same lettering (Figure 2.4). Thus, do not confuse the calculation of dip and strike with the calculation of the "X" direction.

For the XY and ZY sections, therefore, the "X" direction is ALWAYS equal to 90°, and for the XZ section, "X" is equal to [90° + α]. This is illustrated below in Figures 2.2 and 2.5, and is critical in maintaining a data spreadsheet of all thin sections and samples under consideration.

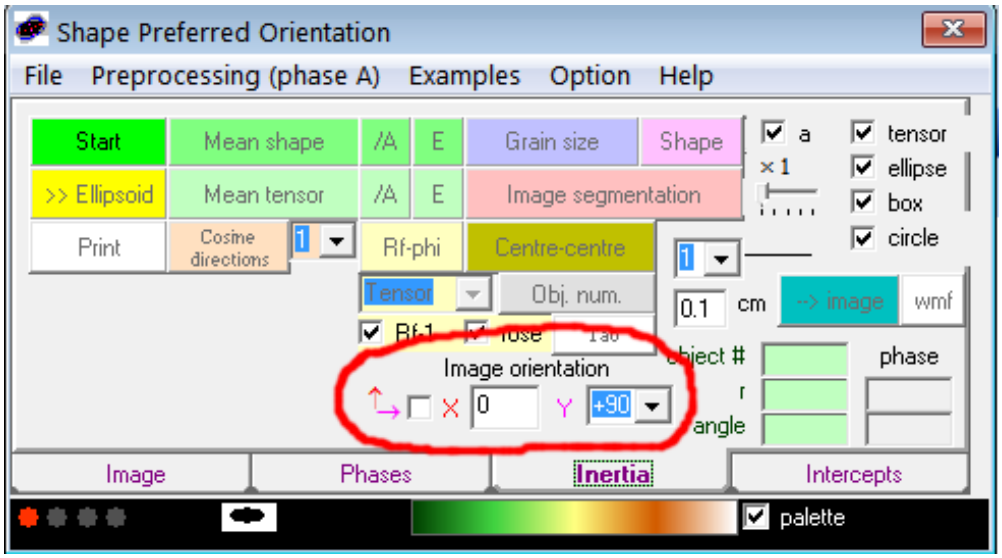

Figure 2.4: Screen print of the SPO-2003 interface, showing the "Image orientation" menu (outlined in red) which involves the "X" and "Y" input for calculating the inertia tensor (see section 5). The box with the two orthogonal arrows must ALWAYS be checked, and the correct "X" and "Y" values are entered.

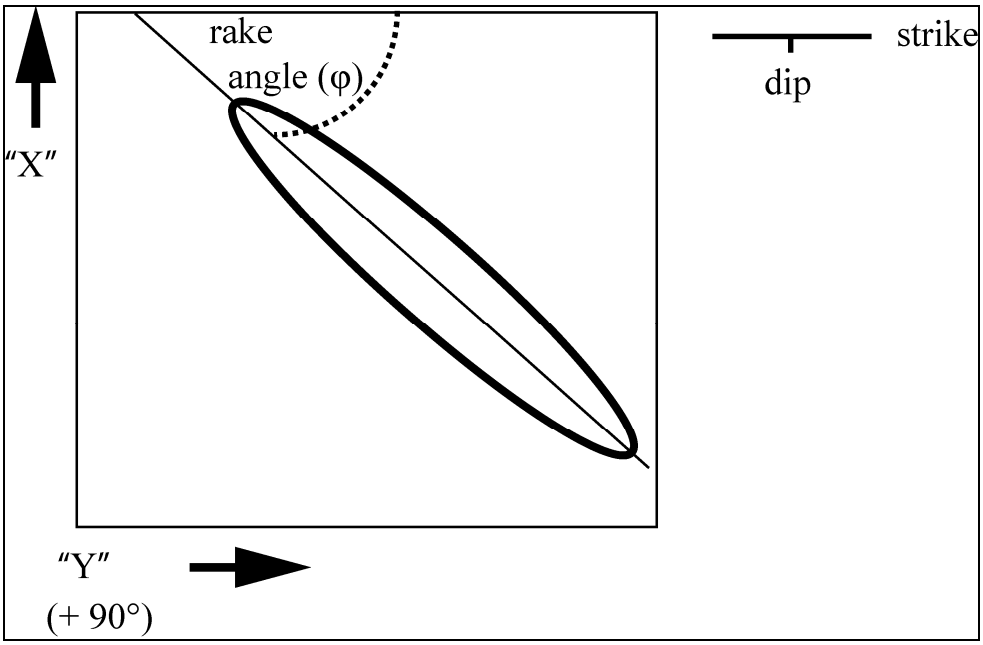

Figure 2.5: Basic illustration of the "X" "Y" convention used in SPO-2003 for an image and the principle of measuring the rake angle (φ) (see also Figure 3.2). Remember that the "X" direction for XY and ZY sections is always 90°, and the "X" direction for XZ sections is always (90° + dip). The strike and dip of each section is not important for SPO-2003, but is critical for use in Ellipsoid-2003 when data from three images are combined. See also Figure 2.2.

Also note in Figures 2.2, 2.3 and 2.6 that notches are cut into particular edges of the thin section. This is done BEFORE affixing the prepared block to the glass slide. The notches provide constant and permanent control on the orientation of the thin section, especially when viewing it under a microscope. See the figure caption for explanation.

The figure below illustrates the notch (black space) as viewed in a thin section of dolerite under crossed polarisers. Note that this a ZY section from a small drill core, and thus the notch indicates the "up" direction, which allows one to know at all times how this image relates to others of the same sample.

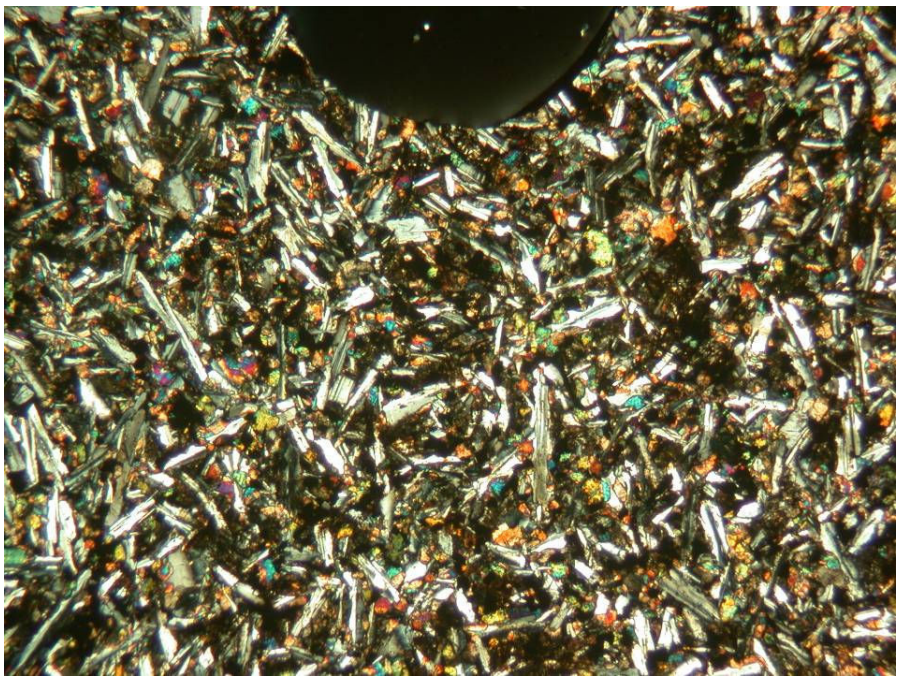

Figure 2.6: ZY section of a dolerite sample (crossed polarisers). Note the notch at the top of the sample which is black (because the glass slide is isotropic). The XY section would be found parallel to the top of the image, and the XZ section parallel to the right-hand edge of the image.

2.3. Orientated block samples

Essentially the same XYZ co-ordinate system can be used for block samples, except for two important features:

1) The use of small notches cut into the resultant sections is paramount. This prevents the inversion of the section once it is mounted and polished down to the required thickness.
2) The viewing direction of the ZY section must be such that the section dips TOWARDS the viewer (this is true of the drill-core procedure as well). The consequence of this is that care must be taken to CORRECTLY determine the strike direction according to the right-hand rule. An easy method for determining this is to realise that the XY and ZY sections ALWAYS dip in opposite directions, and should therefore never have the same strike direction. This is illustrated more clearly below in Figure 2.7.

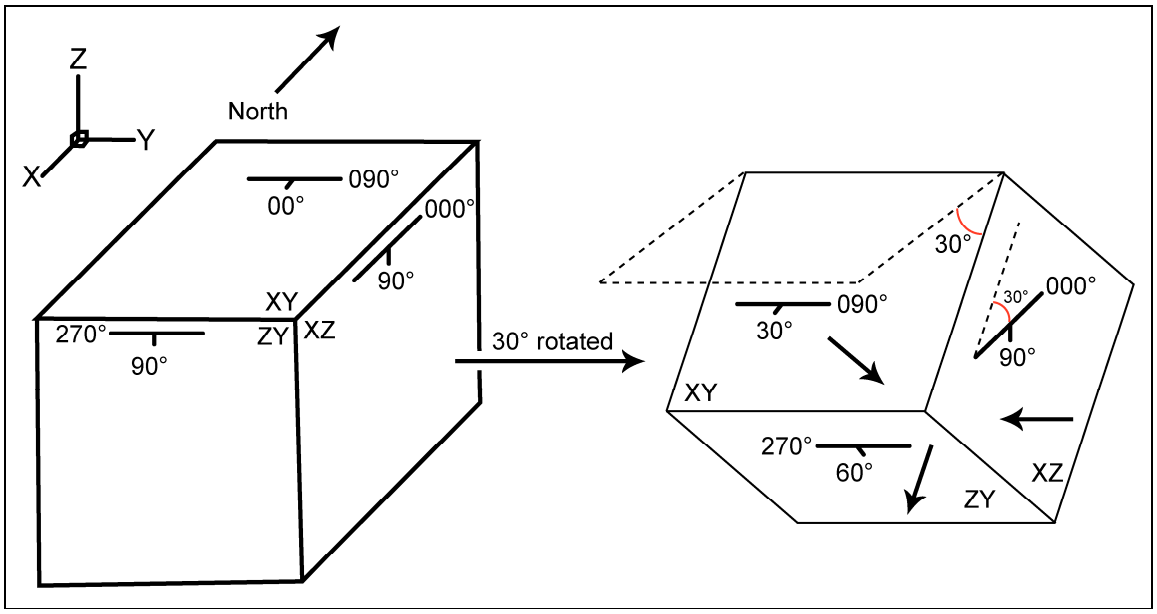

Figure 2.7: Simple block diagrams of orientated block samples. Note that the XYZ co-ordinate system still applies, and an arbitrary "North" direction is given. For a horizontal block, the orientation of the thin sections is shown. Note, in particular, that the ZY section appears to have a "left-handed" strike direction. This is in fact correct, however, given the viewing directions as shown in the rotated diagram on the right. Note in this diagram too that the dip of the XY section (30°) is orthogonal to the dip of ZY section (60°). The dip of the XZ section is always 90°. The 30° angle shown in the XZ section illustrates that the "X" direction is 90°+30°.

The assignment of XY, XZ and ZY planes to a particular face does not have stringent rules, although it is ideal that the top surface of the sample (i.e. as seen in the field) is XY, and the other two faces can be assigned accordingly. If a pervasive/macroscopic fabric is present, it may also be advisable to assign the co-ordinate system faces to planes which are orthogonal to and/or parallel with the fabric element (whether planar or linear).

The use of notches in block samples is critical in order to prevent thin sections becoming inverted in any number of ways, and is essentially the only means of keeping the thin section correctly orientated on the microscope stage when viewing and/or photographing the specimen. A useful method for creating unique notch patterns in thin sections is illustrated below in Figure 2.8.

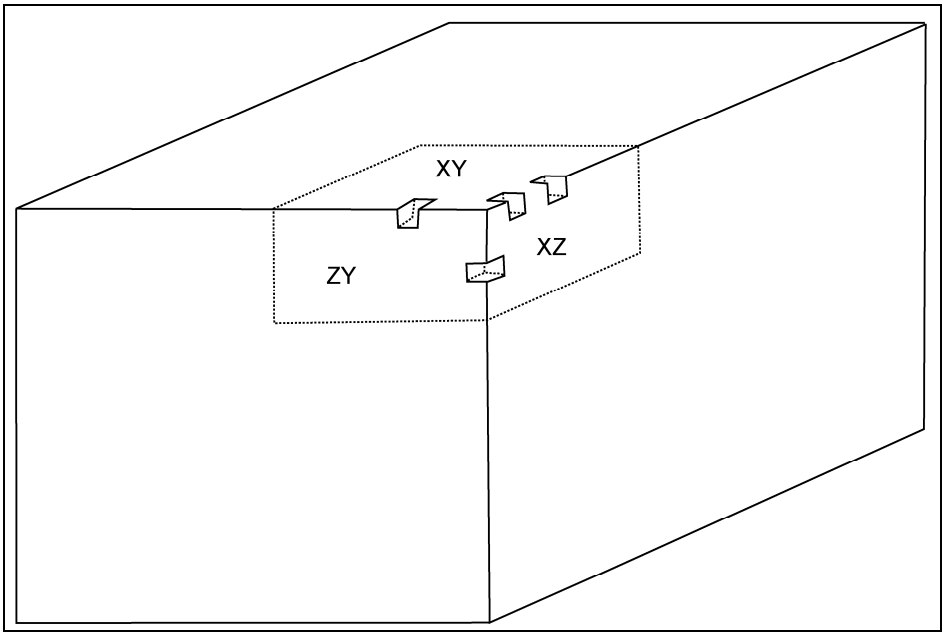

Figure 2.8: Schematic block diagram illustrating a simple means of cutting notches into three orthogonal faces in the XYZ co-ordinate system in order to maintain their unique orientation relative to one another. Knowledge of how the sections relate to one another with these notches also prevents inversion of the faces when producing thin sections, and during viewing under the microscope.

2.4. Errors in Orientation

2.4.1. Measurements

It is clear that an important assumption is made in terms of thin section orientation: namely that the sections are cut so precisely that the simple mathematical relationship in terms of orientation (Figure 2.2) between sections holds true. This is obviously not necessarily the case, as small errors will occur when cutting any of the XYZ faces, especially with large, awkward block samples. However, if each unique face is MEASURED after being cut, there is still a risk of error, as iterative measurements of strike and dip in a sandbox in the laboratory will surely introduce some error, as opposed to single, accurate measurements in the field, the orientations of which are carried through the process of thin section preparation. Thus, it is up to the individual whether measurements in the field are carried through using the simple mathematical relationships outlined above, or whether the XYZ faces are orientated during thin section preparation. Both methods clearly have pros and cons.

2.4.2. Image Inversion

The inversion of an image can happen for many reasons, and as a consequence, results in data being incorrect in orientation by 90° or 180°! As can be seen in Figure 2.9 below, it is impossible to tell which of the ZY sections images (they are identical images) is inverted without the aid of the notches cut into the specimen.

This inversion can happen usually by 1) affixing the specimen “upside-down” to the thin section glass slide and 2) viewing the image incorrectly on the microscope owing to the inversion of images by the optical system (Figure 2.10).

When in any doubt, it is best to re-assemble the sections (as shown in Figure 2.3) to check if the notches in the sections match up correctly.

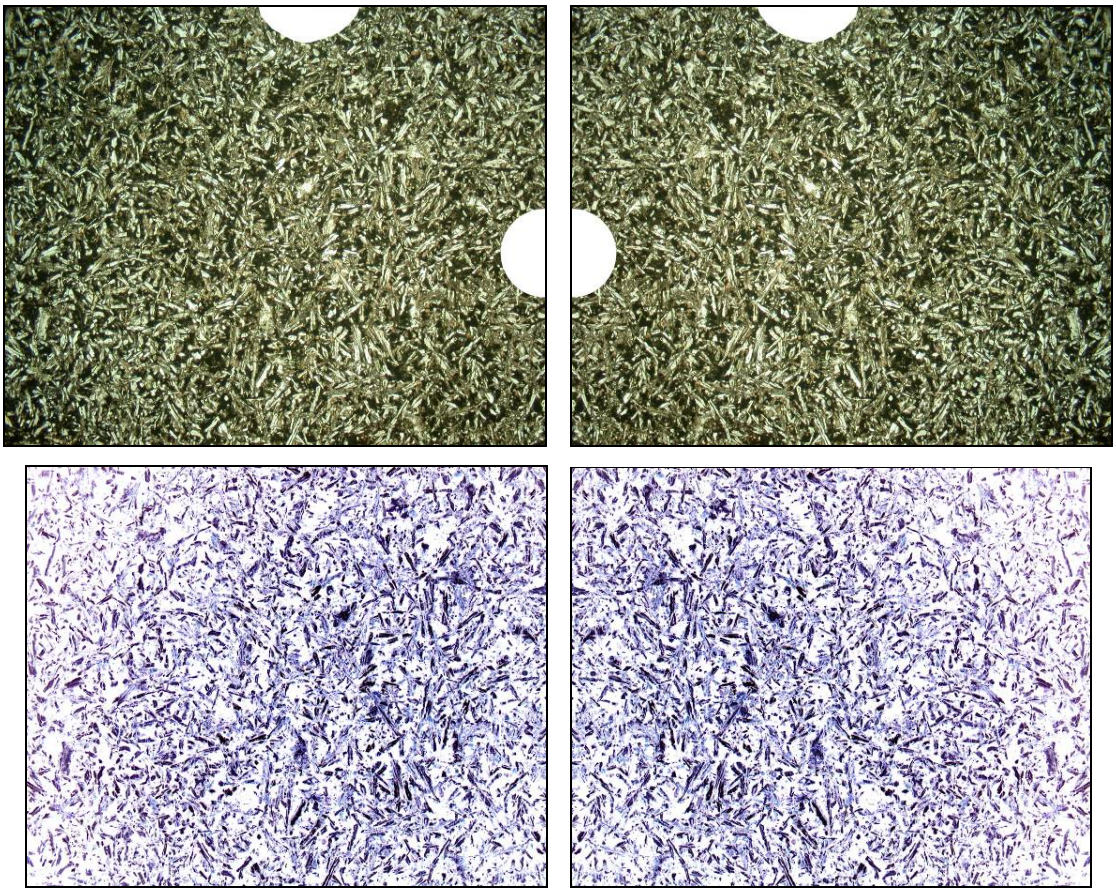

Figure 2.9: Using notches cut into the specimens, it is clear that this ZY section is correctly orientated in the upper left-hand image (see Figure 2.9 above) and inverted in the image on the right. In the lowermost, filtered images, this is not noticeable, because the notches are not present.

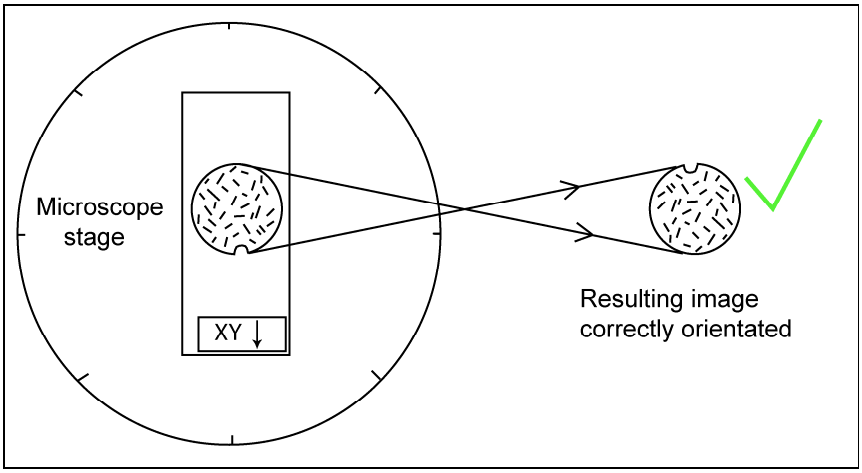

Figure 2.10: Illustration showing how a correctly orientated image results from placing the thin-section on the microscope stage in an apparently incorrect manner (XY section).

3. Maintaining a spreadsheet of SPO data

Significant errors can arise during almost any stage of sample preparation and analysis, especially with regard to always maintaining the known orientation of samples, thin-sections, images etc. However, if data are maintained in a well-organised manner in a spreadsheet (e.g. in Microsoft® Excel®), much of this error can be negated, and errors can be spotted as they appear.

3.1. Basic Layout

It is best to organise a spreadsheet according to the layout of SPO-2003 and Ellipsoid-2003, as illustrated below in Figure 3.1 (and in the spreadsheet template provided on the CD). Note that cells for one sample are divided into three (one per thin section). As discussed above, the "X" direction for XY and ZY is always 90°, and is shown in the table. This direction must, however, be calculated for XZ and entered into the table correctly (hence the yellow highlighting).

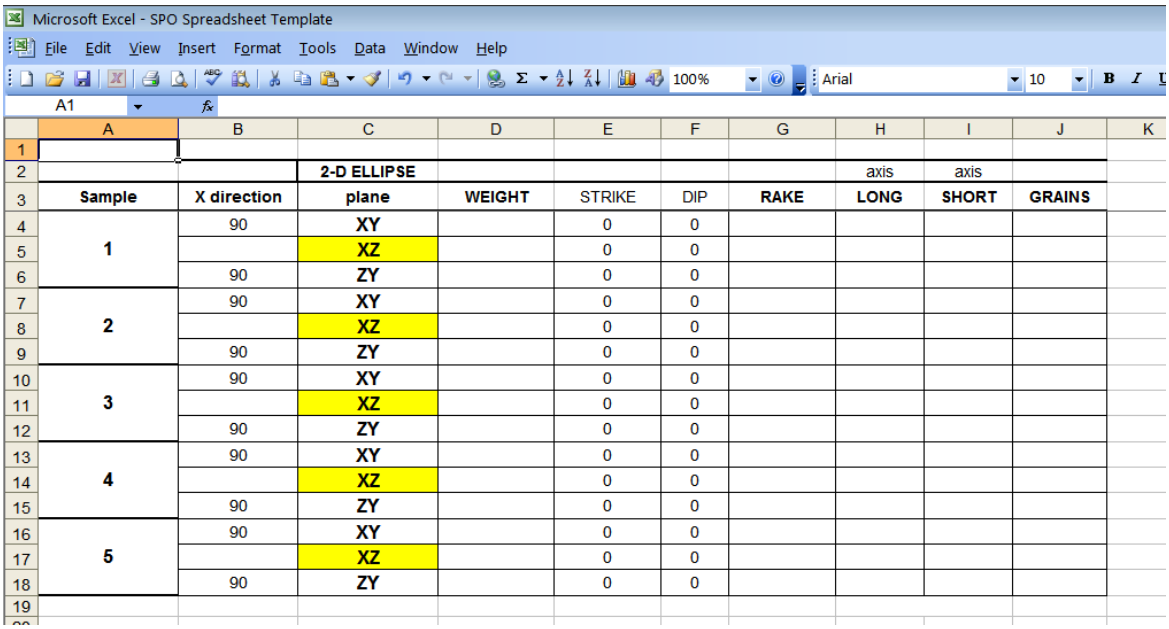

	A	B	C	D	E	F	G	H	I	J	K
1											
2			2-D ELLIPSE					axis	axis		
3	**Sample**	**X direction**	**plane**	**WEIGHT**	STRIKE	DIP	**RAKE**	**LONG**	**SHORT**	**GRAINS**	
4	**1**	90	**XY**		0	0					
5			**XZ**		0	0					
6		90	**ZY**		0	0					
7	**2**	90	**XY**		0	0					
8			**XZ**		0	0					
9		90	**ZY**		0	0					
10	**3**	90	**XY**		0	0					
11			**XZ**		0	0					
12		90	**ZY**		0	0					
13	**4**	90	**XY**		0	0					
14			**XZ**		0	0					
15		90	**ZY**		0	0					
16	**5**	90	**XY**		0	0					
17			**XZ**		0	0					
18		90	**ZY**		0	0					
19											

Figure 3.1: Example of how an Excel® spreadsheet should be constructed for storing SPO and ellipsoid data. Remember that the "X" direction for the XZ sections must be calculated using the dip of the XY section (angle α). The strike and dip values are only needed in Ellipsoid-2003, not in SPO-2003.

It is important to note that at this point it is not necessary to input the strike and dip data into SPO-2003. These data are only used later in Ellipsoid-2003. The only strike and dip data necessary here are those used to calculate the "X" direction for the XZ section, as discussed previously. As a result, the strike and dip columns are left blank or filled with "0". These data can be added manually later, or pasted from another spreadsheet where they are stored.

3.2. Data generated by SPO-2003

There are five major outputs which SPO-2003 generates per image analysed, and these form the headings "weight", "rake", "long", "short" and "grains"

The "weight" heading refers to whether the user wishes to weight thin sections equally (1-1-1) or according to the number of grains in each thin section photomicrograph (hence the heading "grains"). The "rake" angle is calculated as the angle from the top of the image to the average long-axis of the measured fabric in the sample, as shown below in Figure 3.2.

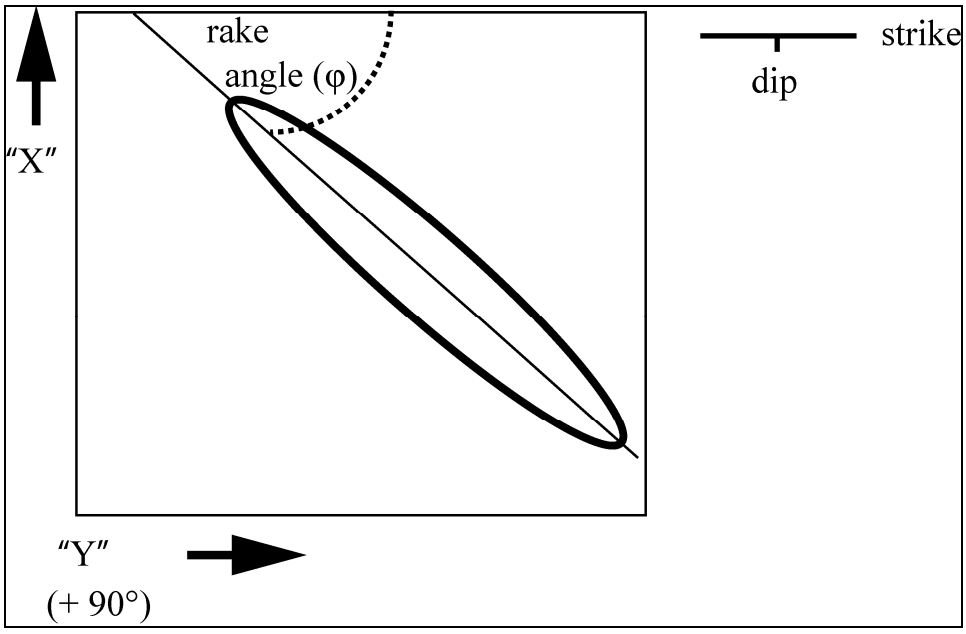

Figure 3.2: Basic illustration of the concept of the rake angle (φ) and the "X" "Y" convention used in SPO-2003 for the analysis of an image.

The terms “long” and “short” refer to the lengths of the axes of the 2-dimensional fabric ellipse determined by SPO-2003 for a single image. Given that the program requires the scale of the image, the axes length are true-to-scale, and therefore not simply a ratio. The “grains” output provides the user with exactly the number of grains which have been analysed in each image.

4. Images and image processing

Without decent and correctly orientated images of the thin sections in question, further analysis of the samples becomes meaningless.

4.1. Orientation & Scale

1) Note that most microscopes, including those with affixed cameras INVERT images about an axis orthogonal to the microscope stage. In other words, the BOTTOM of a thin section (facing the person at the microscope) appears in the TOP of the view/image of that thin section (see Figure 2.11).

Thus it is critical to maintain the correct orientation of the thin section for image analysis. This is again why having notches preserved in the thin sections for analysis is critical, as they assist in maintaining the correct direction during viewing and photographing of the thin section. Note as well that the image capturing device (such as a camera) may affect orientation due to further inversion of an image, or if the camera/camera lens has rotated relative to the microscope stage. This can only be checked by thorough inspection of the setup of the microscope/camera system.

2) The viewing direction of the thin section is important with respect to the mounted side of the specimen on the glass slide. Viewing from the "underside" of the thin section would also result in inversion of the image. It is CRITICAL that it is specified to the technician preparing the thin sections which side of a raw specimen must be affixed to the glass side, and therefore which side will be viewed/photographed using a microscope. This must be done consistently according to the co-ordinate system (e.g. XYZ) across an entire dataset.

3) The scale (horizontal distance across the bottom of the image to be analysed) must be known to the nearest millimetre. SPO-2003 requires this information in centimetres (most images at 2x objective magnification are 9mm across). It is easy to check this using a scale (i.e. ruler) under the objective for a specific magnification to be used. Note, however, that the image capturing device (such as a mounted digital camera) may adjust this distance due

to its own auto-focusing mechanism. Again, check the setup before proceeding with image capturing, and stay consistent with a methodology throughout the analysis of a sample set.

4) It is advisable to only capture three images per sample at a time (i.e. one per thin section). These images should then be downloaded to a hard-disk/laptop immediately. This will avoid any potential confusion, as mixing up images between samples will render any result meaningless. Keep images for each sample in individual folders, and each image MUST have an indication (in the file name) of the section (XY, XZ, ZY) from which it was taken.

4.2. From photomicrographs to Bitmaps

SPO-2003 can ONLY analyse high-quality black-and-white Bitmap images, which are saved from digitally filtered photomicrographs. Most photographic/image software (e.g. Photostudio®) have a "save as" option which allows one to save the image as a Windows® Bitmap, with various options possible for selecting resolution etc. (Figure 4.1).

Figure 4.1: Photomicrograph on the left, with filtered Bitmap image of plagioclase grains of a ZY section on the right. Using circular images reduces edge effects which may distort true grain orientations. Both images are 0.9cm wide.

The grains/vesicles/pore spaces etc. in each section can be digitally filtered using Adobe® Photoshop® or Photostudio® (see CD) into circular Bitmap images in order to remove the remaining phases that are not considered and to reduce edge effects.

This digital filtering can only work when the grains/vesicles etc. have a high contrast with the background of the image (which will be illustrated below). If there is little contrast and/or the fine grain boundaries are of interest, then it is necessary to hand-digitise the features using Corel Draw®, Adobe Illustrator®, ArcGIS® or some similar software. This is evidently more time consuming and potentially subjective, but there simply may not be any other means of filtering out the features of interest from an image.

4.3. Worked Example of Digital Filtering of plagioclase

The example below utilises Photostudio® to convert a thin section photomicrograph into a greyscale bitmap. The figures are not captioned as they form part of the described process.

Step 1: Import image. The image below is taken of an XY section of a drill-core sample of a dolerite under crossed polarisers. Note the higher birefringent pyroxenes surrounded by plagioclase.

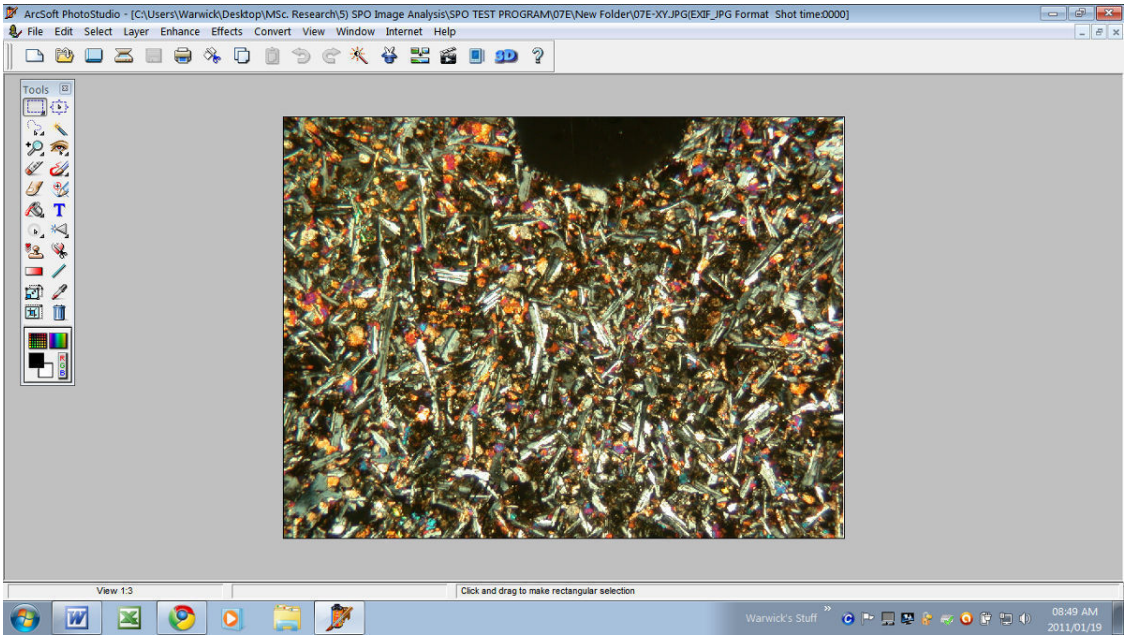

Step 2: Click “enhance” and select “negative”. For this example, it will result in the plagioclase grains becoming darker, and therefore they will ultimately form the bulk of the image, and the light/white background will be removed.

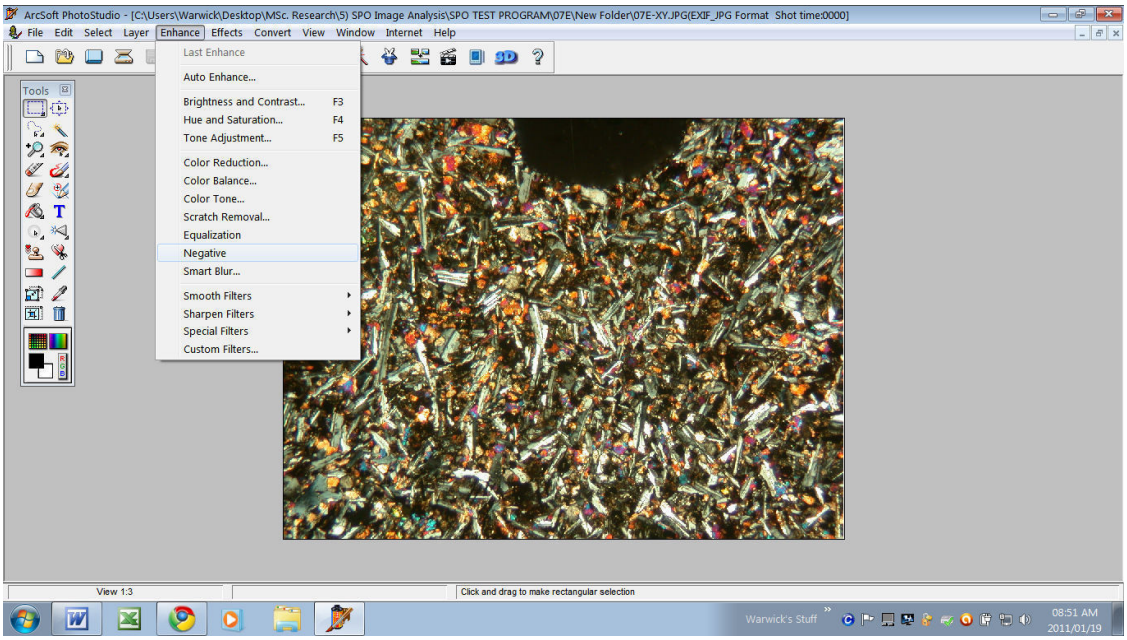

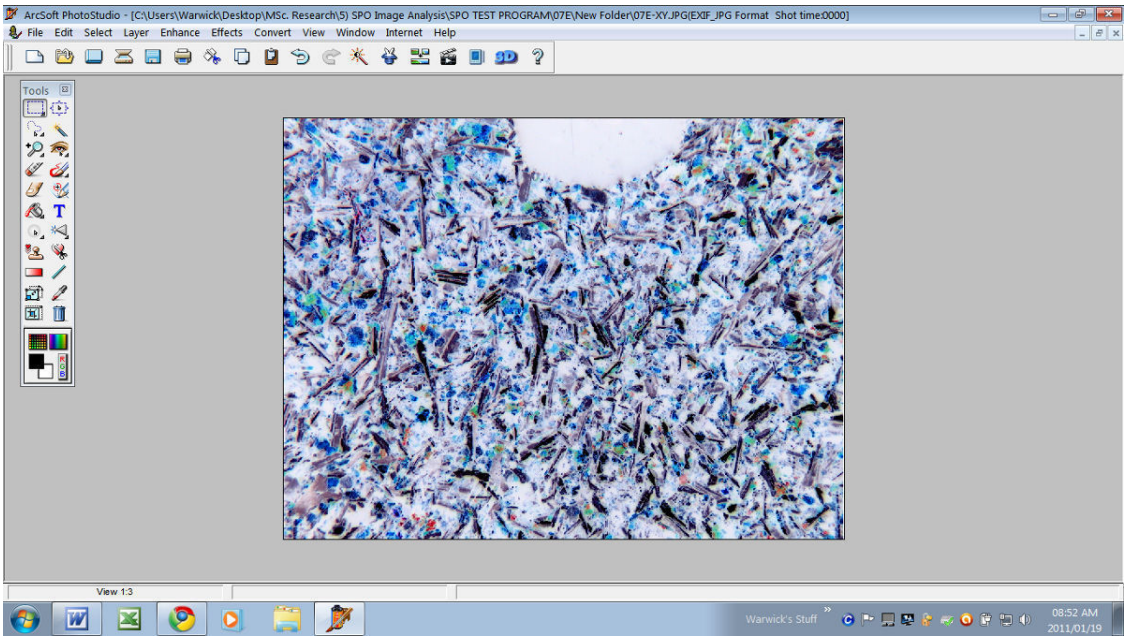

Step 3: Select the "effect browser" (6th button from end of the taskbar). Adjust the brightness and contrast (generally increase both) until the fine-grained background is reduced, without losing the larger, more solid grains.

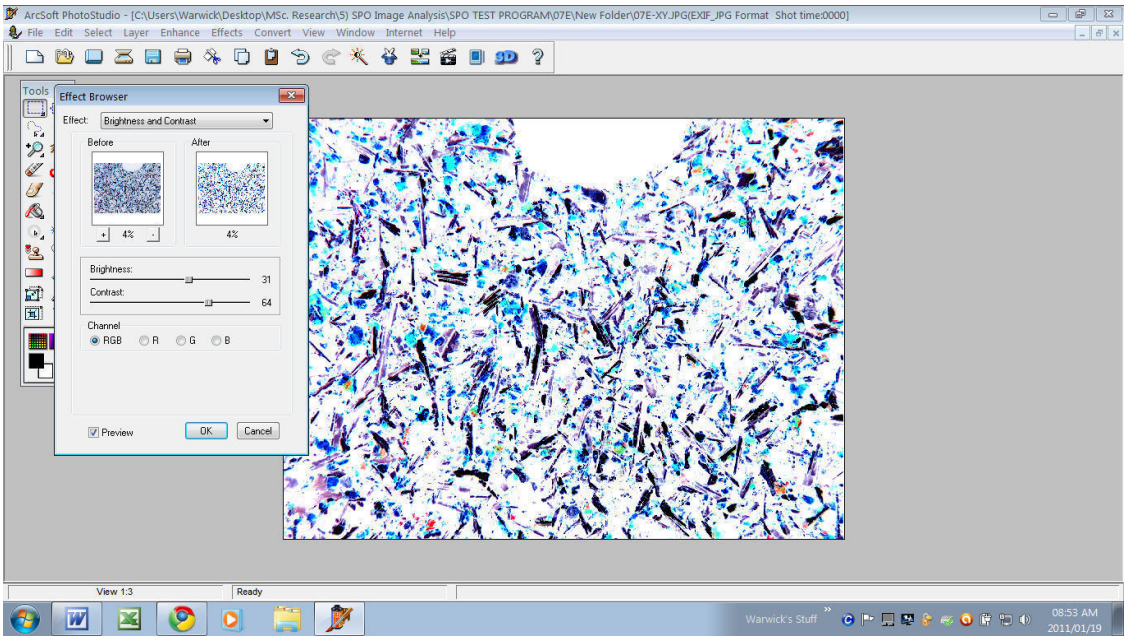

Step 4: Click "convert" to "8-bit greyscale".

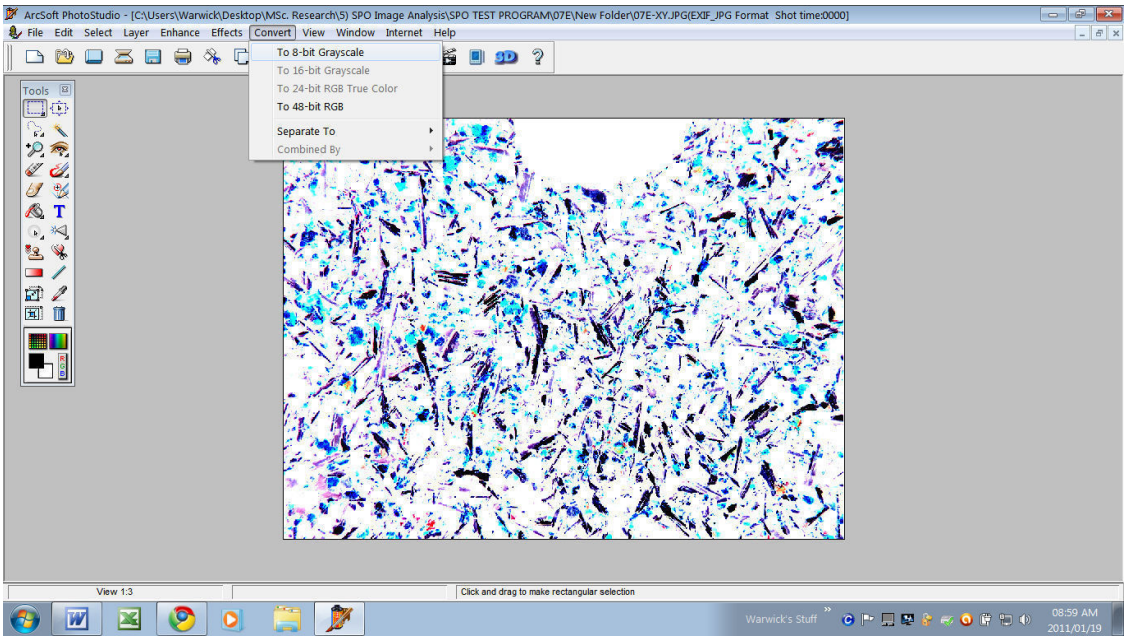

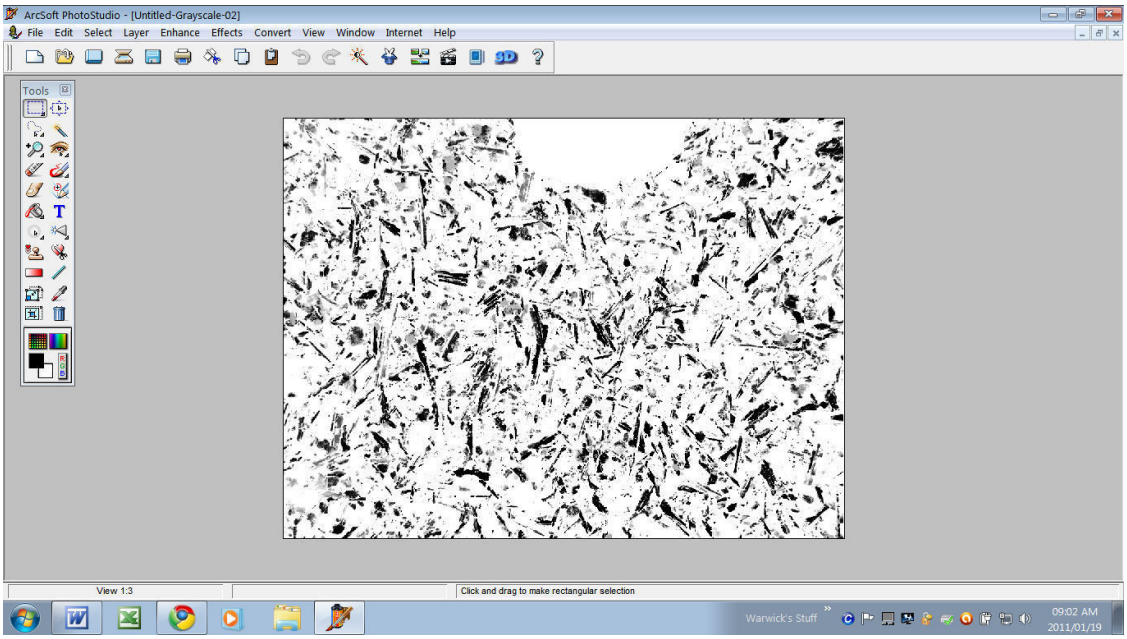

Step 5: Open the effect browser again, and from the drop-down menu select “Threshold”. This function essentially reduces the number of colours in an image. Thus, in a black-and-white image, it removes progressively larger grains from the background. The adjustment of this threshold is very subjective, as it is possible to remove an excessive amount of data from the image, or not remove enough of the background “noise” (see also section 5.2).

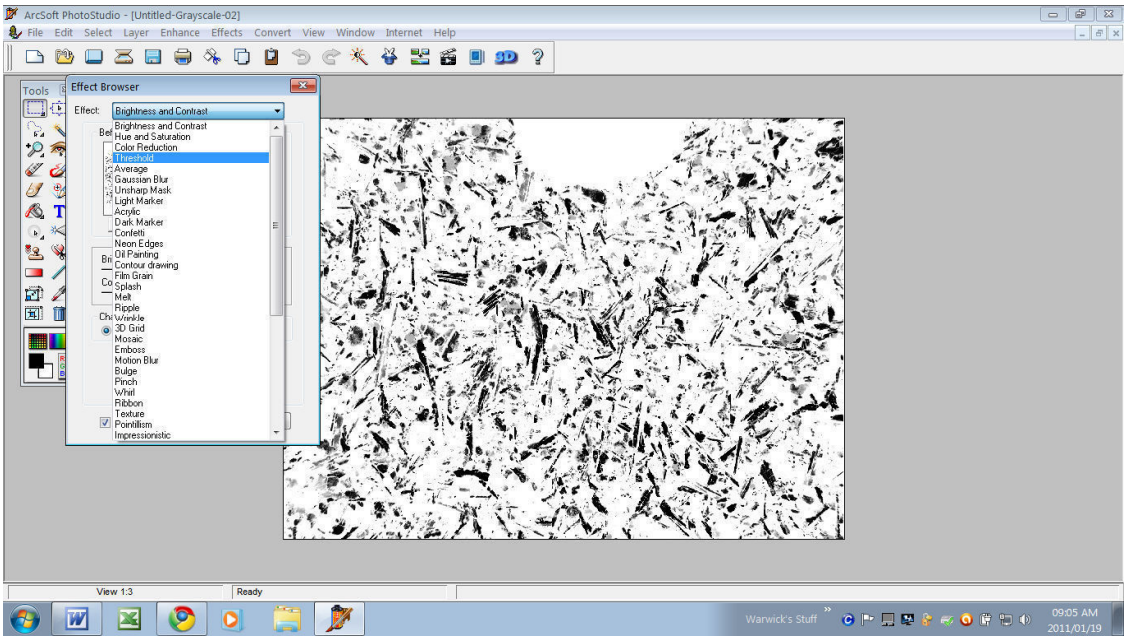

Step 6: From the final image, select a circle (top left button of the free-standing toolbar in the main screen). “Cut” and “Paste” the circular image into a new file (click “file”, “new”).

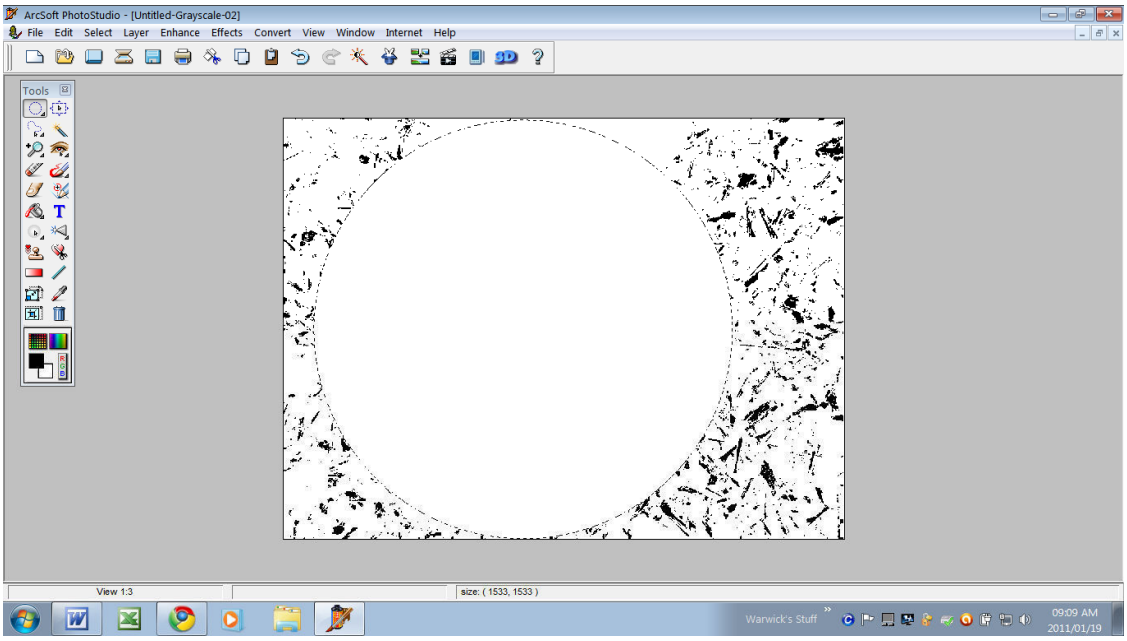

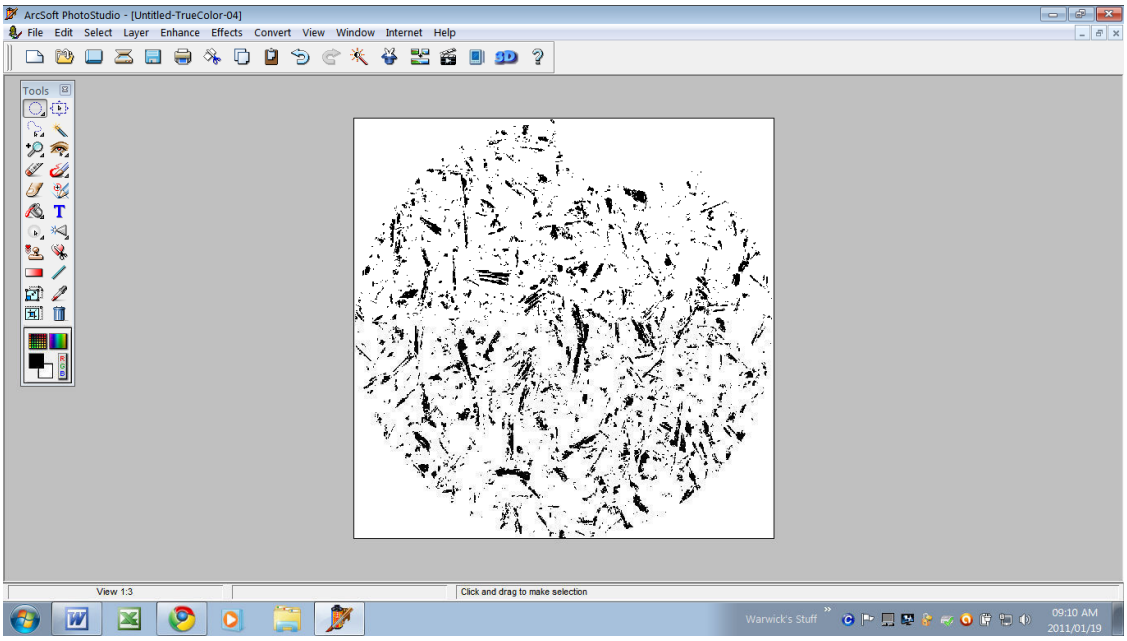

Step 7: Click “file” and “Save-as”, and select “Windows® bitmap” and name the image according to the photomicrograph used.

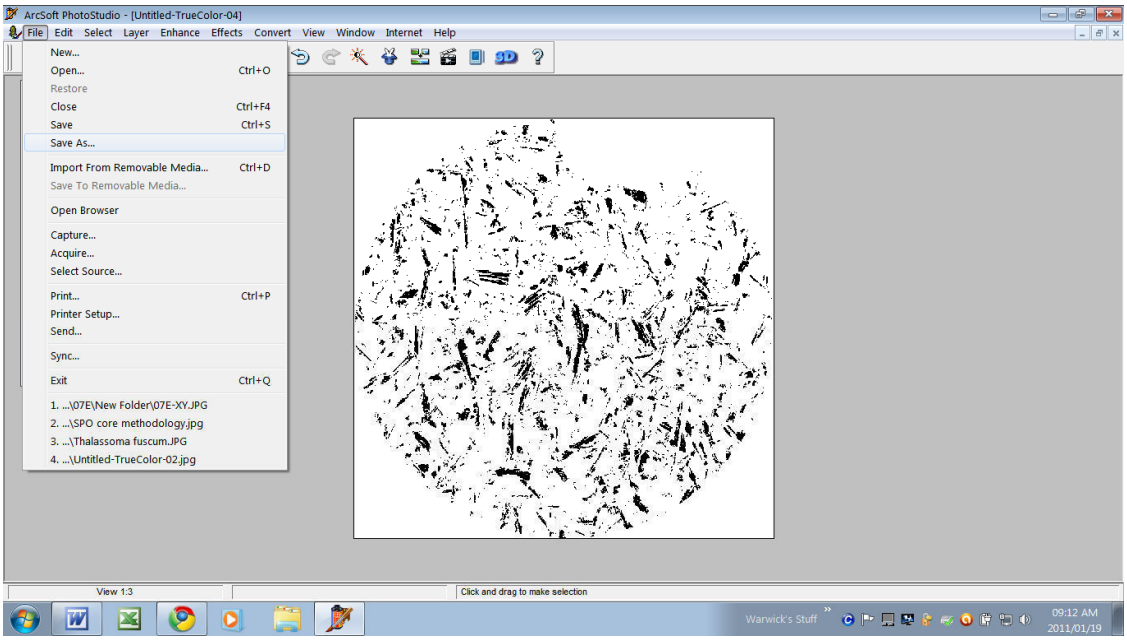

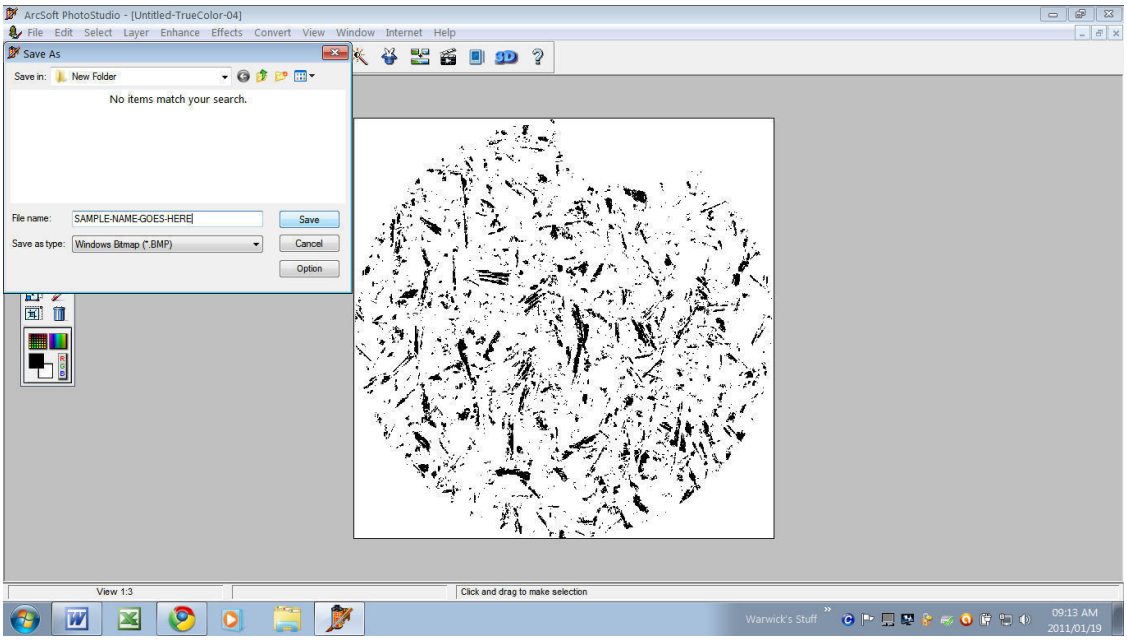

5. Processing samples in 2-dimensions

Whether the final output of data is in 2-D or 3-D, the first step in determining any manner of SPO in a sample(s) is done using the software "SPO-2003".

The program itself has a useful "Help" function which more broadly addresses the fundamental mathematical and geometric theory of the processing. In-depth discussion of this is, however, beyond the scope of the manual. One may refer also to the journal papers which are referenced on the user interface of the software (as shown above).

5.1. Methods in SPO-2003

The SPO-2003 interface has four main tabs: "image", "phases", "inertia" and "intercepts", as shown below in Figure 5.1.

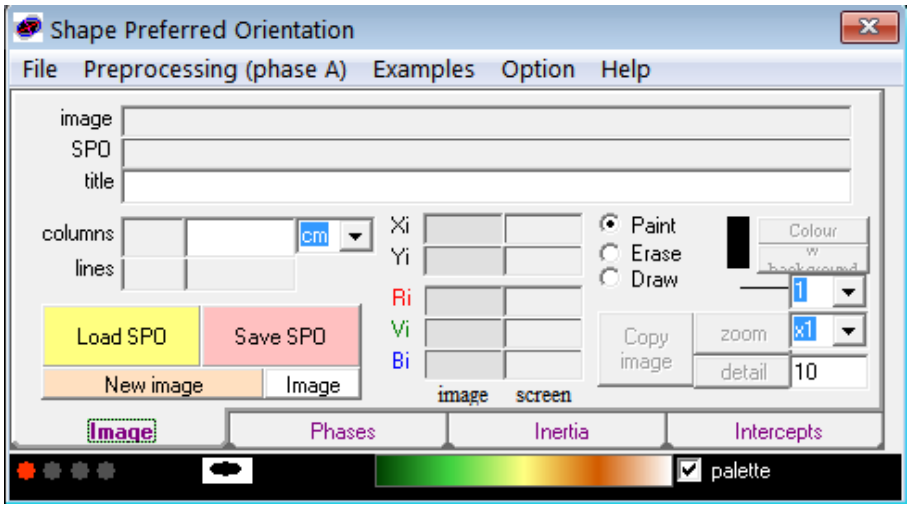

Figure 5.1: User interface of SPO-2003.

The "intercepts" tab allows a user to find a "rose of directions" from analysis of grain boundary intersections. However, it is more common, when one is considering the SPO of grains/grain populations, to utilise the "inertia" interface (Figure 5.2).

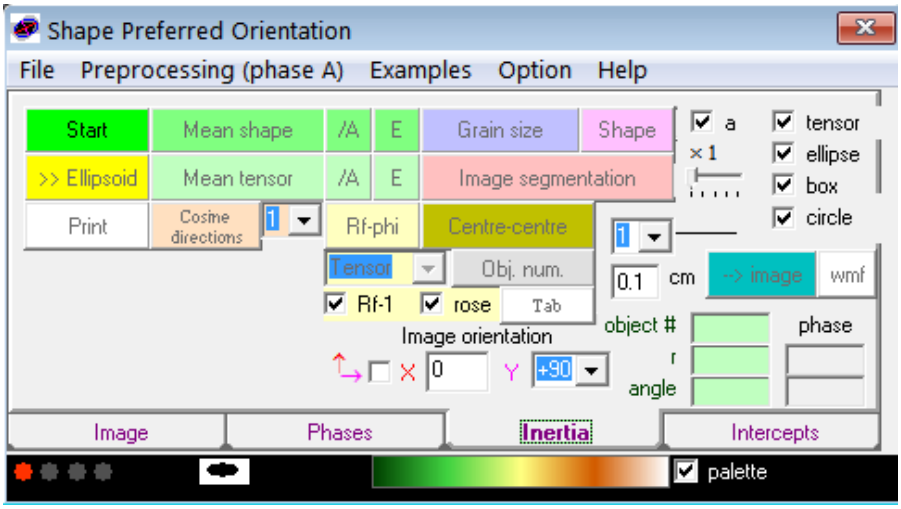

Figure 5.2: The "Inertia" interface of SPO-2003.

From this interface it is possible to perform: Rf-phi analysis, find cosine directions, use the centre-to-centre method and crystal size distribution (CSD). However, this step-by-step guide relates exclusively to finding the mean shape and/or mean tensor for each image, which will be combined later in Ellipsoid-2003. **It is strongly recommended that at this**

point the test sections and accompanying data are used as worked examples, following the method below. Because the correct "answers" are provided, it will be a worthwhile exercise in getting comfortable with the process, and the many steps involved.

Analysing an image:

1) Open bitmap image by clicking "file", "open image" (Figure 5.3). It is possible to adjust the "zoom" (scale) of the image under the "image" tab. Note that once the image is opened, and the **green** "start" button is clicked, a menu will appear asking for the scale in centimetres.

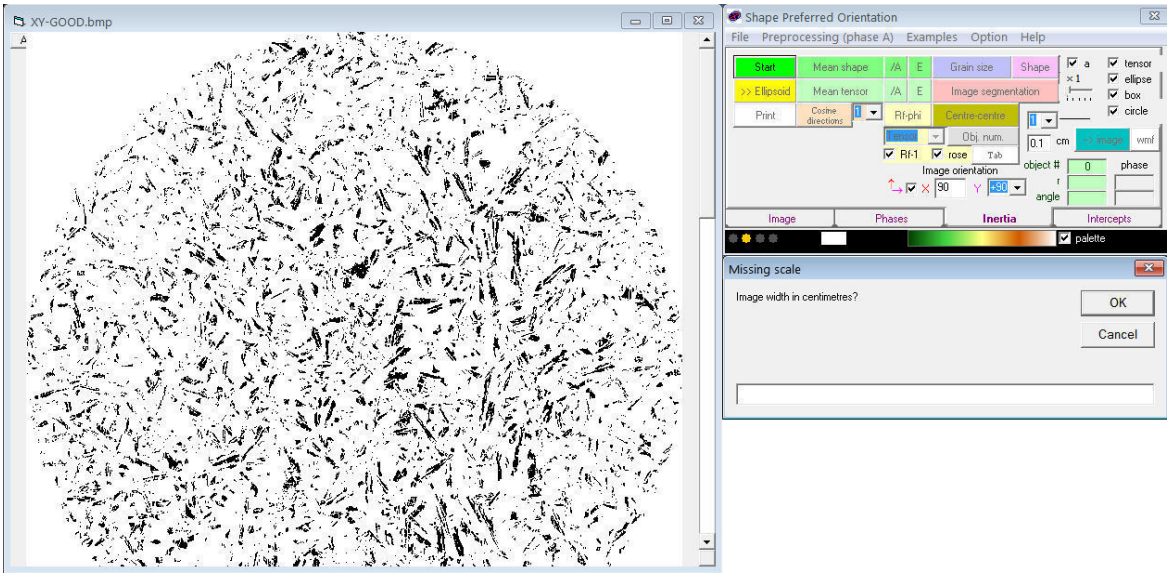

Figure 5.3: Opening a Bitmap image for analysis in SPO-2003. Note the menu on the bottom right which requires input of the image width (to scale).

Note especially the "**X**" and "**Y**" buttons, which must be filled out correctly as discussed above and shown below in Figure 5.4.

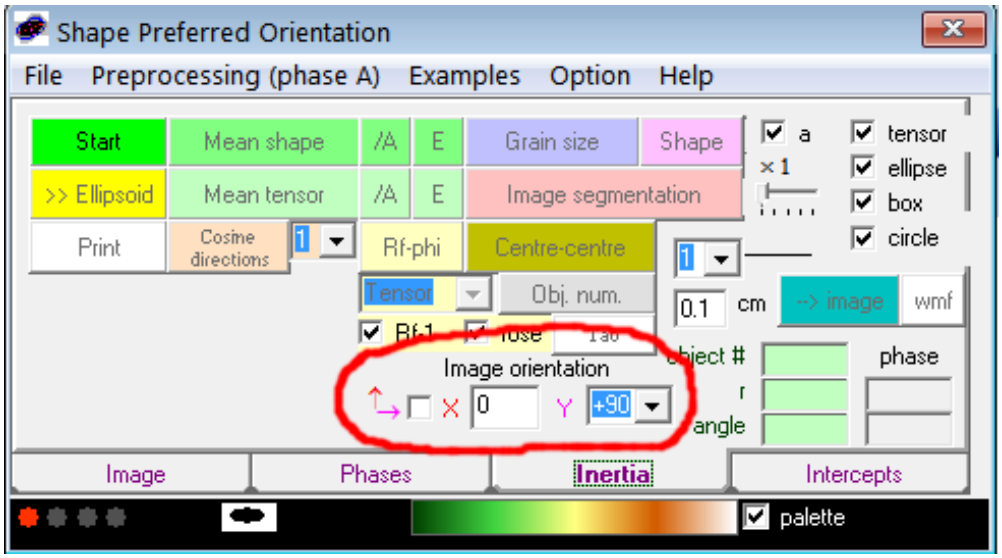

Figure 5.4: Note the X – Y input buttons…

2) Once the "**X**" and "**Y**" input and the scale input is complete, click "OK" (or press enter), and SPO-2003 will digitally render the image in various colours according to a rose of directions…(Figure 5.5).

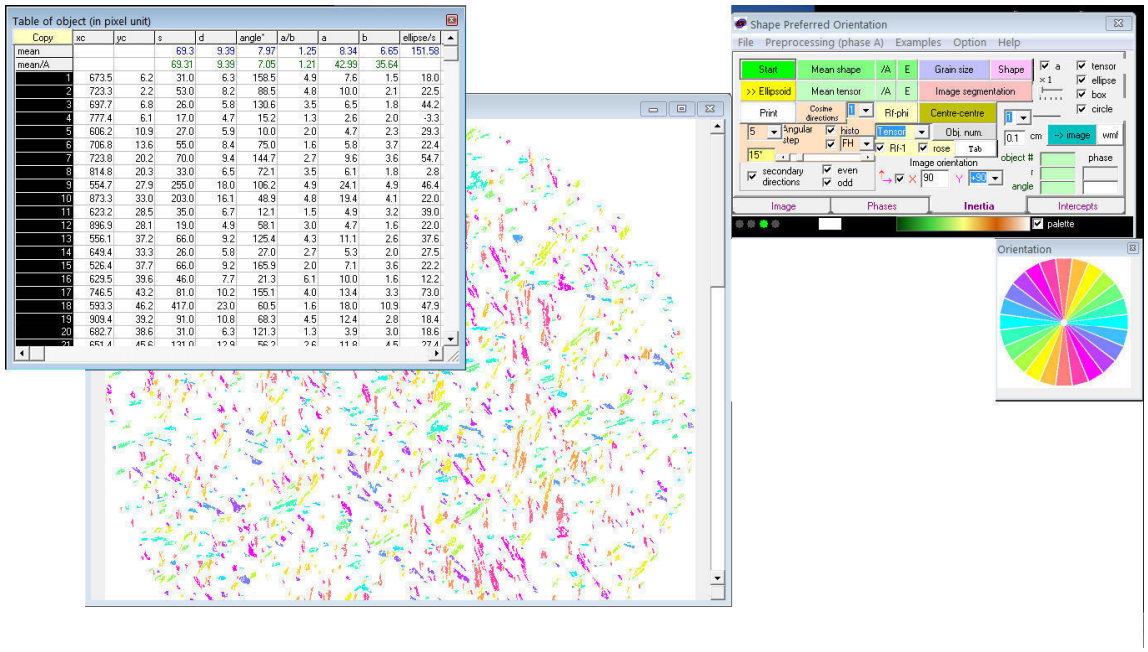

Figure 5.5: Screenprint from SPO-2003 showing the display of digitised and coloured grains in the original bitmap image. The rose of directions corresponds to grain populations of different orientations.

The table which appears provides all the raw data of each grain analysed by the program. In this particular image, 2196 grains have been analysed.

3) It is now possible to view the average tensor/shape ellipse of the fabric in this particular image (see mean shape and mean tensor buttons) (Figure 5.6). The red axis = long axis, pink axis = short axis. The number of grains is indicated, as well as the principal axes lengths, shape ratio, rake angle (e.g. angle X: 97.97°). Remember that the angles given are NOT geographic. They are calculated from the top of the image (horizontal on the screen) which is 00°. This is clear from Figure 5.6, as the "angle X" is 97.97° - i.e. close to vertical on the screen.

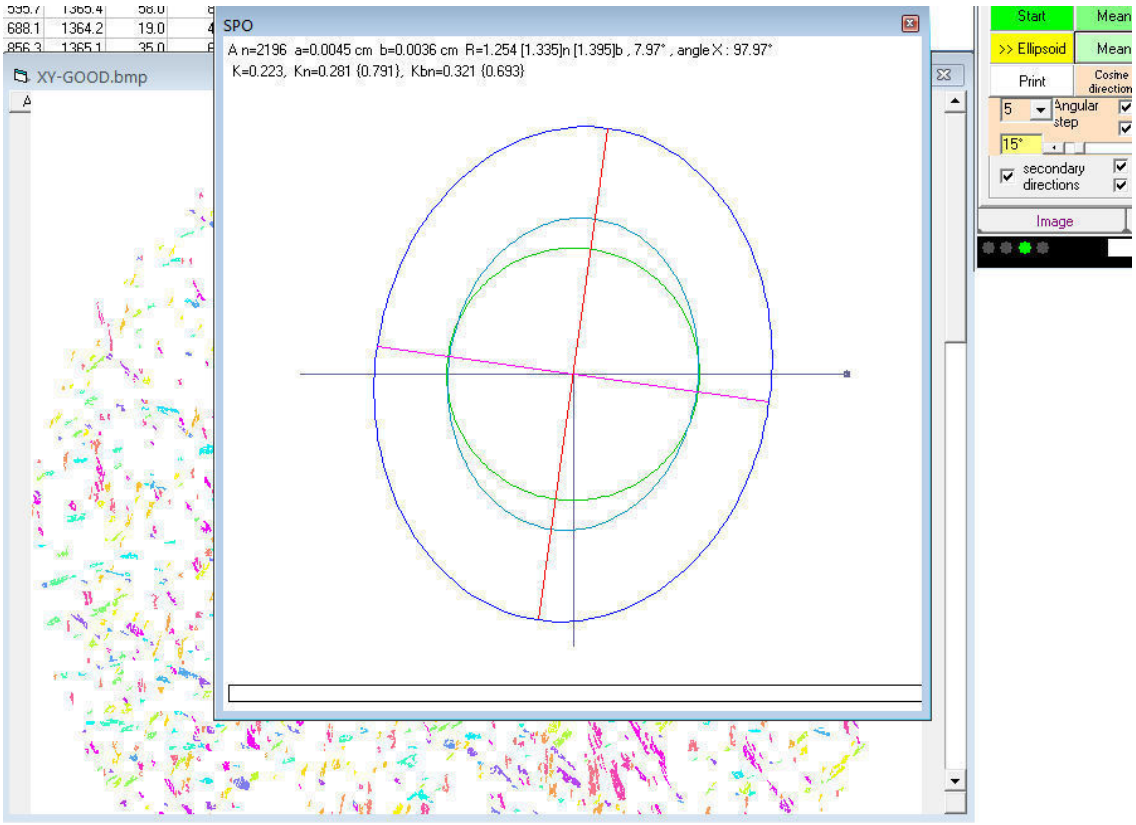

Figure 5.6: Mean tensor (in blue) for the example sample analysed above. Note that the long axis is shown in red, and the short axis in pink. The grey lines show the orientation (strike and dip) of the section. The green line is a perfect circle (i.e. isotropic), which allows for visual comparison with the anisotropic tensor/ellipse.

4) To continue this analysis into Ellipsoid-2003, click the yellow "ellipsoid" button, which will bring up a menu, as shown in Figure 5.7. A quick guide to the relevant options is discussed below this.

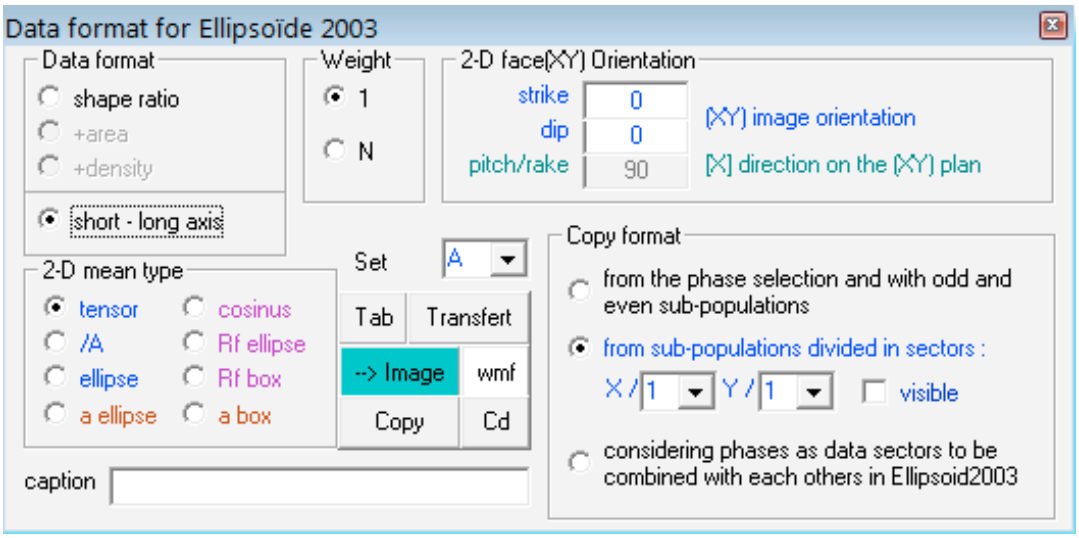

Figure 5.7: Data format menu in SPO-2003 which is used to determine the means of output for later use in Ellipsoid-2003.

Data format : up to the user; "short – long axis" is a better option than shape ratio as other shape parameters may need to be calculated at a later stage.

Weight : 1 = each thin section in the final ellipsoid analysis will be accorded a single weight each ; N = thin sections will be weighted according to the number of grains in each section.

2-D face (XY) Orientation : not necessary to fill anything in here…this data can be added from an Excel® spreadsheet where dip and strike data for the thin sections are stored.

2-D mean type : the "tensor" or "ellipse" options are the standard ways of data input/output of Ellipsoid-2003. Tensor is ideal if comparing this data to AMS for example.

Copy format : last option: "considering phases…combined…in Ellipsoid-2003"

Once the “Copy format” option has been clicked, a blank, single row table should appear. Then click “Transfert” (note incorrect spelling). The relevant data from the image should now appear in the table (Figure 5.8). Then click “copy”, and a menu acknowledging that the data is in the clipboard should appear.

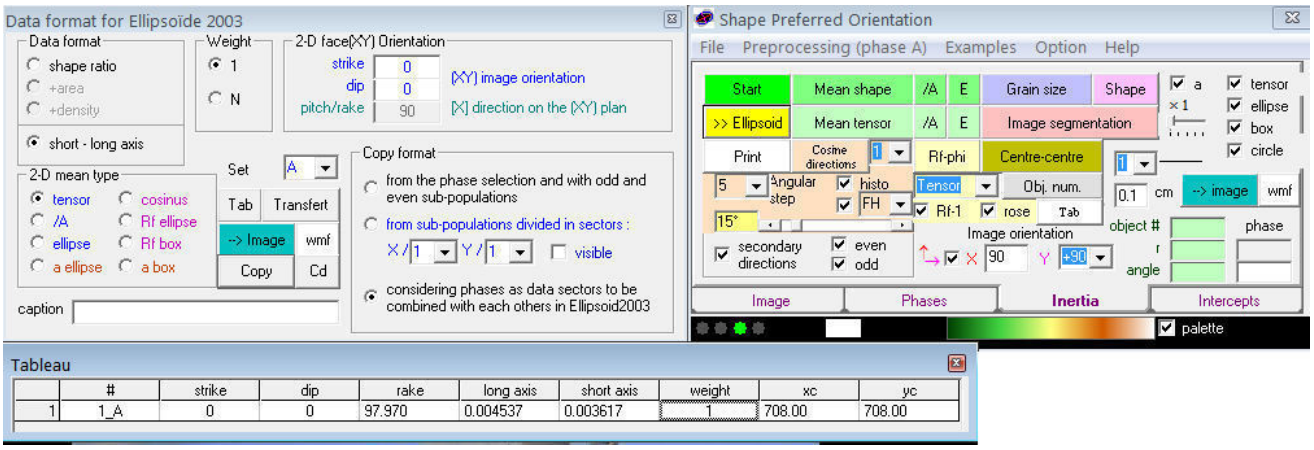

Figure 5.8: Data output table from SPO-2003 (lowermost table) with the relevant rake, long axis and short axis data which can be stored in a spreadsheet for all samples analysed.

Now paste this data into the prepared Excel spreadsheet (Figure 5.9) **making absolutely certain that the data is pasted next to the correct sample/specimen with which the analysed image is associated.** **The “weight” column is not that important at this stage. It is up to the user whether sections will be weighted equally (1) or weighted according to the number of grains (n) per section when analysing three or more sections in Ellipsoid-2003.**

Once again it is necessary to reiterate that once THREE sections for the same sample have been analysed, it is possible to paste this data into Ellipsoid-2003 to find the 3-D fabric orientation and intensity.

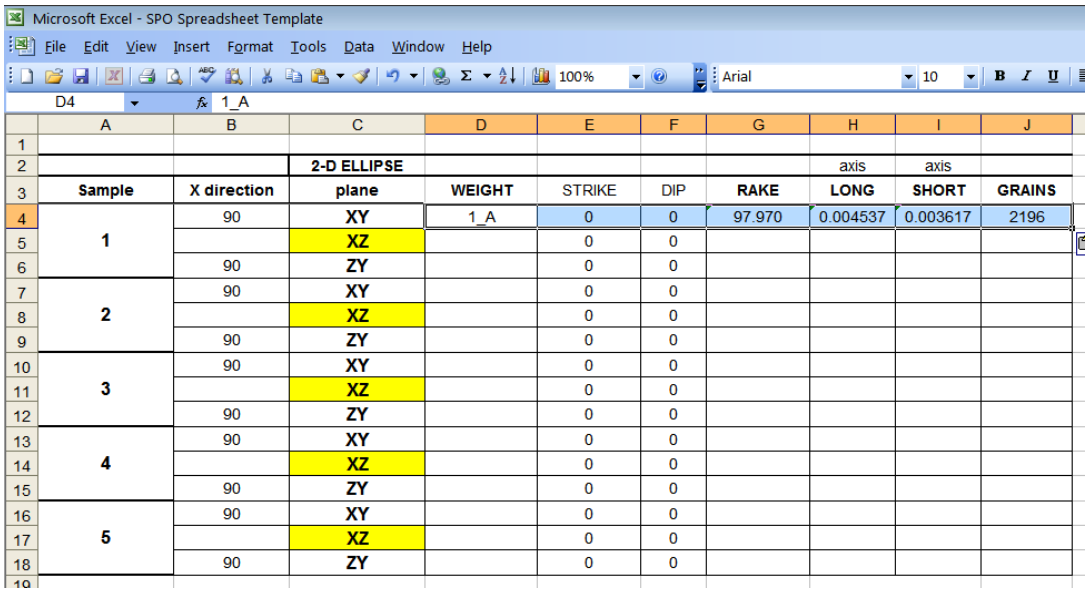

Microsoft Excel - SPO Spreadsheet Template

File Edit View Insert Format Tools Data Window Help

D4 1_A

	A	B	C	D	E	F	G	H	I	J
1										
2			2-D ELLIPSE					axis	axis	
3	Sample	X direction	plane	WEIGHT	STRIKE	DIP	RAKE	LONG	SHORT	GRAINS
4	1	90	XY	1_A	0	0	97.970	0.004537	0.003617	2196
5			XZ		0	0				
6		90	ZY		0	0				
7	2	90	XY		0	0				
8			XZ		0	0				
9		90	ZY		0	0				
10	3	90	XY		0	0				
11			XZ		0	0				
12		90	ZY		0	0				
13	4	90	XY		0	0				
14			XZ		0	0				
15		90	ZY		0	0				
16	5	90	XY		0	0				
17			XZ		0	0				
18		90	ZY		0	0				

Figure 5.9: Excel® spreadsheet of SPO data showing the addition of one thin-section worth of data pasted. It is critical that data is always pasted next to the correct XY, XZ or ZY plane otherwise serious errors will result when using Ellipsoid-2003 later.

5.2. Good Images vs. Bad Images

SPO-2003 is sensitive to populations of grains which share a common orientation. It cannot separate grains which are in contact with each other, but share different orientations. Measurements of such grains will therefore be an average of orientations, which is obviously less than ideal, if not incorrect altogether.

It is up to the user how grains are separated (i.e. digitally filtered vs. hand-selected grains), but in SPO-2003 itself it is possible to quite easily check if data are reliable in a processed image. Below are two bitmap images (Figure 5.10) of the same dolerite thin-section (XY section) processed to lesser and greater degrees of black-and-white "threshold" respectively. The left-hand image is correctly processed, and the right has a grain density which is too high, and is demonstrably so, based on the grain populations determined by SPO-2003 (Figure 5.11).

It is quite clear that the assignment of colour to grain populations is visually useful in determining which image is more reliable. Grains in the right-hand image of Figure 5.11

have become clustered and formed coloured blotches, the orientations of which are not significant with respect to the true petrofabric – represented more accurately by separated grains in the left-hand image.

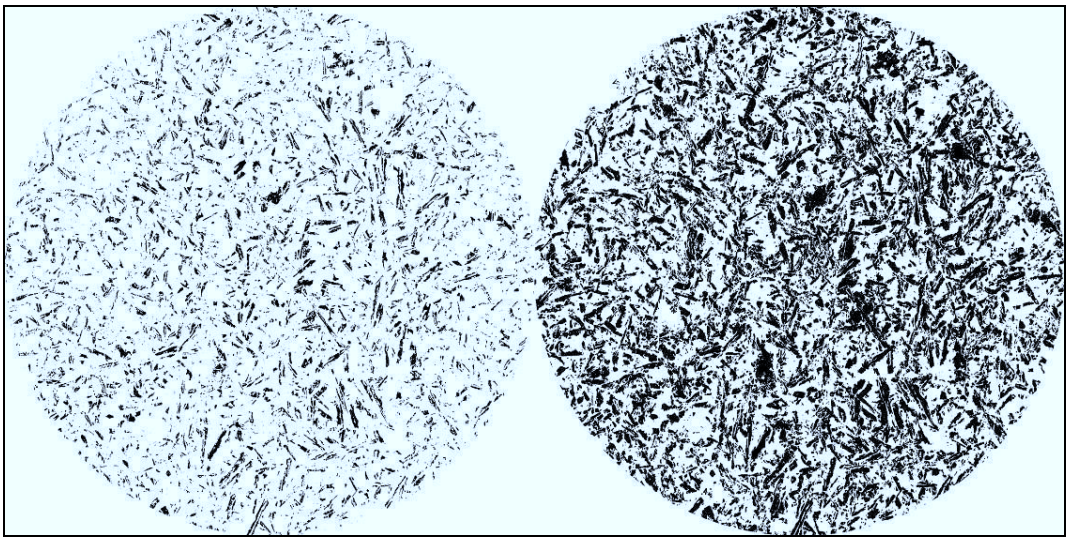

Figure 5.10: Black and white images of an XY section filtered to different levels of colour "threshold".

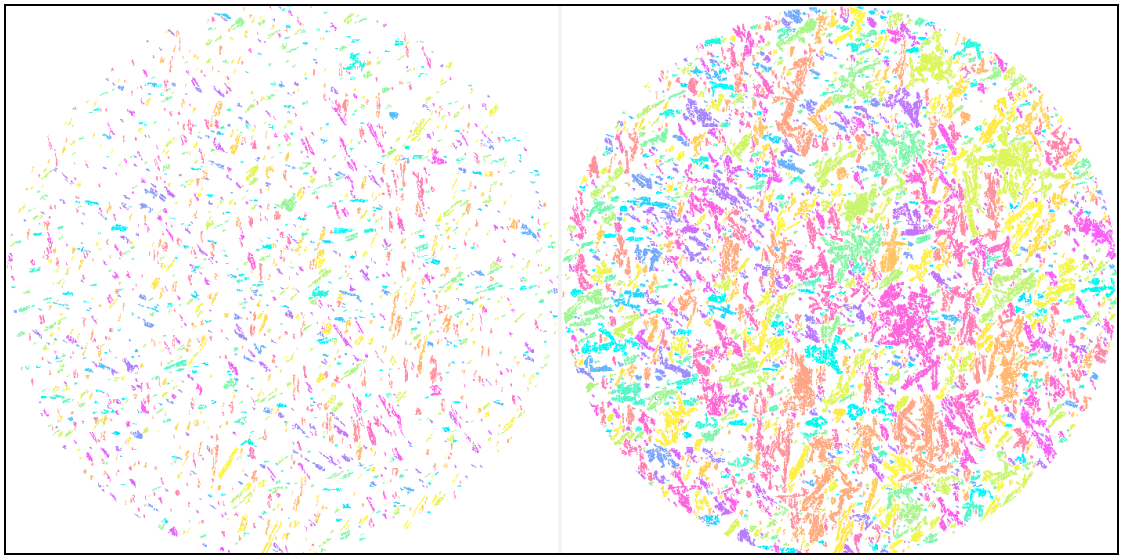

Figure 5.11: Images from Figure 5.10 processed by SPO-2003. Note the "clumping" of grains in the right hand image, which does not reflect the true petrofabric of the sample.

6. Measuring the 3-dimensional Ellipsoid

6.1. Introduction

Using the program "Ellipsoid-2003" it is possible to combine 2-D data from three thin sections (of the same sample) in order to truly define the geographic orientation of a fabric within the sample, as well as measuring physical parameters (intensity, shape etc.) of the fabric. Again, there is a built-in "Help" function which provides further background on many aspects of the analysis and software.

It is ideal to utilise the tabulated data in Excel® from the 2-D analysis for Ellipsoid-2003, as the data can then be entered simply using "copy" and "paste" functions.

6.2. The Ellipsoid-2003 User Interface

The main interface appears as shown below in Figure 6.1. Note that the lowermost table has #, strike, dip, rake etc. shown, which should correspond EXACTLY to the layout of the data table in Excel® used for the 2-D measurements. This facilitates quick and error-free pasting of 2-D data into Ellipsoid-2003 for analysis. Note the "Paste" button on the main interface.

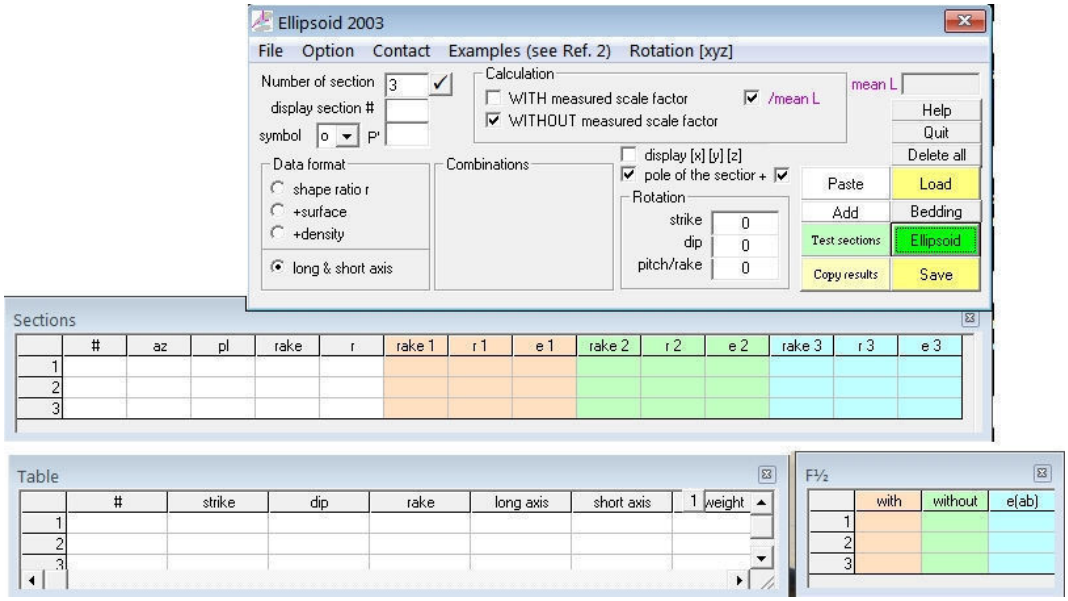

Figure 6.1: User interface of Ellipsoid-2003. See text for discussion of tables and function buttons.

Guide to important function buttons

Number of sections: any number of sections can be added (i.e. across a large dataset if it is necessary to contour data. Note that a MINIMUM of three (3) thin sections are required for the analysis of one sample.

Data format: Generally for one ellipsoid (per sample) it is advisable to use the "long & short axis" option, or the "shape ratio r" option.

Calculation: This option allows the user to proceed with or without a measured scale factor. If the size of the fabric elements/markers is deemed significant to the study, then "WITH

scale factor" can be used. If, however, the size of the fabric elements/markers are too small, or not significant to the study, then one can proceed "WITHOUT scale factor".

In Figures 6.2 and 6.3 below is an illustration of 30 thin sections (i.e. 10 samples) worth of data pasted into "Ellipsoid". Note that the ellipsoid is represented as a lower-hemisphere stereographic projection. The long axis "**A**" is shown in red, the intermediate axis "**B**" in green and the short axis "**C**" in blue. The lengths of these axes are in **bold** text under "Norm. L". The "trend" and "plunge" of these axes is shown below the lengths as well.

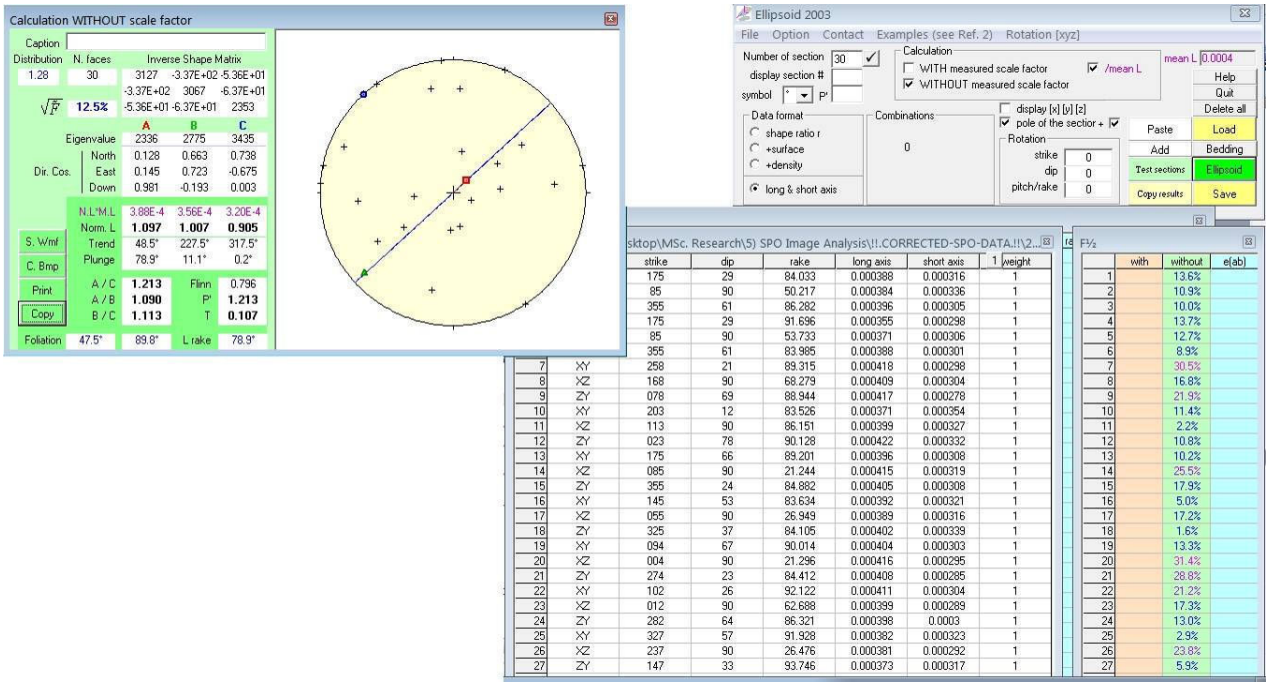

Figure 6.2: User interface of Ellipsoid-2003 showing some analysed data for plagioclase from dolerite dykes (30 thin sections). Note the resultant ellipsoid presented stereographically (lower hemisphere). See also Figure 6.3 below.

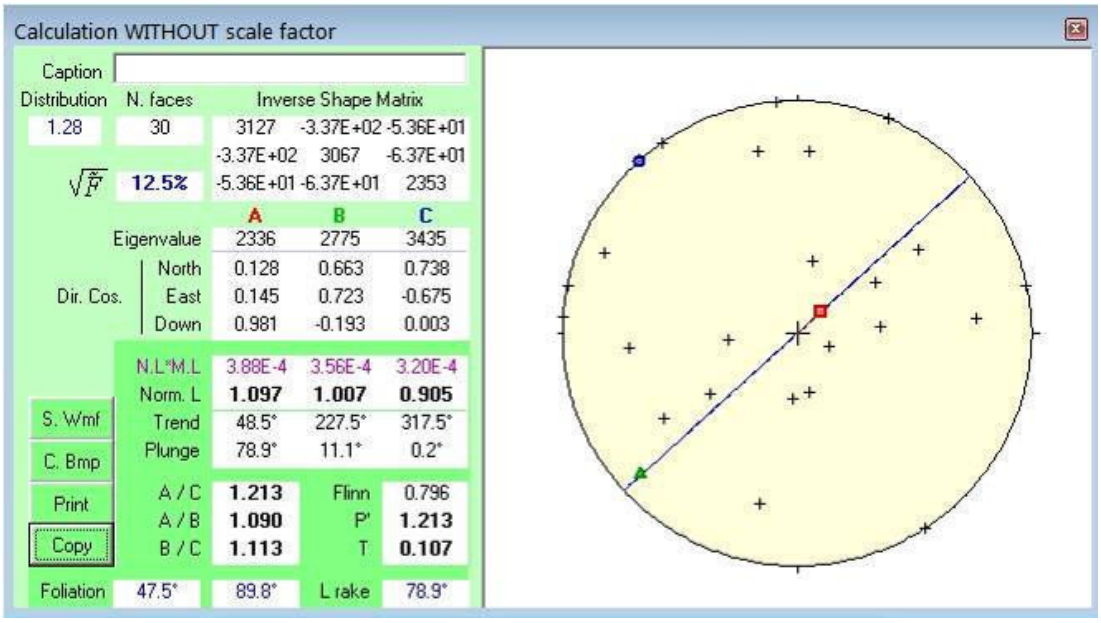

Figure 6.3: Ellipsoid data from 30 thin sections (from Figure 6.2) presented stereographically. Note the three principal axes (red, green and blue) and the NE-SW striking foliation shown in blue. The numerous black crosses (+) on the stereographic projection indicate the orientations of the thin sections (30 in total in this example) measured for this analysis.

6.3. Exporting data from Ellipsoid-2003

Similarly to SPO-2003, it is possible to export data and paste it into a prepared Excel® spreadsheet (preferably the same one in which all SPO and ellipsoid data are kept). Simply click “copy” (bottom left button, Figure 6.3) and then “paste” into Excel®.

N	30		
F	0.125002815		
	A	B	C
nLenght	1.097395872	1.006919495	0.90498
strike	48.452169	227.5042845	317.539
dip	78.85669615	11.14181711	0.17973
aLength	3.88E-04	3.56E-04	3.19653
F-L	47.53968262	89.82026917	78.8581
ac	1.213		
ab	1.09		
bc	1.113		
P	1.213239513		
T	0.107311264		

Figure 6.4: Data pasted directly from Ellipsoid-2003 from 30 thin sections (from Figure 6.2 and 6.3).

Unfortunately, the pasted table is not very clear. The following terms require clarification:

N = number of sections measured
F = error factor (here shown divided by 100)
A = major axis of ellipse
B = intermediate axis
C = minor axis
nLenght = normalised length of each axis (note incorrect spelling)
aLength = actual length (in centimetres) of each axis
Strike = azimuth/plunge angle of axis
Dip = plunge angle of axis

F-L = strike (e.g. 47.53) and dip (e.g. 89.82) of the foliation

P = anisotropy factor (e.g. P for a sphere = 0). This is essentially equivalent to the ratio of long axis to short axis (ac).

T = Shape factor: a measure of whether the ellipsoid is oblate (T>0) or prolate (T<0)

To export images of the ellipsoid, click "S.Wmf" to save a Windows® metafile – these are editable in Adobe Illustrator® or Corel Draw®. "C.Bmp" indicates that a Windows Bitmap can be copied, and then pasted elsewhere.

In addition, it is best to save an ASCII file (.elli) for each sample, as these can be quickly re-opened and examined without having to do any unnecessary re-calculation each time.

The $\sqrt{F}$ factor is an incompatibility index that quantifies the potential misfit between the 2-dimensional sectional ellipses and the 3-dimensional ellipsoid. It is given as a percentage which is analogous to the standard deviation of the population of sectional ellipses. Thus, where values of $\sqrt{F}$ are < 10% the ellipsoid can be considered geologically significant, i.e. it is truly representative of the petrofabric measured.

7. Concluding Remarks

As discussed initially, measuring the shape preferred orientation (SPO) of mineral(s) is a useful means of quantifying the shape, orientation and intensity of a fabric in a rock. Hopefully this manual will be a useful aid in "getting to grips" with the processes and software necessary to measure any kind of SPO in a geological sample. There are several points which must be stressed:

1. Field control is extremely important:
    a. Measurements of any fabric without geological context become scientifically irrelevant.
    b. The orientation of the structure to which the fabric relates; i.e. the orientation of bedding/layering/intrusion margin etc. is just as important as collecting and measuring samples.
    c. Samples must be ORIENTATED – and preferably orientated whilst in the field (be cautious of highly magnetised rock/material if using a magnetic compass/core orientator).
2. One thin section, in one orientation per sample is not significant. To quantify any fabric, even if the orientation is not desired, at least THREE MUTUALLY ORTHOGONAL THIN SECTIONS PER SAMPLE MUST BE ANALYSED.
3. ALWAYS make sure that the thin sections are viewed in the correct orientation (section 2.4.2) and the SCALE of the images is known.
4. Make use of the test sections and the "answers" provided. Doing this will immediately highlight where and how small mistakes arise.
5. Do not simply trust any "answers" which SPO or Ellipsoid provide – scrutinise the input to and the output of data from this, or any other, software.

It cannot be stressed enough how much careful preparation of the methodology, of spreadsheets and of the goal of a particular project will minimise wasted effort. Thus, this type of work should be carried out step-by-step – bearing in mind that any mistakes in any of the steps will render later analysis and/or interpretation incorrect. Do not make mistakes.

8. Bibliography & References

Archanjo, C.J., Launeau, P., 2004. Magma flow inferred from preferred orientations of plagioclase of the Rio Cearf-Mirim dyke swarm (NE Brazil) and its AMS significance. In: Martin-Hernandez, F., Luneburg, C.M., Aubourg, C., Jackson, M. (Eds.), Magnetic Fabric: Methods and applications. Geological Society of London Special Publication 238, 285–298.

Aubourg, C., Giordano, G., Mattei, M., Speranza, F., 2002. Magma flow in sub-aqueous rhyolitic dikes inferred from magnetic fabric analysis (Ponza Island, W. Italy). Physics and Chemistry of the Earth 27, 1263–1272.

Callot, J.P., Guichet, X. 2003. Rock texture and magnetic lineation in dykes: a simple analytical model. Tectonophysics 366, 207–222.

Cañón-Tapia, E., Chávez-Álvarez, M.J., 2004. Theoretical aspects of particle movement in flowing magma: implications for the anisotropy of magnetic susceptibility of dykes. In: Martin-Hernandez F., Luneburg, C.M., Aubourg, C., Jackson, M. (Eds.), Magnetic Fabric: Methods and Applications. Geological Society of London Special Publication 238, 227–249.

Correa-Gomes, L.C., Souza Filho, C.R., Martins, C.J.F.N., Oliveira, E.P., 2001. Development of symmetrical and asymmetrical fabrics in sheet-like igneous bodies: the role of magma flow and wall-rock displacements in theoretical and natural cases. Journal of Structural Geology 23, 1415–1428.

Cruden, A.R., 1990. Flow and fabric development during the diapiric rise of magma. Journal of Geology 98, 681–698.

Ferguson, C.C., 1979. Rotations of elongate rigid particles in slow non-newtonian fluids. Tectonophysics 60, 247–262.

Geoffroy, L., Callot, J.P., Aubourg, C., Moreira, M., 2002. Is the common use of AMS in mafic dykes scientifically correct? Terra Nova 14, 183–190.

Hastie, W.W., Aubourg, C., Watkeys, M.K., 2011. When an 'inverse' fabric is not inverse: an integrated AMS-SPO study in MORB-like dykes. Terra Nova 23, 49–55.

Launeau, P., 2004. Mise en évidence des écoulements magmatiques par analyse d'images 2-D des distributions 3-D d'Orientations Préferentielles de Formes. Bulletin of the Geological Society of France 175, 331–350.

Launeau, P., Cruden, A.R., 1998. Magmatic fabric acquisition mechanisms in a syenite: Results of a combined anisotropy of magnetic susceptibility and image analysis study. Journal of Geophysical Research 103, 5067–5089.

Launeau, P., Robin, P.-Y.F., 1996. Fabric analysis using the intercept method. Tectonophysics 267, 91–119.

Launeau, P., Robin, P.-Y.F., 2005. Determination of fabric & strain ellipsoids from measured sectional ellipses - Implementation and applications. Journal of Structural Geology 27, 2223–2233.

Passchier, C.W., Trouw, R.A.J., 1998. Micro-tectonics. Springer, Berlin, 283pp.

Pollard, D.D., Fletcher, R.C., 2005. Fundamentals of Structural Geology. Cambridge University Press, New York, 512pp.

Philpotts, A.R., Philpotts, D.E., 2007. Upward and downward flow in a camptonite dike as recorded by deformed vesicles and the anisotropy of magnetic susceptibility (AMS). Journal of Volcanology and Geothermal Research 161, 81–94.

Ramsay, J.G., 1989. Emplacement kinematics of a granite diapir: the Chindamora batholith, Zimbabwe. Journal of Structural Geology 11, 191–209.

Willis, D.G., 1977. A kinematic model of preferred orientation. Geological Society of America Bulletin 88, 883–894.

- Appendix E -

1) **Individual Dyke Sketch Maps**

2) **Tabulated Dyke and Sample Data**

3) **Tabulated AMS Data**

4) **Tabulated SPO Data – Plagioclase**

5) **Tabulated SPO Data – Opaque Grains**

1) Individual Dyke Sketch Maps

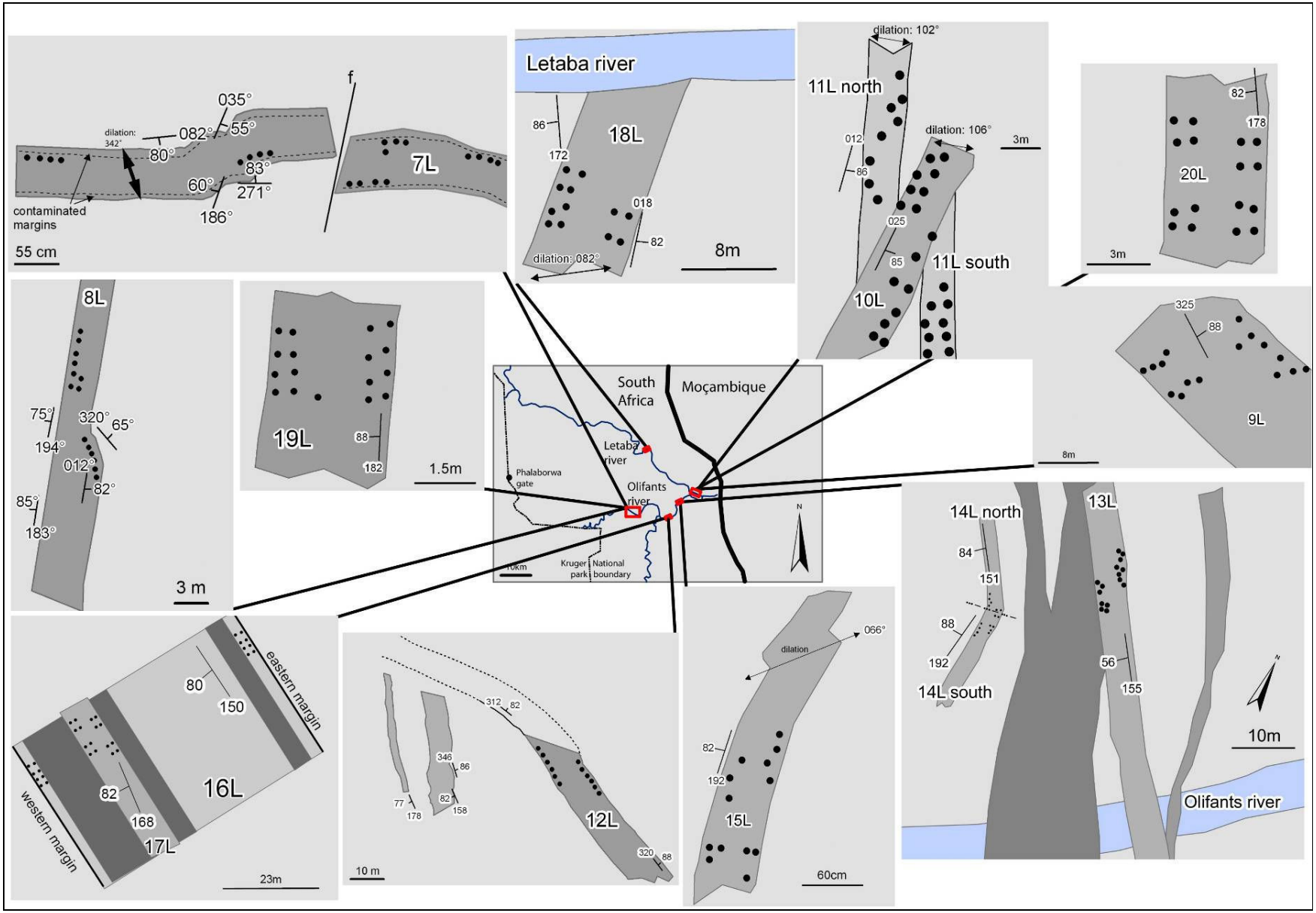

Figure E1: Dykes of the northern Lebombo dyke swarm. Positions of samples are indicated.

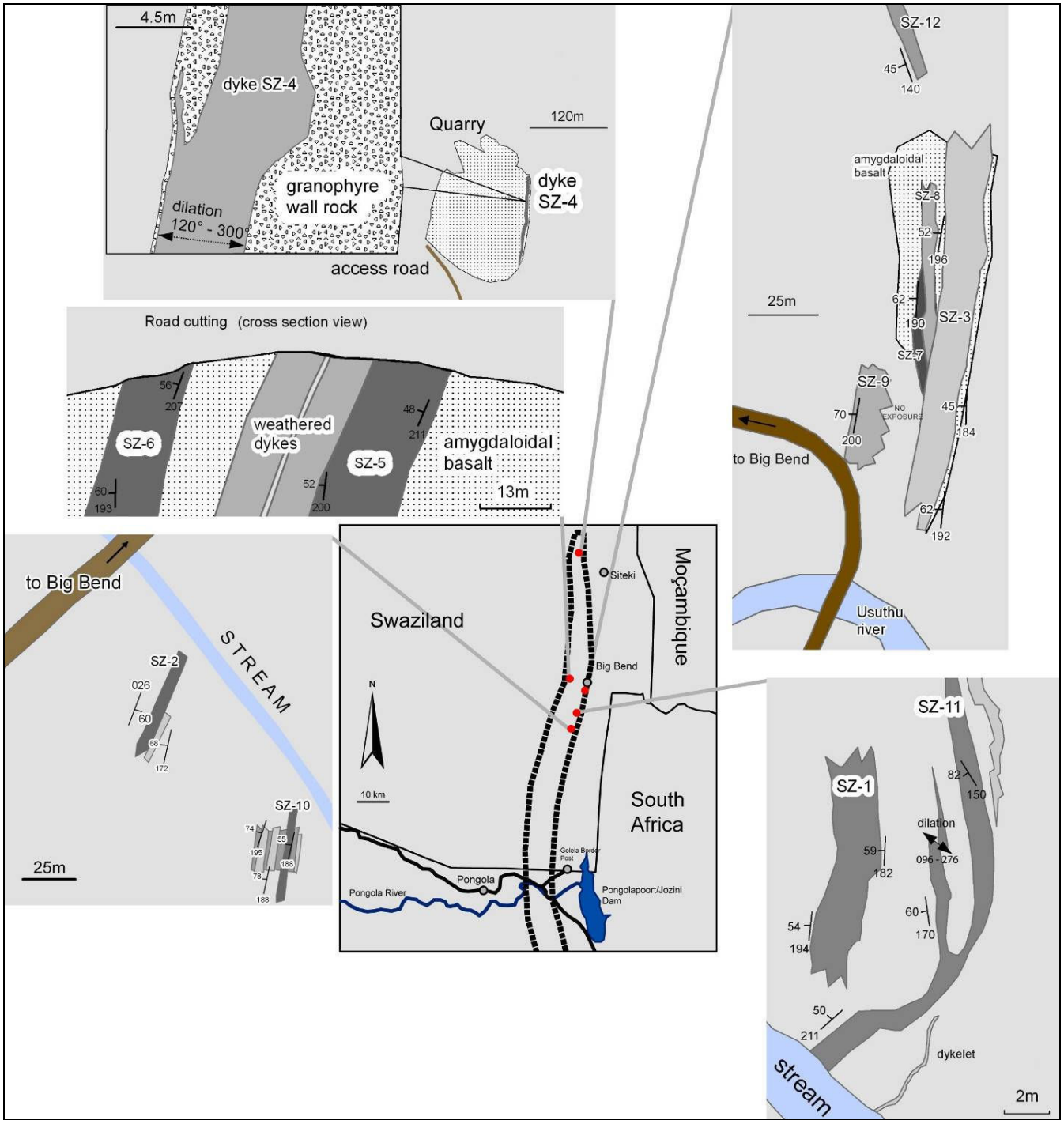

Figure E2: Dykes of the northern Rooi Rand dyke swarm. Note that dykes SZ-5 and SZ-6 are shown in cross-section, and not map view due to their outcrop position in a road cutting.

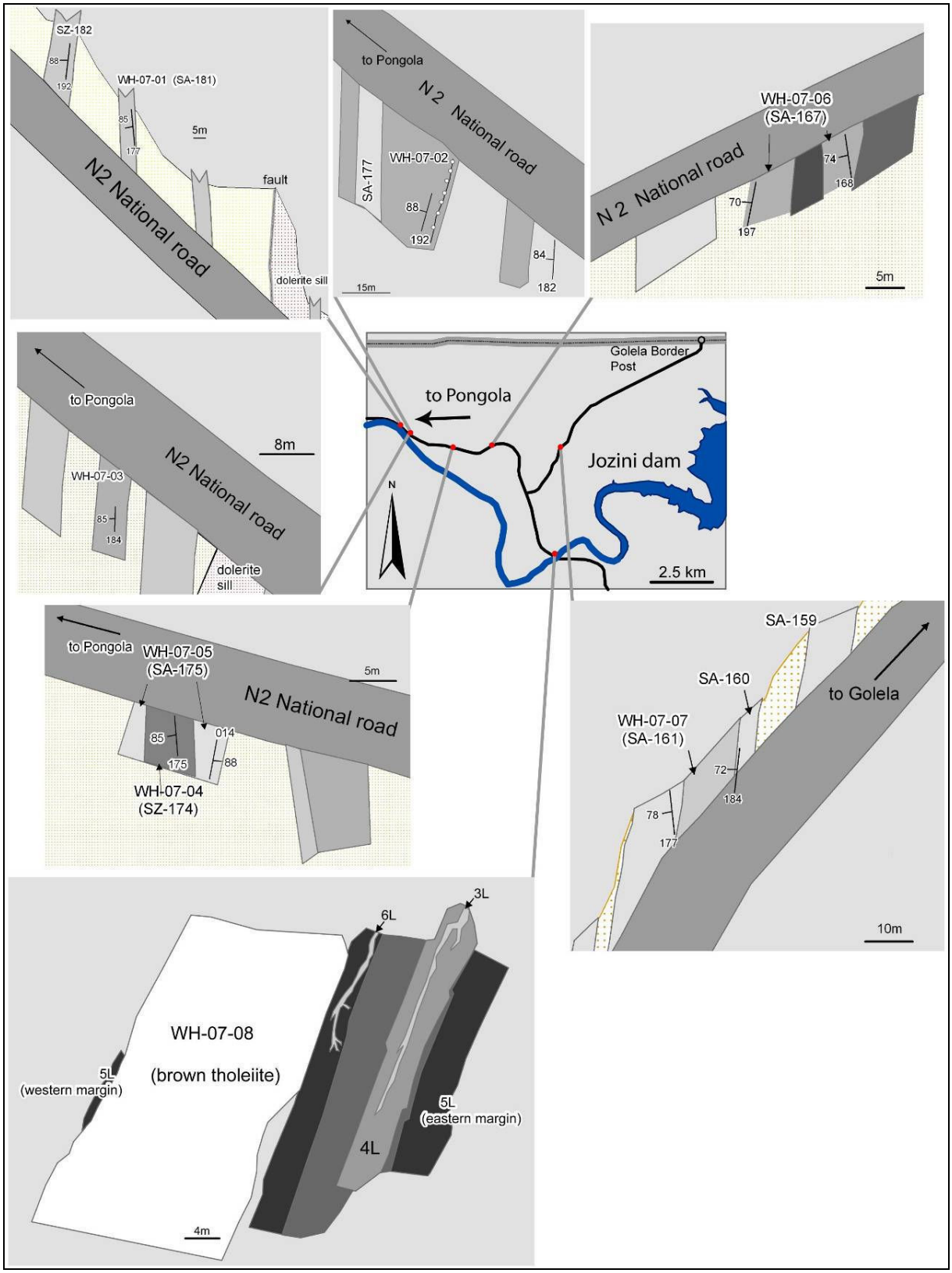

Figure E3: Dykes of the central Rooi Rand dyke swarm. Note that the majority of outcrops are in road cuttings.

2) Tabulated Dyke and Sample Data

Northern Lebombo dyke swarm						
Dyke	*Site*	*Thickness*	*Orientation (dip and strike)*	*Lat. / Long.*	*Dilation direction*	*n*
7L	SOUTH	0.55m	83°/271°	24°02'20.1" S | 31°34'35.5" E (Clarens section)	dil. Plane: 55°/342°	8
	NORTH					8
7L-17-20	NORTH					4
8L	WEST	~3.5m	85°/183°	24°02'14.0" S | 31°34'28.8" E (Clarens section)	020°-200°	8
	EAST		56°/316°			8
9L	WEST	16.8m	88°/325°	23°58'31.0" S | 31°47'37.0" E (Vutamlilo section)	028°-208°	8
	EAST					8
10L	WEST	<3m	85°/025°	23°58'39.6" S | 31°47'53.2" E (Vutamlilo section)	~096°/106°	6
	EAST					9
11L-North	WEST	~2m	86°/012°	23°58'39.6" S | 31°47'53.2" E (Vutamlilo section)	~089°/102°	4
	EAST					4
11L-South	WEST					4
	EAST					5
12L	WEST	~10m	90°/120°	23°58'39.1" S | 31°47'51.5" E (Vutamlilo section)	-	6
	EAST					6
13L-1-4	EAST	5.5m	70°/004°	24°00'01.3" S | 31°45'07.9" E (Olifants Gorge section)	-	4
13L-6-8			74°/115°			3
13L-9-19	WEST		56°/155°			11
14L-NORTH	WEST	2.3m	84°/151°	24°00'01.3" S | 31°45'07.9" E (Olifants Gorge section)	054°-234°	4
	EAST		88°/192°			4
14L-SOUTH	WEST		88°/192°			4
	EAST					4
15L	WEST	0.6m	82°/192°	24°00'01.3" S | 31°45'06.3" E (Olifants Gorge section)	066°-246°	6
	EAST					6
16L	WEST	28m	80°/150°	24°03'02.0" S | 31°43'53.3" E (Balule Camp section)	-	8
	EAST					8
17L	WEST	5.2m	82°/168°	24°03'02.2" S | 31°43'52.3" E (Balule Camp section)	-	8
	EAST					8
18L	WEST	7.5m	82°/018°	23°48'48.7" S | 31°34'52.4" E (Clarens section)	082°-262°	8
	EAST					8
19L	WEST	3m	88°/182°	24°03'30.5" S | 31°42'41.2" E (Balule Camp section)	-	8
	EAST					8
20L	WEST	3.5m	82°/178°	23°48'47.2" S | 31°34'57.1" E (Clarens section)	-	8
	EAST					8
Northern Rooi Rand dyke swarm						
SZ-1	WEST	~2m	52°/192°	26°55'29.7" S | 31°52'14.5" E	-	9
	EAST		55°/181°			11
SZ-2	WEST	~5m	~60°/026°	26°51'35.9" S | 31°51'19.5" E	-	9
	EAST					10
SZ-3	WEST	~5m	~60°/193°	26°51'35.9" S | 31°52'15.4" E	-	16
	EAST		~54°/188°			17
SZ-4	WEST	1.6m	72°/005°	26°28'10.7" S | 31°51'37.9" E	110°-290°	10
	EAST		64°/054°			10
SZ-5	WEST	18m	52°/200°	26°49'08.7" S | 31°52'12.3" E	-	10
	EAST		48°/211°			7
SZ-6	WEST	13m	60°/193°	26°49'08.7" S | 31°52'12.3" E	-	10
	EAST		56°/207°			13
SZ-7	WEST	~0.8m	64°/197°	26°51'35.9" S | 31°54'15.4" E	140°-320°	11
	EAST					10

SZ-8	WEST	1.5m	52°/196°	26°51'35.9" S | 31°54'15.4" E	-	8
	EAST					11
SZ-9	WEST	>2m	70°/200°	26°51'35.9" S | 31°54'15.4" E	-	14
SZ-10	WEST	1.2m	~65°/177°	26°58'02.9" S | 31°51'19.5" E	-	8
	EAST		~57°/183°			6
SZ-11	WEST	0.4m	82°/150°	26°55'29.7" S | 31°52'14.5" E	060°-240°	5
	EAST					5
SZ-12	WEST	1.2m	45°/140°	26°51'35.9" S | 31°54'15.4" E	-	6
Central Rooi Rand dyke swarm						
WH-07-01	WEST	5.85m	85°/177°	27°20'50.3" S | 31°45'53.1" E	-	3
	EAST					2
WH-07-02	EAST	7.6m	88°/192°	27°20'59.2" S | 31°46'05.4" E	-	7
WH-07-03	WEST	5.3m	72°/353°	27°20'56.8" S | 31°46'01.7" E	-	4
WH-07-04	WEST	4.7m	85°/175°	27°21'17.6" S | 31°47'09.7" E	-	7
	EAST					6
WH-07-05	WEST	9.8m	88°/014°	27°21'17.6" S | 31°47'09.7" E	-	7
	EAST					7
WH-07-06	WEST	8.8m	74°/168°	27°21'17.0" S | 31°48'07.6" E	-	7
	EAST					6
WH-07-07	WEST	4.3m	78°/177°	27°21'22.4" S | 31°49'47.9" E	-	7
	EAST		72°/184°			7
WH-07-08	WEST	20.1m	trend: 030°	27°23'37.4" S | 31°49'34.3" E	-	7
	EAST					8
3L	WEST	0.43-0.47m	82°/170°	27°23'37.3" S | 31°49'35.2" E	060°-240°	8
	EAST					9
4L	WEST	4.1m	82°/170°	27°23'37.3" S | 31°49'35.2" E	-	8
	EAST					8
5L	WEST	5.5m	90°/350°	27°23'37.4" S | 31°49'34.3" E	-	8
	EAST					8
6L	WEST	0.62m	90°/030°	27°23'37.3" S | 31°49'35.2" E	-	9
	EAST					9
	EAST					5

3) Tabulated AMS Data

The Northern Lebombo dyke swarm

Dyke	*Site*	*Thickness*	*Orientation (dip and strike)*	*Lat. / Long.*	*Dilation direction*	*n*	*Km (10^{-5} SI Units)*	*K1*	*K3*	*P′*	*T*
7L	WEST	0.55m	83°/271°	24°02'20.1" S | 31°34'35.5" E	dil. Plane: 55°/342°	8	779	68°/103°	22°/275°	1.0443	0.0846
	EAST					8	326	61°/359°	16°/239°	1.0289	0.0805
7L-17-20	EAST					4	76	02°/070°	74°/169°	1.0073	0.2045
8L	WEST	~3.5m	85°/183°	24°02'14.0" S | 31°34'28.8" E	020°-200°	8	2065	85°/001°	04°/208°	1.0501	-0.3780
	EAST		56°/316°			8	3131	76°/244°	10°/109°	1.0504	-0.2624
9L	WEST	16.8m	88°/325°	23°58'31.0" S | 31°47'37.0" E	028°-208°	8	2841	81°/339°	01°/243°	1.0294	0.1724
	EAST					8	2012	71°/321°	01°/055°	1.0350	0.1971
10L	WEST	<3m	85°/025°	23°58'39.6" S | 31°47'53.2" E	~096°/106°	6	5107	55°/204°	03°/299°	1.0251	0.2670
	EAST					9	6323	51°/222°	07°/123°	1.0208	0.3766
11L-North	WEST	~2m	86°/012°	23°58'39.6" S | 31°47'53.2" E	~089°/102°	4	5552	19°/195°	08°/102°	1.0120	-0.0125
	EAST					4	3083	61°/231°	19°/103°	1.0168	0.1300
11L-South	WEST					4	4187	20°/058°	37°/164°	1.0075	0.2508
	EAST					5	3890	05°/025°	66°/284°	1.0104	0.0888
12L	WEST	~10m	90°/120°	23°58'39.1" S | 31°47'51.5" E	-	6	6522	44°/006°	10°/267°	1.0448	0.3008
	EAST					6	5309	17°/321°	16°/226°	1.0268	0.0265
13L-1-4	EAST	5.5m	70°/004°	24°00'01.3" S | 31°45'07.9" E	-	4	4072	23°/172°	66°/334°	1.0195	-0.0988
13L-6-8			74°/115°			3	3182	17°/175°	49°/064°	1.0243	-0.3067
13L-9-19	WEST		56°/155°			11	2811	39°/065°	20°/318°	1.0117	-0.2338
14L-NORTH	WEST	2.3m	84°/151°	24°00'01.3" S | 31°45'07.9" E	054°-234°	4	8194	60°/151°	13°/265°	1.0200	0.3655
	EAST		88°/192°			4	6855	06°/282°	47°/018°	1.0225	0.0040
14L-SOUTH	WEST		88°/192°			4	8666	20°/058°	37°/164°	1.0193	0.0035
	EAST					4	7096	05°/025°	66°/284°	1.0190	0.0763
15L	WEST	0.6m	82°/192°	24°00'01.3" S | 31°45'06.3" E	066°-246°	6	9077	12°/191°	16°/097°	1.0197	0.0268
	EAST					6	10753	26°/085°	64°/254°	1.0232	0.0695
16L	WEST	28m	80°/150°	24°03'02.0" S | 31°43'53.3" E	-	8	5278	02°/145°	71°/240°	1.0190	-0.2118
	EAST					8	6877	15°/322°	17°/057°	1.0394	0.5315
17L	WEST	5.2m	82°/168°	24°03'02.2" S | 31°43'52.3" E	-	8	9816	22°/159°	13°/064°	1.0219	0.1915
	EAST					8	8112	12°/183°	19°/089°	1.0341	0.4210
18L	WEST	7.5m	82°/018°	23°48'48.7" S | 31°34'52.4" E	082°-262°	8	7541	20°/123°	46°/235°	1.0226	0.1485
	EAST					8	7474	25°/296°	52°/168°	1.0144	-0.2844
19L	WEST	3m	88°/182°	24°03'30.5" S | 31°42'41.2" E	-	8	4836	30°/343°	41°/223°	1.0342	-0.1961
	EAST					8	5976	05°/010°	71°/267°	1.0161	-0.1449
20L	WEST	3.5m	82°/178°	23°48'47.2" S | 31°34'57.1" E	-	8	6475	39°/341°	44°/200°	1.0180	-0.2424
	EAST					8	6439	09°/096°	49°/196°	1.0539	-0.3719
					Tot. Spec.	225					

n =number of specimens *P′* = degree of anisotropy *Km* = (kmax + kint + kmin)÷3 *T* = shape factor (oblate/prolate)

The Rooi Rand dyke swarm (Northern region, Swaziland)

Dyke	*Site*	*Thickness*	*Orientation (dip and strike)*	*Lat. / Long.*	*Dilation direction*	*n*	*Km (10^{-5} SI units)*	*K1*	*K3*	*P′*	*T*
SZ-1	WEST	~2m	52°/192°	26°55'29.7" S | 31°52'14.5" E	-	9	6154	25°/193°	11°/098°	1.023	0.400
	EAST		55°/181°			11	4982	19°/194°	14°/099°	1.027	0.026
SZ-2	WEST	~5m	~60°/026°	26°51'35.9" S | 31°51'19.5" E	-	9	3920	46°/195°	07°/293°	1.019	-0.222
	EAST					10	3827	44°/343°	16°/089°	1.026	-0.223
SZ-3	WEST	~5m	~60°/193°	26°51'35.9" S | 31°52'15.4" E	-	16	4259	22°/345°	31°/089°	1.021	0.159
	EAST		~54°/188°			17	5197	37°/322°	38°/089°	1.037	0.039
SZ-4	WEST	1.6m	72°/005°	26°28'10.7" S | 31°51'37.9" E	110°-290°	10	2509	13°/212°	08°/304°	1.036	0.322
	EAST		64°/054°			10	4910	26°/175°	46°/054°	1.017	0.182
SZ-5	WEST	18m	52°/200°	26°49'08.7" S | 31°52'12.3" E	-	10	4117	34°/349°	26°/098°	1.027	-0.079
	EAST		48°/211°			7	2209	45°/347°	29°/112°	1.020	0.121
SZ-6	WEST	13m	60°/193°	26°49'08.7" S | 31°52'12.3" E	-	10	5149	59°/216°	13°/103°	1.023	-0.521
	EAST		56°/207°			13	3678	42°/355°	36°/126°	1.041	0.416
SZ-7	WEST	~0.8m	64°/197°	26°51'35.9" S | 31°54'15.4" E	140°-320°	11	4557	69°/139°	18°/287°	1.036	-0.426
	EAST					10	4038	74°/118°	16°/286°	1.036	-0.301
SZ-8	WEST	1.5m	52°/196°	26°51'35.9" S | 31°54'15.4" E	-	8	5983	47°/184°	05°/088°	1.023	0.137
	EAST					11	4767	71°/154°	04°/256°	1.024	-0.269
SZ-9	WEST	>2m	70°/200°	26°51'35.9" S | 31°54'15.4" E	-	14	6756	71°/310°	15°/091°	1.022	-0.165
SZ-10	WEST	1.2m	~65°/177°	26°58'02.9" S | 31°51'19.5" E	-	8	6330	39°/343°	19°/090°	1.036	0.067
	EAST		~57°/183°			6	5445	28°/033°	16°/294°	1.018	-0.026
SZ-11	WEST	0.4m	82°/150°	26°55'29.7" S | 31°52'14.5" E	060°-240°	5	249	44°/195°	01°/103°	1.010	0.165
	EAST					5	271	51°/206°	05°/109°	1.011	0.504
SZ-12	WEST	1.2m	45°/140°	26°51'35.9" S | 31°54'15.4" E	-	6	3792	06°/344°	52°/082°	1.025	0.230
	EAST					5	3178	05°/156°	53°/060°	1.035	0.087
					Total specimens:	212					

n =number of specimens

Km = (kmax + kint + kmin)/3

P′ = degree of anisotropy

T = shape factor (oblate/prolate)

The Rooi Rand dyke swarm (Central Region, Pongola, South Africa)

Dyke	*Site*	*Thickness*	*Orientation (dip and strike)*	*Lat. / Long.*	*Dilation direction*	*n*	*Km (10^{-5} SI units)*	*K1*	*K3*	*P′*	*T*
WH-07-01	WEST	5.85m	85°/177°	27°20'50.3" S | 31°45'53.1" E	-	3	3466	86°/036°	04°/254°	1.0560	-0.0270
	EAST					2	4397	71°/286°	09°/042°	1.0455	-0.2975
WH-07-02	EAST	7.6m	88°/192°	27°20'59.2" S | 31°46'05.4" E	-	7	70	81°/040°	03°/146°	1.0097	-0.0841
WH-07-03	WEST	5.3m	72°/353°	27°20'56.8" S | 31°46'01.7" E	-	4	2268	62°/033°	15°/272°	1.0578	0.0540
WH-07-04	WEST	4.7m	85°/175°	27°21'17.6" S | 31°47'09.7" E	-	7	3923	63°/320°	11°/072°	1.0546	0.4014
	EAST					6	3162	63°/353°	01°/261°	1.0474	0.0444
WH-07-05	WEST	9.8m	88°/014°	27°21'17.6" S | 31°47'09.7" E	-	7	3223	57°/050°	33°/221°	1.0137	-0.1781
	EAST					7	3374	54°/029°	08°/129°	1.0334	0.1569
WH-07-06	WEST	8.8m	74°/168°	27°21'17.0" S | 31°48'07.6" E	-	7	3536	33°/017°	05°/110°	1.0231	0.5067
	EAST					6	2033	18°/155°	03°/064°	1.0173	-0.0553
WH-07-07	WEST	4.3m	78°/177°	27°21'22.4" S | 31°49'47.9" E	-	7	4176	46°/189°	13°/085°	1.0517	0.2063
	EAST		72°/184°			7	5326	53°/212°	26°/082°	1.0339	-0.0293
WH-07-08	WEST	20.1m	trend: 030°	27°23'37.4" S | 31°49'34.3" E	-	7	1960	46°/334°	18°/083°	1.0337	0.3583
	EAST					8	1661	47°/353°	12°/097°	1.0563	0.4194
3L	WEST	0.43-0.47m	82°/170°	27°23'37.3" S | 31°49'35.2" E	060°-240°	8	3673	13°/071°	10°/135°	1.0196	-0.1469
	EAST					9	3377	76°/294°	11°/079°	1.0203	0.0220
4L	WEST	4.1m	82°/170°	27°23'37.3" S | 31°49'35.2" E	-	8	3161	58°/267°	32°/082°	1.0249	0.0451
	EAST					8	4403	40°/205°	24°/094°	1.0326	-0.0250
5L	WEST	5.5m	90°/350°	27°23'37.4" S | 31°49'34.3" E	-	8	690	06°/007°	13°/099°	1.0194	-0.1444
	EAST					8	3033	28°/028°	42°/270°	1.0193	0.1390
6L	WEST	0.62m	90°/030°	27°23'37.3" S | 31°49'35.2" E	-	9	3092	20°/192°	24°/093°	1.0384	0.6974
	EAST					9	2832	68°/212°	12°/090°	1.0348	0.6123
				Total specimens:		154					

n =number of specimens

Km = (kmax + kint + kmin)/3

P′ = degree of anisotropy

T = shape factor (oblate/prolate)

4) Tabulated SPO Data – Plagioclase

The Northern Lebombo dyke swarm

		2-D ELLIPSE						
Margin	**Sample**	**plane**	**strike °**	**dip °**	**rake °**	**L. axis (cm)**	**S. axis (cm)**	**tot. grains**
east	**9L5B**	**XY**	211	40	109.3	0.001568	0.001402	2198
		XZ	121	90	71.658	0.001557	0.001462	2035
		ZY	31	50	90.867	0.001579	0.001406	2852
	9L8B	**XY**	214	41	126.263	0.001600	0.00141	1297
		XZ	124	90	70.034	0.001550	0.001358	1453
		ZY	34	49	99.617	0.001574	0.001324	2103
west	**9L10A**	**XY**	227	37	91.13	0.001541	0.001333	2650
		XZ	137	90	69.475	0.001531	0.001288	2552
		ZY	47	53	98.593	0.001542	0.001326	2483
	9L16A	**XY**	281	15	75.864	0.001600	0.001525	1996
		XZ	191	90	59.716	0.001579	0.001475	1303
		ZY	101	75	22.036	0.001549	0.001514	1510
east	**10L2A**	**XY**	296	21	98.806	0.001594	0.001295	2457
		XZ	206	90	96.503	0.001423	0.001362	2576
		ZY	116	69	91.805	0.001572	0.001333	3934
	10L7A	**XY**	299	14	99.506	0.001672	0.001386	2426
		XZ	209	90	90.904	0.001494	0.001395	2243
		ZY	119	76	91.254	0.001576	0.001354	2188
west	**10L11C**	**XY**	296	36	95.93	0.001548	0.001323	2206
		XZ	206	90	65.058	0.001628	0.0014	2943
		ZY	116	54	88.353	0.001614	0.001371	2771
	10L16B	**XY**	282	53	94.15	0.001559	0.001379	2533
		XZ	192	90	36.377	0.001546	0.001385	2752
		ZY	102	37	83.522	0.001559	0.001439	2832
east	**15L3A**	**XY**	92	11	87.534	0.001574	0.001499	2486
		XZ	2	90	80.692	0.001684	0.001427	2195
		ZY	272	79	102.763	0.001673	0.001447	2326
	15L5B	**XY**	344	20	86.128	0.001685	0.00148	2240
		XZ	254	90	78.174	0.001648	0.001451	2355
		ZY	164	70	86.123	0.001690	0.001502	2420
west	**15L8**	**XY**	118	26	113.7	0.001652	0.001384	1885
		XZ	28	90	77.213	0.001697	0.001447	1717
		ZY	298	64	85.688	0.001662	0.001475	2134
	15L12B	**XY**	98	14	97.874	0.001566	0.001365	1928

		XZ	8	90	72.731	0.001753	0.001493	2060
		ZY	278	76	89.642	0.001855	0.001505	1324
east	**16L4B**	**XY**	288	18	96.883	0.002181	0.001905	1928
		XZ	198	90	77.515	0.001759	0.00159	2804
		ZY	108	72	102.944	0.001878	0.00157	2968
	16L6	**XY**	336	10	93.057	0.001829	0.001451	2051
		XZ	246	90	85.674	0.001812	0.001494	2419
		ZY	156	80	98.379	0.001761	0.00151	2429
west	**16L9B**	**XY**	297	7	92.985	0.001704	0.001427	3397
		XZ	207	90	87.817	0.001680	0.001458	3208
		ZY	117	83	89.307	0.001630	0.00142	2483
	16L16B	**XY**	63	15	90.703	0.001640	0.001425	2658
		XZ	333	90	79.337	0.001658	0.001482	2418
		ZY	243	75	92.137	0.001742	0.001462	2947
east	**17L3A**	**XY**	262	30	94.612	0.001642	0.0014	1677
		XZ	172	90	63.076	0.001576	0.001429	2012
		ZY	82	60	102.869	0.001704	0.001375	1662
	17L8A	**XY**	10	29	83.345	0.001698	0.001502	2462
		XZ	280	90	58.367	0.001601	0.00145	2434
		ZY	190	61	69.777	0.001612	0.001485	2205
west	**17L10A**	**XY**	106	24	63.222	0.001622	0.001483	2239
		XZ	16	90	66.697	0.001662	0.001459	2438
		ZY	286	66	100.793	0.001619	0.001463	1963
	17L16A	**XY**	12	21	100.756	0.001673	0.001498	2683
		XZ	282	90	75.536	0.001673	0.00151	2388
		ZY	192	69	92.16	0.001643	0.001467	2670
east	**18L2**	**XY**	227	38	128.342	0.006817	0.006184	2596
		XZ	137	90	81.85	0.006553	0.006011	1847
		ZY	47	52	117.565	0.006296	0.005576	1898
	18L6	**XY**	210	27	126.528	0.007403	0.007083	2488
		XZ	120	90	64.862	0.007065	0.006308	2420
		ZY	30	63	102.836	0.00819	0.007495	2545
west	**18L9**	**XY**	256	36	37.619	0.006199	0.006121	2215
		XZ	166	90	74.201	0.006404	0.006147	2031
		ZY	76	54	143.579	0.006657	0.006373	2319
	18L14	**XY**	245	35	68.611	0.006819	0.006669	2243
		XZ	155	90	41.993	0.008038	0.00729	3458
		ZY	65	55	106.461	0.008001	0.007241	3041
east	**19L1**	**XY**	285	19	107.059	0.007105	0.006584	1646
		XZ	195	90	69.541	0.0078	0.007406	1725
		ZY	105	71	113.435	0.007026	0.006134	1890

	19L4	**XY**	84	31	75.516	0.008314	0.006861	1875
		XZ	354	90	13.438	0.007596	0.006215	1881
		ZY	264	59	121.173	0.007744	0.006608	1802
west	**19L12**	**XY**	11	14	102.305	0.007955	0.007787	3016
		XZ	281	90	172.446	0.008095	0.007242	2805
		ZY	191	76	111.025	0.007964	0.007566	2003
	19L14	**XY**	261	40	77.349	0.006865	0.006362	2234
		XZ	171	90	56.707	0.007997	0.007398	3255
		ZY	81	50	90.819	0.006912	0.00671	2135

		3-D ellipsoid							**FOLIATION**				
Margin	**Sample**	**√F**	**D1**	**I1**	**D3**	**I3**	**P'**	**T**	**DEC**	**INC**	**L1**	**L2**	**L3**
east	**9L5B**	0.8%	90	77	230	10	1.1592	0.3514	320	80	1.0660	1.0171	0.9223
	9L8B	1.2%	129	67	250	12	1.2488	0.2133	340	78	1.1077	1.0158	0.8887
west	**9L10A**	6.5%	158	75	55	3	1.2488	-0.1616	145	87	1.1235	0.9882	0.9007
	9L16A	5.4%	169	35	69	14	1.0522	-0.5960	159	76	1.0292	0.9905	0.9809
east	**10L2A**	2.5%	38	60	306	1	1.2429	0.6625	36	89	1.0823	1.0458	0.8835
	10L7A	3.8%	43	74	310	1	1.2284	0.6167	40	89	1.0800	1.0406	0.8898
west	**10L11C**	5.8%	199	70	302	5	1.2405	0.0067	32	85	1.1134	1.0005	0.8977
	10L16B	7.1%	187	36	283	8	1.1375	0.1786	13	82	1.0621	1.0077	0.9344
east	**15L3A**	3.7%	53	76	272	11	1.2012	-0.6176	2	79	1.1096	0.9651	0.9338
	15L5B	6.1%	238	83	337	1	1.1804	0.0603	67	89	1.0846	1.0033	0.9190
west	**15L8**	6.4%	290	77	146	10	1.2439	0.2181	236	80	1.1055	1.0159	0.8904

	15L12B	3.5%	8	72	107	3	1.2828	-0.0413	197	87	1.1343	0.9966	0.8846
east	**16L4B**	3.1%	238	72	120	9	1.2225	0.1763	210	81	1.0985	1.0118	0.8997
	16L6	11.9%	349	85	162	5	1.2728	0.2525	252	85	1.1154	1.0203	0.8788
west	**16L9B**	7.9%	51	88	301	1	1.2355	0.2725	31	89	1.0995	1.0191	0.8924
	16L16B	3.4%	345	81	244	2	1.2217	0.1991	334	88	1.0972	1.0133	0.8995
east	**17L3A**	2.7%	195	59	92	8	1.2695	0.2687	182	82	1.1132	1.0213	0.8796
	17L8A	7.2%	259	50	356	6	1.1424	0.2559	86	84	1.0621	1.0113	0.9310
west	**17L10A**	4.1%	42	69	257	18	1.1699	-0.0230	347	72	1.0822	0.9988	0.9251
	17L16A	4.1%	283	79	26	2	1.1609	0.1709	116	88	1.0725	1.0085	0.9246
east	**18L2**	0.2%	180	58	271	1	1.180	0.538	1	89	1.0669	1.0287	0.9111
	18L6	2.1%	143	61	253	11	1.133	-0.303	343	79	1.0699	0.9877	0.9463
west	**18L9**	1.9%	243	49	146	6	1.056	-0.638	236	84	1.0317	0.9891	0.9799
	18L14	0.9%	174	42	48	33	1.130	-0.536	138	57	1.0714	0.9793	0.9531
east	**19L1**	1.0%	237	53	126	15	1.158	0.113	216	75	1.0731	1.0055	0.9268

	19L4	4.1%	358	10	259	40	1.340	0.073	349	50	1.1529	1.0072	0.8612
west	**19L12**	5.9%	109	2	202	55	1.088	-0.185	292	35	1.0457	0.9948	0.9613
	19L14	5.3%	177	62	60	14	1.086	0.013	150	76	1.0421	1.0003	0.9593

√F = percent error in orientation determination
I = inclination (plunge, in °)
D = declination (azimuth, in °)
DEC = declination (°)
INC = inclination (°)
L denotes axes lengths (cm)

The Rooi Rand dyke swarm (Northern Region, Swaziland)

		2-D ELLIPSE						
Margin	**Sample**	**plane**	**strike**	**dip**	**rake**	**L. axis**	**S. axis**	**tot. grains**
east	**SZ-1BA**	**XY**	029	42	91.574	0.001648	0.00149	3233
		XZ	299	90	41.389	0.001911	0.00154	2861
		ZY	209	48	86.172	0.001988	0.00166	2291
	SZ-1BB	**XY**	029	42	108.24	0.001743	0.00161	3303
		XZ	299	90	41.387	0.001995	0.00168	2649
		ZY	209	48	87.626	0.002045	0.00174	1783
west	**SZ-1LA**	**XY**	175	29	105.17	0.001804	0.00152	2650
		XZ	85	90	60.006	0.001794	0.00162	2330
		ZY	355	61	89.608	0.001752	0.00156	2507
	SZ-1LB	**XY**	175	29	102.5	0.001851	0.00161	2782
		XZ	85	90	60.718	0.001761	0.00167	2955
		ZY	355	61	85.295	0.001724	0.00156	2954
west	**SZ-2BB**	**XY**	258	21	106.46	0.001929	0.00169	2514
		XZ	168	90	80.524	0.001783	0.00157	2919
		ZY	078	69	109.88	0.001825	0.00159	3140
	SZ-2FA	**XY**	203	12	165.39	0.001542	0.00149	2139
		XZ	113	90	88.362	0.001655	0.00146	2610
		ZY	023	78	111.62	0.001619	0.00151	2788
east	**SZ-2GA**	**XY**	328	20	80.033	0.00162	0.00153	2294
		XZ	238	90	61.24	0.001837	0.00173	1990
		ZY	148	70	108.79	0.001603	0.00147	2370
	SZ-2LA	**XY**	321	27	87.476	0.001544	0.00144	2767

		XZ	231	90	59.902	0.001831	0.00168	2256
		ZY	141	063	104.98	0.001508	0.00133	2403
west	**SZ-4BA**	**XY**	175	66	91.896	0.001737	0.001650	2581
		XZ	085	90	42.196	0.001589	0.001431	3199
		ZY	355	24	107.235	0.001557	0.001458	3077
	SZ-4EA	**XY**	145	53	75.414	0.001580	0.001419	2994
		XZ	055	90	53.484	0.001552	0.001416	2873
		ZY	325	37	107.159	0.001628	0.001409	3125
east	**SZ-4HA**	**XY**	185	25	102.695	0.001734	0.001566	2662
		XZ	095	90	85.031	0.001624	0.001495	2948
		ZY	005	65	96.356	0.001577	0.001456	2690
	SZ-4J	**XY**	175	28	89.083	0.001704	0.001556	3544
		XZ	085	90	89.192	0.001615	0.001464	3398
		ZY	355	62	102.471	0.001582	0.001420	3576
west	**SZ-6CA**	**XY**	094	67	93.338	0.001407	0.001353	3052
		XZ	004	90	27.070	0.001809	0.001538	2025
		ZY	274	23	99.511	0.001497	0.001340	3133
	SZ-6EA	**XY**	102	26	113.126	0.001768	0.001683	3782
		XZ	012	90	63.113	0.001573	0.001451	3986
		ZY	282	64	117.527	0.001706	0.001532	3641
east	**SZ-6JA**	**XY**	095	65	129.894	0.001643	0.001454	2270
		XZ	005	90	35.123	0.001617	0.001447	2122
		ZY	275	25	95.328	0.001560	0.001106	2800
	SZ-6JB	**XY**	095	65	110.867	0.001732	0.001422	2540
		XZ	005	90	41.471	0.001538	0.001266	2657
		ZY	275	25	110.087	0.001747	0.001470	2883
west	**SZ-10FA**	**XY**	327	57	84.026	0.001798	0.00171	2383
		XZ	237	90	49.933	0.001786	0.0016	2218
		ZY	147	33	88.62	0.001871	0.00174	2307
	SZ-10FC	**XY**	327	57	47.881	0.001753	0.00166	2294
		XZ	237	90	48.502	0.001879	0.0017	2458
		ZY	147	33	78.917	0.001802	0.00173	2693
east	**SZ-10G**	**XY**	39	48	156.19	0.001857	0.00175	1810
		XZ	309	90	50.042	0.001594	0.00134	2364
		ZY	219	42	119.05	0.001693	0.00148	3032
	SZ-10H	**XY**	354	50	59.46	0.001731	0.00156	2803
		XZ	264	90	48.798	0.001719	0.00148	3019
		ZY	174	40	101.33	0.002178	0.00201	2064

		3-D ellipsoid							FOLIATION				
Margin	**Sample**	**√F**	**D1**	**I1**	**D3**	**I3**	**P'**	**T**	**DEC**	**INC**	**L1**	**L2**	**L3**
east	**SZ-1BA**	5.8%	295	39	29	5	1.273	-0.4239	119	85	1.1430	0.9675	0.9043
	SZ-1BB	3.2%	298	40	45	19	1.226	-0.3701	135	71	1.1185	0.9757	0.9163
west	**SZ-1LA**	5.8%	86	59	191	9	1.202	0.6195	281	81	1.0710	1.0364	0.9009
	SZ-1LB	3.7%	71	67	186	10	1.160	0.7695	276	80	1.0518	1.0355	0.9182
west	**SZ-2BB**	5.4%	218	73	104	7	1.209	0.2212	194	83	1.0912	1.0140	0.9038
	SZ-2FA	1.9%	195	74	98	2	1.134	-0.2884	188	88	1.0702	0.9882	0.9456
east	**SZ-2GA**	1.8%	270	59	141	20	1.106	0.0215	231	70	1.0513	1.0007	0.9505
	SZ-2LA	2.2%	256	58	144	14	1.148	-0.1150	234	76	1.0743	0.9947	0.9358
west	**SZ-4BA**	3.8%	99	46	198	9	1.118	-0.5551	288	81	1.0647	0.9806	0.9578
	SZ-4EA	2.4%	86	56	328	18	1.194	-0.0402	58	72	1.0938	0.9976	0.9164
east	**SZ-4HA**	3.6%	296	86	205	0	1.135	0.1333	295	90	1.0621	1.0056	0.9362
	SZ-4J	2.3%	195	81	5	9	1.162	-0.2119	95	81	1.0828	0.9896	0.9333
west	**SZ-6CA**	4.3%	12	28	107	9	1.173	-0.7795	197	81	1.0958	0.9630	0.9477
	SZ-6EA	2.5%	52	50	311	10	1.136	-0.2606	41	80	1.0708	0.9891	0.9441

east	**SZ-6JA**	9.0%	12	28	115	24	1.345	-0.0377	205	66	1.1615	0.9963	0.8641
	SZ-6JB	7.9%	16	43	122	17	1.310	0.3237	212	73	1.1255	1.0290	0.8635
west	**SZ-10FA**	3.2%	237	54	135	9	1.126	-0.6161	225	81	1.0696	0.9773	0.9566
	SZ-10FC	2.5%	240	52	99	31	1.111	0.1026	189	59	1.0519	1.0036	0.9473
east	**SZ-10G**	2.6%	343	41	100	27	1.223	-0.3437	190	63	1.1162	0.9776	0.9163
	SZ-10H	5.5%	288	55	145	29	1.178	0.0089	235	61	1.0852	1.0005	0.9211

The Rooi Rand dyke swarm (Central Region, Pongola, South Africa)

		2-D ELLIPSE						
Margin	**Sample**	**plane**	**strike**	**dip**	**rake**	**L. axis**	**S. axis**	**tot. grains**
east	**WH-07-05E**	**XY**	268	10	115.19	0.001686	0.001503	2559
		XZ	178	90	76.077	0.001666	0.00149	3567
		ZY	088	80	106.31	0.001793	0.001598	3239
	WH-07-05F	**XY**	179	12	71.276	0.003786	0.003328	810
		XZ	089	90	83.620	0.002362	0.001911	930
		ZY	359	78	100.65	0.003067	0.002527	556
west	**WH-07-05I**	**XY**	264	21	142.55	0.000651	0.000602	407
		XZ	174	90	59.795	0.000357	0.000320	1004
		ZY	084	69	85.222	0.000332	0.000305	1184
	WH-07-05M	**XY**	319	08	86.483	0.00378	0.003106	795
		XZ	229	90	12.656	0.00372	0.003488	649
		ZY	139	82	100.89	0.003612	0.003492	719
east	**WH-07-07I**	**XY**	304	05	143.8	0.003433	0.0032	771
		XZ	214	90	99.5	0.003535	0.003109	760
		ZY	124	85	76.804	0.003475	0.003186	681

	WH-07-07K	**XY**	029	03	60.247	0.001559	0.001411	1047
		XZ	299	90	106.74	0.002816	0.002546	509
		ZY	209	87	90.427	0.003001	0.002822	718
west	**WH-07-07D**	**XY**	070	44	98.425	0.003402	0.002829	765
		XZ	340	90	111.98	0.003362	0.003256	794
		ZY	250	46	86.553	0.003839	0.003327	778
	WH-07-07G	**XY**	219	12	118.25	0.00279	0.002562	604
		XZ	129	90	74.758	0.003011	0.002556	534
		ZY	039	78	72.21	0.002924	0.002515	590
	WH-07-07E	**XY**	077	57	109.67	0.003112	0.002759	472
		XZ	347	90	28.581	0.003396	0.003057	492
		ZY	257	33	68.635	0.001911	0.001707	500
east	**WH-07-08C**	**XY**	084	40	113.31	0.003324	0.002891	490
		XZ	354	90	47.333	0.001551	0.001348	956
		ZY	264	50	124.649	0.001954	0.001840	713
	WH-07-08H	**XY**	060	17	151.33	0.002852	0.00244	407
		XZ	330	90	60.751	0.001686	0.001625	560
		ZY	240	74	115.075	0.001643	0.001538	1036
west	**WH-07-08N**	**XY**	358	12	6.136	0.003296	0.002797	418
		XZ	268	90	72.818	0.002190	0.001578	441
		ZY	178	78	30.971	0.001936	0.001891	408
	WH-07-08O	**XY**	304	20	21.563	0.00348	0.002973	675
		XZ	214	90	66.663	0.003293	0.002893	954
		ZY	124	70	125.62	0.003158	0.003043	590
east	**4L13**	**XY**	020	10	75.360	0.003300	0.003020	837
		XZ	290	90	92.506	0.002828	0.002592	713
		ZY	200	80	84.686	0.001547	0.001367	1049
	4L14	**XY**	031	13	132.199	0.001439	0.001299	1985
		XZ	301	90	74.626	0.001464	0.001212	2255
		ZY	211	77	108.894	0.001396	0.001299	2070
west	**4L3**	**XY**	115	06	81.199	0.002940	0.002261	2162
		XZ	025	90	95.201	0.003004	0.002487	2325
		ZY	295	84	85.169	0.002931	0.002437	2041
	4L10	**XY**	137	00	31.454	0.003026	0.002730	846
		XZ	047	90	106.805	0.002780	0.002370	438
		ZY	317	90	141.281	0.002526	0.002409	574
east	**6L13**	**XY**	056	15	98.940	0.002882	0.002582	992
		XZ	326	90	66.804	0.003248	0.002875	696

		ZY	236	75	96.191	0.002744	0.002357	588
	6L15	**XY**	080	22	84.679	0.002942	0.002409	695
		XZ	350	90	46.687	0.003095	0.002764	1053
		ZY	260	68	93.195	0.002850	0.002460	731
west	**6L4**	**XY**	085	34	99.475	0.001880	0.001683	2562
		XZ	355	90	55.093	0.001807	0.001719	2735
		ZY	265	56	90.558	0.001781	0.001556	3127
	6L6	**XY**	069	30	91.705	0.001699	0.001558	1364
		XZ	339	90	45.905	0.001831	0.001688	1468
		ZY	249	60	59.970	0.001772	0.001632	1422

		3-D ellipsoid							**FOLIATION**				
Margin	**Sample**	**√F**	**D1**	**I1**	**D3**	**I3**	**P'**	**T**	**DEC**	**INC**	**L1**	**L2**	**L3**
east	**WH-07-05E**	4.0%	214	61	118	4	1.183	0.1401	208	86	1.0829	1.0078	0.9163
	WH-07-05F	5.7%	168	80	338	10	1.296	-0.2175	68	80	1.1475	0.9816	0.8878
west	**WH-07-05I**	0.0%	174	60	313	24	1.147	0.1688	43	66	1.0665	1.0077	0.9304
	WH-07-05M	5.2%	225	4	135	8	1.178	-0.2405	225	82	1.0916	0.9871	0.9281
east	**WH-07-07I**	0.6%	86	68	182	3	1.164	-0.2213	272	87	1.0840	0.9890	0.9328
	WH-07-07K	3.1%	93	59	351	7	1.146	0.1297	81	83	1.0672	1.0059	0.9315
west	**WH-07-07D**	0.6%	180	63	74	8	1.216	0.5601	164	82	1.0786	1.0353	0.8955
	WH-07-07G	4.0%	75	71	249	19	1.222	-0.2017	339	71	1.1120	0.9867	0.9114
	WH-07-07E	5.2%	326	35	78	28	1.175	0.2918	168	62	1.0745	1.0156	0.9163
east	**WH-07-08C**	9.9%	20	25	117	15	1.161	0.2848	207	75	1.0690	1.0141	0.9225

	WH-07-08H	4.3%	22	18	115	10	1.171	0.1470	205	80	1.0778	1.0077	0.9207
west	**WH-07-08N**	7.3%	237	68	93	18	1.334	0.5068	183	72	1.1217	1.0478	0.8508
	WH-07-08O	0.1%	308	38	58	23	1.197	0.6559	148	67	1.0680	1.0375	0.9025
east	**4L13**	1.6%	142	86	2	3	1.157	0.0777	92	87	1.0737	1.0038	0.9278
	4L14	6.4%	337	64	83	8	1.200	0.0925	173	82	1.0921	1.0056	0.9106
west	**4L3**	10.3%	204	74	103	3	1.333	0.3636	193	87	1.1312	1.0346	0.8545
	4L10	4.4%	174	47	68	14	1.191	0.0475	158	76	1.0896	1.0028	0.9153
east	**6L13**	3.3%	340	63	247	2	1.201	-0.0410	337	88	1.0972	0.9975	0.9137
	6L15	5.9%	349	33	255	6	1.246	0.2756	345	84	1.1036	1.0202	0.8882
west	**6L4**	0.9%	356	55	94	5	1.161	0.4593	184	85	1.0630	1.0223	0.9202
	6L6	5.5%	316	37	65	23	1.121	0.0402	155	67	1.0580	1.0015	0.9437

5) Tabulated SPO Data – Opaque Grains

The Northern Lebombo dyke swarm

		2-D ELLIPSE						
Margin	**Sample**	**plane**	**strike**	**dip**	**rake**	**L. axis**	**S. axis**	**tot. grains**
east	**9L5B**	**XY**	211	40	97.208	0.00036	0.000309	664
		XZ	121	90	112.31	0.000332	0.000313	490
		ZY	31	50	94.422	0.000368	0.000344	599
	9L8B	**XY**	214	41	85.519	0.000413	0.000366	703
		XZ	124	90	48.629	0.000369	0.000323	1232
		ZY	34	49	84.589	0.000388	0.000302	1368
west	**9L10A**	**XY**	227	37	89.785	0.000367	0.000343	1032
		XZ	137	90	52.045	0.000365	0.000303	1137
		ZY	47	53	79.068	0.000353	0.000331	975
	9L16A	**XY**	281	15	95.235	0.000291	0.000231	1160
		XZ	191	90	79.841	0.000273	0.000218	871
		ZY	101	75	93.405	0.000278	0.000228	881
east	**10L2A**	**XY**	296	21	89.487	0.000401	0.000383	529
		XZ	206	90	68.122	0.000409	0.000334	703
		ZY	116	69	80.302	0.000388	0.000324	797
	10L7A	**XY**	299	14	87.437	0.000393	0.000316	796
		XZ	209	90	76.911	0.000396	0.00035	659
		ZY	119	76	80.468	0.000395	0.000356	598
west	**10L11C**	**XY**	296	36	79.843	0.000388	0.000331	846
		XZ	206	90	54.877	0.000393	0.000305	991
		ZY	116	54	94.894	0.000385	0.000353	672
	10L16B	**XY**	282	53	93.559	0.000427	0.000352	624
		XZ	192	90	42.228	0.000392	0.000327	665
		ZY	102	37	97.41	0.000417	0.000337	604
east	**15L3A**	**XY**	92	11	1.124	0.000392	0.000382	331
		XZ	2	90	1.289	0.000368	0.000333	291
		ZY	272	79	73.755	0.000383	0.000328	407
	15L5B	**XY**	344	20	65.114	0.000437	0.000388	212
		XZ	254	90	74.162	0.000388	0.000337	704
		ZY	164	70	90.506	0.000378	0.000326	530
west	**15L8**	**XY**	118	26	87.286	0.000351	0.000333	790
		XZ	28	90	143.463	0.000359	0.000347	516
		ZY	298	64	88.01	0.000372	0.00033	1043
	15L12B	**XY**	98	14	96.364	0.000392	0.000338	702

		XZ	8	90	72.607	0.000383	0.00035	750
		ZY	278	76	77.607	0.000376	0.000344	568
east	**16L4B**	**XY**	288	18	89.977	0.000381	0.000325	296
		XZ	198	90	70.782	0.000383	0.000302	546
		ZY	108	72	97.051	0.000373	0.000312	465
	16L6	**XY**	336	10	87.896	0.000442	0.000342	779
		XZ	246	90	72.219	0.000496	0.000373	664
		ZY	156	80	93.966	0.000490	0.00036	631
west	**16L9B**	**XY**	297	7	93.597	0.000383	0.000332	877
		XZ	207	90	83.35	0.000397	0.000346	752
		ZY	117	83	96.075	0.000391	0.000344	776
	16L16B	**XY**	63	15	84.082	0.000394	0.000331	295
		XZ	333	90	61.287	0.000408	0.000351	308
		ZY	243	75	84.692	0.000372	0.000314	523
east	**17L3A**	**XY**	262	30	153.955	0.000387	0.000385	399
		XZ	172	90	59.134	0.000408	0.00036	623
		ZY	82	60	91.044	0.000400	0.000345	675
	17L8A	**XY**	10	29	174.633	0.000340	0.000318	455
		XZ	280	90	65.183	0.000348	0.000328	759
		ZY	190	61	90.743	0.000366	0.000313	665
west	**17L10A**	**XY**	106	24	77.009	0.000361	0.00033	443
		XZ	16	90	65.835	0.000364	0.000335	410
		ZY	286	66	89.646	0.000374	0.000368	338
	17L16A	**XY**	12	21	81.904	0.000375	0.000339	494
		XZ	282	90	67.594	0.000414	0.00031	646
		ZY	192	69	82.25	0.000386	0.000351	468
west	**18L9**	**XY**	256	36	101.501	0.005815	0.005554	680
		XZ	166	90	50.242	0.007168	0.005737	766
		ZY	76	54	97.622	0.005175	0.004745	877
	18L14	**XY**	245	35	70.001	0.005324	0.004982	837
		XZ	155	90	13.915	0.004416	0.004301	684
		ZY	65	55	140.147	0.004674	0.00456	917
west	**19L12**	**XY**	11	14	66.462	0.002978	0.002692	860
		XZ	281	90	69.915	0.004021	0.003247	1066
		ZY	191	76	118.585	0.003255	0.00286	1015
	19L14	**XY**	261	40	154.994	0.00543	0.004951	907
		XZ	171	90	9.403	0.004247	0.004093	963
		ZY	81	50	111.095	0.003448	0.003142	804
east	**18L2**	**XY**	227	38	138.029	0.005848	0.005266	585
		XZ	137	90	62.372	0.006047	0.004534	614

		ZY	47	52	171.966	0.005417	0.004483	512
	18L6	**XY**	210	27	129.005	0.005119	0.00483	669
		XZ	120	90	38.428	0.005566	0.004699	615
		ZY	30	63	104.449	0.004288	0.003855	752
east	**19L1**	**XY**	285	19	43.41	0.00316	0.002892	1459
		XZ	195	90	90.627	0.003032	0.002947	401
		ZY	105	71	81.652	0.002812	0.002535	1096
	19L4	**XY**	84	31	39.772	0.003777	0.003296	940
		XZ	354	90	140.387	0.004295	0.003504	729
		ZY	264	59	97.045	0.003917	0.003563	935

√F = percent error in orientation determination
I = inclination (plunge)
D = declination (azimuth)

		3-D ellipsoid							**FOLIATION**				
Margin	**Sample**	**√F**	**D1**	**I1**	**D3**	**I3**	**P'**	**T**	**DEC**	**INC**	**L1**	**L2**	**L3**
east	**9L5B**	2.2%	313	59	221	1	1.161	0.0191	311	89	1.0769	1.0009	0.9277
	9L8B	0.3%	116	48	207	1	1.289	-0.0498	297	89	1.1373	0.9958	0.8830
west	**9L10A**	8.9%	129	51	224	4	1.160	-0.7878	314	86	1.0892	0.9651	0.9513
	9L16A	10.4%	207	84	108	1	1.339	0.2468	198	89	1.1415	1.0240	0.8555
east	**10L2A**	3.5%	184	66	293	8	1.249	-0.7569	23	82	1.1360	0.9499	0.9267
	10L7A	10.7%	185	77	294	4	1.222	0.7242	24	86	1.0725	1.0456	0.8918
west	**10L11C**	13.8%	210	56	102	12	1.256	-0.2135	192	78	1.1289	0.9840	0.9002
	10L16B	7.1%	200	44	290	0	1.313	0.1241	20	90	1.1389	1.0113	0.8682

east	**15L3A**	11.4%	329	47	94	28	1.122	0.1338	184	62	1.0562	1.0051	0.9420
	15L5B	2.8%	263	75	133	9	1.215	0.0204	223	81	1.1015	1.0013	0.9066
west	**15L8**	4.4%	17	80	115	1	1.111	0.5610	205	89	1.0417	1.0190	0.9421
	15L12B	7.0%	346	70	105	10	1.163	0.4837	195	80	1.0628	1.0237	0.9191
east	**16L4B**	9.6%	213	70	109	5	1.289	-0.3429	199	85	1.1488	0.9719	0.8956
	16L6	8.6%	254	68	154	4	1.490	0.0637	244	86	1.2147	1.0085	0.8163
west	**16L9B**	6.9%	239	82	122	4	1.198	0.1755	212	86	1.0881	1.0105	0.9094
	16L16B	5.9%	323	52	55	2	1.243	0.0788	145	88	1.1115	1.0057	0.8946
east	**17L3A**	1.2%	174	59	277	7	1.172	-0.8953	7	83	1.0955	0.9589	0.9519
	17L8A	7.4%	282	63	59	20	1.128	-0.7620	149	70	1.0714	0.9724	0.9598
west	**17L10A**	6.8%	16	65	266	9	1.085	0.3944	356	81	1.0353	1.0106	0.9558
	17L16A	12.9%	273	66	167	7	1.268	-0.6888	257	83	1.1450	0.9507	0.9187
east	**18L2**	19.3%	189	42	297	19	1.243	0.871	27	71	1.071	1.058	0.882
	18L6	1.3%	138	34	260	38	1.214	-0.642	350	52	1.117	0.962	0.931

east	**19L1**	3.3%	166	69	62	5	1.137	0.453	152	85	1.054	1.019	0.931
	19L4	14.1%	134	41	233	11	1.186	-0.555	323	79	1.101	0.970	0.936
west	**18L9**	8.1%	173	48	313	34	1.192	-0.756	43	56	1.106	0.960	0.942
	18L14	2.7%	312	20	59	39	1.066	0.217	149	51	1.030	1.005	0.967
west	**19L12**	9.4%	329	65	156	24	1.235	-0.205	246	66	1.119	0.986	0.907
	19L14	5.7%	209	15	307	27	1.119	-0.354	37	63	1.063	0.987	0.953

The Rooi Rand dyke swarm (Northern Region, Swaziland)

		2-D ELLIPSE						
Margin	**Sample**	**plane**	**strike**	**dip**	**rake**	**L. axis**	**S. axis**	**tot. grains**
east	**SZ-1BA**	**XY**	029	42	101.59	0.000405	0.000333	337
		XZ	299	90	48.925	0.00039	0.000369	484
		ZY	209	48	88.368	0.000363	0.00036	318
	SZ-1BB	**XY**	029	42	83.632	0.00036	0.000312	684
		XZ	299	90	47.184	0.000388	0.000266	662
		ZY	209	48	87.31	0.000361	0.000279	561
west	**SZ-1LA**	**XY**	175	29	84.033	0.000388	0.000316	419
		XZ	85	90	50.217	0.000384	0.000336	372
		ZY	355	61	86.282	0.000396	0.000305	464
	SZ-1LB	**XY**	175	29	91.696	0.000355	0.000298	649
		XZ	85	90	53.733	0.000371	0.000306	512
		ZY	355	61	83.985	0.000388	0.000301	573
east	**SZ-2BB**	**XY**	258	21	89.315	0.000418	0.000298	688
		XZ	168	90	68.279	0.000409	0.000304	431
		ZY	078	69	88.944	0.000417	0.000278	503
	SZ-2FA	**XY**	203	12	83.526	0.000371	0.000354	392
		XZ	113	90	86.151	0.000399	0.000327	431
		ZY	023	78	90.128	0.000422	0.000332	444

west	SZ-2GA	XY	328	20	94.8	0.000362	0.000302	270
		XZ	238	90	70.841	0.000379	0.000295	527
		ZY	148	70	89.659	0.000381	0.00028	551
	SZ-2LA	XY	321	27	91.242	0.00042	0.000288	747
		XZ	231	90	75.002	0.000472	0.000402	357
		ZY	141	063	91.194	0.000414	0.000296	586
west	SZ-4BA	XY	175	66	89.201	0.000396	0.000308	480
		XZ	085	90	21.244	0.000415	0.000319	571
		ZY	355	24	84.882	0.000405	0.000308	591
	SZ-4EA	XY	145	53	83.634	0.000392	0.000321	712
		XZ	055	90	26.949	0.000389	0.000316	599
		ZY	325	37	84.105	0.000402	0.000339	571
east	SZ-4HA	XY	185	25	86.663	0.000440	0.000385	322
		XZ	095	90	62.211	0.000368	0.000310	377
		ZY	005	65	86.461	0.000365	0.000307	435
	SZ-4J	XY	175	28	87.716	0.000409	0.000309	728
		XZ	085	90	49.214	0.00038	0.000331	619
		ZY	355	62	86.321	0.000405	0.000321	729
west	SZ-6CA	XY	094	67	90.014	0.000404	0.000303	954
		XZ	004	90	21.296	0.000416	0.000295	746
		ZY	274	23	84.412	0.000408	0.000285	770
	SZ-6EA	XY	102	26	92.122	0.000411	0.000304	728
		XZ	012	90	62.688	0.000399	0.000289	838
		ZY	282	64	86.321	0.000398	0.0003	748
east	SZ-6JA	XY	095	65	96.861	0.00038	0.000273	283
		XZ	005	90	28.545	0.000391	0.000261	358
		ZY	275	25	93.424	0.000383	0.000233	264
	SZ-6JB	XY	095	65	90.674	0.000373	0.000275	387
		XZ	005	90	22.97	0.000385	0.000249	348
		ZY	275	25	90.944	0.00039	0.000267	432
west	SZ-10FA	XY	327	57	91.928	0.000382	0.000323	622
		XZ	237	90	26.476	0.000381	0.000292	688
		ZY	147	33	93.746	0.000373	0.000317	579
	SZ-10FC	XY	327	57	84.625	0.000378	0.000288	723
		XZ	237	90	28.665	0.000376	0.000278	619
		ZY	147	33	82.505	0.000388	0.00029	712
east	SZ-10G	XY	39	48	84.252	0.000466	0.000427	473
		XZ	309	90	43.523	0.000405	0.000325	703

		ZY	219	42	89.017	0.000444	0.000339	583
	SZ-10H	XY	354	50	84.8	0.000353	0.000317	619
		XZ	264	90	40.771	0.000395	0.000291	977
		ZY	174	40	89.992	0.00037	0.000287	747

		3-D ellipsoid							FOLIATION				
Margin	**Sample**	**√F**	**D1**	**I1**	**D3**	**I3**	**P'**	**T**	**DEC**	**INC**	**L1**	**L2**	**L3**
east	**SZ-1BA**	10.4%	143	41	42	12	1.141	0.3478	132	78	1.0589	1.0151	0.9303
	SZ-1BB	10.2%	296	47	201	5	1.445	-0.4548	291	85	1.2266	0.9476	0.8603
west	**SZ-1LA**	2.8%	79	46	348	0	1.344	0.2564	78	90	1.1427	1.0253	0.8536
	SZ-1LB	4.8%	77	52	175	6	1.346	-0.0058	265	84	1.1601	0.9994	0.8625
east	**SZ-2BB**	8.0%	166	68	257	1	1.630	0.2235	347	89	1.2500	1.0366	0.7718
	SZ-2FA	0.1%	118	86	16	1	1.297	-0.6361	106	89	1.1594	0.9496	0.9083
west	**SZ-2GA**	4.9%	237	71	333	2	1.425	-0.1114	63	88	1.2006	0.9870	0.8439
	SZ-2LA	7.1%	238	86	143	0	1.534	0.5653	233	90	1.1789	1.0794	0.7858
west	**SZ-4BA**	9.7%	81	19	171	1	1.429	0.1156	261	89	1.1861	1.0138	0.8317
	SZ-4EA	9.7%	49	19	318	5	1.295	0.0341	48	85	1.1361	1.0029	0.8776
east	**SZ-4HA**	5.8%	89	61	180	1	1.245	-0.0874	270	89	1.1192	0.9936	0.8992
	SZ-4J	7.2%	80	37	172	1	1.365	0.4747	262	89	1.1345	1.0486	0.8406

west	**SZ-6CA**	10.1%	359	20	90	2	1.577	0.0489	180	88	1.2497	1.0074	0.7943
	SZ-6EA	13.1%	6	62	103	4	1.487	0.1722	193	86	1.2037	1.0228	0.8122
east	**SZ-6JA**	7.1%	8	29	101	6	1.802	0.0216	191	84	1.3369	1.0042	0.7448
	SZ-6JB	12.2%	6	22	96	0	1.657	-0.0173	186	90	1.2873	0.9971	0.7791
west	**SZ-10FA**	11.4%	240	22	330	1	1.299	-0.2280	60	89	1.1495	0.9805	0.8872
	SZ-10FC	11.1%	230	25	139	2	1.480	0.0869	229	88	1.2085	1.0114	0.8182
east	**SZ-10G**	1.5%	308	44	214	4	1.341	-0.4384	304	86	1.1769	0.9593	0.8857
	SZ-10H	6.4%	264	41	169	6	1.388	-0.5107	259	84	1.2014	0.9480	0.8780

The Rooi Rand dyke swarm (Central Region, Pongola, South Africa)

		2-D ELLIPSE						
Margin	**Sample**	**plane**	**strike**	**dip**	**rake**	**L. axis**	**S. axis**	**tot. grains**
east	**WH-07-05E**	**XY**	268	10	175.13	0.000824	0.00079	277
		XZ	178	90	77.527	0.000865	0.000819	273
		ZY	088	80	136.88	0.00086	0.000839	235
	WH-07-05F	**XY**	179	12	127.31	0.000901	0.000897	113
		XZ	089	90	86.913	0.00096	0.000727	89
		ZY	359	78	93.458	0.000865	0.000725	228
west	**WH-07-05I**	**XY**	264	21	102.66	0.000974	0.000911	120
		XZ	174	90	167.96	0.000963	0.000765	113

		ZY	084	69	109.55	0.000965	0.000847	135
	WH-07-05M	**XY**	319	08	88.978	0.004085	0.003368	332
		XZ	229	90	75.709	0.004113	0.003407	220
		ZY	139	82	100.12	0.004219	0.003437	151
east	**WH-07-07I**	**XY**	304	05	95.071	0.003887	0.003383	445
		XZ	214	90	92.34	0.004459	0.003892	261
		ZY	124	85	97.871	0.004372	0.003645	335
	WH-07-07K	**XY**	029	03	85.424	0.004385	0.003591	341
		XZ	299	90	97.023	0.00382	0.003586	193
		ZY	209	87	47.077	0.003976	0.00369	207
west	**WH-07-07D**	**XY**	070	44	89.511	0.003782	0.003521	203
		XZ	340	90	44.856	0.004068	0.003687	442
		ZY	250	46	110.19	0.00371	0.003337	310
	WH-07-07G	**XY**	219	12	100.1	0.004279	0.003859	227
		XZ	129	90	78.67	0.005111	0.004132	263
		ZY	039	78	91.795	0.004124	0.003522	369
	WH-07-07E	**XY**	077	57	80.843	0.004217	0.003704	336
		XZ	347	90	27.9	0.003918	0.00333	520
		ZY	257	33	91.626	0.00375	0.003554	460
east	**WH-07-08C**	**XY**	084	40	93.799	0.000800	0.000689	277
		XZ	354	90	44.402	0.000775	0.000667	324
		ZY	264	50	95.683	0.000450	0.000365	794
	WH-07-08H	**XY**	060	17	116.028	0.000820	0.000765	203
		XZ	330	90	69.135	0.000822	0.000728	261
		ZY	240	74	104.456	0.000742	0.000690	214
west	**WH-07-08N**	**XY**	358	12	92.787	0.000654	0.000563	148
		XZ	268	90	77.130	0.000740	0.000681	334
		ZY	178	78	86.523	0.000715	0.000611	345
	WH-07-08O	**XY**	304	20	78.913	0.000887	0.000749	145
		XZ	214	90	72.456	0.000860	0.000804	186
		ZY	124	70	101.641	0.000859	0.000817	197
east	**4L13**	**XY**	020	10	85.569	0.003813	0.003492	361
		XZ	290	90	76.317	0.003926	0.003553	306
		ZY	200	80	79.288	0.004012	0.003403	359
	4L14	**XY**	031	13	84.758	0.003336	0.002972	215
		XZ	301	90	73.069	0.003333	0.002712	197
		ZY	211	77	89.949	0.003368	0.002713	478
west	**4L3**	**XY**	115	06	81.233	0.003666	0.003362	379

		XZ	025	90	83.300	0.003664	0.003142	133
		ZY	295	84	95.429	0.003494	0.003227	245
	4L10	**XY**	137	00	68.852	0.003485	0.003211	352
		XZ	047	90	92.547	0.003748	0.003379	313
		ZY	317	90	89.643	0.004231	0.003795	310
east	**6L13**	**XY**	056	15	96.591	0.004168	0.003397	377
		XZ	326	90	64.515	0.006855	0.005803	120
		ZY	236	75	87.500	0.004209	0.003496	529
	6L15	**XY**	080	22	96.223	0.003976	0.003651	321
		XZ	350	90	60.409	0.003601	0.003281	320
		ZY	260	68	88.984	0.003986	0.003494	236
west	**6L4**	**XY**	085	34	85.404	0.004124	0.003623	460
		XZ	355	90	54.780	0.003958	0.003471	523
		ZY	265	56	98.179	0.003728	0.003333	496
	6L6	**XY**	069	30	148.222	0.000866	0.000838	158
		XZ	339	90	67.256	0.000962	0.000945	134
		ZY	249	60	91.091	0.000897	0.000839	146

		3-D ellipsoid						**FOLIATION**					
Margin	**Sample**	**√F**	**D1**	**I1**	**D3**	**I3**	**P'**	**T**	**DEC**	**INC**	**L1**	**L2**	**L3**
east	**WH-07-05E**	0.7%	251	47	354	12	1.063	0.1771	84	78	1.0292	1.0036	0.9681
	WH-07-05F	3.9%	142	87	261	2	1.310	-0.7904	351	88	1.1678	0.9374	0.9135
west	**WH-07-05I**	11.7%	4	3	96	34	1.215	-0.2215	186	56	1.1090	0.9859	0.9147
	WH-07-05M	8.0%	253	71	138	8	1.307	0.1053	228	82	1.1375	1.0094	0.8709
east	**WH-07-07I**	4.1%	336	83	131	7	1.242	0.0678	221	83	1.1115	1.0049	0.8953
	WH-07-07K	11.5%	116	15	19	21	1.153	0.6688	109	69	1.0530	1.0301	0.9219
west	**WH-07-07D**	4.1%	2	43	260	12	1.140	-0.1720	350	78	1.0715	0.9925	0.9403

	WH-07-07G	6.7%	136	79	234	2	1.247	-0.3587	324	88	1.1286	0.9745	0.9092
	WH-07-07E	10.5%	346	22	249	16	1.149	-0.0262	339	74	1.0728	0.9988	0.9333
east	**WH-07-08C**	3.9%	1	42	270	1	1.274	0.0394	0	89	1.1269	1.0032	0.8845
	WH-07-08H	4.6%	356	61	96	6	1.135	-0.1651	186	84	1.0685	0.9931	0.9424
west	**WH-07-08N**	3.4%	255	77	1	4	1.206	0.4164	91	86	1.0815	1.0256	0.9016
	WH-07-08O	8.2%	11	45	111	10	1.143	0.7603	201	80	1.0467	1.0315	0.9262
east	**4L13**	1.5%	255	72	14	9	1.193	-0.0626	104	81	1.0941	0.9963	0.9174
	4L14	4.4%	300	72	205	2	1.295	-0.2847	295	88	1.1497	0.9761	0.8911
west	**4L3**	7.3%	51	83	278	5	1.150	-0.3218	8	85	1.0789	0.9854	0.9406
	4L10	2.5%	219	87	112	1	1.151	0.0101	202	89	1.0724	1.0005	0.9321
east	**6L13**	7.4%	326	58	64	5	1.291	0.2174	154	85	1.1244	1.0185	0.8732
	6L15	1.9%	349	59	86	4	1.161	-0.0299	176	86	1.0781	0.9985	0.9290
west	**6L4**	6.9%	5	54	263	9	1.176	0.0977	353	81	1.0815	1.0053	0.9198
	6L6	3.0%	340	63	106	16	1.059	0.0510	196	74	1.0284	1.0010	0.9714